IAEA
International Atomic Energy Agency

INDC(CCP)-0460 Rev
Distr. G+J

INDC International Nuclear Data Committee

Neutron Activation Cross Sections Measured at KRI in Neutron Energy Region 13.4 – 14.9 MeV

A.A. Filatenkov

St. Petersburg, Russia

December 2016

IAEA Nuclear Data Section, Vienna International Centre, A-1400 Vienna, Austria

Selected INDC documents may be downloaded in electronic form from
http://www-nds.iaea.org/publications/
or sent as an e-mail attachment.
Requests for hardcopy or e-mail transmittal should be directed to
nds.contact-point@iaea.org
or to:

Nuclear Data Section
International Atomic Energy Agency
Vienna International Centre
PO Box 100
A-1400 Vienna
Austria

Produced by the IAEA in Austria
December 2016

INDC(CCP)-0460 Rev
Distr. G+J

Neutron Activation Cross Sections Measured at KRI in Neutron Energy Region 13.4 – 14.9 MeV

A.A. Filatenkov

St. Petersburg, Russia

December 2016

Abstract

Results of measurements carried out at KRI for reaction cross sections induced by neutrons with energy around 14 MeV are gathered in the present publication. In total, 1547 experimental cross section values obtained for 242 reactions are given in Tables and Figures of this paper. All the recollected measurement results have been recalculated using the latest reference data on properties of target nuclei and reaction products. Also the reference cross-section values used in KRI experiments earlier were changed by the corresponding values taken from the recent IRDFF v1.05 evaluation. The revised experimental results supersede the corresponding KRI data published earlier. The work was sponsored by NDS of IAEA.

TABLE OF CONTENTS

1. INTRODUCTION

The present work is aimed for taking together results of the systematic activation cross section measurement for the reactions of importance for fusion and other applications. The experiments were carried out on the edge of the 20th – 21st centuries by a group of experimentalists at the Khlopin Radium Institute (KRI). The most important data were earlier published in [1 – 5].

Most KRI measurements were performed in the standard, rigidly fixed conditions that provided decreasing the random data uncertainties. The systematic uncertainty component related to the instrumentation used was reduced by obtaining the cross sections that are known with high accuracy using the same conditions.

When it was possible, the cross-sections for the excitation of metastable and ground states of the product nuclide were measured separately. In total, the **1547** experimental cross-section values obtained for **242** reactions are presented in Tables and Figures of this paper.

All the collected data has been revised with the latest reference parameters [26 – 29] which are the reference cross-sections, isotopic abundance of the target nuclei, and half-lives and gamma intensities of the reaction products. In this paper, the uncertainty contributions of the reference data are given explicitly in an additional column of the Tables that contain the cross-section measurement results. This was done to facilitate a possible next result recalculation that will be required if the reference data would be further changed.

One page for one reaction was chosen as the format of the experimental data presentation. There are the numeric information on measurement results given in Tables and the intercomparison of available experimental data and evaluations demonstrated in Figures. The relevant decay schemes and numeric decay data used are presented on the corresponding pages too.

The reference cross-section data on $^{27}Al(n, \alpha)^{24}Na$ and $^{93}Nb(n,2n)^{92m}Nb$ is tabulated in Attachment. Both the new IRDFF v1.05 values used in this paper and the old KRI values used earlier are given in the Attachment Tables.

In the report body, the applied experimental methods are described in detail. Some original methods developed for special measurements are also considered.

The experimental data values given in Tables supersede the corresponding experimental KRI data published earlier.

The work was sponsored by NDS of IAEA.

The full report text of the present version is available as:

https://www-nds.iaea.org/publications/indc/indc-ccp-0460/

Some misprints revealed in the report version of March 2016 have been corrected in the present version (December 2016). The author thanks very much Marina Mikhailukova who noted and reported these errors to me.

The revealed and corrected misprints are shown in the table lower.

Mistakes revealed in the version of March 2016 and corrected in the present version

Page number	**Position in the list**	**Version of March 2016**	**Version of December 2016**
p.37	Data table for ^{29}Si(n, 2p)^{28}Mg, incident energy E_n	14.8	14.80
p.39	Table at the page bottom, ^{39}K abundance	95.2581 *44*	93.2581 *44*
p.104	Data table for ^{nat}Mo(n, x)^{96}Nb	Data of columns 2,3,4 corresponds to the real data of columns 1,2,3 but the real data of column 4 is absent	Corrected
p.105	Data table for ^{nat}Mo(n, x)^{97}Nb	Data of columns 2,3,4 corresponds to the real data of columns 1,2,3 but the real data of column 4 is absent	Corrected
p.123	Table at the page bottom, reaction product $T_{1/2}$	35.36 d *6*	35.36 h *6*
p.126	Table at the page bottom, reaction product	^{105}Rh	^{105}Ru
p.137	Table at the page bottom, reaction product $T_{1/2}$	7.45 h *1*	7.45 d *1*
p.208	Table at the page bottom, reaction product $T_{1/2}$	42.39 h *6*	42.39 d *6*
p.275	Data table for ^{27}Al(n, α)^{24}Na reference cross section	Data at 13.48 MeV are absent.	Corrected
p.276	Data table for ^{93}Nb(n, 2n)^{92m}Nb reference cross section	Data at 13.48 MeV are absent.	Corrected.

2. EXPERIMENTAL PROCEDURES

Activation cross-section measurements were carried out using a conventional, widely used scheme: irradiation – cooling – gamma counting. Briefly, the main features of the measurements considered are as follows:

a) most reaction cross sections were measured at several neutron energy values inside the interval 13.4 – 14.9 MeV;

b) the ^{27}Al(n, α)^{24}Na and ^{93}Nb(n, 2n)^{92m}Nb reaction cross sections known with the accuracy of 0.4 – 0.8% were used for the neutron fluence determination as the reference data;

c) the geometry of irradiation and gamma counting was fixed for most measurements, and some standard reaction cross sections known with an accuracy of 1 – 2% were also measured in the same conditions;

d) the scattered neutron contribution was minimized by the use of thin-wall constructions and air cooling of the target;

e) the changes of neutron flux during irradiation were measured by two independent scintillation detectors. One of them was continuously scanning around the target and monitoring both angular and energy distributions of neutrons;

f) the neutron field parameters were calculated in detail using a special code that took into account the real target properties and experimental geometry.

g) the data accumulation, treatment and presentation were computerized. All information about the measurements was stored in a structured data bank provided with service codes.

h) some efforts were made to create a computer code that could estimate the gamma radiation of samples irradiated by neutrons. This code was used as an auxiliary tool for choosing the optimal parameters of measurements.

The issues outlined above are considered in more detail in the following section of this paper.

2.1. Neutron irradiation

A Neutron Generator NG-400 (of ICT type) was used for sample irradiation with neutrons produced in the T(d, n)^{4}He reaction. Depending on requirements of the particular experiment, the accelerating voltage was 220 - 320 kV, the deuteron current was 0.01 - 0.5 mA and the Ti-T target thickness was 1 – 2 mg/cm^2.

The irradiation arrangement is shown in Fig. 2.1.1. The samples were gathered into assemblies that were mounted relative to the beam direction at the angles of 0, 40, 60, 80, 100, 120 and 140 degrees (the ring No. 1 for seven assemblies) or at 0, 40, 60, 75, 91, 107, 125 and 150 degrees (the ring No. 2 for eight assemblies). In this arrangement, the neutron energy interval 13.4 - 14.9 MeV was covered at the accelerator parameters indicated above.

A special attention was paid to minimizing the contribution of scattered neutrons to the primary neutron spectrum. The accelerator target chamber was constructed using thin details that have the wall thickness of 0.2 - 0.5 mm. The target warm was withdrawn by a focused air jet. The sample holder was also made from thin-wall constructions where the maximal thickness had the sample assemblies (~1 – 3 mm). Additionally, the role of scattered neutrons was reduced by using during irradiations a short target - sample distance (30 mm) that was much less than the distance between the target and other massive elements of the accelerator and experimental hall.

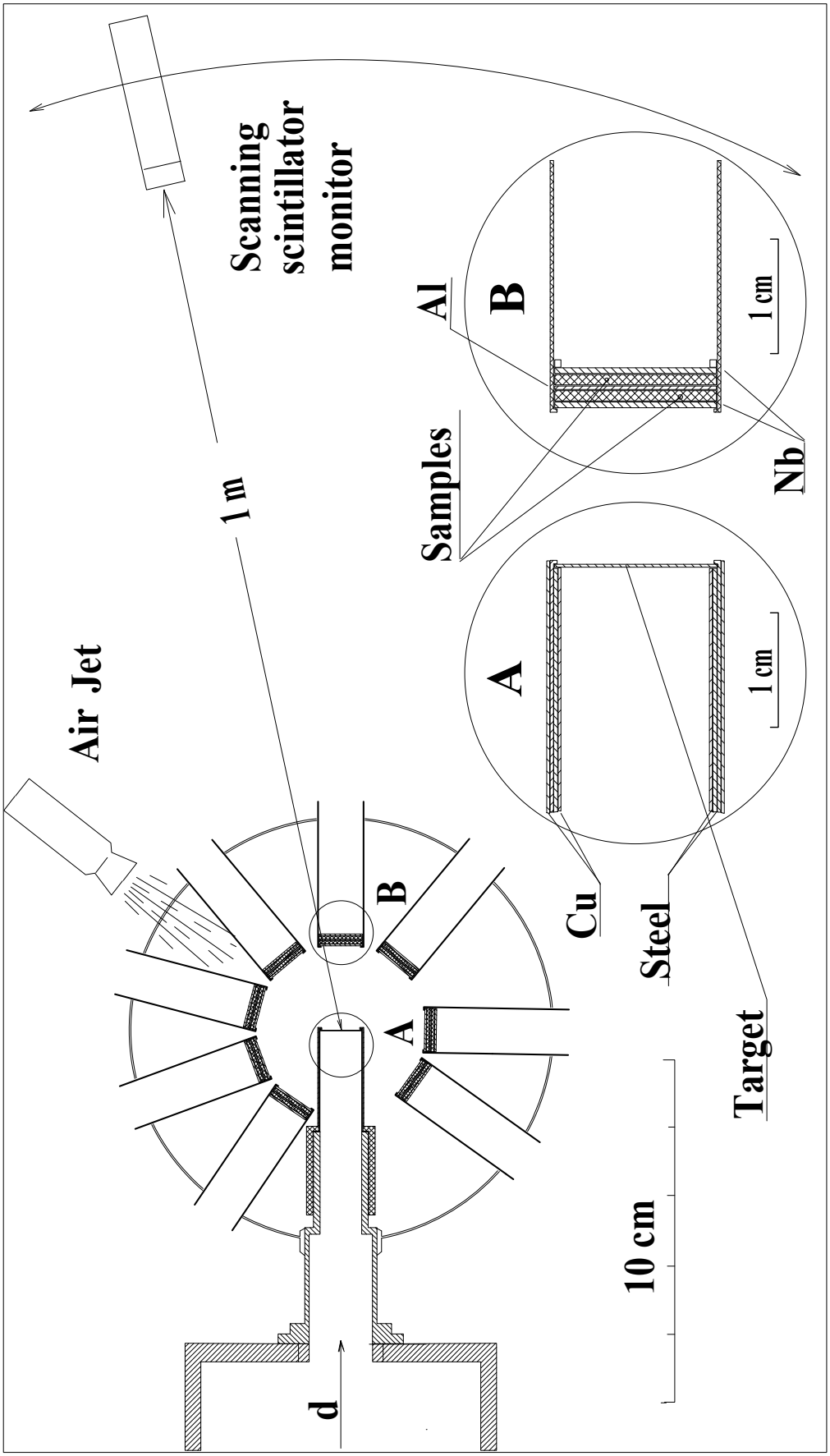

Fig. 2.1.1. Near target arrangement.

Typically, 2 - 4 different materials were irradiated simultaneously. The samples were gathered in packets in which the first and the last positions were occupied by the monitor foils (Al or Nb). Occasionally, an additional monitor foil was inserted in the middle of the assembly. The fluence data determined by all monitor foils were treated jointly taking into account the real foil distance to the neutron source, the angular distribution of d-T neutrons and the real law of neutron flux reduction with distance. This decreased the uncorrelated part of monitor errors by a factor approximately 2 - 3 in comparison with the conventional method where the fluence is independently determined for each packet. The method is described in more detail below.

Variations of the neutron flux during irradiation were measured by two independent scintillation detectors, one of which was fixed rigidly and the other one was rotated around the target at the distance 1 m, over the angular range from -160 to +120 degrees. A standard period of 20 s was set for a rotation cycle, however, if necessary, that could be changed from 5 s to 2 min.

Detailed information on the angular and energy distribution of neutrons, and their variations during the irradiation, was written to a PC disk and used later during data processing.

2.2. Calculation of neutron field parameters

The space and energy distributions of neutrons generated in the $^{3}H(d,n)^{4}He$ reaction were calculated with taking into account the realistic experimental conditions, such as finite sizes of the beam and the sample, inhomogeneity of the tritium distribution in the target, changes of the energy and angle parameters of the beam due to slowing down, etc. As the base model, the method described in [20] was used. In the present work, this approach was extended to the events of non-coaxial geometry.

Calculations described are very important when the sizes of the irradiated samples are comparable with the sample distance to the neutron source. There are a number of circumstances when the samples are to be placed in close proximity to the target. This could be necessary, for example, if the measured cross-section is small or if the reaction product has long half-life or low gamma-ray intensity or if only a small amount of material is available for irradiation, etc.

Additionally, it is worth noticing that the role of scattered neutrons which distort the original neutron field is much less near the target.

Last but not least, the allocation of the irradiated samples close to the target allows accumulating the needed neutron fluence without excessive activation of the target chamber, accelerator elements, etc.

Some examples of calculation results are shown below. The dependence of neutron field parameters on the irradiation geometry is presented in Figs. 2.3.1 – 2.3.4. The influence of deuteron energy on neutron characteristics is shown in Figs. 2.3.5 – 2.3.6.

Most noticably, the finite geometry effects appear in a remarkable broadening of neutron energy distribution near 90° (Fig. 2.3.2) and in significant deviation of neutron flux changing with distance from the ***1/r²*** law (Fig. 2.3.4).

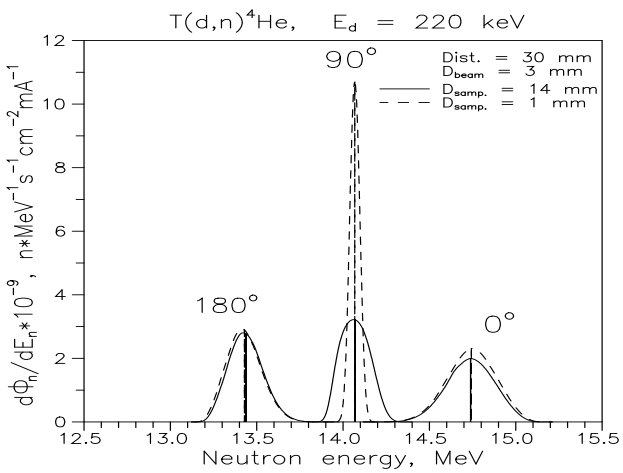

Fig. 2.3.1. Neutron spectra calculated for different sample diameters, 14 and 1 mm. Beam diameter is 3 mm and sample-to-target distance is 30 mm.

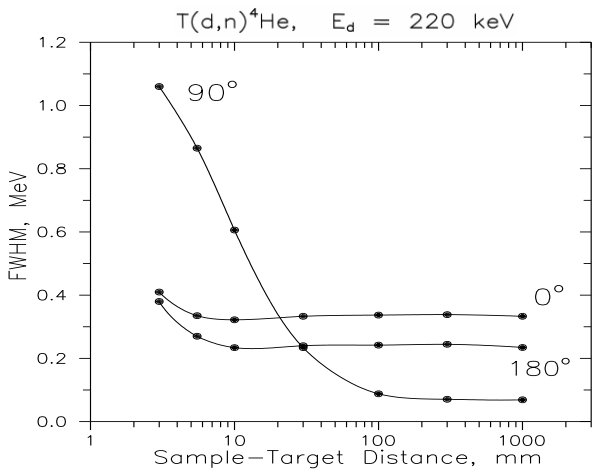

Fig. 2.3.2. Neutron spectrum full width at half of maximum (FWHM) dependence on the sample-to-target distance. Beam diameter is 3 mm and sample diameter is 14 mm.

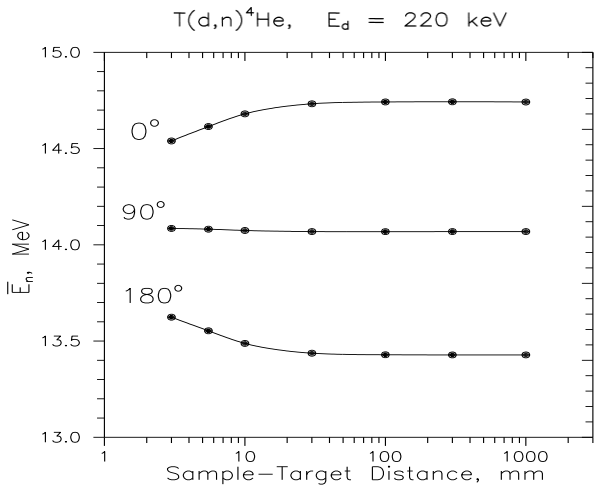

Fig. 2.3.3. Dependence of the averaged neutron energy on the sample-to-target distance. Sample diameter is 14 mm.

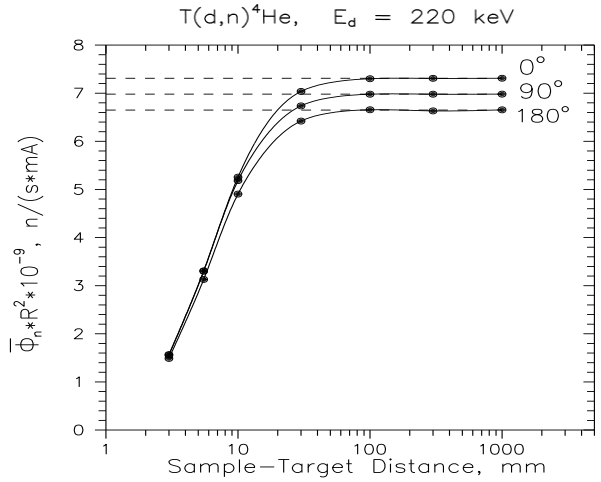

Fig. 2.3.4. Change of the averaged neutron flux multiplied by the squared distance to target. Sample diameter is 14 mm.

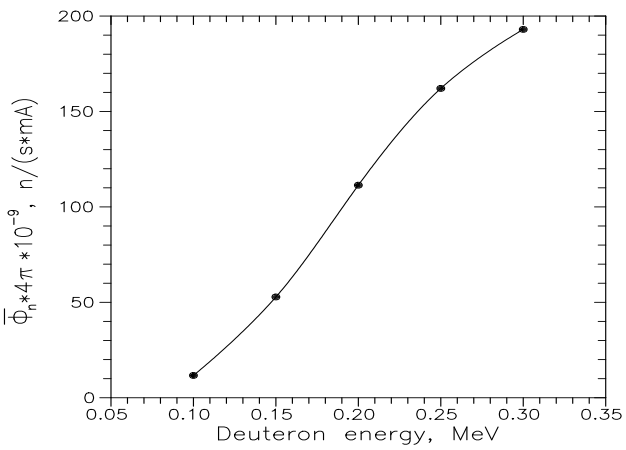

Fig. 2.3.5. The energy dependence of the 4π-solid angle integrated neutron flux.

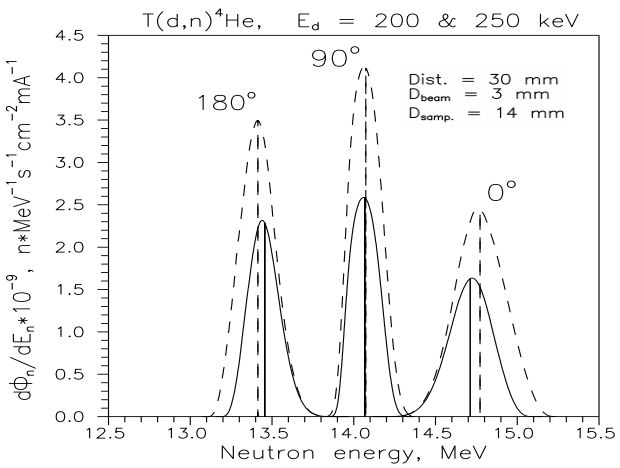

Fig. 2.3.6. Neutron spectra calculated for different deuteron energies (solid line corresponds to E_d = 200 keV).

The real FWHMs are about of 200 keV for every irradiation angle at the sample-to-target distance 30 mm. Although the neutron energy spread is remarkable, it does not influence the cross sections measured because the change of the majority of cross sections around the neutron energy 14 MeV is smooth and can be well approximated by the linear dependence. It is worth mention that the method of the cross section approximation by linearization was successfully used in our previous publications.

Generally, if the cross section change is linear and the neutron energy distribution is symmetric then the average neutron energy is the value that sufficiently characterizes the cross section measured. These conditions are valid almost everywhere in the present measurements. This is why the uncertainty of the average neutron energy (not FWHM!) is given in our present data illustrated in the Figures.

2.3. Reference cross sections

Cross-sections measured in the present work were determined relatively to the reference cross-sections which are either ^{27}Al(n,α)^{24}Na, or ^{93}Nb(n,2n)^{92m}Nb, or both. The second reaction was favorable in practice because the ^{92m}Nb has eminently suitable decay properties: one dominant gamma-line 934.4 keV that is in the well calibrated region of gamma detector and the convenient half-life 10.15 d which provides gamma counting without hurrying. The ^{27}Al(n,α)^{24}Na reaction was the preferred reference at short irradiations.

Systematic cross-section measurements of reactions induced by 14-MeV neutrons were started at KRI in the early 1990s. At that time, improvements in nuclear data libraries were demanded, and several projects for conducting new experiments and extending evaluations were initiated. The ^{27}Al(n,α)^{24}Na cross-section around neutron energy 14 MeV has remained stable throughout the period of nuclear data revision. This is illustrated with the Fig. 2.2.1.

As can be seen in the Fig. 2.2.1 the "old" ^{27}Al(n,α)^{24}Na cross-section values used at KRI measurements as the reference ones are in the good agreement with each of the modern evaluations. Most closely, the KRI data are to FENDL-3.0 and IRDFF v.1.05 evaluations.

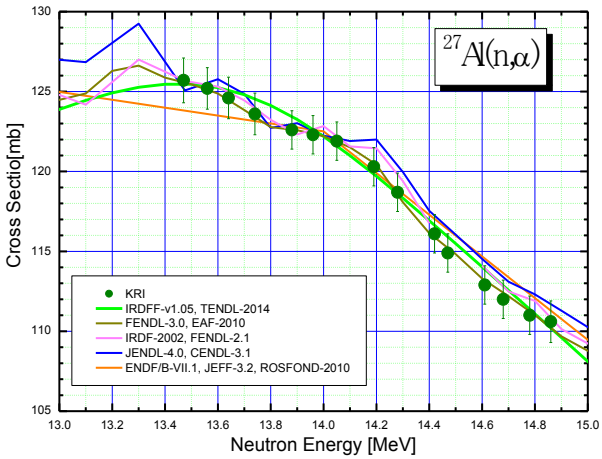

Fig. 2.2.1. Modern evaluations of the ^{27}Al(n,α)^{24}Na cross section in comparison with the data used at KRI measurements as the reference cross-section values.

The situation with the ^{93}Nb(n,2n)^{92m}Nb cross-section evaluation was quite different when the systematic cross-section measurements were started at KRI. Firstly, the experimental data was scattered widely (see Fig. 2.2.2). Secondly, there are only few evaluations that contained the split data for the ground and isomeric states. Therefore, obtaining ^{93}Nb(n,2n)^{92m}Nb cross-section data reliable enough for use as reference values during the determination of other measured cross-sections was a rather complicated problem.

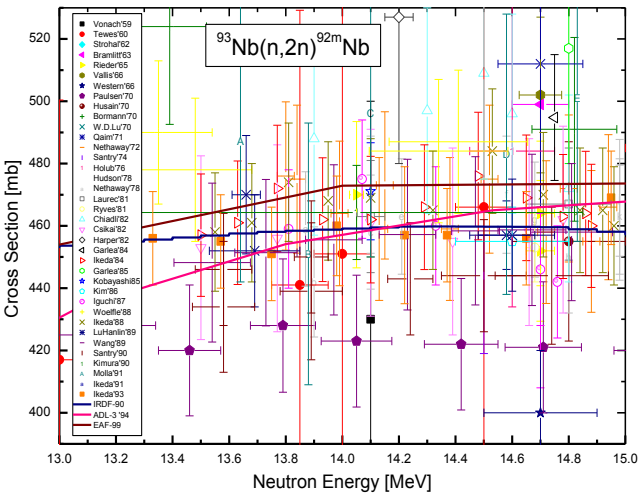

Fig. 2.2.2. The ^{93}Nb(n,2n)^{92m}Nb cross section data of EXFOR and Neutron Libraries in the time when the KRI systematic cross-section measurement was started.

In the circumstances outlined above, it was decided to bind the ^{93}Nb(n,2n)^{92m}Nb cross section that was studied insufficiently to the ^{27}Al(n,α)^{24}Na cross section that was known more precisely.

A large body of ratios of the ^{93}Nb(n,2n)^{92m}Nb to the ^{27}Al(n,α)^{24}Na cross sections were obtained during the initial stages of our measurements, as most of the KRI standard sample assemblies contained both niobium and aluminum foils that were sandwiched with the irradiated samples,

e.g. **Nb** - sample X1 - **Al** - sample X2 - **Nb**
or **Al** - sample Y1 - **Nb** - sample Y2 - **Al**.

About of 20 independent ratio values were obtained using the model described above for all neutron energies. The ratios were

averaged to reduce random uncertainty in the data. Then the ^{93}Nb(n,2n)^{92m}Nb values were tabulated and used as the reference cross-section standard of the KRI measurements.

A good quality of the ^{93}Nb(n,2n)^{92m}Nb cross-section data used in the KRI experiments is confirmed by the contemporary evaluations shown in Fig. 2.2.3.

^{27}Al(n,α)^{24}Na and ^{93}Nb(n,2n)^{92m}Nb reference cross-sections were stated once, at the very beginning of KRI experiments. These remained unchangeable during the total cycle of the KRI activation cross-section measurements.

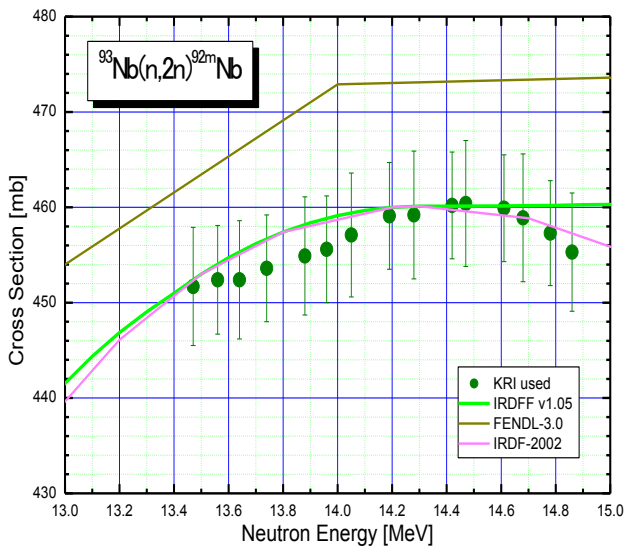

Fig. 2.2.3. Contemporary evaluations of ^{93}Nb(n,2n)^{92m}Nb cross-section in comparison with the data used during KRI measurements as reference cross-section values.

One of the aims of this paper is to bring the reference decay and cross-section data used at KRI activation cross-section measurements into compliance with recommendations of up-to-date evaluated data files. Using this opportunity, the old (KRI) ^{27}Al(n,α)^{24}Na and ^{93}Nb(n,2n)^{92m}Nb reference cross-section data should be changed with the values of the modern evaluations.

IRDFF v1.05 seems to be most preferable for this purpose because this evaluation is one of the latest (released 09 October, 2014), and contains detailed information on both cross-sections and uncertainties. Additionally, the IRDFF v1.05 data for the two cross-sections considered here are in a total accordance with the data of the last available TENDL-2014 evaluation. Furthemore, the IRDFF v1.05 data for ^{27}Al(n,α)^{24}Na and ^{93}Nb(n,2n)^{92m}Nb cross-sections agree well with the reference data used at the KRI measurements. (Fig. 2.2.1 and Fig. 2.2.3). This means that the exchange of the old reference data (KRI) with new ones (IRDFF v1.05) does not cause a drastic change in the KRI activation data published earlier.

The old and the new reference cross-section data are tabulated in Table I and Table II of ATTACHMENT (pp.275-276).

2.4. Gamma counting

Two detectors were used for γ-counting of irradiated samples. These were a Ge(Li)-detector of the 160 cm^3 sensitive volume and the energy resolution 4.0 keV at E_γ = 1332.5 keV, and a HPGe-detector that had a relative efficiency 24.7% and energy resolution of 1.8 keV at E_γ = 1332.5 keV. The HPGe-detector had a thin beryllium entrance window that extends the energy interval of gamma rays acceptable to detection up to 5 keV.

The detectors were enclosed in heavy shields consisting of consecutive layers of the lead, cadmium and steel (the Ge(Li) shield) or lead, copper and aluminum (the HPGe shield). The typical background gamma spectra of the shielded detectors are shown in Fig. 2.4.1.

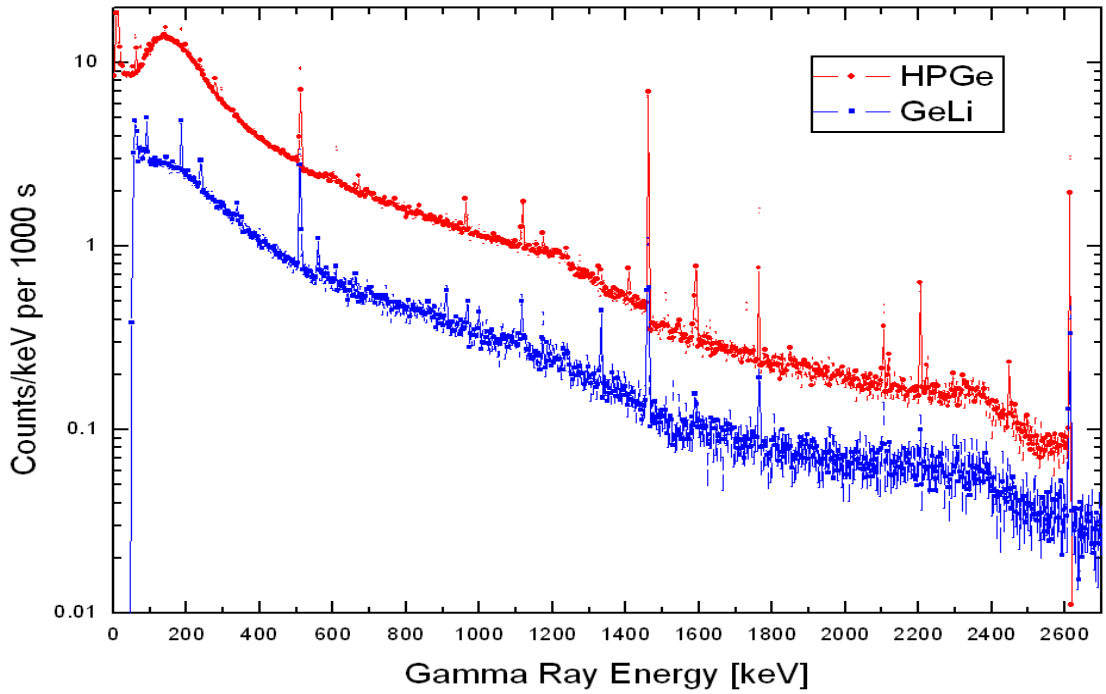

Fig. 2.4.1. Background count rate of the shielded HPGe- and Ge(Li)-detectors used in the experiment.

A thorough knowledge of background spectrum details is often required for an accurate determination of low activities. To provide a good statistics of background spectra, these were measured by many small portions using the time windows when the detectors were free of other gamma measurements. In order to avoid broadening the peaks during summation of disconnected portions, a certain procedure was developed. First, the energy scale of every spectrum was recalibrated using well known background peak positions. Then, the spectra were deformed to the unified energy scale (e.g. 0.5 keV per channel as in Fig. 2.4.1) by a special computer code. After this, the spectra portions were summed. The background spectra shown in Fig. 2.4.1 corresponds to the total exposition of approximately 20 days for the HPGe and 9 days for the Ge(Li) detectors.

The relative full-energy peak efficiencies of the detectors were measured at different distances from the detector using the standard gamma sources (OSGI) as well as several radioactive nuclides produced at the Neutron Generator. The dependence of efficiency on energy and distance were approximated by analytical formulas. Two distance points were calibrated most carefully and set to the standard counting points for which the absolute full-energy peak efficiency was determined. The distances from the upper surface of the detector cup to the lower side of the sample were 33 and 112 mm for these two points. The absolute full-energy peak efficiency measured at the remote point for the HPGe detector is presented in Fig. 2.4.2.

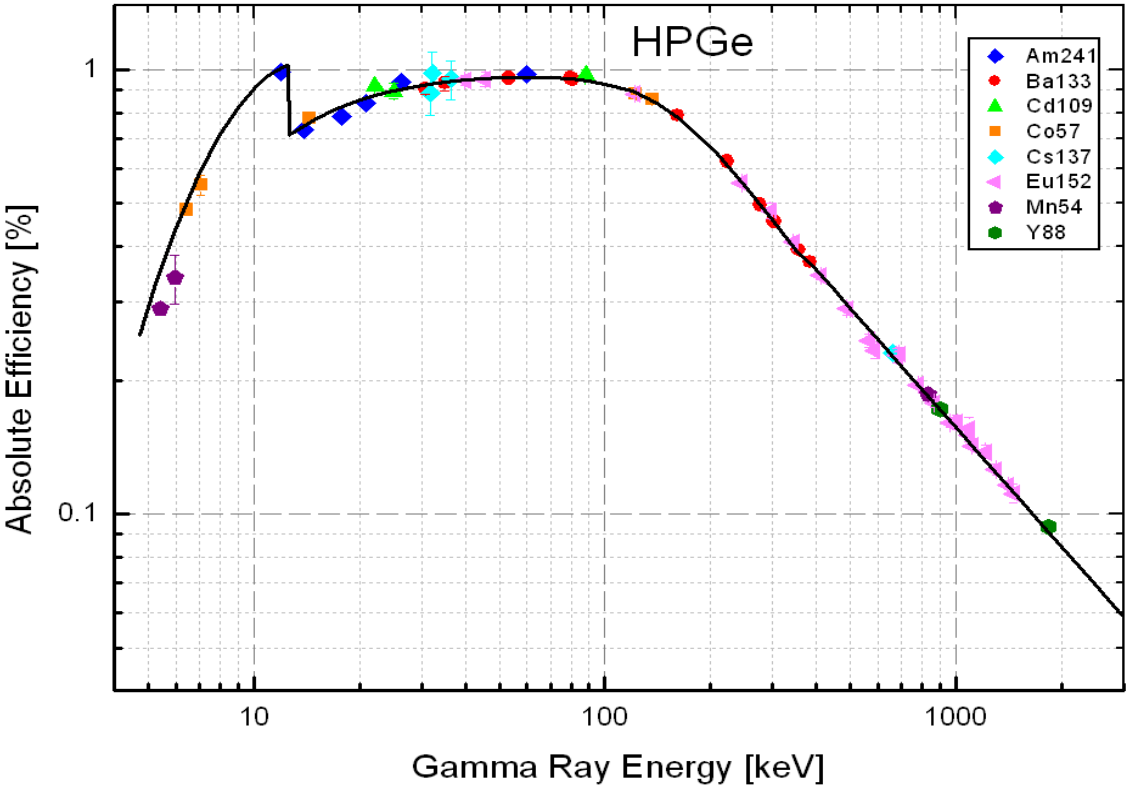

Fig. 2.4.2. Absolute full-energy peak efficiency of the high purity germanium (HPGe) detector with the thin beryllium entrance measured at the distance of 112 mm from the detector cover top. A black solid curve is the analytical efficiency approximation used in activation cross-section calculations.

The HPGe detector used in the experiment had not only good energy resolution but also high registration efficiency, especially in the region of low gamma energies. The detector was operated in complicated measurements, e.g., detection of low activities embedded in high background.

The high detector sensitivity that is an undoubtedly positive property often has a negative effect related to the simultaneous registration of X-rays and other gamma-rays emitted in cascade with the defined gamma-line. The pulses correlated in time are summed in the detector and leave the peak area. The full-energy peak efficiency should then be corrected for the effect of gamma cascades.

The total registration efficiency is needed for calculation of gamma coincidence corrections. Experimental measurements of this quantity require the use of mono-energetic gamma sources. However, the sources of this category such as ^{241}Am, ^{109}Cd, ^{139}Ce, ^{203}Hg, ^{137}Cs, ^{54}Mn and others are, strictly speaking, not mono-energetic because they emit the X-Rays also. These are registered by the HPGe detector and should be excluded by an additional correction procedure.

The problem of the total gamma registration efficiency could be solved by means of MCNP emulations. In the calculations we carried out, the real geometry of gamma counting was modeled. This included gamma detector crystal, detector capsule, sample holder, shield layers and other details. The MCNP emulations were performed for both HPGe- and Ge(Li)- detectors and also for both 112 mm and 33 mm standard gamma counting positions.

Results of MCNP calculations performed for the Ge(Li) detector is shown in Fig. 2.4.3. A gamma radiation source was supposed to be placed in the standard measurement point distanced at 33 mm from the top of the detector capsule.

It is seen in in Fig. 2.4.3 that the full-energy peak efficiencies calculated by means of MCNP are in a good agreement with those measured experimentally. Besides, it was discovered that the emulated response functions of various gamma sources correlate closely with corresponding gamma spectra measured in experiments. These facts could be considered as a strong evidence for the reliability of the total efficiency calculated by MCNP and, therefore, the accuracy of corrections for gamma cascade summing that was calculated in the present measurements.

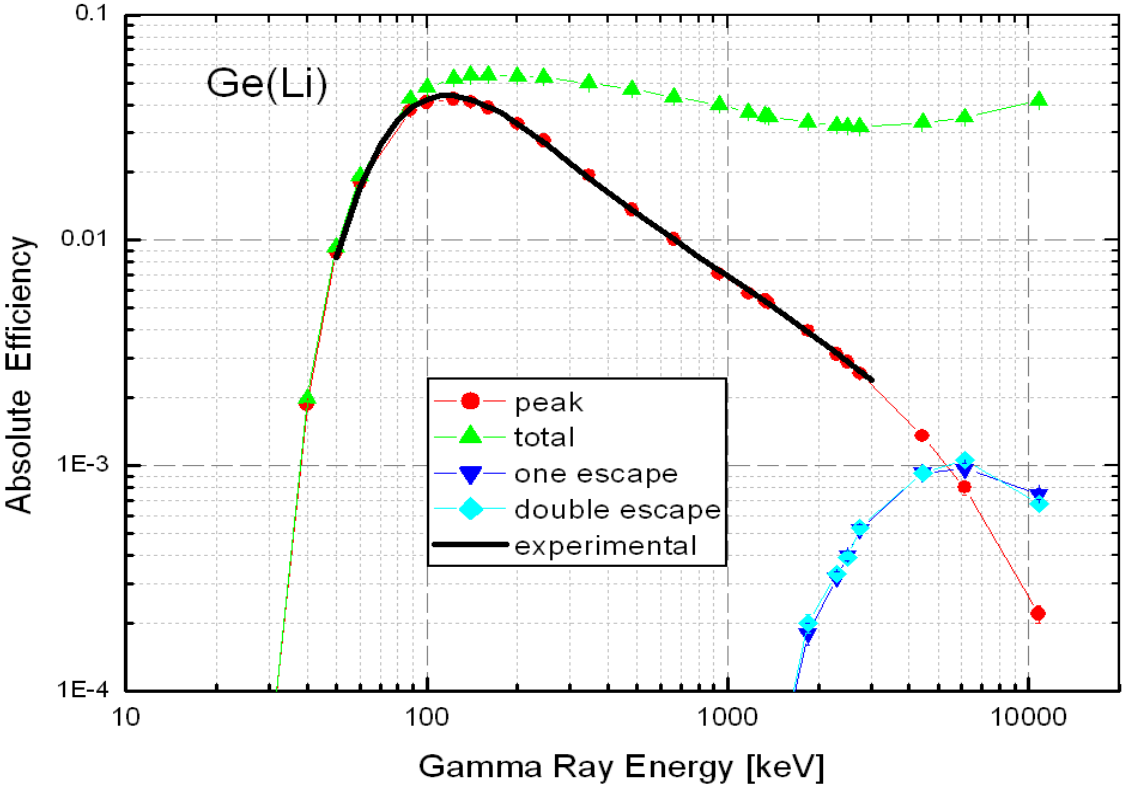

Fig. 2.4.3. Absolute total, full-energy peak, one escape and double escape gamma efficiencies of the Ge(Li) detector calculated with MCNP for the distance of 33 mm from the detector cover top. A black solid curve is an approximation of the full-energy peak efficiency measured experimentally. The colored points correspond to the results of MCNP calculations,

One more conclusion can be drawn from the comparison of the calculated and measured characteristics of the detectors presented in Fig. 2.4.2 and Fig. 2.4.3. This concerns the accuracy of the full-energy peak efficiency. Since the methods used in the experiment and the MCNP calculation were totally independent, then the analysis of small differences between results of the two different approaches can shorten the uncertainty of the gamma peak efficiency approximation by the value $\Delta\varepsilon_\gamma \leq 1.2\%$ for both detectors and almost for the total gamma ray energy interval that was used in the measurements. A little uncertainty increasing was only admitted at the ends of the used gamma energy region.

After processing the gamma spectra of the samples activated by neutrons, the procedure of activation cross-section determination was started.

2.5. Algorithm of cross section determination

By definition, the cross section of the nuclear reaction **A(n, x)B** is determined by the relation:

$$\sigma_{AB} = \frac{N_B}{N_A \cdot \Phi_n}, \tag{2.5.1}$$

where N_B is the number of nuclei **B** produced in the reaction;

N_A is the number of the target sample nuclei **A**;

Φ_n is the neutron fluence accumulated by the sample.

Now, consider the procedures used to determine each of the three values in the formula (2.5.1).

2.5.1. Determination of the target nuclei amount

The number of the initial nuclei, N_A, is connected with the mass of the sample through:

$$N_A = \frac{m \cdot Aw \cdot p_1 \cdot p_2}{At}, \tag{2.5.2}$$

where m is the sample mass, [g];

Aw is the Avogadro's number;

p_1 is the abundance of the isotope A in the chemical element;

p_2 is the share of the chemical elements in the chemical formula;

At is the atomic weight of atoms of the sample, [a.e.m];

2.5.2. Neutron fluence determination

There are several methods used to determine the integrated flux. The approach used in this work involves the use of ratios, whereby many uncertainty factors can be cancelled and the total data uncertainty is diminished.

In this approach, the integrated neutron fluence accumulated by the reference sample is determined as:

$$\Phi_n = \frac{N_{rB}}{N_{rA} \cdot \sigma_{rAB}}, \tag{2.5.3}$$

where the formula is similar to (2.5.1) and "*r*" means "reference".

Usually, σ_{rAB} is known with good accuracy; N_{rA} and N_{rB} should be determined by the same procedures as N_A and N_B.

The fluence accumulated by each sample depends on the sample position in the assembly. This dependence is described by the $1/r^2$ -law if the neutron scattering and sizes of sample and target can be neglected. For close geometry, as shown in chapter 2.3, the accumulated fluence

changes with distance more slowly (see Fig. 2.3.4, for example). More correctly, the dependence $1/r^a$ would be used, where $a \le 2$.

For the actual conditions of the experiment (the target-sample distance is 30 mm, beam diameter 5 mm, diameter of the sample 14 mm, and sample thickness 1 mm), it was estimated that $a \approx 1.97$ which approximates closely to the “normal” value 2. Nevertheless, for more generality, let us consider that:

$$\Phi_n \sim 1/r^a \tag{2.5.4}$$

To simplify the following formulas one can introduce a new variable, the so called "reverse fluence" φ_n that is connected with the normal fluence Φ_n by:

$$\varphi = \Phi_n^{-\frac{1}{a}} \tag{2.5.5}$$

Then the reverse fluence $\varphi(r_i)$, accumulated by the sample i, placed at the distance r_i from the neutron source will be calculated as:

$$\varphi(r_i) = \varphi(r_1) \cdot \frac{r_i}{r_1} \tag{2.5.6}$$

where $\varphi(r_1)$ is the reverse fluence accumulated by the reference sample located at the distance r_1 from the neutron source.

Often, as in the present case, the two reference foils occupy the first and last positions in the assembly. For them,

$$\begin{cases} \varphi(r_1) = \varphi_0 \cdot r_1 \\ \varphi(r_2) = \varphi_0 \cdot r_2 \end{cases} \tag{2.5.7}$$

where φ_0 is the reverse fluence at the unitary distance from the neutron source;

r_1 and r_2 are the positions of the two reference foils.

The solution of the system (2.5.7) is equivalent to drawing a straight line in the plane $\{r, \varphi_n\}$. The straight line goes out from the point $[0,0]$ and must pass through the regions of two other points with coordinates $[r_1, \varphi(r_1)]$ and $[r_2, \varphi(r_2)]$ with minimal deviations. It is natural to use the method of weighted least squares for finding the slope of the line φ_0 :

$$w_1 \cdot [\varphi(r_1) - \varphi_0 \cdot r_1]^2 + w_2 \cdot [\varphi(r_2) - \varphi_0 \cdot r_2]^2 = \min \tag{2.5.8}$$

where w_1 and w_2 are the weights of measurements for the first and second reference samples.

Then,

$$\varphi_0 = \frac{w_1 \cdot \varphi(r_1) \cdot r_1 + w_2 \cdot \varphi(r_2) \cdot r_2}{w_1 \cdot r_1^{\,2} + w_2 \cdot r_2^{\,2}} \tag{2.5.9}$$

The reverse fluence accumulated by the sample located at the distance r_i will be determined as:

$$\varphi(r_i) = \varphi_0 \cdot r_i \tag{2.5.10}$$

If n sample assemblies arranged at different angles to the deuteron beam are irradiated simultaneously (as shown in Fig. 2.1.1) and every assembly contains two reference foils, then we will have a system of n equations like (2.5.8).

$$w_{1k} \cdot [\varphi(r_{1k}) - \varphi_0 \cdot r_{1k}]^2 + w_{2k} \cdot [\varphi(r_{2k}) - \varphi_0 \cdot r_{2k}]^2 = \min \tag{2.5.11}$$

where k runs from 1 to n.

Additionally, it is necessary to take into account that the effective center of the accelerator beam can be shifted from the geometrical center of the target. This will cause a change to the distance set used in the formulas above. The real distance from the neutron source to the sample, r_{ik}^*, is connected with the mechanically fixed distance, r_{ik}, from the target to the sample through:

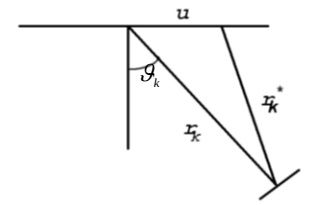

Fig. 2.5.1. The target vicinity

$$r_{ik}^{*2} = r_{ik}^2 + u^2 + 2r_{ik} \cdot u \cdot \sin(\vartheta_k) \tag{2.5.12}$$

where u is the beam shift projection on the plane of sample assemblies;

ϑ_k is the angle between the beam direction and the assembly k axis.

Additionally, the neutron source anisotropy $V(\varphi)$ is to be considered. This is defined as:

$$V(\vartheta) = \frac{\Phi(\vartheta)}{\Phi_0} \tag{2.5.13}$$

where $\Phi(\vartheta)$ is the fluence of neutrons emitted in direction ϑ, and Φ_0 is the mean neutron fluence:

$$\Phi_0 = \frac{N_{n\_tot}}{4\pi} \tag{2.5.14}$$

where N_{n_tot} is the total number of neutrons emitted in all directions during the irradiation.

The “anisotropic reverse fluence”, φ_k^*, is bound with the “isotropic reverse fluence”, φ_k with relation:

$$\varphi_k^* = \varphi_k \cdot V_k^{-\frac{1}{a}} \tag{2.5.15}$$

where the index k corresponds to the angle ϑ_k.

Finally, the system of n equations which corresponds to the zero approach (2.5.11) can be rewritten with the modified variables:

$$w_{1k} \cdot [\varphi_k^{*}(r_{1k}^{*}) - \varphi_{0k} \cdot r_{1k}^{*}]^2 + w_{2k} \cdot [\varphi_k^{*}(r_{2k}^{*}) - \varphi_{0k} \cdot r_{2k}^{*}]^2 = \min \qquad (2.5.16)$$

where k runs from 1 to n.

The variables marked with asterisk include the information on neutron source anisotropy and the possible shift of the beam position on the target. Therefore, the equations (2.5.16) describe the problem more realistic.

The system (2.5.16) has no analytical solution similar to (2.5.9). However, it can be easily solved with a computer using an iteration procedure. As a result, the total number of neutrons emitted during the irradiation time, N_{n_tot}, and the real position of the beam on the target, u, will be deduced. It is worth noting that for determination of these two parameters, more than two independent equations are used. This means, the uncorrelated error of the neutron fluence determination decreases $\sqrt{n_r - 2}$ times, where n_r is the number of reference samples.

Finally, the neutron fluence accumulated by the i-sample in the k-assembly will be calculated by the formulas:

$$\varphi_{ik} = \varphi_{0k} \cdot r_{ik}^{*} \qquad (2.5.17)$$

$$\varphi_{ok} = [\Phi_0 \cdot V(\vartheta_k)]^{-\frac{1}{a}} \qquad (2.5.18)$$

$$r_{ik}^{*2} = \sqrt{r_{ik}^2 + u^2 + 2r_{ik} \cdot u \cdot \sin(\varphi_k)} \qquad (2.5.19)$$

2.5.3. Determination of the amount of nuclei produced in the reaction

As indicated above, this analysis is restricted to activation cross section measurements. In this case, we need to know the number of nuclei of type **B,** N_B, that were produced in the reaction studied (formula 2.5.1). It is related to the induced sample activity, A_B, measured experimentally through the simple relation:

$$A_B = \lambda_B \cdot N_B \qquad (2.5.20)$$

where λ_B is the decay constant.

The formula (2.5.20) would be quite enough for determination of the N_B value if all the **B**-nuclei were produced by a very short neutron flash and the sample activity was measured very quickly, just at the moment of the flash. Unfortunately, this ideal situation can never happen.

Firstly, the nuclei we are interested in are radioactive and amount of them is changing in the time according to the radioactive decay law:

$$N_B(t) = N_B(t_{00}) \cdot e^{-\lambda_B \cdot t} \qquad (2.5.21)$$

where $N_B(t_{00})$ is the number of **B**-nuclei produced in the neutron flash;
t is the time gone after the irradiation moment.

Secondly, various nuclei are generated at the neutron irradiation of the sample. Some of them can also produce the **B**-nuclei in the process of own decay. These are "**B**-parents". Let us denote the **B**-parents by index B^m (mother). Then, the change in the time of the **B**-nuclei amount will be expressed by the more complicated dependence:

$$N_B(t) = N_B(t_{00}) \cdot e^{-\lambda_B \cdot t} \cdot \left[1 + \frac{\sigma_{B^m}}{\sigma_B} \cdot \alpha \cdot \frac{\lambda_{B^m}}{\lambda_{B^m} - \lambda_B} \cdot \left(1 - e^{-(\lambda_{B^m} - \lambda_B) \cdot t} \right) \right] \tag{2.5.22}$$

where σ_{B^m} and σ_B are cross-sections of production of the corresponding nuclei at neutron irradiation;

α is a part of mother nuclide decays that is resulting in generation of **B**-nuclides;

λ_{B^m} and λ_B are decay constants of the corresponding nuclei .

The formula (2.5.22) covers almost all situations that have practical significance because the production of the radioactive chains consisting of three or more members is rather unusual for irradiations involving fast neutrons.

Generally speaking, the ratio $\frac{\sigma_{B^m}}{\sigma_B}$ is unknown and has to be determined from experimental data. Moreover, it may depend on neutron energy and, hence, is specific for each sample packet. There are a number of methods for its determination.

The situation is most easy when decays of the mother and daughter nuclei are accompanied by emission of gamma rays having different spectra. If the mother nuclide does not indicate itself by specific gamma radiation then the measurement of the decay curve shape can be used. Several gamma spectra are to be repeatedly counted for every sample in this case. The accurate σ_{B^m} data taken from other experiments or evaluations would be also sufficient for solution of the problem.

At the present stage let us assume that the mother-to-daughter cross section ratio is deduced already and try to consider in more detail the sample activity determination. The immediate result of gamma counting is the gamma peak area, $P(E_\gamma)$. It is related to the amount of **B**-nuclei as:

$$P(E_\gamma) = Y(E_\gamma) \cdot \varepsilon(E_\gamma) \cdot \lambda_B \cdot \int_{t_1^{cnt}}^{t_2^{cnt}} N_B(t^{cnt} - t_{00}) \cdot dt^{cnt} \tag{2.5.23}$$

where t_1^{cnt}, t_2^{cnt} are the times of the beginning and the end of gamma counting;

t^{cnt} is the time of gamma counting $t_1^{cnt} \le t^{cnt} \le t_2^{cnt}$;

$Y(E_\gamma)$ is the yield of the relevant gamma line with energy E_λ;

$\varepsilon(E_\gamma)$ is the absolute peak efficiency of the gamma detector.

Formula (2.5.23) is written as if all the **B**-nuclei were produced at the time moment t_{00}. In reality, the sample irradiation was extended from t_1^{irr} to t_2^{irr}, and the irradiation intensity could vary arbitrary as $\phi_n(t^{irr})$. To take this into account we can write:

$$P(E_\gamma) = \frac{Y(E_\gamma) \cdot \varepsilon(E_\gamma) \cdot \lambda_B \cdot \int_{t_1^{irr}}^{t_2^{irr}} dt^{irr} \int_{t_1^{cnt}}^{t_2^{cnt}} \phi_n(t^{irr}) \cdot N_B(t^{cnt} - t^{irr}) \cdot dt^{cnt}}{\int_{t_1^{irr}}^{t_2^{irr}} \phi_n(t^{irr}) \cdot dt^{irr}} \tag{2.5.24}$$

Then, gathering the previous formulas we can obtain finally:

$$P_k\left(E_\gamma\right)=Y\left(E_\gamma\right)\cdot\varepsilon\left(E_\gamma\right)\cdot\left(t_{2k}^{cnt}-t_{1k}^{cnt}\right)\cdot\sigma_B\cdot N_A\cdot\Phi_n\cdot\lambda_B\cdot F_k\left(B,B^m,\phi\right) \qquad (2.5.25)$$

where: $P_k\left(E_\gamma\right)$ is the E_γ peak area determined at the kth gamma counting;

$Y(E_\gamma)$ is the yield (intensity) of the relevant gamma line with energy E_γ;

$\varepsilon(E_\gamma)$ is the absolute peak efficiency of the gamma detector;

$\left(t_{2k}^{cnt}-t_{1k}^{cnt}\right)$ is the exposition of the kth gamma counting;

σ_B is the cross section of the reaction **A**(n, x)**B**;

N_A is the number of **A**-nuclei in the sample;

Φ_n is the neutron fluence accumulated by the sample;

λ_B is the decay constant of the **B**-nuclei;

$F_k\left(B,B^m,\phi\right)$ is the term responsible for non-ideality of the experiment. It is defined as:

$$F_k\left(B,B^m,\phi\right)=\frac{\int_{t_1^{irr}}^{t_2^{irr}}dt^{irr}\int_{t_1^{cnt}}^{t_2^{cnt}}\phi_n(t^{irr})\cdot e^{-\lambda_B\cdot(t_k^{cnt}-t^{irr})}\cdot\left[1+\frac{\sigma_{B^m}}{\sigma_B}\cdot\alpha\cdot\frac{\lambda_{B^m}}{\lambda_{B^m}-\lambda_B}\cdot\left(1-e^{-(\lambda_{B^m}-\lambda_B)\cdot(t_k^{cnt}-t^{irr})}\right)\right]dt^{cnt}}{\left(t_{2k}^{cnt}-t_{1k}^{cnt}\right)\cdot\int_{t_1^{irr}}^{t_2^{irr}}\phi_n(t^{irr})\cdot dt^{irr}} \qquad (2.5.26)$$

The total algorithm of the activation cross-section determination described in the chapter (2.5) has been implemented in a computer code that was used at the KRI experiments. It should be noted that the algorithm described above is a generalization and includes many effects usually regarded as corrections. This allows data processing in a standard way that enhances the productivity of set-up and the reliability of results. Additionally, careful calculation of geometrical factors and detailed measurement of detector characteristics allow experiments to be undertaken with "close" geometries leading to optimization of the use of neutron flux generated by the Neutron Generator.

2.6. Cross section uncertainties

Uncertainties of many parameters contribute to the total uncertainty of the measured cross-section. The most important of them are as follows:

- decay data – (0.01% – 35%);
- area of γ-peak – (1% – 40%);
- efficiency of γ-detector – (1.2% – 1.5%);
- corrections for self-absorption and γ-cascade summing – (0.01% – 8.5%);
- reference cross sections used for neutron fluence determination – (0.4% – 0.8%);
- sample mass – (0.01% – 0.1%);
- isotopic abundance – (0.01% – 7.5%).

The contribution of uncertainties of other parameters is small and can be neglected. The total relative uncertainty of an individual cross section can be calculated in the standard way assuming that the uncertainty contributors are independent.

In some cases, the Monte-Carlo method was used for the uncertainty calculation. For this, the input parameters of the computer code that followed the formula (2.5.25) were considered as random variables having normal distributions with dispersions correspondent to uncertainties of the formula (2.5.25) parameters. Calculations were repeated for every new randomized set of the input parameters many times. The dispersion of the calculation results was taken as the output parameter uncertainty.

The Monte-Carlo procedure was used when the uncertainty contribution of the correction factor $F_k\left(B, B^m, \phi\right)$ defined by the formula (2.5.26) could not be neglected. Also, this method was used at calculations of isomeric ratios (sub-paragraph 2.7.2).

The Tables in Chapter 3 that contain the experimental data where a separate column was reserved for the reference data uncertainties ($\Delta\sigma_{ref}$) that are bound with the outer databases and are mainly independent on the experiment quality. The reference uncertainties were defined as:

$$\Delta\sigma_{ref} = \sqrt{(\Delta CS_{ref})^2 + \left(\Delta I_{abu}\right)^2 + (\Delta Y_\gamma)^2 + (\alpha_d \cdot \Delta T_{1/2})^2} \qquad (2.6.1)$$

NOTE! All the uncertainties in (2.6.1) are **the relative uncertainties!**

where ΔCS_{ref} is the relative uncertainty of the reference cross section;

ΔI_{abu} is the relative uncertainty of the target isotope abundance;

ΔY_γ is the minimal relative uncertainty of the used gamma intensities;

$\Delta T_{1/2}$ is the relative uncertainty of the half life of the reaction product;

α_d is the correction factor responsible for the decay during irradiation, cooling and gamma counting.

The last parameter α_d is not easy to calculate exactly because the uncertainty arising during decays is involved in the factor $F_k\left(B, B^m, \phi\right)$ in a complicated form. The α_d values used in calculation of the reference data uncertainties are given in the text explicitly. The values I_{abu}, Y_γ and $T_{1/2}$ used for ΔCS_{ref} calculation are marked in the "decay data used" Tables by the bold font.

2.7. Examples of special measurements

As previously noted this paper uses one page for one reaction data presentation. Sometimes, the space reserved is not sufficient for a clear description of the experiment peculiarities. Some specific methods used in the nonstandard or problematic situations are in detail considered in the present chapter.

The main method of the activation cross section determination used in our work is tightly bound with the measurement of the induced gamma activity. However, some reaction products do not reveal themselves by emitting the gamma-rays that could be registered by the conventional gamma detectors. Nevertheless, the corresponding cross sections can be measured sometimes. In the next two sub-paragraphs, *2.7.1* and *2.7.2*, methods are described that were applied to cross-section determination for the reactions that do not produce the gamma emitting nuclides.

Another difficulty in the reaction cross-section determination can emerge in the situation where the products of the different reactions have the common decay paths. An example of resolving a similar problem is considered in sub-paragraph *2.7.3.*

Modification of the set-up made for the adaptation of it to the measurement of short-lived activities is described in subparagraph *2.7.4.*

Additional details of the pioneer cross-section measurement carried out with the ^{241}Am, the material of high radio-activity, are presented in sub-paragraph *2.7.5.*

2.7.1. Determination of isomeric ratios using analysis of the decay curve shape

It was shown in the chapter 2.5 that two generations of the produced radioactive nuclei are always considered at the cross-section calculation in our work. The time behavior of the induced radioactivity is described then by:

$$N_B(t) = N_B(t_{00}) \cdot e^{-\lambda_B \cdot t} \cdot \left[1 + \frac{\sigma_{B^m}}{\sigma_B} \cdot \alpha \cdot \frac{\lambda_{B^m}}{\lambda_{B^m} - \lambda_B} \cdot \left(1 - e^{-(\lambda_{B^m} - \lambda_B) \cdot t} \right) \right] \qquad (2.5.22)$$

where the formula terms denoted by "***B***" are the parameters related to the assigned nuclide produced at neutron irradiation immediately, and the terms denoted by "$\boldsymbol{B^m}$" are related to the "mother" nuclide that produces the nuclide "***B***" in the decay process. It is significant that the "mother" nuclide is also produced at neutron irradiation.

The unknown ratio $\frac{\sigma_{B^m}}{\sigma_B}$ can be obtained from the analysis of the decay curve shape described by the formula (2.5.22). In Fig. 2.7.1.1, it is illustrated the work of the computer code that was written for determination of this ratio, or more exactly, the value that is more convenient to use, i.e. the Isomeric Ratio (IR) that is defined as:

$$IR \equiv \frac{\sigma_{B^m}}{\sigma_B + \sigma_{B^m}} \qquad (2.7.1.1)$$

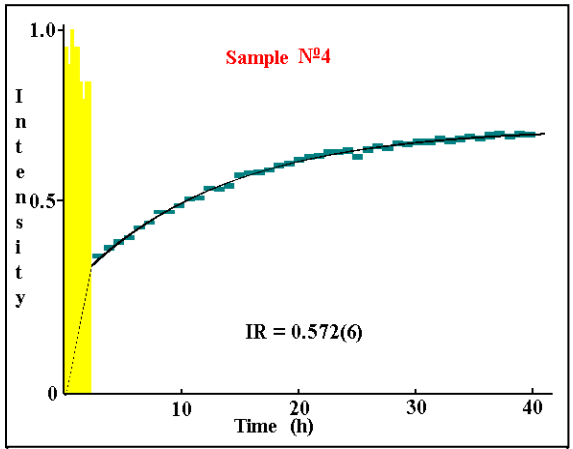

Fig. 2.7.1.1. Screen copy of working computer code that determines Isomeric Ratio (IR) using the decay curve shape analysis.

Interrelations between the cross-section ratio used in (2.5.22) and the isomeric ratio (2.7.1.1) are easy and everybody can write these on one's own.

It is worth emphasizing two important advantages of the IR determination described here. Firstly, high accuracy of IR can be obtained since only the relative activity change is analyzed. Consequently, many uncertainty sources such as the neutron monitor cross sections, sample mass, isotope abundance, reference gamma intensity, gamma self absorption, gamma spectrometer efficiency, etc. are excluded. Secondly, excitation cross-sections can be deduced for states which do not emit measurable radiation.

Fig. 2.7.1.1 relates to the measurement of ^{58}Ni(n, p)^{58m,g}Co cross sections. The metastable state ^{58m}Co populates the ground state ^{58g}Co via the isomeric transition which is strongly converted and cannot be registered by the gamma detector. The ^{58m}Co half-life is 9.10 h. The ^{58g}Co half-life is 70.86 d, and it emits gamma rays 810.8 keV with the probability 99.45%. The gamma-line is observable well. The change of the 810.8 keV count rate was used for analysis.

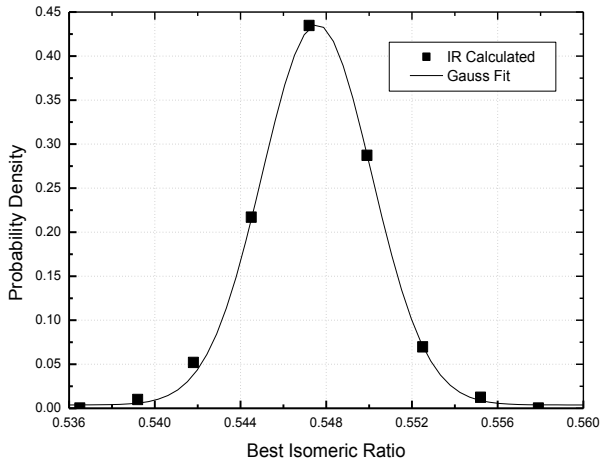

Fig. 2.7.1.2. Distribution of the IR values calculated with different input sets varied within own uncertainties. IR=0.547(5)

The best isomeric ratio was deduced in a computer code by the least squares method. For the IR uncertainty determination, the Monte-Carlo method was applied where the input data were varied inside own uncertainties that were suggested to have the normal distribution. In other words, the IR value was repeatedly calculated thousands of times with every new input parameter set that was generated from the original one by random Gauss scattering within own uncertainties of every input parameter such as the gamma peak area, time of gamma counting, half-lives of the metastable and ground states, neutron irradiation intensity, time of irradiation, etc. Then, the set of the IR values obtained was treated in a conventional way for determination of the average IR value and its dispersion. The work of the computer code is illustrated by Fig. 2.7.1.2.

The described method of the isomeric ratio determination was developed for studying the ^{58}Ni(n, p)^{58m,g}Co and ^{59}Co(n, 2n)^{58m,g}Co reactions but was extended later to other similar situations.

2.7.2. Isomeric ratio measurement using β-particles registered by γ-detector

It was shown in the previous sub-paragraph that the isomeric ratio can be obtained from the analysis of the decay curve shape. The method has the important advantage because it does not require the complicated absolute calibrations, calculation of numerous corrections but needs only the high registration stability of the parameter the count rate change of which is measured. This parameter could be, for example, the β-particle intensity.

Really, the β-particles with the energy more than approximately 0.5 MeV go free through the thin entrance window and are directly registered by the HPGe detector we used. The problem was to separate the signals produced by original β-particles from those generated by Compton- and other electrons in the gamma detector. The reaction ^{93}Nb(n, α)^{90m,g}Y proved to have the appropriate properties for the considered method application.

Firstly, there are only few reactions that produce considerable radiation in the niobium samples irradiated by neutrons. These reactions are ^{93}Nb(n, 2n)^{92m}Nb ($T_{1/2}$ = 10.15 d), ^{93}Nb(n, α)^{90m}Y ($T_{1/2}$ = 0.133 d) and ^{93}Nb(n, α)^{90g}Y ($T_{1/2}$ = 2.67 d). Secondly, the β-particles of the

^{90g}Y-decay have the high end-point energy of 2280 keV. Thirdly, the main part of gamma radiation emitted by irradiated niobium has the lower energy (E_γ < 480 keV for ^{90m}Y, E_γ < 950 keV for ^{92m}Nb and no gammas for ^{90g}Y).

Hence, the detector pulse height region (950 keV<E<1460 keV) is favorable for determination of the β-particle contribution. The region is limited from the left by the most intensive gamma-rays of the reaction products, and from the right by the prominent gamma-rays of the background.

Unfortunately, the chosen range of interest does not contain exclusively the unchangeably background and the changeably β-particle contribution. The ^{92m}Nb 1847.5 keV weak gamma-rays that have the intensity 0.85% per decay are admixed to this region also. It was necessary to take into account their changeable contribution as well.

For this, every niobium sample irradiated by neutrons was counted many times during several days after irradiation. A special computer code was created that divided the measured pulse height spectra into the components that have different time behavior. Three constituents were searched for: the background (unchanged in time), production of the ^{92m}Nb decay ($T_{1/2}$ = 10.15 d) and production of the ^{90g}Y decay ($T_{1/2}$ = 2.671 d). The dividing procedure was applied to the spectra with cooling time more than 2 days.

The three separated components of the total pulse height spectra obtained in such a way are shown in Fig. 2.7.2.1. The component intensities are normed to the two day cooling time. Also, the detector response functions emulated by MCNP are presented in Fig. 2.7.2.1. These were calculated for the β-particles of ^{90g}Y and for the 1847.5 keV gamma rays of ^{92m}Nb.

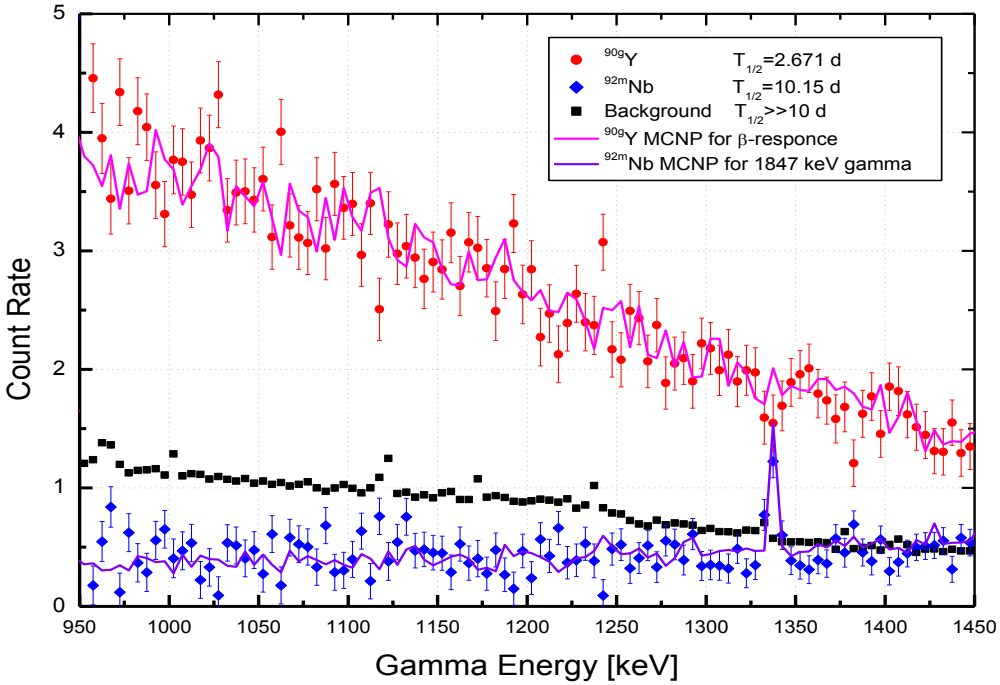

Fig. 2.7.2.1. Three pulse-height distribution components that have the different time behavior. Component points were extracted from the spectra counted for the Nb sample in the time interval of 2 – 10 days after irradiation. The solid lines are the corresponding response functions calculated by MCNP.

As it is seen in Fig. 2.7.2.1, the components extracted from the experimental spectra and the response functions calculated by MCNP are in a good agreement. Even the single-escape peak at E_γ = 1336 keV is equally reproduced in both amplitude distributions of the ^{92m}Nb constituent. A close match between the pulse height distributions extracted from the experimental spectra using a priory information on the expected time behavior of the spectra components and the detector

response functions to the corresponding radiations calculated by MCNP can be considered as an additional evidence for the correctness of the separation procedure we used.

So, if from the total number of pulses counted in the region 960 keV – 1450 keV are subtracted the number of background events and the number of events produced in ^{92m}Nb decay then the rest amount should be proportional to the number of β-particles emitted in the ^{90g}Y-decay.

The background was measured with high accuracy earlier (Fig. 2.4.1 on p.10). Long gamma counting made for every sample after 12 – 16 days after irradiation (when ^{90g}Y decayed) allowed the experimental determination of the ^{92m}Nb contribution in the region of interest. For further applications, it was linked to the intensity of the main gamma peak of ^{92m}Nb with the energy of 934.4 keV. The result was also confirmed by MCNP calculations.

Fig. 2.7.2.2 demonstrates an example of the time behavior of the ^{90g}Y beta radiation intensity measured by the method described above (red points). The red solid line corresponds to the calculated decay curve of ^{90g}Y ($T_{1/2}$ = 64.10 h) that have "a mother", ^{90m}Y ($T_{1/2}$ = 3.244 h) produced with the probability that corresponds to the isomeric ratio value ***IR***=0.43.

Simultaneously, areas of several gamma peaks were determined in the spectra measured by the same detector. For completeness, the changing of count rates of the 934.4 keV peak of ^{92m}Nb, the 479.5 keV peak of ^{90m}Y and the 1461.0 keV background peak are given in Fig. 2.7.2.2 also. Solid lines show the corresponding decay curves.

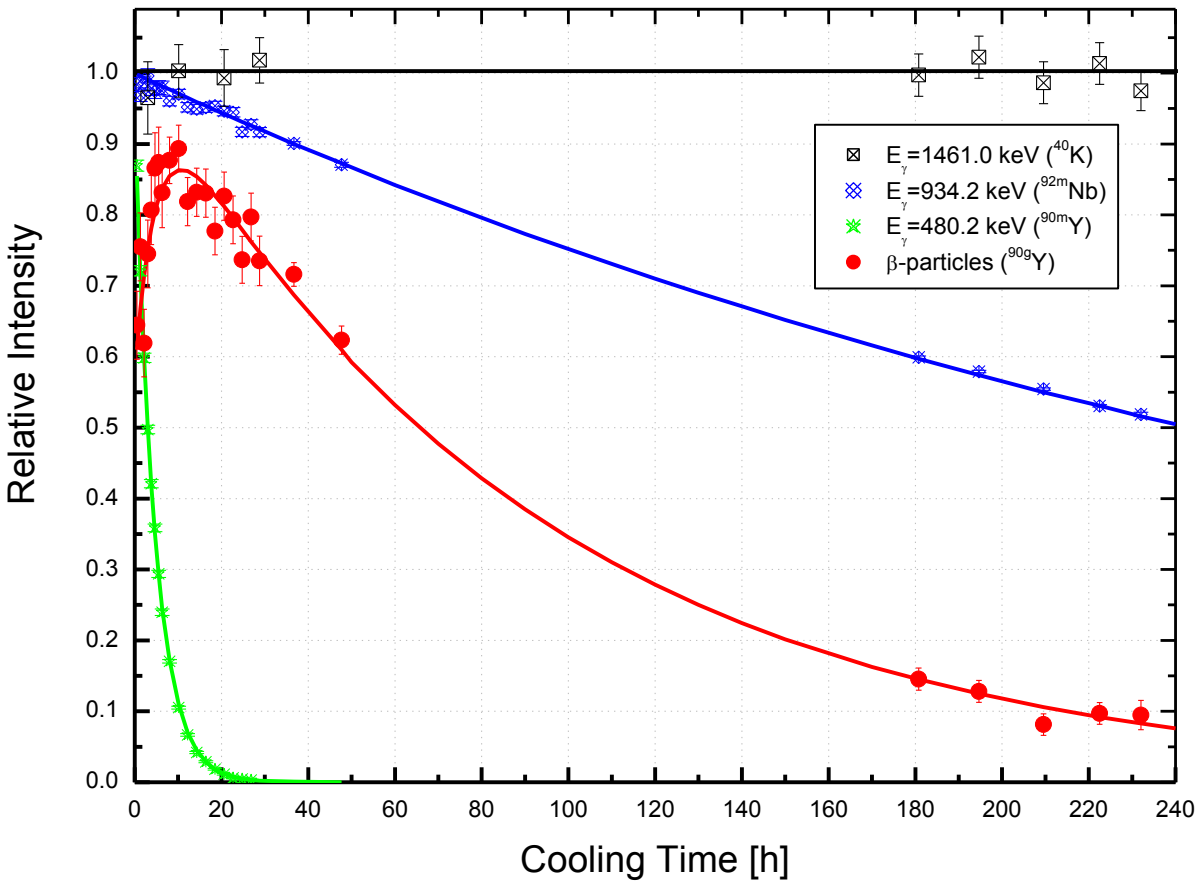

Fig. 2.7.2.2. Measured and calculated decay curves obtained for the Nb sample irradiated by neutrons of 14.86 MeV.

The isomeric ratio for reaction ^{93}Nb(n, α)^{90g,m}Y was determined as the best fit of the curve produced by formula (2.5.22) (solid red line) to the experimental points (red circles) that are the relative intensities of β-particles counted by the HPGe detector. For more detail see previous sub-paragraph, where isomeric ratio determination using the analysis of the decay curve is described.

The experimental results of the $^{93}Nb(n, \alpha)^{90g,m}Y$ cross sections are presented in p. 94-95.

2.7.3. Cross section separation for reactions that result in the common product

The problem is considered via the example of ^{50}V(n, α)^{47}Sc and ^{51}V(n, n'α)^{47}Sc reactions.

A very low abundance of ^{50}V (0.25%) in natural vanadium made it necessary to purchase an enriched sample. The sample used in the work had an enrichment of 17% for ^{50}V. It was quite enough for reliable measuring the ^{50}V(n, n'α)^{46}Sc cross section but for the ^{50}V(n, α)^{47}Sc cross section the contribution of the ^{51}V(n, n'α)^{47}Sc reaction could not be ignored. To solve the problem, a sample of natural abundance was included in the assembly, back-to-back to the enriched sample. The summarized cross-section of the ^{47}Sc production in vanadium (σ_V) was exclusively measured for both samples. The individual values of the cross sections ^{50}V(n, α)^{47}Sc (σ_{50}) and ^{51}V(n, n'α)^{47}Sc (σ_{51}) were determined as a solution of the system of two equations with two variables:

$$\sigma_{50} \cdot v_{50}^1 + \sigma_{51} \cdot v_{51}^1 = \sigma_V^1 \qquad (2.7.3.1)$$

$$\sigma_{50} \cdot v_{50}^2 + \sigma_{51} \cdot v_{51}^2 = \sigma_V^2 \qquad (2.7.3.2)$$

where v_{50}^1 and v_{51}^1 – are shares of isotopes ^{50}V and ^{51}V in vanadium of the first sample;
v_{50}^2 and v_{51}^2 – are shares of isotopes ^{50}V and ^{51}V in vanadium of the second sample;
σ_V^1 is the summarized cross section (V(n, x)^{47}Sc) obtained for the first sample;
σ_V^2 is the summarized cross section (V(n, x)^{47}Sc) obtained for the second sample.

The solution of the equation system is well known:

$$\sigma_{50} = \frac{\sigma_V^1 \cdot v_{51}^2 - \sigma_V^2 \cdot v_{51}^1}{v_{50}^1 \cdot v_{51}^2 - v_{50}^2 \cdot v_{51}^1} \qquad (2.7.3.3)$$

$$\sigma_{51} = \frac{\sigma_V^2 \cdot v_{50}^1 - \sigma_V^1 \cdot v_{50}^2}{v_{50}^1 \cdot v_{51}^2 - v_{50}^2 \cdot v_{51}^1} \qquad (2.7.3.4)$$

If we recollect that $v_{50}^1 + v_{51}^1 = 1$ and $v_{50}^2 + v_{51}^2 = 1$ then the view of the equation system solution can be simplified:

$$\sigma_{50} = \frac{\sigma_V^1 \cdot v_{51}^2 - \sigma_V^2 \cdot v_{51}^1}{v_{51}^2 - v_{51}^1} \qquad (2.7.3.5)$$

$$\sigma_{51} = \frac{\sigma_V^2 \cdot v_{50}^1 - \sigma_V^1 \cdot v_{50}^2}{v_{50}^1 - v_{50}^2} \qquad (2.7.3.6)$$

The experimental results of the ^{50}V(n, α)^{47}Sc and ^{51}V(n, n'α)^{47}Sc cross sections are presented in p. 43-44.

2.7.4. Measurement of short lived reaction products

To extend the region of nuclear reaction cross-sections measured at KRI to the reactions that generate short-lived nuclei, the set-up was modified. A system of quick sample transportation from the measuring room to the neutron target and back was designed, made, and tested in experimental conditions. The time needed for transportation of the sample to the neutron target or to the gamma detector was about 2 s. The sample arrival and departure moments were determined by means of two sensor units which were connected with a computer via a CAMAC module. Time uncertainties of sample irradiation and gamma counting were estimated to be less than 0.5 s.

2.7.5. Measurement of ^{241}Am cross sections

Conversion and utilization of long-lived radioactive products and, especially, actinide elements are among the most important problems of nuclear industry. Given the significance of this issue, experimental data on nuclear cross-sections are scanty or often nonexistent in this field.

In this chapter, one of the first successful attempts for measuring neutron cross-sections on ^{241}Am is described. These measurements were very difficult from the experimental point of view. For example, the natural gamma activity of a ^{241}Am sample used was about 10^8 Bq but the induced gamma activity of the most probable (n, 2n) reaction product was expected to be of order of 100 Bq. Other reactions that were planned to measure were yet less probable. Additionally, some relevant gamma peaks could be masked by the numerous gamma peaks generated by fission fragments.

The first problem to resolve was the suppression of intensive natural gamma radiation of americium samples. For this purpose, a leaden container with the 5 mm walls was used from the beginning. This was later changed to a cadmium screen because the gamma absorption in cadmium dependes more steeply on gamma energy near 100 keV, and this provides a higher registration efficiency for the cadmium absorber in the region of 100–300 keV at the equivalent suppression of 60 keV gamma radiation.

The second problem was the container had to be sealed absolutely reliably for neutron irradiation and gamma counting but could be easily unpacked for radiochemical cleaning of the samples in order to provide repeated use of a very expensive material and its final return to a host laboratory. The container and the near-detector arrangement are shown in Fig. 2.7.5.1.

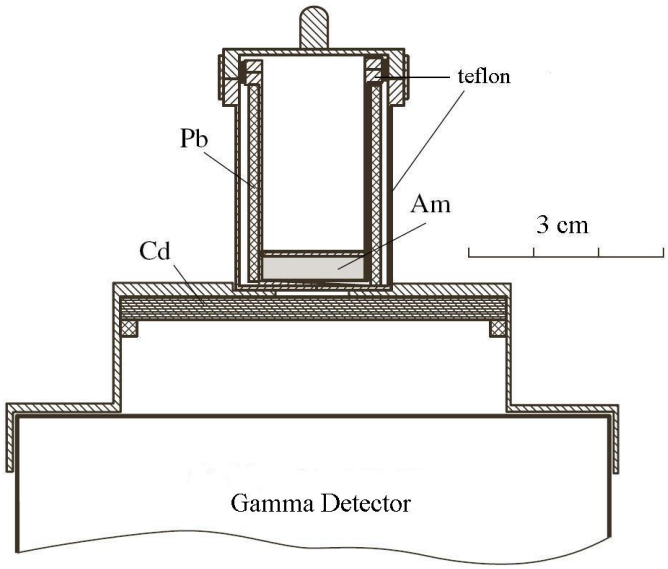

Fig. 2.7.5.1. Geometry for gamma counting. The thickness of cadmium absorber was 3.5 mm. The lead tube was used to shield the gamma-detector from scattered gamma-radiation.

The third problem was detector calibration. To determine the efficiency for gamma counting with the lead container used at the beginning of experiment, we carried out measurements for a ^{92m}Nb sample with a well determined activity which was placed inside the container in the position of the geometric center of the Am sample. Since the gamma radiation energies of ^{92m}Nb and ^{240}Am, the product of ^{241}Am(n, 2n)^{240}Am reaction, are near, any corrections for the efficiency registration difference were small. In particular, the difference in absorption of gamma rays with energies of 934.2 keV (^{92m}Nb) and 987.8 keV (^{240}Am) by the lead container bottom was -1.8%; the difference in gamma counting efficiency without the container was +5.3%. The efficiency difference related to the form of samples and self-absorption was -0.5%. Thus, the total difference in gamma counting efficiency of 934.2 keV (^{92m}Nb) and 987.8 keV (^{240}Am) was only 4.0%.

The dependence of gamma radiation attenuation values on the cadmium absorber thickness in the geometry presented in Fig. 2.7.5.1 was determined experimentally using a kit of three standard gamma sources (^{241}Am, ^{109}Cd and ^{152}Eu) which were placed in the position of the studied americium sample. The absorption values measured experimentally were compared with those calculated by the simple formula:

$$C = e^{-\mu \cdot d} \qquad (2.7.5.1)$$

where C is the attenuation value;
μ is the attenuation coefficient, [mg/cm^2]$^{-1}$
d is the absorber thickness, [mg/cm^2]

The comparison results are shown in Fig. 2.7.5.2 where it is seen that the simple formula (2.7.5.1) describes the real gamma ray attenuation rather well at energies above 200 keV that cover the whole region of interest in the experiment on the neutron induced activation cross-section measurement for ^{241}Am. The deficit of the calculated attenuation values at lower gamma energies appears to be associated with the oblique tracks that become important in this case.

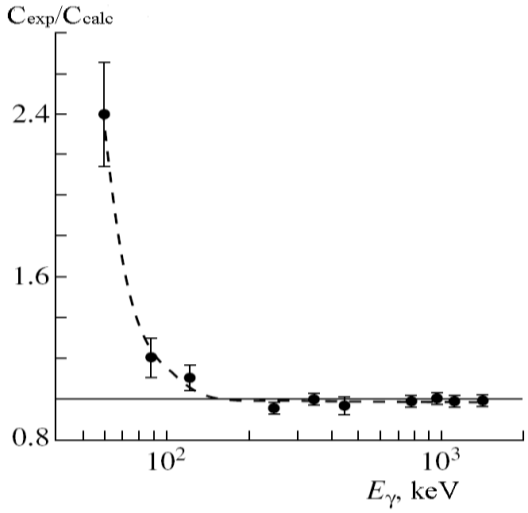

Fig. 2.7.5.2. Ratio of the measured gamma ray attenuation to the calculated one in dependence on gamma energy. The cadmium absorber thickness is 3.5 mm.

The main part of the natural gamma radiation of ^{241}Am that has the energy 60 keV and less, was reliably suppressed by the constructions described above. However, some gamma-rays associated the with natural radioactive decay having higher energies and the intensities of order of 10^{-6} per decay were clearly observed in the gamma spectra counted with a non-irradiated americium sample. An example of such spectrum is shown in Fig. 2.7.5.3.

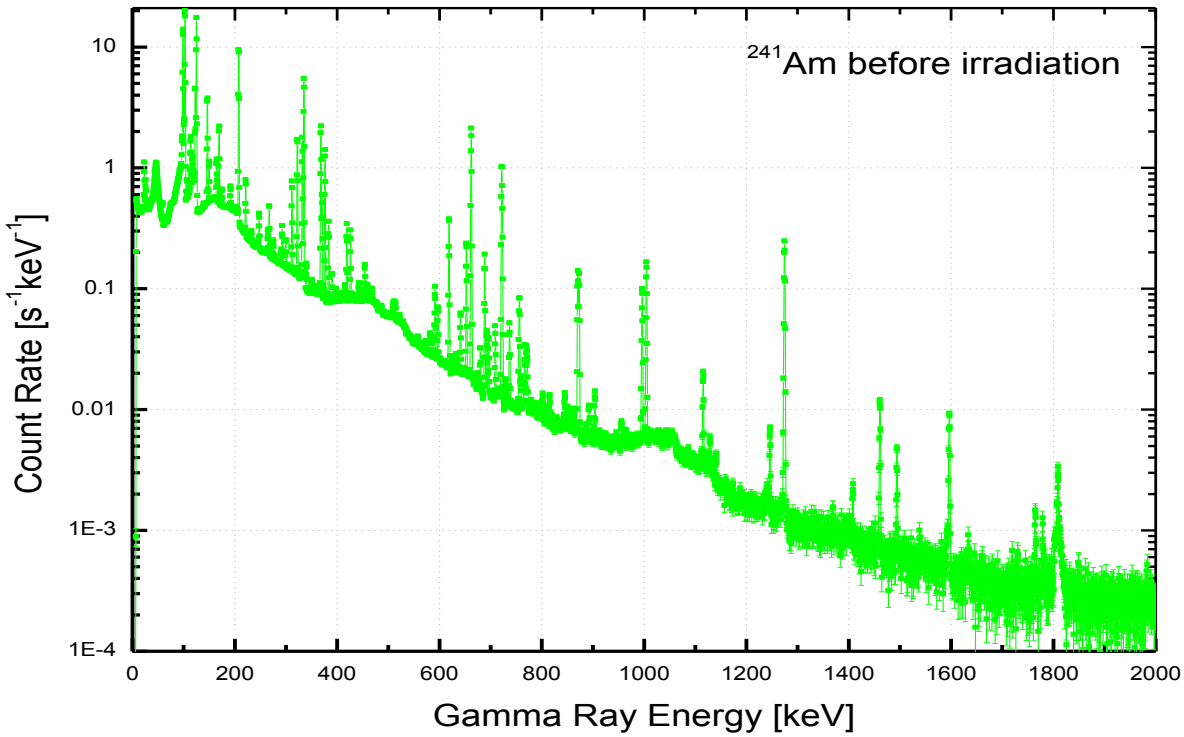

Fig. 2.7.5.3. Gamma spectrum of a non-irradiated Am-sample counted by the HPGe detector shielded from low-energy gamma radiation with cadmium absorber of 3.5 mm thickness.

The additional background gamma radiation shown in Fig. 2.7.5.3 has not only a negative but also a positive role because energies and intensities of the gamma rays that accompany the ^{241}Am natural decay are well known. The inclusion of the corresponding information into the process of the gamma detector efficiency calibration made the data on efficiency more accurate and reliable.

Besides, the absolute intensity values of the ^{241}Am natural gammas can be used for the determination of the sample mass.

The samples were prepared from an aqueous solution or from americium nitrate. The dimensions of the volume filled with the solution or americium nitrate varied between 8 and 16 mm in diameter and between 1.0 and 3.5 mm in height. Two standard niobium foils used for the neutron fluence determination, were fastened to the front and back surfaces of the inner container (Fig. 2.7.5.1).

The samples were of high purity. According to the certificate, the total concentration of alien fissile elements in the samples did not exceed 0.1%. However, for the present experiment, isotopic purity requirements were much higher. The stringent limitations concerned the possible admixture of the other americium isotopes, ^{242m}Am and ^{243}Am, because the products of their natural decay emit the same gamma rays as ^{239}Am and ^{238}Np, the products of ^{241}Am(n, 3n)^{239}Am and ^{241}Am(n, α)^{238}Np reactions. The available experimental conditions (neutron flux, duration of irradiation and gamma counting) determined an upper limit on permissible admixture of other americium isotopes as 10^{-7} g/g. To make sure that the samples meet such conditions, a long gamma counting was carried out with the freshly prepared sample. No traces of other americium isotopes were revealed in the accumulated gamma spectra. The upper limit of possible content of ^{242m}Am and ^{243}Am isotopes in the samples was estimated as less than 10^{-8} g/g.

For determination of neutron induced activation cross-sections, six irradiations were carried out with nine Am-samples. Typically, the irradiations lasted from 1 to 17 hours, and the total fluence accumulated by samples varied from (1 to 10)$*10^{13}$ n/cm^2.

The gamma spectra of the irradiated samples were found to be very complex. They contained hundreds of gamma peaks, most of which belonged to the fission fragments. In order to increase the peak identification reliability, the peak half-lives were also analyzed. For this, every irradiated sample was counted several times during 200 h after irradiation.

For the ^{241}Am(n, 2n)^{240}Am reaction, two gamma peaks were to be observed: $E_{\gamma 1}$=987.8 keV and $I_{\gamma 1}$=72.2%, and $E_{\gamma 2}$=888.9 keV and $I_{\gamma 2}$=24.7%. These peaks were revealed in the spectra, where their intensity ratio corresponded to the values given above, and their half lives were equal to 50.8 h which coincides with the half life of ^{240}Am. (Fig. 2.7.5.4). Therefore, the ^{241}Am(n, 2n)^{240}Am cross sections could be reliably calculated using the standard procedures without any complications. The data obtained is presented on p. 273 of this paper.

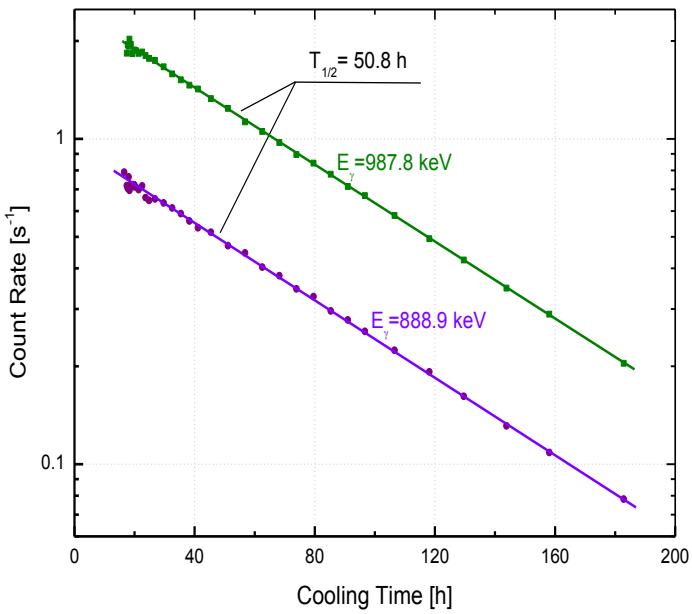

Fig. 2.7.5.4. Decay curves for the gamma rays 888.9 keV and 987.8 keV that were identified as the ^{240}Am decay gammas.

For the ^{241}Am(n, 3n)^{239}Am cross section measurement, the experimental conditions were more sophisticated than for the reaction considered above. There were many factors that contributed to making this experiment more difficult, such as the smaller cross section, the smaller intensities of the ^{239}Am gamma radiation; the lower energies of the gamma rays emitted, the higher background level in this region of

gamma spectra. In addition, the interference probability with some gamma rays of the ^{241}Am natural decay or with some gammas of the numerous fission fragments is higher. These factors arose in reality during the experiment.

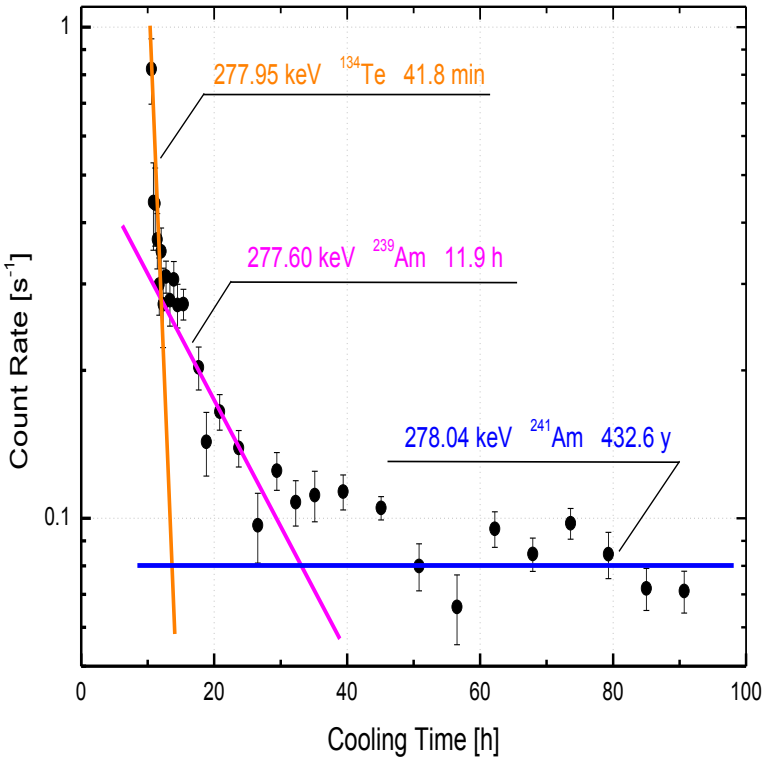

Fig. 2.7.5.5. Decay curves for the gamma rays with energies close to 277.6 keV. The magenta solid line corresponds to the ^{239}Am decay gammas.

Three candidates were selected for ^{239}Am radiation identification:

$E_{\gamma 1}$=226.4 keV and $I_{\gamma 1}$=3.3%;
$E_{\gamma 2}$=228.2 keV and $I_{\gamma 2}$=11.3%;
$E_{\gamma 3}$=277.6 keV and $I_{\gamma 3}$=15.0%.

The first two candidates proved to be totally masked by very intensive gamma radiation of the ^{132}Te with E_{γ}=228.2 keV and $T_{1/2}$ =3.20 d.

The third candidate was also not simple. The decay curve for gamma radiation with the appropriate energy could not be approximated by the straight line in the logarithmic scale as was done for gamma rays of the ^{241}Am(n, 2n)^{240}Am reaction. The studied decay curve consists of three contributions (shown in Fig. 2.7.5.5). Happily, half-lives of the contributors are very different, and the component related to the ^{241}Am(n, 3n)^{239}Am reaction was determined without significant additional uncertainty. The cross-section data obtained are presented on p.272.

The ^{241}Am(n, α)^{238}Np cross-section was most difficult for measuring because of its small magnitude that was expected to be of order of 1 mb. Remember that the fission cross section at neutron energy 14 MeV is about 2500 mb. Using tables of evaluated cumulative fission fragment yields one can estimate that more than 300 fission fragments are produced with the cross-section of 10 mb or higher at neutron irradiation of ^{241}Am. Really, several hundreds of gamma peaks were revealed during processing of gamma spectra of irradiated americium samples. Most of them were identified as fission fragment gamma rays.

The best region for observation of the ^{238}Np decay gamma radiation proved to be the region around E_{γ} = 1028.5 keV that is shown in Fig. 2.7.5.6. There are not observed any intensive gamma peaks that could mask a very weak radiation of the ^{241}Am(n, α)^{238}Np reaction. In Fig. 2.7.5.6, the range (1028.5±1.5) keV where

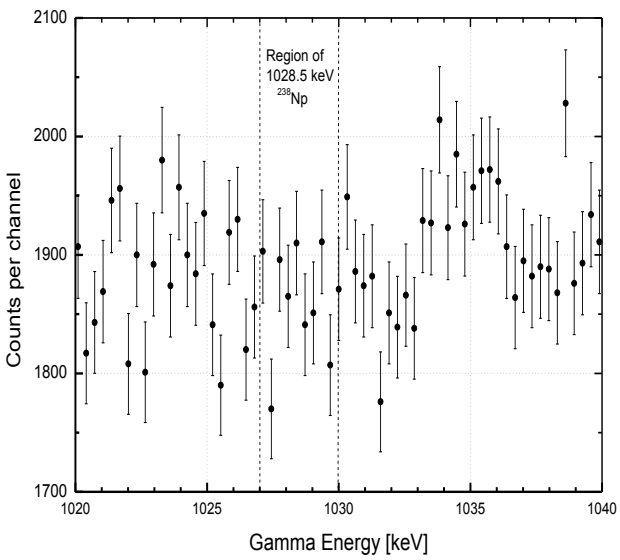

Fig. 2.7.5.6. Fragment of the gamma spectrum in the vicinity of E_{γ} = 1028.5 keV that was expected in the ^{238}Np decay. Gamma counting was started at 60 h after irradiation and was carried out during 100 h

one of the biggest gamma peaks of ^{238}Np was to be observed is marked out by the dashed lines. Since no peak can be detected there the region between the dashed lines was interpreted as the background. The possible 1028.5 keV peak area was set as being less than 3 background statistical uncertainties that resulted in the upper limit of the ^{241}Am(n, α)^{238}Np cross section presented on p.271.

A significant volume of information about the fission fragmens was obtained in this experiment as a byproduct of the irradiations. Since we had about two hundred decay curves for different gamma peaks obtained during eight days after irradiation, we were able to identify many gamma peaks belonging to fission fragments. Some examples of these decay curves are presented in Fig. 2.7.5.7 together with the identification results.

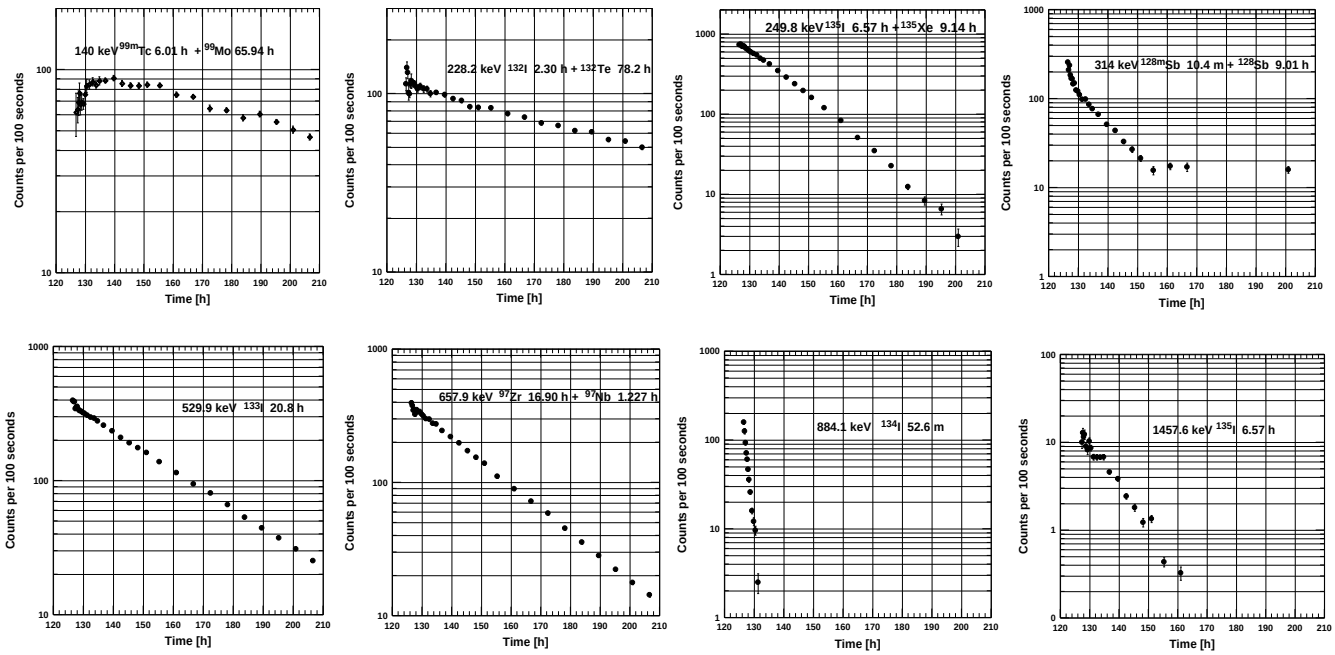

Fig. 2.7.5.7. Several decay curves of nuclides identified as fission fragments of ^{241}Am irradiated by neutrons.

It can be noted that some curves have a shape which is inherent to nuclide chains. These figures are correspondingly marked.

About twenty fission fragment yields were also obtained in the data processing. However, the fission data was considered as a byproduct of the main experiment on the ^{241}Am(n, 2n)^{240}Am, ^{241}Am(n, 3n)^{240}Am and ^{241}Am(n, α)^{238}Np cross section measurement and therefore is not included in the present paper.

3. EXPERIMENTAL RESULTS

The experimental data obtained at KRI Neutron Generator NG-400 in neutron energy region 13.4 – 14.9 MeV are presented in the following pages. As discussed earlier a format showing “one reaction on one page” was chosen for the data presentation. The page structure is as follows:

Reaction name is in the page header.

A Table with experimental results is placed in the top left of the page. The Table consists of four columns: the neutron energy (E_n [MeV]), the reaction cross-section (σ [mb]), the cross-section total uncertainty ($\pm\Delta\sigma_{total}$ [%]) and the cross-section reference uncertainty ($\pm\Delta\sigma_{ref}$ [%]). The last column data is the uncertainty contributed by the reference data used for the cross-section calculation. A rule of $\Delta\sigma_{ref}$ calculation is previously described on p. 19. The correction factor α_d used in $\Delta\sigma_{ref}$ calculation is given in the last line of the Table. This line contains also an indication of the reference cross-section used.

To the right of the Table, a Figure is allocated where the present data are compared with results of other experiments and with available evaluations.

Under the Table and Figure, necessary comments and explanations are given to the experimental results presented.

Reference decay data used for the cross-section calculation is in the table at the page bottom. This includes the half-life of the reaction product, the energy and intensity of the gamma-lines used during data processing. The target isotop abundance used is given in this table too.

In addition, a picture showing the decay scheme of the nuclides related to studied reaction is placed near the table with the reference decay data. The picture is a copy fragment of relevant schemes presented in the Handbook “Tables of Isotopes” by Richard B. Firestone issued in 1996 [25]. Note that the half-life values presented in the picture may differ from the half-life values presented in the table with the reference decay data. The difference reflects the progress in Nuclear Structure Data that has happened over the last twenty years. **It should be underlined that the latest decay data given in the table at the page bottom were used in the process of the cross section calculation**.

^{23}Na(n, 2n)^{22}Na

^{23}Na(n,2n)^{22}Na			
E_n [MeV]	σ [mb]	$\pm\Delta\sigma_{total}$ [%]	$\pm\Delta\sigma_{ref}$ [%]
13.56	4.58	*21.1*	*0.600*
13.74	9.83	*9.95*	*0.599*
13.96	14.1	*7.78*	*0.570*
14.19	21.9	*6.76*	*0.554*
14.42	29.8	*6.26*	*0.558*
14.61	32.3	*5.13*	*0.573*
14.78	37.7	*4.39*	*0.573*
Ref. CS is ^{93}Nb(n,2n)^{92m}Nb;			α_d = *1.1*

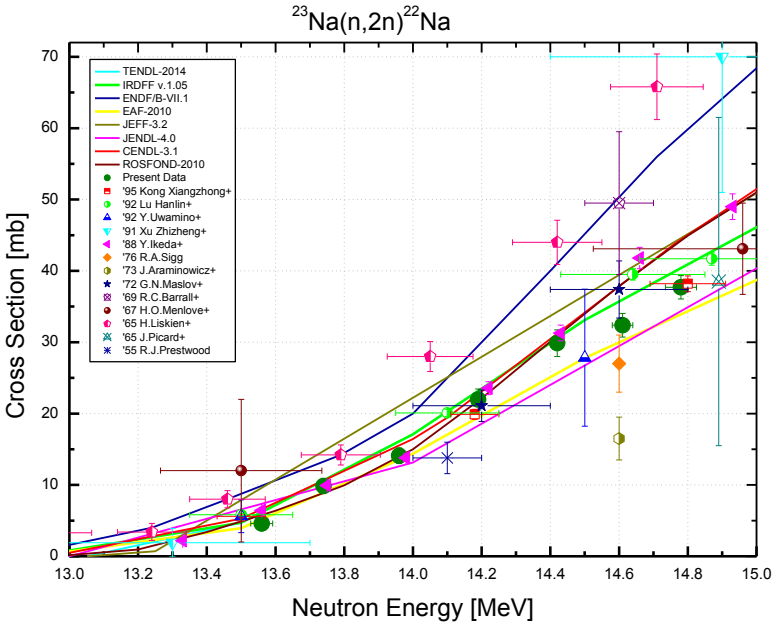

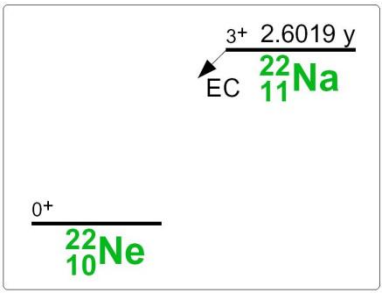

Decay data used for **^{23}Na(n,2n)^{22}Na**.

Target nucleus	**Abundance [%]**	**Chemical form**	**Reaction product**	**$T_{1/2}$**	**E_γ [keV]**	**Y_γ [%]**
^{23}Na	**100**	NaCl	^{22}Na	**2.6018 y** *22*	**1274.5**	**99.940** *14*

^{26}Mg(n, α)^{23}Ne

^{26}Mg(n,α)^{23}Ne			
E_n [MeV]	σ [mb]	$\pm\Delta\sigma_{total}$ [%]	$\pm\Delta\sigma_{ref}$ [%]
13.72	52.7	*5.08*	*4.03*
13.95	53.0	*6.38*	*4.03*
14.23	51.9	*4.52*	*4.02*
14.50	49.1	*7.74*	*4.01*
14.72	55.9	*5.48*	*4.01*
14.85	51.3	*4.13*	*4.02*
Ref. CS is ^{27}Al(n, α)^{24}Na;			α_d = *1.9*

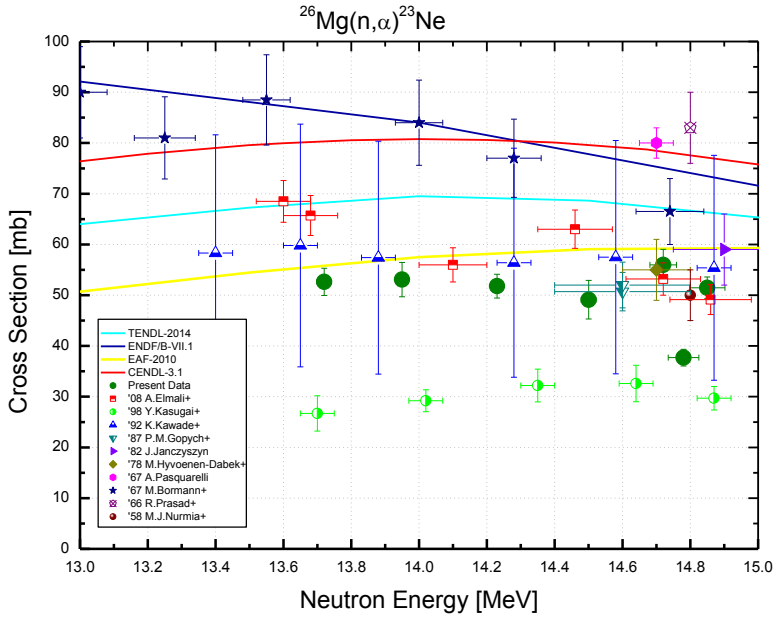

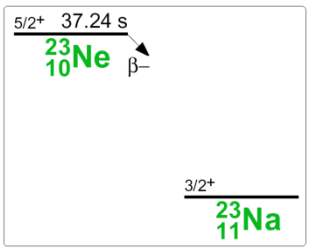

Decay data used for **^{26}Mg(n,α)^{23}Ne**.

Target nucleus	**Abundance [%]**	**Chemical form**	**Reaction product**	**$T_{1/2}$**	**E_γ [keV]**	**Y_γ [%]**
^{26}Mg	**11.01** *3*	Mg-metal	^{23}Ne	**37.24 s** *12*	**440.0**	**33.0** *13*

^{27}Al(n, p)^{27}Mg

^{27}Al(n,p)^{27}Mg			
E_n [MeV]	σ [mb]	$\pm\Delta\sigma_{total}$ [%]	$\pm\Delta\sigma_{ref}$ [%]
13.47	79.7	*2.03*	*0.830*
13.66	74.6	*2.00*	*0.576*
13.88	76.6	*1.97*	*0.545*
14.04	71.8	*2.09*	*0.514*
14.26	71.0	*1.94*	*0.472*
14.44	72.0	*1.90*	*0.443*
14.63	67.1	*2.07*	*0.451*
14.81	64.0	*1.94*	*0.490*
Ref. CS is ^{27}Al(n, α)^{24}Na;			α_d = *1.8*

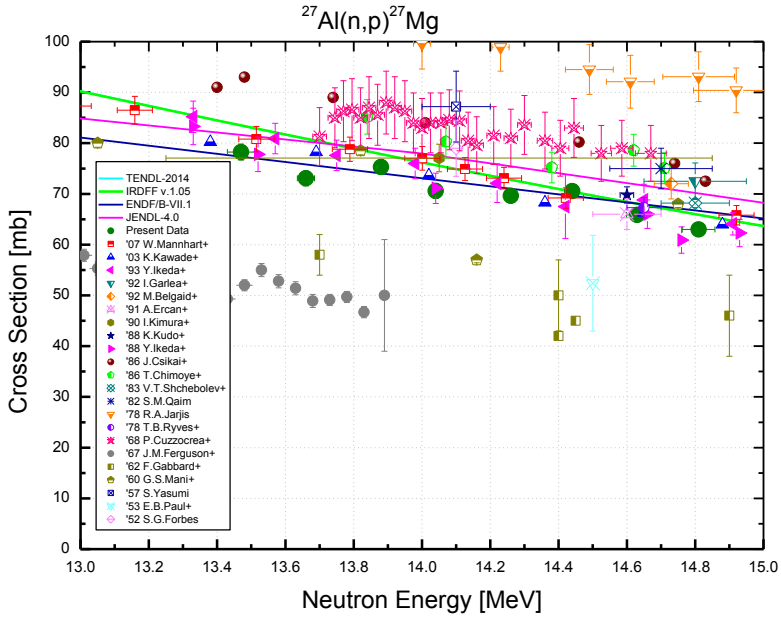

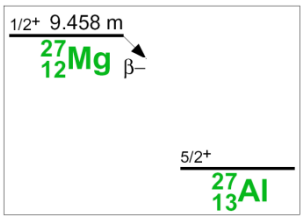

Decay data used for **^{27}Al(n,p)^{27}Mg**.

Target nucleus	**Abundance [%]**	**Chemical form**	**Reaction product**	**$T_{1/2}$**	**E_γ [keV]**	**Y_γ [%]**
^{27}Al	**100**	Al-metal	^{27}Mg	**9.458 m** *12*	**843.8**	**71.80** *2*
					1014.5	28.20 *2*

^{27}Al(n, 2n)^{26g}Al

^{27}Al(n,2n)^{26g}Al			
E_n [MeV]	σ [mb]	$\pm\Delta\sigma_{total}$ [%]	$\pm\Delta\sigma_{ref}$ [%]
13.68	0.15	*66.7*	*0.592*
13.74	0.55	*18.1*	*0.591*
13.87	3.12	*12.8*	*0.561*
14.07	6.73	*7.35*	*0.546*
14.29	12.5	*6.26*	*0.543*
14.48	18.5	*6.91*	*0.550*
14.70	25.0	*5.06*	*0.565*
14.84	30.9	*5.75*	*0.589*
Ref. CS is ^{93}Nb(n,2n)^{92m}Nb; $\alpha_d = 1.0$			

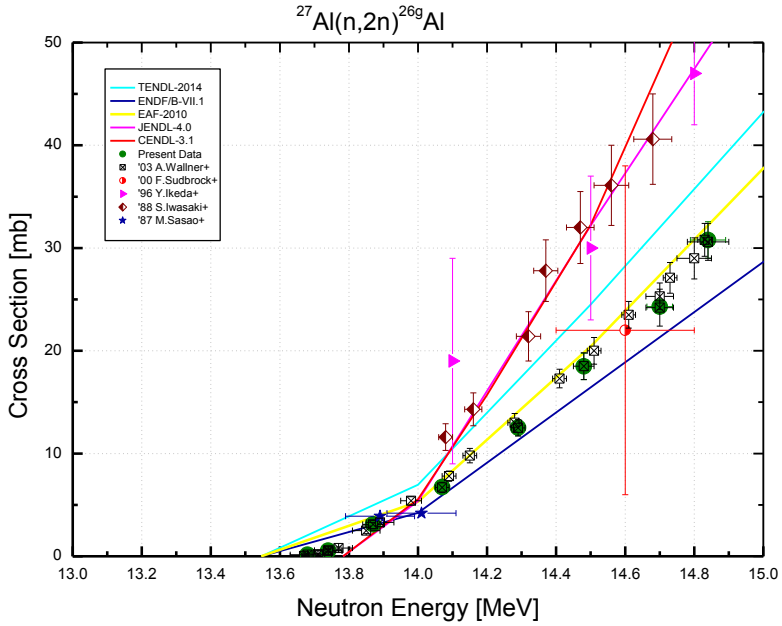

The aluminum samples were irradiated at KRI, and the accumulated neutron fluence was determined using KRI methods. A very long half-life of ^{26}Al made the gamma counting of the irradiated aluminum samples ineffective. It was not done. The gamma-ray energy and intensity given in the table at the page bottom are presented for the sake of information completeness but were not used in this experiment.

The amount of ^{26}Al produced during the irradiations was measured via accelerator mass spectrometry (AMS) with the Vienna Environmental Research Accelerator (VERA) in the frame of IRK-KRI collaboration.

More exhaustively, the experiment on the ^{27}Al(n,2n)^{26g}Al cross section measurement is described in [5].

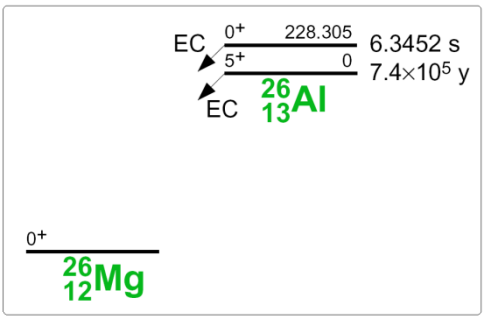

Decay data used for **^{27}Al(n,2n)^{26g}Al**.

Target nucleus	**Abundance [%]**	**Chemical form**	**Reaction product**	**$T_{1/2}$**	**E_γ [keV]**	**Y_γ [%]**
^{27}Al	**100**	Al-metal	^{26}Al	$7.17\cdot10^5$ y *24*	1808.7	99.76 *4*

^{28}Si(n, p)^{28}Al

^{28}Si(n,p)^{28}Al			
E_n [MeV]	σ [mb]	$\pm\Delta\sigma_{total}$ [%]	$\pm\Delta\sigma_{ref}$ [%]
13.47	269	*4.02*	*0.813*
13.88	283	*4.55*	*0.520*
14.26	270	*4.35*	*0.443*
14.63	264	*4.10*	*0.420*
14.81	220	*6.27*	*0.462*
Ref. CS is ^{27}Al(n, α)^{24}Na;			α_d = *1.8*

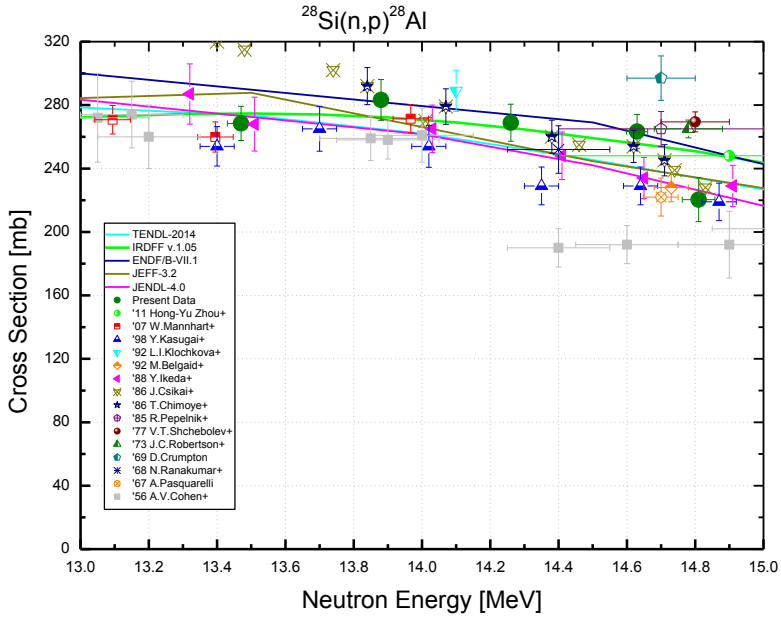

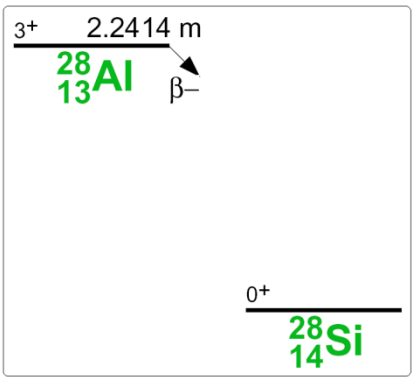

Decay data used for **^{28}Si(n,p)^{28}Al**.

Target nucleus	Abundance [%]	Chemical form	Reaction product	$T_{1/2}$	E_γ [keV]	Y_γ [%]
^{28}Si	**92.223** *19*	Si-crystal	^{28}Al	**2.245 m** *2*	**1779.0**	**100**

^{29}Si(n, 2p)^{28}Mg

^{29}Si(n,2p)^{28}Mg		
E_n [MeV]	σ [mb]	$\pm\Delta\sigma_{total}$ [%]
14.80	$<1.5\cdot10^{-4}$	33.3
Ref. CS is ^{93}Nb(n,2n)^{92m}Nb		

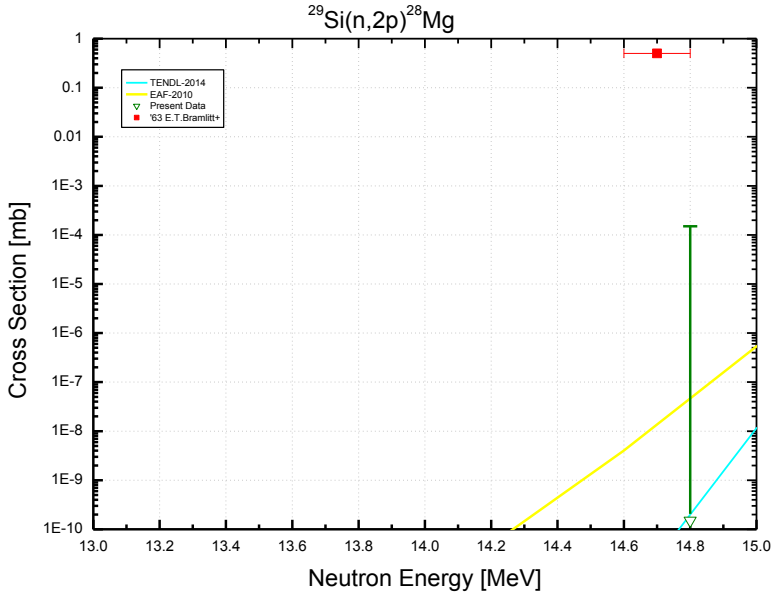

No peaks were revealed in gamma spectra of irradiated silicon samples that could be identified as peaks belonging to ^{28}Mg. Therefore, only the upper limit of the ^{29}Si(n,2p)^{28}Mg cross section was obtained that was set to be equal to three background uncertainties calculated for regions of the expected gamma peaks.

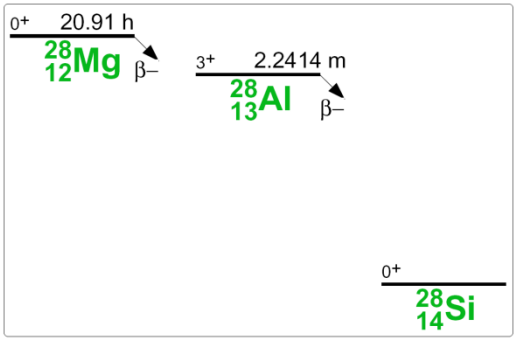

Decay data used for **^{29}Si(n,2p)^{28}Mg**.

Target nucleus	Abundance [%]	Chemical form	Reaction product	$T_{1/2}$	E_γ [keV]	Y_γ [%]
^{29}Si	**4.685** *8*	Si-crystal	^{28}Mg	**20.915 h** *9*	**400.6**	**35.9** *10*
					941.7	36.3 *10*
					1342.2	54.0 *16*
					1779.0	100

^{30}Si(n, α)^{27}Mg

^{30}Si(n,α)^{27}Mg			
E_n [MeV]	σ [mb]	$\pm\Delta\sigma_{total}$ [%]	$\pm\Delta\sigma_{ref}$ [%]
13.47	60.8	*9.85*	*0.894*
13.66	62.4	*6.69*	*0.665*
13.88	62.3	*5.88*	*0.639*
14.04	66.3	*5.46*	*0.613*
14.44	67.8	*5.99*	*0.554*
14.63	71.8	*5.51*	*0.560*
14.81	70.7	*4.79*	*0.592*
Ref. CS is ^{27}Al(n, α)^{24}Na;			$\alpha_d = 1.5$

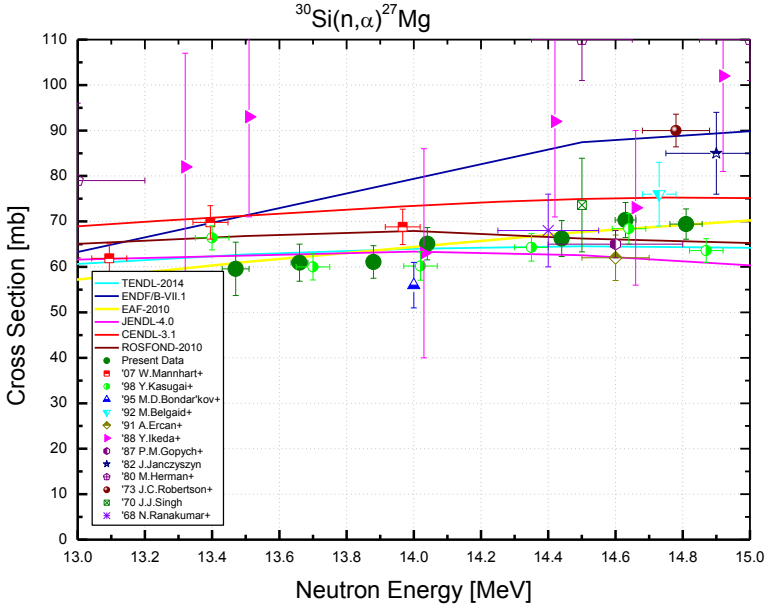

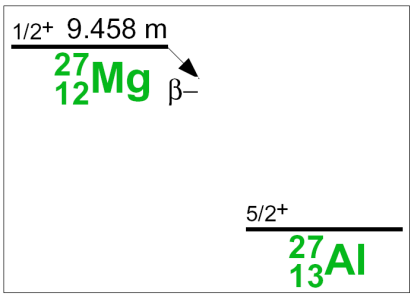

Decay data used for **^{30}Si(n,α)^{27}Mg**.

Target nucleus	Abundance [%]	Chemical form	Reaction product	$T_{1/2}$	E_γ [keV]	Y_γ [%]
^{30}Si	**3.092** *11*	Si-crystal	^{27}Mg	**9.458 m** *12*	**843.8**	**71.80** *2*
					1014.5	28.20 *2*

^{39}K(n, 2n)^{38g}K

^{39}K(n,2n)^{38g}K			
E_n [MeV]	σ [mb]	$\pm\Delta\sigma_{total}$ [%]	$\pm\Delta\sigma_{ref}$ [%]
13.48	0.034	*44.1*	*0.872*
13.65	0.241	*12.5*	*0.636*
13.87	0.685	*5.82*	*0.608*
14.07	1.39	*10.8*	*0.582*
14.27	2.50	*5.12*	*0.544*
14.46	3.11	*5.10*	*0.519*
14.66	4.55	*5.44*	*0.526*
14.85	5.35	*5.48*	*0.561*
Ref. CS is ^{27}Al(n, α)^{24}Na;			α_d = *1.5*

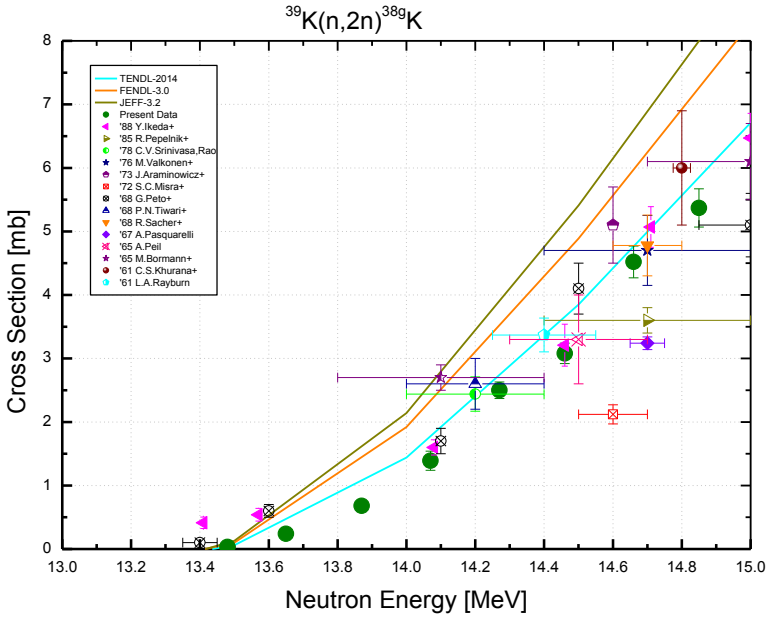

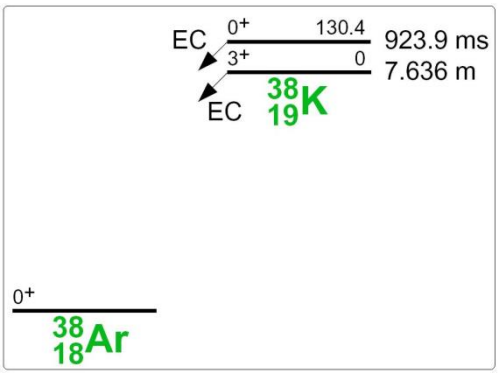

Decay data used for **^{39}K(n,2n)^{38g}K**.

Target nucleus	Abundance [%]	Chemical form	Reaction product	$T_{1/2}$	E_γ [keV]	Y_γ [%]
^{39}K	**93.2581** ***44***	KNO_3	^{38g}K	**7.636 m** ***18***	**2167.5**	**99.858** ***13***

^{41}K(n, α)^{38}Cl

^{41}K(n,α)^{38}Cl			
E_n [MeV]	σ [mb]	$\pm\Delta\sigma_{total}$ [%]	$\pm\Delta\sigma_{ref}$ [%]
13.48	36.4	5.28	2.26
13.65	34.0	5.45	2.18
13.87	33.0	5.06	2.17
14.07	33.1	4.65	2.16
14.27	31.2	5.01	2.15
14.46	31.9	5.26	2.15
14.66	28.5	5.66	2.15
14.85	28.6	5.19	2.16
Ref. CS is ^{27}Al(n, α)^{24}Na;			$\alpha_d = 1.5$

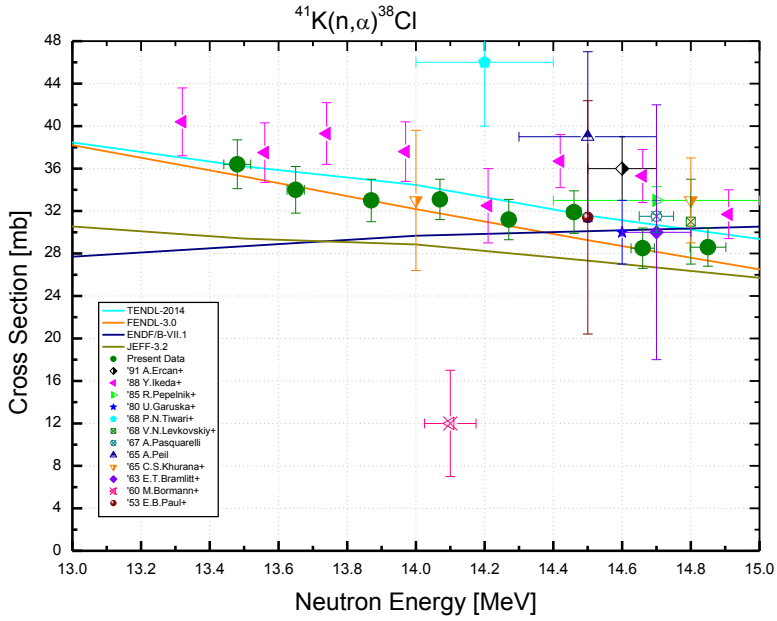

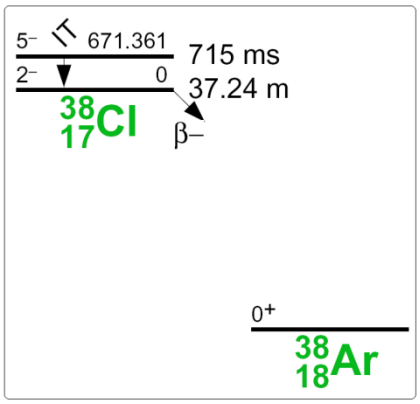

Decay data used for **^{41}K(n,α)^{38}Cl**.

Target nucleus	Abundance [%]	Chemical form	Reaction product	$T_{1/2}$	E_γ [keV]	Y_γ [%]
^{41}K	**6.7302** *44*	KNO_3	^{38}Cl	**37.24 m** *5*	**1642.4**	**33.3** *7*
					2167.5	44.4 *9*

^{41}K(n, p)^{41}Ar

^{41}K(n,p)^{41}Ar			
E_n [MeV]	σ [mb]	$\pm\Delta\sigma_{total}$ [%]	$\pm\Delta\sigma_{ref}$ [%]
13.48	55.3	*4.45*	*0.803*
13.65	56.2	*4.19*	*0.536*
13.87	51.8	*4.79*	*0.503*
14.07	53.4	*4.40*	*0.471*
14.27	50.3	*4.27*	*0.423*
14.46	49.6	*4.16*	*0.391*
14.66	50.3	*3.89*	*0.400*
14.85	46.5	*4.15*	*0.445*
Ref. CS is ^{27}Al(n, α)^{24}Na;			α_d = *1.8*

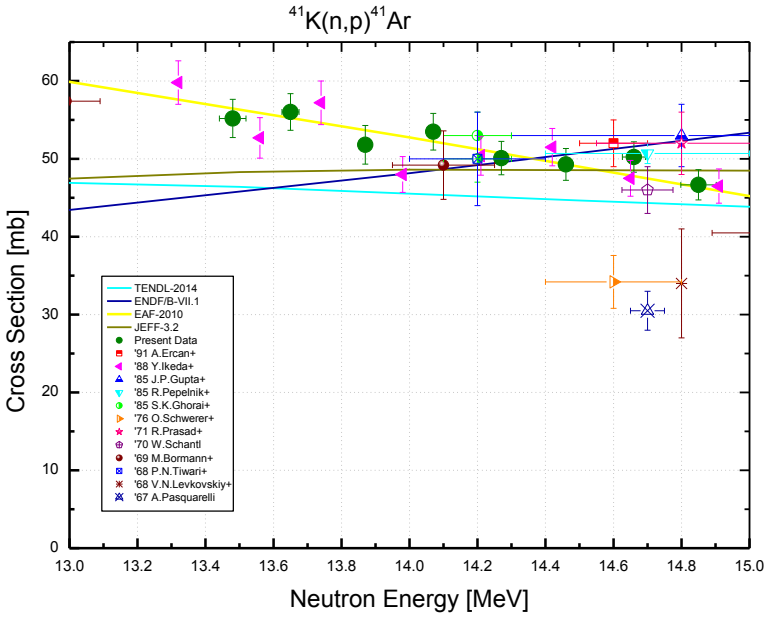

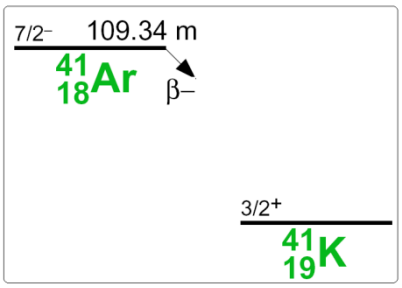

Decay data used for **^{41}K(n,p)^{41}Ar**.

Target nucleus	Abundance [%]	Chemical form	Reaction product	$T_{1/2}$	E_γ [keV]	Y_γ [%]
^{41}K	**6.7302** *44*	KNO_3	^{41}Ar	**109.61 m** *4*	**1293.6**	**99.16** *2*

^{50}V(n, nα)^{46}Sc

^{50}V(n,nα)^{46}Sc			
E_n [MeV]	σ [mb]	$\pm\Delta\sigma_{total}$ [%]	$\pm\Delta\sigma_{ref}$ [%]
13.65	0.026	*76.9*	*0.837*
14.82	0.262	*23.0*	*0.834*
Ref. CS is ^{93}Nb(n,2n)^{92m}Nb;			α_d = *1.1*

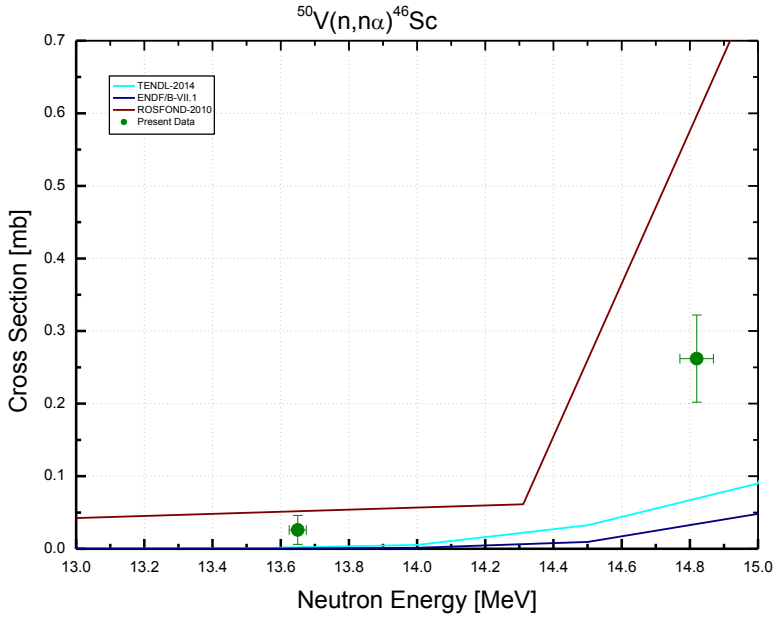

Two samples enriched with V-50 were used. The total mass of V-50 in the samples was 6.94 mg.

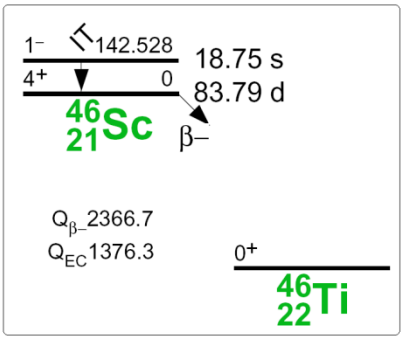

Decay data used for **^{50}V(n,nα)^{46}Sc.**

Target nucleus	Abundance [%]	Chemical form	Reaction product	$T_{1/2}$	E_γ [keV]	Y_γ [%]
^{50}V	***17.0** *1*	V_2O_5	^{46}Sc	**83.79 d** *4*	**889.3**	**99.984** *1*
					1120.5	99.987 *1*

* - refer to samples enriched with V-50

^{50}V(n, α)^{47}Sc

^{50}V(n,α)^{47}Sc			
E_n [MeV]	σ [mb]	$\pm\Delta\sigma_{total}$ [%]	$\pm\Delta\sigma_{ref}$ [%]
13.65	34.2	*3.62*	*1.77*
14.82	40.3	*3.81*	*1.77*
Ref. CS is ^{93}Nb(n,2n)^{92m}Nb;			α_d = *1.1*

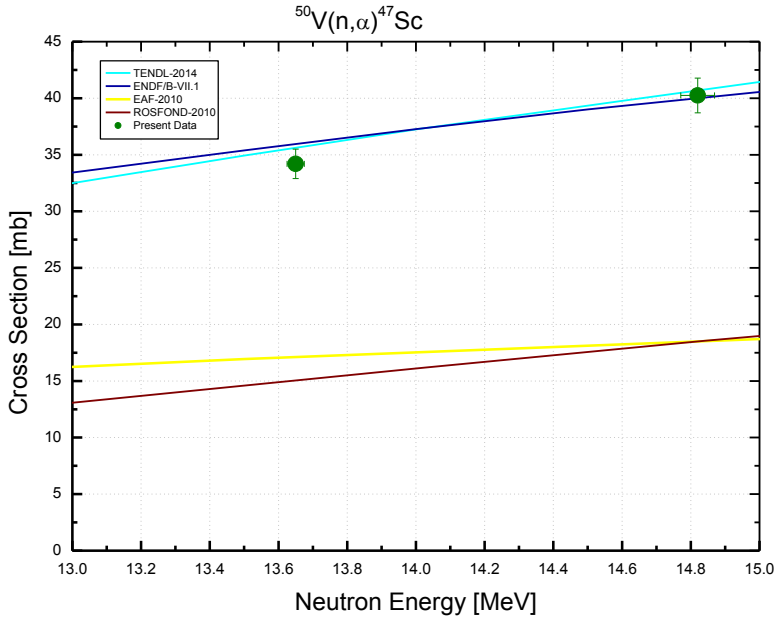

The ^{50}V abundance in the natural vanadium is only 0.25%. Samples enriched with ^{50}V to 17% were purchased for this experiment. Gamma counting of the irradiated samples provided the determination of amount of ^{47}Sc nuclei but could not divide the contributions of ^{50}V(n,α)^{47}Sc and ^{51}V(n,n'α)^{47}Sc reactions both of which were responsible for ^{47}Sc production. To resolve the problem, a second sample with a natural mixture of two vanadium isotopes was irradiated simultaneously. In more detail, the separation method of the ^{50}V(n,α)^{47}Sc and the ^{51}V(n,n'α)^{47}Sc cross-sections is described on p.25.

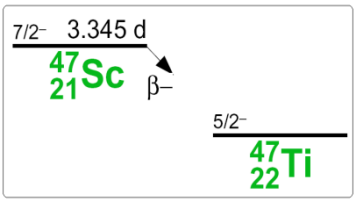

Decay data used for **^{50}V(n,α)^{47}Sc**.

Target nucleus	Abundance [%]	Chemical form	Reaction product	$T_{1/2}$	E_γ [keV]	Y_γ [%]
^{50}V	***17.0** ***1*** *(sep)*	V_2O_5	^{47}Sc	**3.3492 d** ***6***	**159.4**	**68.3** ***4***
	0.250 *4* *(nat)*	V-metal				

* -refer to samples enriched with V-50

^{51}V(n, nα)^{47}Sc

^{51}V(n,nα)^{47}Sc			
E_n [MeV]	σ [mb]	$\pm\Delta\sigma_{total}$ [%]	$\pm\Delta\sigma_{ref}$ [%]
13.65	0.007	*95.3*	*1.77*
14.82	0.024	*37.5*	*1.77*
Ref. CS is ^{93}Nb(n,2n)^{92m}Nb;			α_d = *1.1*

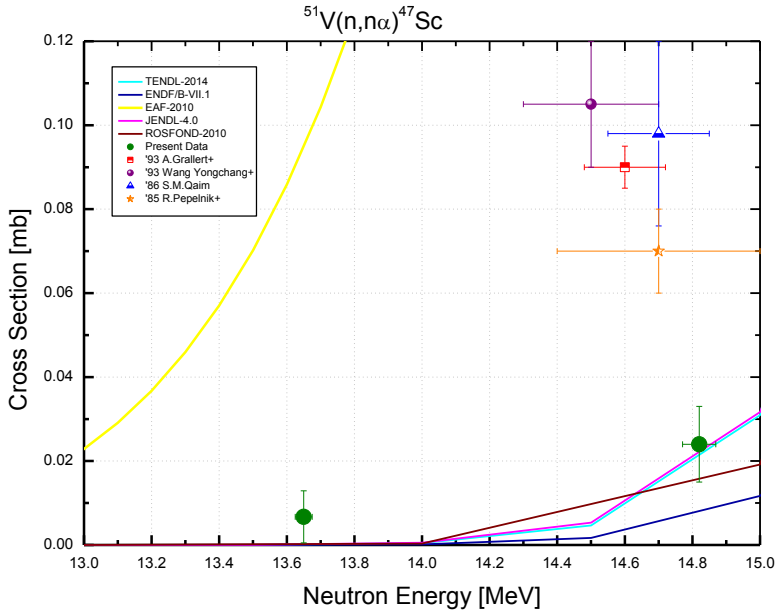

The contribution of the ^{50}V(n,α)^{47}Sc reaction considered in the previous page was deduced by the method described on p.25.

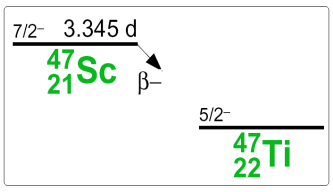

Decay data used for **^{51}V(n,nα)^{47}Sc**.

Target nucleus	**Abundance [%]**	**Chemical form**	**Reaction product**	**$T_{1/2}$**	**E_γ [keV]**	**Y_γ [%]**
^{51}V	**99.750** *4 (nat)*	V-metal	^{47}Sc	**3.3492 d** *6*	**159.4**	**68.3** *4*
	83.0 *1 (sep)*	V_2O_5				

^{51}V(n, α)^{48}Sc

^{51}V(n,α)^{48}Sc			
E_n [MeV]	σ [mb]	$\pm\Delta\sigma_{total}$ [%]	$\pm\Delta\sigma_{ref}$ [%]
13.56	14.6	*2.90*	*0.873*
13.74	15.1	*3.50*	*0.872*
13.96	15.1	*3.64*	*0.853*
14.19	16.6	*3.07*	*0.842*
14.42	16.9	*3.13*	*0.844*
14.61	17.5	*3.55*	*0.854*
14.78	18.4	*3.11*	*0.854*
14.82	18.6	*2.41*	*0.870*
Ref. CS is ^{93}Nb(n,2n)^{92m}Nb;			α_d = *1.1*

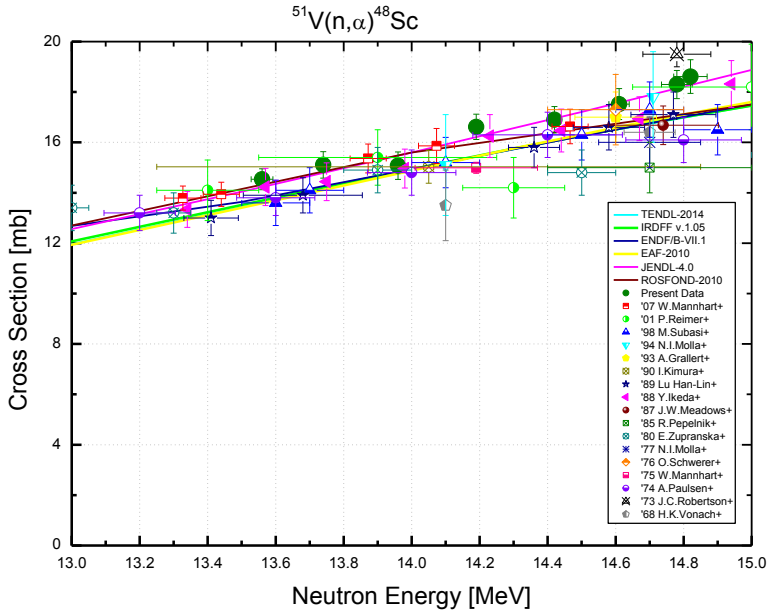

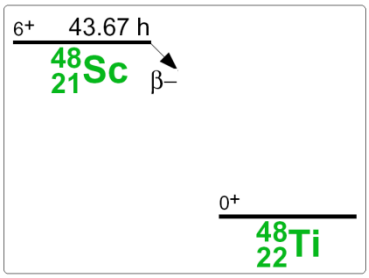

Decay data used for **^{51}V(n,α)^{48}Sc**.

Target nucleus	Abundance [%]	Chemical form	Reaction product	$T_{1/2}$	E_γ [keV]	Y_γ [%]
^{51}V	**99.750** *4*	V-metal	^{48}Sc	**43.67 h** *9*	**983.5**	**100.1** *6*
					1037.5	97.6 *7*
					1312.1	100.1 *7*

^{55}Mn(n, α)^{52}V

^{55}Mn(n,α)^{52}V			
E_n [MeV]	σ [mb]	$\pm\Delta\sigma_{total}$ [%]	$\pm\Delta\sigma_{ref}$ [%]
13.47	20.6	*3.77*	*1.63*
13.66	21.0	*4.18*	*1.52*
13.88	22.8	*4.31*	*1.50*
14.04	22.7	*4.28*	*1.49*
14.26	22.9	*4.23*	*1.48*
14.44	23.5	*3.70*	*1.47*
14.63	23.7	*3.66*	*1.47*
14.81	22.8	*4.21*	*1.48*
Ref. CS is ^{27}Al(n, α)^{24}Na;			$\alpha_d = 1.8$

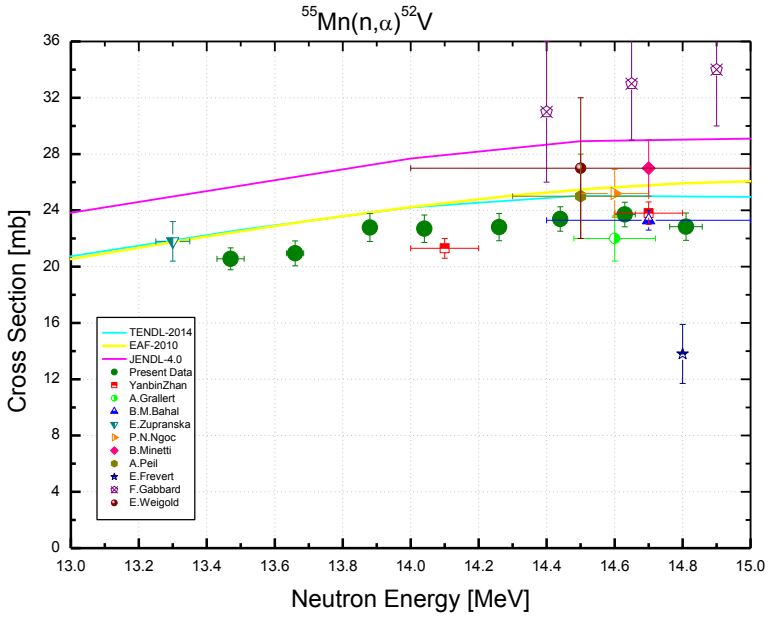

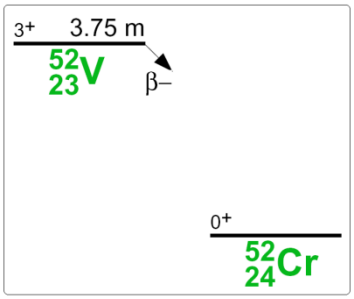

Decay data used for **^{55}Mn(n,α)^{52}V.**

Target nucleus	Abundance [%]	Chemical form	Reaction product	$T_{1/2}$	E_γ [keV]	Y_γ [%]
^{55}Mn	**100**	$KMnO_4$	^{52}V	**3.743 m** *5*	**1434.1**	**100.0** *14*

^{55}Mn(n, 2n)^{54}Mn

^{55}Mn(n,2n)^{54}Mn			
E_n [MeV]	σ [mb]	$\pm\Delta\sigma_{total}$ [%]	$\pm\Delta\sigma_{ref}$ [%]
13.56	622	*4.04*	*0.597*
13.74	636	*3.97*	*0.595*
13.96	661	*3.97*	*0.567*
14.19	709	*3.65*	*0.550*
14.42	740	*3.63*	*0.554*
14.61	764	*3.37*	*0.569*
14.78	786	*3.42*	*0.569*
Ref. CS is ^{93}Nb(n,2n)^{92m}Nb;			α_d = *1.1*

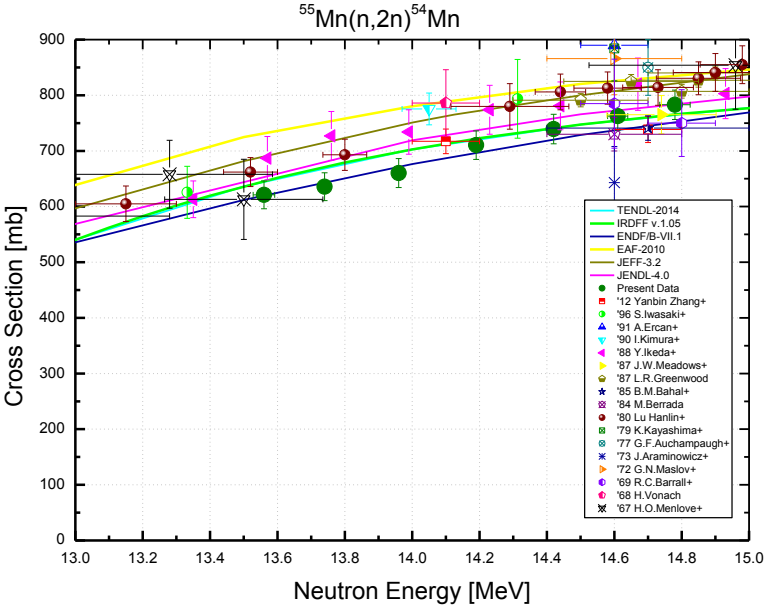

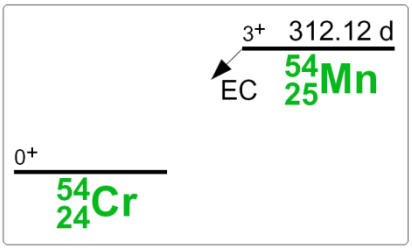

Decay data used for **^{55}Mn(n,2n)^{54}Mn**.

Target nucleus	Abundance [%]	Chemical form	Reaction product	$T_{1/2}$	E_γ [keV]	Y_γ [%]
^{55}Mn	**100**	$KMnO_4$	^{54}Mn	**312.2 d** *2*	**834.8**	**99.976** *1*

^{54}Fe(n, p)^{54}Mn

^{54}Fe(n,p)^{54}Mn			
E_n [MeV]	σ [mb]	$\pm\Delta\sigma_{total}$ [%]	$\pm\Delta\sigma_{ref}$ [%]
13.56	389	*5.53*	*0.603*
13.74	352	*5.87*	*0.602*
13.96	328	*6.01*	*0.573*
14.19	328	*5.99*	*0.557*
14.42	315	*5.58*	*0.561*
14.61	262	*11.0*	*0.576*
14.78	300	*7.28*	*0.576*
Ref. CS is ^{93}Nb(n,2n)^{92m}Nb;			α_d = *1.1*

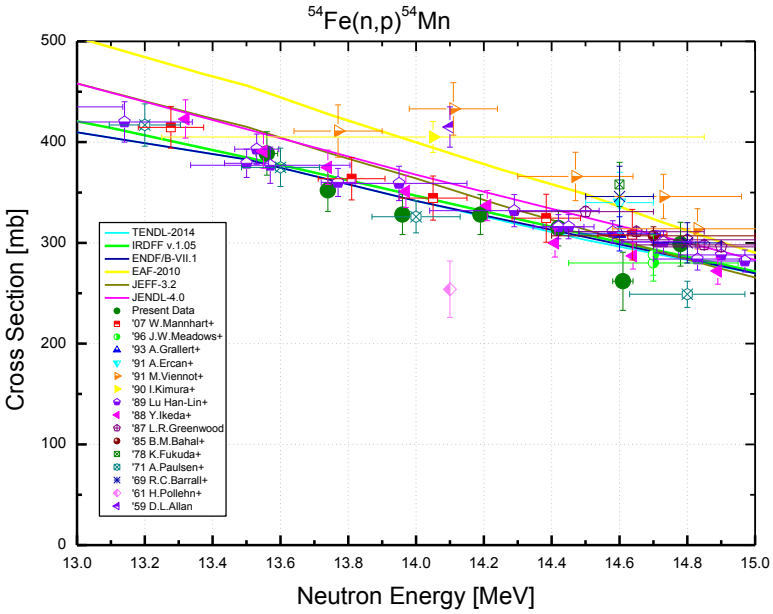

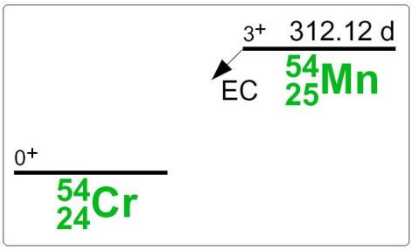

Decay data used for **^{54}Fe(n,p)^{54}Mn**.

Target nucleus	Abundance [%]	Chemical form	Reaction product	$T_{1/2}$	E_γ [keV]	Y_γ [%]
^{54}Fe	**5.845** *35*	Fe-metal	^{54}Mn	**312.2 d** *2*	**834.8**	**99.976** *1*

^{56}Fe(n, p)^{56}Mn

^{56}Fe(n,p)^{56}Mn			
E_n [MeV]	σ [mb]	$\pm\Delta\sigma_{total}$ [%]	$\pm\Delta\sigma_{ref}$ [%]
13.56	115.8	*3.47*	*0.595*
13.74	116.1	*3.57*	*0.593*
13.96	112.6	*1.85*	*0.564*
14.19	114.0	*1.91*	*0.548*
14.42	109.0	*2.12*	*0.552*
14.61	105.9	*1.89*	*0.567*
14.78	104.6	*1.83*	*0.567*
Ref. CS is ^{93}Nb(n,2n)^{92m}Nb;			$\alpha_d = 1.4$

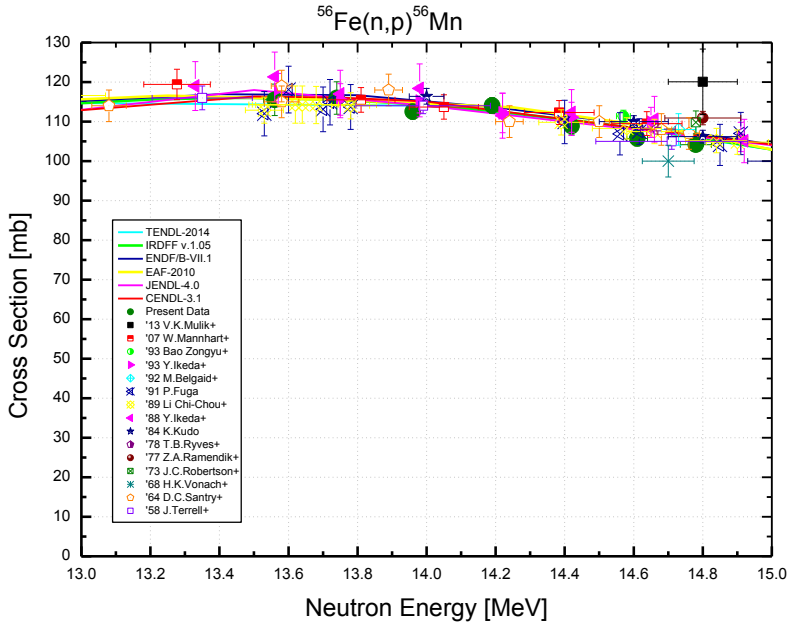

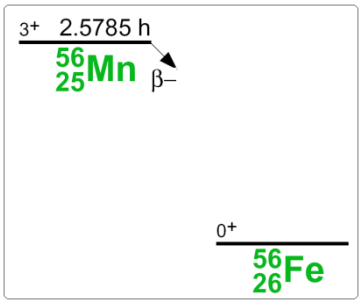

Decay data used for **^{56}Fe(n,p)^{56}Mn.**

Target Nucleus	Abundance [%]	Chemical form	Reaction product	$T_{1/2}$	E_γ [keV]	Y_γ [%]
^{56}Fe	**91.754** ***36***	Fe-metal	^{56}Mn	**2.5789 h** ***1***	**846.8**	**99.85** ***3***
					1810.7	26.9 *4*
					2113.1	14.2 *3*

^{57}Fe(n, p)^{57}Mn

^{57}Fe(n,p)^{57}Mn			
E_n [MeV]	σ [mb]	$\pm\Delta\sigma_{total}$ [%]	$\pm\Delta\sigma_{ref}$ [%]
13.68	87.3	*35.9*	*35.9*
13.95	81.8	*36.2*	*35.9*
14.23	85.0	*35.9*	*35.9*
14.50	87.2	*36.3*	*35.9*
14.72	86.1	*36.1*	*35.9*
14.83	86.9	*35.9*	*35.9*
Ref. CS is ^{27}Al(n, α)^{24}Na;			$\alpha_d = 1.7$

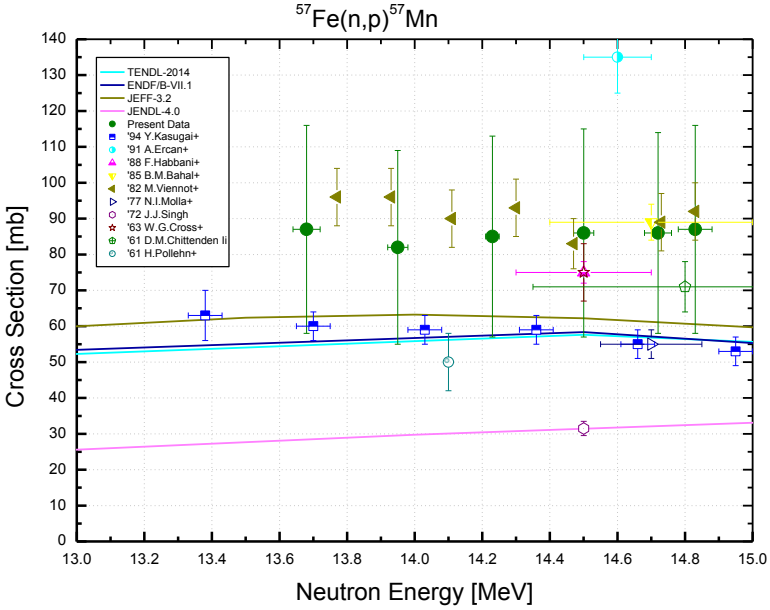

The set-up for measurement of short-lived activities was used. (p.25).

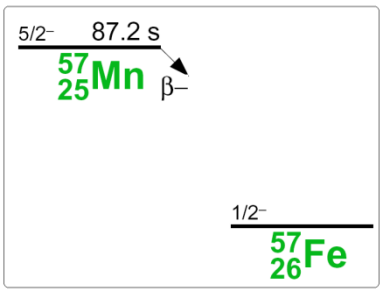

Decay data used **^{57}Fe(n,p)^{57}Mn.**

Target nucleus	**Abundance [%]**	**Chemical form**	**Reaction product**	**$T_{1/2}$**	**E_γ [keV]**	**Y_γ [%]**
^{57}Fe	**2.119** ***10***	Fe-metal	^{57}Mn	**85.4 s** ***18***	**122.1**	**14** ***5***
					692.0	5.5 *21*

^{59}Co(n, α)^{56}Mn

^{59}Co(n,α)^{56}Mn			
E_n [MeV]	σ [mb]	$\pm\Delta\sigma_{total}$ [%]	$\pm\Delta\sigma_{ref}$ [%]
13.56	31.4	*2.90*	*0.593*
13.74	31.3	*2.41*	*0.592*
13.96	31.9	*2.89*	*0.563*
14.19	31.5	*2.37*	*0.547*
14.42	31.9	*2.30*	*0.551*
14.61	31.5	*2.34*	*0.566*
14.78	32.3	*2.36*	*0.566*
Ref. CS is ^{93}Nb(n,2n)^{92m}Nb;			$\alpha_d = 1.4$

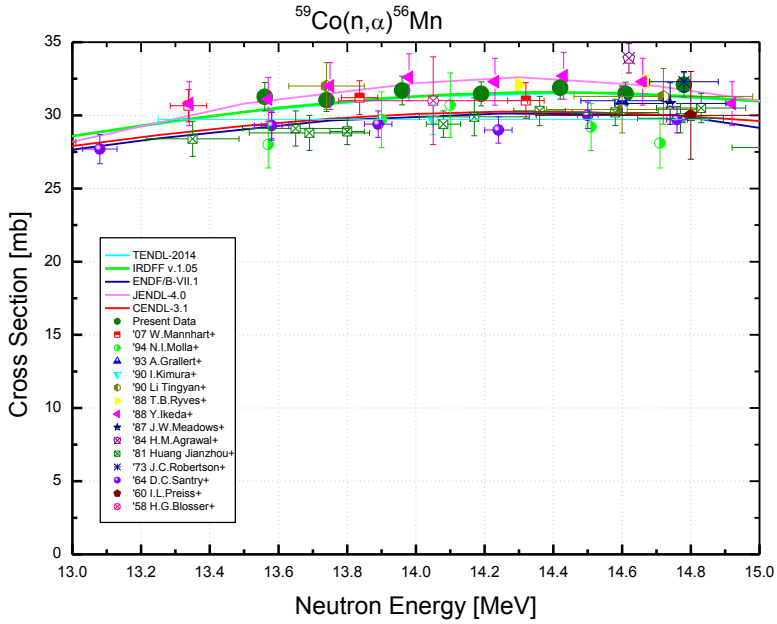

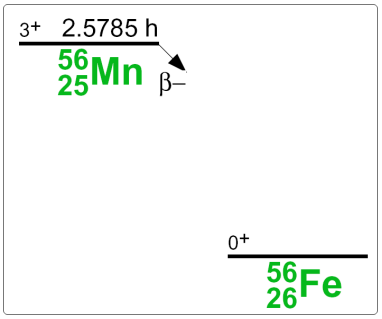

Decay data used for **^{59}Co(n,α)^{56}Mn**.

Target Nucleus	Abundance [%]	Chemical form	Reaction product	$T_{1/2}$	E_γ [keV]	Y_γ [%]
^{59}Co	**100**	Co-metal	^{56}Mn	**2.5789 h** *1*	**846.8**	**99.85** *3*
					1810.7	26.9 *4*
					2113.1	14.2 *3*

^{59}Co(n, p)^{59}Fe

^{59}Co(n,p)^{59}Fe			
E_n [MeV]	σ [mb]	$\pm\Delta\sigma_{total}$ [%]	$\pm\Delta\sigma_{ref}$ [%]
13.56	53.2	*3.25*	*3.24*
13.74	52.8	*3.28*	*3.24*
13.96	51.4	*3.29*	*3.24*
14.19	51.7	*3.35*	*3.23*
14.42	47.8	*3.28*	*3.23*
14.61	46.2	*3.25*	*3.24*
14.78	47.5	*3.25*	*3.24*
Ref. CS is ^{93}Nb(n,2n)^{92m}Nb;			α_d = *1.2*

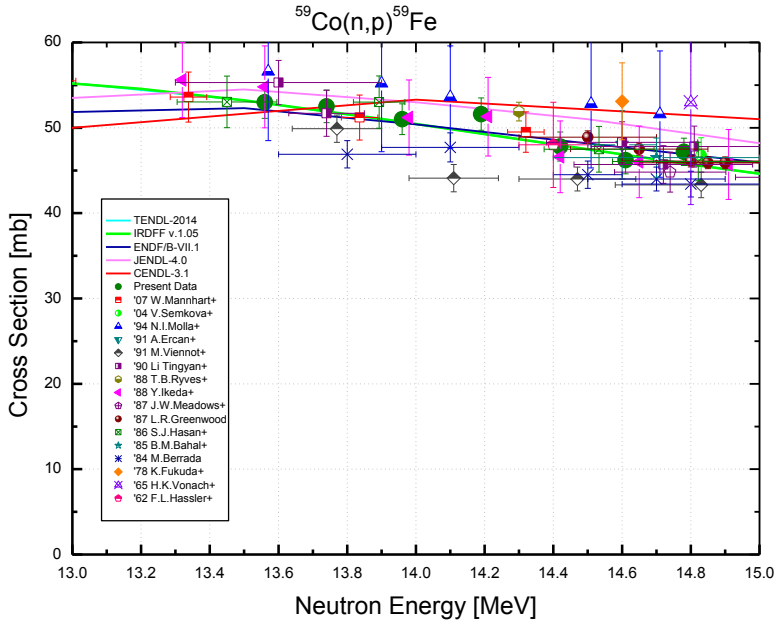

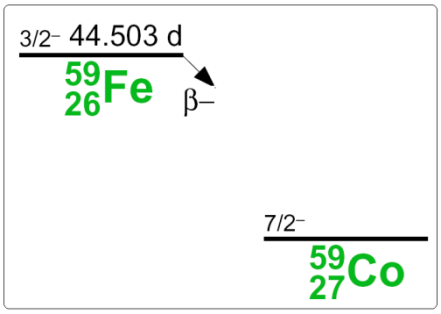

Decay data used for **^{59}Co(n,p)^{59}Fe**.

Target nucleus	Abundance [%]	Chemical form	Reaction product	$T_{1/2}$	E_γ [keV]	Y_γ [%]
^{59}Co	**100**	Co-metal	^{59}Fe	**44.495 d** *9*	**1099.2**	**56.5** *18*
					1291.6	43.2 *14*

^{59}Co(n, 2n)^{58}Co

^{59}Co(n,2n)^{58}Co			
E_n [MeV]	σ [mb]	$\pm\Delta\sigma_{total}$ [%]	$\pm\Delta\sigma_{ref}$ [%]
13.56	593	*3.40*	*0.601*
13.74	635	*3.17*	*0.600*
13.96	666	*3.64*	*0.571*
14.19	673	*3.58*	*0.555*
14.42	732	*3.26*	*0.559*
14.61	735	*3.53*	*0.574*
14.78	740	*3.40*	*0.574*
Ref. CS is ^{93}Nb(n,2n)^{92m}Nb;			α_d = *1.2*

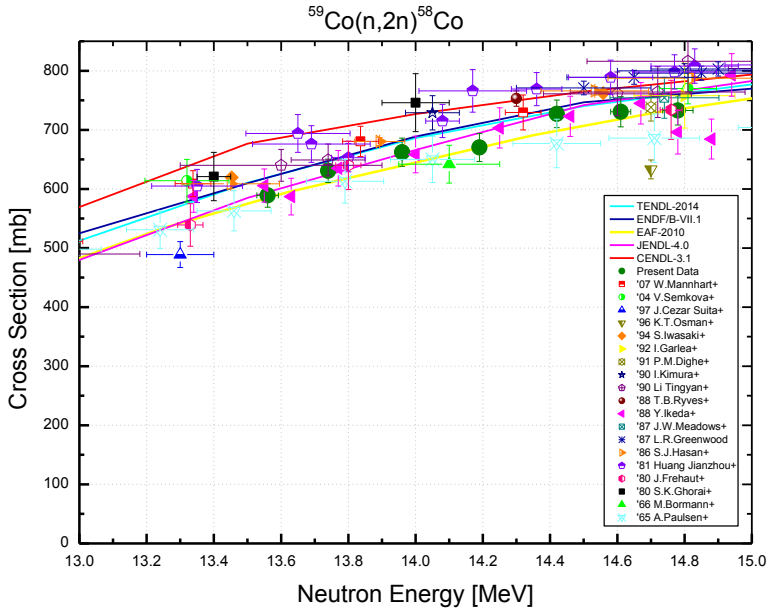

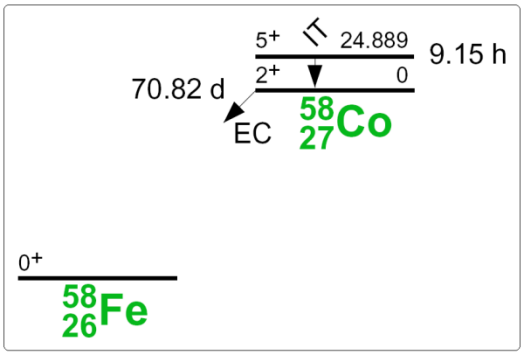

Decay data used for **^{59}Co(n,2n)^{58}Co**.

Target nucleus	Abundance [%]	Chemical form	Reaction product	$T_{1/2}$	E_γ [keV]	Y_γ [%]
^{59}Co	**100**	Co-metal	^{58}Co	**70.86 d** *6*	**810.8**	**99.450** *10*

^{59}Co(n, 2n)^{58m}Co

^{59}Co(n,2n)^{58m}Co		
E_n [MeV]	σ [mb]	$\pm\Delta\sigma_{total}$ [%]
13.56	390	*3.92*
13.74	416	*3.69*
13.96	436	*4.08*
14.19	440	*4.03*
14.42	477	*3.77*
14.61	479	*4.05*
14.78	481	*3.98*
Ref. CS is ^{93}Nb(n,2n)^{92m}Nb		

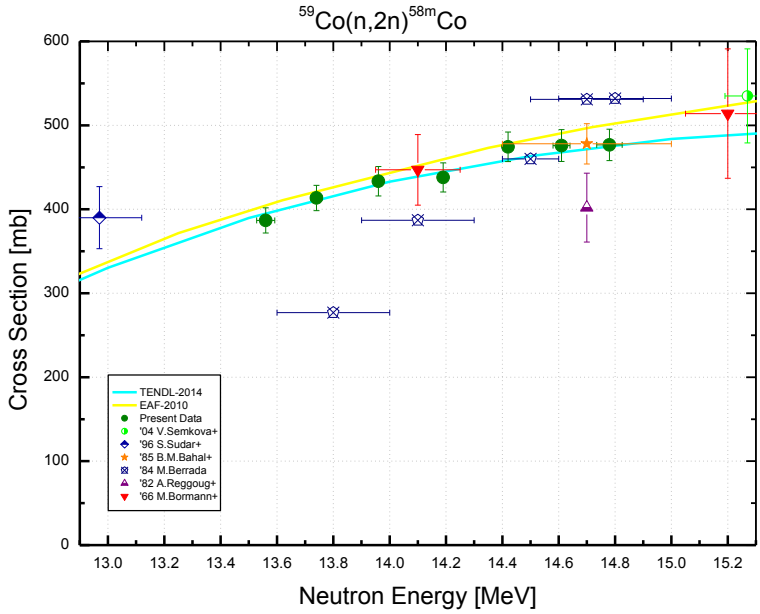

The ^{59}Co(n,2n)^{58m}Co cross section was not measured directly but is the product of two other values measured immediately, the ^{59}Co(n,2n)^{58}Co cross section presented in the previous page and the isomeric ratio, i.e. $\sigma_m/(\sigma_m + \sigma_g)$, that was determined from the analysis of the 810.8 keV gamma decay curve. The method used for the isomeric ratio determination is described in detail earlier (pp. 20-21). The obtained isomeric ratio values were approximated by the straight line:

$$IR = a \cdot (E_n - E_0) + b$$

where $a = -0.005 \pm 0.009\ MeV^{-1}$

$b = 0.654 \pm 0.012$

$E_0 = 14.08\ MeV$

The straight line parameters were determined by the least squares methods.

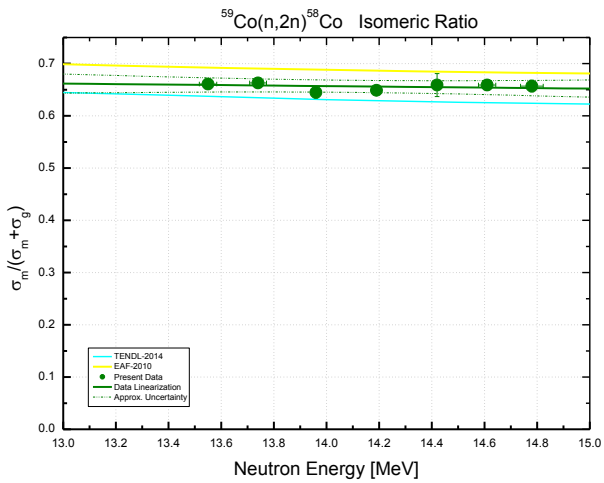

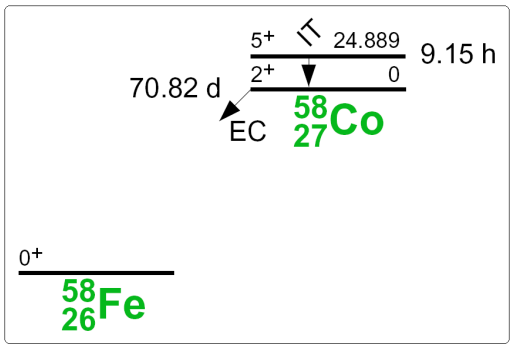

Decay data used for **^{59}Co(n,2n)^{58m}Co**.

Target nucleus	Reaction product	$T_{1/2}$	E_γ [keV]
^{59}Co	^{58m}Co	**9.10 h** *9*	—
	^{58g}Co	**70.86 d** *6*	**810.8**

^{58}Ni[(n, np) + (n, d)]^{57}Co

^{58}Ni(n,x)^{57}Co			
E_n [MeV]	σ [mb]	$\pm\Delta\sigma_{total}$ [%]	$\pm\Delta\sigma_{ref}$ [%]
13.47	512	*5.54*	*0.663*
13.56	540	*4.89*	*0.626*
13.64	551	*3.82*	*0.626*
13.74	574	*2.59*	*0.624*
13.88	565	*5.57*	*0.596*
13.96	593	*2.85*	*0.597*
14.05	600	*4.15*	*0.582*
14.19	638	*2.78*	*0.581*
14.28	638	*4.02*	*0.579*
14.42	656	*4.91*	*0.585*
14.47	649	*4.74*	*0.585*
14.61	676	*2.91*	*0.600*
14.68	660	*4.99*	*0.600*
14.78	683	*3.98*	*0.600*
14.86	689	*3.92*	*0.622*
Ref. CS is ^{93}Nb(n,2n)^{92m}Nb;			α_d = *1.2*

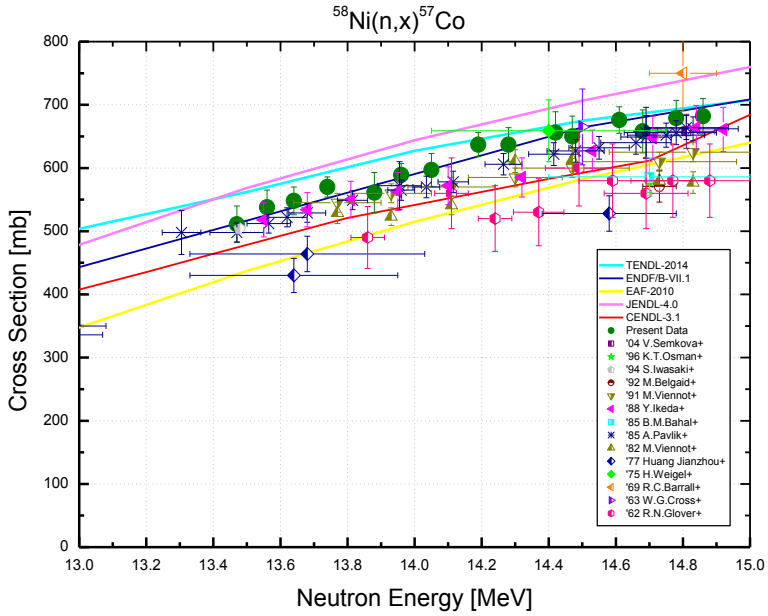

. . . . . .

The data was corrected for the contribution of the ^{58}Ni(n,2n)^{57}Ni cross section.

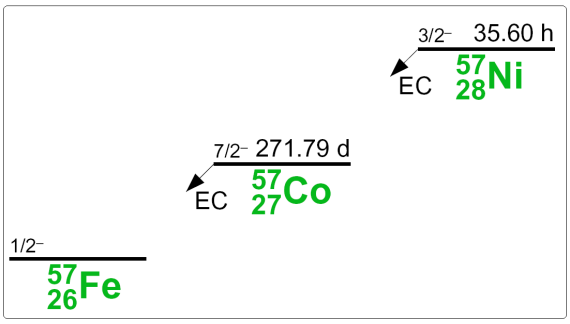

Decay data used for **^{58}Ni(n,x)^{57}Co**.

Target nucleus	Abundance [%]	Chemical form	Reaction product	$T_{1/2}$	E_γ [keV]	Y_γ [%]
^{58}Ni	**68.0769** *89*	Ni-metal	^{57}Co	**271.74 d** *6*	**122.1**	**85.60** *17*
					136.5	10.68 *8*

^{58}Ni(n, p)^{58}Co

^{58}Ni(n,p)^{58}Co			
E_n [MeV]	σ [mb]	$\pm\Delta\sigma_{total}$ [%]	$\pm\Delta\sigma_{ref}$ [%]
13.47	424	*6.54*	*0.640*
13.56	418	*3.19*	*0.601*
13.64	399	*4.92*	*0.602*
13.74	388	*4.04*	*0.600*
13.88	379	*6.57*	*0.570*
13.96	364	*4.61*	*0.571*
14.05	355	*4.96*	*0.556*
14.19	332	*4.10*	*0.555*
14.28	342	*5.74*	*0.553*
14.42	316	*4.33*	*0.559*
14.47	317	*4.90*	*0.559*
14.61	294	*4.67*	*0.574*
14.68	295	*5.99*	*0.574*
14.78	279	*4.22*	*0.574*
14.86	278	*6.11*	*0.598*
Ref. CS is ^{93}Nb(n,2n)^{92m}Nb;			$\alpha_d = 1.2$

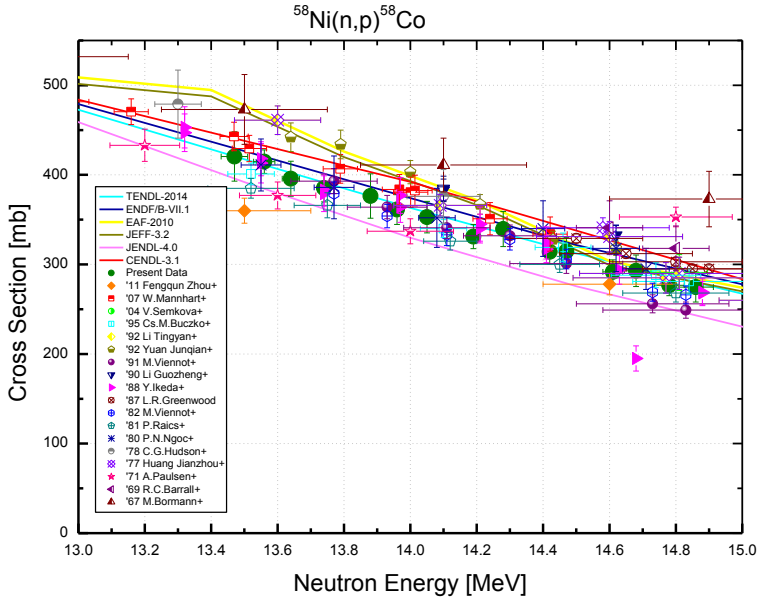

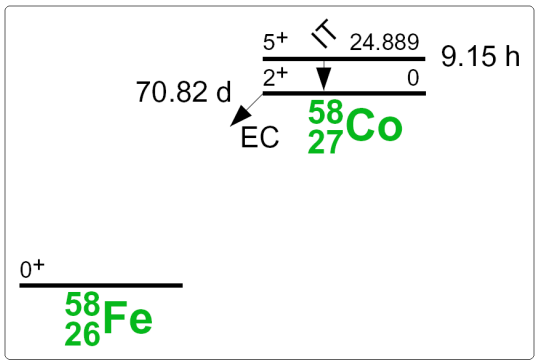

Decay data used for **^{58}Ni(n,p)^{58}Co.**

Target nucleus	Abundance [%]	Chemical form	Reaction product	$T_{1/2}$	E_γ [keV]	Y_γ [%]
^{58}Ni	**68.0769** ***89***	Ni-metal	^{58}Co	**70.86 d** ***6***	**810.8**	**99.450** ***10***

^{58}Ni(n, p)^{58m}Co

^{58}Ni(n,p)^{58m}Co		
E_n [MeV]	σ [mb]	$\pm\Delta\sigma_{total}$ [%]
13.47	228	*6.62*
13.56	226	*3.34*
13.64	216	*5.02*
13.74	211	*4.15*
13.88	207	*6.63*
13.96	199	*4.70*
14.05	195	*5.04*
14.19	184	*4.20*
14.28	189	*5.82*
14.42	176	*4.42*
14.47	177	*4.99*
14.61	165	*4.77*
14.68	166	*6.07*
14.78	157	*4.33*
14.86	157	*6.19*
Ref. CS is ^{93}Nb(n,2n)^{92m}Nb		

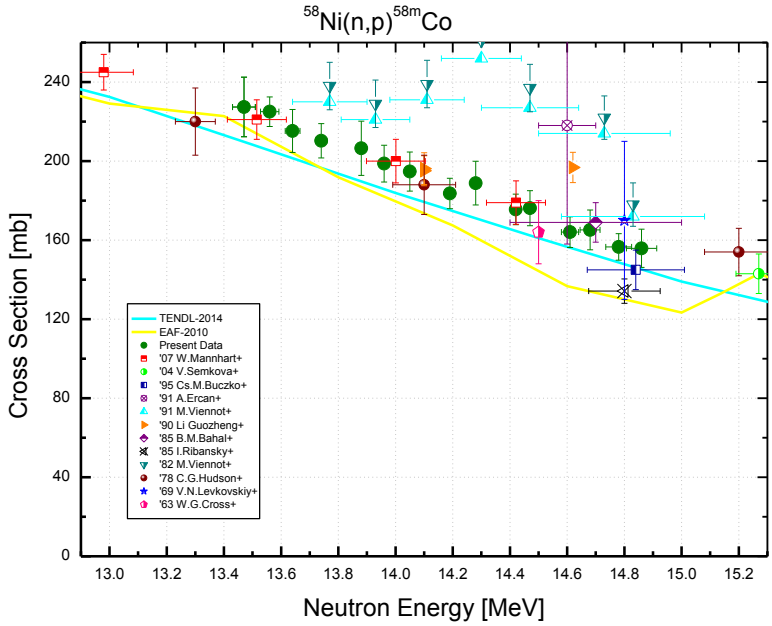

The ^{58}Ni(n, p)^{58m}Co cross section was not measured directly but is the product of two other values measured immediately, the ^{58}Ni(n, p)^{58}Co cross section presented in the previous page and the isomeric ratio, i.e. $\sigma_m/(\sigma_m + \sigma_g)$, that was determined from the analysis of the 810.8 keV gamma decay curve. The method used for the isomeric ratio determination is described in detail earlier (pp. 20-21). The obtained isomeric ratio values were approximated by the straight line:

$$IR = a \cdot (E_n - E_0) + b$$

where $a = 0.0191 \pm 0.0037\ MeV^{-1}$

$b = 0.550 \pm 0.005$

$E_0 = 14.07\ MeV$

The straight line parameters were determined by the least squares methods.

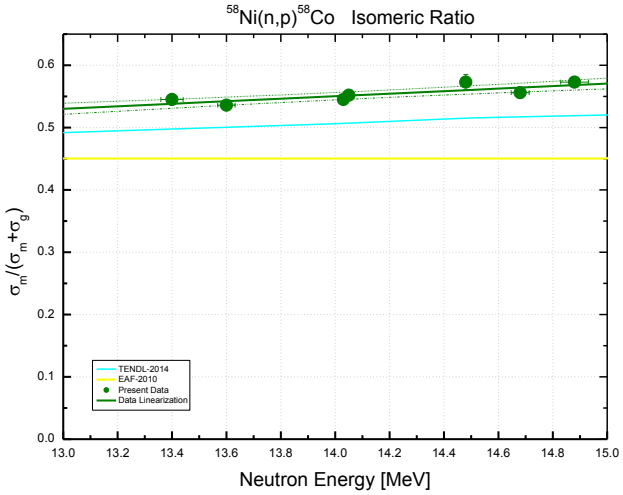

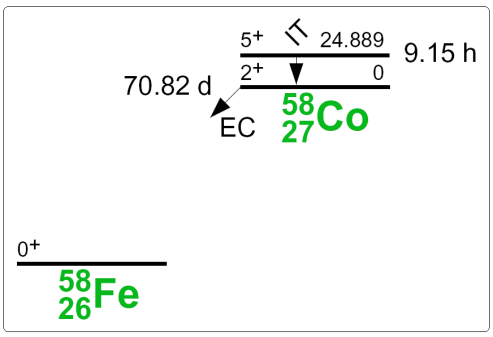

Decay data used for **^{58}Ni(n,p)^{58m}Co**.

Target nucleus	**Reaction product**	**$T_{1/2}$**	**E_γ [keV]**
^{58}Ni	^{58m}Co	9.10 h *9*	—
	^{58g}Co	70.86 d *6*	810.8

^{58}Ni(n, 2n)^{57}Ni

^{58}Ni(n,2n)^{57}Ni			
E_n [MeV]	σ [mb]	$\pm\Delta\sigma_{total}$ [%]	$\pm\Delta\sigma_{ref}$ [%]
13.47	11.5	*4.17*	*3.01*
13.56	12.6	*4.56*	*3.00*
13.64	14.6	*3.82*	*3.00*
13.74	15.4	*4.35*	*3.00*
13.88	19.7	*4.02*	*3.00*
13.96	20.2	*4.12*	*3.00*
14.05	23.5	*3.81*	*2.99*
14.19	25.1	*5.89*	*2.99*
14.28	27.8	*4.30*	*2.99*
14.42	29.8	*4.59*	*3.00*
14.47	32.9	*3.63*	*3.00*
14.61	33.4	*3.65*	*3.00*
14.68	36.0	*3.81*	*3.00*
14.78	35.9	*3.81*	*3.00*
14.86	39.5	*3.71*	*3.00*
Ref. CS is ^{93}Nb(n,2n)^{92m}Nb;			α_d = *1.2*

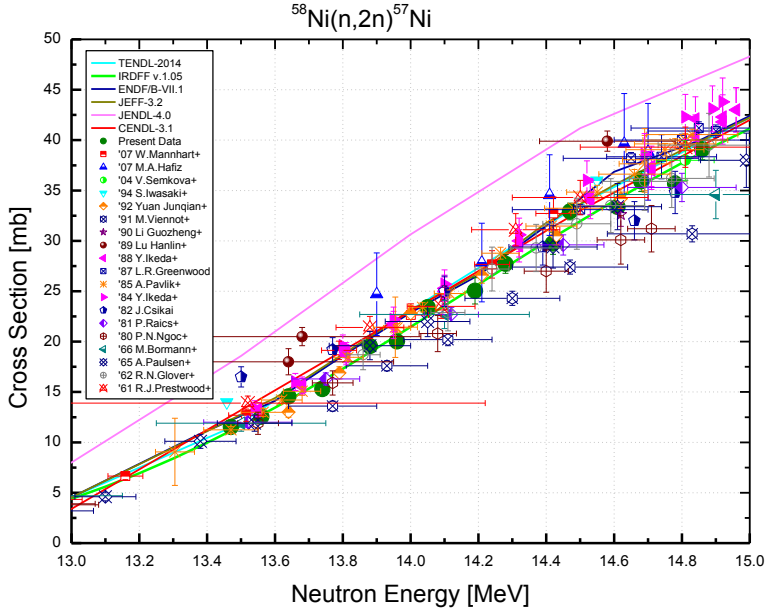

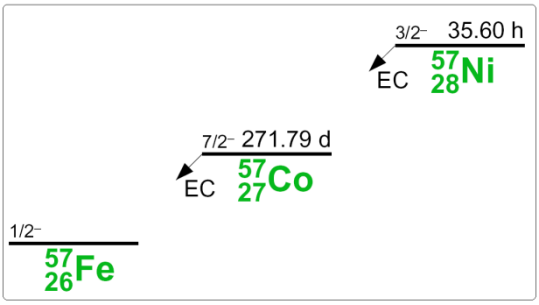

Decay data used for **^{58}Ni(n,2n)^{57}Ni**.

Target Nucleus	Abundance [%]	Chemical form	Reaction product	$T_{1/2}$	E_γ [keV]	Y_γ [%]
^{58}Ni	**68.0769** *89*	Ni-metal	^{57}Ni	**35.60 h** *6*	127.2	16.7 *5*
					1377.6	**81.7** *24*
					1919.5	12.3 *4*

^{60}Ni(n, p)^{60}Co

^{60}Ni(n,p)^{60}Co			
E_n [MeV]	σ [mb]	$\pm\Delta\sigma_{total}$ [%]	$\pm\Delta\sigma_{ref}$ [%]
13.47	167	*3.32*	*0.633*
13.64	160	*3.97*	*0.594*
13.88	158	*2.87*	*0.562*
14.05	158	*2.61*	*0.547*
14.28	155	*2.64*	*0.544*
14.44	151	*4.01*	*0.551*
14.63	143	*4.84*	*0.566*
14.86	138	*4.52*	*0.590*
Ref. CS is ^{93}Nb(n,2n)^{92m}Nb;			α_d = *1.2*

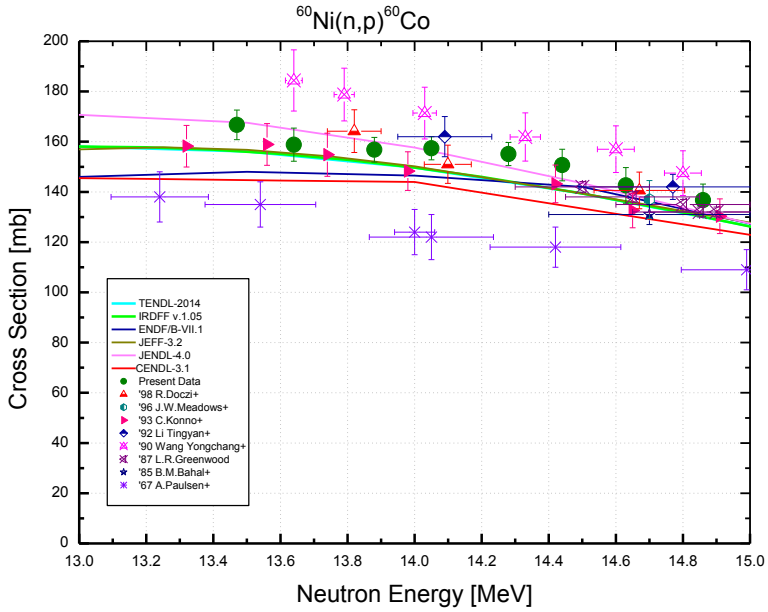

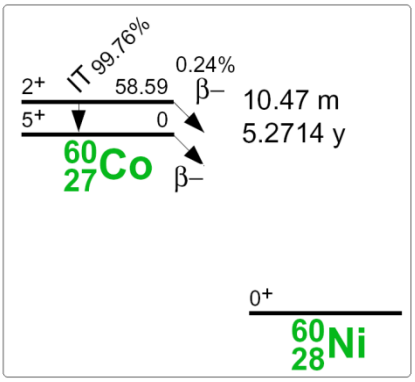

Decay data used for **^{60}Ni(n,p)^{60}Co**.

Target nucleus	Abundance [%]	Chemical form	Reaction product	$T_{1/2}$	E_γ [keV]	Y_γ [%]
^{58}Ni	**26.2231** *77*	Ni-metal	^{60}Co	**1925.28 d** *14*	1173.2	99.85 *3*
					1332.5	**99.9826** *6*

^{63}Cu(n, α)^{60}Co

^{63}Cu(n,α)^{60}Co			
E_n [MeV]	σ [mb]	$\pm\Delta\sigma_{total}$ [%]	$\pm\Delta\sigma_{ref}$ [%]
13.47	47.6	*5.55*	*0.634*
13.64	45.9	*3.28*	*0.595*
13.88	45.9	*5.34*	*0.563*
14.05	45.7	*2.78*	*0.548*
14.28	45.9	*2.74*	*0.545*
14.44	46.1	*3.49*	*0.552*
14.63	43.3	*3.28*	*0.567*
14.86	42.8	*2.82*	*0.590*
Ref. CS is ^{93}Nb(n,2n)^{92m}Nb;			α_d = *1.2*

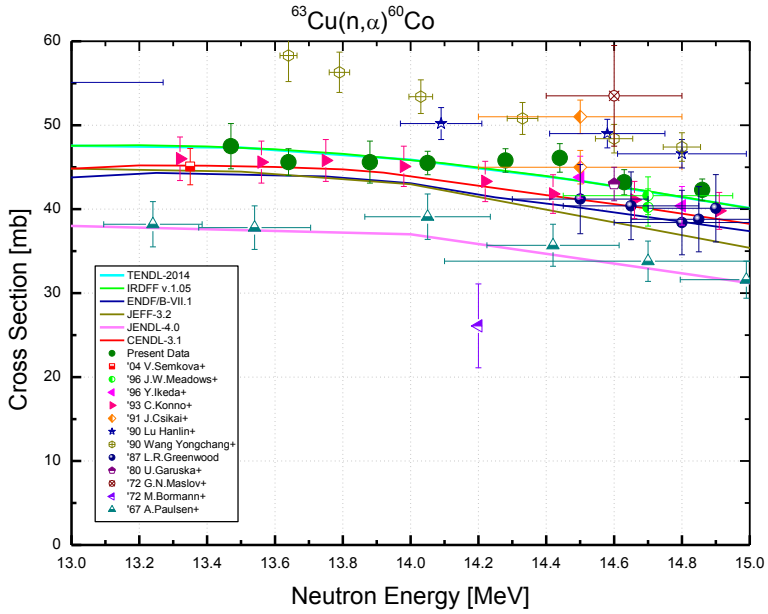

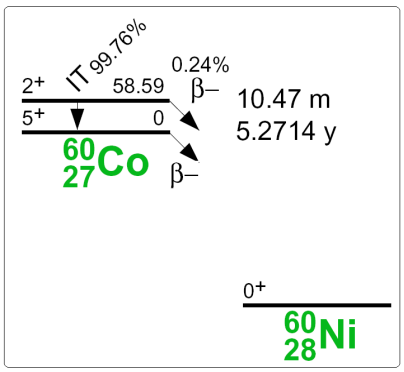

Decay data used for **^{63}Cu(n,α)^{60}Co**.

Target nucleus	Abundance [%]	Chemical form	Reaction product	$T_{1/2}$	E_γ [keV]	Y_γ [%]
^{63}Cu	**69.17** *3*	Cu-metal	^{60}Co	**1925.28 d** *14*	1173.2	99.85 *3*
					1332.5	**99.9826** *6*

^{65}Cu(n, p)^{65}Ni

^{65}Cu(n,p)^{65}Ni			
E_n [MeV]	σ [mb]	$\pm\Delta\sigma_{total}$ [%]	$\pm\Delta\sigma_{ref}$ [%]
13.56	22.4	*3.20*	*1.03*
13.74	20.4	*6.16*	*1.03*
13.96	21.6	*4.09*	*1.02*
14.19	20.5	*5.56*	*1.01*
14.42	20.4	*3.30*	*1.01*
14.61	21.5	*2.81*	*1.02*
14.78	20.7	*4.08*	*1.02*
Ref. CS is ^{93}Nb(n,2n)^{92m}Nb;			α_d = *1.2*

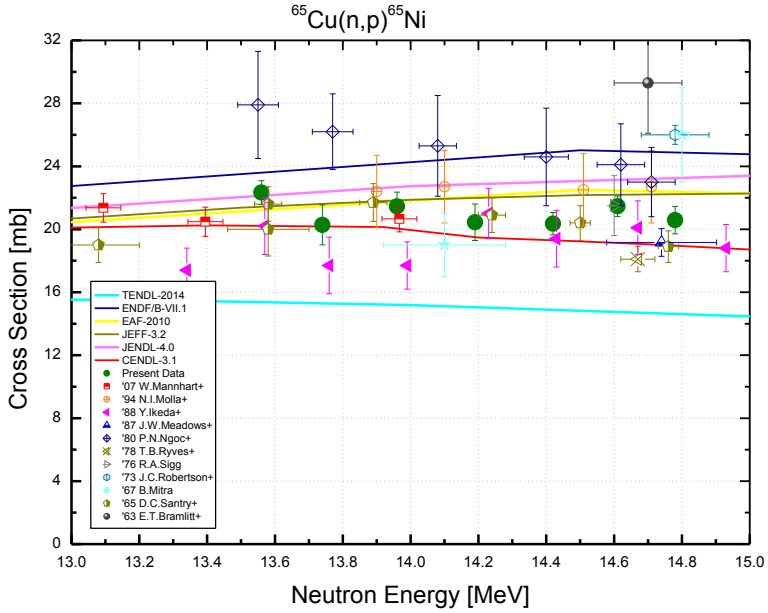

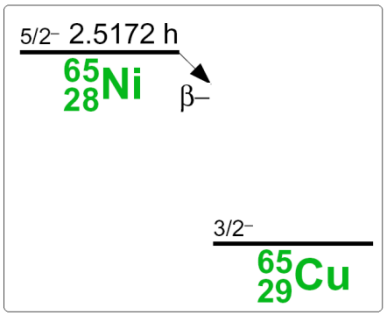

Decay data used for **^{65}Cu(n,p)^{65}Ni**.

Target nucleus	Abundance [%]	Chemical form	Reaction product	$T_{1/2}$	E_γ [keV]	Y_γ [%]
^{65}Cu	**30.83** *3*	Cu-metal	^{65}Ni	**2.5175 h** *5*	366.3	4.81 *6*
					1115.5	**15.43** *13*
					1481.8	23.59 *14*

^{65}Cu(n, 2n)^{64}Cu

^{65}Cu(n,2n)^{64}Cu			
E_n [MeV]	σ [mb]	$\pm\Delta\sigma_{total}$ [%]	$\pm\Delta\sigma_{ref}$ [%]
13.56	834	*5.85*	*2.39*
13.74	865	*4.25*	*2.39*
13.96	921	*6.73*	*2.39*
14.19	865	*4.23*	*2.38*
14.42	948	*4.49*	*2.38*
14.61	900	*4.18*	*2.39*
14.78	967	*5.16*	*2.39*
Ref. CS is ^{93}Nb(n,2n)^{92m}Nb;			α_d = *1.2*

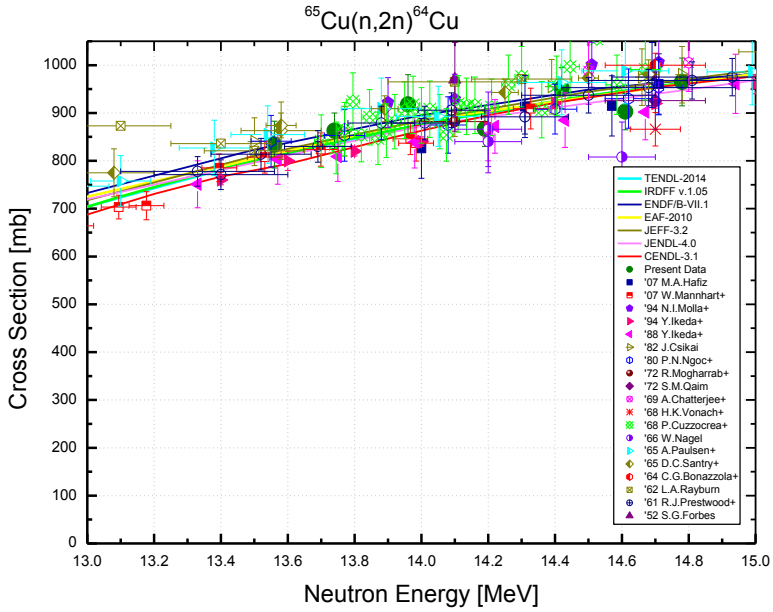

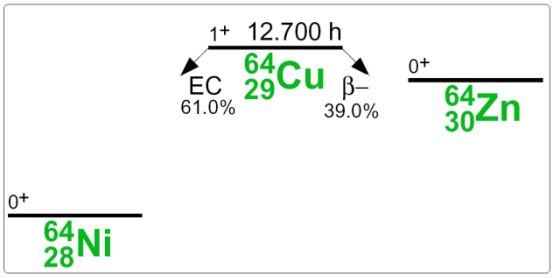

Decay data used for **^{65}Cu(n,2n)^{64}Cu**.

Target nucleus	Abundance [%]	Chemical form	Reaction product	$T_{1/2}$	E_γ [keV]	Y_γ [%]
^{65}Cu	**30.83** *3*	Cu-metal	^{64}Cu	**12.701 h** *2*	**1345.8**	**0.475** *11*

^{64}Zn(n, 2n)^{63}Zn

^{64}Zn(n,2n)^{63}Zn			
E_n [MeV]	σ [mb]	$\pm\Delta\sigma_{total}$ [%]	$\pm\Delta\sigma_{ref}$ [%]
13.47	58.5	*7.87*	*3.81*
13.66	60.4	*8.33*	*3.76*
13.88	81.9	*6.38*	*3.76*
14.04	98.2	*7.12*	*3.75*
14.26	119	*6.72*	*3.75*
14.44	145	*6.22*	*3.74*
14.63	147	*7.52*	*3.74*
14.81	160	*7.47*	*3.75*
Ref. CS is ^{27}Al(n, α)^{24}Na;			$\alpha_d = 1.7$

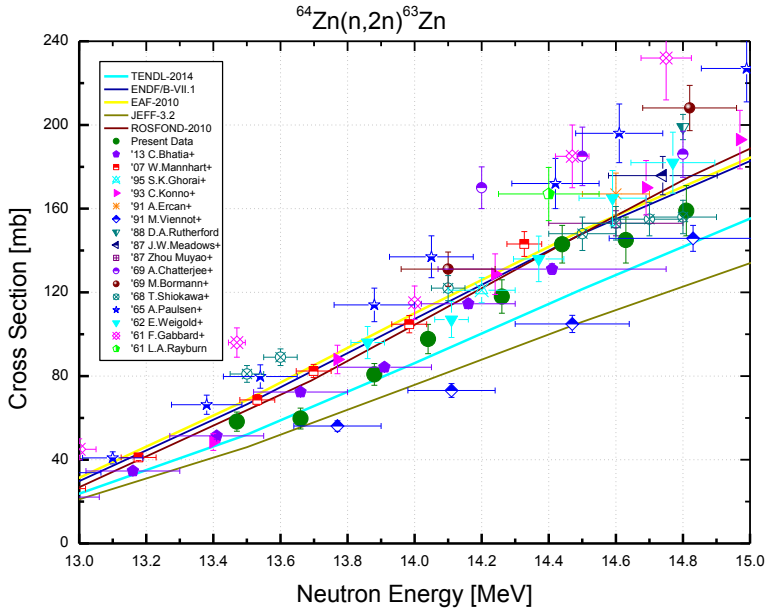

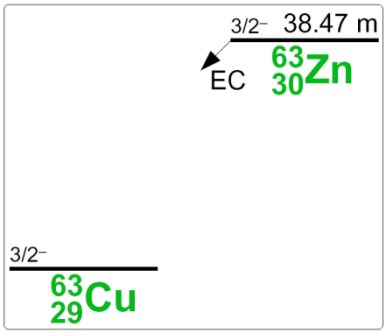

Decay data used for **^{64}Zn(n,2n)^{63}Zn**.

Target nucleus	Abundance [%]	Chemical form	Reaction product	$T_{1/2}$	E_γ [keV]	Y_γ [%]
^{64}Zn	**48.27** *32*	Zn-metal	^{54}Mn	**38.47 m** *5*	**669.6**	**8.2** *3*
					962.1	6.5 *4*

^{68}Zn(n, p)^{68m}Cu

^{68}Zn(n,p)^{68m}Cu			
E_n [MeV]	σ [mb]	$\pm\Delta\sigma_{total}$ [%]	$\pm\Delta\sigma_{ref}$ [%]
13.47	3.42	*5.61*	*3.46*
13.66	3.58	*5.92*	*3.41*
13.88	3.77	*7.23*	*3.40*
14.04	4.32	*5.47*	*3.40*
14.26	4.59	*9.69*	*3.39*
14.44	4.54	*6.11*	*3.39*
14.63	4.60	*6.93*	*3.39*
14.81	4.38	*6.30*	*3.39*
Ref. CS is ^{27}Al(n, α)^{24}Na;			α_d = *1.8*

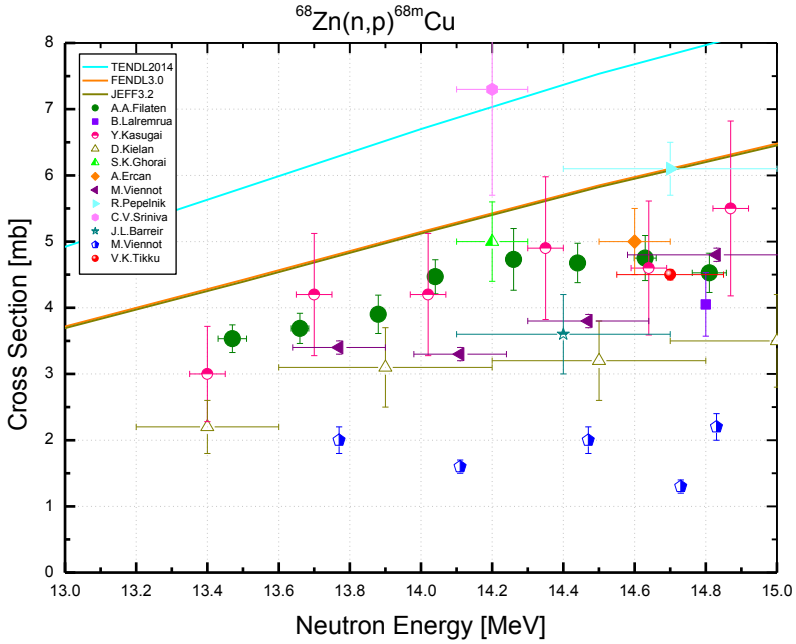

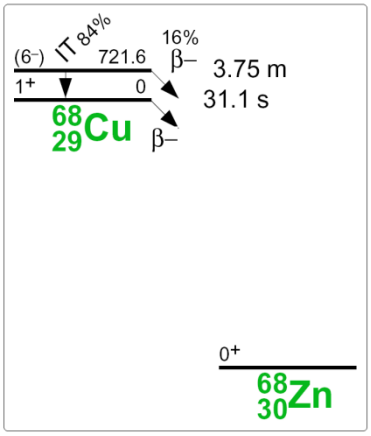

Decay data used for **^{68}Zn(n,p)^{68m}Cu**.

Target nucleus	Abundance [%]	Chemical form	Reaction product	$T_{1/2}$	E_γ [keV]	Y_γ [%]
^{68}Zn	**19.02** *12*	Zn-metal	^{68m}Cu	**3.75 m** *5*	**526.4**	**74.8** *17*

^{74}Ge(n, p)^{74}Ga

^{74}Ge(n, p)^{74}Ga			
E_n [MeV]	σ [mb]	$\pm\Delta\sigma_{total}$ [%]	$\pm\Delta\sigma_{ref}$ [%]
13.48	8.49	*11.7*	*2.54*
13.68	8.27	*10.8*	*2.47*
13.75	9.68	*15.6*	*2.47*
13.95	9.15	*8.95*	*2.46*
14.25	10.1	*7.87*	*2.44*
14.50	10.8	*14.0*	*2.44*
14.72	12.4	*8.89*	*2.44*
14.88	11.8	*4.25*	*2.45*
Ref. CS is ^{27}Al(n, α)^{24}Na;			α_d = *1.6*

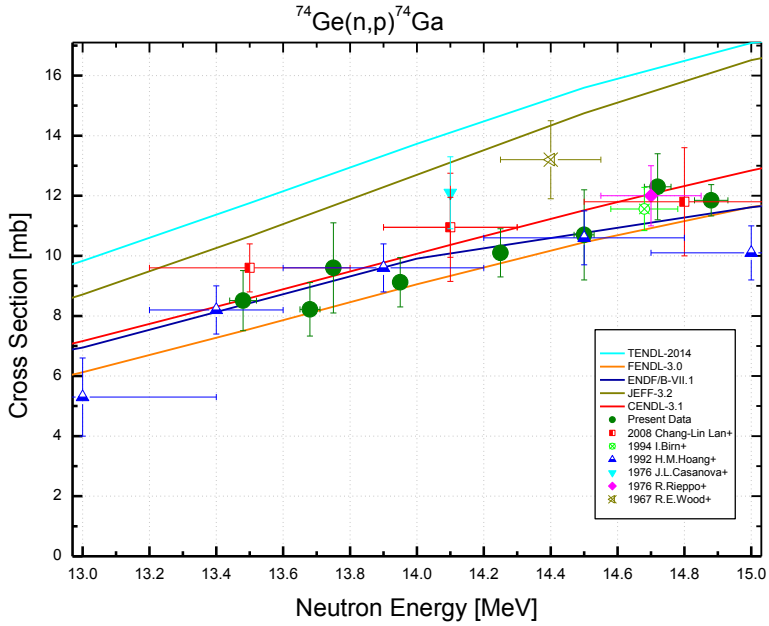

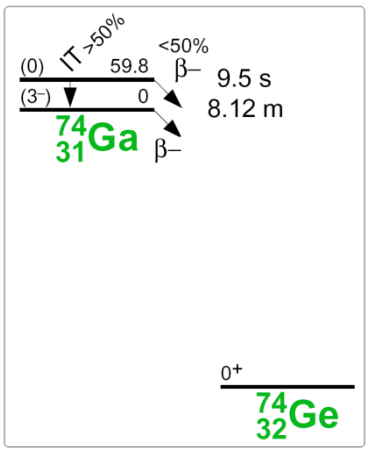

Decay data used for **^{74}Ge(n, p)^{74}Ga**.

Target nucleus	Abundance [%]	Chemical form	Reaction product	$T_{1/2}$	E_γ [keV]	Y_γ [%]
^{74}Ge	**36.72** ***15***	Ge-crystal	^{74}Ga	**8.12 m** ***12***	**595.9**	**91.8** ***2***

^{74}Se(n, p)^{74}As

^{74}Se(n, p)^{74}As			
E_n [MeV]	σ [mb]	$\pm\Delta\sigma_{total}$ [%]	$\pm\Delta\sigma_{ref}$ [%]
13.49	163	*8.89*	*6.84*
13.89	171	*9.11*	*6.81*
14.26	167	*8.03*	*6.80*
14.44	137	*44.1*	*6.80*
14.81	134	*14.7*	*6.80*
Ref. CS is ^{27}Al(n, α)^{24}Na;			$\alpha_d = 1.2$

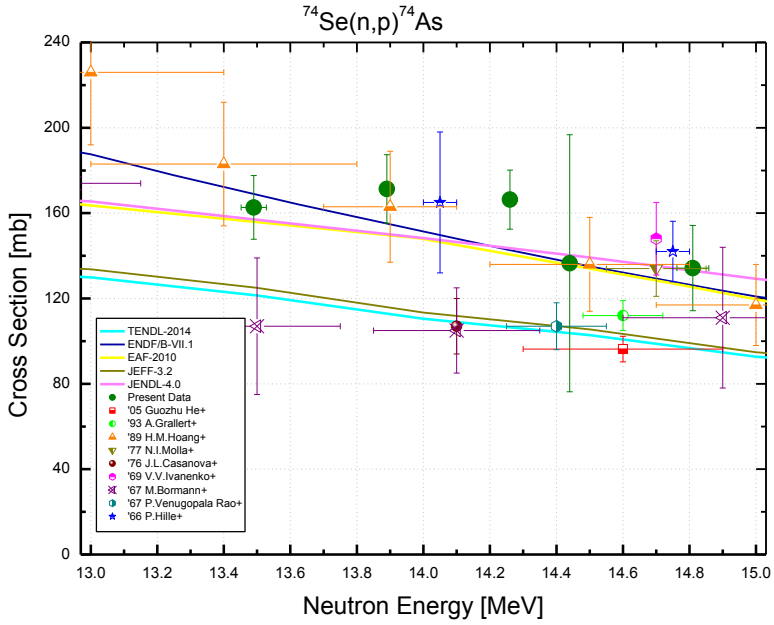

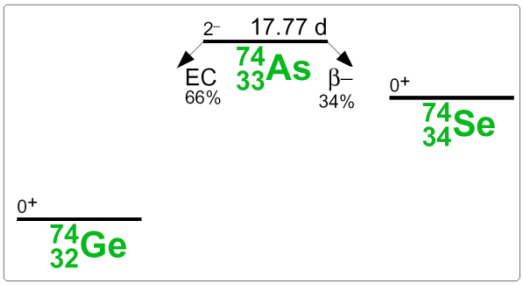

Decay data used for **^{74}Se(n, p)^{74}As.**

Target Nucleus	Abundance [%]	Chemical form	Reaction product	$T_{1/2}$	E_γ [keV]	Y_γ [%]
^{74}Se	**0.89** *4*	Se-crystal	^{74}As	**17.77 d** *2*	**595.8**	**59** *3*

^{74}Se(n, 2n)^{73m}Se

^{74}Se(n, 2n)^{73m}Se			
E_n [MeV]	σ [mb]	$\pm\Delta\sigma_{total}$ [%]	$\pm\Delta\sigma_{ref}$ [%]
13.49	71.9	*22.1*	*10.1*
13.89	108	*15.6*	*10.0*
14.05	116	*25.7*	*10.0*
14.26	166	*11.7*	*10.0*
14.44	169	*14.6*	*10.0*
14.81	212	*13.9*	*10.0*
Ref. CS is ^{27}Al(n, α)^{24}Na;			$\alpha_d = 1.2$

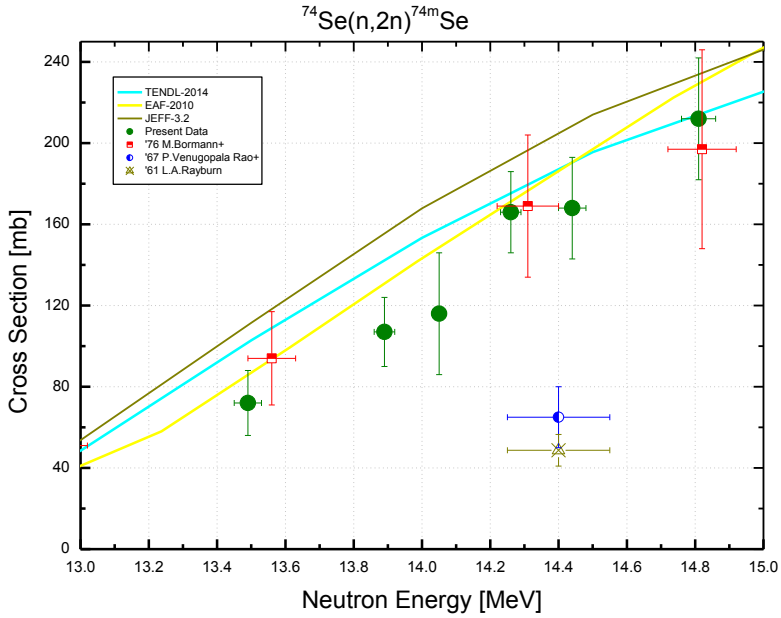

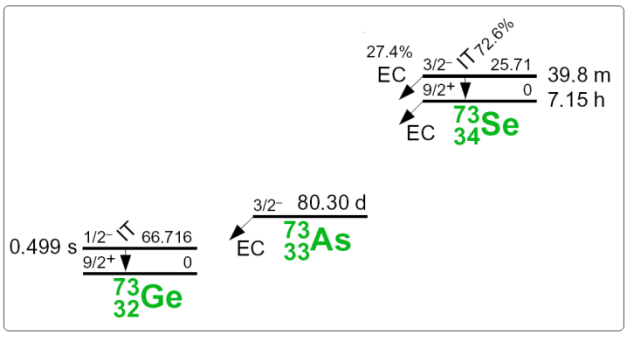

Decay data used for **^{74}Se(n, 2n)^{73m}Se**.

Target nucleus	Abundance [%]	Chemical form	Reaction product	$T_{1/2}$	E_γ [keV]	Y_γ [%]
^{74}Se	**0.89** *4*	Se-crystal	^{73m}Se	**39.8 m** *13*	84.0	2.03 *19*
					253.7	**2.36** *19*
					393.4	1.63 *13*

^{74}Se(n, 2n)^{73g}Se

^{74}Se(n, 2n)^{73g}Se			
E_n [MeV]	σ [mb]	$\pm\Delta\sigma_{total}$ [%]	$\pm\Delta\sigma_{ref}$ [%]
13.49	98.9	*15.1*	*4.87*
13.89	164	*10.4*	*4.83*
14.05	155	*16.1*	*4.82*
14.26	205	*9.71*	*4.82*
14.44	196	*12.8*	*4.82*
14.81	230	*13.0*	*4.82*
Ref. CS is ^{27}Al(n, α)^{24}Na;			$\alpha_d = 1.2$

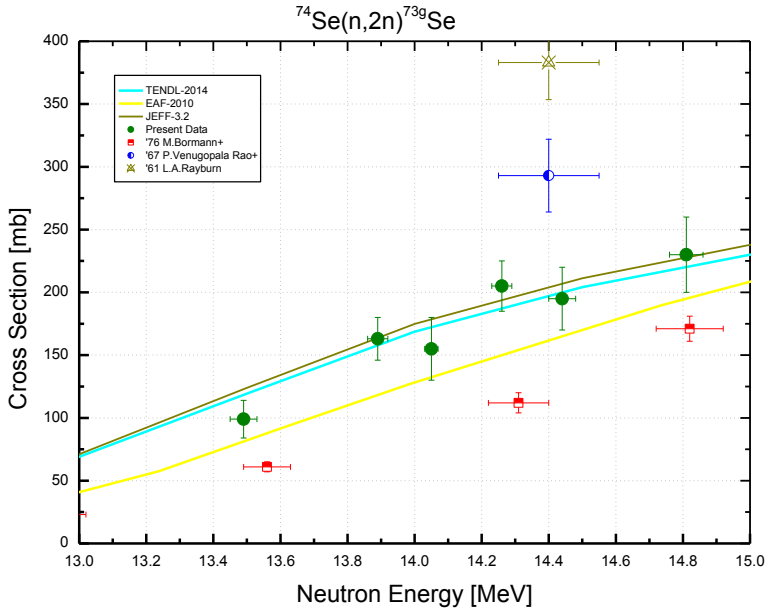

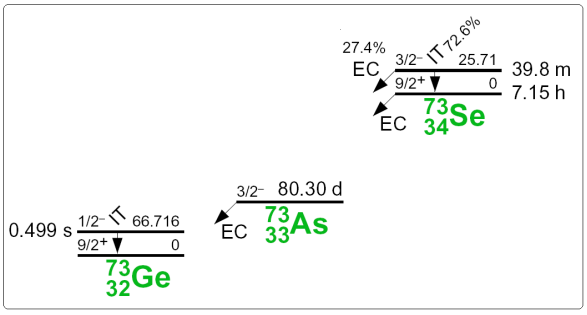

Decay data used for **^{74}Se(n, 2n)^{73g}Se.**

Target Nucleus	Abundance [%]	Chemical form	Reaction product	$T_{1/2}$	E_γ [keV]	Y_γ [%]
^{74}Se	**0.89** ***4***	Se-crystal	^{73g}Se	**7.15 h** ***8***	**361.2**	**97.0** ***10***

^{74}Se(n, 2n)^{73}Se

^{74}Se(n, 2n)^{73}Se		
E_n [MeV]	σ [mb]	$\pm\Delta\sigma_{total}$ *[%]*
13.49	171	*13.1*
13.89	272	*9.35*
14.05	270	*14.7*
14.26	370	*8.14*
14.44	365	*10.1*
14.81	442	*10.0*
Ref. CS is ^{27}Al(n, α)^{24}Na		

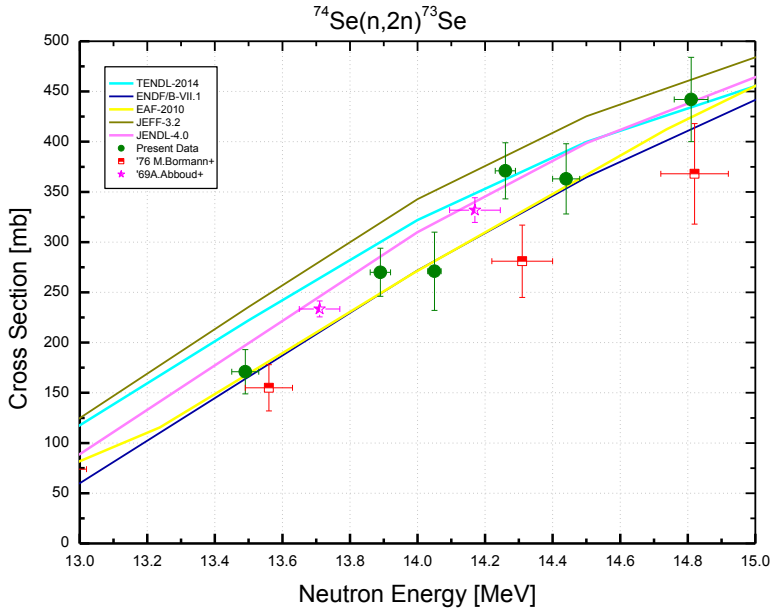

This is the sum of two cross sections measured independently: ^{74}Se(n, 2n)^{73m}Se and ^{74}Se(n, 2n)^{73g}Se.

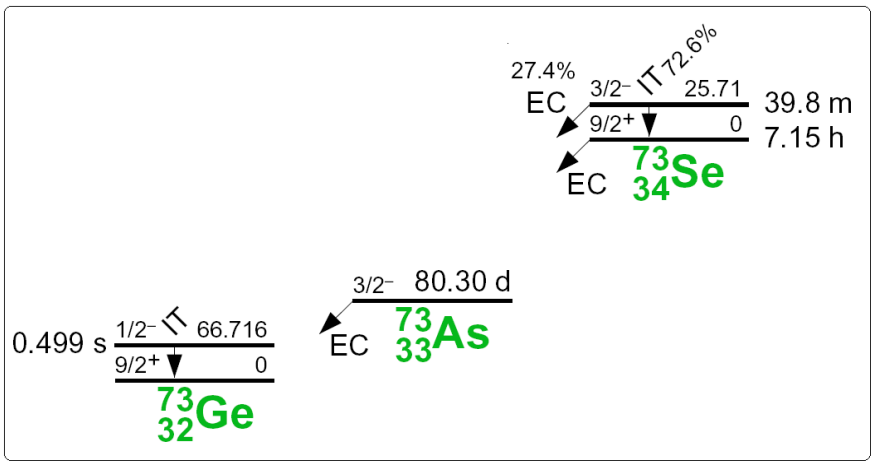

^{76}Se(n, p)^{76}As

^{76}Se(n, p)^{76}As			
E_n [MeV]	σ [mb]	$\pm\Delta\sigma_{total}$ [%]	$\pm\Delta\sigma_{ref}$ [%]
13.49	45.9	*6.18*	*5.49*
13.89	49.7	*6.37*	*5.45*
14.05	47.5	*8.94*	*5.45*
14.26	52.2	*6.42*	*5.45*
14.44	50.5	*7.01*	*5.44*
14.81	54.4	*7.91*	*5.45*
Ref. CS is ^{27}Al(n, α)^{24}Na;			$\alpha_d = 1.2$

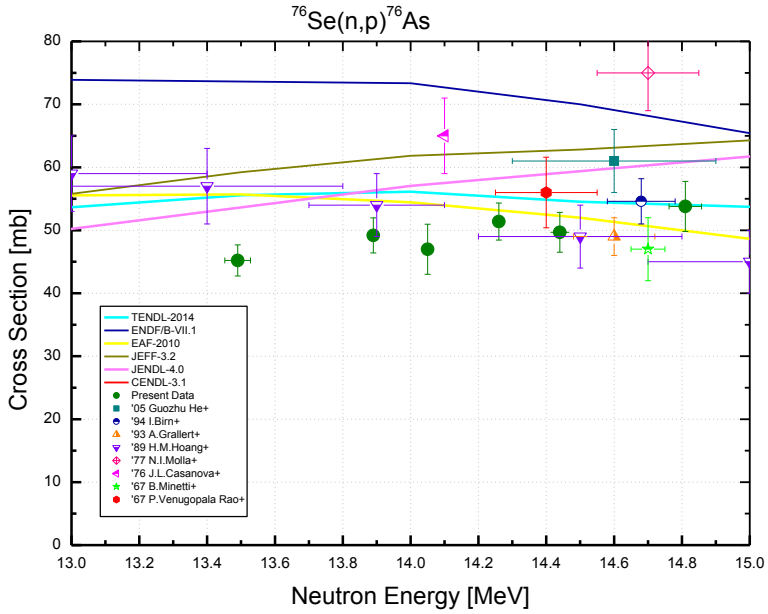

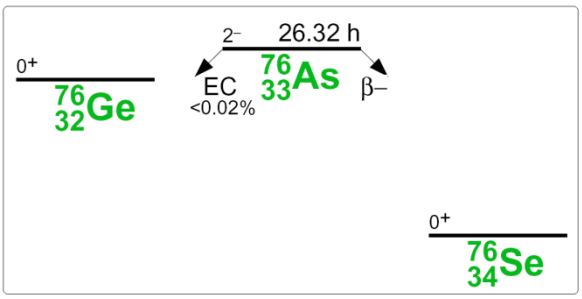

Decay data used for **^{76}Se(n, p)^{76}As.**

Target nucleus	Abundance [%]	Chemical form	Reaction product	$T_{1/2}$	E_γ [keV]	Y_γ [%]
^{76}Se	**9.37** *29*	Se-crystal	^{76}As	**26.24 h** *9*	**559.1**	**45** *2*
					657.0	6.2 *4*

^{76}Se(n, 2n)^{75}Se

^{76}Se(n, 2n)^{75}Se			
E_n [MeV]	σ [mb]	$\pm\Delta\sigma_{total}$ [%]	$\pm\Delta\sigma_{ref}$ [%]
13.49	625	*6.21*	*3.27*
13.89	807	*5.40*	*3.21*
14.05	736	*12.1*	*3.20*
14.26	870	*6.69*	*3.20*
14.44	844	*10.6*	*3.19*
14.81	988	*6.35*	*3.20*
Ref. CS is ^{27}Al(n, α)^{24}Na;			$\alpha_d = 1.2$

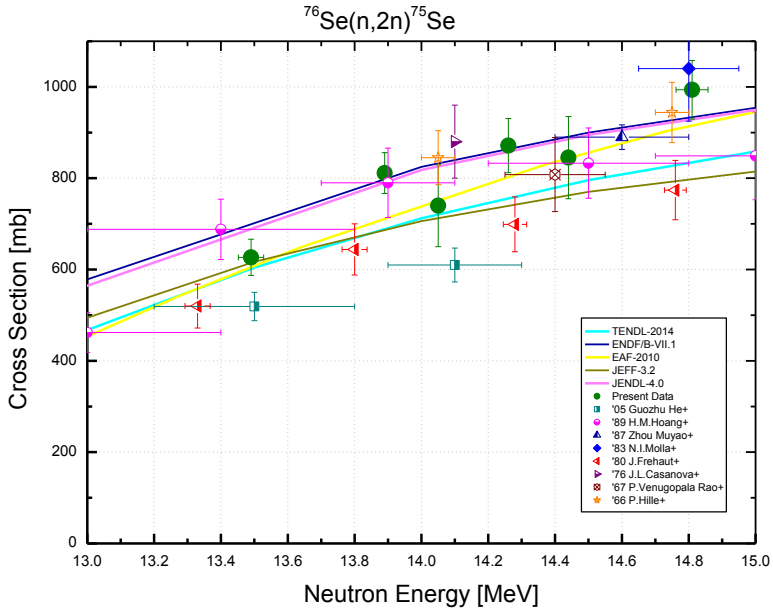

Decay data used for **^{76}Se(n, 2n)^{75}Se**.

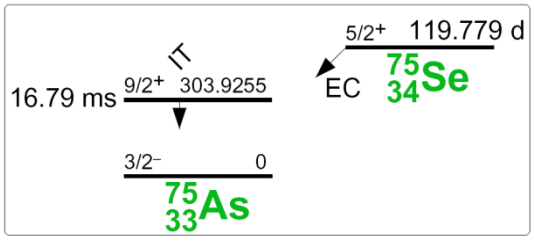

Target nucleus	Abundance [%]	Chemical form	Reaction product	$T_{1/2}$	E_γ [keV]	Y_γ [%]
^{76}Se	**9.37** *29*	Se-crystal	^{75}Se	**119.78 d** *5*	121.1	17.20 *12*
					136.0	**58.5** *4*
					279.5	25.02 *18*

^{77}Se(n, p)^{77}As

^{77}Se(n, p)^{77}As			
E_n [MeV]	σ [mb]	$\pm\Delta\sigma_{total}$ [%]	$\pm\Delta\sigma_{ref}$ [%]
13.49	56.9	*26.4*	*15.3*
13.89	65.3	*27.7*	*15.2*
14.05	54.8	*29.1*	*15.2*
14.26	67.8	*25.1*	*15.2*
14.44	65.4	*23.1*	*15.2*
14.81	76.9	*26.0*	*15.2*
Ref. CS is ^{27}Al(n, α)^{24}Na;			α_d = *1.2*

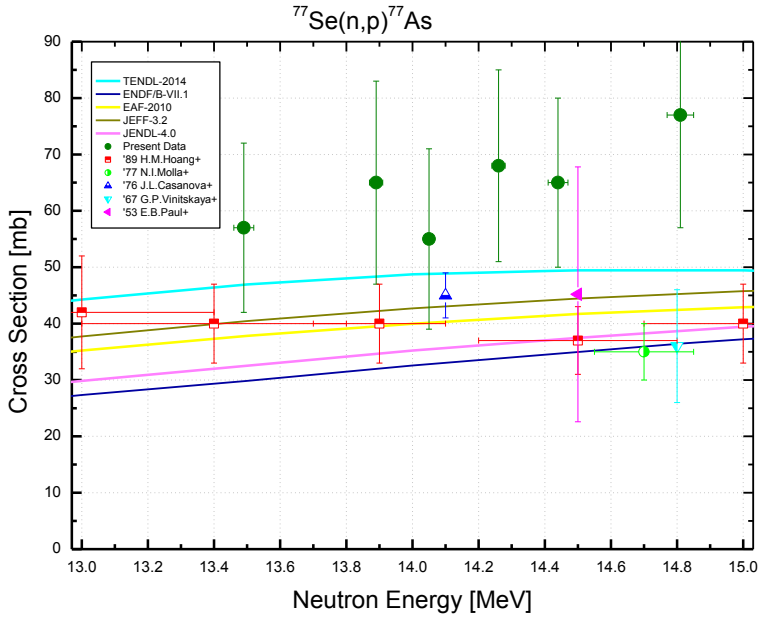

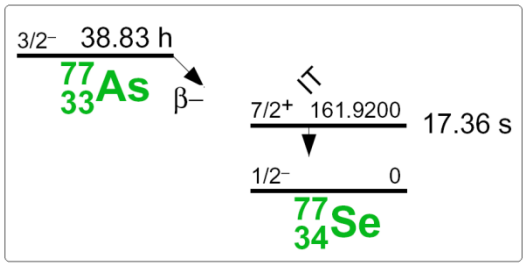

Decay data used for **^{77}Se(n, p)^{77}As**.

Target nucleus	Abundance [%]	Chemical form	Reaction product	$T_{1/2}$	E_γ [keV]	Y_γ [%]
^{77}Se	**7.63** ***16***	Se-crystal	^{77}As	**38.79 h** ***5***	**239.0**	**1.59** ***24***
					249.8	0.39 *6*
					520.7	0.56 *9*

^{78}Se(n, α)^{75}Ge

^{78}Se(n, α)^{75}Ge			
E_n [MeV]	σ [mb]	$\pm\Delta\sigma_{total}$ [%]	$\pm\Delta\sigma_{ref}$ [%]
13.49	7.59	*17.1*	*10.2*
13.89	6.44	*20.3*	*10.2*
14.26	9.09	*15.4*	*10.2*
14.81	10.0	*20.0*	*10.2*
Ref. CS is ^{27}Al(n, α)^{24}Na;			α_d = *1.2*

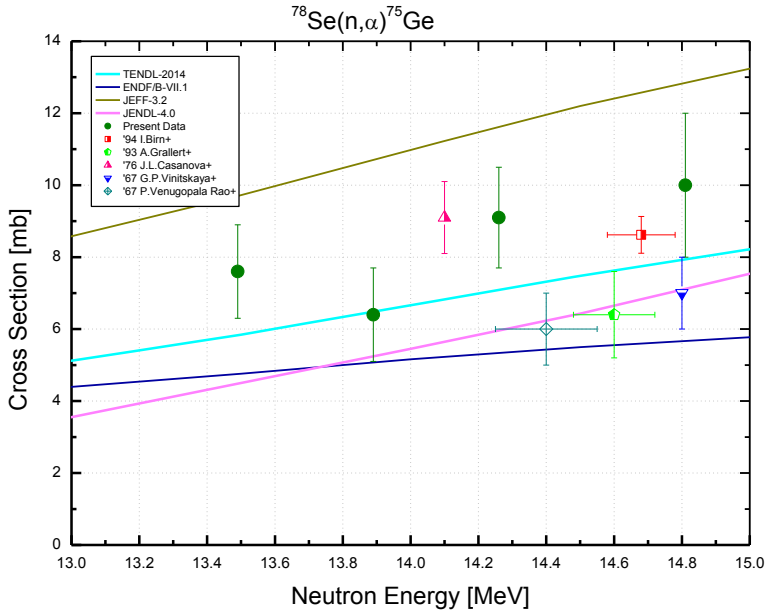

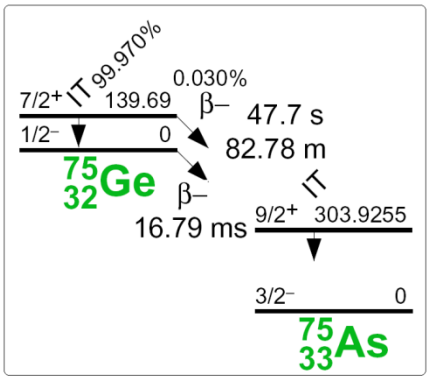

Decay data used for **^{78}Se(n, α)^{75}Ge**.

Target nucleus	Abundance [%]	Chemical form	Reaction product	$T_{1/2}$	E_γ [keV]	Y_γ [%]
^{78}Se	**23.77** ***28***	Se-crystal	^{75}Ge	**82.78 m** ***6***	**198.6**	**1.19** ***12***

^{78}Se(n, p)^{78}As

^{78}Se(n, p)^{78}As			
E_n [MeV]	σ [mb]	$\pm\Delta\sigma_{total}$ [%]	$\pm\Delta\sigma_{ref}$ [%]
13.49	16.2	*11.8*	*11.2*
13.89	17.8	*11.3*	*11.2*
14.05	17.7	*11.3*	*11.2*
14.26	20.3	*11.3*	*11.2*
14.44	19.1	*11.6*	*11.2*
14.64	22.9	*11.3*	*11.2*
14.81	21.2	*11.3*	*11.2*
14.84	20.4	*11.3*	*11.2*
Ref. CS is ^{27}Al(n, α)^{24}Na;			α_d = *1.2*

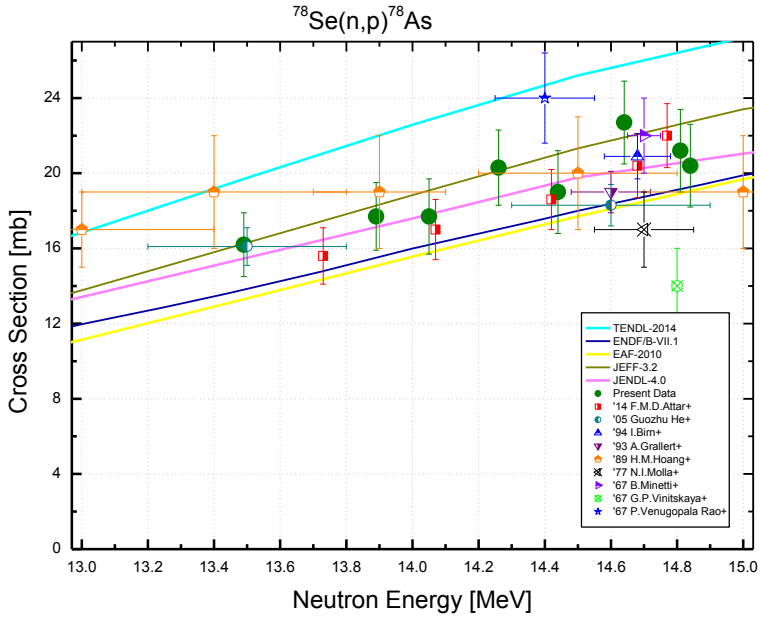

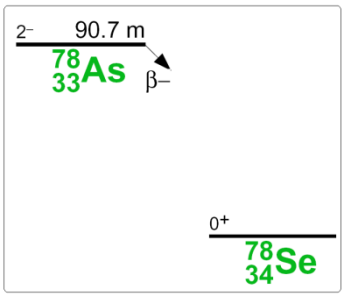

Decay data used for **^{78}Se(n, p)^{78}As**.

Target nucleus	Abundance [%]	Chemical form	Reaction product	$T_{1/2}$	E_γ [keV]	Y_γ [%]
^{78}Se	**23.77** ***28***	Se-crystal	^{78}As	**90.7 m** ***2***	**613.8**	**54** ***6***
					694.9	16.7 *22*
					1308.7	13.0 *18*

^{80}Se(n, α)$^{77(g+0.19m)}$Ge

^{80}Se(n, α)$^{77(g+0.19m)}$Ge			
E_n [MeV]	σ [mb]	$\pm\Delta\sigma_{total}$ [%]	$\pm\Delta\sigma_{ref}$ [%]
13.49	2.07	*5.80*	*1.48*
13.89	2.49	*5.64*	*1.34*
14.05	2.26	*8.80*	*1.33*
14.26	2.76	*5.76*	*1.31*
14.44	2.71	*7.42*	*1.30*
14.81	3.05	*6.19*	*1.32*
Ref. CS is ^{27}Al(n, α)^{24}Na;			α_d = *1.2*

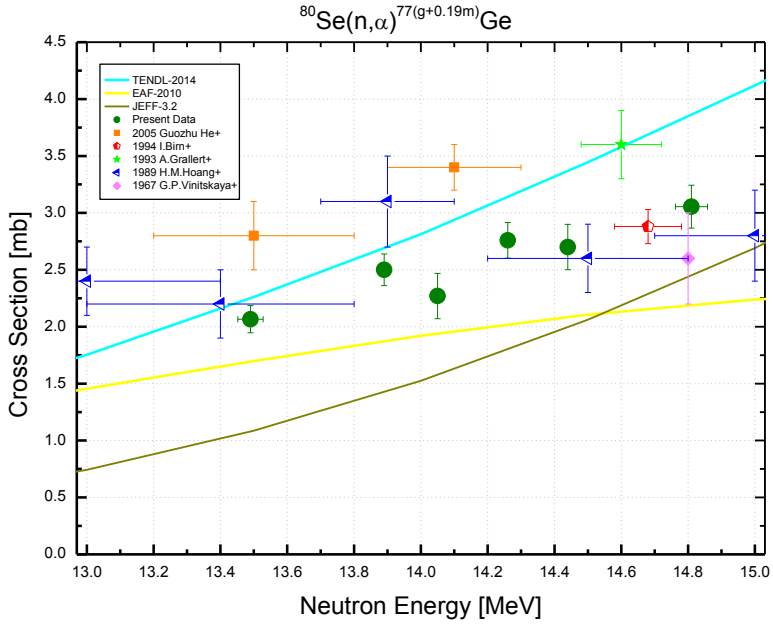

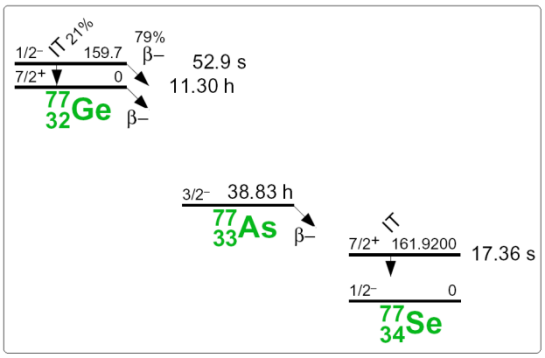

Decay data used for **^{80}Se(n, α)^{77}Ge**.

Target nucleus	Abundance [%]	Chemical form	Reaction product	$T_{1/2}$	E_γ [keV]	Y_γ [%]
^{80}Se	**49.61** *41*	Se-crystal	^{77}Ge	**11.211 h** *3*	**264.5**	**53.3** *5*
					367.5	14.5 *7*
					416.4	22.7 *11*
					557.9	16.8 *10*

^{80}Se(n, p)^{80}As

^{80}Se(n, p)^{80}As			
E_n [MeV]	σ [mb]	$\pm\Delta\sigma_{total}$ [%]	$\pm\Delta\sigma_{ref}$ [%]
13.58	8.40	*13.1*	*12.2*
13.68	8.45	*16.6*	*12.2*
13.75	10.4	*15.5*	*12.2*
13.95	9.03	*18.9*	*12.2*
14.23	9.28	*13.9*	*12.2*
14.50	11.1	*12.7*	*12.2*
14.72	12.1	*16.6*	*12.2*
14.80	11.2	*29.4*	*12.2*
Ref. CS is ^{27}Al(n, α)^{24}Na;			α_d = *1.9*

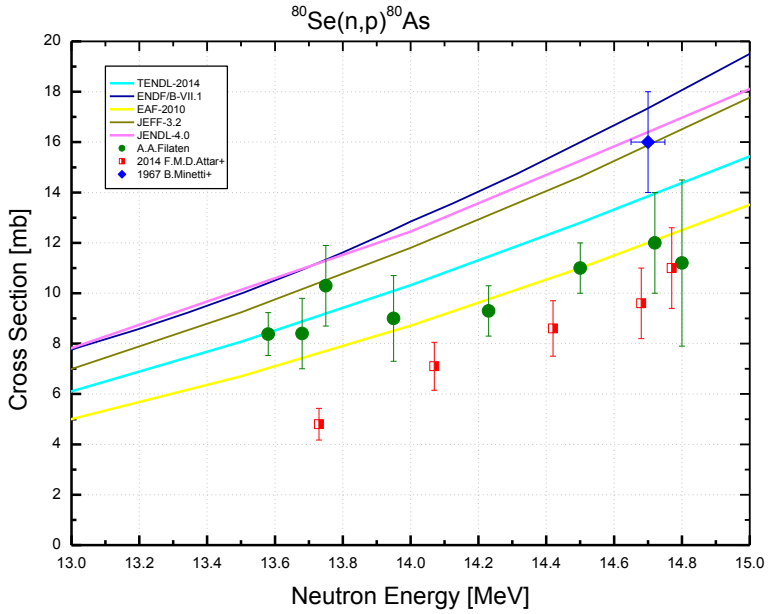

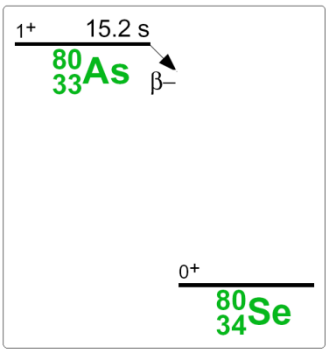

Decay data used for **^{80}Se(n, p)^{80}As**.

Target nucleus	Abundance [%]	Chemical form	Reaction product	$T_{1/2}$	E_γ [keV]	Y_γ [%]
^{80}Se	**49.61** ***41***	Se-crystal	^{80}As	**15.2 s** ***2***	**666.2**	**42** ***5***

^{80}Se(n, 2n)^{79m}Se

^{80}Se(n, 2n)^{79m}Se			
E_n [MeV]	σ [mb]	$\pm\Delta\sigma_{total}$ [%]	$\pm\Delta\sigma_{ref}$ [%]
14.05	213	*7.30*	*1.02*
14.64	213	*11.4*	*0.99*
14.84	242	*9.77*	*1.01*
Ref. CS is ^{27}Al(n, α)^{24}Na;			α_d = *1.5*

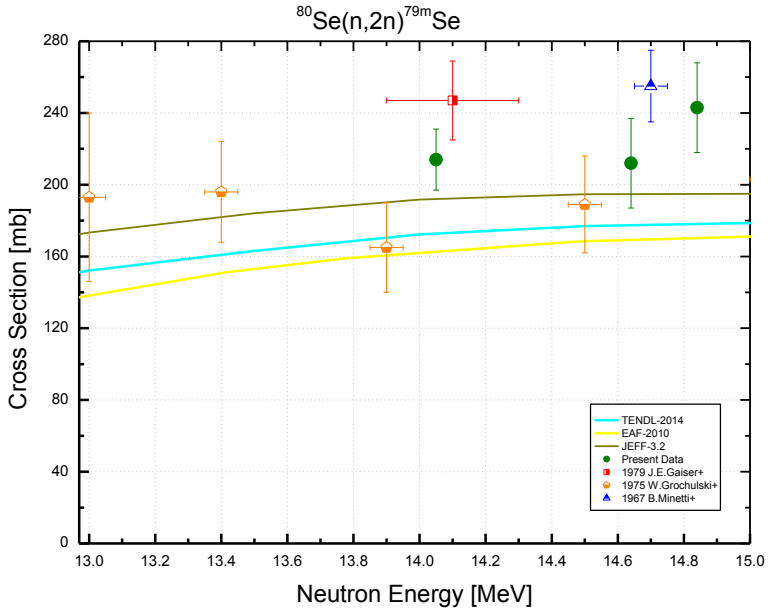

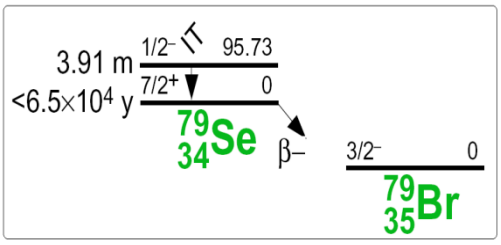

Decay data used for **^{80}Se(n, 2n)^{79m}Se**.

Target nucleus	Abundance [%]	Chemical form	Reaction product	$T_{1/2}$	E_γ [keV]	Y_γ [%]
^{80}Se	**49.61** *41*	Se-crystal	^{79m}Se	**3.92 m** *1*	**95.7**	**9.6192** *11*

^{82}Se(n, 2n)^{81m}Se

^{82}Se(n, 2n)^{81m}Se			
E_n [MeV]	σ [mb]	$\pm\Delta\sigma_{total}$ [%]	$\pm\Delta\sigma_{ref}$ [%]
13.49	1017	*15.5*	*3.53*
13.89	1108	*15.3*	*3.48*
14.05	933	*16.8*	*3.47*
14.26	1162	*14.5*	*3.47*
14.44	967	*17.5*	*3.46*
14.64	1090	*15.6*	*3.46*
14.81	1277	*16.4*	*3.47*
14.84	1119	*23.3*	*3.47*
Ref. CS is ^{27}Al(n, α)^{24}Na;			$\alpha_d = 1.4$

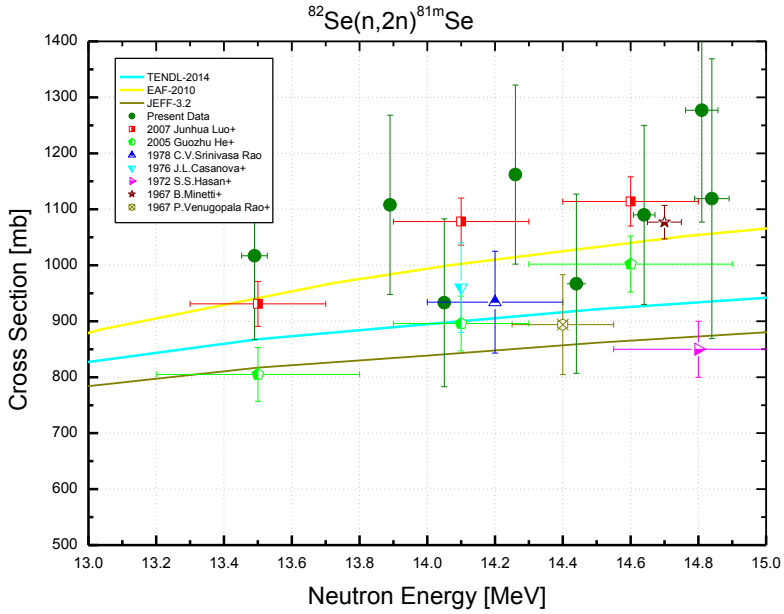

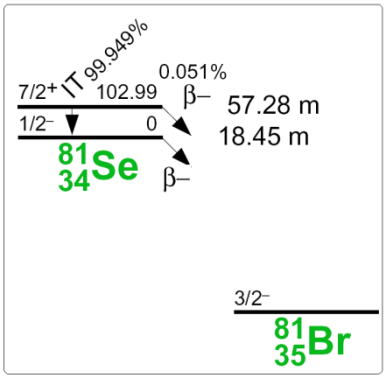

Decay data used for **^{82}Se(n, 2n)^{81m}Se**.

Target nucleus	Abundance [%]	Chemical form	Reaction product	$T_{1/2}$	E_γ [keV]	Y_γ [%]
^{82}Se	**8.73** *22*	Se-crystal	^{81m}Se	**57.28 m** *2*	**103.0**	**12.8** *3*

^{82}Se(n, 2n)^{81g}Se

^{82}Se(n, 2n)^{81g}Se			
E_n [MeV]	σ [mb]	$\pm\Delta\sigma_{total}$ [%]	$\pm\Delta\sigma_{ref}$ [%]
13.49	343	*11.5*	*11.1*
13.89	375	*13.2*	*11.1*
14.05	323	*21.2*	*11.1*
14.26	392	*15.0*	*11.1*
14.44	395	*25.0*	*11.1*
14.64	416	*19.1*	*11.1*
14.81	456	*21.5*	*11.1*
14.84	372	*26.3*	*11.1*
Ref. CS is ^{27}Al(n, α)^{24}Na;			α_d = *1.9*

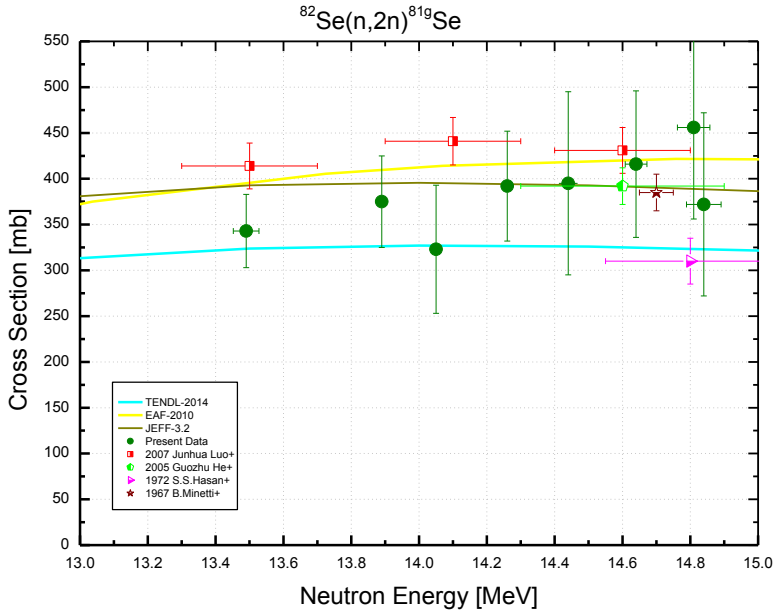

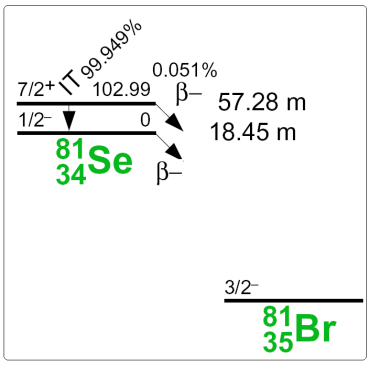

Decay data used for **^{82}Se(n, 2n)^{81g}Se**.

Target nucleus	Abundance [%]	Chemical form	Reaction product	$T_{1/2}$	E_γ [keV]	Y_γ [%]
^{82}Se	**8.73** *22*	Se-crystal	^{81g}Se	**18.45 m** *12*	**290.0**	**0.56** *6*

^{82}Se(n, 2n)^{81}Se

^{82}Se(n, 2n)^{81}Se		
E_n [MeV]	σ [mb]	$\pm\Delta\sigma_{total}$ *[%]*
13.49	1361	*12.0*
13.89	1484	*12.0*
14.05	1256	*13.7*
14.26	1554	*11.6*
14.44	1363	*14.4*
14.64	1506	*12.5*
14.81	1734	*13.4*
14.84	1491	*18.7*
Ref. CS is ^{27}Al(n, α)^{24}Na		

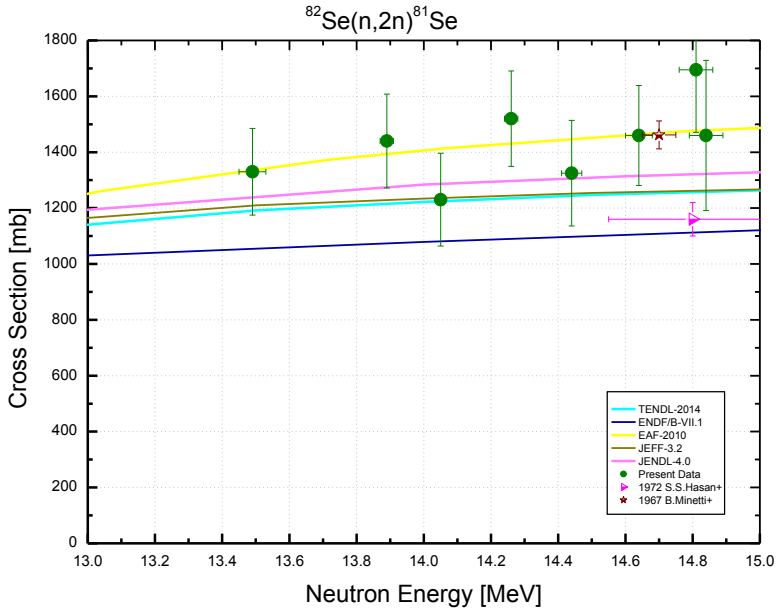

This is the sum of two cross sections measured independently: ^{82}Se(n, 2n)^{81m}Se and ^{82}Se(n, 2n)^{81g}Se.

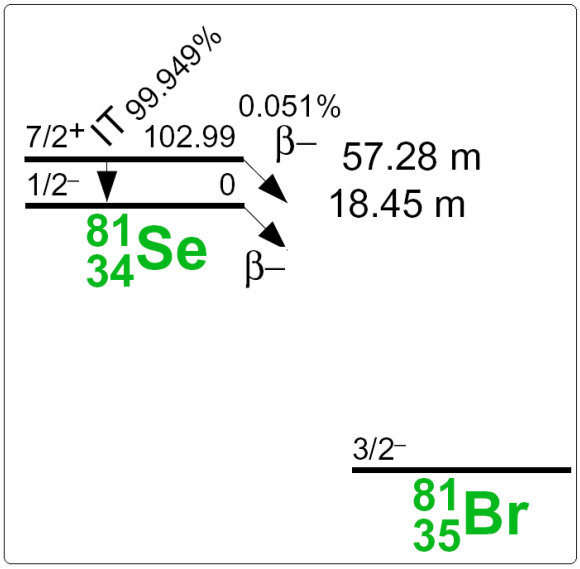

^{88}Sr(n, α)^{85m}Kr

^{88}Sr(n, α)^{85m}Kr			
E_n [MeV]	σ [mb]	$\pm\Delta\sigma_{total}$ [%]	$\pm\Delta\sigma_{ref}$ [%]
13.47	0.801	*9.77*	*1.57*
13.64	1.04	*8.46*	*1.46*
13.88	1.07	*7.23*	*1.44*
14.05	1.24	*6.93*	*1.43*
14.28	1.30	*7.37*	*1.42*
14.47	1.38	*7.01*	*1.41*
14.68	1.53	*6.94*	*1.41*
14.86	1.61	*5.78*	*1.43*
Ref. CS is ^{27}Al(n, α)^{24}Na;			$\alpha_d = 1.5$

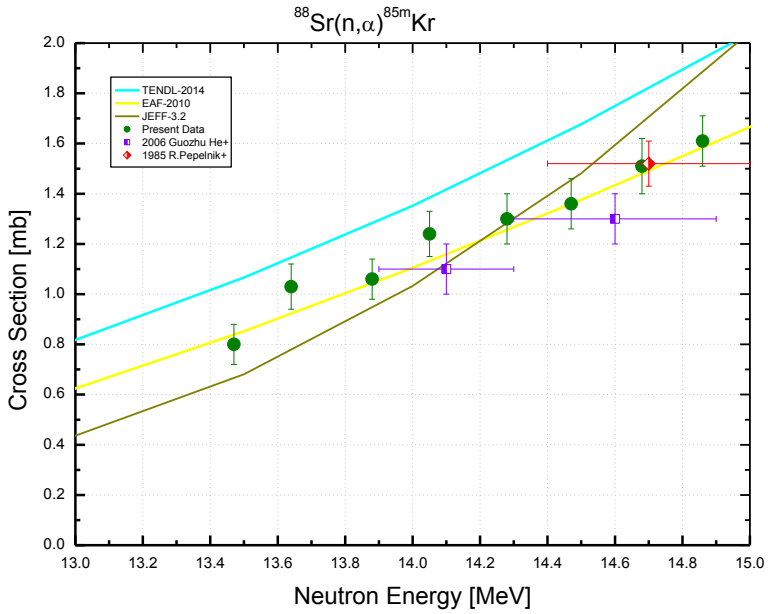

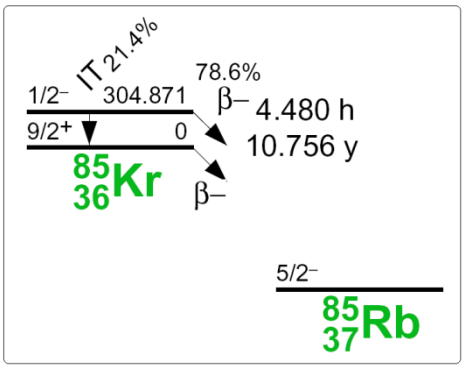

Decay data used for **^{88}Sr(n, α)^{85m}Kr**.

Target nucleus	Abundance [%]	Chemical form	Reaction product	$T_{1/2}$	E_γ [keV]	Y_γ [%]
^{88}Sr	*99.94 *3*	$SrCO_3$	^{85m}Kr	**4.480 h *8***	**151.2**	**75.2 *10***

*– refer to samples with separated isotopes of Strontium

^{88}Sr(n, 2n)^{87m}Sr

^{88}Sr(n, 2n)^{87m}Sr			
E_n [MeV]	σ [mb]	$\pm\Delta\sigma_{total}$ [%]	$\pm\Delta\sigma_{ref}$ [%]
13.47	174	*6.28*	*1.06*
13.64	197	*5.55*	*0.872*
13.88	216	*6.03*	*0.852*
14.05	225	*5.26*	*0.833*
14.28	241	*4.92*	*0.808*
14.47	249	*4.79*	*0.787*
14.68	270	*6.28*	*0.792*
14.86	278	*4.93*	*0.819*
Ref. CS is ^{27}Al(n, α)^{24}Na;			α_d = *1.5*

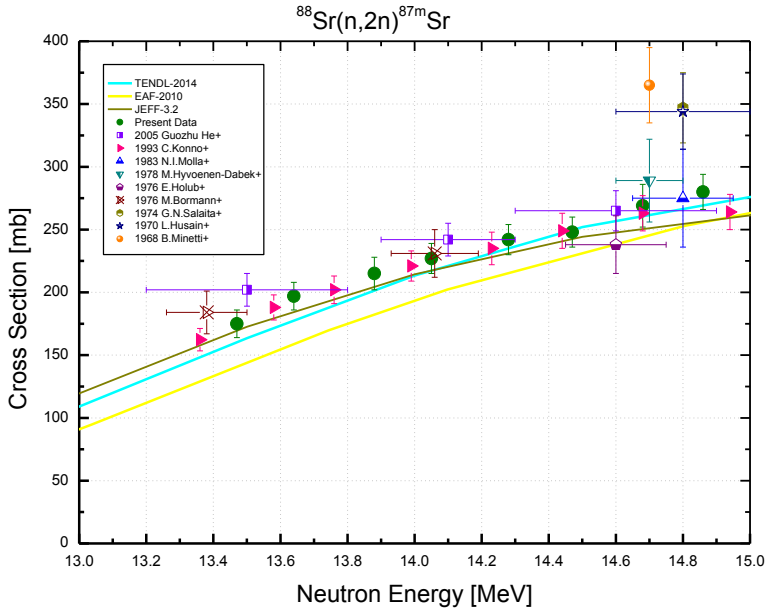

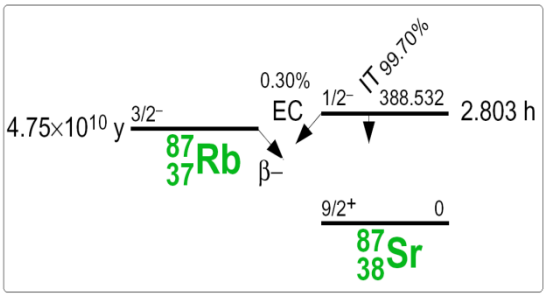

Decay data used for **^{88}Sr(n, 2n)^{87m}Sr**

Target nucleus	Abundance [%]	Chemical form	Reaction product	$T_{1/2}$	E_γ [keV]	Y_γ [%]
^{88}Sr	*99.94 *3*	$SrCO_3$	^{87m}Sr	**2.815 h** *12*	**388.5**	**82.19** *22*

* – refer to samples with separated isotopes of Strontium

^{89}Y(n, α)^{86m}Rb

^{89}Y(n, α)^{86m}Rb			
E_n [MeV]	σ [mb]	$\pm\Delta\sigma_{total}$ [%]	$\pm\Delta\sigma_{ref}$ [%]
13.47	1.03	*25.2*	*0.914*
13.65	1.19	*14.3*	*0.691*
13.88	1.31	*14.6*	*0.666*
14.04	1.32	*14.4*	*0.641*
14.26	1.60	*18.7*	*0.608*
14.43	1.82	*8.79*	*0.585*
14.62	1.85	*9.73*	*0.591*
14.78	2.00	*9.49*	*0.590*
Ref. CS is ^{27}Al(n, α)^{24}Na;			$\alpha_d = 1.5$

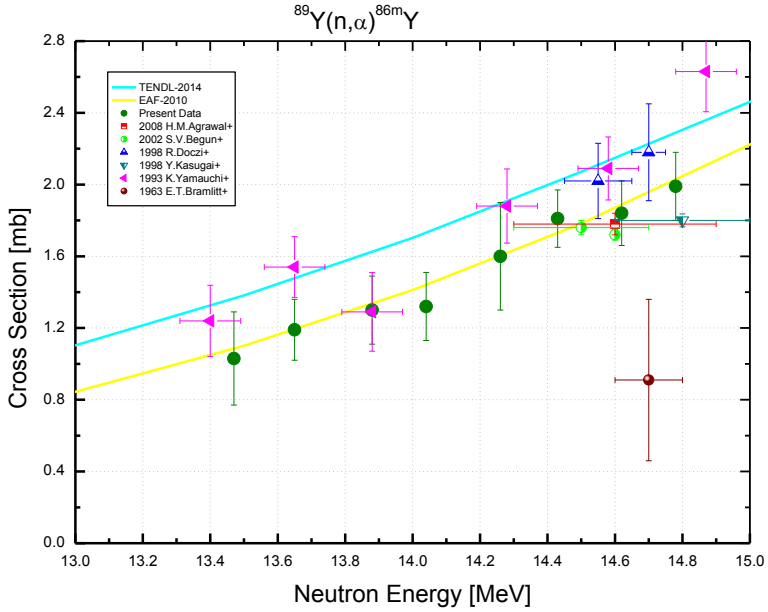

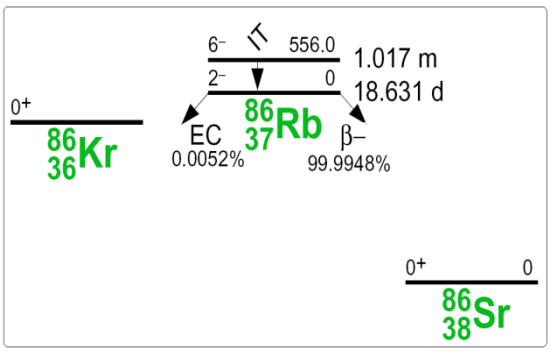

Decay data used for **^{89}Y(n, α)^{86m}Rb**.

Target nucleus	Abundance [%]	Chemical form	Reaction product	$T_{1/2}$	E_γ [keV]	Y_γ [%]
^{89}Y	**100**	Y-metal	^{86m}Rb	**1.017 m** *3*	**556.1**	**98.20** *6*

^{89}Y(n, α)^{86}Rb

^{89}Y(n, α)^{86}Rb			
E_n [MeV]	σ [mb]	$\pm\Delta\sigma_{total}$ [%]	$\pm\Delta\sigma_{ref}$ [%]
13.47	4.42	*17.2*	*0.792*
13.65	5.85	*16.5*	*0.761*
13.88	5.68	*17.7*	*0.736*
14.04	5.59	*17.9*	*0.726*
14.28	6.58	*18.2*	*0.723*
14.47	6.24	*19.2*	*0.728*
14.68	7.34	*15.0*	*0.740*
14.86	7.43	*16.3*	*0.758*
Ref. CS is ^{93}Nb(n,2n)^{92m}Nb;			α_d = *1.2*

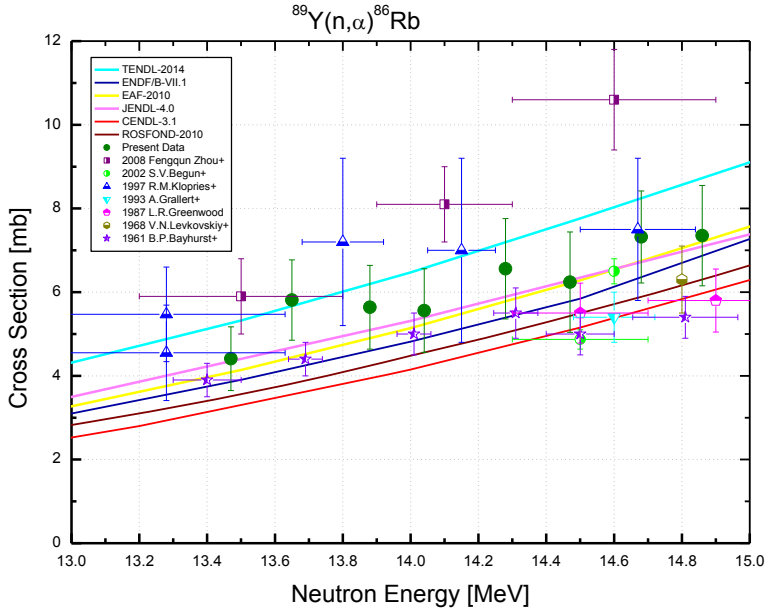

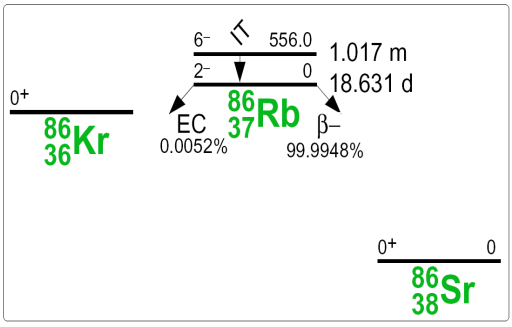

Decay data used for **^{89}Y(n, α)^{86}Rb**.

Target Nucleus	Abundance [%]	Chemical form	Reaction product	$T_{1/2}$	E_γ [keV]	Y_γ [%]
^{89}Y	**100**	Y-metal	^{86m}Rb	**18.642 d** *18*	**1077.0**	**8.64** *4*

^{89}Y(n, 2n)^{88}Y

^{89}Y(n, 2n)^{88}Y			
E_n [MeV]	σ [mb]	$\pm\Delta\sigma_{total}$ [%]	$\pm\Delta\sigma_{ref}$ [%]
13.47	681	*2.84*	*0.709*
13.64	729	*2.92*	*0.674*
13.88	797	*3.04*	*0.646*
14.05	891	*2.99*	*0.634*
14.28	904	*2.79*	*0.631*
14.47	960	*2.60*	*0.637*
14.68	980	*2.76*	*0.650*
14.86	1042	*2.64*	*0.671*
Ref. CS is ^{93}Nb(n,2n)^{92m}Nb;			α_d = *1.1*

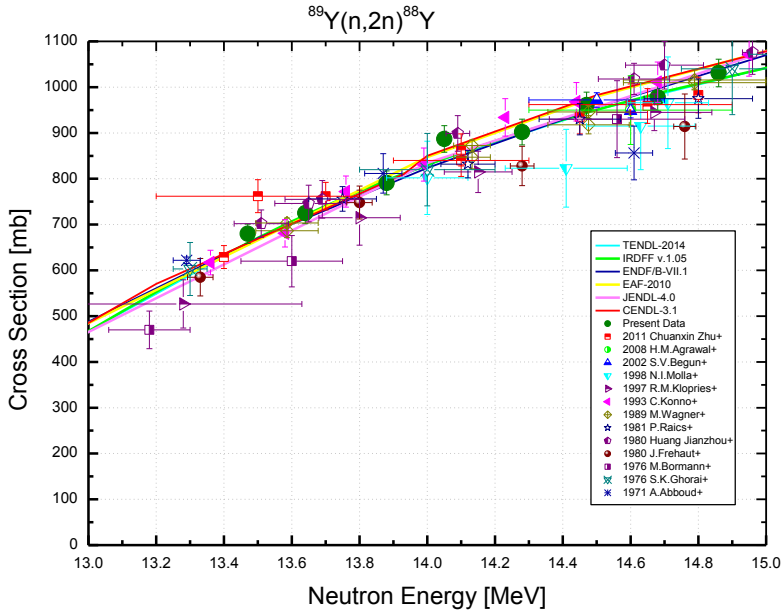

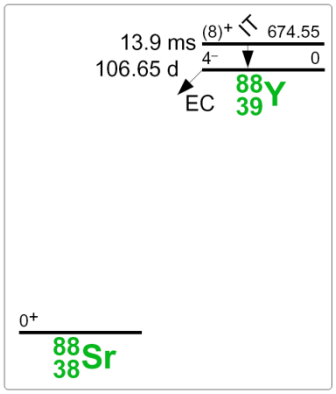

Decay data used for **^{89}Y(n, 2n)^{88}Y**.

Target nucleus	Abundance [%]	Chemical form	Reaction product	$T_{1/2}$	E_γ [keV]	Y_γ [%]
^{89}Y	**100**	Y-metal	^{88}Y	**106.626 d** *21*	**898.0**	**93.7** *3*
					1836.1	99.2 *3*

^{90}Zr(n, α)^{87m}Sr

^{90}Zr(n, α)^{87m}Sr			
E_n [MeV]	σ [mb]	$\pm\Delta\sigma_{total}$ [%]	$\pm\Delta\sigma_{ref}$ [%]
13.56	3.48	*8.55*	*1.30*
13.74	3.50	*7.68*	*1.30*
13.96	3.69	*5.65*	*1.28*
14.19	3.97	*6.98*	*1.28*
14.42	4.03	*6.62*	*1.28*
14.61	3.97	*10.24*	*1.28*
14.78	4.08	*5.61*	*1.28*
Ref. CS is ^{93}Nb(n,2n)^{92m}Nb;			α_d = *1.4*

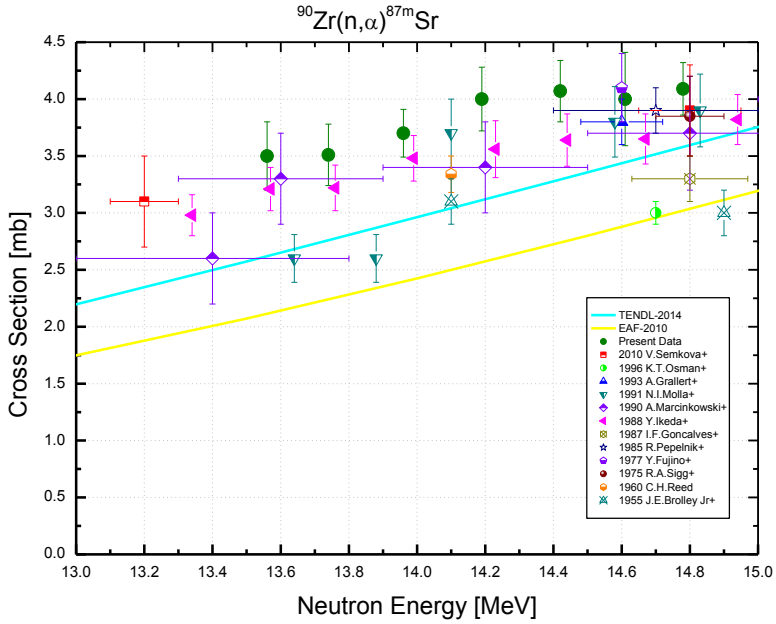

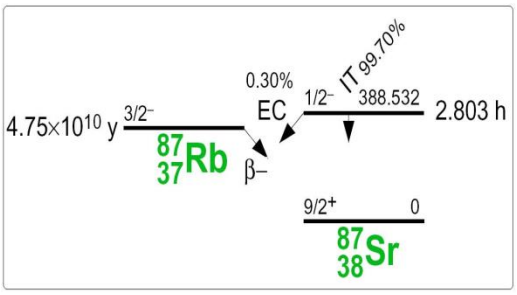

Decay data used for **^{90}Zr(n, α)^{87m}Sr**.

Target Nucleus	Abundance [%]	Chemical form	Reaction product	$T_{1/2}$	E_γ [keV]	Y_γ [%]
^{90}Zr	**51.45** ***40***	Zr-metal	^{87m}Sr	**2.815 h** ***12***	**388.5**	**82.3** ***5***

^{90}Zr(n, p)^{90m}Y

^{90}Zr(n, p)^{90m}Y			
E_n [MeV]	σ [mb]	$\pm\Delta\sigma_{total}$ [%]	$\pm\Delta\sigma_{ref}$ [%]
13.56	10.7	*5.00*	*2.84*
13.74	11.2	*5.07*	*2.84*
13.96	11.8	*4.75*	*2.83*
14.19	11.9	*5.49*	*2.83*
14.42	12.3	*5.14*	*2.83*
14.61	12.0	*4.12*	*2.83*
14.78	12.3	*4.34*	*2.83*
Ref. CS is ^{93}Nb(n,2n)^{92m}Nb;			α_d = *1.4*

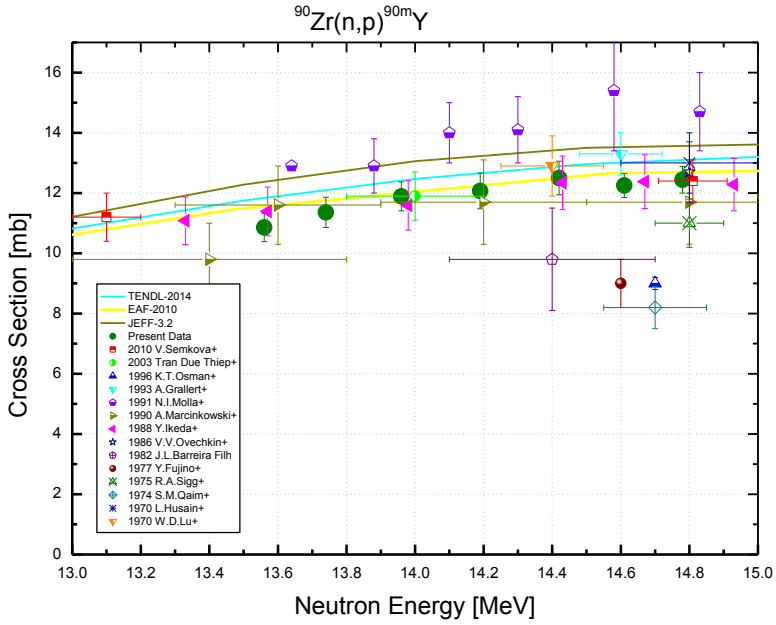

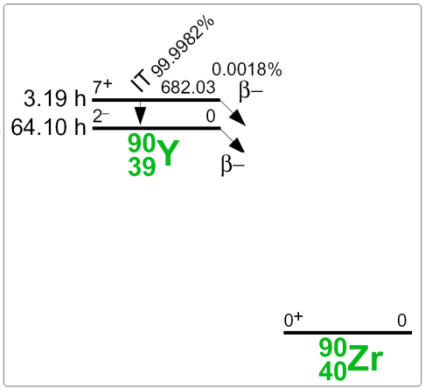

Decay data used for **^{90}Zr(n, p)^{90m}Y.**

Target nucleus	Abundance [%]	Chemical form	Reaction product	$T_{1/2}$	E_γ [keV]	Y_γ [%]
^{90}Zr	**51.45** *40*	Zr-metal	^{90m}Y	**3.19 h** *6*	**202.5**	**97.3** *4*
					479.5	90.74 *5*

^{90}Zr[(n, np) + (n, d)]^{89m}Y

^{90}Zr(n, x)^{89m}Y			
E_n [MeV]	σ [mb]	$\pm\Delta\sigma_{total}$ [%]	$\pm\Delta\sigma_{ref}$ [%]
13.58	22.8	*13.6*	*0.94*
13.72	26.0	*8.09*	*0.94*
13.95	31.1	*9.64*	*0.92*
14.25	32.3	*7.06*	*0.88*
14.72	51.3	*10.1*	*0.87*
14.85	44.8	*5.23*	*0.89*
Ref. CS is ^{27}Al(n, α)^{24}Na;			α_d = *1.5*

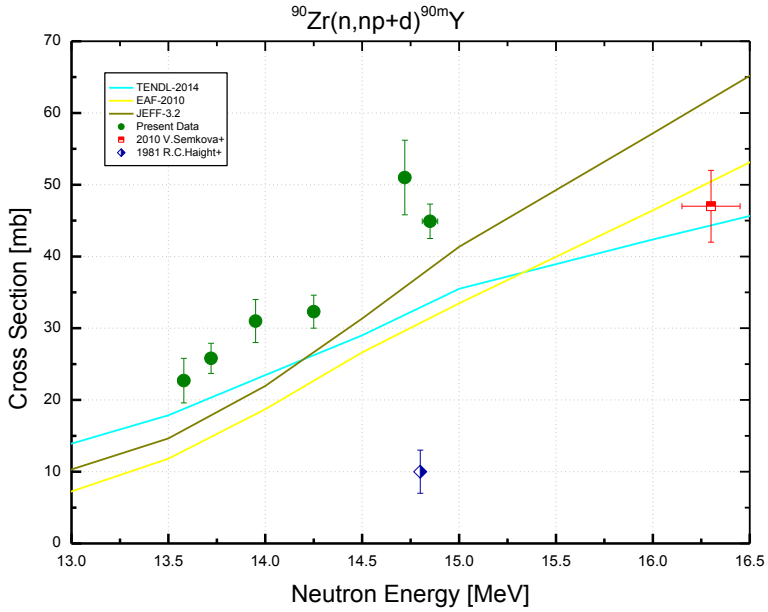

The set-up modified for short-lived activity measurement was used (p.25).

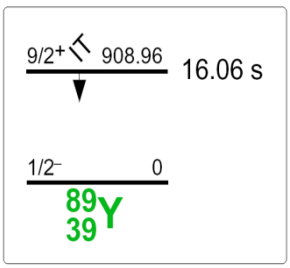

Decay data used for **^{90}Zr(n, x)^{89m}Y**

Target Nucleus	Abundance [%]	Chemical form	Reaction product	$T_{1/2}$	E_γ [keV]	Y_γ [%]
^{90}Zr	**51.45** *40*	Zr-metal	^{90m}Y	**15.663 s** *5*	**909.0**	**99.16** *3*

^{90}Zr(n, 2n)^{89m}Zr

^{90}Zr(n, 2n)^{89m}Zr			
E_n [MeV]	σ [mb]	$\pm\Delta\sigma_{total}$ [%]	$\pm\Delta\sigma_{ref}$ [%]
13.47	30.6	*2.63*	*1.186*
13.66	40.1	*3.04*	*1.024*
13.88	62.9	*2.53*	*1.007*
14.04	77.2	*2.68*	*0.991*
14.26	91.8	*2.88*	*0.970*
14.44	116.4	*2.43*	*0.956*
14.63	124.6	*2.51*	*0.959*
14.81	141.1	*2.42*	*0.979*
Ref. CS is ^{27}Al(n, α)^{24}Na;			α_d = *1.5*

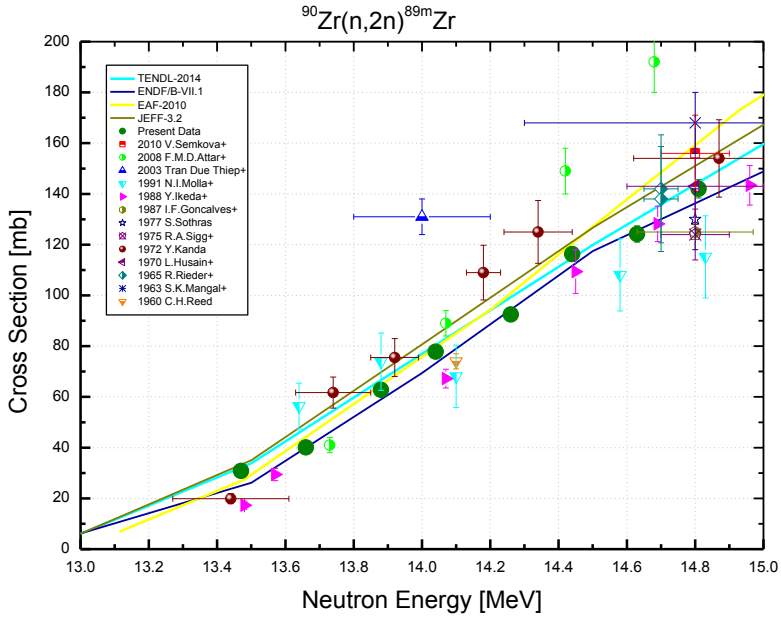

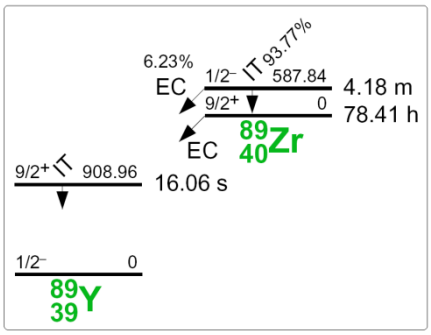

Decay data used for **^{90}Zr(n, 2n)^{89m}Zr**.

Target nucleus	Abundance [%]	Chemical form	Reaction product	$T_{1/2}$	E_γ [keV]	Y_γ [%]
^{90}Zr	**51.45** *40*	Zr-metal	^{89m}Zr	**4.161 m** *10*	**587.8**	**89.62** *17*
					1507.4	6.06 *18*

^{90}Zr(n, 2n)^{89}Zr

^{90}Zr(n, 2n)^{89}Zr			
E_n [MeV]	σ [mb]	$\pm\Delta\sigma_{total}$ [%]	$\pm\Delta\sigma_{ref}$ [%]
13.56	452	*2.09*	*0.992*
13.74	505	*1.86*	*0.992*
13.96	586	*1.93*	*0.975*
14.19	646	*1.88*	*0.965*
14.42	710	*1.99*	*0.967*
14.61	747	*2.03*	*0.976*
14.78	785	*1.94*	*0.976*
Ref. CS is ^{93}Nb(n,2n)^{92m}Nb;			α_d = *1.1*

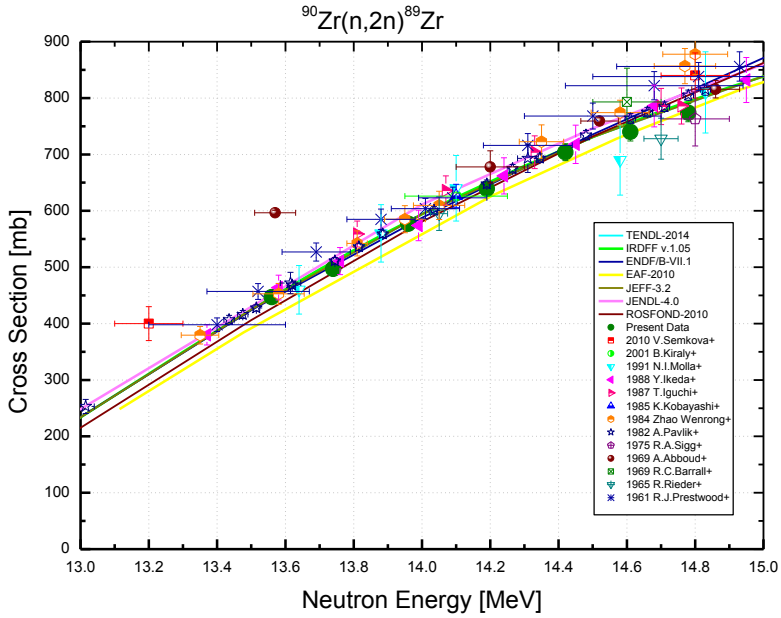

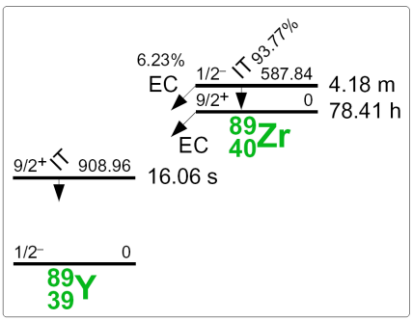

Decay data used for **^{90}Zr(n, 2n)^{89}Zr**.

Target nucleus	Abundance [%]	Chemical form	Reaction product	$T_{1/2}$	E_γ [keV]	Y_γ [%]
^{90}Zr	**51.45** *40*	Zr-metal	^{89}Zr	**78.41 h** *12*	**909.1**	**99.04** *3*

^{92}Zr(n, p)^{92}Y

^{92}Zr(n, p)^{92}Y			
E_n [MeV]	σ [mb]	$\pm\Delta\sigma_{total}$ [%]	$\pm\Delta\sigma_{ref}$ [%]
13.56	14.3	*15.0*	*10.8*
13.74	16.5	*13.9*	*10.8*
13.96	19.7	*12.9*	*10.8*
14.19	18.7	*12.4*	*10.8*
14.42	19.6	*12.0*	*10.8*
14.61	22.9	*11.7*	*10.8*
14.78	20.6	*12.4*	*10.8*
Ref. CS is ^{93}Nb(n,2n)^{92m}Nb;			α_d = *1.1*

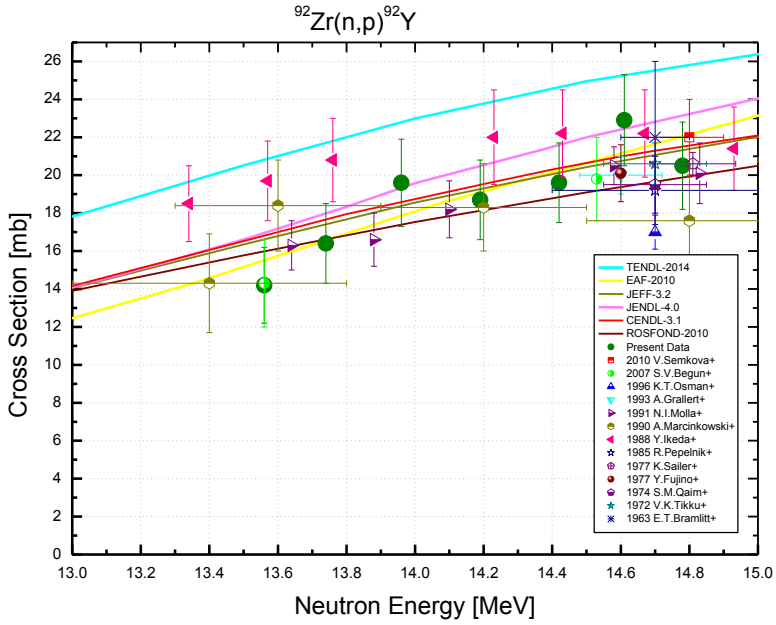

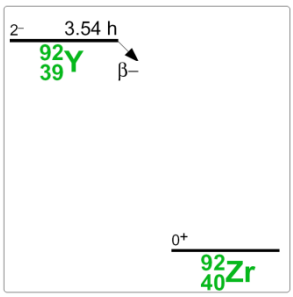

Decay data used for **^{92}Zr(n, p)^{92}Y**.

Target nucleus	Abundance [%]	Chemical form	Reaction product	$T_{1/2}$	E_γ [keV]	Y_γ [%]
^{92}Zr	**17.15** *8*	Zr-metal	^{92}Y	**3.54 h** *1*	**934.5**	**13.9** *15*
					1405.4	4.8 *5*

^{94}Zr(n, α)^{91}Sr

^{94}Zr(n, α)^{91}Sr			
E_n [MeV]	σ [mb]	$\pm\Delta\sigma_{total}$ [%]	$\pm\Delta\sigma_{ref}$ [%]
13.56	4.21	*12.0*	*3.85*
13.74	4.53	*10.0*	*3.85*
13.96	4.76	*7.74*	*3.84*
14.19	4.62	*10.2*	*3.84*
14.42	4.89	*9.24*	*3.84*
14.61	4.99	*10.2*	*3.84*
14.78	5.32	*7.39*	*3.84*
Ref. CS is ^{93}Nb(n,2n)^{92m}Nb;			α_d = *1.1*

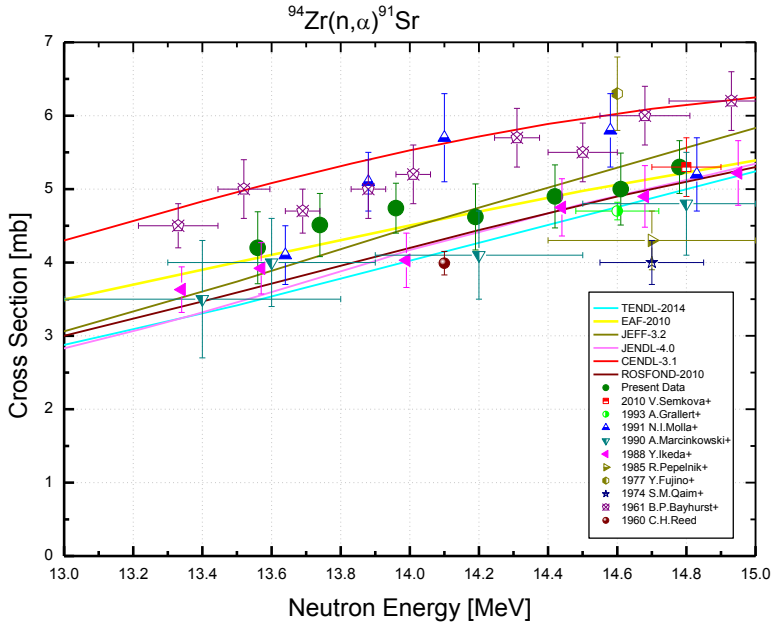

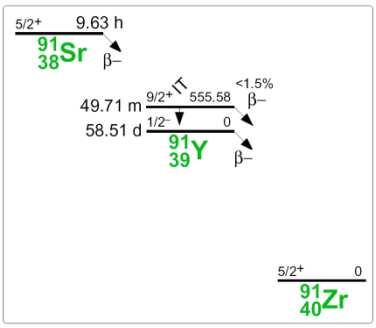

Decay data used for **^{94}Zr(n, α)^{91}Sr**.

Target nucleus	Abundance [%]	Chemical form	Reaction product	$T_{1/2}$	E_γ [keV]	Y_γ [%]
^{94}Zr	**17.38** ***28***	Zr-metal	^{91}Sr	**9.65 h** ***6***	**749.8**	**23.7** ***8***
					1024.3	33.5 *11*

^{96}Zr(n, 2n)^{95}Zr

^{96}Zr(n, 2n)^{95}Zr			
E_n [MeV]	σ [mb]	$\pm\Delta\sigma_{total}$ [%]	$\pm\Delta\sigma_{ref}$ [%]
13.56	1630	*7.17*	*3.29*
13.74	1614	*10.0*	*3.29*
13.96	1594	*5.76*	*3.29*
14.19	1543	*5.16*	*3.29*
14.42	1629	*9.62*	*3.29*
14.61	1628	*10.6*	*3.29*
14.78	1620	*6.23*	*3.29*
Ref. CS is ^{93}Nb(n,2n)^{92m}Nb;			α_d = *1.1*

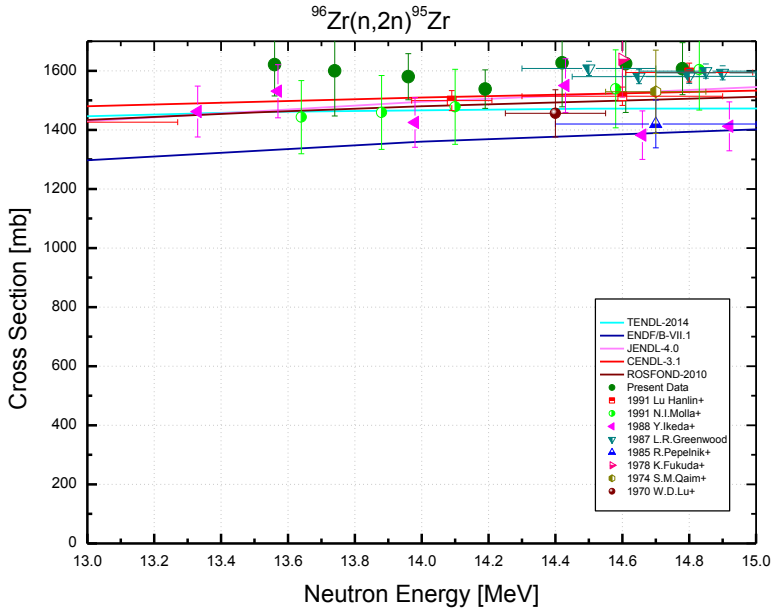

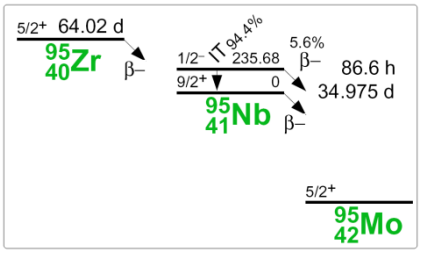

Decay data used for **^{96}Zr(n, 2n)^{95}Zr**.

Target nucleus	Abundance [%]	Chemical form	Reaction product	$T_{1/2}$	E_γ [keV]	Y_γ [%]
^{96}Zr	**2.80** *9*	Zr-metal	^{95}Zr	**64.032 d** *6*	724.2	44.27 *22*
					756.7	**54.38** *22*

^{93}Nb(n, α)^{90m}Y

^{93}Nb(n, α)^{90m}Y			
E_n [MeV]	σ [mb]	$\pm\Delta\sigma_{total}$ [%]	$\pm\Delta\sigma_{ref}$ [%]
13.47	5.03	*4.38*	*2.71*
13.56	4.81	*7.18*	*2.70*
13.66	5.15	*4.49*	*2.70*
13.74	5.15	*5.89*	*2.70*
13.88	5.28	*5.40*	*2.69*
13.96	5.35	*6.56*	*2.69*
14.05	5.68	*5.22*	*2.69*
14.19	5.68	*5.88*	*2.69*
14.27	5.61	*4.18*	*2.69*
14.42	5.58	*4.55*	*2.69*
14.47	5.85	*5.07*	*2.69*
14.61	5.80	*5.93*	*2.69*
14.68	5.74	*6.10*	*2.69*
14.78	5.81	*6.59*	*2.69*
14.86	5.84	*4.12*	*2.70*
Ref. CS is ^{93}Nb(n,2n)^{92m}Nb;			$\alpha_d = 1.4$

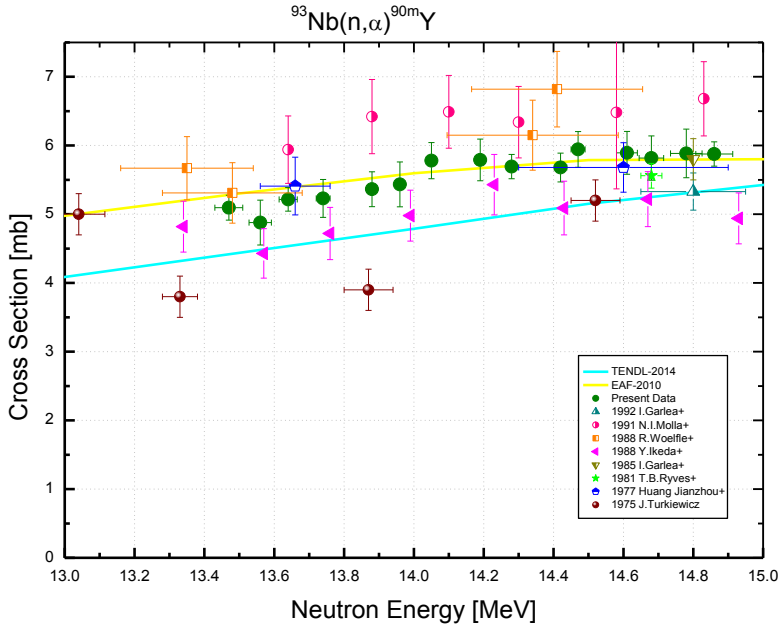

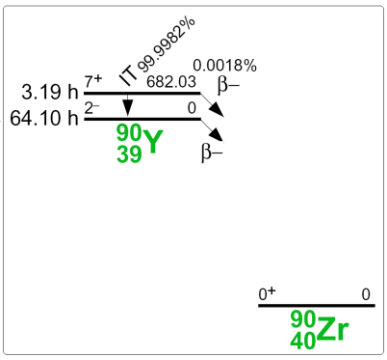

Decay data used for **^{93}Nb(n, α)^{90m}Y**.

Target nucleus	Abundance [%]	Chemical form	Reaction product	$T_{1/2}$	E_γ [keV]	Y_γ [%]
^{93}Nb	**100**	Nb-metal	^{90m}Y	**3.19 h** *6*	202.5	97.3 *4*
					472.5	**90.74** *5*

^{93}Nb(n, α)^{90}Y

^{93}Nb(n, α)^{90}Y		
E_n [MeV]	σ [mb]	$\pm\Delta\sigma_{total}$ [%]
13.47	12.2	*7.45*
13.56	11.6	*9.14*
13.66	12.4	*6.96*
13.74	12.3	*7.74*
13.88	12.6	*7.15*
13.96	12.7	*8.00*
14.05	13.5	*6.89*
14.19	13.4	*7.43*
14.27	13.2	*6.25*
14.42	13.1	*6.74*
14.47	13.7	*7.20*
14.61	13.5	*8.14*
14.68	13.3	*8.45*
14.78	13.5	*9.09*
14.86	13.5	*7.79*
Ref. CS is ^{93}Nb(n,2n)^{92m}Nb		

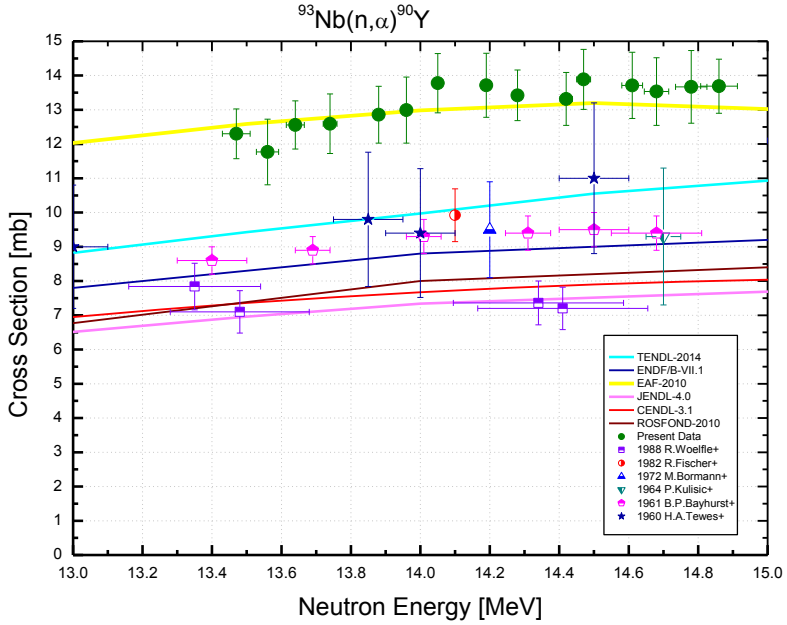

The ^{93}Nb(n, α)^{90}Y cross section was not measured directly but is the product of two other values measured immediately, the ^{93}Nb(n, α)^{90m}Y cross section presented in the previous page and the isomeric ratio *IR*, i.e. $\sigma_m/(\sigma_m + \sigma_g)$, that was determined from the analysis of the time behavior of the continuous spectrum component corresponded to the ^{90}Y β-particles that were registered by the HPGe detector with thin entrance window. The experiment is described in detail earlier (pp. 21 – 24). The obtained isomeric ratio values were approximated by the straight line in the used neutron energy interval:

$$IR(E_n)=a\cdot(E_n-E_0)+b$$

where $a = 0.013\pm0.027\ MeV^{-1}$

$b = 0.422\pm0.019$

$E_0 = 14.07\ MeV$

The straight line parameters were determined by the least squares methods.

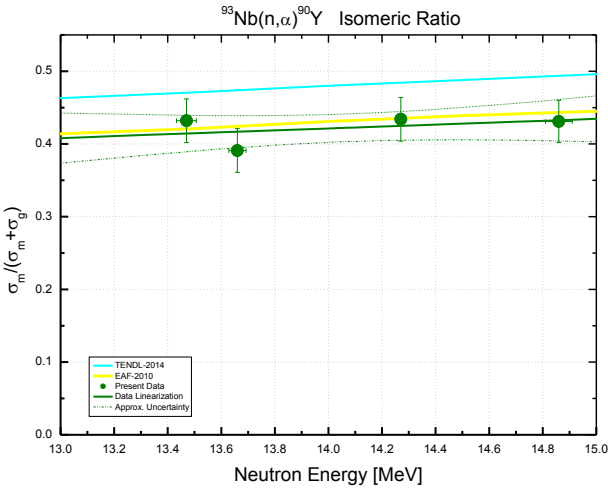

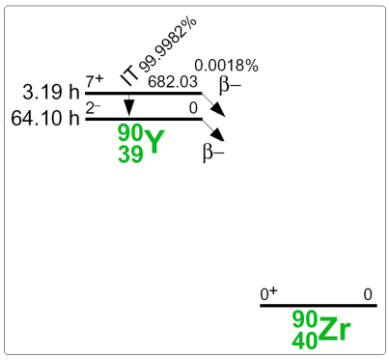

Decay data used for **^{93}Nb(n, α)^{90}Y**

Target nucleus	Reaction product	$T_{1/2}$	$E_{\beta\ max}$ [keV]
^{93}Nb	^{90m}Y	**3.19 h** *6*	—
	^{90g}Y	**64.00 h** *21*	2278.7

^{92}Mo(n, α)^{89m}Zr

^{92}Mo(n, α)^{89m}Zr			
E_n [MeV]	σ [mb]	$\pm\Delta\sigma_{total}$ [%]	$\pm\Delta\sigma_{ref}$ [%]
13.47	6.40	*4.69*	*2.42*
13.66	6.12	*6.71*	*2.35*
13.88	6.71	*5.08*	*2.34*
14.04	6.58	*6.40*	*2.33*
14.26	6.51	*6.74*	*2.33*
14.44	7.20	*8.48*	*2.32*
14.63	6.87	*4.83*	*2.32*
14.81	6.72	*8.54*	*2.33*
Ref. CS is ^{27}Al(n, α)^{24}Na;			α_d = *1.9*

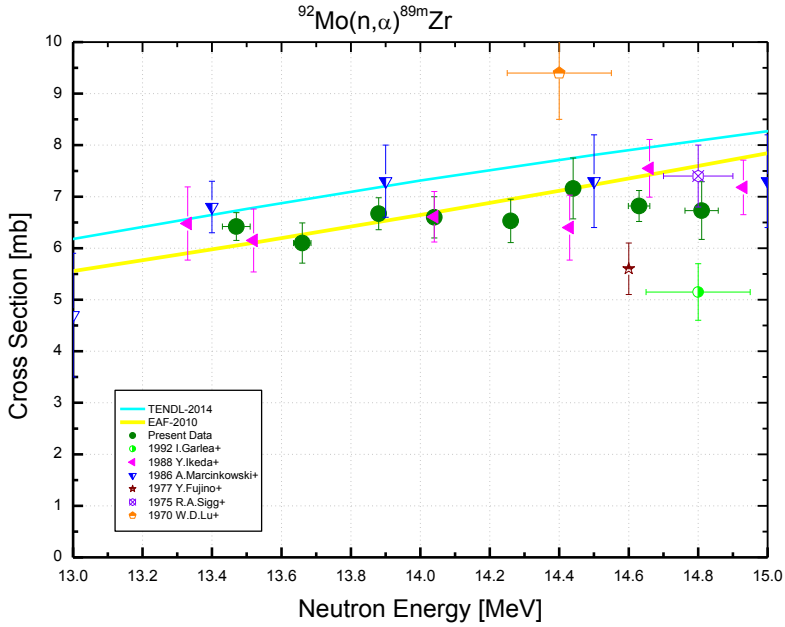

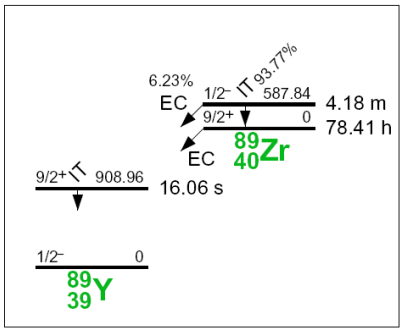

Decay data used for **^{92}Mo(n, α)^{89m}Zr**.

Target nucleus	Abundance [%]	Chemical form	Reaction product	$T_{1/2}$	E_γ [keV]	Y_γ [%]
^{92}Mo	**14.77** *31*	Mo-metal	^{89m}Zr	**4.161 m** *10*	**587.8**	**89.62** *17*
					1507.4	6.06 *18*

^{92}Mo(n, α)^{89}Zr

^{92}Mo(n, α)^{89}Zr			
E_n [MeV]	σ [mb]	$\pm\Delta\sigma_{total}$ [%]	$\pm\Delta\sigma_{ref}$ [%]
13.47	21.4	*6.43*	*2.33*
13.65	22.7	*4.44*	*2.32*
13.87	23.4	*4.35*	*2.31*
14.05	24.2	*4.18*	*2.31*
14.28	24.5	*4.13*	*2.31*
14.44	25.4	*4.39*	*2.31*
14.64	26.1	*4.31*	*2.31*
14.82	27.0	*5.61*	*2.32*
Ref. CS is ^{93}Nb(n,2n)^{92m}Nb;			$\alpha_d = 1.2$

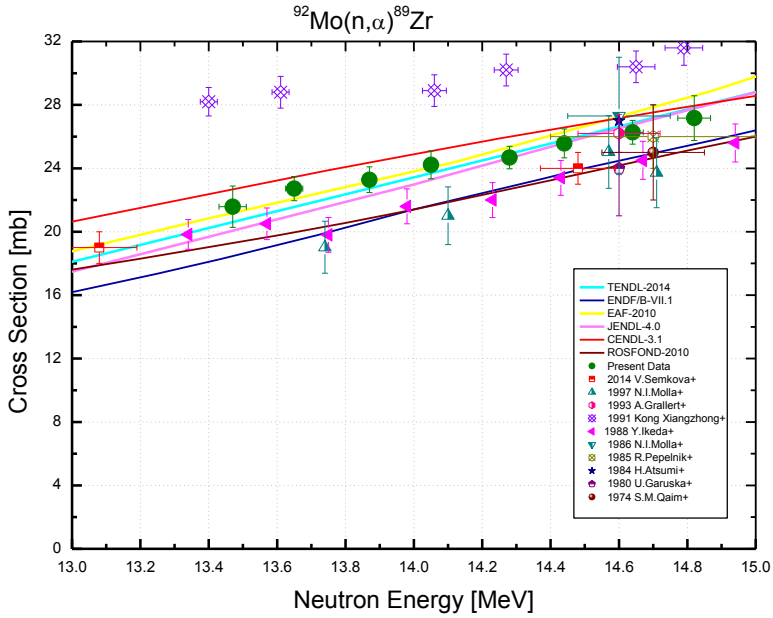

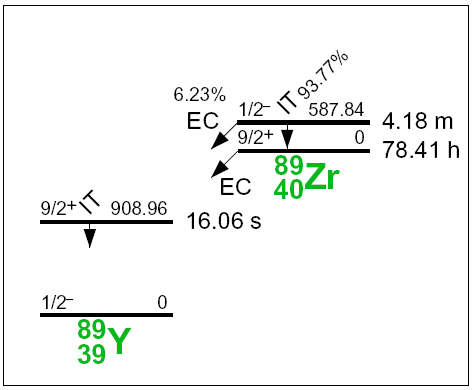

Decay data used for **^{92}Mo(n, α)^{89}Zr**.

Target nucleus	Abundance [%]	Chemical form	Reaction product	$T_{1/2}$	E_γ [keV]	Y_γ [%]
^{92}Mo	**14.77** ***31***	Mo-metal	^{89}Zr	**78.41 h** ***12***	**909.1**	**99.04** ***3***

^{92}Mo(n, 2n)^{91m}Mo

^{92}Mo(n, 2n)^{91m}Mo			
E_n [MeV]	σ [mb]	$\pm\Delta\sigma_{total}$ [%]	$\pm\Delta\sigma_{ref}$ [%]
13.66	1.44	*41.8*	*5.23*
13.88	3.70	*16.8*	*5.23*
14.04	6.41	*13.0*	*5.22*
14.26	11.0	*12.4*	*5.22*
14.44	16.3	*14.1*	*5.22*
14.64	22.6	*13.1*	*5.22*
14.81	26.8	*12.5*	*5.22*
Ref. CS is ^{27}Al(n, α)^{24}Na;			α_d = *1.9*

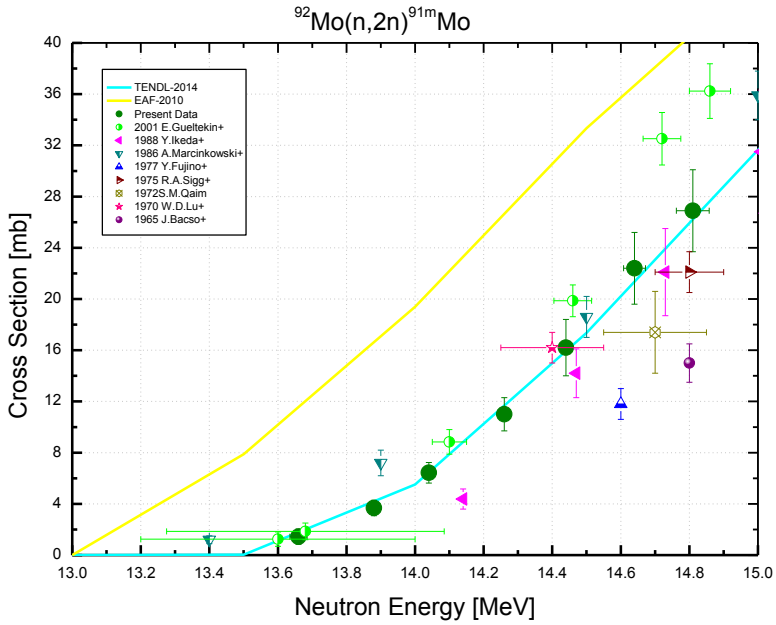

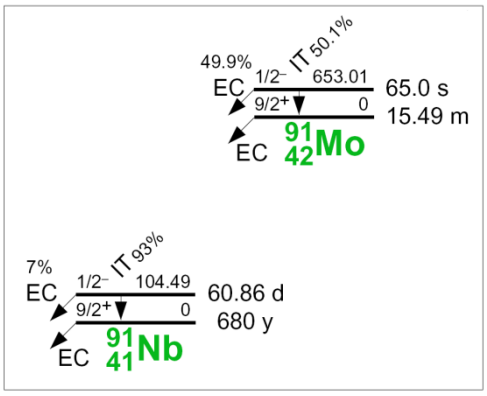

Decay data used for **^{92}Mo(n, 2n)^{91m}Mo**.

Target nucleus	Abundance [%]	Chemical form	Reaction product	$T_{1/2}$	E_γ [keV]	Y_γ [%]
^{92}Mo	**14.77** ***31***	Mo-metal	^{91m}Mo	**64.6 s** ***6***	**652.9**	**48.2** ***21***
					1208.1	18.6 *14*
					1508.0	24.2 *18*

^{92}Mo[(n, np) + (n, d)]^{91m}Nb

^{92}Mo(n, x)^{91m}Nb			
E_n [MeV]	σ [mb]	$\pm\Delta\sigma_{total}$ [%]	$\pm\Delta\sigma_{ref}$ [%]
13.48	201	*8.81*	*2.84*
13.67	222	*8.45*	*2.83*
13.88	231	*8.12*	*2.82*
14.06	244	*8.10*	*2.82*
14.28	250	*7.87*	*2.82*
14.46	242	*8.10*	*2.82*
14.67	249	*8.29*	*2.82*
14.83	245	*8.87*	*2.83*
Ref. CS is ^{93}Nb(n,2n)^{92m}Nb;			$\alpha_d = 1.2$

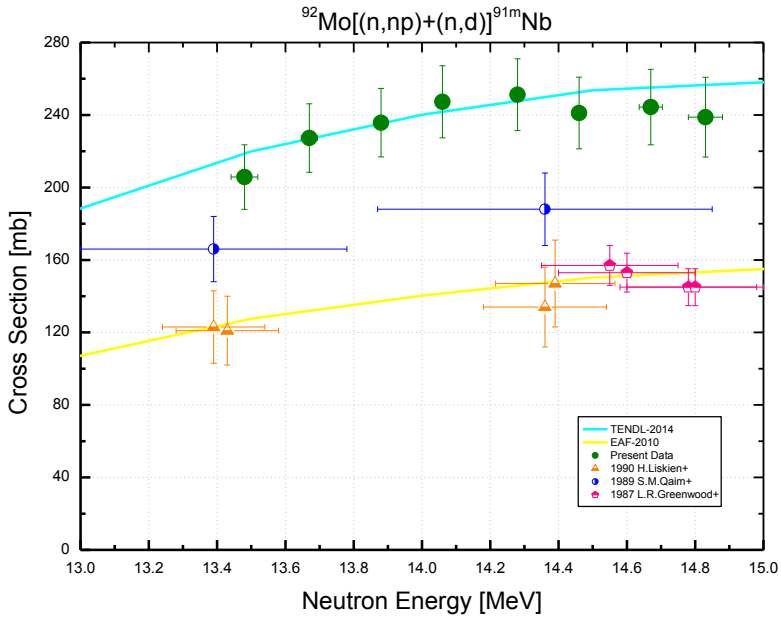

The intensity of the 104.6 keV γ-transition that discharges the metastable state ½⁻ of the ^{91}Nb was measured in the experiment. The ^{91m}Nb half-life is 60.86 d. Additionally, this metastable state is popupated via EC decay of the ^{91m}Mo state with the probability of (0.50 ± 0.16) and half-life of 64.6 s. The ^{91m}Mo excited state is produced in the ^{92}Mo(n, 2n)^{91m}Mo reaction which cross section was measured independently. The corresponding data are presented in the previous page. The cross section data for the ^{92}Mo[(n,np)+(n,d)]^{91m}Nb presented in this page were obtained with the correction for the contribution of the ^{92}Mo(n, 2n)^{91m}Mo reaction into population of the metastable state ^{91m}Mo.

The decay of the ^{91}Mo ground state does not contribute to the ^{91m}Nb 104.6 keV state excitation.

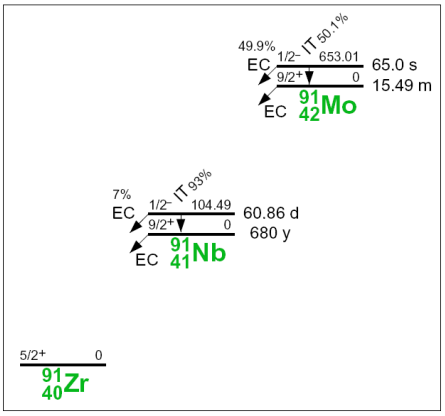

Decay data used for **^{92}Mo(n, x)^{91m}Nb**.

Target nucleus	Abundance [%]	Chemical form	Reaction product	$T_{1/2}$	E_γ [keV]	Y_γ [%]
^{92}Mo	**14.77** ***31***	Mo-metal	^{91m}Nb	**60.86 d** ***22***	**104.6**	**0.574** ***9***

^{92}Mo(n, p)^{92m}Nb

^{92}Mo(n, p)^{92m}Nb			
E_n [MeV]	σ [mb]	$\pm\Delta\sigma_{total}$ [%]	$\pm\Delta\sigma_{ref}$ [%]
13.47	77.4	*4.18*	*2.84*
13.65	75.7	*6.56*	*2.83*
13.88	73.2	*4.56*	*2.82*
14.05	72.0	*4.20*	*2.82*
14.27	66.8	*4.48*	*2.82*
14.44	63.1	*3.87*	*2.82*
14.64	61.5	*4.58*	*2.82*
14.81	58.8	*3.69*	*2.83*
Ref. CS is ^{93}Nb(n,2n)^{92m}Nb;			$\alpha_d = 1.2$

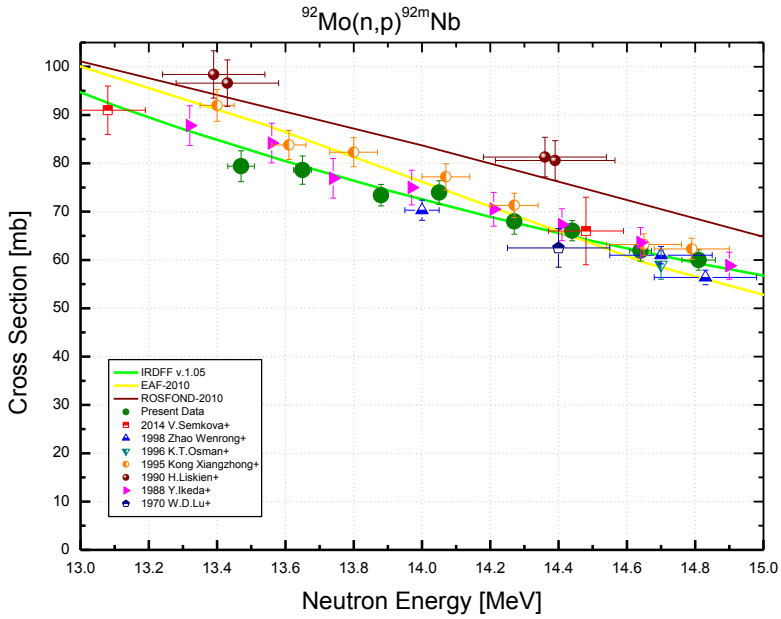

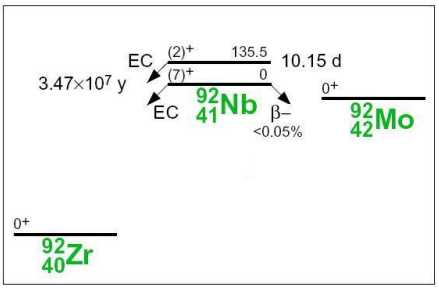

Decay data used for **^{92}Mo(n, p)^{92m}Nb**.

Target nucleus	Abundance [%]	Chemical form	Reaction product	$T_{1/2}$	E_γ [keV]	Y_γ [%]
^{92}Mo	**14.77** *31*	Mo-metal	^{92m}Nb	**10.15 d** *2*	**934.4**	**99.15** *4*

^{94}Mo(n, 2n)^{93m}Mo

^{94}Mo(n, 2n)^{93m}Mo			
E_n [MeV]	σ [mb]	$\pm\Delta\sigma_{total}$ [%]	$\pm\Delta\sigma_{ref}$ [%]
13.64	1.59	*9.29*	*2.20*
13.87	2.24	*4.06*	*2.19*
14.05	2.98	*9.59*	*2.19*
14.28	3.88	*8.81*	*2.19*
14.44	4.60	*8.92*	*2.19*
14.64	5.86	*10.1*	*2.19*
Ref. CS is ^{93}Nb(n,2n)^{92m}Nb;			$\alpha_d = 1.6$

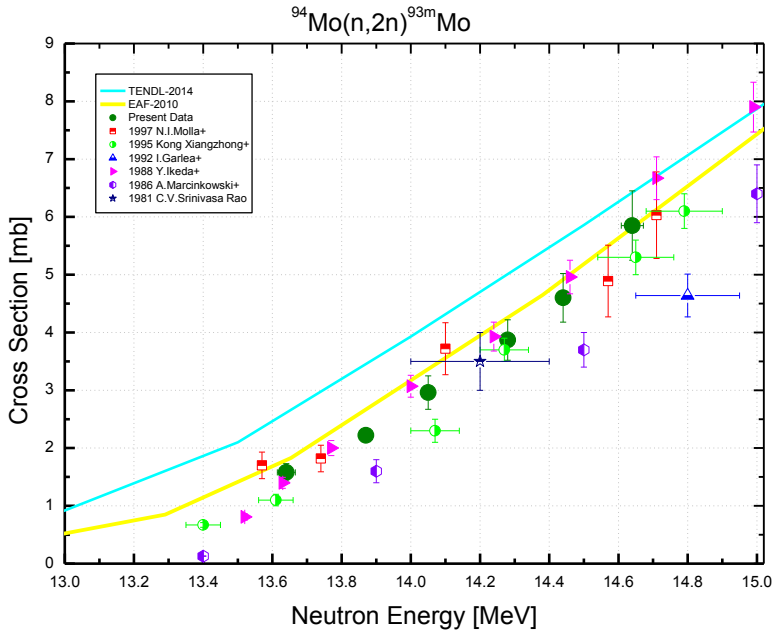

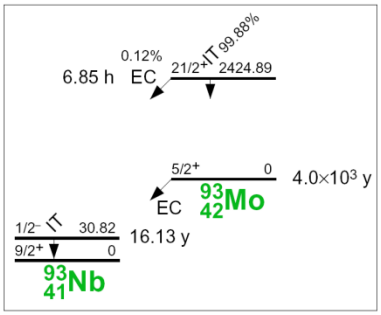

Decay data used for **^{94}Mo(n, 2n)^{93m}Mo**.

Target nucleus	Abundance [%]	Chemical form	Reaction product	$T_{1/2}$	E_γ [keV]	Y_γ [%]
^{94}Mo	**9.23** *10*	Mo-metal	^{93m}Mo	**6.85 h** *7*	263.0	57.4 *11*
					684.7	**99.9** *8*
					1477.1	99.1 *11*

^{nat}Mo(n, x)^{95}Nb

^{nat}Mo(n, x)^{95}Nb			
E_n [MeV]	σ [mb]	$\pm\Delta\sigma_{total}$ [%]	$\pm\Delta\sigma_{ref}$ [%]
13.48	5.48	*3.89*	*0.63*
13.64	5.71	*3.14*	*0.59*
13.87	5.91	*3.67*	*0.56*
14.05	6.19	*3.28*	*0.55*
14.28	6.27	*3.25*	*0.54*
14.45	6.56	*3.38*	*0.55*
14.64	6.56	*3.38*	*0.56*
14.82	6.81	*3.80*	*0.59*
Ref. CS is ^{93}Nb(n,2n)^{92m}Nb;			$\alpha_d = 1.2$

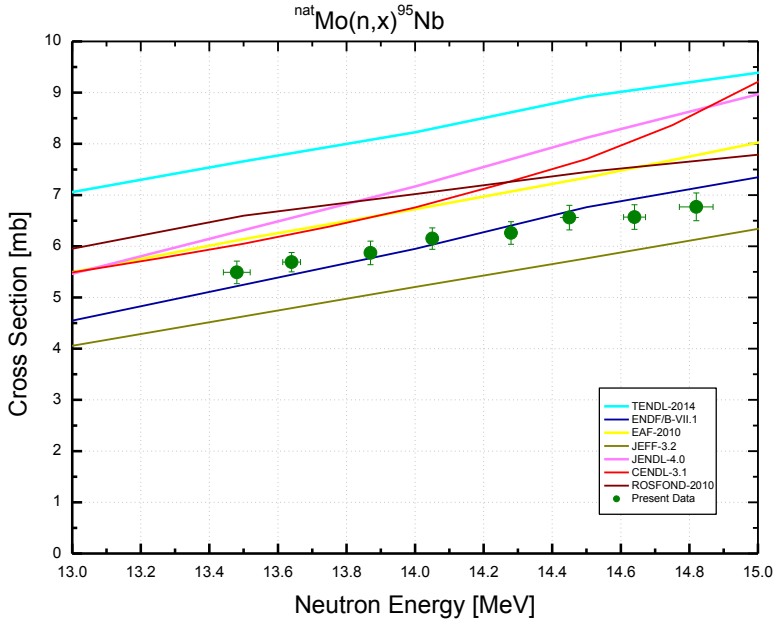

The samples made of natural molybdenum were used. Several reactions can contribute to the production of ^{95}Nb:

^{95}Mo(n, p)^{95}Nb – is the most probable reaction, >80%;

^{96}Mo(n, x)^{95}Nb – the possible contribution is changing, approximately, from 1 to 15%; the evaluations are very scattered (see Figure to the right where the ratio of ^{96}Mo(n, x)^{95}Nb cross-section to this of ^{95}Mo(n, p)^{95}Nb is shown);

^{98}Mo(n, α)^{95}Zr → ^{95}Nb – the contribution is small due to the long half-live of ^{95}Zr.

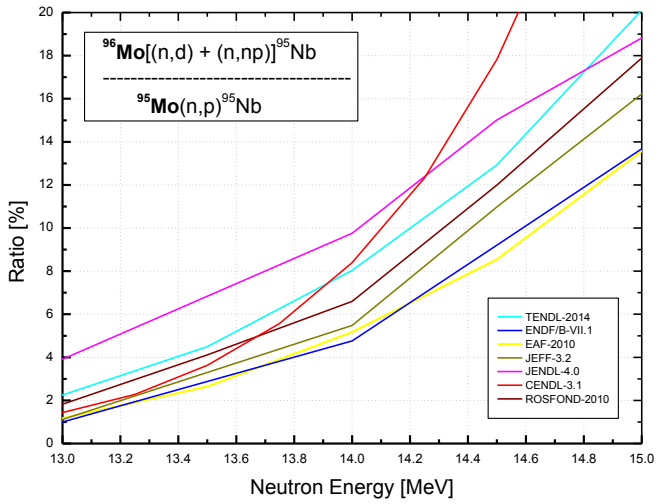

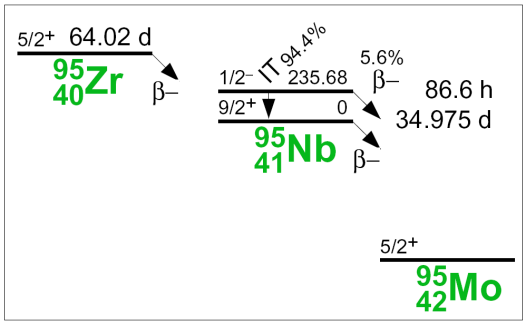

Decay data used for **^{nat}Mo(n, x)^{95}Nb**.

Target nucleus	Abundance [%]	Chemical form	Reaction product	$T_{1/2}$	E_γ [keV]	Y_γ [%]
^{95}Mo	**15.84** *11*	Mo-metal	^{95}Nb	**34.991 d** *6*	**765.8**	**99.808** *7*
^{96}Mo	**16.67** *15*					

^{nat}Mo(n, x)^{95m}Nb

^{nat}Mo(n, x)^{95m}Nb			
E_n [MeV]	σ [mb]	$\pm\Delta\sigma_{total}$ [%]	$\pm\Delta\sigma_{ref}$ [%]
13.48	1.30	*9.44*	*1.34*
13.64	1.20	*9.76*	*1.33*
13.87	1.29	*9.50*	*1.31*
14.05	1.30	*9.78*	*1.31*
14.28	1.41	*10.55*	*1.30*
14.45	1.38	*8.75*	*1.31*
14.64	1.57	*8.70*	*1.31*
14.82	1.49	*8.20*	*1.32*
Ref. CS is ^{93}Nb(n,2n)^{92m}Nb;			$\alpha_d = 1.2$

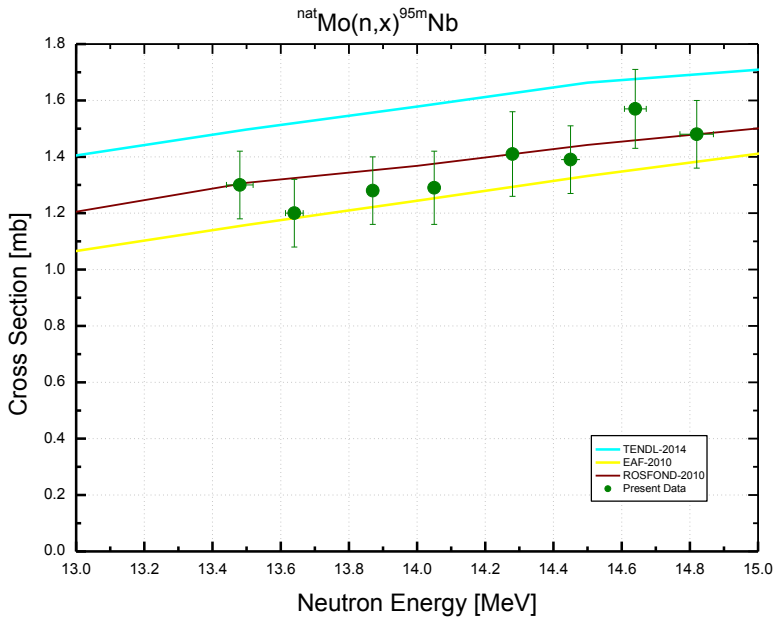

The samples made of natural molybdenum were used. Several reactions can contribute to the production of ^{95m}Nb:

- ^{95}Mo(n, p)^{95m}Nb – is the most probable reaction, >80%;
- ^{96}Mo(n, x)^{95m}Nb – the possible contribution is changing, approximately, from 2 to 20%; the evaluations are very scattered (see Figure to the right where the ratio of ^{96}Mo(n, x)^{95m}Nb cross-section to this of ^{95}Mo(n, p)^{95m}Nb is shown);
- ^{98}Mo(n, α)^{95}Zr → ^{95m}Nb – could be neglected since only 1.08% of ^{95}Zr decays to ^{95m}Nb. Besides, the gamma counting was done in the first days after irradiation.

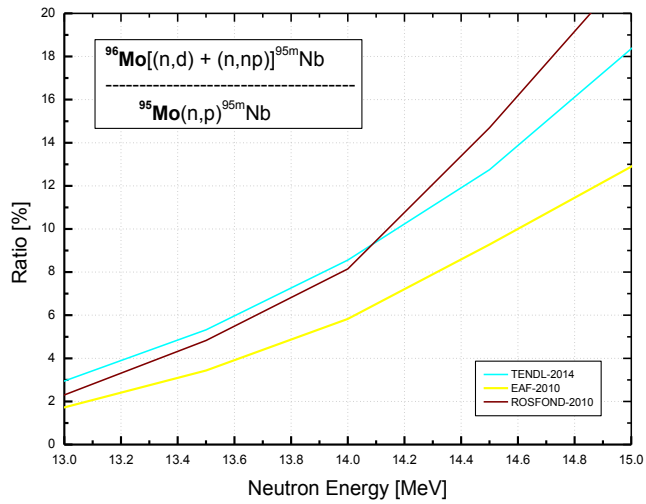

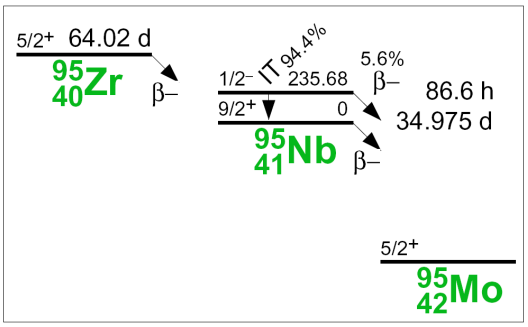

Decay data used for **^{nat}Mo(n, x)^{95m}Nb**.

Target nucleus	Abundance [%]	Chemical form	Reaction product	$T_{1/2}$	E_γ [keV]	Y_γ [%]
^{95}Mo	**15.84** *11*	Mo-metal	^{95m}Nb	**3.61 d** *3*	**235.7**	**25.0 8**
^{96}Mo	**16.67** *15*					

^{nat}Mo(n, x)^{96}Nb

^{nat}Mo(n, x)^{96}Nb			
E_n [MeV]	σ [mb]	$\pm\Delta\sigma_{total}$ [%]	$\pm\Delta\sigma_{ref}$ [%]
13.64	2.95	*4.97*	*0.80*
13.87	3.12	*5.36*	*0.78*
14.05	3.36	*4.33*	*0.77*
14.28	3.46	*4.18*	*0.77*
14.44	3.55	*4.05*	*0.77*
14.64	3.79	*4.32*	*0.78*
Ref. CS is ^{93}Nb(n,2n)^{92m}Nb;			$\alpha_d = 1.2$

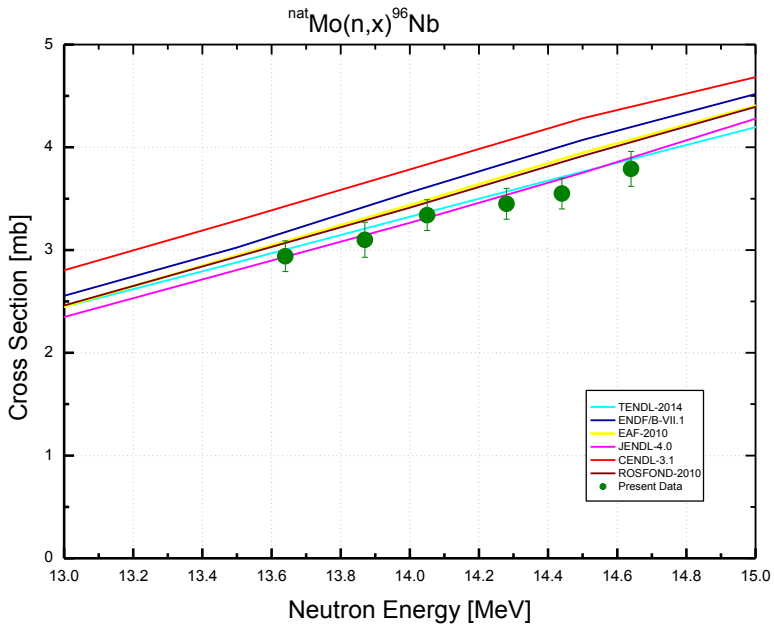

The samples made of natural molybdenum were used. Several reactions can contribute to the production of ^{96}Nb:

^{96}Mo(n, p)^{96}Nb – is the most probable reaction, >90%;

^{97}Mo(n, x)^{96}Nb – the possible contribution is changing, approximately, from 1 to 8%; the evaluations are scattered (see Figure to the right where the ratio of ^{97}Mo(n, x)^{96}Nb cross-section to this of ^{96}Mo(n, p)^{96}Nb is shown).

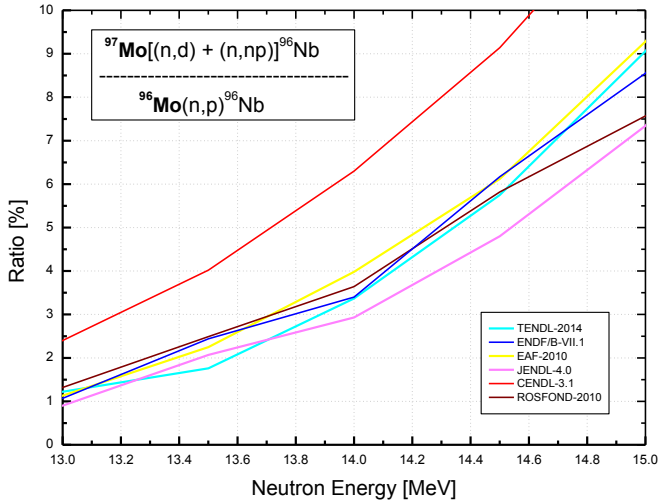

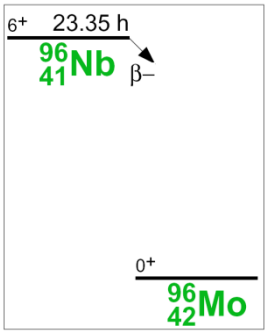

Decay data used for **^{nat}Mo(n, x)^{96}Nb**.

Target nucleus	Abundance [%]	Chemical form	Reaction product	$T_{1/2}$	E_γ [keV]	Y_γ [%]
^{96}Mo	**16.67** *15*	Mo-metal	^{96}Nb	**23.35 h** *5*	568.9	58.0 *3*
^{97}Mo	**9.60** *14*				**1200.2**	**19.97** *10*

^{nat}Mo(n, x)^{97}Nb

^{nat}Mo(n, x)^{97}Nb			
E_n [MeV]	σ [mb]	$\pm\Delta\sigma_{total}$ [%]	$\pm\Delta\sigma_{ref}$ [%]
13.48	1.42	*12.0*	*1.59*
13.64	1.44	*18.0*	*1.57*
13.87	1.51	*15.2*	*1.56*
14.05	1.62	*3.97*	*1.56*
14.28	1.70	*6.63*	*1.56*
14.45	1.74	*10.9*	*1.56*
14.64	1.86	*4.98*	*1.56*
14.82	2.02	*5.09*	*1.57*
Ref. CS is ^{27}Al(n, α)^{24}Na;			$\alpha_d = 1.5$

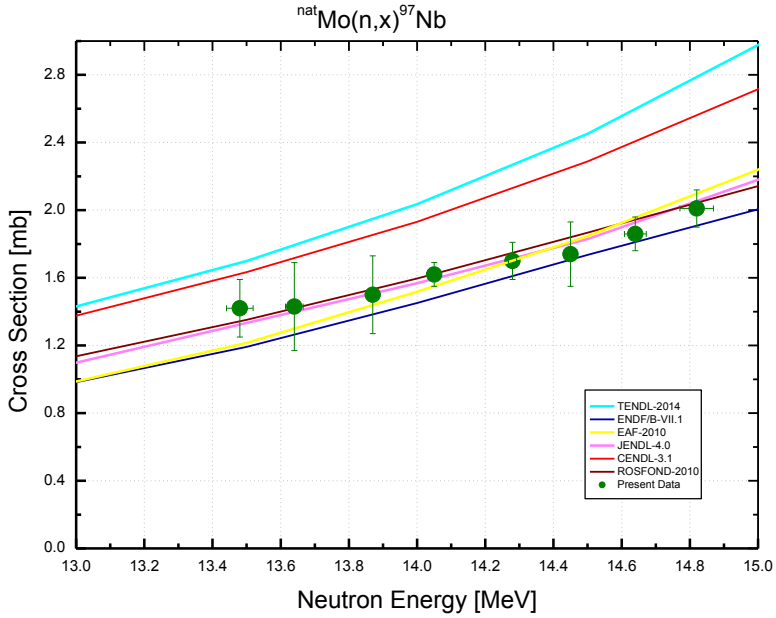

The samples made of natural molybdenum were used. Several reactions can contribute to the production of ^{97}Nb:

- ^{97}Mo(n, p)^{97}Nb – is the most probable reaction, >75%;
- ^{98}Mo(n, x)^{97}Nb – the possible contribution is changing with neutron energy, approximately, from 1 to 25%; the evaluations are very scattered (see Figure to the right where the ratio of ^{98}Mo(n, x)^{97}Nb cross-section to this of ^{97}Mo(n, p)^{97}Nb is shown);
- ^{100}Mo(n, α)^{97}Zr → ^{97}Nb – the contribution is small due to the half-life of ^{97}Zr which is much more than the half-life of ^{97}Nb.

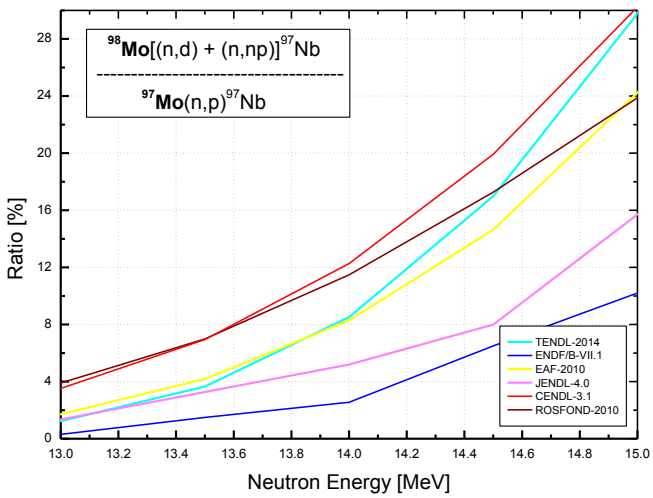

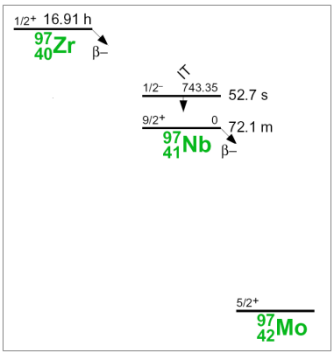

Decay data used for **^{nat}Mo(n, x)^{97}Nb**.

Target nucleus	Abundance [%]	Chemical form	Reaction product	$T_{1/2}$	E_γ [keV]	Y_γ [%]
^{97}Mo	**9.60** *14*	Mo-metal	^{97}Nb	**72.1 m** *7*	**657.9**	**98.23** *8*
^{98}Mo	**24.39** *37*					

^{98}Mo(n, α)^{95}Zr

^{98}Mo(n, α)^{95}Zr			
E_n [MeV]	σ [mb]	$\pm\Delta\sigma_{total}$ [%]	$\pm\Delta\sigma_{ref}$ [%]
13.47	4.97	*6.01*	*1.31*
13.64	5.07	*6.92*	*1.29*
13.88	5.30	*8.52*	*1.28*
14.05	5.94	*5.36*	*1.27*
14.28	5.87	*7.64*	*1.27*
14.47	6.55	*5.44*	*1.27*
14.68	6.34	*4.83*	*1.28*
14.86	6.69	*4.95*	*1.29*
Ref. CS is ^{93}Nb(n,2n)^{92m}Nb;			$\alpha_d = 1.2$

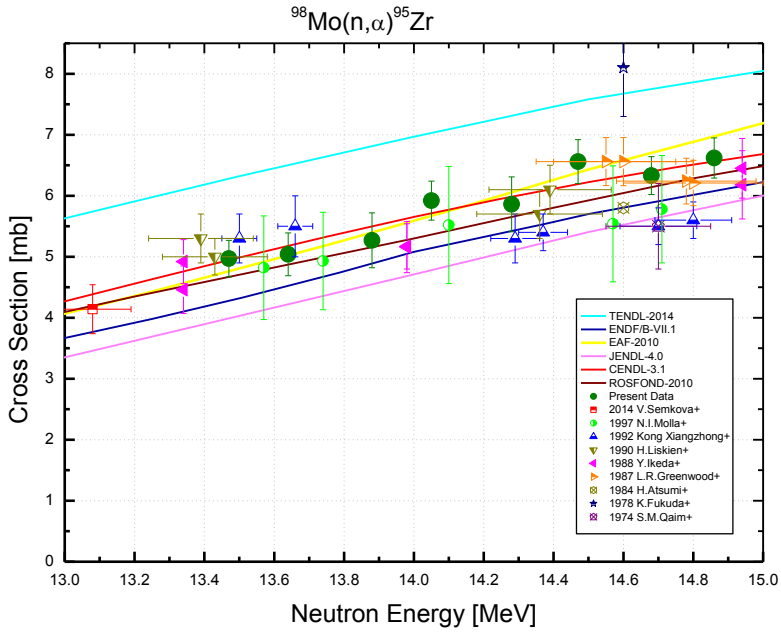

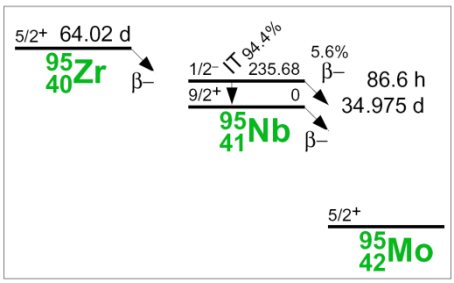

Decay data used for **^{98}Mo(n, α)^{95}Zr**.

Target nucleus	Abundance [%]	Chemical form	Reaction product	$T_{1/2}$	E_γ [keV]	Y_γ [%]
^{98}Mo	**24.19** *26*	Mo-metal	^{95}Zr	**64.032 d** *6*	724.2	44.27 *22*
					756.7	**54.38** *22*

^{98}Mo(n, p)^{98m}Nb

^{98}Mo(n, p)^{98m}Nb			
E_n [MeV]	σ [mb]	$\pm\Delta\sigma_{total}$ [%]	$\pm\Delta\sigma_{ref}$ [%]
13.48	3.48	*14.2*	*1.84*
13.64	4.01	*15.0*	*1.74*
13.87	4.12	*8.71*	*1.73*
14.05	4.14	*5.41*	*1.72*
14.28	4.34	*8.66*	*1.71*
14.45	4.78	*10.6*	*1.70*
14.64	4.58	*6.26*	*1.71*
14.82	4.75	*8.71*	*1.72*
Ref. CS is ^{27}Al(n, α)^{24}Na;			$\alpha_d = 1.6$

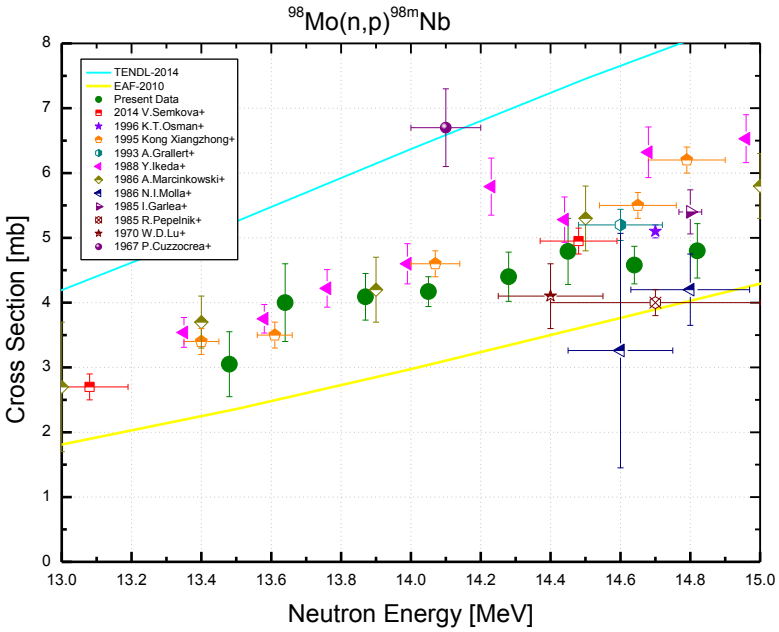

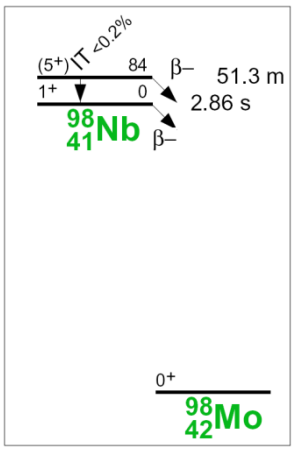

Decay data used for **^{98}Mo(n, p)^{98m}Nb**.

Target nucleus	Abundance [%]	Chemical form	Reaction product	$T_{1/2}$	E_γ [keV]	Y_γ [%]
^{98}Mo	**24.19** *26*	Mo-metal	^{98m}Nb	**51.3 m** *4*	722.6	73.8 *15*
					787.4	**93.4** *2*

^{100}Mo(n, α)^{97}Zr

^{100}Mo(n, α)^{97}Zr			
E_n [MeV]	σ [mb]	$\pm\Delta\sigma_{total}$ [%]	$\pm\Delta\sigma_{ref}$ [%]
13.64	2.21	*5.08*	*2.16*
14.28	2.51	*5.60*	*2.15*
14.44	2.74	*5.48*	*2.15*
Ref. CS is ^{93}Nb(n,2n)^{92m}Nb;			α_d = *1.7*

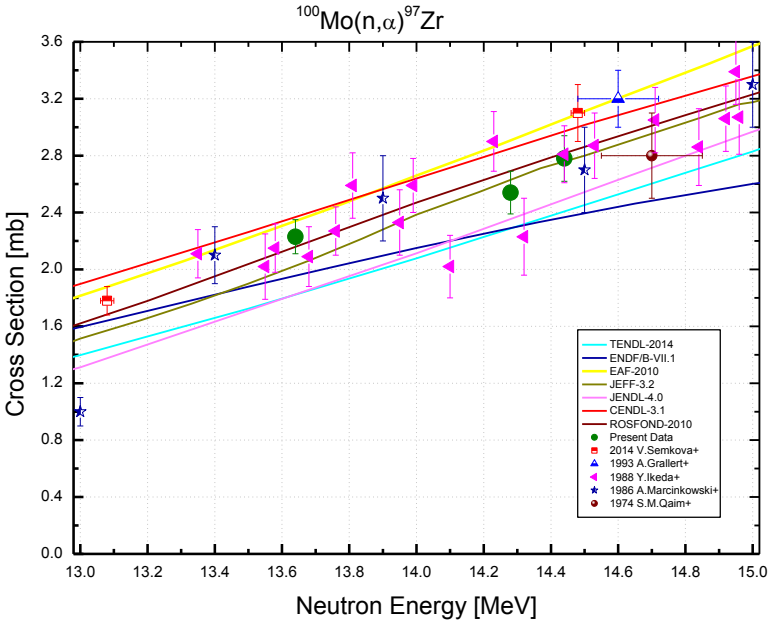

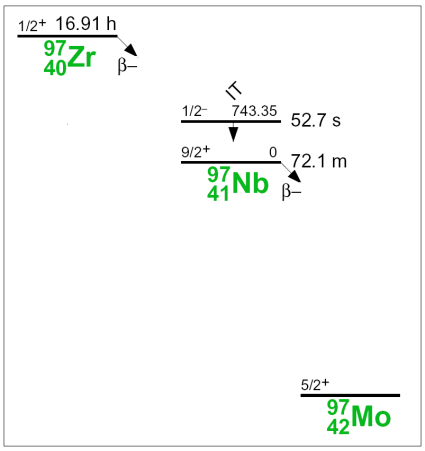

Decay data used for **^{100}Mo(n, α)^{97}Zr.**

Target nucleus	Abundance [%]	Chemical form	Reaction product	$T_{1/2}$	E_γ [keV]	Y_γ [%]
^{100}Mo	**9.67** ***20***	Mo-metal	^{97}Zr	**16.749 h** ***8***	**743.4**	**93.09** ***16***

^{100}Mo(n, 2n)^{99}Mo

^{100}Mo(n, 2n)^{99}Mo			
E_n [MeV]	σ [mb]	$\pm\Delta\sigma_{total}$ [%]	$\pm\Delta\sigma_{ref}$ [%]
13.47	1472	*3.64*	*2.81*
13.64	1409	*3.62*	*2.80*
13.87	1414	*3.29*	*2.80*
14.05	1447	*3.63*	*2.79*
14.28	1419	*3.29*	*2.79*
14.44	1427	*3.52*	*2.79*
14.64	1406	*3.36*	*2.80*
14.86	1454	*3.19*	*2.80*
Ref. CS is ^{93}Nb(n,2n)^{92m}Nb;			$\alpha_d = 1.2$

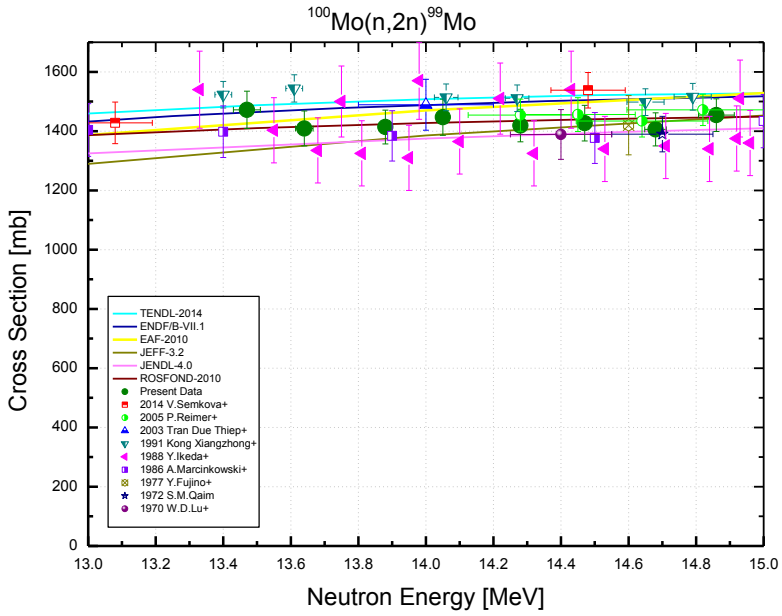

Formally, the ^{100}Mo(n, x)^{99}Nb is also contributed to production of ^{99}Mo because the ^{99}Nb has a short half-life. The cross-section of the ^{100}Mo(n, x)^{99}Nb reaction is evaluated as 0.8 mb approximately that is much less than the cross section of the studied ^{100}Mo(n, 2n)^{99}Mo reaction. Therefore, the contribution of the ^{100}Mo(n, x)^{99}Nb was ignored.

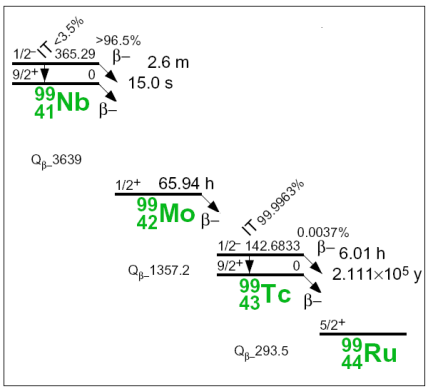

Decay data used for **^{100}Mo(n, 2n)^{99}Mo**.

Target nucleus	Abundance [%]	Chemical form	Reaction product	$T_{1/2}$	E_γ [keV]	Y_γ [%]
^{100}Mo	**9.67** *20*	Mo-metal	^{99}Mo	**65.976 h** *24*	181.1	6.14 *12*
					739.5	**12.26** *22*

^{99}Tc(n, nα)^{95}Nb

^{99}Tc(n, nα)^{95}Nb			
E_n [MeV]	σ [mb]	$\pm\Delta\sigma_{total}$ [%]	$\pm\Delta\sigma_{ref}$ [%]
13.88	0.43	*27.9*	*0.562*
14.47	0.64	*21.8*	*0.551*
14.68	0.98	*12.2*	*0.566*
14.80	1.22	*9.85*	*0.566*
Ref. CS is ^{93}Nb(n,2n)^{92m}Nb;			α_d = *1.6*

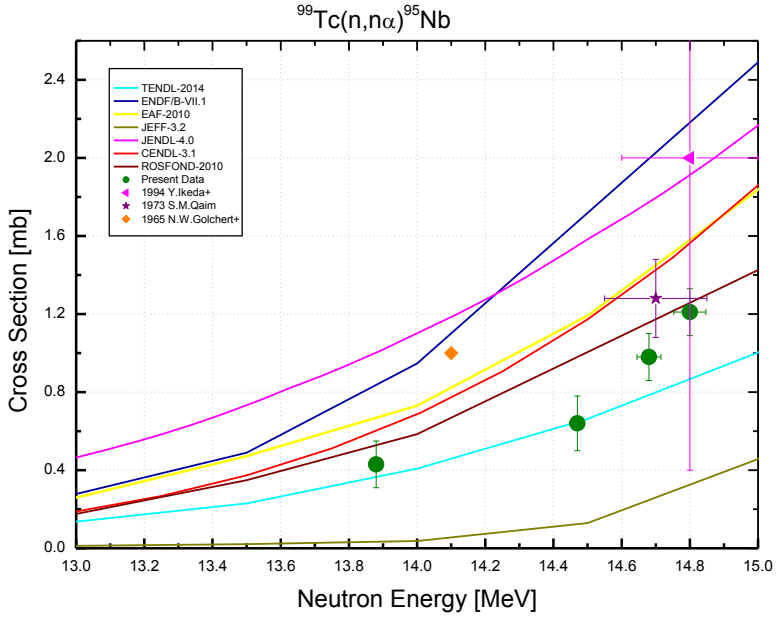

In the experiment, ^{95}Nb ground state decay was measured. The ground state is also populated by an isomeric transition from a metastable state with the probability ***IT*** = 94.4% (see the decay scheme lower). The cooling time was ~ 20 days, and about 5.6% of the ^{95m}Nb excitation fell out of the measured ^{95}Nb total exciatation. Let us estimate the lost value.

Isomeric ratio (or brunching ratio that is just the same) is defined as: $\boldsymbol{IR = \sigma_m/(\sigma_m+\sigma_g)}$
It is estimated in available evaluations as:

IR(JEFF) ~ 0.07; ***IR***(EAF) ~ 0.06; ***IR***(TENDL) ~ 0.04

Assume that ***IR*** = 0.05.

The loss of the ground state population is then 0.05∗0.056 ≈ 0.003 of the total value that was used for the ^{99}Tc(n, nα)^{95}Nb cross-section determination. This was neglected.

In addition, the samples may contain ^{98}Tc with admissible level no more than 0.0008. The ^{98}Tc(n, α)^{95}Nb cross-sections are evaluated in available evaluations as (12 – 22) mb that are resulted in possible contributions of about (0.010 - 0.018) mb. The estimated contributions were not subtracted from the data presented but were added to the uncertainties.

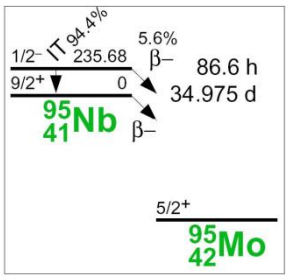

Decay data used for **^{99}Tc(n, nα)^{95}Nb**.

Target nucleus	Abundance [%]	Chemical form	Reaction product	$T_{1/2}$	E_γ [keV]	Y_γ [%]
^{99}Tc	**99.92** *2*	Tc-metal	^{95}Nb	**34.991 d** *6*	**765.8**	**99.808** *7*
^{98}Tc	0.08 *2*					

^{99}Tc(n, α)^{96}Nb

^{99}Tc(n, α)^{96}Nb			
E_n [MeV]	σ [mb]	$\pm\Delta\sigma_{total}$ [%]	$\pm\Delta\sigma_{ref}$ [%]
13.47	5.28	*4.58*	*0.847*
13.88	5.97	*4.90*	*0.795*
14.47	6.04	*4.79*	*0.787*
14.68	6.39	*4.51*	*0.798*
14.80	6.34	*4.62*	*0.798*
Ref. CS is ^{93}Nb(n,2n)^{92m}Nb;			α_d = *1.2*

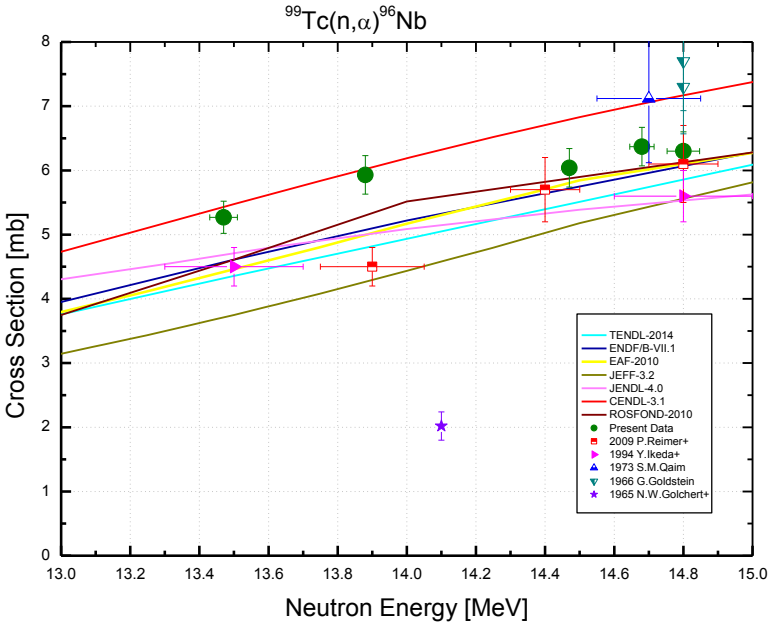

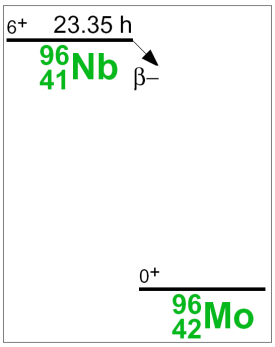

Decay data used for **^{99}Tc(n, α)^{96}Nb**.

Target nucleus	Abundance [%]	Chemical form	Reaction product	$T_{1/2}$	E_γ [keV]	Y_γ [%]
^{99}Tc	**99.92** *2*	Tc-metal	^{96}Nb	**23.35 h** *5*	568.9	58.0 *3*
					1200.2	**19.97** *10*

^{99}Tc(n, 2p)^{98m}Nb

^{99}Tc(n, 2p)^{98m}Nb		
E_n [MeV]	σ [mb]	$\pm\Delta\sigma_{total}$ *[%]*
14.80	<0.00015	*33.3*
Ref. CS is ^{93}Nb(n,2n)^{92m}Nb		

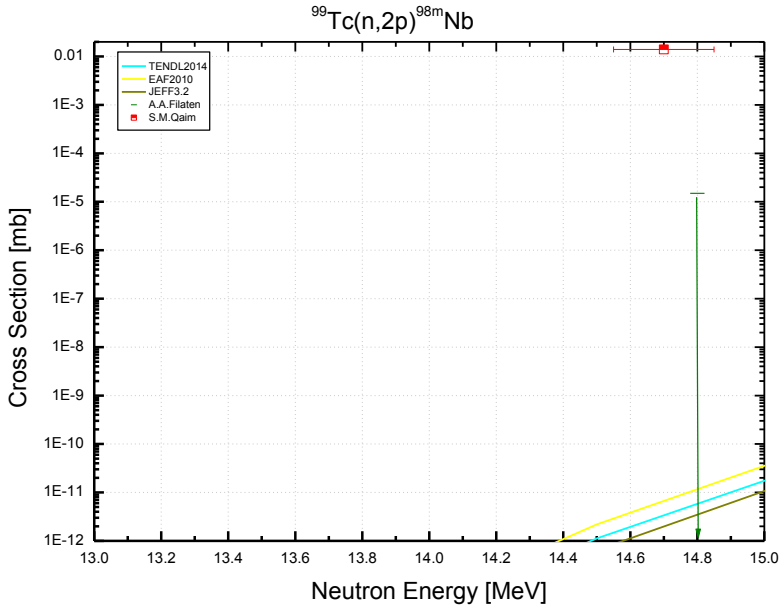

It was questionable the possibility of experimental measurement of an extremely small cross-section expected for (n,2p) reaction. Although samples were irradiated and counted in very close geometries no statistically significant peaks were revealed in the spectra. The upper limit of the cross section value was set to the 3 statistical uncertainties.

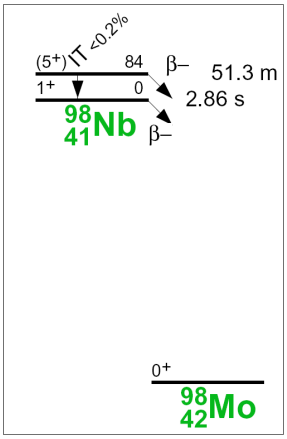

Decay data used for ^{99}Tc(n, 2p)^{98m}Nb.

Target nucleus	Abundance [%]	Chemical form	Reaction product	$T_{1/2}$	E_γ [keV]	Y_γ [%]
^{99}Tc	**99.92** *2*	Tc-metal	^{98m}Nb	**51.3 m** *4*	722.6	73.8 *15*
					787.4	**93.4** *2*

^{99}Tc(n, p)^{99}Mo

^{99}Tc(n, p)^{99}Mo			
E_n [MeV]	σ [mb]	$\pm\Delta\sigma_{total}$ [%]	$\pm\Delta\sigma_{ref}$ [%]
13.47	13.5	*7.25*	*1.90*
13.88	15.3	*7.08*	*1.88*
14.47	14.9	*7.16*	*1.88*
14.68	16.2	*5.98*	*1.88*
14.80	15.3	*6.38*	*1.88*
Ref. CS is ^{93}Nb(n,2n)^{92m}Nb;			$\alpha_d = 1.2$

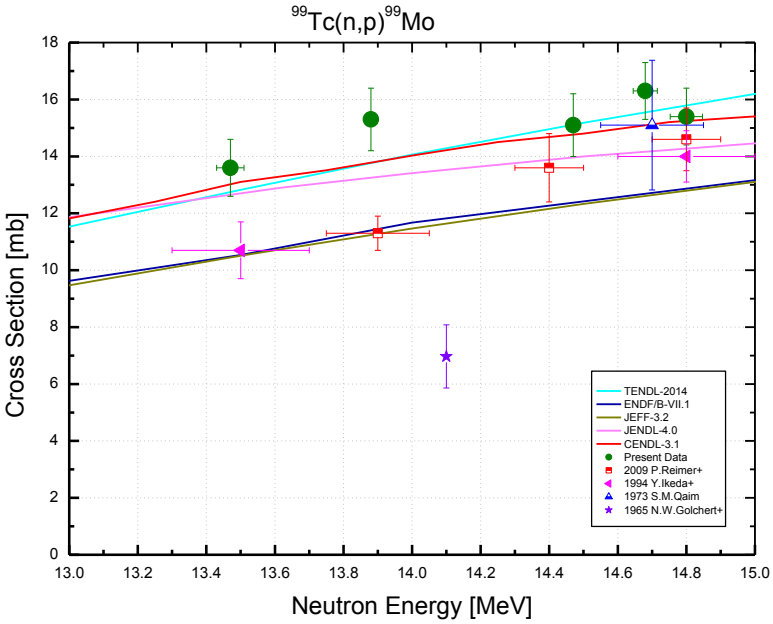

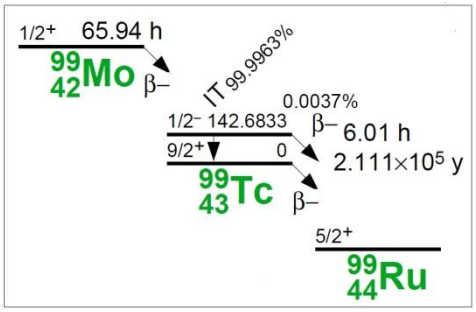

Decay data used for **^{99}Tc(n, p)^{99}Mo**.

Target nucleus	Abundance [%]	Chemical form	Reaction product	$T_{1/2}$	E_γ [keV]	Y_γ [%]
^{99}Tc	**99.92** *2*	Tc-metal	^{99}Mo	**65.976 h** *24*	181.1	6.14 *12*
					739.5	**12.26** *22*

^{103}Rh(n, nα)^{99m}Tc

^{103}Rh(n, nα)^{99m}Tc			
E_n [MeV]	σ [mb]	$\pm\Delta\sigma_{total}$ [%]	$\pm\Delta\sigma_{ref}$ [%]
13.68	0.050	*9.09*	*4.53*
13.88	0.068	*8.52*	*4.53*
14.05	0.109	*10.2*	*4.53*
14.47	0.147	*6.92*	*4.53*
14.86	0.238	*6.05*	*4.53*
Ref. CS is ^{93}Nb(n,2n)^{92m}Nb;			$\alpha_d = 1.8$

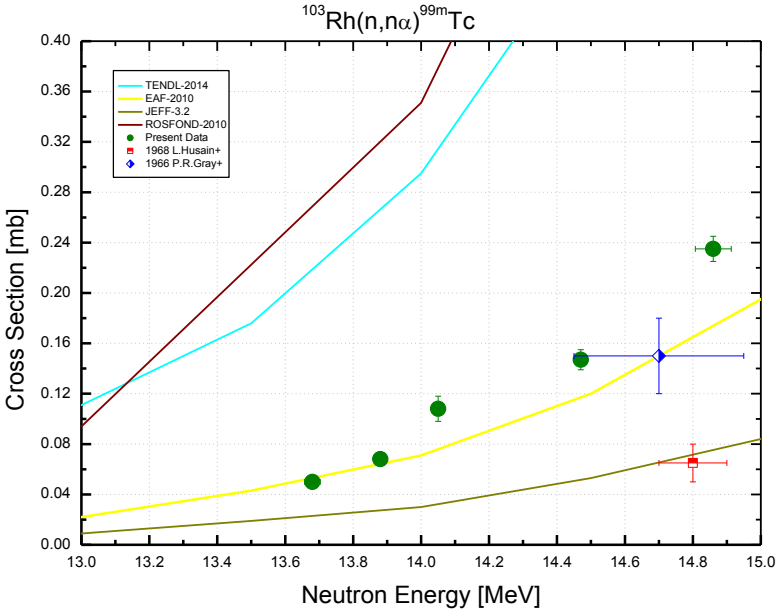

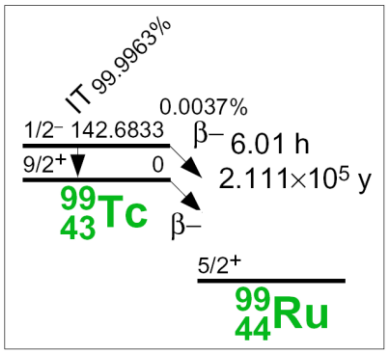

Decay data used for **^{103}Rh(n, nα)^{99m}Tc**.

Target nucleus	Abundance [%]	Chemical form	Reaction product	$T_{1/2}$	E_γ [keV]	Y_γ [%]
^{103}Rh	**100**	Rh-metal	^{99m}Tc	**6.0067 h** *5*	**140.5**	**89** *4*

^{103}Rh(n, p)^{103}Ru

^{103}Rh(n, p)^{103}Ru			
E_n [MeV]	σ [mb]	$\pm\Delta\sigma_{total}$ [%]	$\pm\Delta\sigma_{ref}$ [%]
13.68	20.9	*6.12*	*4.53*
13.88	21.1	*5.76*	*4.53*
14.05	21.2	*7.12*	*4.53*
14.47	21.2	*5.71*	*4.53*
14.86	22.2	*5.64*	*4.53*
Ref. CS is ^{93}Nb(n,2n)^{92m}Nb;			$\alpha_d = 1.2$

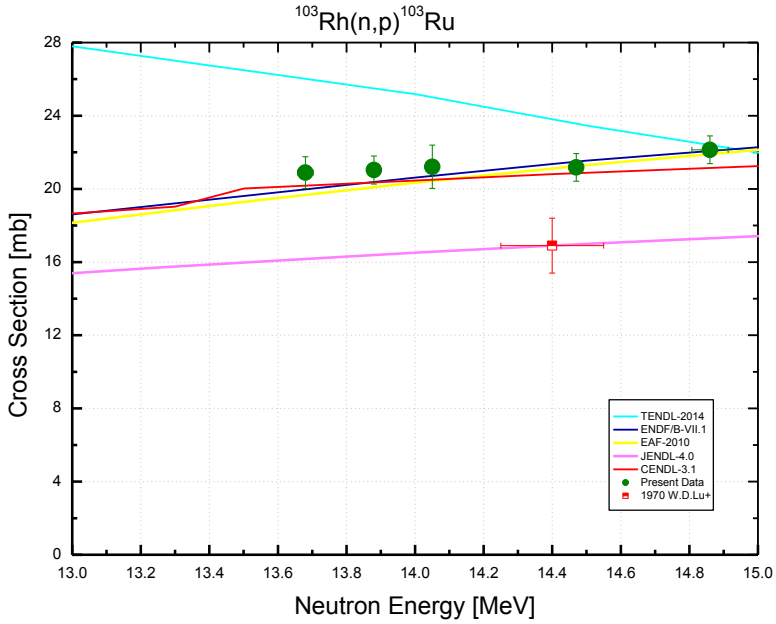

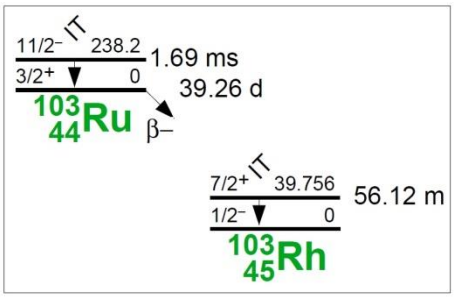

Decay data used for **^{103}Rh(n, p)^{103}Ru**.

Target nucleus	**Abundance [%]**	**Chemical form**	**Reaction product**	**$T_{1/2}$**	**E_γ [keV]**	**Y_γ [%]**
^{103}Rh	**100**	Rh-metal	^{103}Ru	**39.247 d** *13*	**497.1**	**91.0** *12*

^{103}Rh(n, 2n)^{102m}Rh

^{103}Rh(n, 2n)^{102m}Rh			
E_n [MeV]	σ [mb]	$\pm\Delta\sigma_{total}$ [%]	$\pm\Delta\sigma_{ref}$ [%]
13.68	575	*4.74*	*4.59*
13.88	579	*4.72*	*4.59*
14.05	633	*6.03*	*4.59*
14.47	617	*4.70*	*4.59*
14.86	652	*4.79*	*4.59*
Ref. CS is ^{93}Nb(n,2n)^{92m}Nb;			α_d = *1.1*

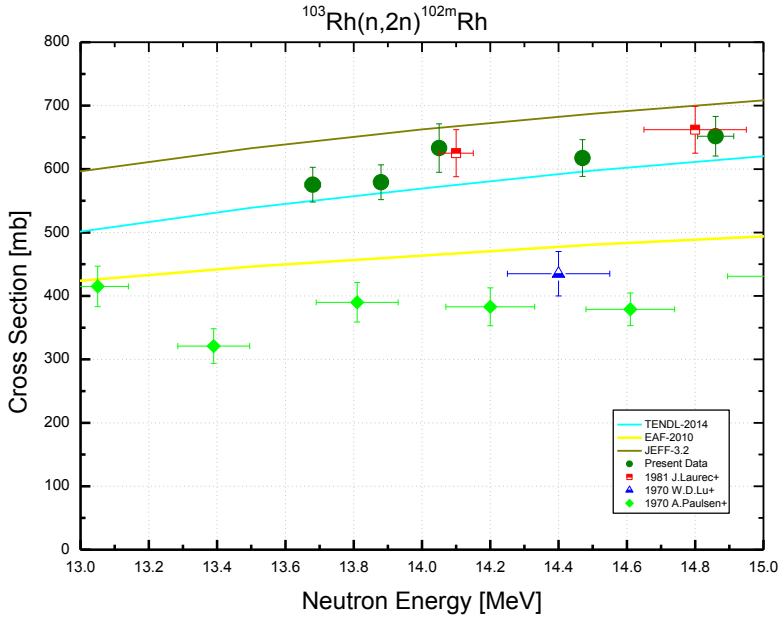

The old data were corrected for the change of the half-life used. The old value was 2.9 y, the new one is 3.742 y.

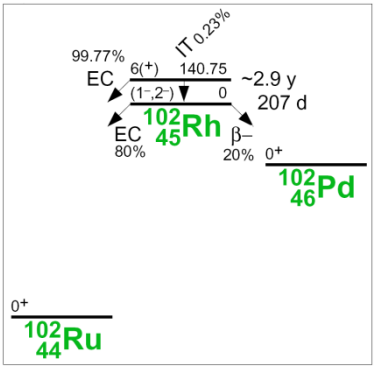

Decay data used for **^{103}Rh(n, 2n)^{102m}Rh**.

Target nucleus	Abundance [%]	Chemical form	Reaction product	$T_{1/2}$	E_γ [keV]	Y_γ [%]
^{103}Rh	**100**	Rh-metal	^{102m}Rh	**3.742 y *10***	**697.5**	**44.0 *20***
					766.8	34.0 *20*
					1112.8	19.0 *10*

^{103}Rh(n, 2n)^{102g}Rh

^{103}Rh(n, 2n)^{102g}Rh			
E_n [MeV]	σ [mb]	$\pm\Delta\sigma_{total}$ [%]	$\pm\Delta\sigma_{ref}$ [%]
13.68	648	*8.74*	*6.99*
13.88	694	*8.90*	*6.99*
14.05	687	*11.78*	*6.99*
14.47	678	*8.58*	*6.99*
14.86	731	*8.50*	*6.99*
Ref. CS is ^{93}Nb(n,2n)^{92m}Nb;			$\alpha_d = 1.2$

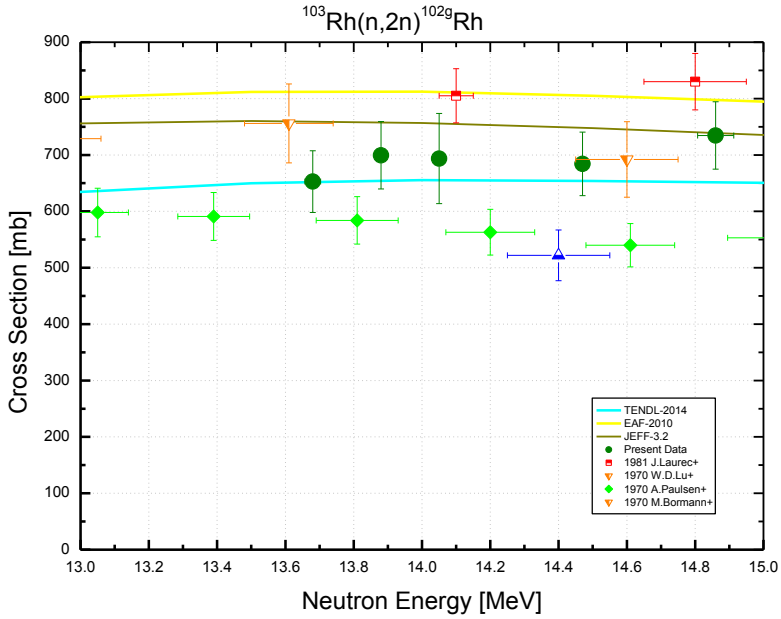

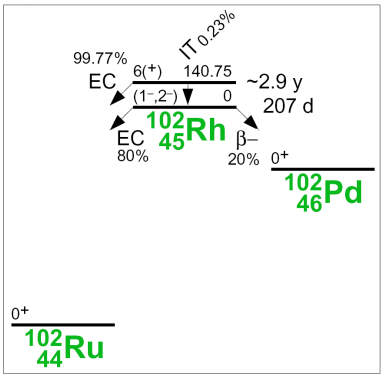

Decay data used for **^{103}Rh(n, 2n)^{102g}Rh**.

Target nucleus	Abundance [%]	Chemical form	Reaction product	$T_{1/2}$	E_γ [keV]	Y_γ [%]
^{103}Rh	**100**	Rh-metal	^{102g}Rh	**207.3 d** *17*	**468.6**	**2.90** *20*

^{103}Rh(n, 2n)^{102}Rh

^{103}Rh(n, 2n)^{102}Rh		
E_n [MeV]	σ [mb]	$\pm\Delta\sigma_{total}$ [%]
13.68	1225	*6.03*
13.88	1273	*6.18*
14.05	1320	*8.06*
14.47	1296	*5.92*
14.86	1386	*5.91*
Ref. CS is ^{93}Nb(n,2n)^{92m}Nb		

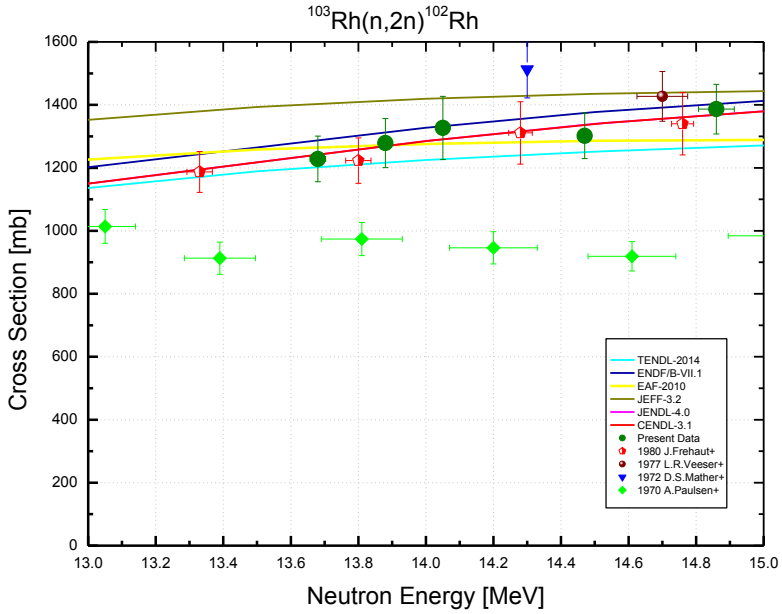

The present experimental data for ^{103}Rh(n, 2n)^{102}Rh cross-section are the sum of the ^{103}Rh(n, 2n)^{102m}Rh and ^{103}Rh(n, 2n)^{102g}Rh cross-sections measured independently and presented on the previous pages. This was done for extending the comparative base becase most evaluations contain the data for the reaction cross-sections without splitting between ground and metastable state excitations.

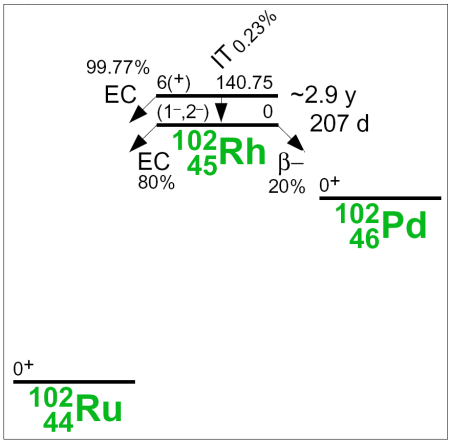

^{102}Pd(n, 2n)^{101}Pd

^{102}Pd(n, 2n)^{101}Pd			
E_n [MeV]	σ [mb]	$\pm\Delta\sigma_{total}$ [%]	$\pm\Delta\sigma_{ref}$ [%]
13.46	837	5.65	4.46
13.64	867	6.76	4.45
13.88	921	6.64	4.45
14.05	980	5.14	4.44
14.28	1026	6.81	4.44
14.48	1028	4.98	4.44
14.68	1033	6.87	4.45
14.87	1065	5.29	4.45
Ref. CS is ^{93}Nb(n,2n)^{92m}Nb;			$\alpha_d = 1.5$

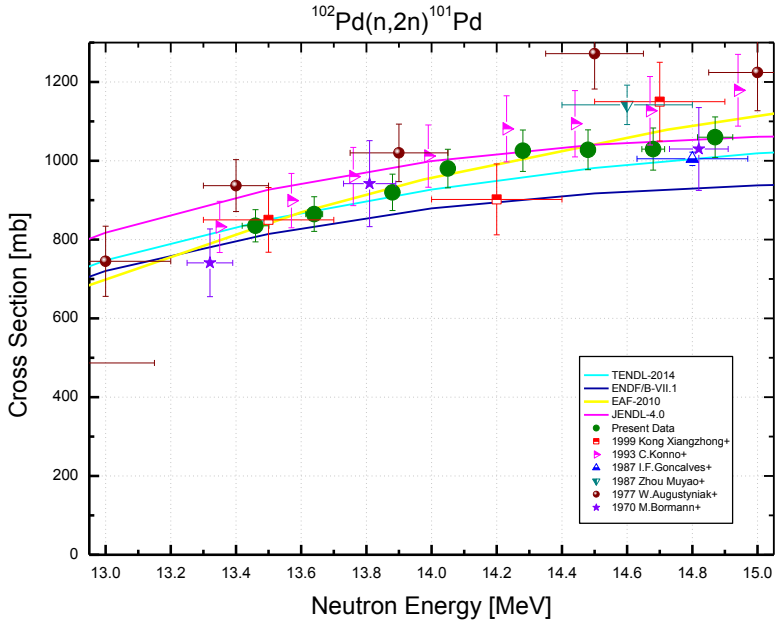

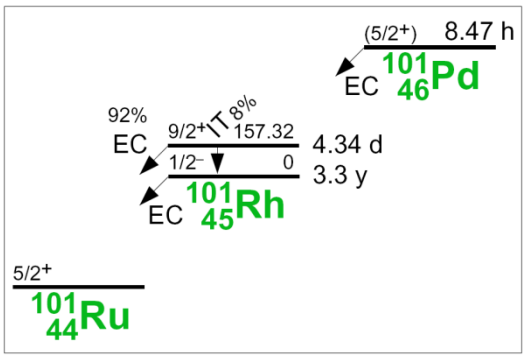

Decay data used for **^{102}Pd(n, 2n)^{101}Pd**.

Target nucleus	Abundance [%]	Chemical form	Reaction product	$T_{1/2}$	E_γ [keV]	Y_γ [%]
^{102}Pd	**1.02** *1*	Pd-metal	^{101}Pd	**8.47 h** *6*	269.7	6.4 *3*
					296.3	**19.2** *8*
					590.4	12.1 *5*

^{102}Pd[(n, np) + (n, d)]^{101m}Rh

^{102}Pd(n, x)^{101m}Rh			
E_n [MeV]	σ [mb]	$\pm\Delta\sigma_{total}$ [%]	$\pm\Delta\sigma_{ref}$ [%]
13.46	217	*23.3*	*5.08*
13.64	256	*32.7*	*5.08*
13.88	303	*31.1*	*5.07*
14.06	274	*22.4*	*5.07*
14.28	294	*33.8*	*5.07*
14.48	315	*18.6*	*5.07*
14.68	332	*31.4*	*5.07*
14.87	333	*19.8*	*5.08*
Ref. CS is ^{93}Nb(n,2n)^{92m}Nb;			α_d = *1.2*

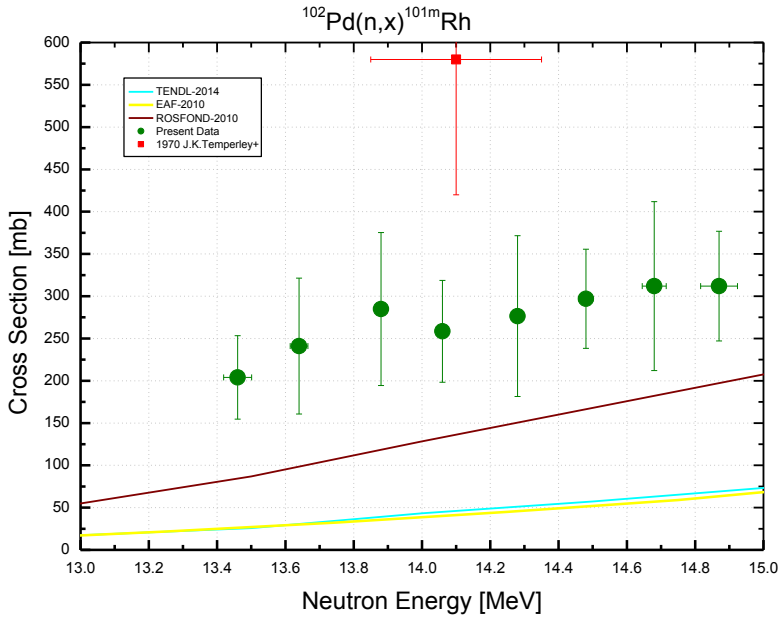

The data was corrected for decay of the ^{101}Pd produced in the ^{102}Pd(n, 2n)^{101}Pd reaction.

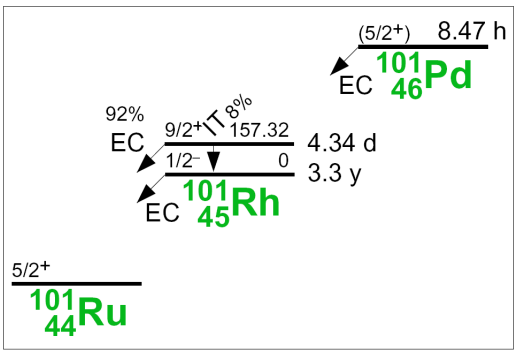

Decay data used for **^{102}Pd(n, x)^{101m}Rh**.

Target nucleus	**Abundance [%]**	**Chemical form**	**Reaction product**	**$T_{1/2}$**	**E_γ [keV]**	**Y_γ [%]**
^{102}Pd	**1.02** *1*	Pd-metal	^{101m}Rh	**4.34 d** *1*	**306.9**	**81** *4*

^{102}Pd[(n, np) + (n, d)]^{101g}Rh

^{102}Pd(n, x)^{101g}Rh			
E_n [MeV]	σ [mb]	$\pm\Delta\sigma_{total}$ [%]	$\pm\Delta\sigma_{ref}$ [%]
13.45	37.0	*70.3*	*13.7*
14.05	34.2	*61.8*	*13.7*
14.49	42.0	*95.2*	*13.7*
Ref. CS is ^{93}Nb(n,2n)^{92m}Nb;			α_d = *1.2*

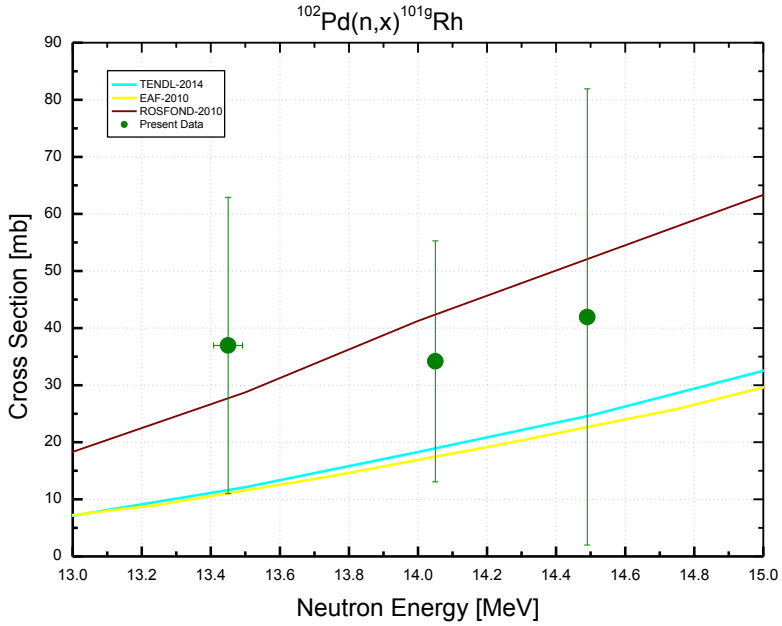

The data were corrected for decay of the ^{101}Pd produced in the ^{102}Pd(n, 2n)^{101}Pd reaction.

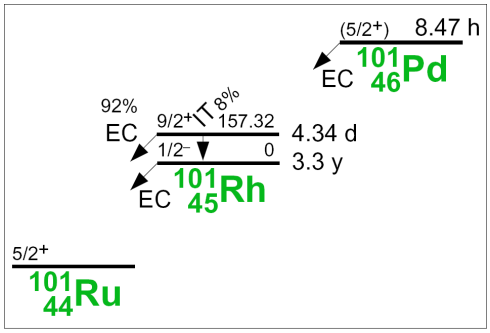

Decay data used for **^{102}Pd(n, x)^{101g}Rh**.

Target nucleus	Abundance [%]	Chemical form	Reaction product	$T_{1/2}$	E_γ [keV]	Y_γ [%]
^{102}Pd	**1.02** *1*	Pd-metal	^{101g}Rh	**3.3 y** *3*	127.2	68 *6*
					198.0	**73** *6*
					325.2	11.8 *10*

^{102}Pd[(n, np) + (n, d)]^{101}Rh

^{102}Pd(n, x)^{101}Rh		
E_n [MeV]	σ [mb]	$\pm\Delta\sigma_{total}$ *[%]*
13.45	241	*26.4*
14.05	293	*24.2*
14.49	339	*24.3*
Ref. CS is ^{93}Nb(n,2n)^{92m}Nb		

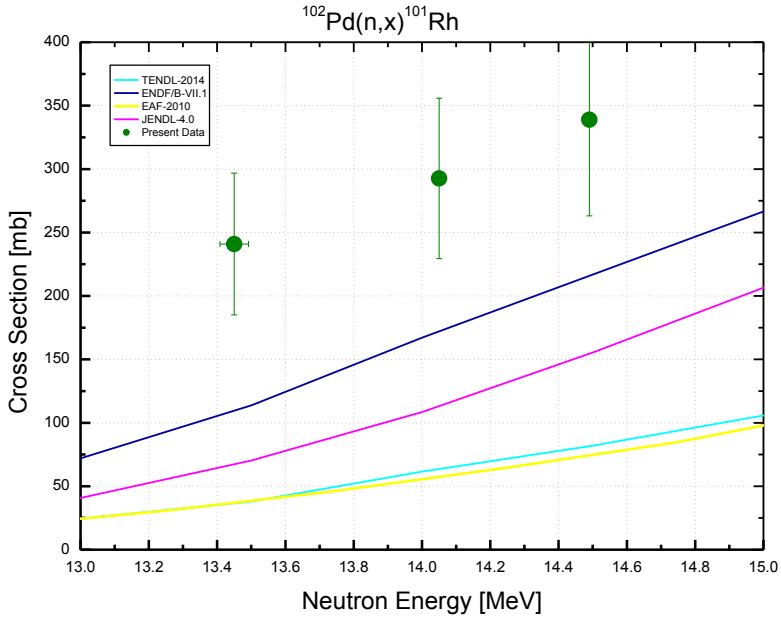

This is the sum of the ^{102}Pd(n, x)^{102m}Rh + ^{102}Pd(n, x)^{102g}Rh cross sections measured independently and presented on the previous pages.

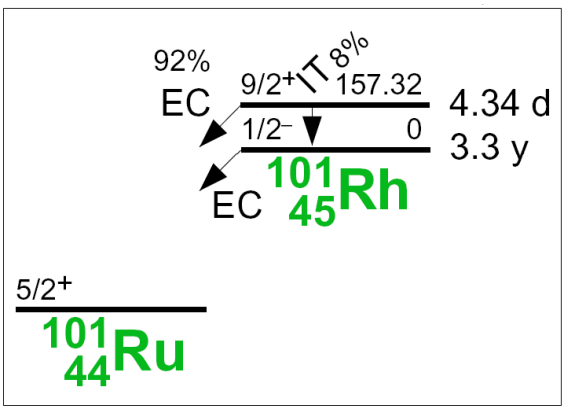

^{105}Pd(n, p)^{105}Rh

^{105}Pd(n, p)^{105}Rh			
E_n [MeV]	σ [mb]	$\pm\Delta\sigma_{total}$ [%]	$\pm\Delta\sigma_{ref}$ [%]
13.45	30.0	*5.87*	*3.23*
14.05	34.4	*4.49*	*3.22*
14.49	38.1	*4.00*	*3.22*
14.88	42.0	*3.65*	*3.22*
Ref. CS is ^{93}Nb(n,2n)^{92m}Nb;			α_d = *1.2*

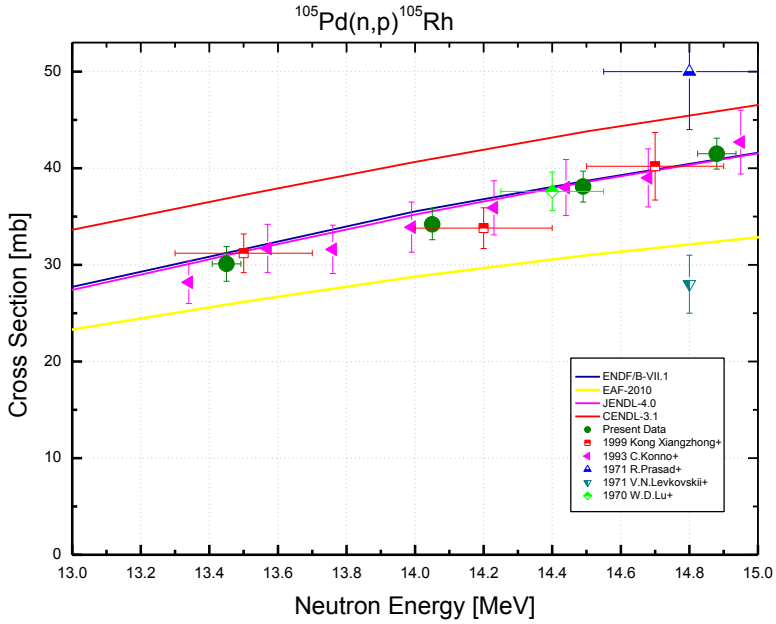

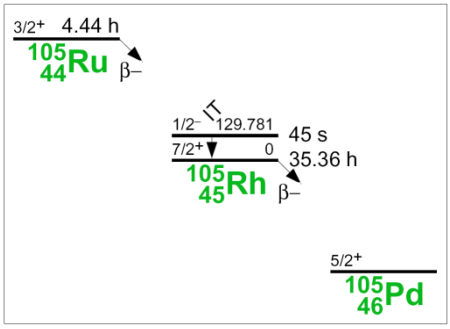

Decay data used for **^{105}Pd(n, p)^{105}Rh**.

Target nucleus	Abundance [%]	Chemical form	Reaction product	$T_{1/2}$	E_γ [keV]	Y_γ [%]
^{105}Pd	**22.33** *8*	Pd-metal	^{105}Rh	**35.36 h** *6*	306.1	5.1 *3*
					318.9	**19.1** *6*

^{106}Pd(n, α)^{103}Ru

^{106}Pd(n, α)^{103}Ru			
E_n [MeV]	σ [mb]	$\pm\Delta\sigma_{total}$ [%]	$\pm\Delta\sigma_{ref}$ [%]
13.46	4.12	*3.91*	*1.47*
13.64	4.63	*12.6*	*1.45*
13.88	4.83	*16.3*	*1.44*
14.06	4.92	*3.06*	*1.43*
14.28	4.91	*11.8*	*1.43*
14.48	5.49	*3.14*	*1.43*
14.68	5.41	*8.65*	*1.44*
14.87	6.26	*3.36*	*1.45*
Ref. CS is ^{93}Nb(n,2n)^{92m}Nb;			α_d = *1.2*

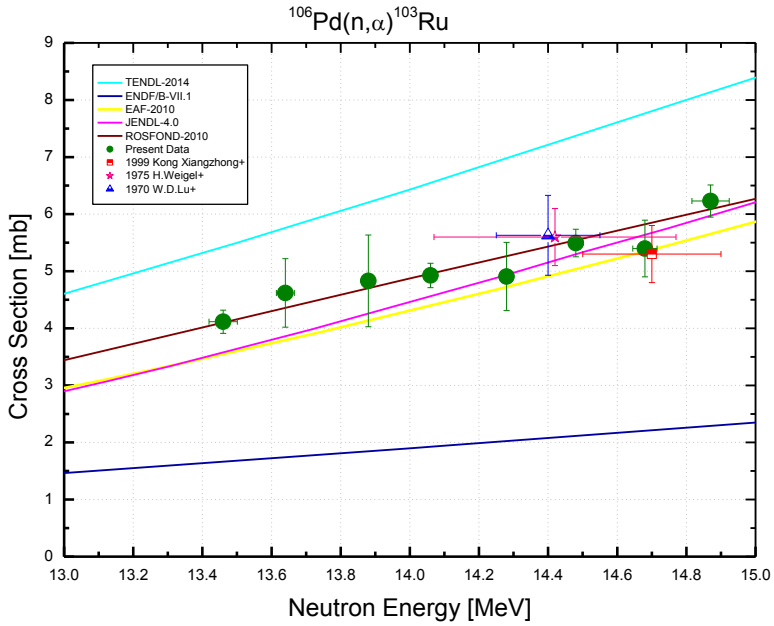

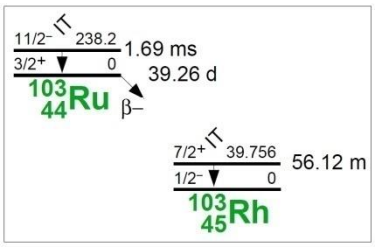

Decay data used for **^{106}Pd(n, α)^{103}Ru.**

Target nucleus	Abundance [%]	Chemical form	Reaction product	$T_{1/2}$	E_γ [keV]	Y_γ [%]
^{106}Pd	**27.33** *3*	Pd-metal	^{103}Ru	**39.247 d** *13*	**497.1**	**91.0** *12*

^{106}Pd(n, p)^{106m}Rh

^{106}Pd(n, p)^{106m}Rh			
E_n [MeV]	σ [mb]	$\pm\Delta\sigma_{total}$ [%]	$\pm\Delta\sigma_{ref}$ [%]
13.46	6.64	*5.90*	*5.71*
13.64	6.95	*6.84*	*5.71*
13.88	8.04	*6.65*	*5.70*
14.05	7.80	*5.91*	*5.70*
14.28	8.10	*6.67*	*5.70*
14.48	8.85	*6.07*	*5.70*
14.68	9.45	*6.77*	*5.70*
14.86	9.77	*6.92*	*5.71*
Ref. CS is ^{93}Nb(n,2n)^{92m}Nb;			α_d = *1.2*

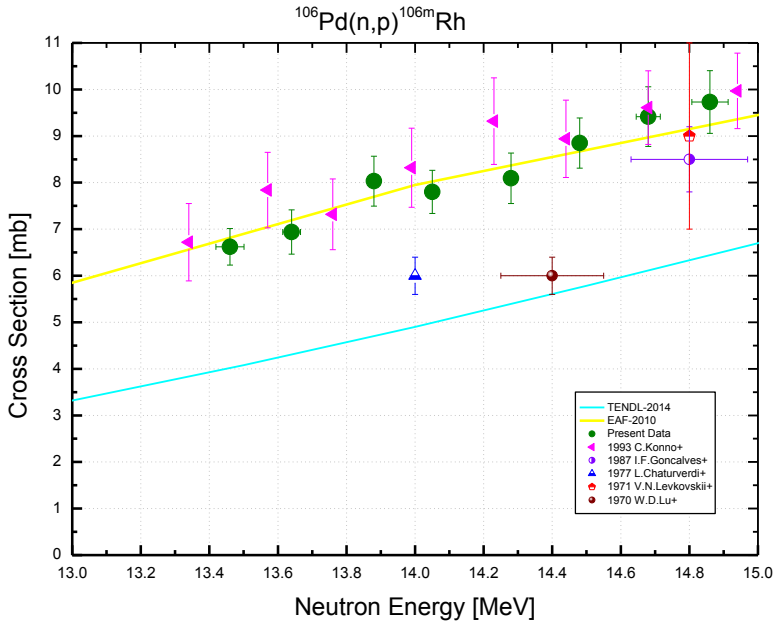

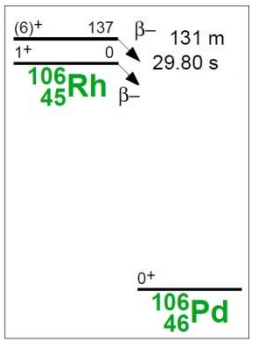

Decay data used for **^{106}Pd(n, p)^{106m}Rh**.

Target nucleus	**Abundance [%]**	**Chemical form**	**Reaction product**	**$T_{1/2}$**	**E_γ [keV]**	**Y_γ [%]**
^{106}Pd	**27.33** *3*	Pd-metal	^{106m}Rh	**131 m** *2*	**450.8**	**24.2** *13*
					616.1	20.2 *14*
					717.2	28.9 *16*
					1046.7	30.4 *16*

^{108}Pd(n, α)^{105}Ru

^{108}Pd(n, α)^{105}Ru			
E_n [MeV]	σ [mb]	$\pm\Delta\sigma_{total}$ [%]	$\pm\Delta\sigma_{ref}$ [%]
13.46	1.94	*6.22*	*3.31*
13.64	2.37	*13.1*	*3.30*
13.88	2.40	*13.4*	*3.30*
14.06	2.35	*6.01*	*3.29*
14.28	2.88	*13.2*	*3.29*
14.48	3.03	*7.34*	*3.29*
14.68	3.26	*9.44*	*3.30*
14.87	3.74	*12.9*	*3.30*
Ref. CS is ^{93}Nb(n,2n)^{92m}Nb;			α_d = *1.2*

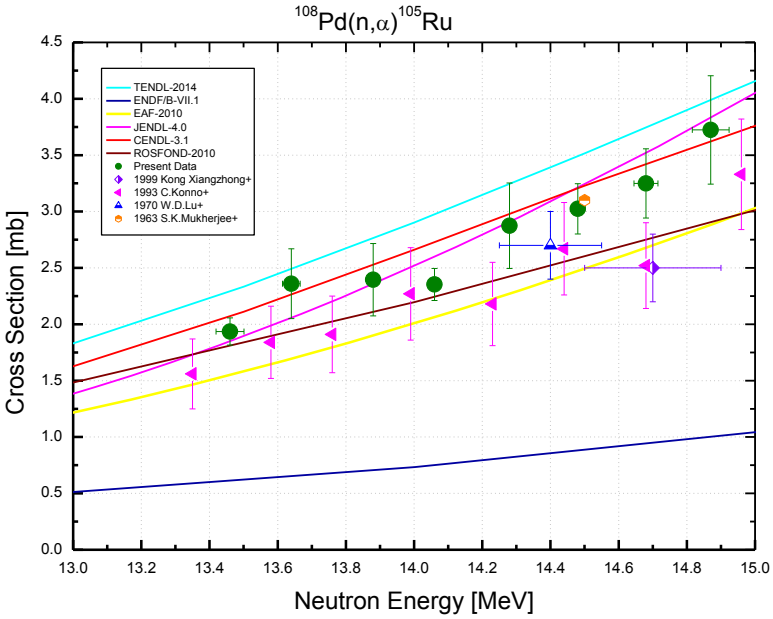

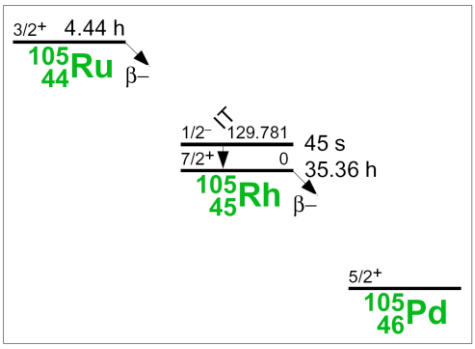

Decay data used for **^{108}Pd(n, α)^{105}Ru**.

Target nucleus	Abundance [%]	Chemical form	Reaction product	$T_{1/2}$	E_γ [keV]	Y_γ [%]
^{108}Pd	**26.46** *9*	Pd-metal	^{105}Ru	**4.44 h** *2*	469.4	17.5 *6*
					676.4	**15.7** *5*

^{110}Pd(n, 2n)^{109}Pd

^{110}Pd(n, 2n)^{109}Pd			
E_n [MeV]	σ [mb]	$\pm\Delta\sigma_{total}$ [%]	$\pm\Delta\sigma_{ref}$ [%]
13.45	1549	*12.9*	*11.2*
14.05	1314	*15.2*	*11.2*
14.49	1392	*14.3*	*11.2*
14.88	1566	*12.9*	*11.2*
Ref. CS is ^{93}Nb(n,2n)^{92m}Nb;			α_d = *1.2*

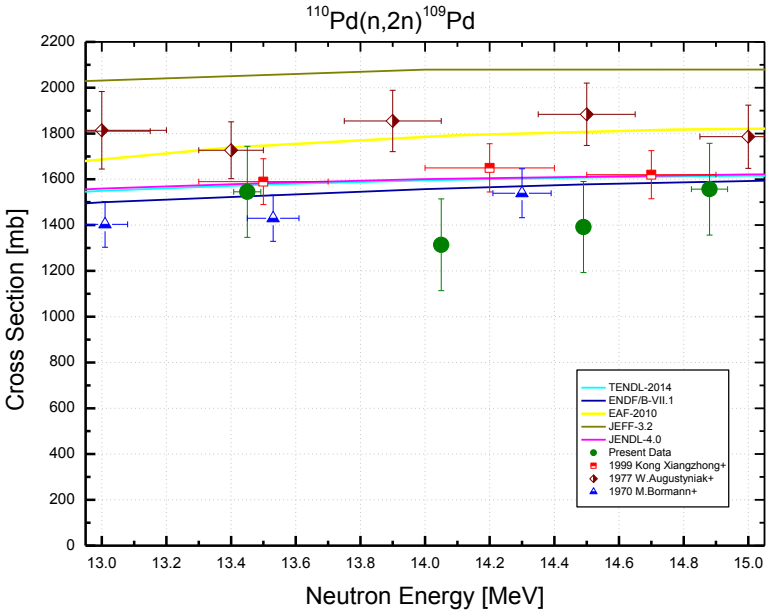

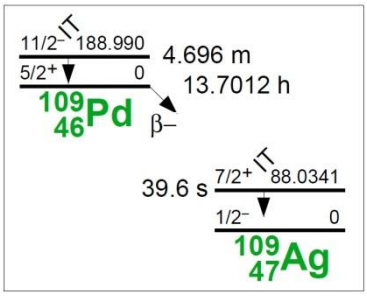

Decay data used for **^{110}Pd(n, 2n)^{109}Pd.**

Target nucleus	Abundance [%]	Chemical form	Reaction product	$T_{1/2}$	E_γ [keV]	Y_γ [%]
^{110}Pd	**11.72** *9*	Pd-metal	^{109}Pd	**13.7012 h** *24*	**88.0**	**3.6** *4*

^{107}Ag(n, 2n)^{106m}Ag

^{107}Ag(n, 2n)^{106m}Ag			
E_n [MeV]	σ [mb]	$\pm\Delta\sigma_{total}$ [%]	$\pm\Delta\sigma_{ref}$ [%]
13.74	545	*3.34*	*2.57*
13.96	582	*3.29*	*2.56*
14.19	603	*3.32*	*2.56*
14.42	593	*3.38*	*2.56*
14.61	600	*3.34*	*2.56*
14.78	603	*3.17*	*2.56*
Ref. CS is ^{93}Nb(n,2n)^{92m}Nb;			α_d = *1.2*

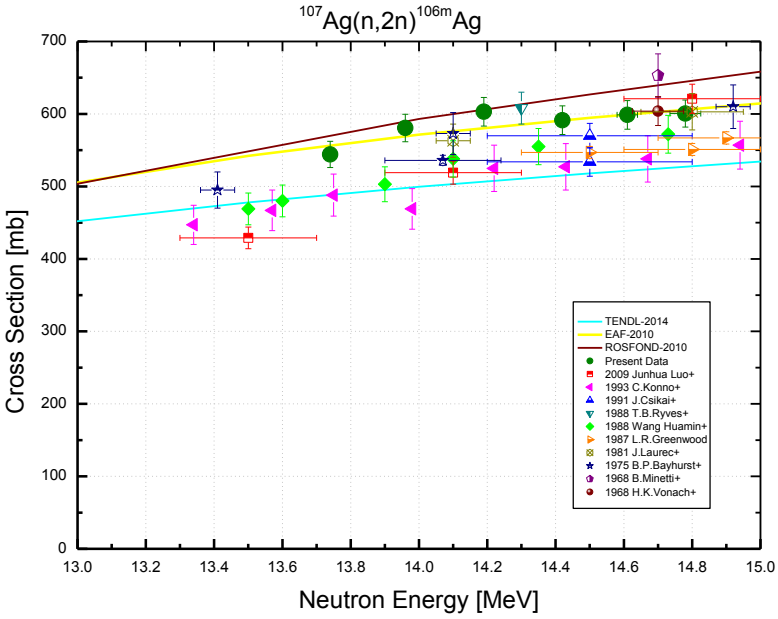

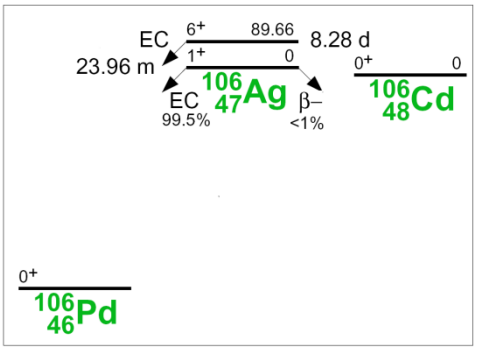

Decay data used for **^{107}Ag(n, 2n)^{106m}Ag**.

Target nucleus	Abundance [%]	Chemical form	Reaction product	$T_{1/2}$	E_γ [keV]	Y_γ [%]
^{107}Ag	**51.839** *8*	Ag-metal	^{106m}Ag	**8.28 d** *2*	**451.0**	**28.2** *7*
					616.2	21.6 *6*
					717.3	28.9 *8*
					1045.8	29.6 *10*

^{109}Ag(n, 2n)^{108m}Ag

^{109}Ag(n, 2n)^{108m}Ag			
E_n [MeV]	σ [mb]	$\pm\Delta\sigma_{total}$ [%]	$\pm\Delta\sigma_{ref}$ [%]
13.70	667	*6.20*	*2.26*
14.10	718	*5.74*	*2.25*
14.50	727	*5.63*	*2.25*
14.80	747	*5.51*	*2.26*
Ref. CS is ^{93}Nb(n,2n)^{92m}Nb;		α_d = *1.01*	

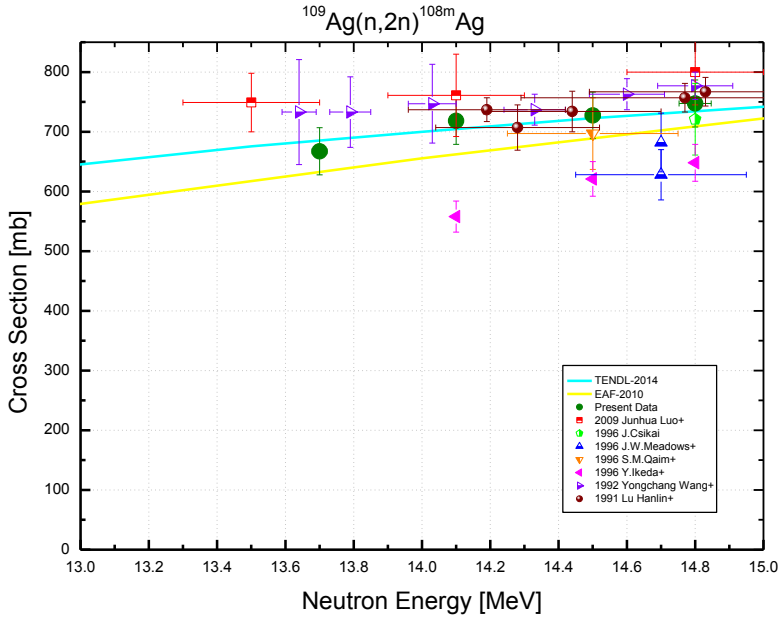

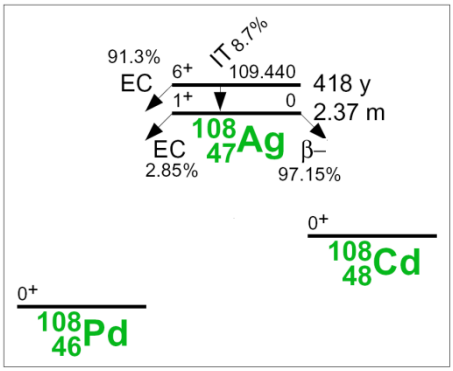

Decay data used for **^{109}Ag(n, 2n)^{108m}Ag**.

Target nucleus	Abundance [%]	Chemical Form	Reaction product	$T_{1/2}$	E_γ [keV]	Y_γ [%]
^{109}Ag	*99.4 *1*	Ag-metal	^{108m}Ag	**438 y *9***	**433.9**	**90.5 *6***
					614.3	89.8 *19*
					722.9	90.8 *19*

* - refer to samples enriched by Silver-109

^{106}Cd(n, x)^{105}Ag+^{106}Cd(n, 2n)^{105}Cd

^{106}Cd(n, x)^{105}Ag+^{106}Cd(n, 2n)^{105}Cd			
E_n [MeV]	σ [mb]	$\pm\Delta\sigma_{total}$ [%]	$\pm\Delta\sigma_{ref}$ [%]
13.45	815	*7.98*	*7.26*
13.56	920	*13.6*	*7.26*
13.74	900	*10.0*	*7.26*
13.88	905	*7.73*	*7.25*
13.96	960	*9.38*	*7.25*
14.19	1070	*11.2*	*7.25*
14.43	1085	*7.37*	*7.25*
14.63	1080	*7.41*	*7.25*
14.78	1250	*9.60*	*7.26*
14.88	1170	*7.69*	*7.26*
Ref. CS is ^{93}Nb(n,2n)^{92m}Nb;			$\alpha_d = 1.2$

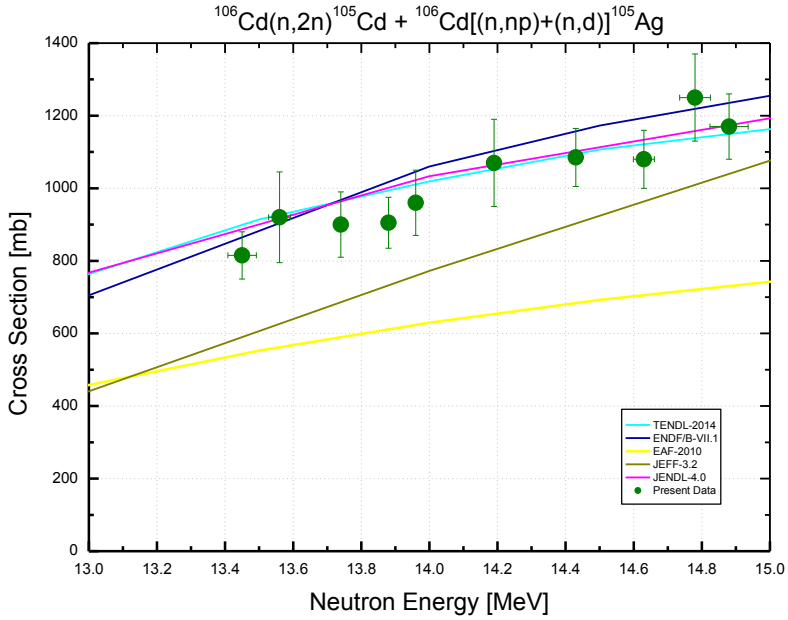

The ^{105}Ag production cross section is presented in this page. It was measured using the ^{105}Ag γ-rays given in the Table at the page bottom. Since the ^{105}Ag half live is 41.29 d, the irradiation, cooling and gamma counting were comparatively long at more than several hours. Under these conditions not only the ^{106}Cd(n, x)^{105}Ag cross-section is measured (here (n, x) is the sum of (n, d) and (n, np) reactions) but also ^{106}Cd(n, 2n)^{105}Cd is added to the measurement result because the ^{105}Cd half-life is 55.5 min and practically all the ^{105}Cd nuclei decay into the ^{105}Ag after cooling time more than 5 hours.

The ^{106}Cd(n, 2n)^{105}Cd was separately measured in short irradiations that were accompanied by short cooling time and short gamma countings of less than 1 h. The data obtained for the ^{106}Cd(n, 2n)^{105}Cd cross section are presented on the next page.

To reduce errors, the ^{106}Cd(n, 2n)^{105}Cd cross section was approximated by a polynom of the second order before subtracting it from the total ^{105}Ag production cross section to determine the ^{106}Cd(n, x)^{105}Ag cross section shown two pages later.

In this page data Table, the total ^{105}Ag production cross section is presented that was measured under the conditions described above. The experimental data agree well with the corresponding cross section sums taken from evaluations. At least, this is valid for three of five available evaluations.

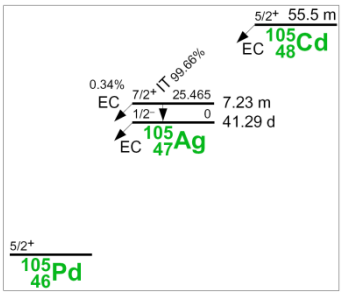

Decay data of **^{105}Ag**

Target nucleus	Abundance [%]	Chemical Form	Reaction product	$T_{1/2}$	E_γ [keV]	Y_γ [%]
^{106}Cd	**1.25** *6*	Cd-metal	^{105}Ag	**41.29 d** *7*	280.4	30.2 *17*
					644.5	**11.1** *6*
					650.7	2.54 *4*
					1087.9	3.85 *17*

^{106}Cd(n, 2n)^{105}Cd

^{106}Cd(n, 2n)^{105}Cd			
E_n [MeV]	σ [mb]	$\pm\Delta\sigma_{total}$ [%]	$\pm\Delta\sigma_{ref}$ [%]
13.47	398	*9.22*	*8.01*
13.64	441	*10.0*	*8.01*
13.88	457	*9.18*	*8.01*
14.05	485	*8.21*	*8.01*
14.28	478	*10.0*	*8.01*
14.47	545	*9.82*	*8.01*
14.68	521	*8.10*	*8.01*
14.81	543	*8.14*	*8.01*
14.86	559	*10.4*	*8.01*
Ref. CS is ^{93}Nb(n,2n)^{92m}Nb;			α_d = *1.5*

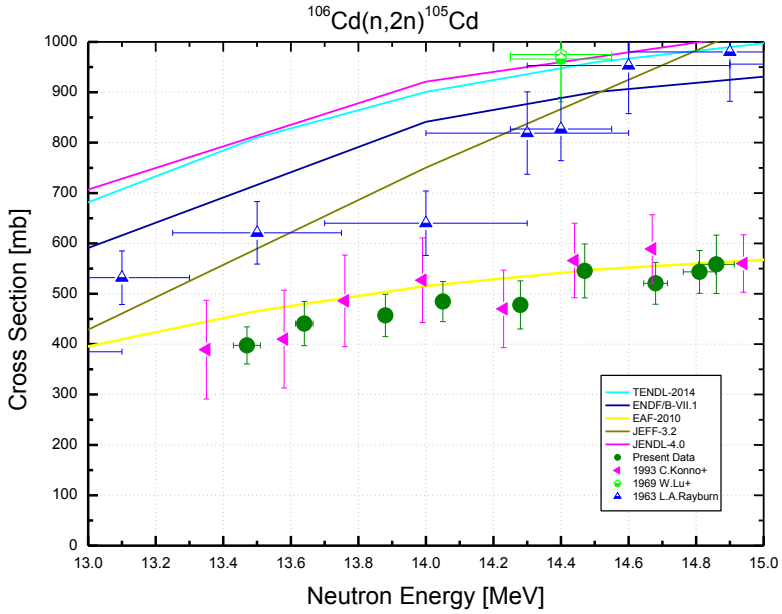

The present data on ^{106}Cd(n, 2n)^{105}Cd cross sections agree well with the latest experimental data [22] obtained for this reaction in JAERI. However, the old experiments carried out in sixties of the past century gave the results that are almost two times higher, and most evaluations follow the old data.

It seems desirable to pay more attention to the recent experimental data that were performed independently but are in a good agreement.

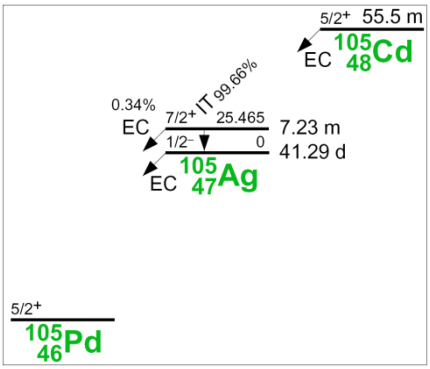

Decay data used for **^{106}Cd(n, 2n)^{105}Cd**.

Target nucleus	Abundance [%]	Chemical Form	Reaction product	$T_{1/2}$	E_γ [keV]	Y_γ [%]
^{106}Cd	**1.25** *6*	Cd-metal	^{105}Cd	**55.5 m** *4*	648.5	1.57 *11*
					961.8	**4.7** *3*
					1302.5	4.1 *3*
					1693.3	3.54 *24*

^{106}Cd[(n, np)+(n,d)]^{105}Ag

^{106}Cd(n, x)^{105}Ag		
E_n [MeV]	σ [mb]	$\pm\Delta\sigma_{total}$ [%]
13.45	415	*15.4*
13.56	499	*25.1*
13.74	463	*19.6*
13.88	446	*15.5*
13.96	496	*17.6*
14.19	582	*20.5*
14.43	577	*14.1*
14.63	543	*13.7*
14.78	712	*16.2*
14.88	606	*15.2*
Ref. CS is ^{93}Nb(n,2n)^{92m}Nb		

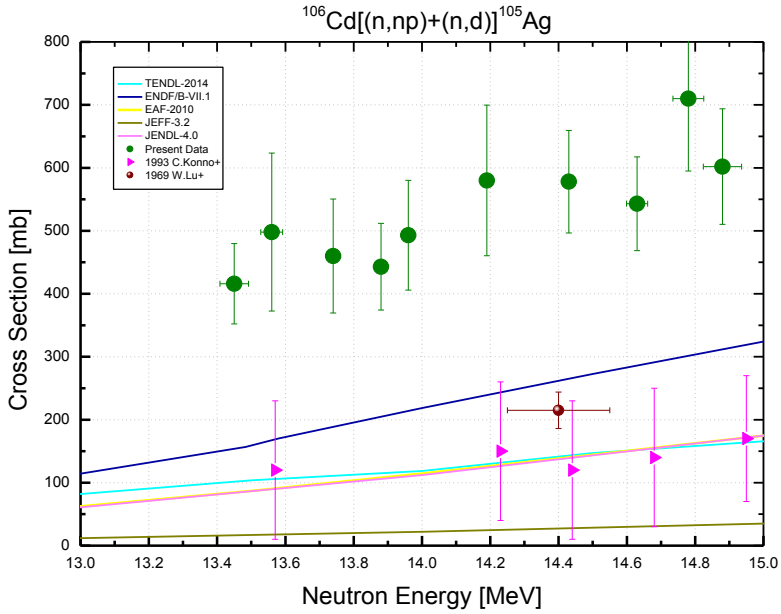

The present data are the result of subtracting the ^{106}Cd(n, 2n)^{105}Cd cross-sections given in the previous page from the ^{105}Ag production cross-section discussed two pages earlier. The data are shown in the Table and in the Figure above (olive circles in the Figure).

In the same way, the data of Konno at al. [22] were obtained (magenta triangles in the Figure). The disagreement between these two data sets is obvious.

A possible cause of the observed cross section difference may be the difference in the reference decay data used. So, the γ-ray 443.00 keV with the intensity 17.1% was taken in [22]. According to the recent evaluations [26], the intensity 10.5% is recommended for the gamma-line 443.37 keV. If the gamma intensity would be changed to the recently recommended value then the agreement between the two cross-section data sets will be much better.

In our experiment, four γ-rays were used, and the cross-section data calculated for any one of the γ-lines agrees within errors with the results for any other γ-ray. The γ-line with the energy about 443 kev was not included in the list of the analysed γ-rays.

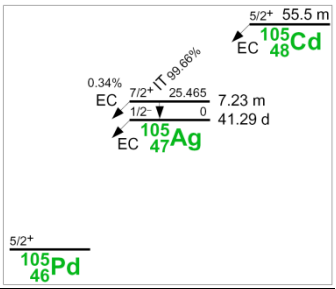

Decay data used for CS **^{106}Cd(n, x)^{105}Ag**.

Target nucleus	**Abundance [%]**	**Chemical Form**	**Reaction product**	**$T_{1/2}$**	**E_γ [keV]**	**Y_γ [%]**
^{106}Cd	**1.25** *6*	Cd-metal	^{105}Ag	**41.29 d** *7*	280.4	30.2 *17*
					644.5	**11.1** *6*
					650.7	2.54 *4*
					1087.9	3.85 *17*

^{106}Cd(n, p)^{106m}Ag

^{106}Cd(n, p)^{106m}Ag			
E_n [MeV]	σ [mb]	$\pm\Delta\sigma_{total}$ [%]	$\pm\Delta\sigma_{ref}$ [%]
13.45	46.3	*4.85*	*5.45*
13.88	48.0	*5.13*	*5.44*
14.44	44.9	*6.43*	*5.44*
14.64	44.7	*8.78*	*5.45*
14.88	43.1	*5.82*	*5.45*
Ref. CS is ^{93}Nb(n,2n)^{92m}Nb;			$\alpha_d = 1.2$

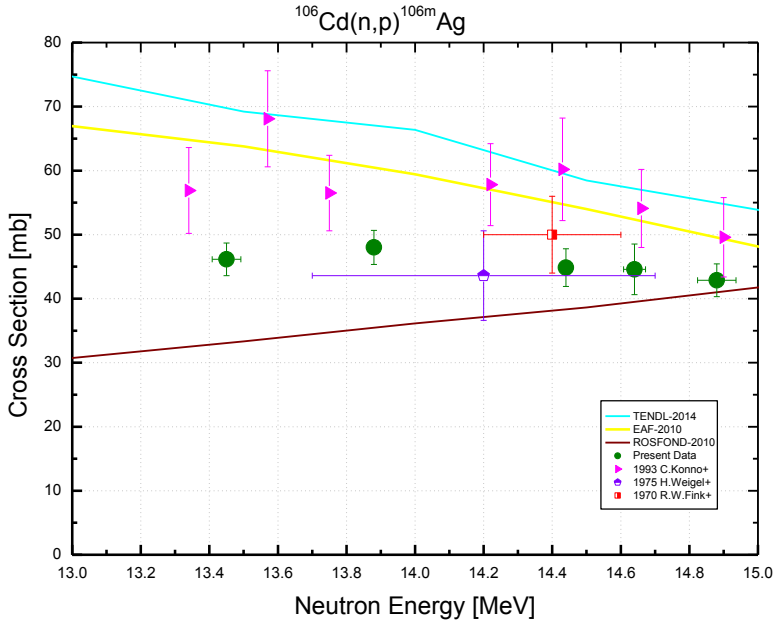

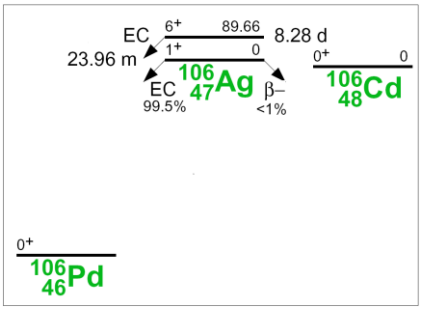

Decay data used for **^{106}Cd(n, p)^{106m}Ag**.

Target nucleus	Abundance [%]	Chemical Form	Reaction product	$T_{1/2}$	E_γ [keV]	Y_γ [%]
^{106}Cd	**1.25** *6*	Cd-metal	^{106m}Ag	**8.28 d** *2*	429.6	13.2 *4*
					451.0	**28.2** *7*
					824.7	15.3 *4*
					1527.6	16.3 *13*

^{108}Cd(n, 2n)^{107}Cd

^{108}Cd(n, 2n)^{107}Cd			
E_n [MeV]	σ [mb]	$\pm\Delta\sigma_{total}$ [%]	$\pm\Delta\sigma_{ref}$ [%]
13.45	1107	*16.8*	*7.26*
13.88	1317	*20.5*	*7.25*
14.44	1164	*7.29*	*7.25*
14.64	1493	*7.45*	*7.25*
14.81	1372	*5.40*	*7.25*
Ref. CS is ^{93}Nb(n,2n)^{92m}Nb;			α_d = *1.2*

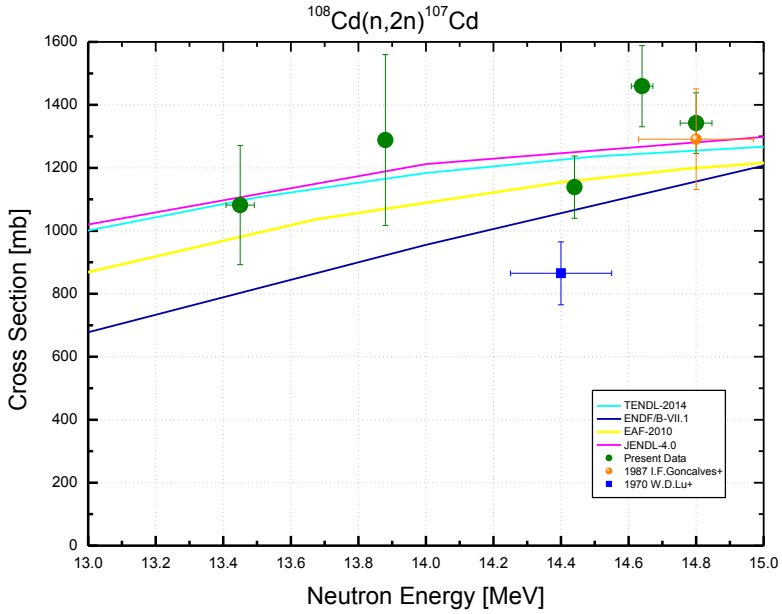

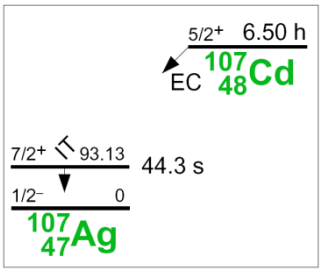

Decay data used for **^{108}Cd(n, 2n)^{107}Cd**.

Target nucleus	Abundance [%]	Chemical Form	Reaction product	$T_{1/2}$	E_γ [keV]	Y_γ [%]
^{108}Cd	**0.89** *3*	Cd-metal	^{107}Cd	**6.50 h** *2*	**93.1**	**4.7** *3*

^{110}Cd(n, p)^{110m}Ag

^{110}Cd(n, p)^{110m}Ag			
E_n [MeV]	σ [mb]	$\pm\Delta\sigma_{total}$ [%]	$\pm\Delta\sigma_{ref}$ [%]
13.45	6.01	*4.34*	*1.58*
13.88	6.63	*3.80*	*1.55*
14.44	8.27	*4.70*	*1.55*
14.64	8.52	*4.56*	*1.55*
14.88	9.52	*7.07*	*1.56*
Ref. CS is ^{93}Nb(n,2n)^{92m}Nb;			$\alpha_d = 1.2$

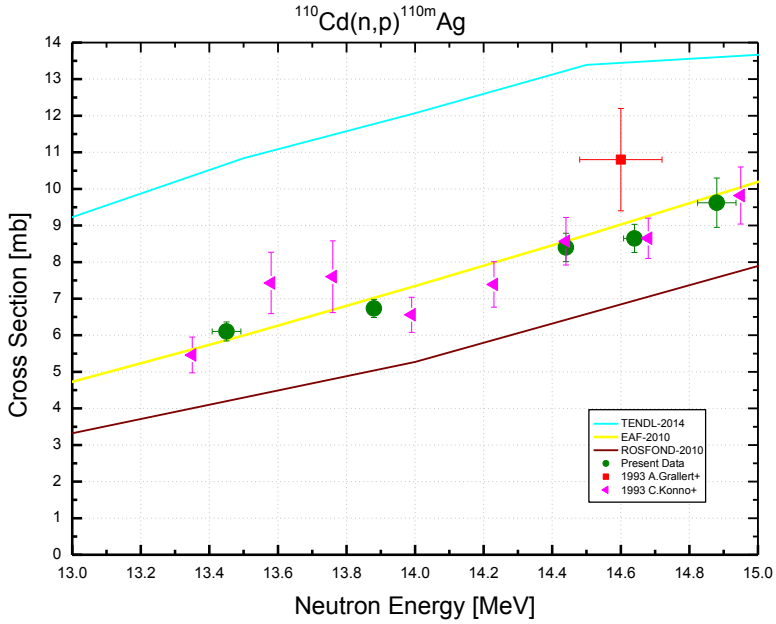

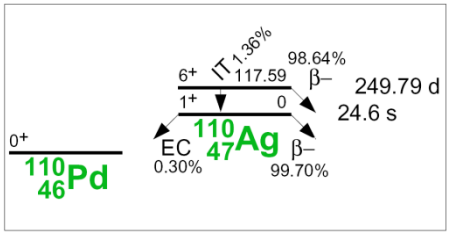

Decay data used for **^{110}Cd(n, p)^{110m}Ag**.

Target nucleus	Abundance [%]	Chemical Form	Reaction product	$T_{1/2}$	E_γ [keV]	Y_γ [%]
^{110}Cd	**12.49** ***18***	Cd-metal	^{110m}Ag	**249.83 d** ***4***	**657.8**	**95.61** ***9***
					884.7	75.0 *11*
					937.5	35.0 *3*
					1384.3	25.1 *5*

^{110}Cd(n, 2n)^{109}Cd

^{110}Cd(n, 2n)^{109}Cd			
E_n [MeV]	σ [mb]	$\pm\Delta\sigma_{total}$ [%]	$\pm\Delta\sigma_{ref}$ [%]
13.45	1319	*13.6*	*3.38*
13.88	1485	*18.5*	*3.37*
14.44	1527	*10.2*	*3.36*
14.64	1598	*8.59*	*3.37*
Ref. CS is ^{93}Nb(n,2n)^{92m}Nb;			α_d = *1.2*

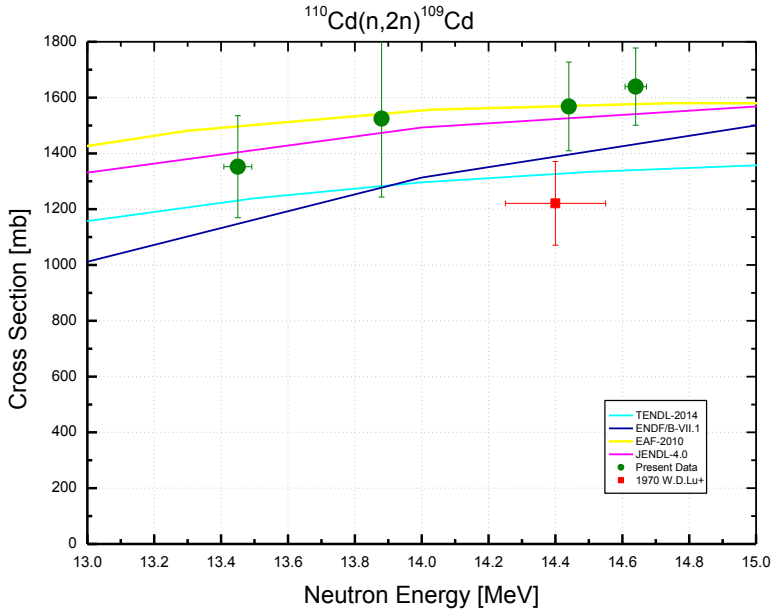

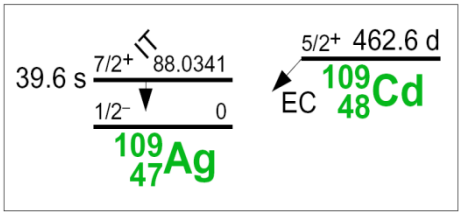

Decay data used for **^{110}Cd(n, 2n)^{109}Cd**.

Target nucleus	Abundance [%]	Chemical Form	Reaction product	$T_{1/2}$	E_γ [keV]	Y_γ [%]
^{110}Cd	**12.49** ***18***	Cd-metal	^{109}Cd	**461.4 d** ***12***	**88.0**	**3.70** ***11***

^{111}Cd(n, p)^{111}Ag

^{111}Cd(n, p)^{111}Ag			
E_n [MeV]	σ [mb]	$\pm\Delta\sigma_{total}$ [%]	$\pm\Delta\sigma_{ref}$ [%]
13.45	20.3	*11.8*	*4.62*
13.88	23.4	*12.8*	*4.61*
14.44	23.9	*7.86*	*4.61*
14.64	26.6	*7.04*	*4.61*
14.88	31.0	*7.04*	*4.62*
Ref. CS is ^{93}Nb(n,2n)^{92m}Nb;			$\alpha_d = 1.2$

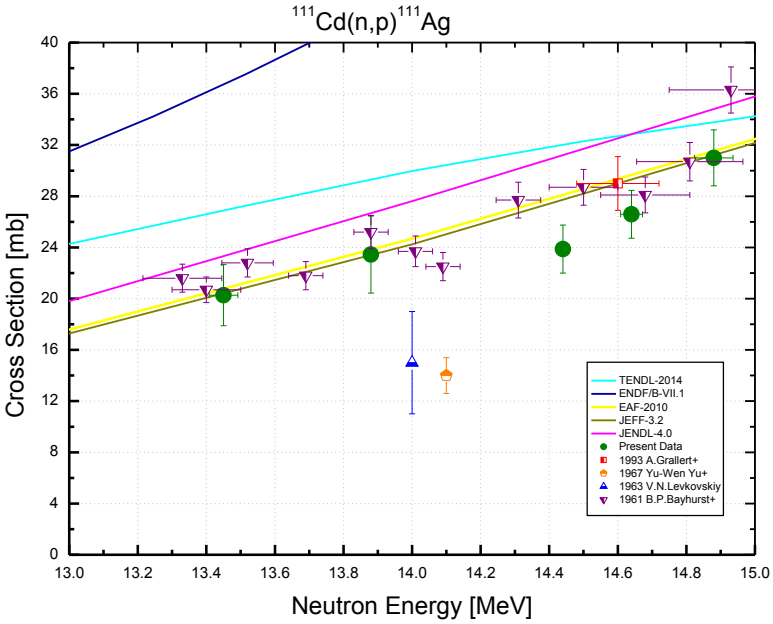

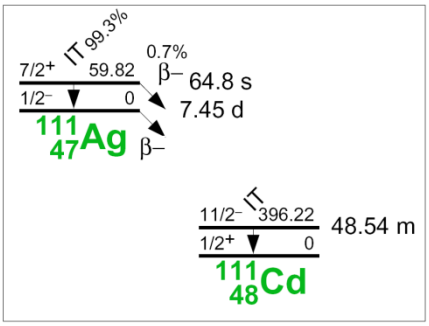

Decay data used for **^{111}Cd(n, p)^{111}Ag**.

Target nucleus	Abundance [%]	Chemical Form	Reaction product	$T_{1/2}$	E_γ [keV]	Y_γ [%]
^{111}Cd	**12.80** *12*	Cd-metal	^{111}Ag	**7.45 d** *1*	245.4	1.24 *9*
					342.1	**6.7** *3*

^{112}Cd(n, α)^{109}Pd

^{112}Cd(n, α)^{109}Pd			
E_n [MeV]	σ [mb]	$\pm\Delta\sigma_{total}$ [%]	$\pm\Delta\sigma_{ref}$ [%]
13.45	3.40	*35.3*	*11.2*
13.88	2.34	*29.3*	*11.2*
14.44	3.80	*23.7*	*11.2*
14.64	3.81	*26.3*	*11.2*
14.88	4.86	*27.1*	*11.2*
Ref. CS is ^{93}Nb(n,2n)^{92m}Nb;			α_d = *1.2*

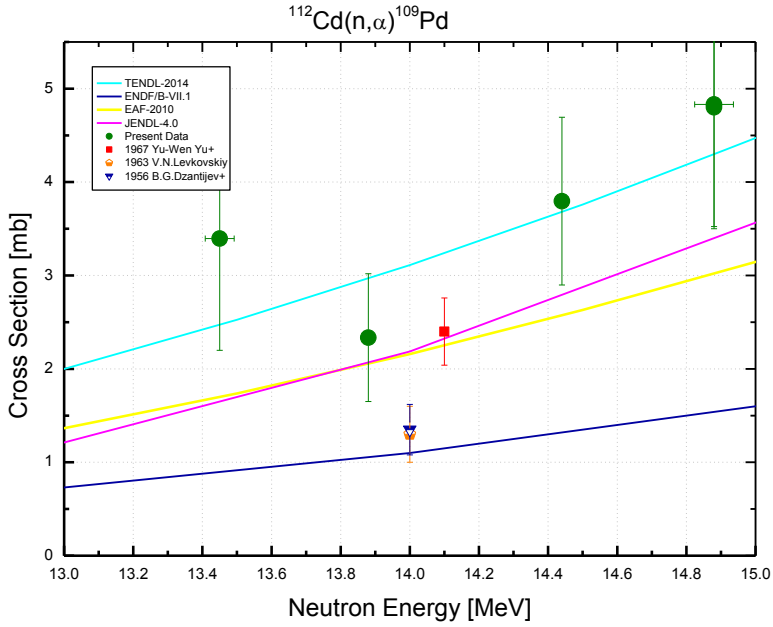

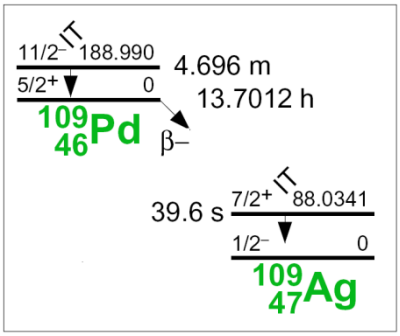

Decay data used for **^{112}Cd(n, α)^{109}Pd**.

Target nucleus	**Abundance [%]**	**Chemical Form**	**Reaction product**	**$T_{1/2}$**	**E_γ [keV]**	**Y_γ [%]**
^{112}Cd	**24.13** ***21***	Cd-metal	^{109}Pd	**13.7012 h** ***24***	**88.0**	**3.6** ***4***

^{112}Cd(n, p)^{112}Ag

^{112}Cd(n, p)^{112}Ag			
E_n [MeV]	σ [mb]	$\pm\Delta\sigma_{total}$ [%]	$\pm\Delta\sigma_{ref}$ [%]
13.46	10.0	*9.00*	*7.07*
13.64	10.4	*9.54*	*7.06*
13.89	12.8	*8.50*	*7.06*
14.05	13.6	*9.56*	*7.06*
14.28	14.7	*8.08*	*7.06*
14.47	14.6	*8.13*	*7.06*
14.68	16.9	*7.60*	*7.06*
14.81	16.5	*8.76*	*7.06*
14.86	15.4	*7.75*	*7.06*
Ref. CS is ^{93}Nb(n,2n)^{92m}Nb;			α_d = *1.2*

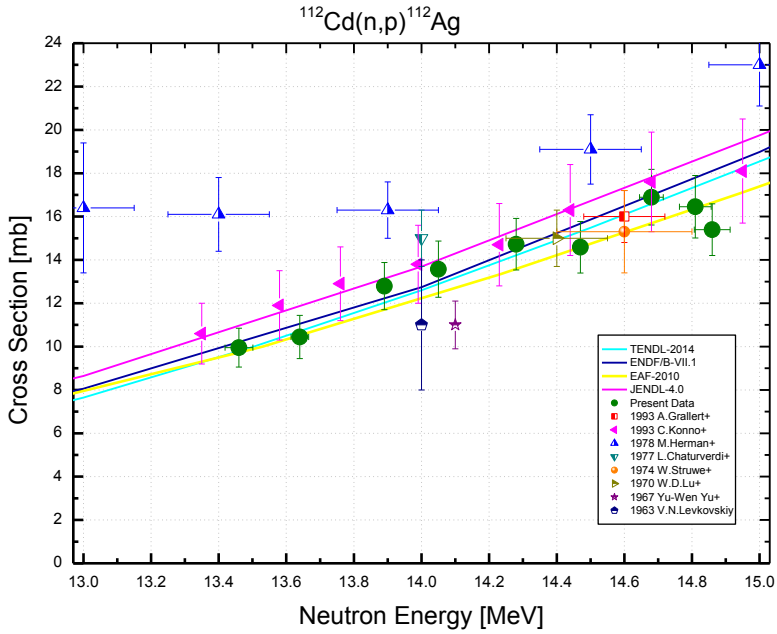

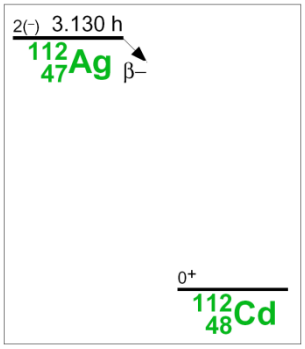

Decay data used for **^{112}Cd(n, p)^{112}Ag**.

Target nucleus	**Abundance [%]**	**Chemical Form**	**Reaction product**	**$T_{1/2}$**	**E_γ [keV]**	**Y_γ [%]**
^{112}Cd	**24.13** ***21***	Cd-metal	^{112}Ag	**3.130 h** ***8***	**617.5**	**43** ***5***

^{112}Cd(n, 2n)^{111m}Cd

^{112}Cd(n, 2n)^{111m}Cd			
E_n [MeV]	σ [mb]	$\pm\Delta\sigma_{total}$ [%]	$\pm\Delta\sigma_{ref}$ [%]
13.47	641	*8.02*	*6.28*
13.64	628	*9.37*	*6.28*
13.88	638	*8.12*	*6.28*
14.05	630	*7.89*	*6.27*
14.28	593	*9.89*	*6.27*
14.47	634	*8.10*	*6.27*
14.68	647	*7.48*	*6.28*
14.81	695	*6.39*	*6.28*
14.86	647	*6.73*	*6.28*
Ref. CS is ^{93}Nb(n,2n)^{92m}Nb;			α_d = *1.2*

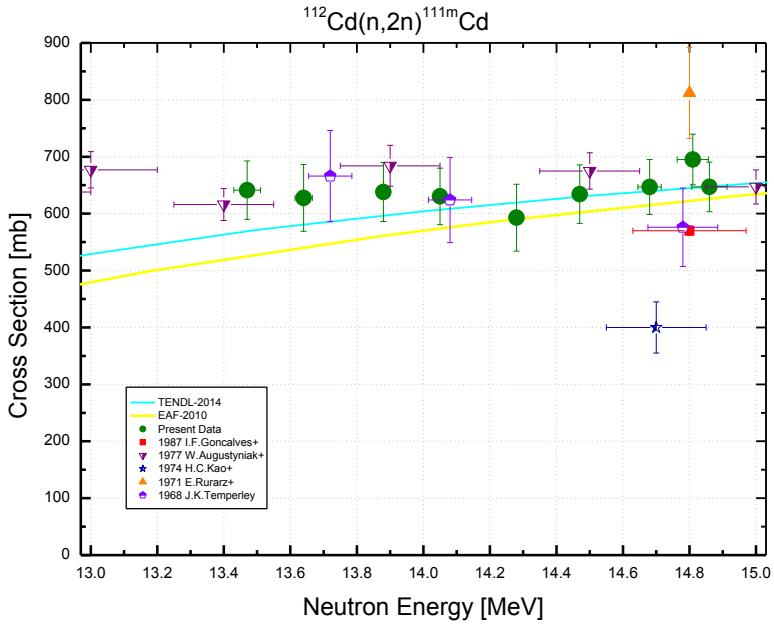

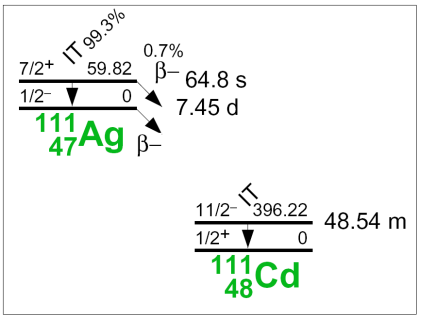

Decay data used for **^{112}Cd(n, 2n)^{111m}Cd**.

Target nucleus	Abundance [%]	Chemical Form	Reaction product	$T_{1/2}$	E_γ [keV]	Y_γ [%]
^{112}Cd	**24.13** *21*	Cd-metal	^{111m}Cd	**48.50 m** *9*	**150.8**	**29.1** *18*
					245.4	94 *7*

^{113}Cd(n, p)^{113}Ag

^{113}Cd(n, p)^{113}Ag			
E_n [MeV]	σ [mb]	$\pm\Delta\sigma_{total}$ [%]	$\pm\Delta\sigma_{ref}$ [%]
13.45	10.8	*11.1*	*3.41*
13.88	13.8	*10.9*	*3.40*
14.44	15.0	*12.6*	*3.40*
14.64	19.0	*9.93*	*3.40*
14.81	19.8	*9.50*	*3.40*
14.88	22.3	*10.3*	*3.40*
Ref. CS is ^{93}Nb(n,2n)^{92m}Nb;			α_d = *1.2*

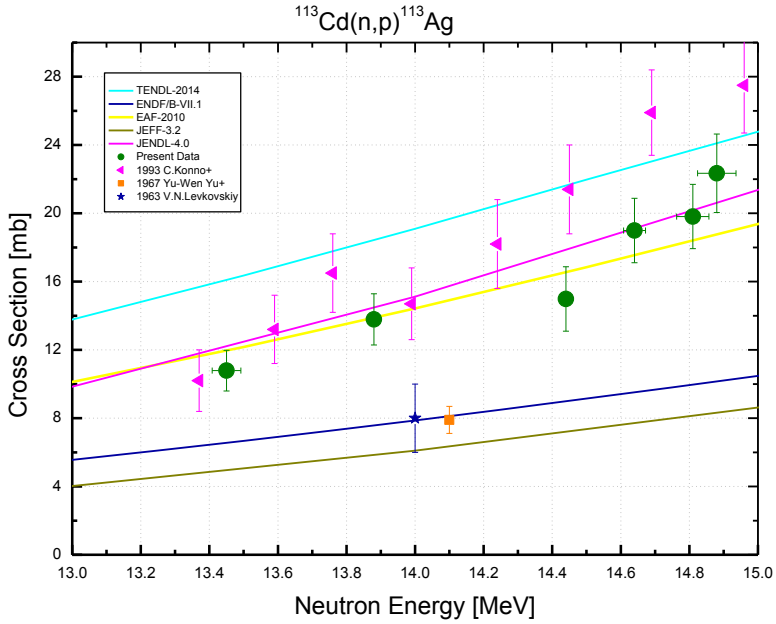

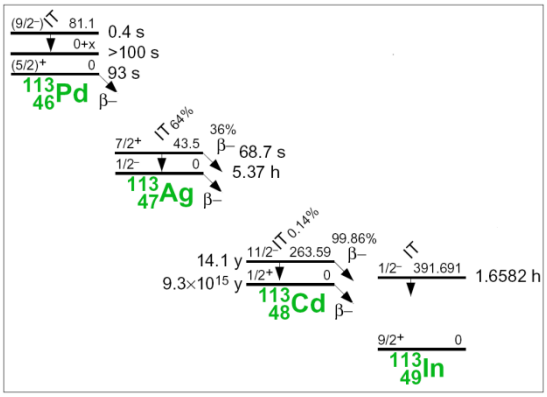

Decay data used for **^{113}Cd(n, p)^{113}Ag**.

Target nucleus	Abundance [%]	Chemical Form	Reaction product	$T_{1/2}$	E_γ [keV]	Y_γ [%]
^{113}Cd	**12.22** *12*	Cd-metal	^{113}Ag	**5.37 h** *5*	**298.6**	**10.0** *3*

^{114}Cd(n, α)^{111m}Pd

^{114}Cd(n, α)^{111m}Pd			
E_n [MeV]	σ [mb]	$\pm\Delta\sigma_{total}$ [%]	$\pm\Delta\sigma_{ref}$ [%]
13.45	0.155	*18.5*	*11.2*
13.88	0.156	*18.5*	*11.2*
14.44	0.237	*34.1*	*11.2*
14.64	0.288	*14.6*	*11.2*
14.81	0.222	*39.8*	*11.2*
14.88	0.298	*24.6*	*11.2*
Ref. CS is ^{93}Nb(n,2n)^{92m}Nb;			$\alpha_d = 1.2$

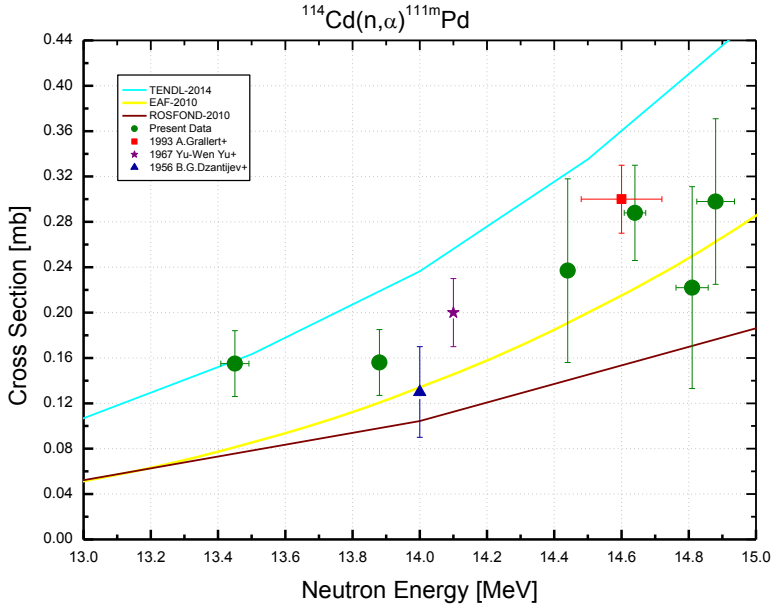

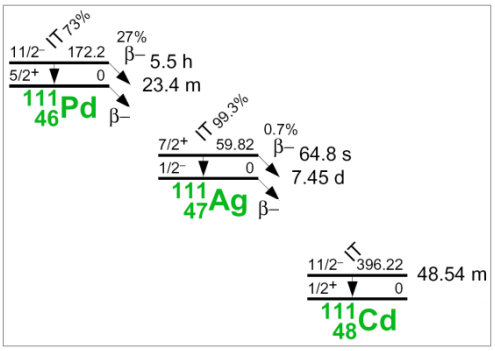

Decay data used for **^{114}Cd(n, α)^{111m}Pd.**

Target nucleus	Abundance [%]	Chemical Form	Reaction product	$T_{1/2}$	E_γ [keV]	Y_γ [%]
^{114}Cd	**28.73** *42*	Cd-metal	^{111m}Pd	**5.5 h** *1*	**172.2**	**46** *5*

^{116}Cd(n, 2n)^{115g}Cd

^{116}Cd(n, 2n)^{115g}Cd			
E_n [MeV]	σ [mb]	$\pm\Delta\sigma_{total}$ [%]	$\pm\Delta\sigma_{ref}$ [%]
13.45	793	*3.51*	*3.31*
13.56	851	*3.46*	*3.30*
13.74	837	*3.31*	*3.30*
13.88	814	*3.56*	*3.30*
13.96	828	*5.63*	*3.30*
14.19	829	*3.43*	*3.29*
14.43	809	*3.45*	*3.29*
14.63	807	*3.85*	*3.30*
14.80	794	*3.56*	*3.30*
14.88	818	*4.15*	*3.30*
Ref. CS is ^{93}Nb(n,2n)^{92m}Nb;		α_d = *1.2*	

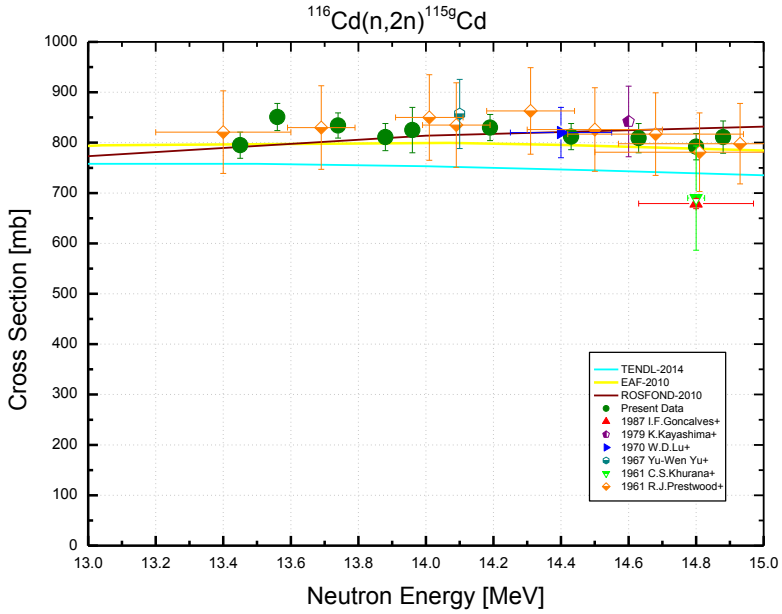

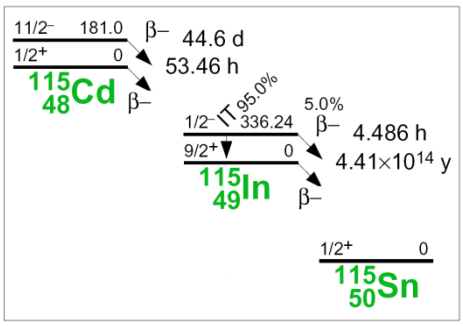

Decay data used for **^{116}Cd(n, 2n)^{115g}Cd**.

Target nucleus	Abundance [%]	Chemical Form	Reaction product	$T_{1/2}$	E_γ [keV]	Y_γ [%]
^{116}Cd	**7.49** ***18***	Cd-metal	^{115g}Cd	**53.46 h** ***5***	492.4	8.03 *18*
					527.9	**27.5** ***6***

^{116}Cd(n, 2n)^{115m}Cd

^{116}Cd(n, 2n)^{115m}Cd			
E_n [MeV]	σ [mb]	$\pm\Delta\sigma_{total}$ [%]	$\pm\Delta\sigma_{ref}$ [%]
13.45	503	*35.8*	*35.1*
13.56	621	*42.7*	*35.1*
13.74	705	*41.1*	*35.1*
13.88	511	*35.5*	*35.1*
13.96	591	*43.5*	*35.1*
14.19	590	*43.3*	*35.1*
14.44	559	*34.8*	*35.1*
14.64	530	*36.8*	*35.1*
14.88	526	*37.5*	*35.1*
Ref. CS is ^{93}Nb(n,2n)^{92m}Nb;			$\alpha_d = 1.2$

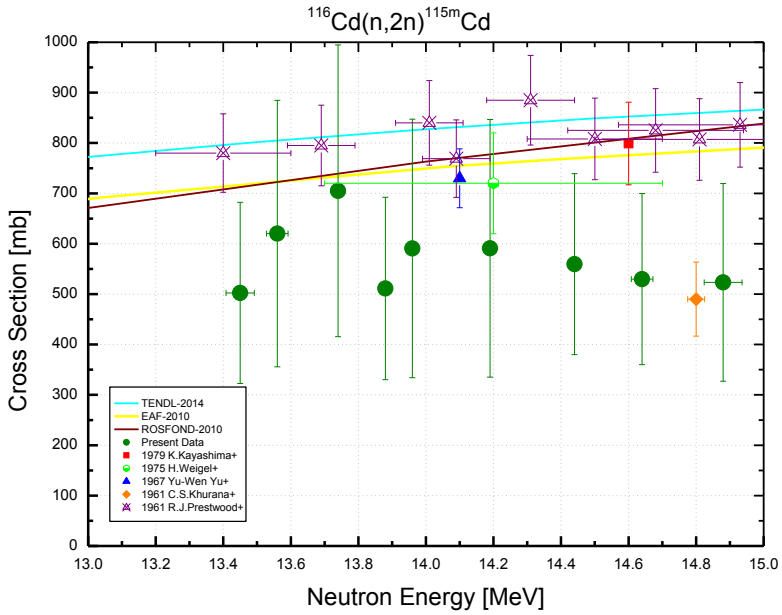

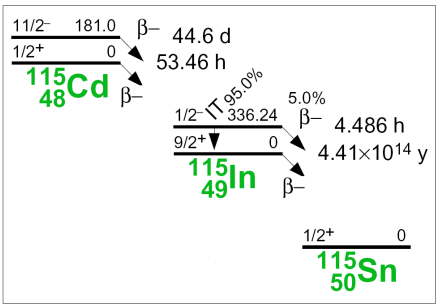

Decay data used for **^{116}Cd(n, 2n)^{115m}Cd**.

Target nucleus	Abundance [%]	Chemical Form	Reaction product	$T_{1/2}$	E_γ [keV]	Y_γ [%]
^{116}Cd	**7.49** ***18***	Cd-metal	^{115m}Cd	**44.56 d** ***24***	484.5	0.29 *10*
					933.8	**2.0** ***7***
					1290.6	0.9 *3*

^{116}Cd(n, 2n)^{115}Cd

^{116}Cd(n, 2n)^{115}Cd		
E_n [MeV]	σ [mb]	$\pm\Delta\sigma_{total}$ *[%]*
13.45	1296	*14.2*
13.56	1472	*18.2*
13.74	1542	*19.0*
13.88	1325	*13.9*
13.96	1418	*18.5*
14.19	1418	*18.2*
14.44	1368	*14.5*
14.63	1337	*14.9*
14.88	1320	*15.2*
Ref. CS is ^{93}Nb(n,2n)^{92m}Nb		

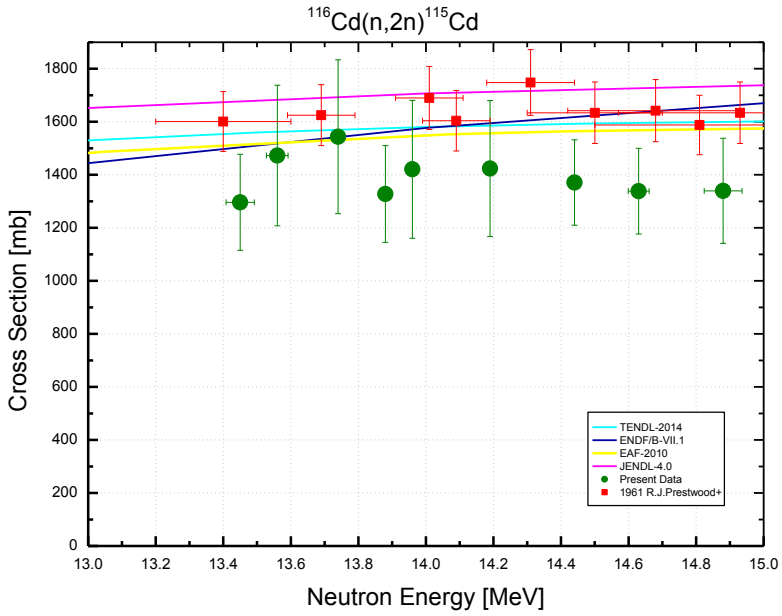

This is the sum of the ^{116}Cd(n, 2n)^{115m}Cd and ^{116}Cd(n, 2n)^{115g}Cd cross sections measured independently and presented on previous pages.

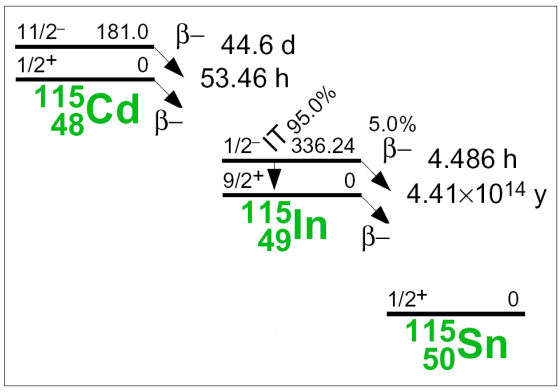

^{113}In(n, n')^{113m}In

^{113}In(n, n')^{113m}In			
E_n [MeV]	σ [mb]	$\pm\Delta\sigma_{total}$ [%]	$\pm\Delta\sigma_{ref}$ [%]
13.56	73.7	*6.69*	*1.34*
13.74	60.9	*8.18*	*1.33*
13.96	68.4	*8.60*	*1.32*
14.19	59.4	*7.85*	*1.31*
14.42	52.5	*10.2*	*1.32*
14.61	54.2	*11.4*	*1.32*
14.78	51.9	*11.1*	*1.33*
Ref. CS is ^{93}Nb(n,2n)^{92m}Nb;			$\alpha_d = 1.6$

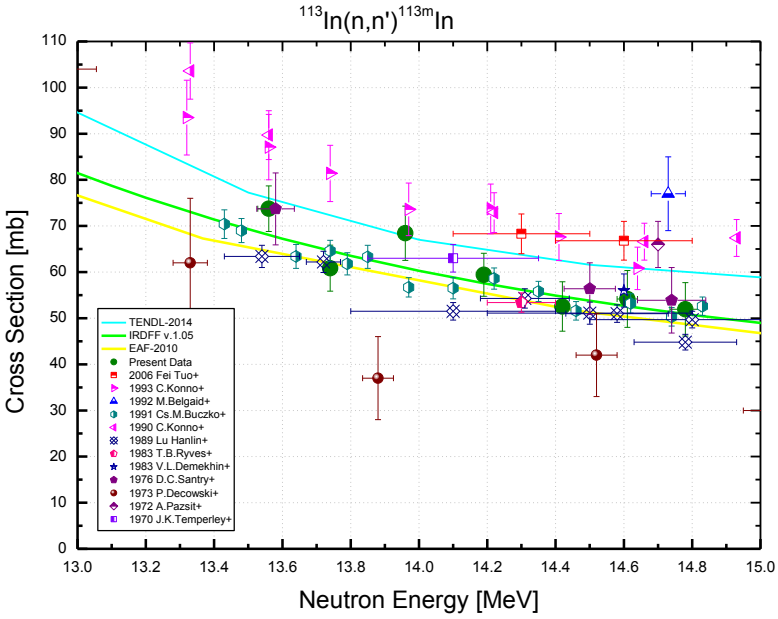

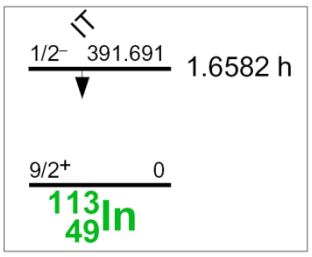

Decay data used for **^{113}In(n, n')^{113m}In**.

Target nucleus	Abundance [%]	Chemical form	Reaction product	$T_{1/2}$	E_γ [keV]	Y_γ [%]
^{113}In	**4.29** *5*	In-metal	^{113m}In	**99.476 m** *23*	**391.7**	**64.94** *17*

^{115}In(n, α)^{112}Ag

^{115}In(n, α)^{112}Ag			
E_n [MeV]	σ [mb]	$\pm\Delta\sigma_{total}$ [%]	$\pm\Delta\sigma_{ref}$ [%]
13.56	1.66	*15.9*	*11.6*
13.74	1.92	*16.3*	*11.6*
13.96	2.03	*14.6*	*11.6*
14.19	2.29	*14.5*	*11.6*
14.42	2.04	*14.0*	*11.6*
14.61	2.25	*14.0*	*11.6*
14.78	2.58	*13.9*	*11.6*
Ref. CS is ^{93}Nb(n,2n)^{92m}Nb;			$\alpha_d = 1.3$

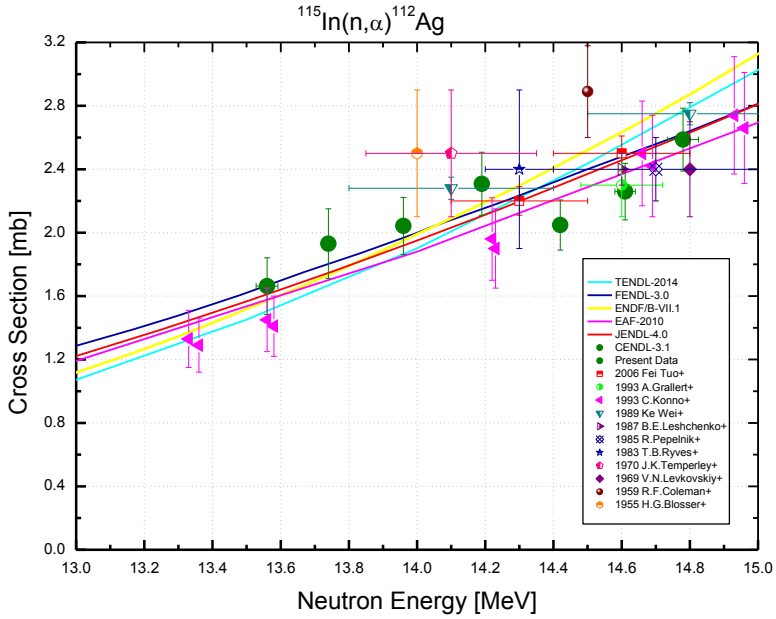

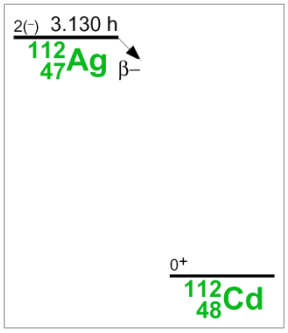

Decay data used for **^{115}In(n, α)^{112}Ag**.

Target nucleus	Abundance [%]	Chemical form	Reaction product	$T_{1/2}$	E_γ [keV]	Y_γ [%]
^{115}In	**95.71** *5*	In-metal	^{112}Ag	**3.130 h** *8*	**617.4**	**43** *5*

^{115}In(n, p)^{115m}Cd

^{115}In(n, p)^{115m}Cd			
E_n [MeV]	σ [mb]	$\pm\Delta\sigma_{total}$ [%]	$\pm\Delta\sigma_{ref}$ [%]
13.47	3.99	*40.1*	*35.0*
13.64	4.10	*39.9*	*35.0*
13.88	4.87	*39.0*	*35.0*
14.05	5.07	*38.9*	*35.0*
14.28	5.16	*38.8*	*35.0*
14.47	5.19	*38.8*	*35.0*
14.68	5.60	*38.6*	*35.0*
14.86	6.13	*38.4*	*35.0*
Ref. CS is ^{93}Nb(n,2n)^{92m}Nb;			α_d = *1.1*

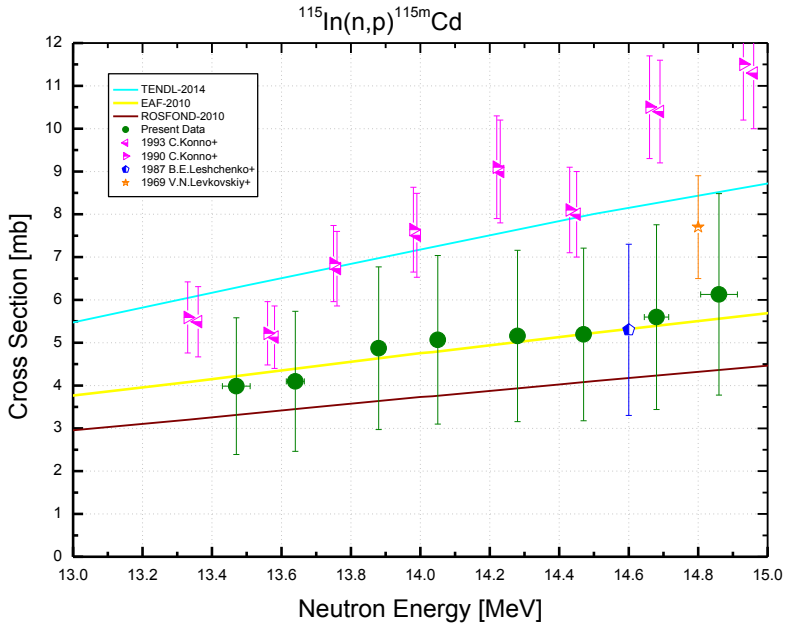

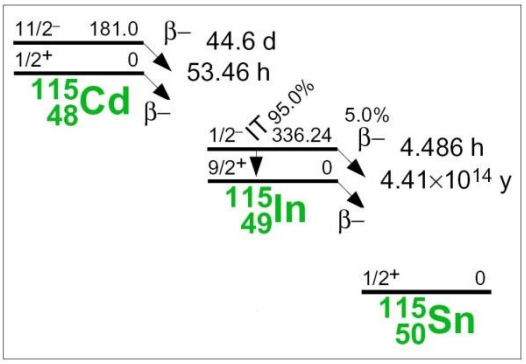

Decay data used for **^{115}In(n, p)^{115m}Cd**.

Target nucleus	Abundance [%]	Chemical form	Reaction product	$T_{1/2}$	E_γ [keV]	Y_γ [%]
^{115}In	**95.71** *5*	In-metal	^{115m}Cd	**44.56 d** *24*	**933.8**	**2.0** *7*

^{115}In(n, p)^{115g}Cd

^{115}In(n, p)^{115g}Cd			
E_n [MeV]	σ [mb]	$\pm\Delta\sigma_{total}$ [%]	$\pm\Delta\sigma_{ref}$ [%]
13.47	3.90	*9.67*	*2.27*
13.64	3.83	*5.12*	*2.26*
13.88	4.33	*4.26*	*2.26*
14.05	4.64	*8.79*	*2.25*
14.28	4.79	*6.59*	*2.25*
14.47	4.93	*3.87*	*2.25*
14.68	4.97	*3.84*	*2.26*
14.86	5.18	*3.48*	*2.26*
Ref. CS is ^{93}Nb(n,2n)^{92m}Nb;			α_d = *1.2*

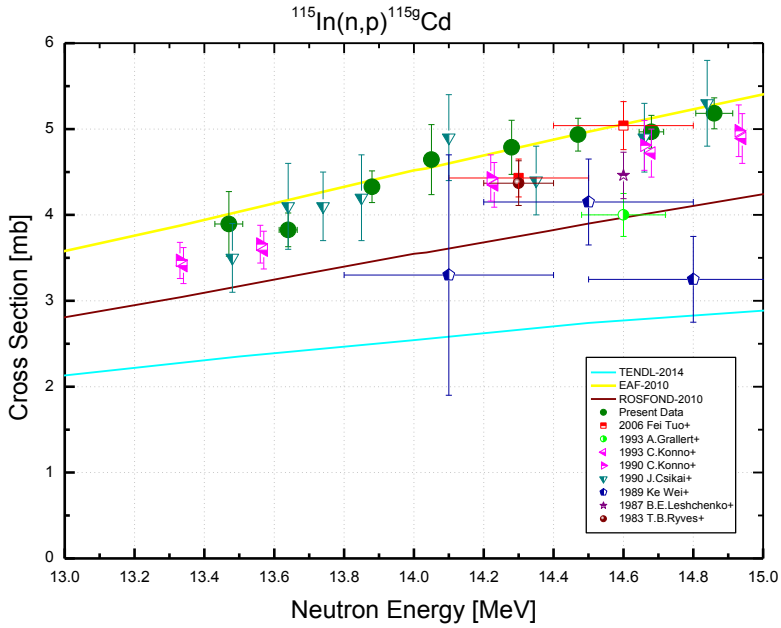

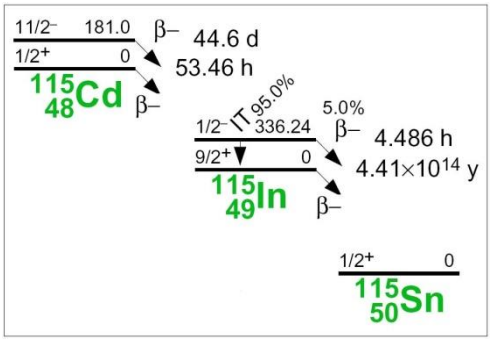

Decay data used for **^{115}In(n, p)^{115g}Cd**.

Target nucleus	Abundance [%]	Chemical form	Reaction product	$T_{1/2}$	E_γ [keV]	Y_γ [%]
^{115}In	**95.71** *5*	In-metal	^{115g}Cd	**53.46 h** *5*	492.4	8.03 *18*
					527.9	**27.5** *6*

^{115}In(n, p)^{115}Cd

^{115}In(n, p)^{115}Cd		
E_n [MeV]	σ [mb]	$\pm\Delta\sigma_{total}$ *[%]*
13.47	7.88	*24.4*
13.64	7.92	*22.8*
13.88	9.20	*22.4*
14.05	9.71	*23.9*
14.28	9.95	*22.9*
14.47	10.1	*21.5*
14.68	10.6	*22.0*
14.86	11.3	*22.2*
Ref. CS	^{93}Nb(n,2n)^{92m}Nb	

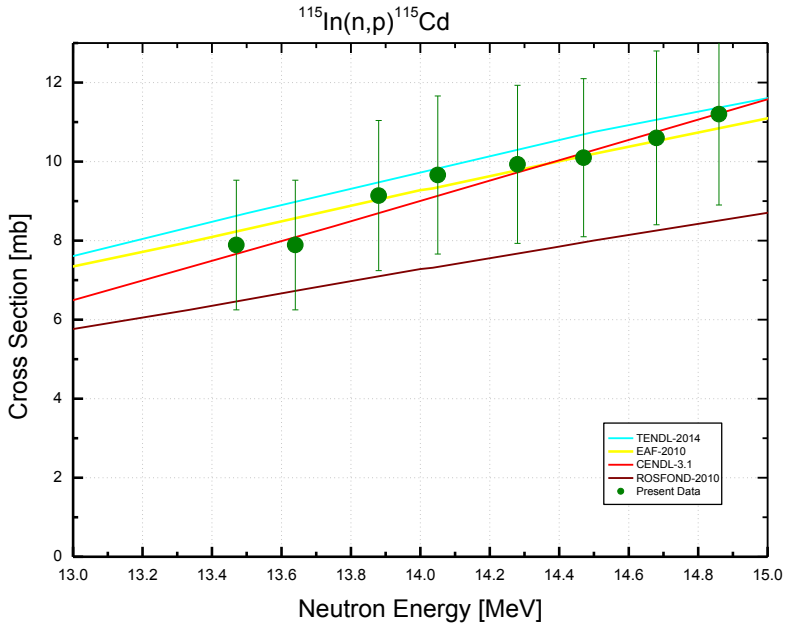

This is the sum of the ^{115}In(n, p)^{115m}Cd and ^{115}In(n, p)^{115g}Cd cross-sections measured independently and presented on previous pages.

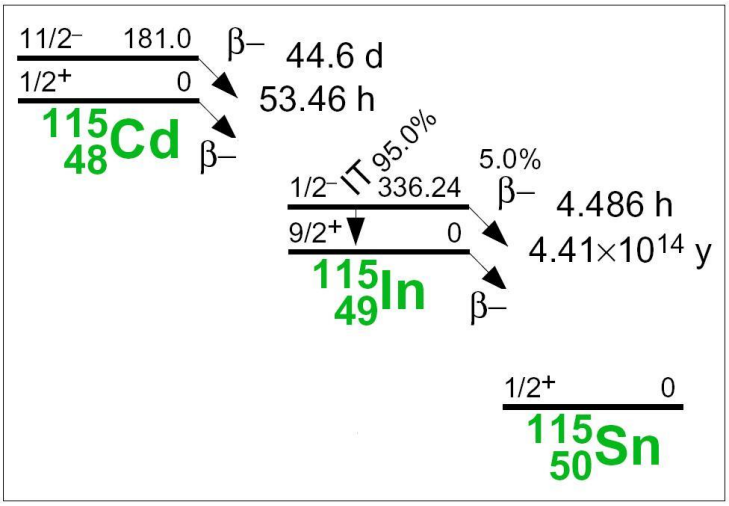

^{115}In(n, n')^{115m}In

^{115}In(n, n')^{115m}In			
E_n [MeV]	σ [mb]	$\pm\Delta\sigma_{total}$ [%]	$\pm\Delta\sigma_{ref}$ [%]
13.56	79.4	*5.42*	*4.84*
13.74	72.4	*5.71*	*4.84*
13.96	67.8	*4.60*	*4.84*
14.19	64.7	*5.93*	*4.84*
14.42	61.8	*4.86*	*4.84*
14.61	62.0	*4.85*	*4.84*
14.78	59.1	*4.94*	*4.84*
Ref. CS is ^{93}Nb(n,2n)^{92m}Nb;			$\alpha_d = 1.5$

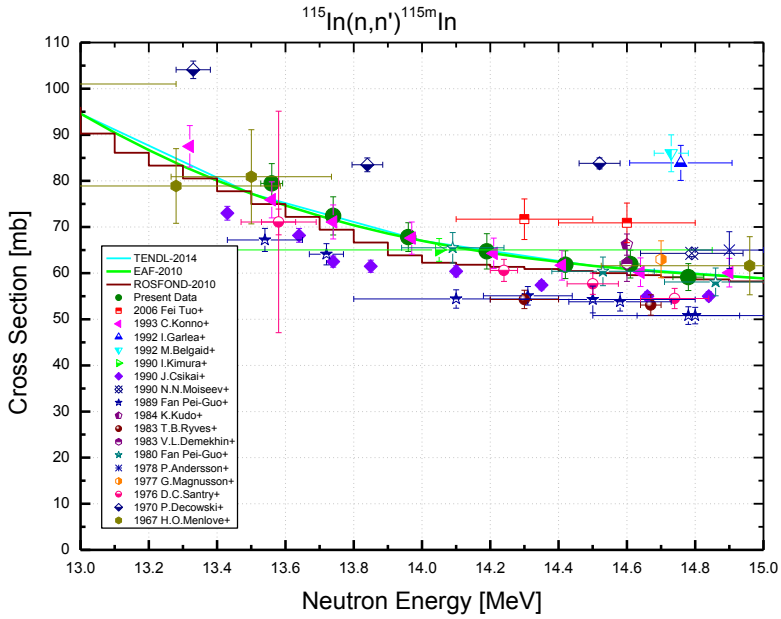

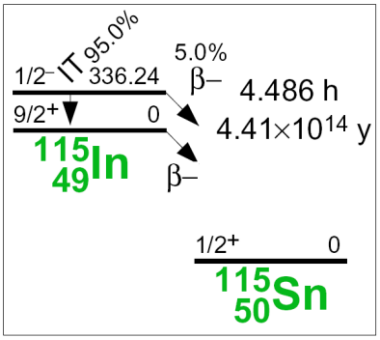

Decay data used for **^{115}In(n, n')^{115m}In.**

Target nucleus	Abundance [%]	Chemical form	Reaction product	$T_{1/2}$	E_γ [keV]	Y_γ [%]
^{115}In	**95.71** *5*	In-metal	^{115m}In	**4.486 h** *4*	**336.2**	**45.8** *22*

^{115}In(n, 2n)^{114m}In

^{115}In(n, 2n)^{114m}In			
E_n [MeV]	σ [mb]	$\pm\Delta\sigma_{total}$ [%]	$\pm\Delta\sigma_{ref}$ [%]
13.56	1228	*5.78*	*4.17*
13.74	1242	*8.05*	*6.99*
13.96	1328	*4.89*	*2.82*
14.19	1331	*9.02*	*8.08*
14.42	1314	*5.18*	*3.28*
14.61	1426	*7.01*	*5.76*
14.78	1249	*6.81*	*5.51*
Ref. CS is ^{93}Nb(n,2n)^{92m}Nb;			$\alpha_d = 1.2$

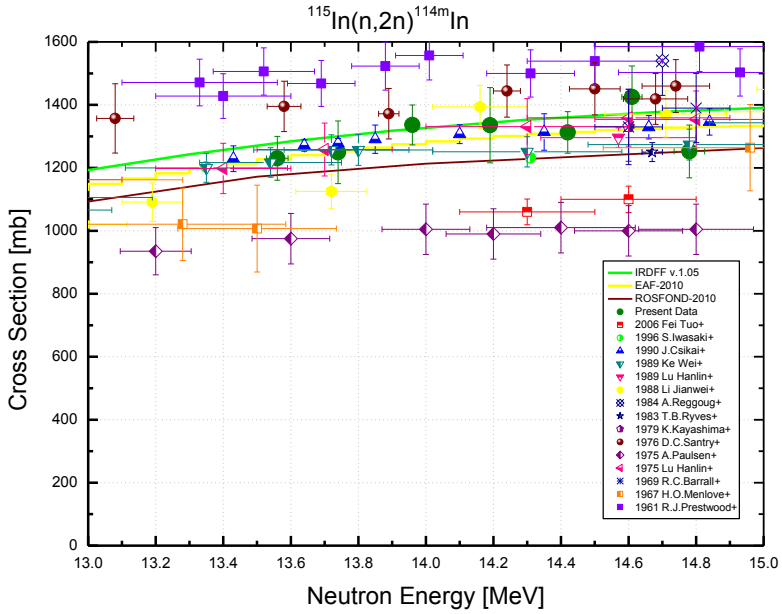

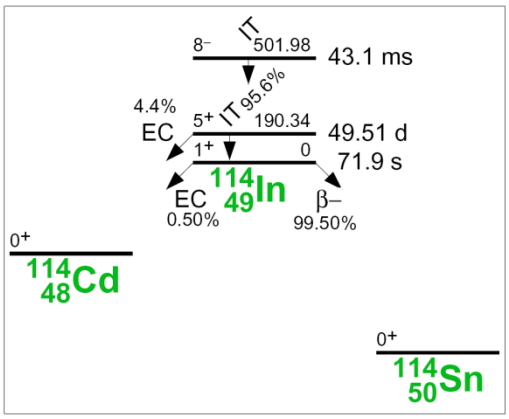

Decay data used for **^{115}In(n, 2n)^{114m}In.**

Target nucleus	Abundance [%]	Chemical form	Reaction product	$T_{1/2}$	E_γ [keV]	Y_γ [%]
^{115}In	**95.71** *5*	In-metal	^{114m}In	**49.51 d** *1*	**190.3**	**15.56** *15*
					558.4	4.4 *4*
					725.2	4.4 *4*

^{112}Sn(n, 2n)^{111}Sn

^{112}Sn(n, 2n)^{111}Sn			
E_n [MeV]	σ [mb]	$\pm\Delta\sigma_{total}$ [%]	$\pm\Delta\sigma_{ref}$ [%]
13.47	641	*19.8*	*15.4*
14.05	764	*15.5*	*15.4*
14.28	691	*19.0*	*15.4*
14.68	772	*16.3*	*15.4*
14.81	865	*16.8*	*15.4*
14.88	804	*17.0*	*15.4*
Ref. CS is ^{27}Al(n, α)^{24}Na;			$\alpha_d = 2.3$

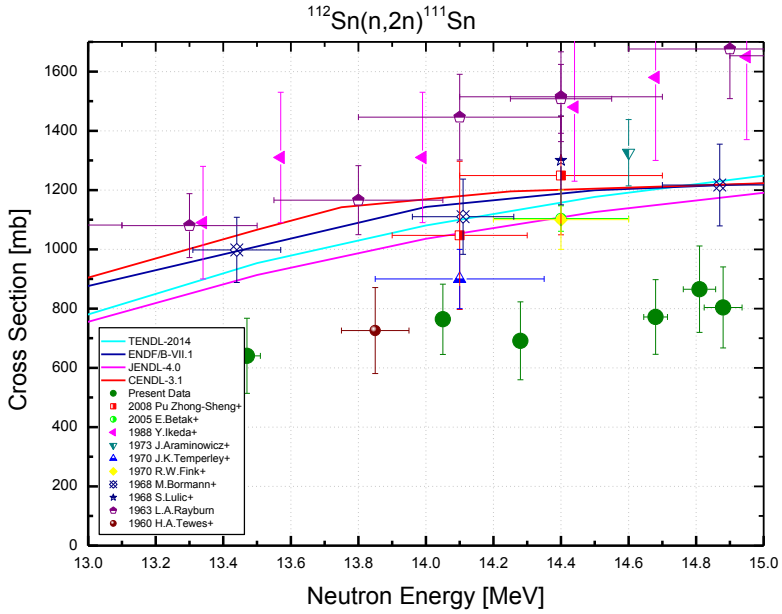

One of the possible reasons for the discrepancy of the present cros-sections with the data of [21] may be a difference in the reference data. For example, the 761.2 keV intensity was 0.66 in [21] but it is 1.48 in the present work, and this value agrees with intensities of other gamma lines observed in the present experiment.

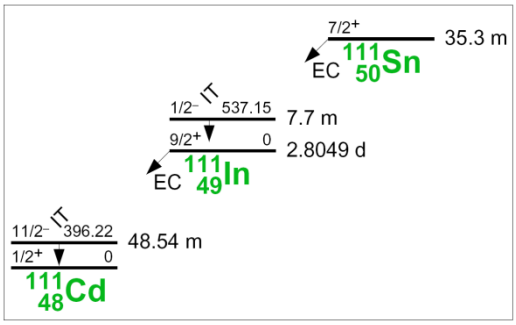

Decay data used **^{112}Sn(n, 2n)^{111}Sn**.

Target nucleus	**Abundance [%]**	**Chemical form**	**Reaction product**	**$T_{1/2}$**	**E_γ [keV]**	**Y_γ [%]**
^{112}Sn	**0.97** *1*	Sn-metal	^{111}Sn	**35.3 m** *6*	762.0	1.48 *23*
					1153.0	**2.7** *4*
					1610.5	1.31 *20*
					1914.7	2.0 *3*

^{112}Sn[(n, np)+(n, d)]^{111}In

^{112}Sn(n, x)^{111}In			
E_n [MeV]	σ [mb]	$\pm\Delta\sigma_{total}$ [%]	$\pm\Delta\sigma_{ref}$ [%]
13.45	235	*46.8*	*1.68*
13.88	269	*43.1*	*1.56*
14.05	293	*39.2*	*1.55*
14.28	370	*32.3*	*1.54*
14.49	347	*36.1*	*1.53*
14.69	386	*31.3*	*1.53*
14.81	392	*33.3*	*1.55*
14.88	409	*31.8*	*1.54*
Ref. CS is ^{27}Al(n, α)^{24}Na;			α_d = *1.2*

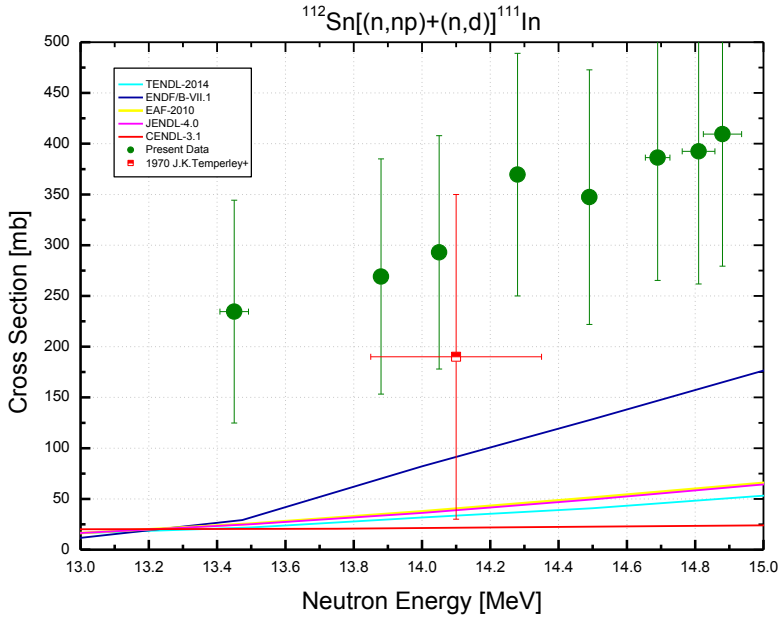

The amount of ^{111}In nuclei was measured next day after irradiation. The cross-section of the ^{112}Sn[(n, np)+(n, d)]^{111}In reaction was determined as the difference between the total ^{111}In production cross-section and the ^{112}Sn(n, 2n)^{111}Sn cross-section.

The comparatively large relative uncertainty of the data obtained is the consequence of this subtraction.

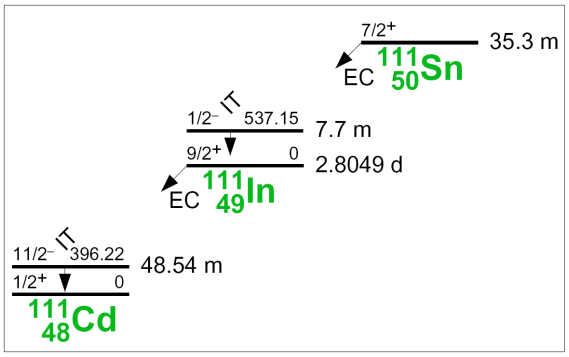

Decay data used for **^{112}Sn(n, x)^{111}In**.

Target nucleus	**Abundance [%]**	**Chemical form**	**Reaction product**	**$T_{1/2}$**	**E_γ [keV]**	**Y_γ [%]**
^{112}Sn	**0.97** *1*	Sn-metal	^{111}In	**2.8047 d** *4*	171.3	90.7 *9*
					245.3	**94.1** *10*

^{114}Sn(n, 2n)^{113}Sn

^{114}Sn(n, 2n)^{113}Sn			
E_n [MeV]	σ [mb]	$\pm\Delta\sigma_{total}$ [%]	$\pm\Delta\sigma_{ref}$ [%]
13.47	1004	*5.51*	*1.73*
13.88	1073	*3.65*	*1.61*
14.05	1115	*3.47*	*1.61*
14.28	1183	*5.64*	*1.59*
14.49	1200	*2.93*	*1.58*
14.70	1262	*5.90*	*1.59*
14.88	1268	*3.05*	*1.60*
Ref. CS is ^{27}Al(n, α)^{24}Na;			$\alpha_d = 1.2$

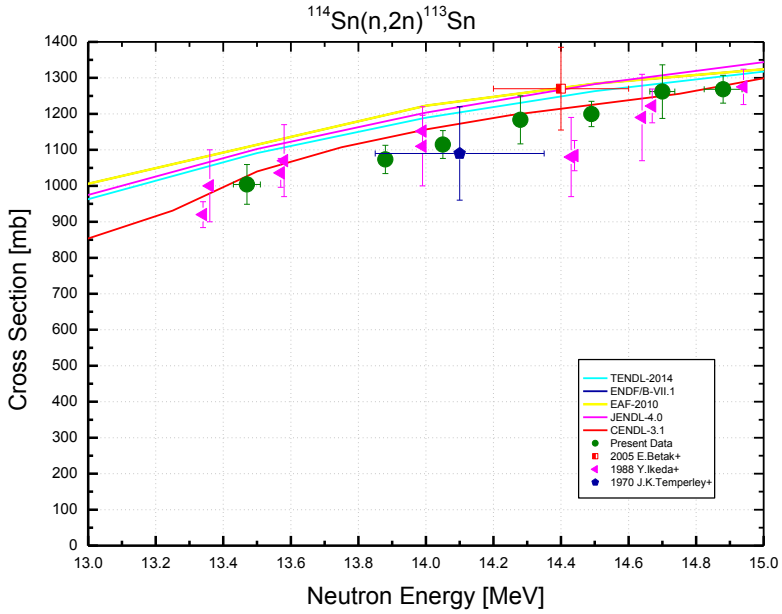

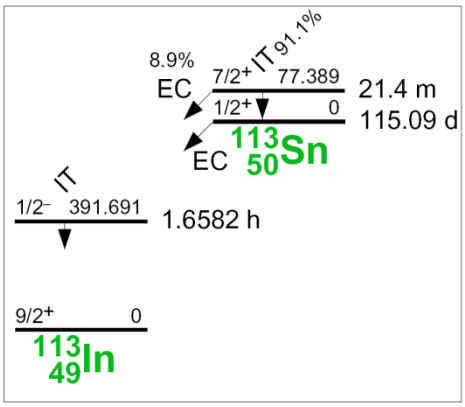

Decay data used for **^{114}Sn(n, 2n)^{113}Sn**.

Target nucleus	Abundance [%]	Chemical form	Reaction product	$T_{1/2}$	E_γ [keV]	Y_γ [%]
^{114}Sn	**0.66** *1*	Sn-metal	^{113}Sn	**115.09 d** *3*	**391.7**	**64.97** *17*

^{116}Sn(n, p)^{116m}In

^{116}Sn(n, p)^{116m}In			
E_n [MeV]	σ [mb]	$\pm\Delta\sigma_{total}$ [%]	$\pm\Delta\sigma_{ref}$ [%]
14.05	9.64	*3.73*	*1.70*
14.28	11.2	*5.27*	*1.68*
14.68	11.6	*3.13*	*1.68*
14.81	12.4	*4.92*	*1.69*
14.88	12.5	*2.84*	*1.69*
Ref. CS is ^{27}Al(n, α)^{24}Na;			$\alpha_d = 1.7$

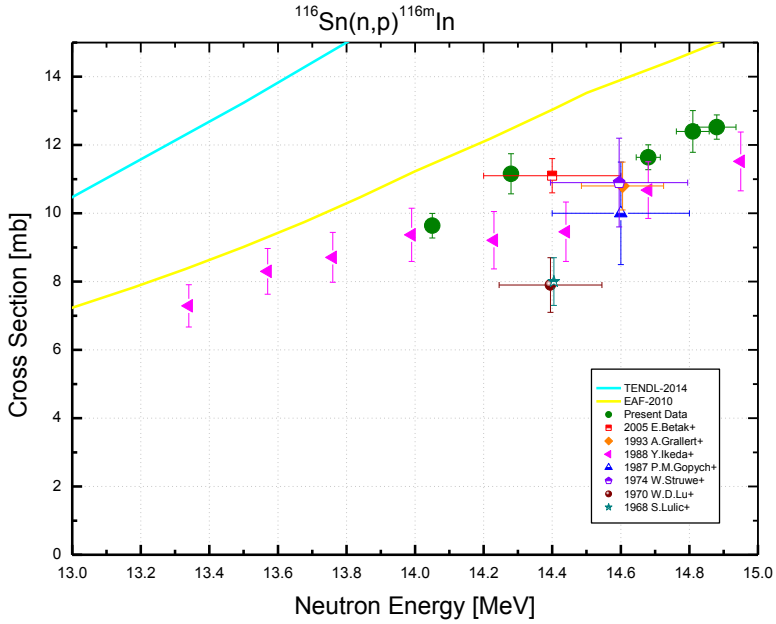

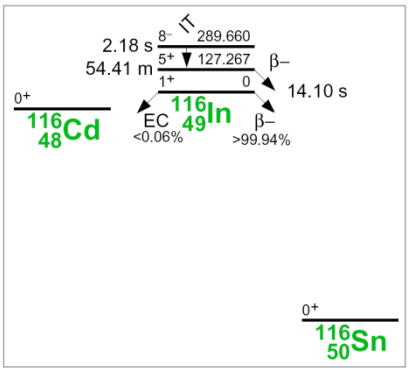

Decay data used for **^{116}Sn(n, p)^{116m}In.**

Target nucleus	Abundance [%]	Chemical form	Reaction product	$T_{1/2}$	E_γ [keV]	Y_γ [%]
^{116}Sn	**14.54** *9*	Sn-metal	^{116m}In	**54.29 m** *17*	416.9	27.2 *4*
					1097.3	58.5 *8*
					1293.6	**84.8** *12*

^{117}Sn(n, p)^{117m}In

^{117}Sn(n, p)^{117m}In			
E_n [MeV]	σ [mb]	$\pm\Delta\sigma_{total}$ [%]	$\pm\Delta\sigma_{ref}$ [%]
13.45	3.79	*7.86*	*4.37*
14.28	4.07	*16.4*	*4.32*
14.68	4.25	*15.6*	*4.32*
14.81	3.49	*25.8*	*4.32*
14.88	4.62	*12.0*	*4.32*
Ref. CS is ^{27}Al(n, α)^{24}Na;			α_d = *1.3*

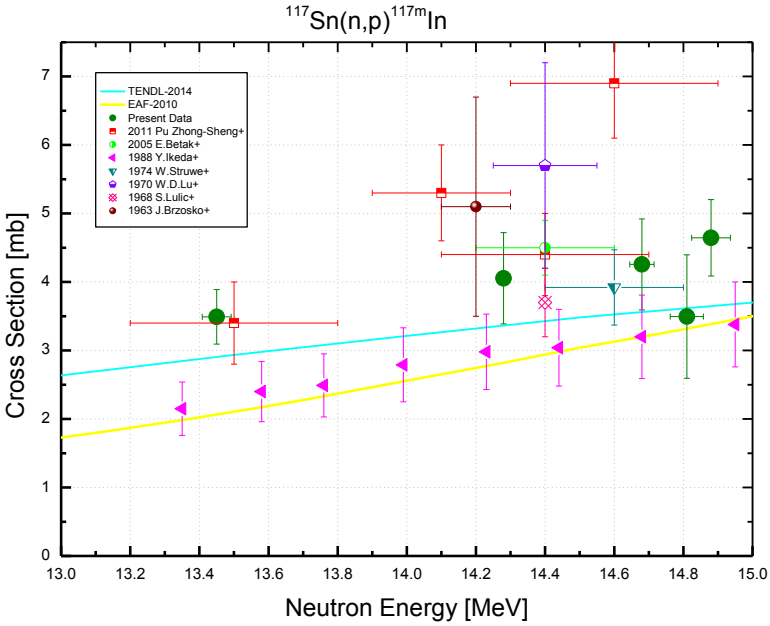

The contribution of ^{120}Sn(n, α)^{117}Cd reaction to population of the ^{117m}In level via ^{117}Cd decay was estimated as <1% that is several times less than the data uncertainty. This contribution was not accounted for.

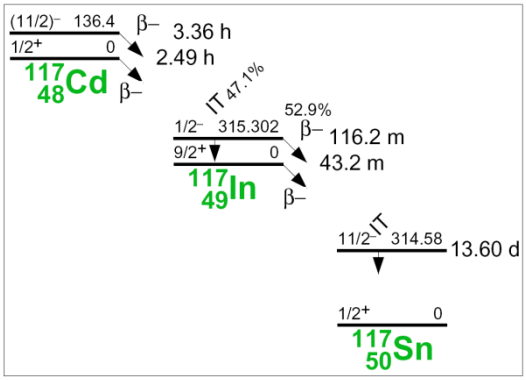

Decay data used for **^{117}Sn(n, p)^{117m}In**.

Target nucleus	Abundance [%]	Chemical form	Reaction product	$T_{1/2}$	E_γ [keV]	Y_γ [%]
^{117}Sn	**7.68** *7*	Sn-metal	^{117m}In	**116.2 m** *3*	**315.3**	**19.1** *8*

^{117}Sn(n, p)^{117g}In

^{117}Sn(n, p)^{117g}In			
E_n [MeV]	σ [mb]	$\pm\Delta\sigma_{total}$ [%]	$\pm\Delta\sigma_{ref}$ [%]
13.47	6.11	*11.4*	*10.1*
14.05	8.32	*10.8*	*10.1*
14.28	10.2	*10.7*	*10.1*
14.68	11.4	*10.6*	*10.1*
14.81	12.4	*10.4*	*10.1*
14.88	13.4	*10.3*	*10.1*
Ref. CS is ^{27}Al(n, α)^{24}Na;			$\alpha_d = 1.6$

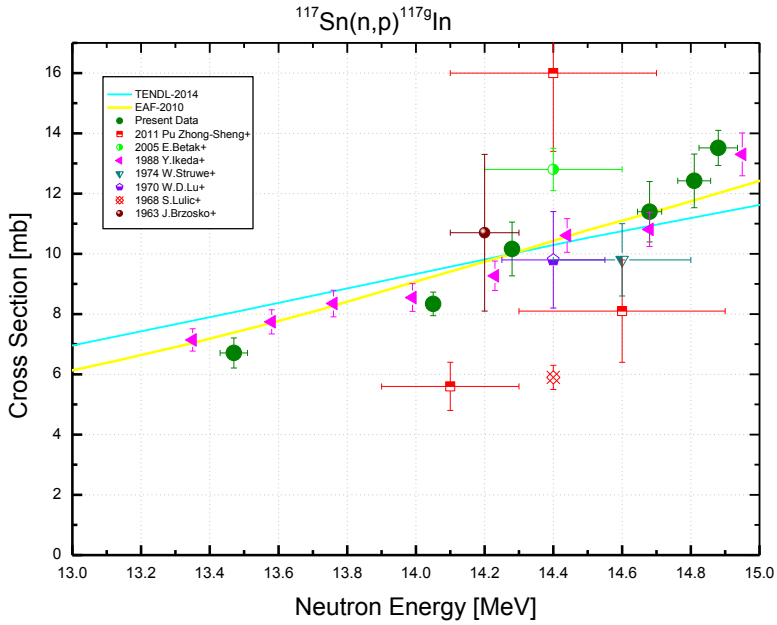

The contribution of ^{120}Sn(n, α)^{117}Cd reaction to population of the ^{117}In ground state via ^{117}Cd decay was estimated as <1% that is several times less than the data uncertainty. This contribution was not accounted for.

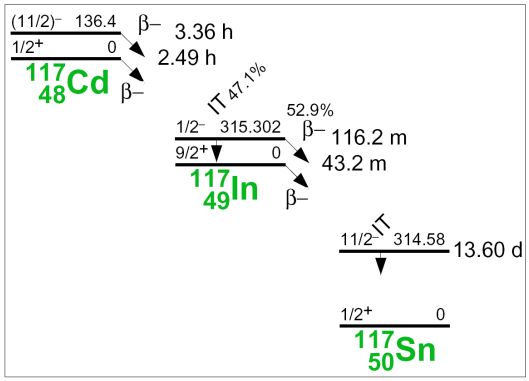

Decay data used for **^{117}Sn(n, p)^{117g}In**.

Target nucleus	Abundance [%]	Chemical form	Reaction product	$T_{1/2}$	E_γ [keV]	Y_γ [%]
^{117}Sn	**7.68** *7*	Sn-metal	^{117g}In	**43.2 m** *3*	**552.9**	**100** *10*

^{117}Sn(n, p)^{117}In

^{117}Sn(n, p)^{117}In		
E_n [MeV]	σ [mb]	$\pm\Delta\sigma_{total}$ [%]
13.46	10.2	*7.64*
14.28	14.2	*8.97*
14.68	15.7	*8.76*
14.81	15.9	*9.17*
14.88	18.2	*5.12*
Ref. CS is ^{27}Al(n, α)^{24}Na		

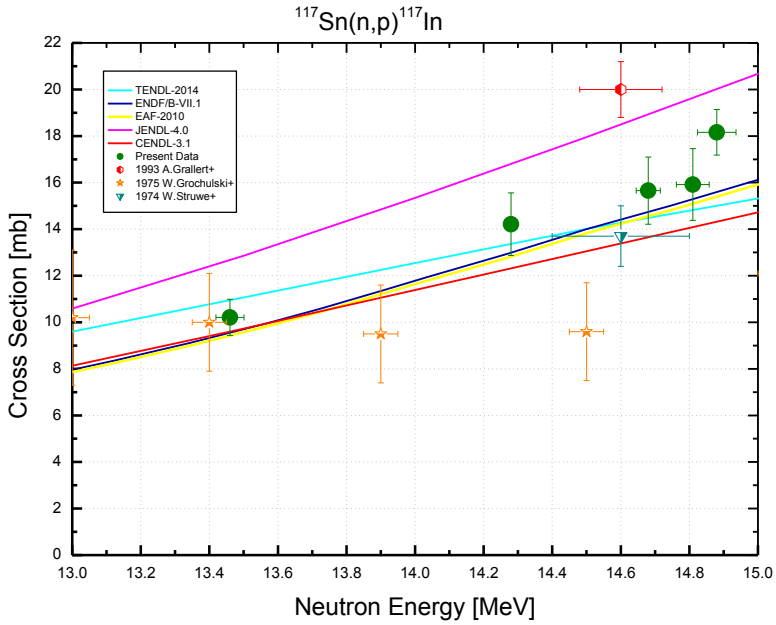

This is the sum of the ^{117}Sn(n, p)^{117m}In and ^{117}Sn(n, p)^{117g}In cross-sections measured independently and presented on the previous pages. The cross-section was not corrected for the contribution of ^{120}Sn(n, α)^{117}Cd reaction which was estimated to be less than 1% that is several times less than the data uncertainty.

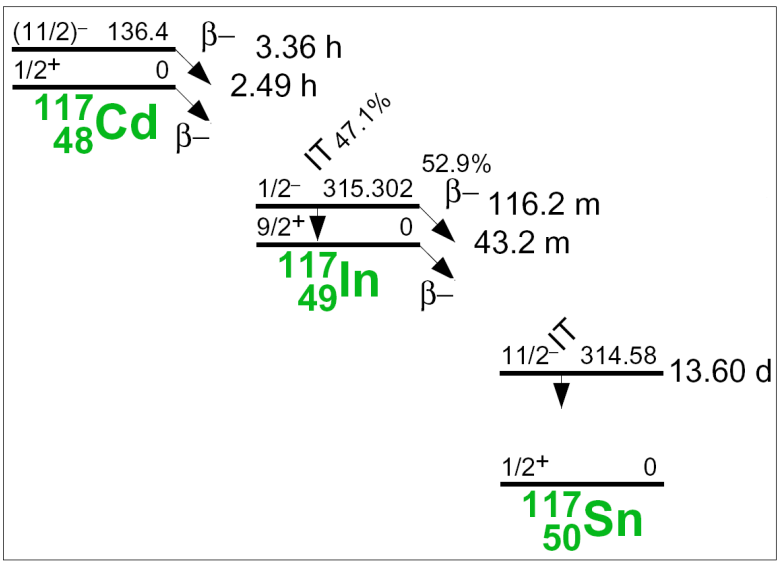

^{118}Sn(n, 2n)^{117m}Sn

^{118}Sn(n, 2n)^{117m}Sn			
E_n [MeV]	σ [mb]	$\pm\Delta\sigma_{total}$ [%]	$\pm\Delta\sigma_{ref}$ [%]
13.45	813	*4.72*	*1.08*
14.05	838	*5.78*	*0.87*
14.28	880	*4.65*	*0.84*
14.69	897	*4.07*	*0.83*
14.81	908	*6.54*	*1.80*
14.88	893	*3.30*	*0.85*
Ref. CS is ^{27}Al(n, α)^{24}Na;			α_d = *1.2*

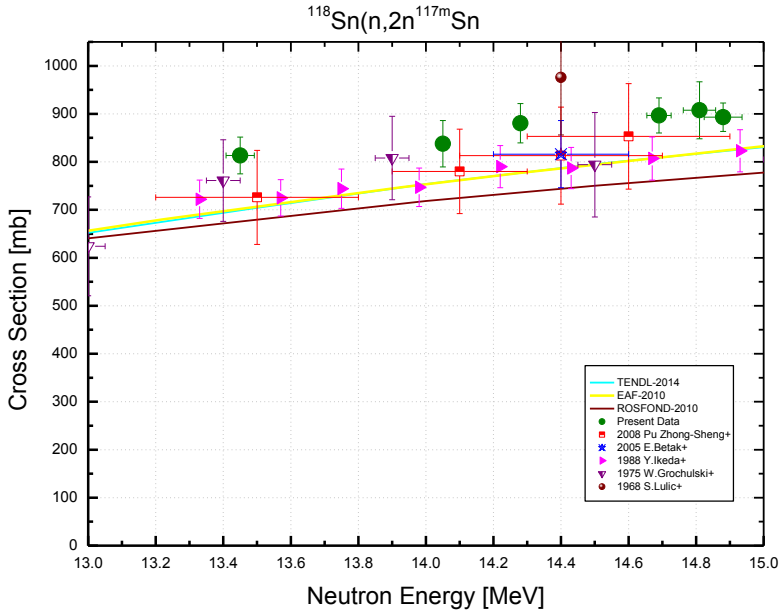

According to the decay schema fragment shown on this page lower, the metastable state ^{117m}Sn (E^*=314.58 keV, $T_{1/2}$=14.00 d, I^π=11/2$^-$) is populated not only in the ^{118}Sn(n, 2n)^{117m}Sn reaction but also via the processes ^{117}Sn(n, p)^{117}In→^{117m}Sn and ^{120}Sn(n, α)^{117}Cd→^{117}In→^{117m}Sn. This contributon is small because most ^{117}In nuclei decay to the ^{117}Sn levels which have the lower spin values. The population of the metastable level ^{117m}Sn with I^π=11/2$^-$ during the ^{117}In decay is less than 0.5%.

The total contribution of the reactions mentioned above was estimated as less as 0.01% relatively to the ^{118}Sn(n, 2n)^{117m}Sn cross-section and was neglected.

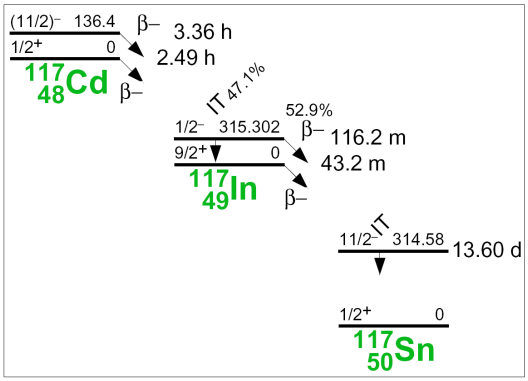

Decay data used for **^{118}Sn(n, 2n)^{117m}Sn**.

Target nucleus	**Abundance [%]**	**Chemical form**	**Reaction product**	**$T_{1/2}$**	**E_γ [keV]**	**Y_γ [%]**
^{118}Sn	**24.22** *9*	Sn-metal	^{117m}Sn	**14.00 d** *5*	**158.6**	**86.4** *4*

^{118}Sn(n, α)^{115g}Cd

^{118}Sn(n, α)^{115g}Cd			
E_n [MeV]	σ [mb]	$\pm\Delta\sigma_{total}$ [%]	$\pm\Delta\sigma_{ref}$ [%]
13.47	0.59	*13.5*	*2.36*
13.88	0.716	*5.57*	*2.27*
14.05	0.710	*4.13*	*2.26*
14.28	0.81	*18.5*	*2.25*
14.49	0.88	*36.3*	*2.25*
14.70	1.06	*18.1*	*2.25*
14.88	1.12	*3.41*	*2.26*
Ref. CS is ^{27}Al(n, α)^{24}Na;			α_d = *1.9*

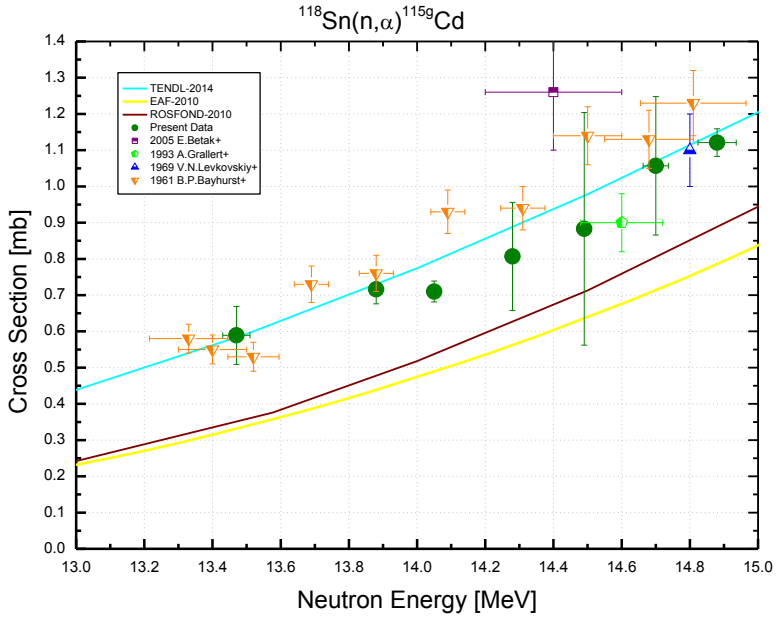

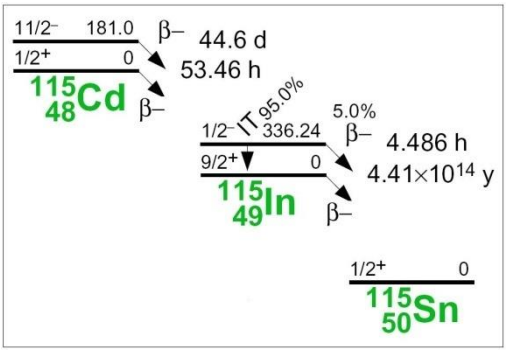

Decay data used for **^{118}Sn(n, α)^{115g}Cd**.

Target nucleus	Abundance [%]	Chemical form	Reaction product	$T_{1/2}$	E_γ [keV]	Y_γ [%]
^{118}Sn	**24.22** *9*	Sn-metal	^{115g}Cd	**53.46 h** *5*	492.4	8.03 *18*
					527.9	**27.5** *6*

^{120}Sn(n, α)^{117m}Cd

^{120}Sn(n, α)^{117m}Cd			
E_n [MeV]	σ [mb]	$\pm\Delta\sigma_{total}$ [%]	$\pm\Delta\sigma_{ref}$ [%]
13.47	0.100	*20.0*	*3.40*
13.88	0.121	*25.0*	*3.35*
14.05	0.120	*25.0*	*3.34*
14.28	0.159	*37.5*	*3.34*
Ref. CS is ^{27}Al(n, α)^{24}Na;			α_d = *1.8*

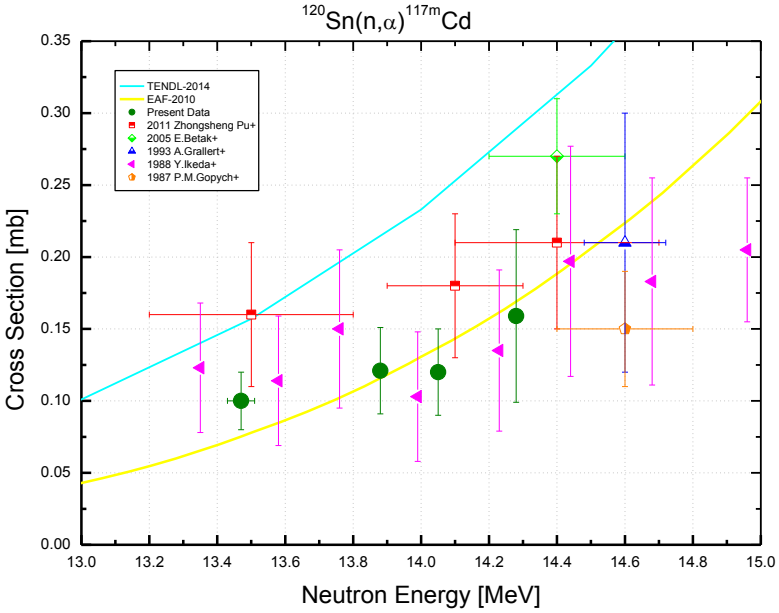

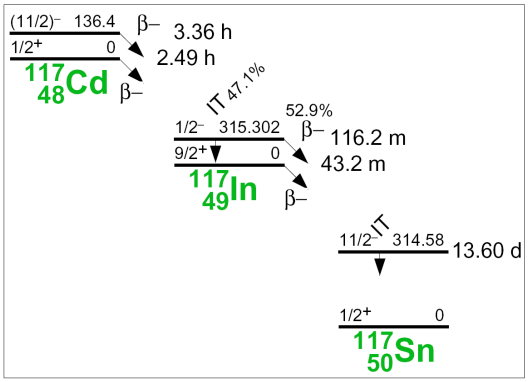

Decay data used for **^{120}Sn(n, α)^{117m}Cd**.

Target nucleus	Abundance [%]	Chemical form	Reaction product	$T_{1/2}$	E_γ [keV]	Y_γ [%]
^{120}Sn	**32.58** *9*	Sn-metal	^{117m}Cd	**3.36 h** *5*	564.4	14.7 *8*
					1066.0	23.1 *7*
					1997.3	**26.2** *5*

^{120}Sn(n, α)^{117g}Cd

^{120}Sn(n, α)^{117g}Cd			
E_n [MeV]	σ [mb]	$\pm\Delta\sigma_{total}$ [%]	$\pm\Delta\sigma_{ref}$ [%]
13.47	0.120	*16.6*	*4.55*
13.88	0.174	*13.8*	*4.51*
14.05	0.246	*22.3*	*4.51*
Ref. CS is ^{27}Al(n, α)^{24}Na;			α_d = *1.9*

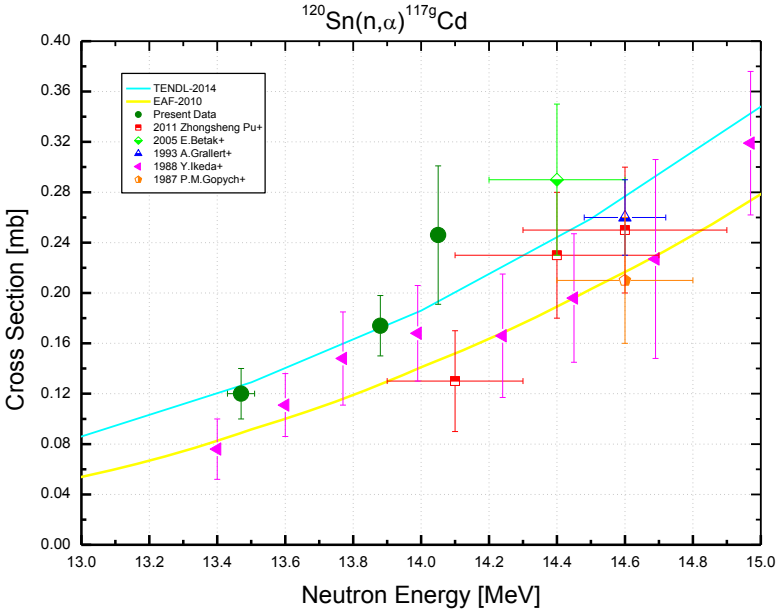

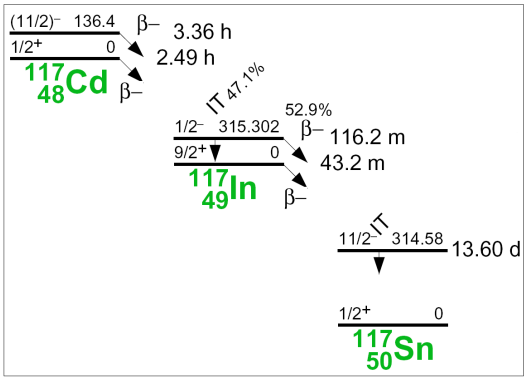

Decay data used for **^{120}Sn(n, α)^{117g}Cd.**

Target nucleus	Abundance [%]	Chemical form	Reaction product	$T_{1/2}$	E_γ [keV]	Y_γ [%]
^{120}Sn	**32.58** *9*	Sn-metal	^{117g}Cd	**2.49 h** *4*	**1303.3**	**18.4** *6*
					1576.6	11.2 *4*

^{120}Sn(n, α)^{117}Cd

^{120}Sn(n, α)^{117}Cd		
E_n [MeV]	σ [mb]	$\pm\Delta\sigma_{total}$ [%]
13.47	0.220	*12.8*
13.88	0.295	*13.1*
14.05	0.366	*17.1*
Ref. CS is ^{27}Al(n, α)^{24}Na		

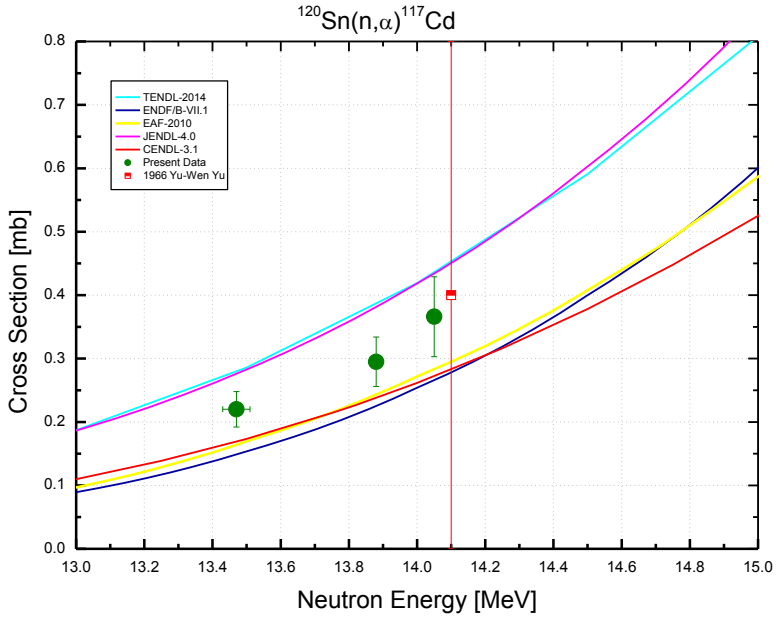

This is the sum of the ^{120}Sn(n, α)^{117m}Cd and ^{120}Sn(n, α)^{117g}Cd cross sections measured independently and presented on previous pages.

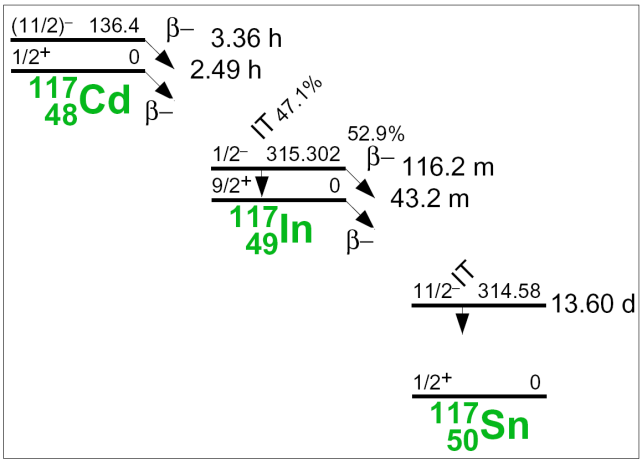

^{120}Sn(n, 2n)^{119m}Sn

^{120}Sn(n, 2n)^{119m}Sn			
E_n [MeV]	σ [mb]	$\pm\Delta\sigma_{total}$ [%]	$\pm\Delta\sigma_{ref}$ [%]
13.45	612	*8.27*	*1.64*
13.88	701	*7.86*	*1.52*
14.05	704	*7.74*	*1.51*
14.28	679	*7.89*	*1.49*
14.49	738	*7.60*	*1.48*
14.70	662	*7.84*	*1.49*
14.88	719	*7.54*	*1.50*
Ref. CS is ^{27}Al(n, α)^{24}Na;			$\alpha_d = 1.9$

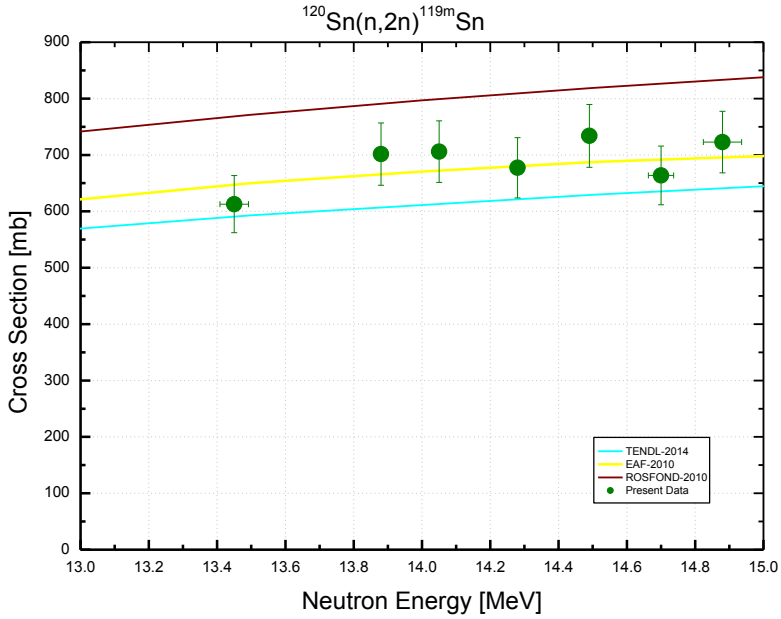

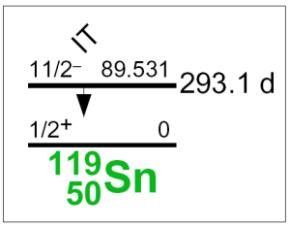

Decay data used for **^{120}Sn(n, 2n)^{119m}Sn**.

Target nucleus	Abundance [%]	Chemical form	Reaction product	$T_{1/2}$	E_γ [keV]	Y_γ [%]
^{120}Sn	**32.58** *9*	Sn-metal	^{119m}Sn	**293.1 d** *7*	**23.875**	**16.50** *22*
					25.044	7.9289 *7*
					25.271	14.8392 *11*

^{124}Sn(n, 2n)^{123g}Sn

^{124}Sn(n, 2n)^{123g}Sn			
E_n [MeV]	σ [mb]	$\pm\Delta\sigma_{total}$ [%]	$\pm\Delta\sigma_{ref}$ [%]
13.45	1214	*17.6*	*16.7*
13.88	1256	*18.7*	*16.7*
14.05	1331	*19.4*	*16.7*
14.28	1299	*19.2*	*16.7*
14.49	1253	*18.3*	*16.7*
14.70	1228	*17.0*	*16.7*
14.88	1315	*19.1*	*16.7*
Ref. CS is ^{27}Al(n, α)^{24}Na;			$\alpha_d = 1.5$

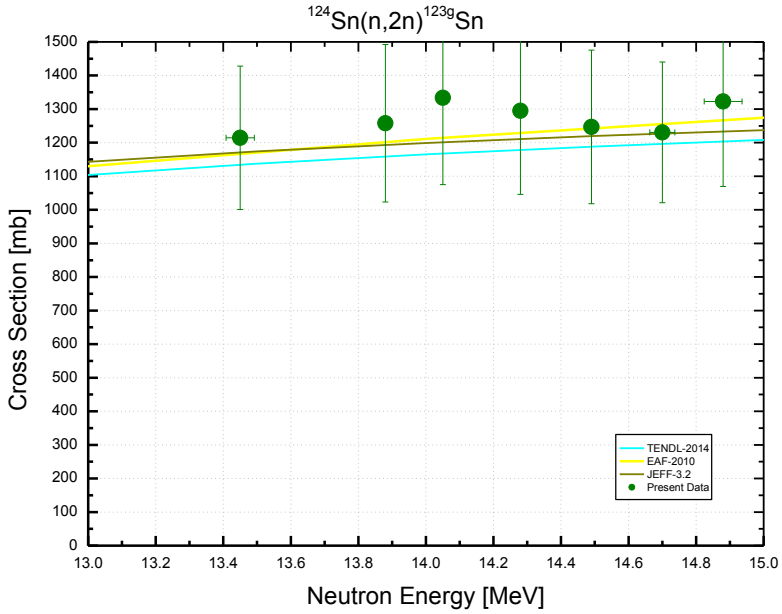

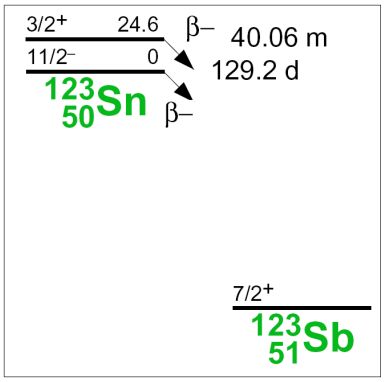

Decay data used for **^{124}Sn(n, 2n)^{123g}Sn**.

Target nucleus	Abundance [%]	Chemical form	Reaction product	$T_{1/2}$	E_γ [keV]	Y_γ [%]
^{124}Sn	**5.79** *5*	Sn-metal	^{123g}Sn	**129.2 d** *4*	**1088.6**	**0.60** *10*

^{124}Sn(n, 2n)^{123m}Sn

^{124}Sn(n, 2n)^{123m}Sn			
E_n [MeV]	σ [mb]	$\pm\Delta\sigma_{total}$ [%]	$\pm\Delta\sigma_{ref}$ [%]
13.45	565	*6.67*	*1.27*
13.88	592	*6.06*	*1.10*
14.05	599	*5.76*	*1.09*
14.28	630	*9.48*	*1.07*
14.49	634	*5.15*	*1.05*
14.70	595	*6.63*	*1.07*
14.88	646	*3.69*	*1.08*
Ref. CS is ^{27}Al(n, α)^{24}Na;			$\alpha_d = 1.9$

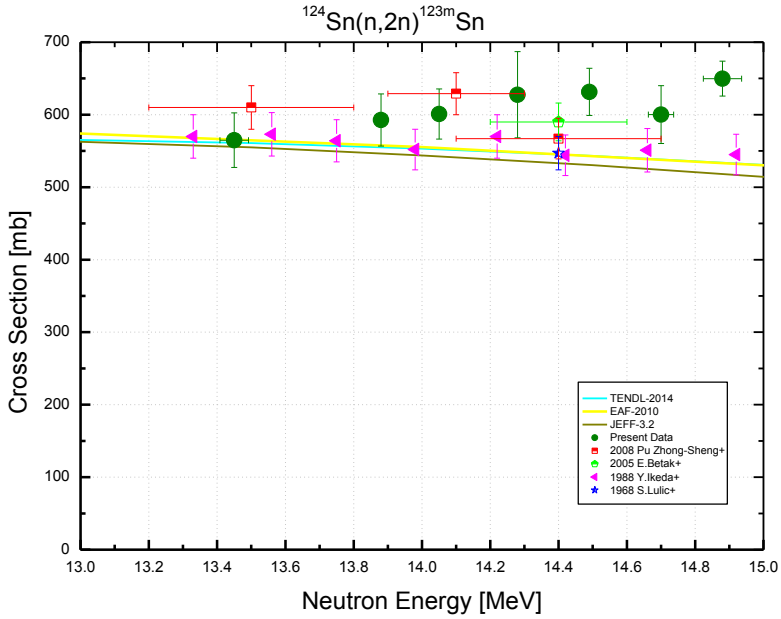

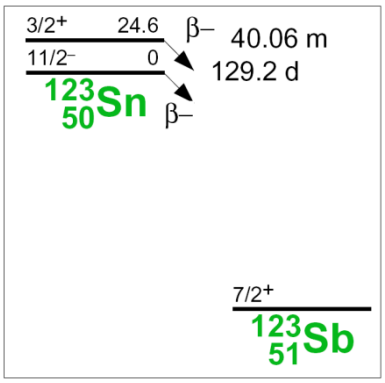

Decay data used for **^{124}Sn(n, 2n)^{123m}Sn**.

Target nucleus	**Abundance [%]**	**Chemical form**	**Reaction product**	**$T_{1/2}$**	**E_γ [keV]**	**Y_γ [%]**
^{124}Sn	**5.79** *5*	Sn-metal	^{123m}Sn	**40.06 m** *1*	**160.3**	**85.7** *4*

^{124}Sn(n, 2n)^{123}Sn

^{124}Sn(n, 2n)^{123}Sn		
E_n [MeV]	σ [mb]	$\pm\Delta\sigma_{total}$ [%]
13.45	1779	*12.2*
13.88	1848	*12.8*
14.05	1930	*13.5*
14.28	1929	*13.3*
14.49	1862	*11.4*
14.70	1961	*12.9*
14.88	1779	*12.2*
Ref. CS is ^{27}Al(n, α)^{24}Na		

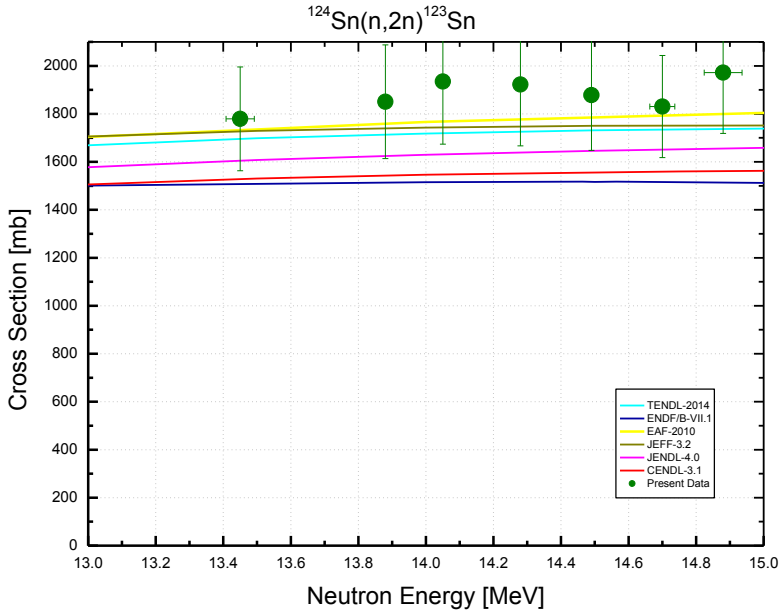

This is the sum of the ^{124}Sn(n, 2n)^{123m}Sn and ^{124}Sn(n, 2n)^{123g}Sn cross-sections measured independently and presented on the previous pages.

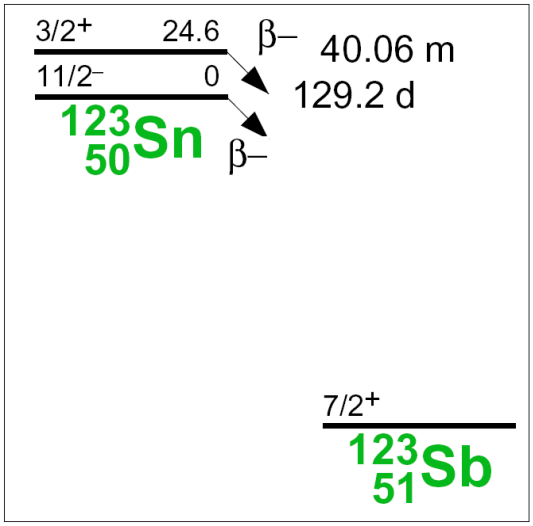

^{120}Te(n, 2n)^{119m}Te

^{120}Te(n, 2n)^{119m}Te			
E_n [MeV]	σ [mb]	$\pm\Delta\sigma_{total}$ [%]	$\pm\Delta\sigma_{ref}$ [%]
13.48	403	*19.8*	*2.60*
13.67	461	*9.95*	*2.59*
14.06	550	*8.88*	*2.58*
14.28	526	*8.68*	*2.58*
14.46	559	*8.85*	*2.58*
14.67	586	*9.14*	*2.58*
14.83	616	*8.41*	*2.59*
Ref. CS is ^{93}Nb(n,2n)^{92m}Nb;			$\alpha_d = 1.1$

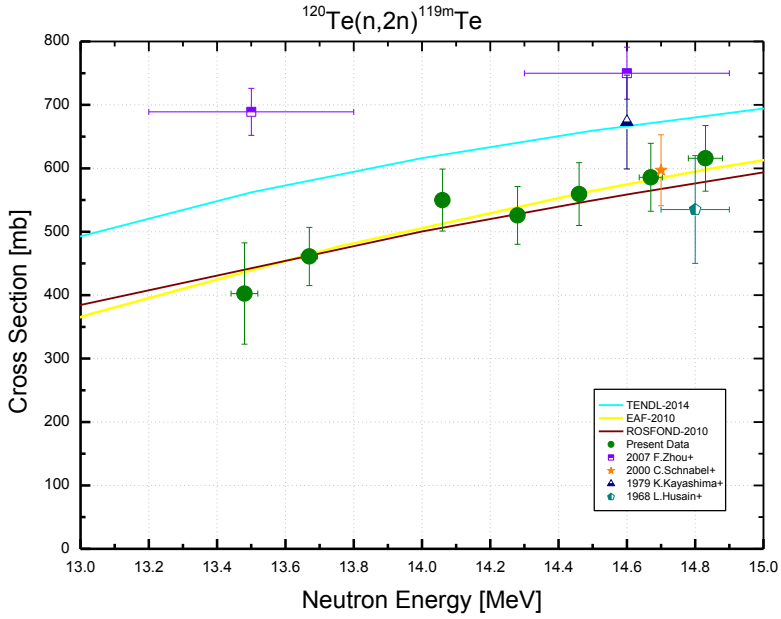

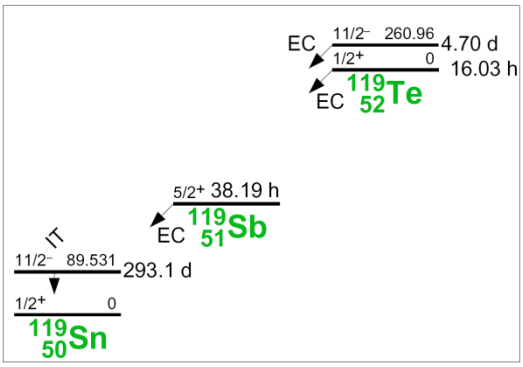

Decay data used for **^{120}Te(n, 2n)^{119m}Te**.

Target nucleus	Abundance [%]	Chemical form	Reaction product	$T_{1/2}$	E_γ [keV]	Y_γ [%]
^{120}Te	**0.096** *2*	TeO_2	^{119m}Te	**4.70 d** *4*	153.6	66 *3*
					270.5	28.0 *4*
					1212.7	**66.1** *3*

^{120}Te(n, 2n)^{119g}Te

^{120}Te(n, 2n)^{119g}Te			
E_n [MeV]	σ [mb]	$\pm\Delta\sigma_{total}$ [%]	$\pm\Delta\sigma_{ref}$ [%]
13.48	542	*8.21*	*2.30*
13.67	551	*8.11*	*2.29*
14.06	604	*7.56*	*2.28*
14.28	611	*7.61*	*2.28*
14.46	629	*7.68*	*2.28*
14.67	642	*7.69*	*2.28*
14.83	660	*7.52*	*2.29*
Ref. CS is ^{93}Nb(n,2n)^{92m}Nb;			$\alpha_d = 1.4$

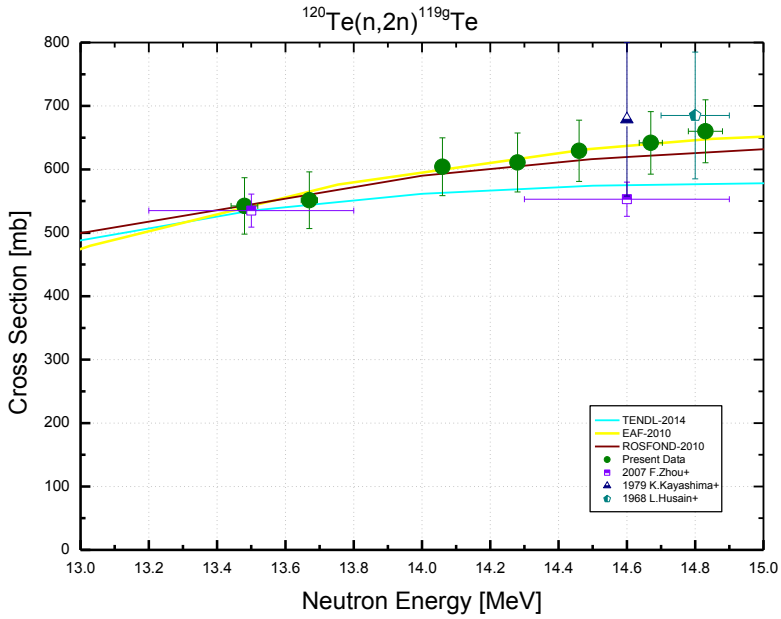

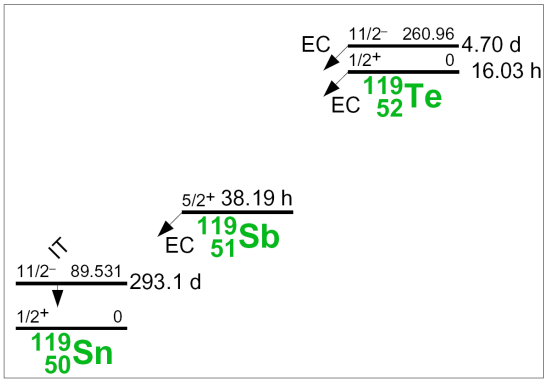

Decay data used for **^{120}Te(n, 2n)^{119g}Te**.

Target nucleus	Abundance [%]	Chemical form	Reaction product	$T_{1/2}$	E_γ [keV]	Y_γ [%]
^{120}Te	**0.096** *2*	TeO_2	^{119g}Te	**16.05 h** *5*	**644.0**	**84.1** *5*
					699.9	10.1 *5*

^{120}Te(n, 2n)^{119}Te

^{120}Te(n, 2n)^{119}Te		
E_n [MeV]	σ [mb]	$\pm\Delta\sigma_{total}$ *[%]*
13.48	945	*9.63*
13.67	1012	*6.28*
14.06	1154	*5.73*
14.28	1137	*5.67*
14.46	1189	*5.76*
14.67	1228	*5.87*
14.83	1276	*5.56*
Ref. CS	^{93}Nb(n,2n)^{92m}Nb	

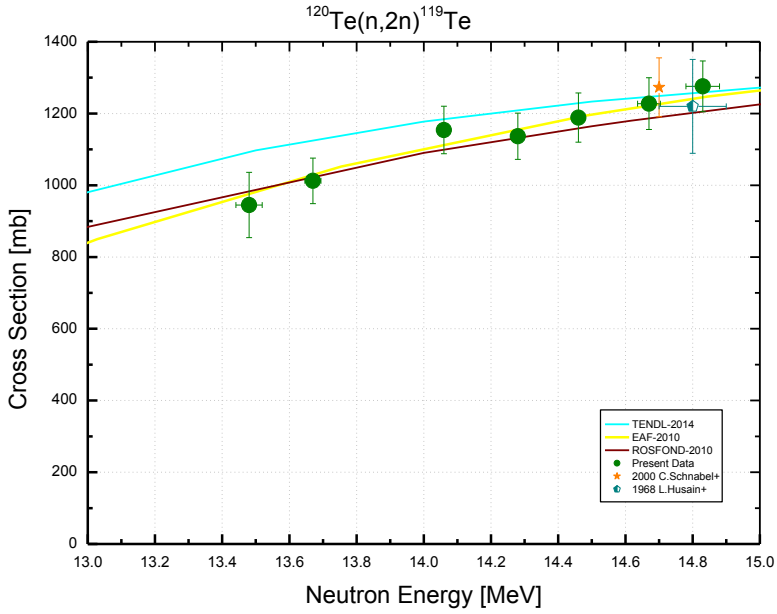

This is the sum of the ^{120}Te(n, 2n)^{119m}Te and ^{120}Te(n, 2n)^{119g}Te cross sections measured independently and presented on the previous pages.

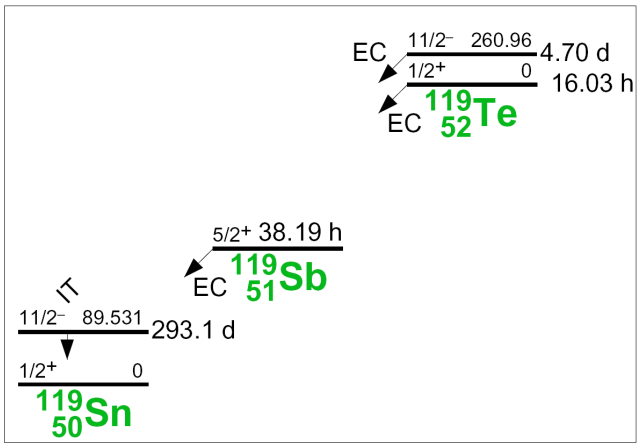

^{122}Te(n, p)^{122}Sb

^{122}Te(n, p)^{122}Sb			
E_n [MeV]	σ [mb]	$\pm\Delta\sigma_{total}$ [%]	$\pm\Delta\sigma_{ref}$ [%]
13.48	11.0	*7.72*	*0.70*
13.67	13.5	*6.42*	*0.66*
14.06	14.3	*5.92*	*0.62*
14.28	13.9	*6.10*	*0.62*
14.46	14.4	*6.11*	*0.62*
14.67	15.5	*6.21*	*0.64*
14.83	16.5	*5.72*	*0.66*
Ref. CS is ^{93}Nb(n,2n)^{92m}Nb;			$\alpha_d = 1.2$

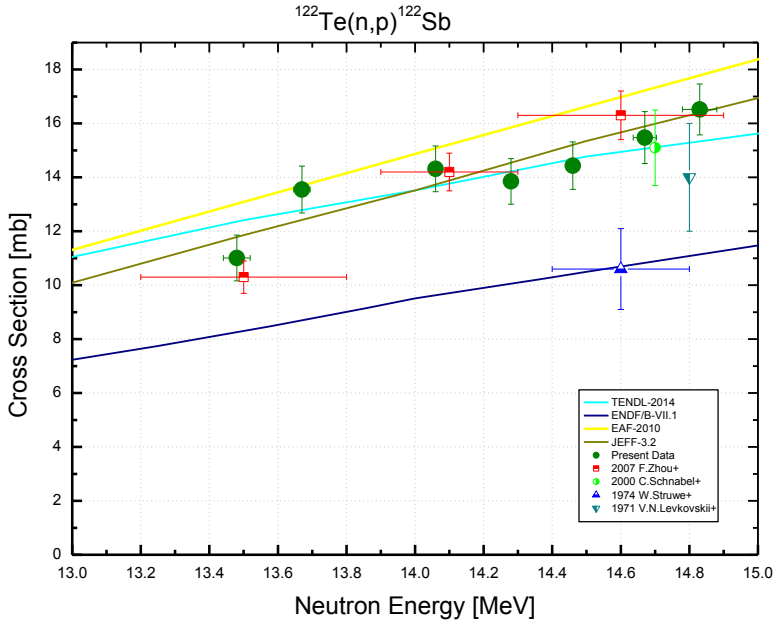

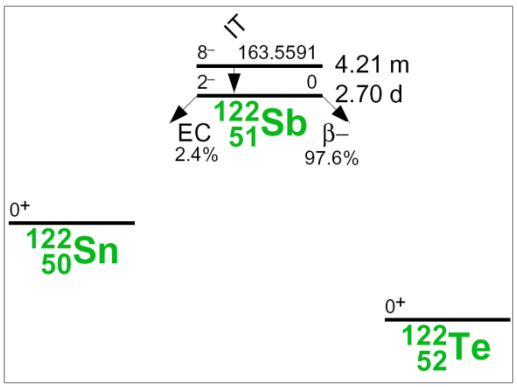

Decay data used for **^{122}Te(n, p)^{122}Sb**.

Target nucleus	Abundance [%]	Chemical form	Reaction product	$T_{1/2}$	E_γ [keV]	Y_γ [%]
^{122}Te	**2.603** *4*	TeO_2	^{122}Sb	**2.7238 d** *2*	**564.2**	**70.68** *18*

^{122}Te(n, 2n)^{121m}Te

^{122}Te(n, 2n)^{121m}Te			
E_n [MeV]	σ [mb]	$\pm\Delta\sigma_{total}$ [%]	$\pm\Delta\sigma_{ref}$ [%]
13.67	694.0	*10.1*	*1.49*
14.06	761.0	*9.17*	*1.47*
14.28	845.3	*8.21*	*1.47*
14.46	835.1	*8.29*	*1.47*
14.67	767.7	*9.03*	*1.48*
14.83	825.0	*8.45*	*1.49*
Ref. CS is ^{93}Nb(n,2n)^{92m}Nb;			$\alpha_d = 1.2$

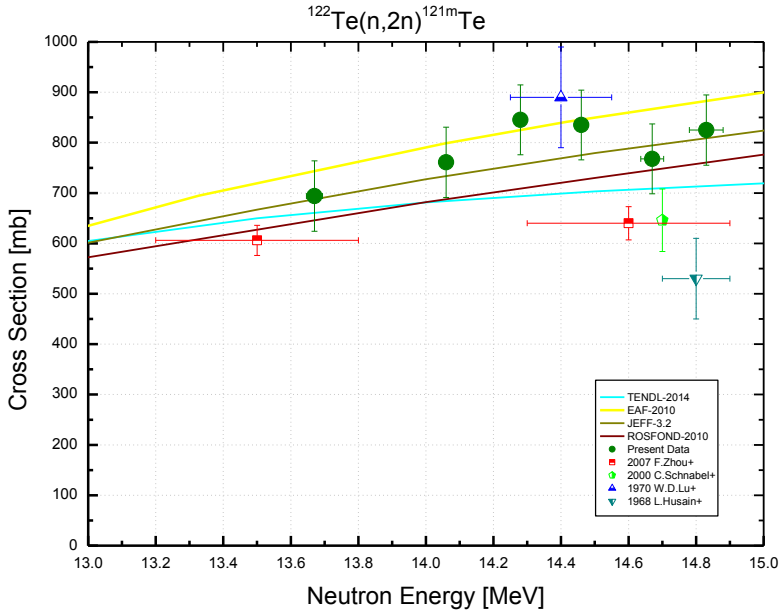

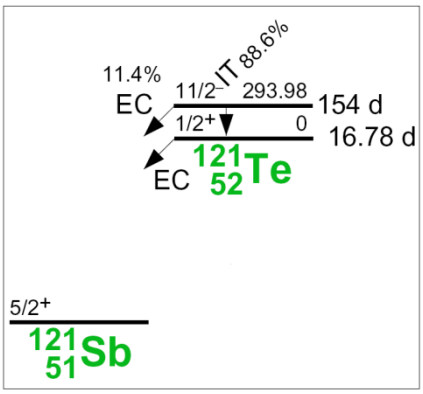

Decay data used for **^{122}Te(n, 2n)^{121m}Te**.

Target nucleus	Abundance [%]	Chemical form	Reaction product	$T_{1/2}$	E_γ [keV]	Y_γ [%]
^{122}Te	**2.603** *4*	TeO_2	^{121m}Te	**164.2 d** *8*	**212.2**	**81.5** *10*

^{122}Te(n, 2n)^{121g}Te

^{122}Te(n, 2n)^{121g}Te			
E_n [MeV]	σ [mb]	$\pm\Delta\sigma_{total}$ [%]	$\pm\Delta\sigma_{ref}$ [%]
13.67	649.8	*9.20*	*2.82*
14.06	749.9	*7.95*	*2.81*
14.28	668.0	*9.67*	*2.81*
14.46	755.2	*8.65*	*2.81*
14.67	719.8	*8.95*	*2.81*
14.83	678.1	*8.82*	*2.82*
Ref. CS is ^{93}Nb(n,2n)^{92m}Nb;			$\alpha_d = 1.3$

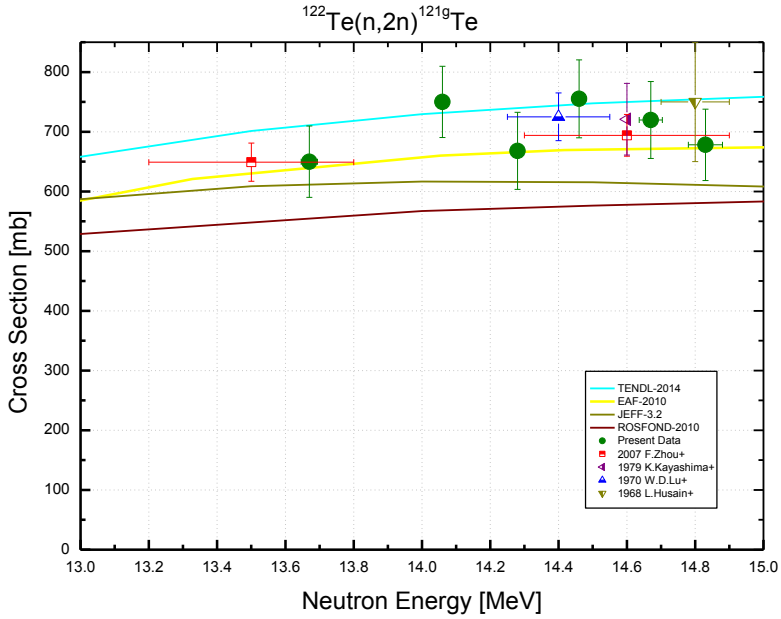

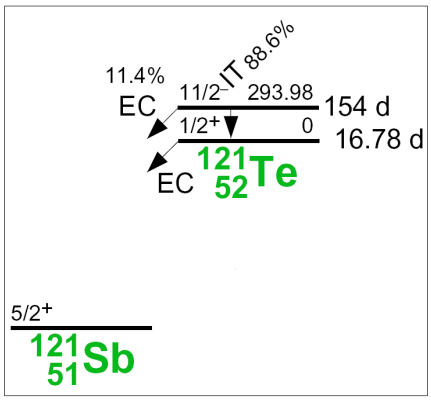

Decay data used for **^{122}Te(n, 2n)^{121g}Te**.

Target nucleus	Abundance [%]	Chemical form	Reaction product	$T_{1/2}$	E_γ [keV]	Y_γ [%]
^{122}Te	**2.603** *4*	TeO_2	^{121g}Te	**19.17 d** *4*	507.6	17.7 *5*
					573.1	**80.4** *22*

^{122}Te(n, 2n)^{121}Te

^{122}Te(n, 2n)^{121}Te		
E_n [MeV]	σ [mb]	$\pm\Delta\sigma_{total}$ *[%]*
13.67	1344	*6.79*
14.06	1511	*6.02*
14.28	1513	*6.21*
14.46	1590	*5.92*
14.67	1488	*6.30*
14.83	1503	*6.05*
Ref. CS	^{93}Nb(n,2n)^{92m}Nb	

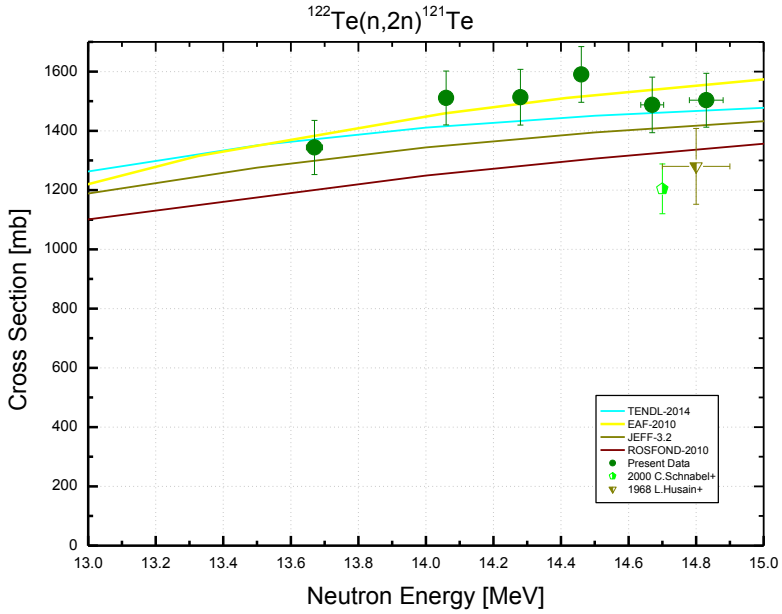

This is the sum of the ^{122}Te(n, 2n)^{121m}Te and ^{122}Te(n, 2n)^{121g}Te cross sections measured independently and presented on the previous pages.

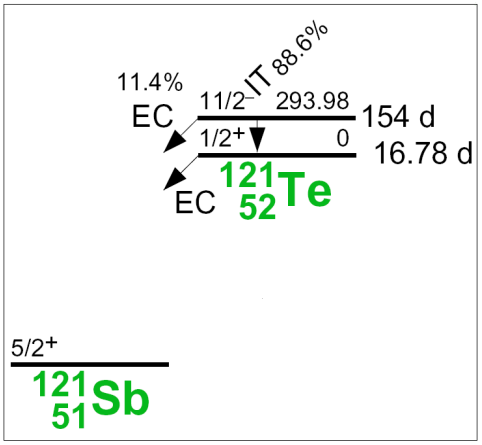

^{124}Te(n, 2n)^{123m}Te

^{124}Te(n, 2n)^{123m}Te			
E_n [MeV]	σ [mb]	$\pm\Delta\sigma_{total}$ [%]	$\pm\Delta\sigma_{ref}$ [%]
13.48	742	*7.99*	*3.06*
13.67	811	*8.09*	*3.05*
14.06	851	*7.46*	*3.04*
14.28	821	*8.21*	*3.04*
14.46	869	*7.26*	*3.04*
14.67	868	*7.27*	*3.05*
14.83	926	*7.40*	*3.05*
Ref. CS is ^{93}Nb(n,2n)^{92m}Nb;			α_d = *1.1*

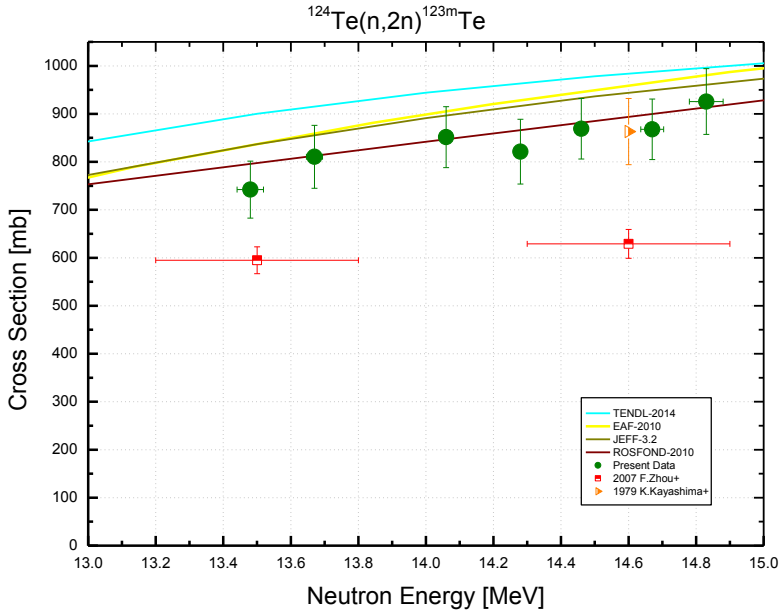

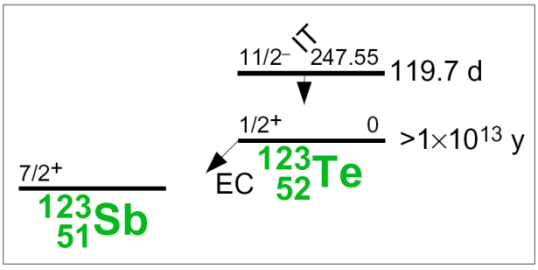

Decay data used for **^{124}Te(n, 2n)^{123m}Te**.

Target nucleus	Abundance [%]	Chemical form	Reaction product	$T_{1/2}$	E_γ [keV]	Y_γ [%]
^{124}Te	**4.74** ***14***	TeO_2	^{123m}Te	**119.2 d** ***1***	**159.0**	**84.0** ***4***

^{126}Te(n, 2n)^{125m}Te

^{126}Te(n, 2n)^{125m}Te			
E_n [MeV]	σ [mb]	$\pm\Delta\sigma_{total}$ [%]	$\pm\Delta\sigma_{ref}$ [%]
13.67	945	*17.0*	*1.65*
14.06	1214	*18.2*	*1.63*
14.28	1009	*15.8*	*1.63*
14.46	1107	*12.6*	*1.63*
14.67	940	*18.0*	*1.64*
Ref. CS is ^{93}Nb(n,2n)^{92m}Nb;			$\alpha_d = 1.2$

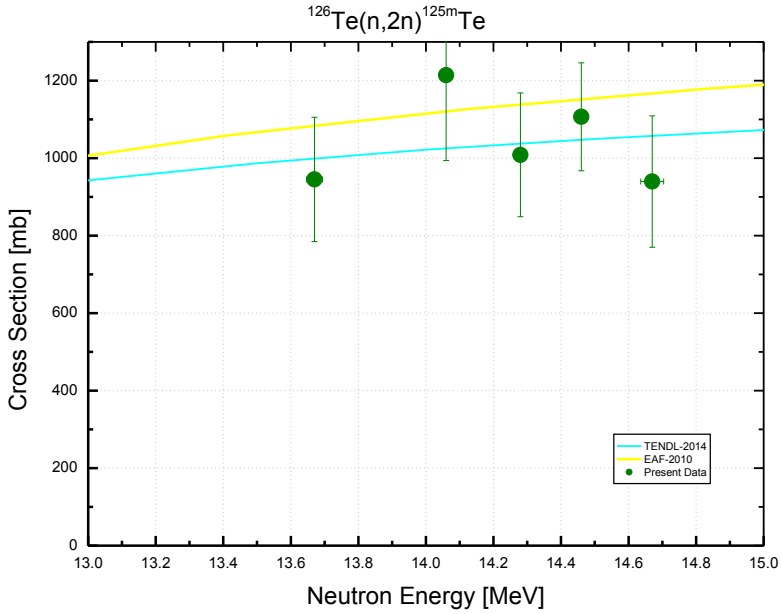

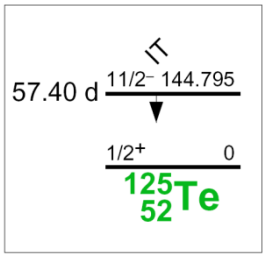

Decay data used for **^{126}Te(n, 2n)^{125m}Te**.

Target nucleus	Abundance [%]	Chemical form	Reaction product	$T_{1/2}$	E_γ [keV]	Y_γ [%]
^{126}Te	**18.84** *25*	TeO_2	^{125m}Te	**57.40 d** *15*	**109.3**	**0.280** *3*

^{128}Te(n, p)^{128g}Sb

^{128}Te(n, p)^{128g}Sb			
E_n [MeV]	σ [mb]	$\pm\Delta\sigma_{total}$ [%]	$\pm\Delta\sigma_{ref}$ [%]
13.48	0.594	*10.0*	*6.63*
13.67	0.640	*9.35*	*6.63*
14.06	0.831	*7.16*	*6.62*
14.28	0.931	*6.34*	*6.62*
14.46	1.049	*6.56*	*6.62*
14.67	1.115	*5.70*	*6.62*
14.83	1.253	*5.08*	*6.63*
Ref. CS is ^{93}Nb(n,2n)^{92m}Nb;			$\alpha_d = 1.6$

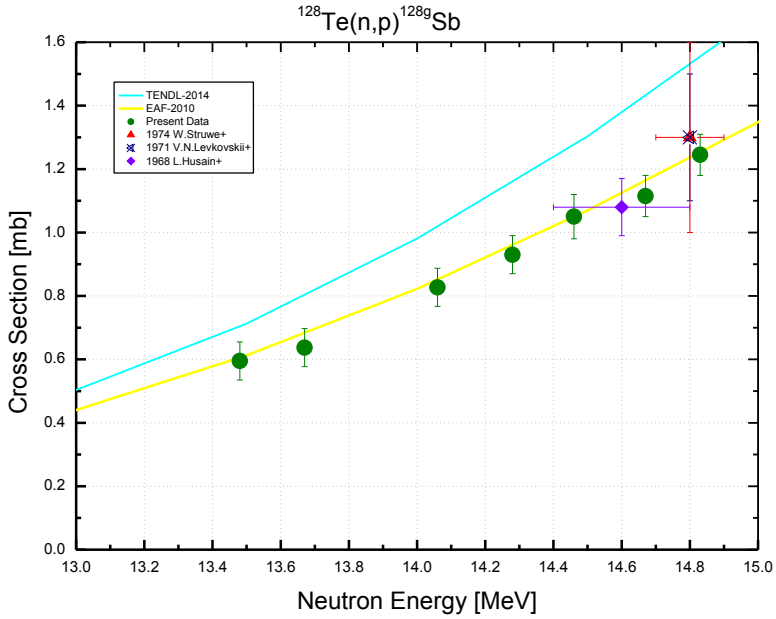

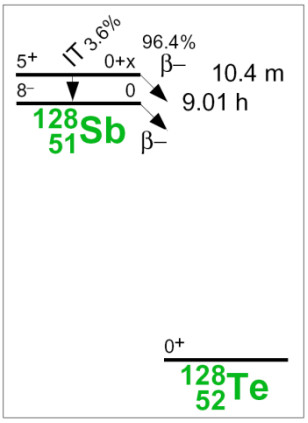

Decay data used for **^{128}Te(n, p)^{128g}Sb**.

Target nucleus	Abundance [%]	Chemical form	Reaction product	$T_{1/2}$	E_γ [keV]	Y_γ [%]
^{128}Te	**31.74** *8*	TeO_2	^{128g}Sb	**9.05 h** *4*	**314.1**	**61** *4*
					526.5	45 *3*
					743.7	100 *7*
					754.0	100 *7*

^{128}Te(n, 2n)^{127g}Te

^{128}Te(n, 2n)^{127g}Te			
E_n [MeV]	σ [mb]	$\pm\Delta\sigma_{total}$ [%]	$\pm\Delta\sigma_{ref}$ [%]
13.48	534	*7.39*	*3.30*
13.67	548	*6.30*	*3.29*
14.06	543	*7.31*	*3.28*
14.28	554	*7.13*	*3.28*
14.46	567	*6.94*	*3.28*
14.67	569	*6.03*	*3.28*
14.83	586	*6.76*	*3.29*
Ref. CS is ^{93}Nb(n,2n)^{92m}Nb;			$\alpha_d = 1.7$

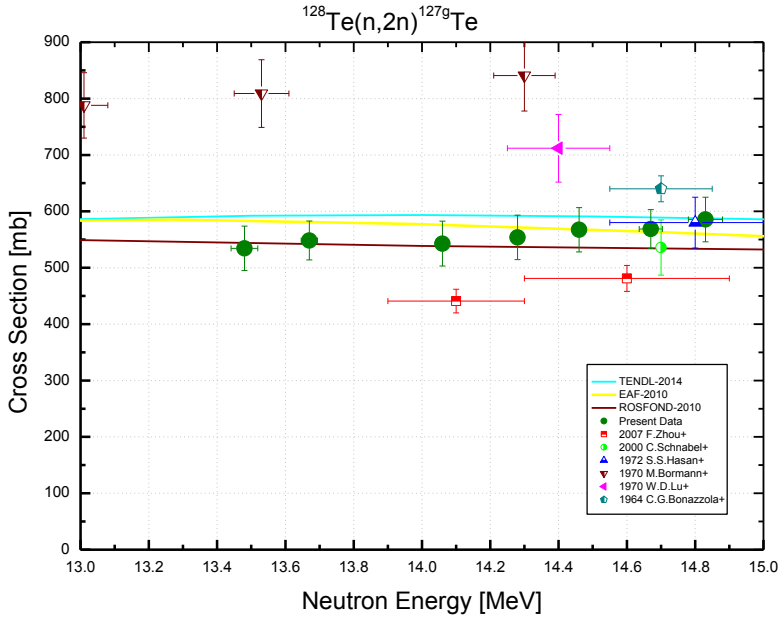

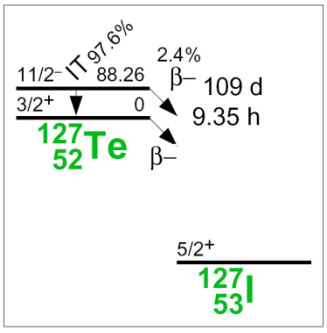

Decay data used for **^{128}Te(n, 2n)^{127g}Te**.

Target nucleus	Abundance [%]	Chemical form	Reaction product	$T_{1/2}$	E_γ [keV]	Y_γ [%]
^{128}Te	**31.74** *8*	TeO_2	^{127g}Te	**9.35 h** *7*	360.3	0.135 *14*
					417.9	**0.99** *10*

^{130}Te(n, 2n)^{129m}Te

^{130}Te(n, 2n)^{129m}Te			
E_n [MeV]	σ [mb]	$\pm\Delta\sigma_{total}$ [%]	$\pm\Delta\sigma_{ref}$ [%]
13.48	1001	*4.96*	*3.90*
13.67	984	*5.91*	*3.89*
14.06	1035	*4.91*	*3.88*
14.28	1042	*4.66*	*3.88*
14.46	1069	*4.32*	*3.88*
14.67	1097	*4.11*	*3.89*
14.83	1132	*4.55*	*3.89*
Ref. CS is ^{93}Nb(n,2n)^{92m}Nb;		α_d = *1.5*	

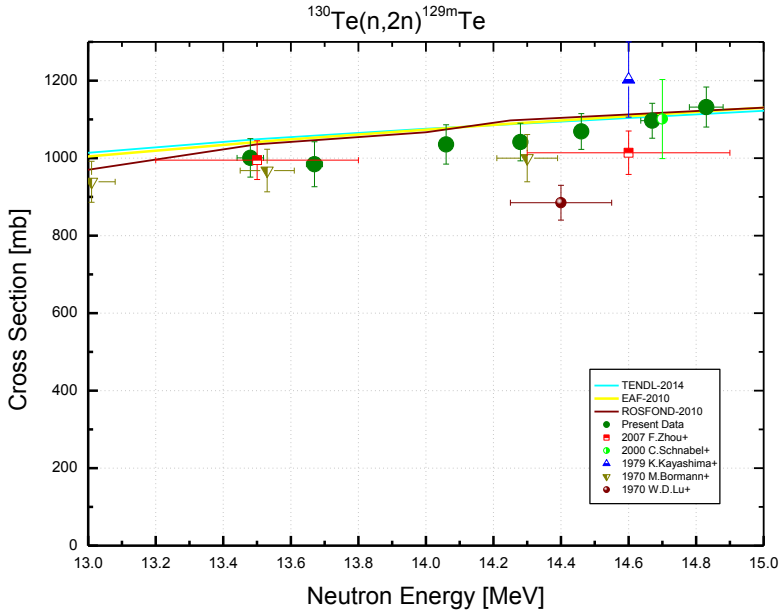

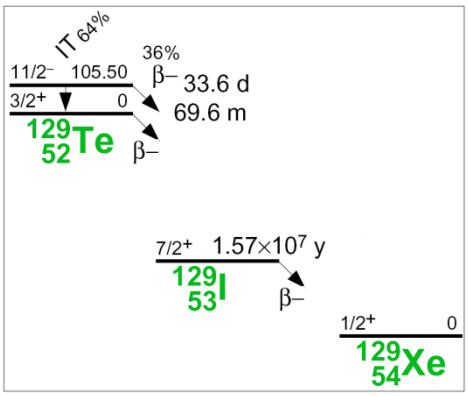

Decay data used for **^{130}Te(n, 2n)^{129m}Te**.

Target nucleus	Abundance [%]	Chemical form	Reaction product	$T_{1/2}$	E_γ [keV]	Y_γ [%]
^{130}Te	**34.08** *62*	TeO_2	^{129m}Te	**33.6 d** *1*	**729.6**	**0.70** *14*

^{130}Te(n, 2n)^{129g}Te

^{130}Te(n, 2n)^{129g}Te			
E_n [MeV]	σ [mb]	$\pm\Delta\sigma_{total}$ [%]	$\pm\Delta\sigma_{ref}$ [%]
13.48	637	*9.33*	*7.33*
13.67	637	*9.39*	*7.33*
14.06	647	*10.0*	*7.33*
14.28	653	*9.90*	*7.33*
14.46	665	*10.4*	*7.33*
14.67	683	*10.2*	*7.33*
14.83	677	*10.3*	*7.33*
Ref. CS is ^{93}Nb(n,2n)^{92m}Nb;			$\alpha_d = 1.6$

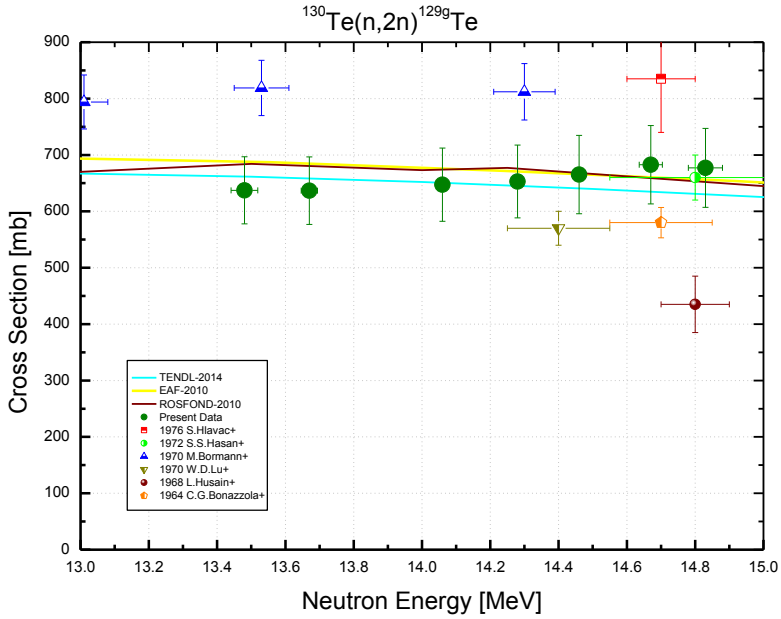

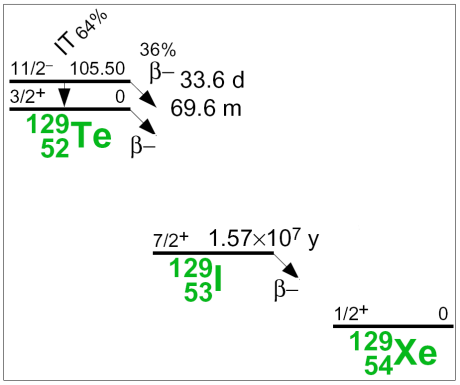

Decay data used for **^{130}Te(n, 2n)^{129g}Te**.

Target nucleus	Abundance [%]	Chemical form	Reaction product	$T_{1/2}$	E_γ [keV]	Y_γ [%]
^{130}Te	**34.08** *62*	TeO_2	^{129g}Te	**69.6 m** *3*	**459.6**	**7.7** *6*
					487.4	1.42 *10*

^{130}Te(n, 2n)^{129}Te

^{130}Te(n, 2n)^{129}Te		
E_n [MeV]	σ [mb]	$\pm\Delta\sigma_{total}$ *[%]*
13.48	1638	*4.66*
13.67	1621	*5.08*
14.06	1683	*4.83*
14.28	1695	*4.70*
14.46	1734	*4.74*
14.67	1779	*4.58*
14.83	1809	*4.73*
Ref. CS	^{93}Nb(n,2n)^{92m}Nb	

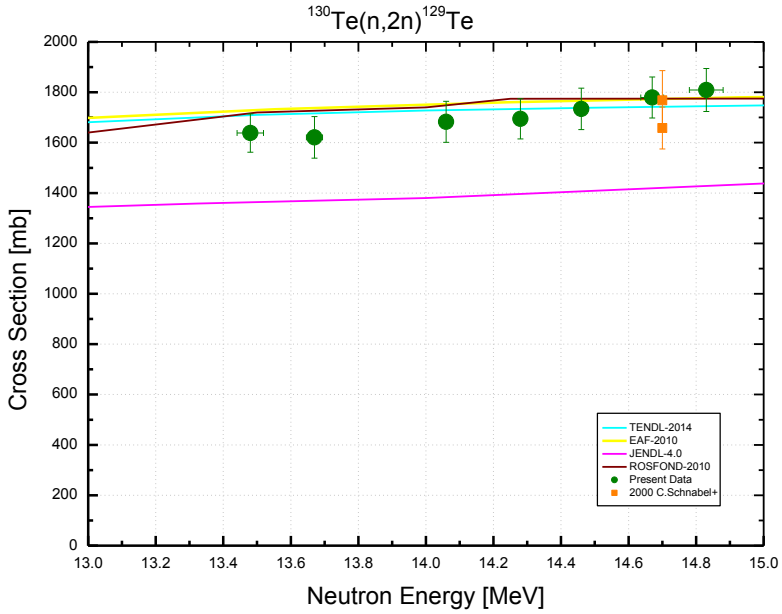

This is the sum of the ^{130}Te(n, 2n)^{129m}Te and ^{130}Te(n, 2n)^{129g}Te cross sections measured independently and presented on the previous pages.

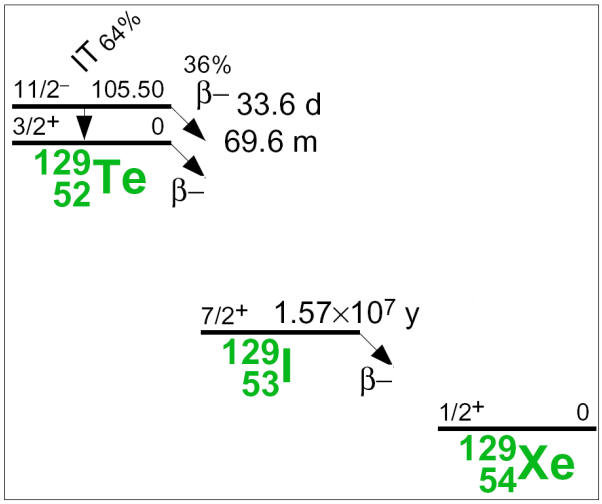

^{138}Ba(n, α)^{135m}Xe

^{138}Ba(n, α)^{135m}Xe			
E_n [MeV]	σ [mb]	$\pm\Delta\sigma_{total}$ [%]	$\pm\Delta\sigma_{ref}$ [%]
13.47	0.73	*8.18*	*1.08*
13.66	0.72	*9.69*	*0.90*
13.88	0.87	*6.92*	*0.88*
14.04	0.79	*8.81*	*0.87*
14.26	0.98	*7.08*	*0.84*
14.44	0.98	*6.04*	*0.82*
14.63	0.99	*6.04*	*0.83*
14.81	1.11	*5.30*	*0.85*
Ref. CS is ^{27}Al(n, α)^{24}Na;			α_d = *1.9*

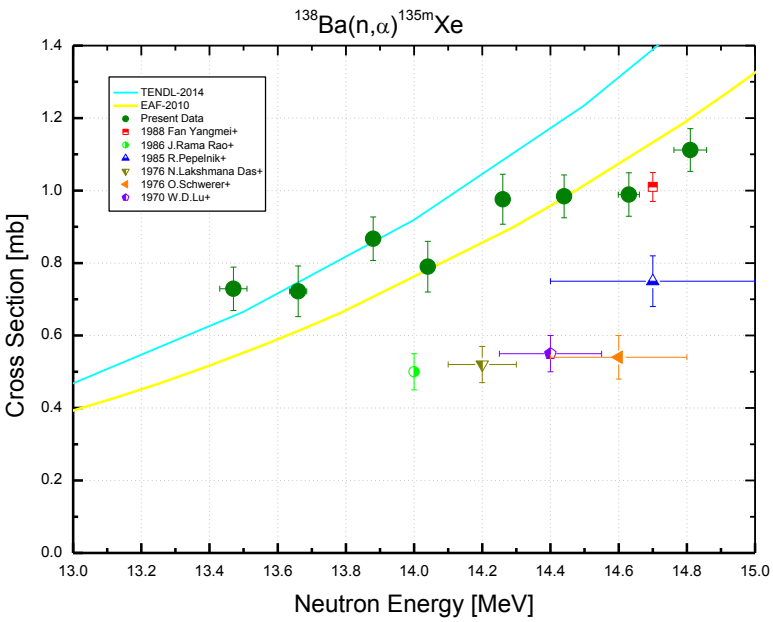

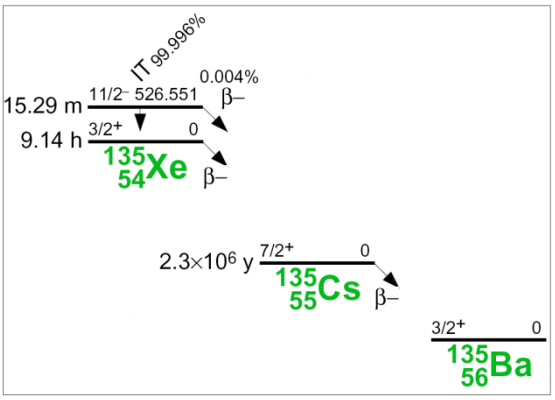

Decay data used for **^{138}Ba(n, α)^{135m}Xe**.

Target nucleus	Abundance [%]	Chemical form	Reaction product	$T_{1/2}$	E_γ [keV]	Y_γ [%]
^{138}Ba	***99.8** *1*	$BaCO_3$	^{135m}Xe	**15.29 m** *5*	**526.6**	**80.4** *3*

* – refer to samples with separated isotopes of Barium

^{138}Ba(n, α)^{135}Xe

^{138}Ba(n, α)^{135}Xe			
E_n [MeV]	σ [mb]	$\pm\Delta\sigma_{total}$ [%]	$\pm\Delta\sigma_{ref}$ [%]
13.47	1.86	*5.86*	*3.44*
13.66	2.05	*6.29*	*3.39*
13.88	2.29	*6.55*	*3.38*
14.04	2.21	*6.73*	*3.38*
14.26	2.39	*6.18*	*3.37*
14.44	2.64	*6.39*	*3.37*
14.63	2.57	*6.59*	*3.37*
14.81	2.71	*6.18*	*3.38*
Ref. CS is ^{27}Al(n, α)^{24}Na;			$\alpha_d = 1.4$

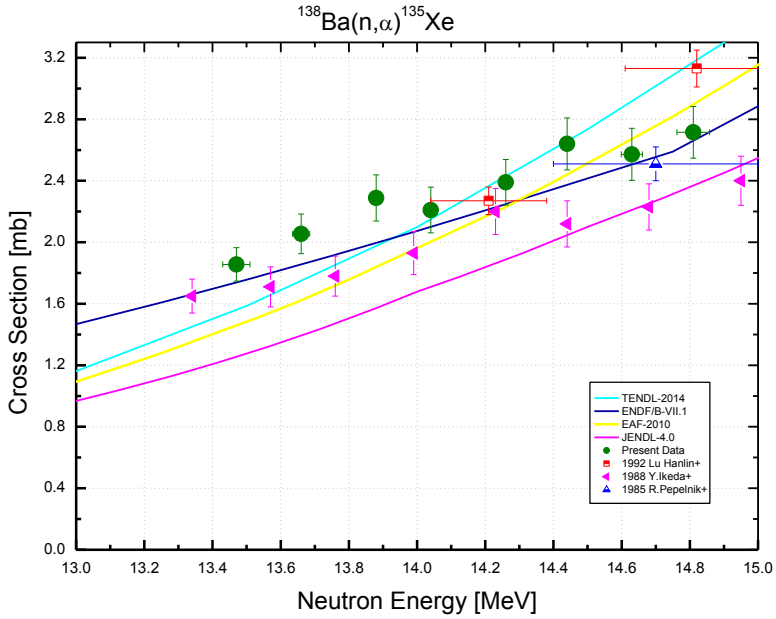

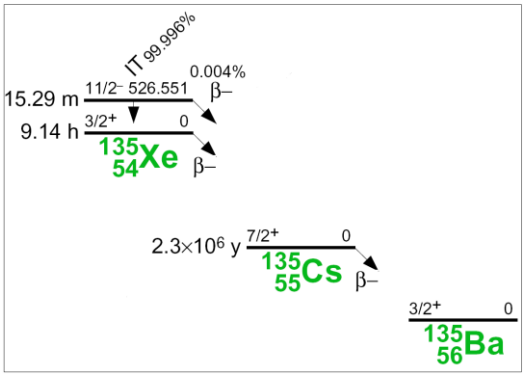

Decay data used for **^{138}Ba(n, α)^{135}Xe**.

Target nucleus	Abundance [%]	Chemical form	Reaction product	$T_{1/2}$	E_γ [keV]	Y_γ [%]
^{138}Ba	***99.8** *1*	$BaCO_3$	^{135}Xe	**9.14 h** *2*	**249.8**	**90** *3*
					608.2	2.90 *13*

* – refer to samples with separated isotopes of Barium

^{138}Ba[(n, np)+(n, d)]^{137}Cs

^{138}Ba(n, x)^{137}Cs			
E_n [MeV]	σ [mb]	$\pm\Delta\sigma_{total}$ [%]	$\pm\Delta\sigma_{ref}$ [%]
13.73	0.36	*19.4*	*0.70*
14.73	1.21	*11.5*	*0.69*
Ref. CS is ^{93}Nb(n,2n)^{92m}Nb;			α_d = *1.01*

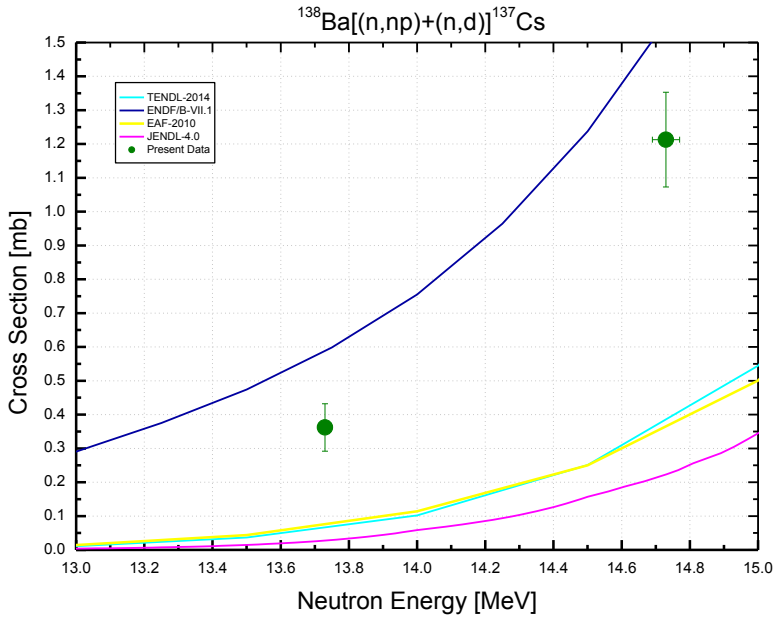

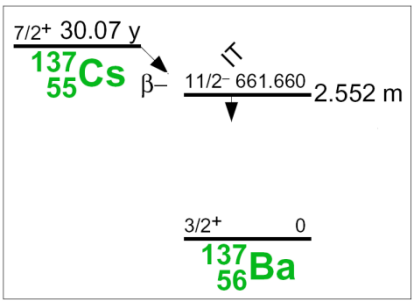

Decay data used for **^{138}Ba(n, x)^{137}Cs**.

Target nucleus	Abundance [%]	Chemical form	Reaction product	$T_{1/2}$	E_γ [keV]	Y_γ [%]
^{138}Ba	**71.698** *42*	$BaCO_3$	^{137}Cs	**30.08 y** *9*	**661.7**	**85.10** *20*

^{138}Ba(n, p)^{138}Cs

^{138}Ba(n, p)^{138}Cs			
E_n [MeV]	σ [mb]	$\pm\Delta\sigma_{total}$ [%]	$\pm\Delta\sigma_{ref}$ [%]
13.47	1.60	*7.46*	*2.28*
13.66	1.76	*6.77*	*2.20*
13.88	2.11	*6.64*	*2.19*
14.04	2.14	*6.48*	*2.19*
14.26	2.26	*5.65*	*2.18*
14.44	2.61	*5.29*	*2.17*
14.63	2.76	*5.01*	*2.17*
14.81	2.92	*5.38*	*2.18*
Ref. CS is ^{27}Al(n, α)^{24}Na;			$\alpha_d = 1.6$

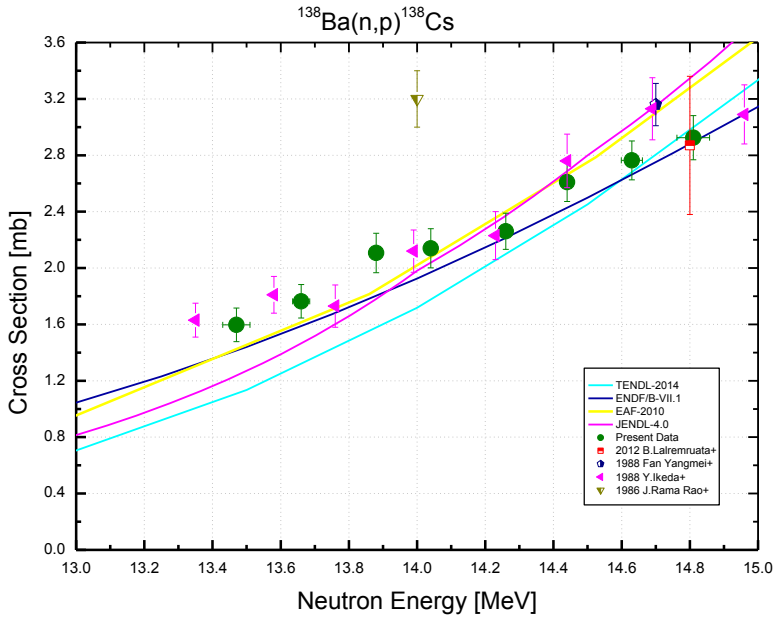

Only (81±2)% of the ^{138m}Cs metastable state decay to the ^{138g}Cs ground state. Strictly speaking, **the cross section [^{138}Ba(n, p)^{138g}Cs + 0.81∗(^{138}Ba(n, p)^{138m}Cs)] was measured in the experiment**.

The difference with the ^{138}Ba(n, p)$^{138(m+g)}$Cs cross-section evaluations presented in the Figure is 0.19*^{138}Ba(n, p)^{138m}Cs. This value can be estimated using EAF-2010 and TENDL-2014 evaluations that contain the data for the metastable state. The difference should be approximately 0.2 – 0.3 mb.

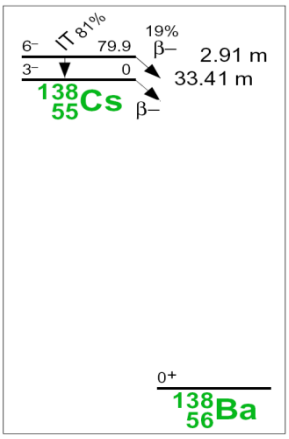

Decay data used for **^{138}Ba(n, p)^{138}Cs**.

Target nucleus	Abundance [%]	Chemical form	Reaction product	$T_{1/2}$	E_γ [keV]	Y_γ [%]
^{138}Ba	*99.8 *1*	$BaCO_3$	^{138}Cs	**33.41 m *18***	**462.8**	**30.7 *6***
					1009.8	29.8 *6*
					1435.9	76.3 *16*
					2218.0	15.2 *3*

* – refer to samples with separated isotopes of Barium

^{138}Ba(n, 2n)^{137m}Ba

^{138}Ba(n, 2n)^{137m}Ba			
E_n [MeV]	σ [mb]	$\pm\Delta\sigma_{total}$ [%]	$\pm\Delta\sigma_{ref}$ [%]
13.47	794	*3.81*	*0.808*
13.64	773	*3.80*	*0.543*
13.88	806	*4.29*	*0.511*
14.05	818	*4.06*	*0.484*
14.28	831	*5.07*	*0.434*
14.47	889	*3.59*	*0.401*
14.68	882	*3.75*	*0.410*
14.81	899	*3.87*	*0.459*
14.86	940	*3.57*	*0.459*
Ref. CS is ^{27}Al(n, α)^{24}Na;			$\alpha_d = 1.9$

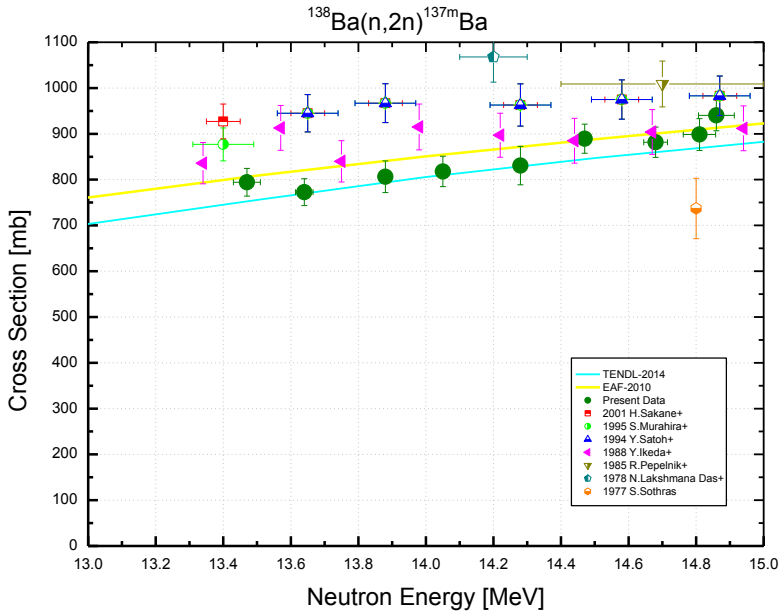

^{138}Ba(n, np)^{137}Cs contribution is neglected because of the little cross section and the very long half life.

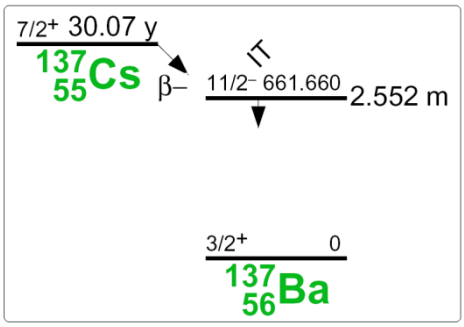

Decay data used for **^{138}Ba(n, 2n)^{137m}Ba**.

Target nucleus	Abundance [%]	Chemical form	Reaction product	$T_{1/2}$	E_γ [keV]	Y_γ [%]
^{138}Ba	*99.8 *1*	$BaCO_3$	^{137m}Ba	**2.552 m** *1*	**661.7**	**89.90** *14*

* – refer to samples with separated isotopes of Barium

^{136}Ce(n, 2n)^{135}Ce

^{136}Ce(n, 2n)^{135}Ce			
E_n [MeV]	σ [mb]	$\pm\Delta\sigma_{total}$ [%]	$\pm\Delta\sigma_{ref}$ [%]
13.47	1288	*7.12*	*4.48*
13.64	1324	*7.11*	*4.48*
13.88	1349	*7.22*	*4.47*
14.05	1406	*7.05*	*4.47*
14.28	1452	*7.21*	*4.47*
14.47	1478	*7.20*	*4.47*
14.68	1500	*7.17*	*4.47*
14.86	1542	*7.01*	*4.48*
Ref. CS is ^{93}Nb(n,2n)^{92m}Nb;			$\alpha_d = 1.3$

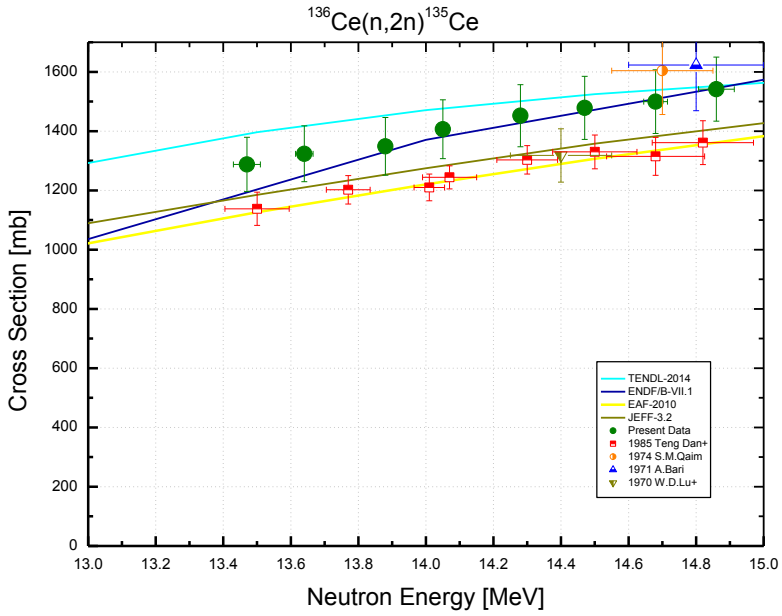

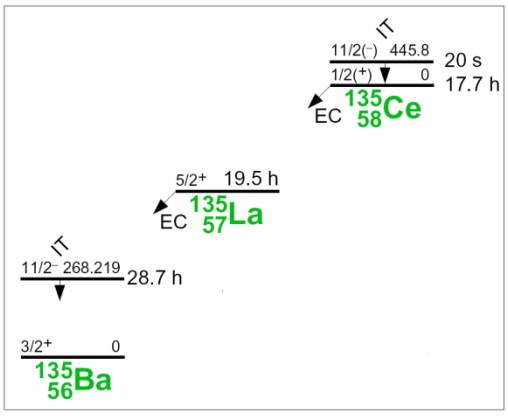

Decay data used for **^{136}Ce(n, 2n)^{135}Ce**.

Target nucleus	Abundance [%]	Chemical form	Reaction product	$T_{1/2}$	E_γ [keV]	Y_γ [%]
^{136}Ce	**0.185** *2*	CeO_2	^{135}Ce	**17.7 h** *3*	518.1	13.6 *6*
					572.3	10.4 *4*
					577.1	5.14 *19*
					783.6	**10.6** *4*

^{138}Ce(n, 2n)^{137m}Ce

^{138}Ce(n, 2n)^{137m}Ce			
E_n [MeV]	σ [mb]	$\pm\Delta\sigma_{total}$ [%]	$\pm\Delta\sigma_{ref}$ [%]
13.47	732	*7.41*	*4.17*
13.64	803	*7.41*	*4.17*
13.88	875	*7.39*	*4.16*
14.05	929	*7.48*	*4.16*
14.28	843	*7.63*	*4.16*
14.47	867	*7.97*	*4.16*
14.68	945	*7.84*	*4.16*
14.86	928	*8.04*	*4.17*
Ref. CS is ^{93}Nb(n,2n)^{92m}Nb;			$\alpha_d = 1.4$

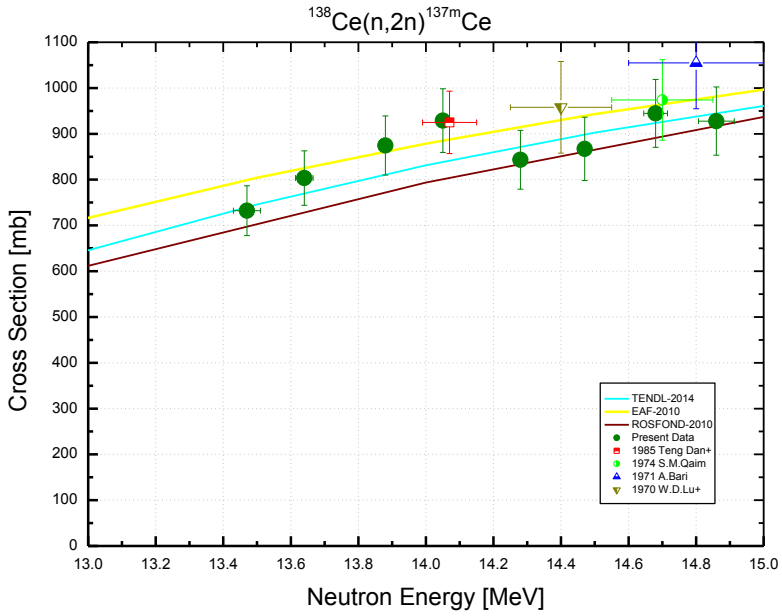

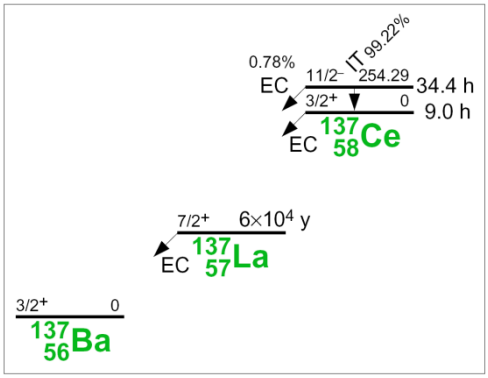

Decay data used for **^{138}Ce(n, 2n)^{137m}Ce**.

Target nucleus	Abundance [%]	Chemical form	Reaction product	$T_{1/2}$	E_γ [keV]	Y_γ [%]
^{138}Ce	**0.251** *2*	CeO_2	^{137m}Ce	**34.4 h** *3*	**254.3**	**11.1** *4*

^{140}Ce(n, p)^{140}La

^{140}Ce(n, p)^{140}La			
E_n [MeV]	σ [mb]	$\pm\Delta\sigma_{total}$ [%]	$\pm\Delta\sigma_{ref}$ [%]
13.47	5.55	*3.78*	*1.60*
13.64	5.82	*3.61*	*1.58*
13.88	6.35	*3.28*	*1.57*
14.05	6.78	*3.20*	*1.57*
14.28	7.00	*3.07*	*1.57*
14.47	7.44	*2.99*	*1.57*
14.68	7.75	*2.99*	*1.57*
14.86	7.98	*2.91*	*1.58*
Ref. CS is ^{93}Nb(n,2n)^{92m}Nb;			α_d = *1.2*

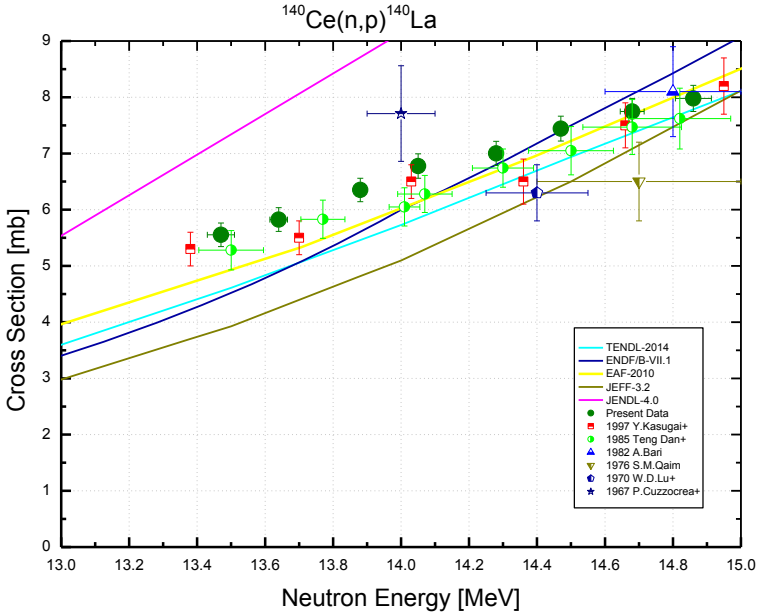

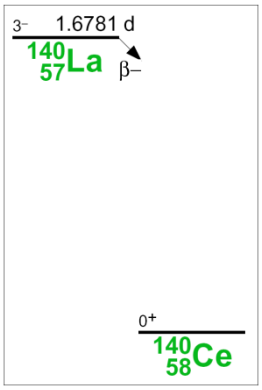

Decay data used for **^{140}Ce(n, p)^{140}La**.

Target nucleus	Abundance [%]	Chemical form	Reaction product	$T_{1/2}$	E_γ [keV]	Y_γ [%]
^{140}Ce	**88.450** ***51***	CeO_2	^{140}La	**1.67855 d** ***12***	328.8	20.3 *3*
					487.0	45.5 *6*
					815.8	23.28 *19*
					1596.2	**95.4** ***14***

^{140}Ce(n, 2n)^{139}Ce

^{140}Ce(n, 2n)^{139}Ce			
E_n [MeV]	σ [mb]	$\pm\Delta\sigma_{total}$ [%]	$\pm\Delta\sigma_{ref}$ [%]
13.47	1683	*6.12*	*0.634*
13.64	1714	*6.34*	*0.596*
13.88	1724	*6.31*	*0.565*
14.05	1779	*6.10*	*0.550*
14.28	1750	*6.18*	*0.547*
14.47	1793	*6.29*	*0.553*
14.68	1802	*6.26*	*0.568*
14.86	1806	*6.29*	*0.591*
Ref. CS is ^{93}Nb(n,2n)^{92m}Nb;			$\alpha_d = 1.05$

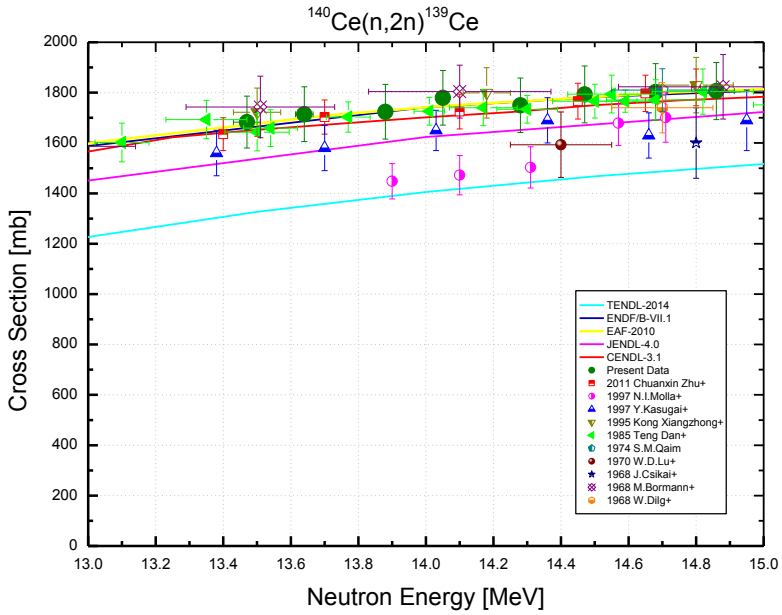

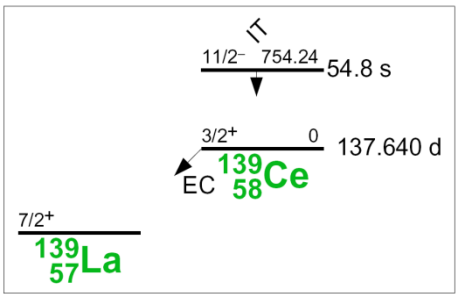

Decay data used for **^{140}Ce(n, 2n)^{139}Ce**.

Target nucleus	Abundance [%]	Chemical form	Reaction product	$T_{1/2}$	E_γ [keV]	Y_γ [%]
^{140}Ce	**88.450** *51*	CeO_2	^{139}Ce	**137.641 d** *20*	**165.9**	**79.89** *2*

^{142}Ce(n, 2n)^{141}Ce

^{142}Ce(n, 2n)^{141}Ce			
E_n [MeV]	σ [mb]	$\pm\Delta\sigma_{total}$ [%]	$\pm\Delta\sigma_{ref}$ [%]
13.47	1958	*6.53*	*0.88*
13.64	1988	*6.46*	*0.86*
13.88	1952	*6.60*	*0.84*
14.05	1990	*6.46*	*0.83*
14.28	1933	*6.63*	*0.82*
14.47	1918	*6.66*	*0.83*
14.68	1899	*6.73*	*0.84*
14.86	1872	*8.52*	*0.85*
Ref. CS is ^{93}Nb(n,2n)^{92m}Nb;			$\alpha_d = 1.1$

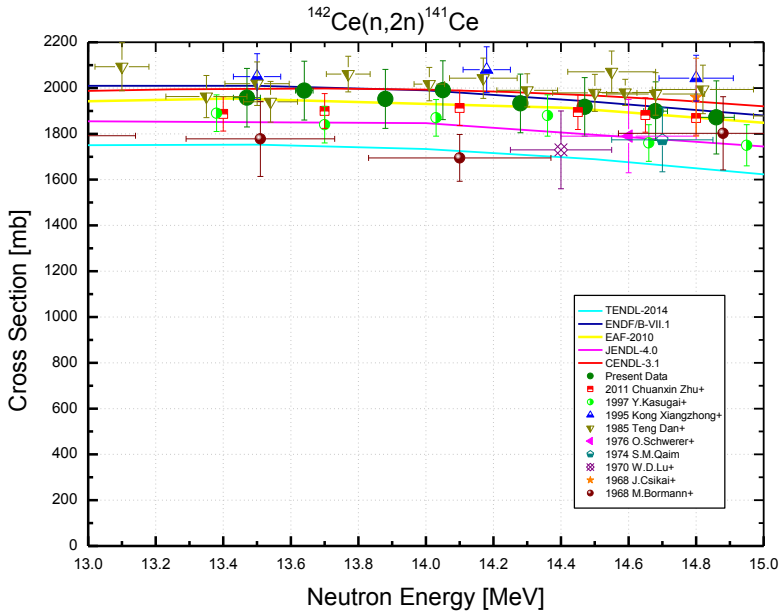

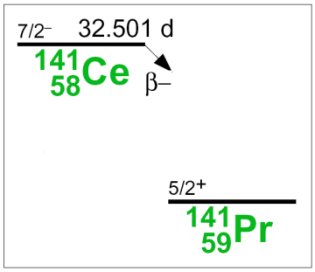

Decay data used for **^{142}Ce(n, 2n)^{141}Ce**.

Target nucleus	Abundance [%]	Chemical form	Reaction product	$T_{1/2}$	E_γ [keV]	Y_γ [%]
^{142}Ce	**11.114** *51*	CeO_2	^{141}Ce	**32.511 d** *13*	**145.4**	**48.4** *3*

^{151}Eu(n, α)^{148m}Pm

^{151}Eu(n, α)^{148m}Pm			
E_n [MeV]	σ [mb]	$\pm\Delta\sigma_{total}$ [%]	$\pm\Delta\sigma_{ref}$ [%]
13.47	1.76	*10.7*	*1.23*
13.56	1.82	*15.9*	*1.22*
13.68	1.89	*10.6*	*1.21*
13.74	2.14	*12.2*	*1.21*
13.88	1.88	*10.6*	*1.20*
13.96	1.90	*12.1*	*1.20*
14.05	1.97	*9.11*	*1.19*
14.19	2.20	*10.9*	*1.19*
14.26	1.89	*10.0*	*1.19*
14.42	1.98	*11.6*	*1.19*
14.47	2.17	*8.67*	*1.19*
14.61	2.41	*14.9*	*1.20*
14.68	2.28	*11.3*	*1.20*
14.78	2.02	*9.88*	*1.21*
14.86	2.19	*12.3*	*1.21*
Ref. CS is ^{93}Nb(n,2n)^{92m}Nb;			α_d = *1.1*

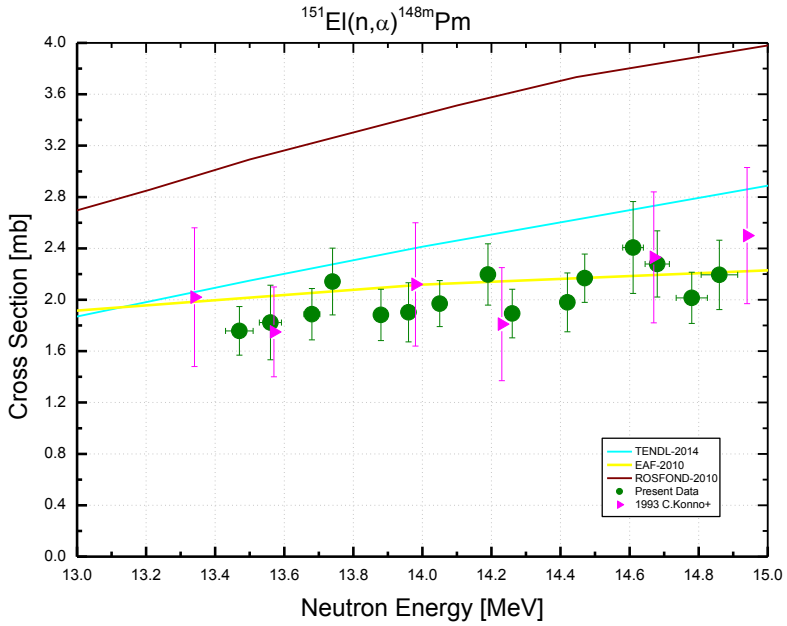

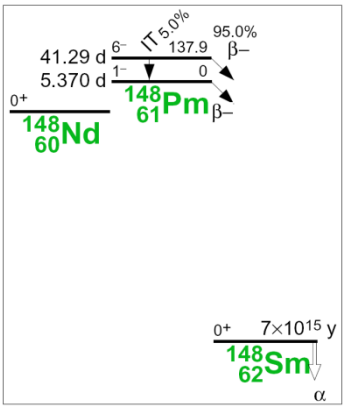

Decay data used for **^{151}Eu(n, α)^{148m}Pm.**

Target nucleus	Abundance [%]	Chemical form	Reaction product	$T_{1/2}$	E_γ [keV]	Y_γ [%]
^{151}Eu	**47.81** *6*	Eu_2O_3	^{148m}Pm	**41.29 d** *11*	550.3	94.9 *12*
	*97.5 *1*				**630.0**	**89.0** *9*
					725.7	32.8 *4*

* – refer to samples with separated isotopes of Europium

^{151}Eu(n, α)^{148g}Pm

^{151}Eu(n, α)^{148g}Pm			
E_n [MeV]	σ [mb]	$\pm\Delta\sigma_{total}$ [%]	$\pm\Delta\sigma_{ref}$ [%]
13.47	1.62	*11.1*	*2.35*
13.64	1.79	*10.0*	*2.34*
13.88	1.79	*10.6*	*2.33*
14.05	1.84	*10.3*	*2.33*
14.28	1.92	*10.3*	*2.33*
14.47	1.72	*10.4*	*2.33*
14.68	1.92	*9.82*	*2.33*
14.86	1.83	*9.81*	*2.34*
Ref. CS is ^{93}Nb(n,2n)^{92m}Nb;			α_d = *1.3*

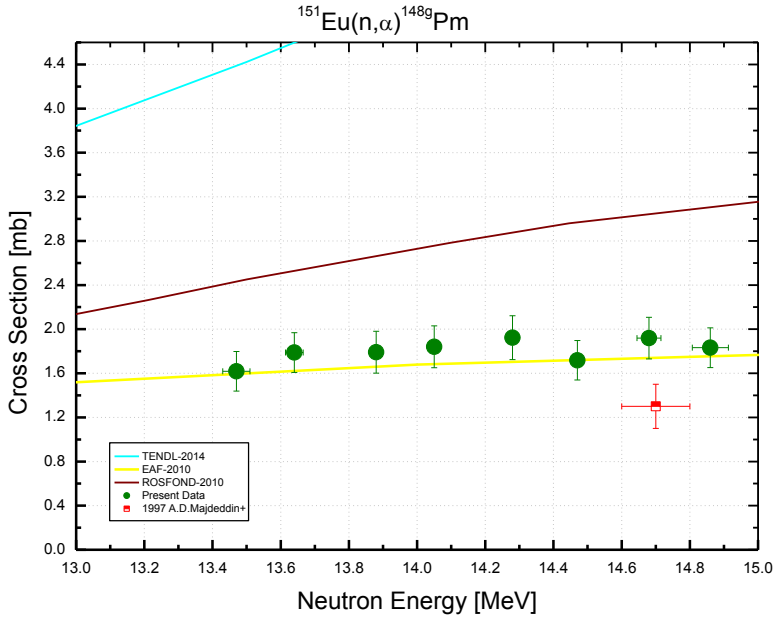

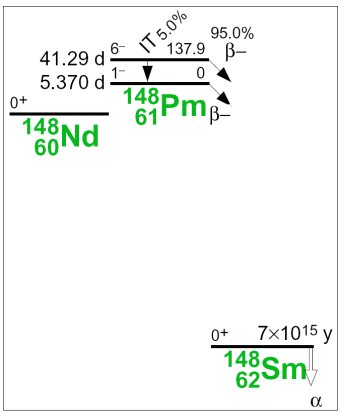

Decay data used for **^{151}Eu(n, α)^{148g}Pm.**

Target nucleus	Abundance [%]	Chemical form	Reaction product	$T_{1/2}$	E_γ [keV]	Y_γ [%]
^{151}Eu	**47.81** *6* *97.5 *1*	Eu_2O_3	^{148g}Pm	**5.368 d** *7*	**1465.1**	**22.2** *5*

* – refer to samples with separated isotopes of Europium

^{151}Eu(n, α)^{148}Pm

^{151}Eu(n, α)^{148}Pm		
E_n [MeV]	σ [mb]	$\pm\Delta\sigma_{total}$ [%]
13.47	3.38	*7.66*
13.66	3.68	*7.26*
13.88	3.67	*7.47*
14.05	3.81	*6.80*
14.27	3.82	*7.14*
14.47	3.89	*6.62*
14.68	4.20	*7.57*
14.86	4.03	*8.02*
Ref. CS is ^{93}Nb(n,2n)^{92m}Nb		

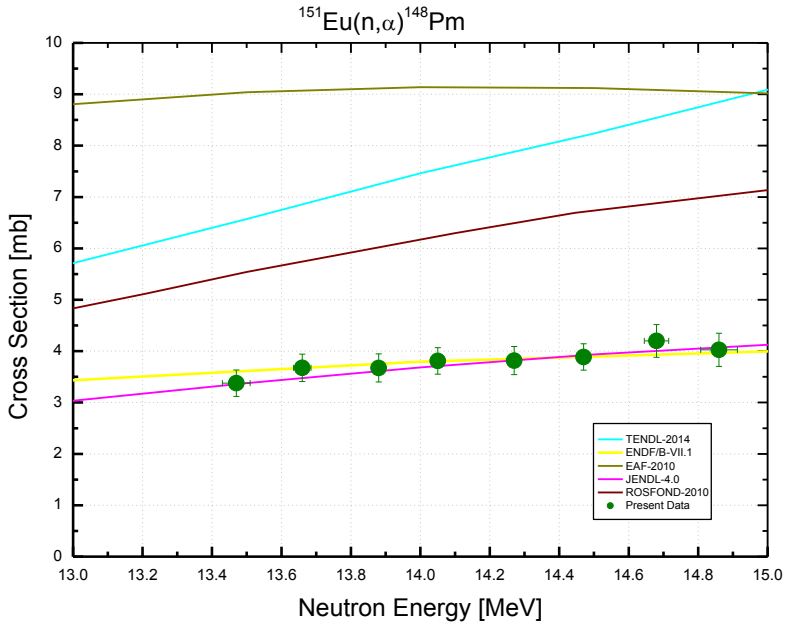

This is the sum of the ^{151}Eu(n, α)^{148m}Pm and ^{151}Eu(n, α)^{148g}Pm cross sections measured independently and presented on the previous pages.

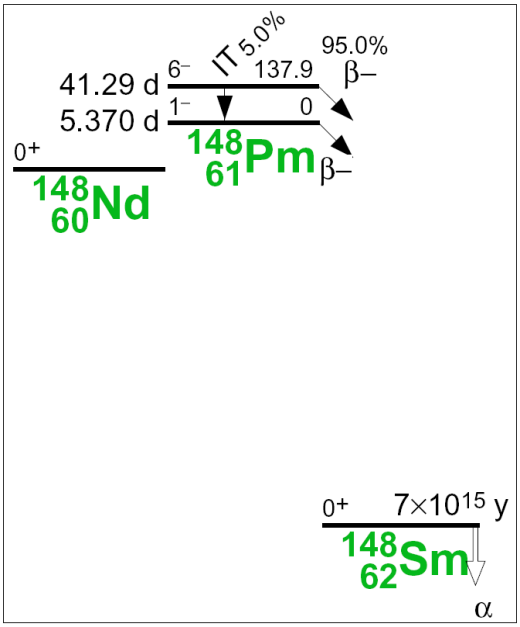

^{151}Eu(n, 3n)^{149}Eu

^{151}Eu(n, 3n)^{149}Eu			
E_n [MeV]	σ [mb]	$\pm\Delta\sigma_{total}$ [%]	$\pm\Delta\sigma_{ref}$ [%]
14.65	0.20	*100*	*1.83*
14.81	1.27	*19.0*	*1.84*
Ref. CS is ^{93}Nb(n,2n)^{92m}Nb;			α_d = *1.1*

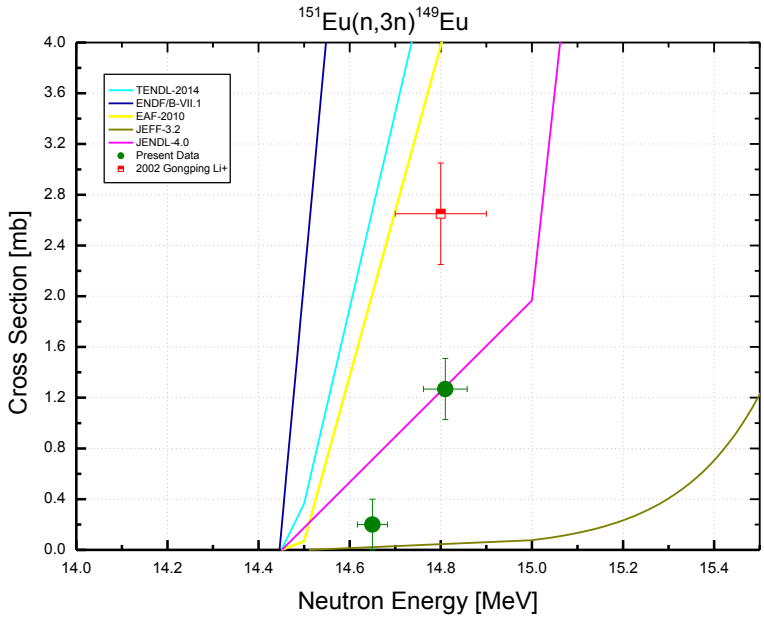

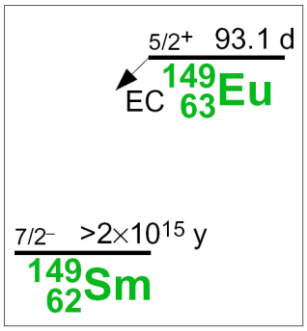

Decay data used for **^{151}Eu(n, 3n)^{149}Eu**.

Target nucleus	Abundance [%]	Chemical form	Reaction product	$T_{1/2}$	E_γ [keV]	Y_γ [%]
^{151}Eu	**47.81** *6*	Eu_2O_3	^{149}Eu	**93.1 d** *4*	**277.1**	**3.56** *6*
					327.5	4.03 *12*

^{151}Eu(n, 2n)^{150m}Eu

^{151}Eu(n, 2n)^{150m}Eu			
E_n [MeV]	σ [mb]	$\pm\Delta\sigma_{total}$ [%]	$\pm\Delta\sigma_{ref}$ [%]
13.56	501	*20.0*	*20.0*
13.74	501	*19.6*	*20.0*
13.96	501	*20.0*	*20.0*
14.19	506	*20.2*	*20.0*
14.42	519	*21.1*	*20.0*
14.61	496	*19.7*	*20.0*
14.78	507	*20.7*	*20.0*
Ref. CS is ^{93}Nb(n,2n)^{92m}Nb;			$\alpha_d = 1.5$

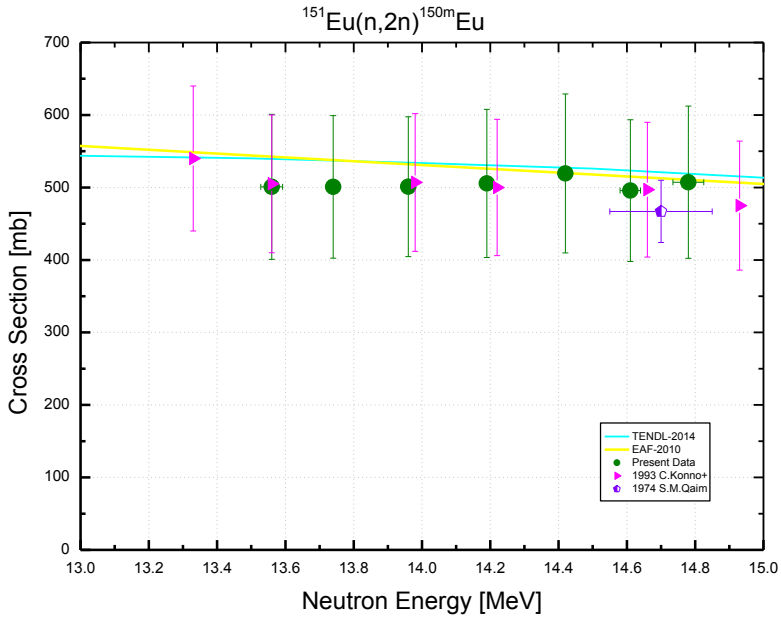

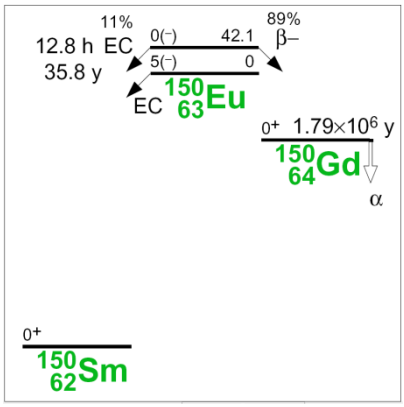

Decay data used for **^{151}Eu(n, 2n)^{150m}Eu**.

Target nucleus	Abundance [%]	Chemical form	Reaction product	$T_{1/2}$	E_γ [keV]	Y_γ [%]
^{151}Eu	**47.81** *6* *97.5 *1*	Eu_2O_3	^{150m}Eu	**12.8 h** *1*	**333.9**	**4.0** *8*
					406.5	2.8 *6*

* – refer to samples with separated isotopes of Europium

^{151}Eu(n, 2n)^{150g}Eu

^{151}Eu(n, 2n)^{150g}Eu			
E_n [MeV]	σ [mb]	$\pm\Delta\sigma_{total}$ [%]	$\pm\Delta\sigma_{ref}$ [%]
13.56	1129	*5.47*	*2.56*
13.74	1174	*5.01*	*2.55*
13.96	1144	*5.41*	*2.55*
14.19	1095	*5.74*	*2.55*
14.42	1125	*4.92*	*2.55*
14.61	1139	*4.67*	*2.55*
14.78	1221	*4.26*	*2.55*
Ref. CS is ^{93}Nb(n,2n)^{92m}Nb;		α_d = *1.01*	

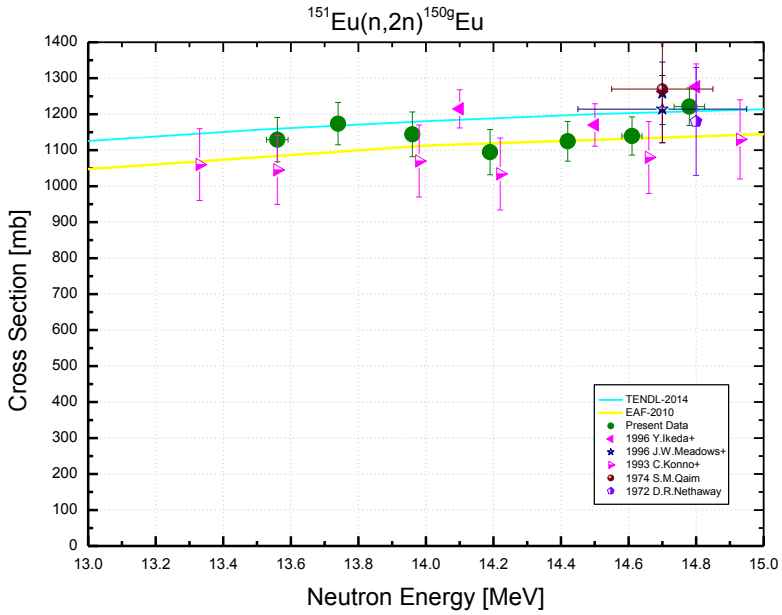

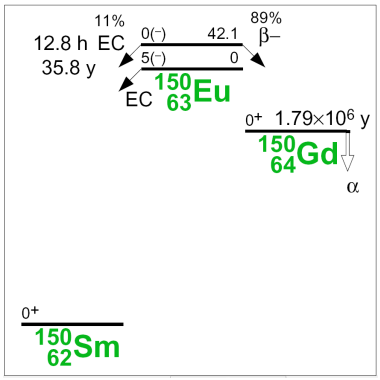

Decay data used for **^{151}Eu(n, 2n)^{150g}Eu**.

Target nucleus	Abundance [%]	Chemical form	Reaction product	$T_{1/2}$	E_γ [keV]	Y_γ [%]
^{151}Eu	**47.81** *6* *97.5 *1*	Eu_2O_3	^{150g}Eu	**36.9 y** *9*	**334.0**	**95.2** *20*
					439.4	79.6 *16*
					584.3	52.1 *14*

* – refer to samples with separated isotopes of Europium

^{151}Eu(n, 2n)^{150}Eu

^{151}Eu(n, 2n)^{150}Eu		
E_n [MeV]	σ [mb]	$\pm\Delta\sigma_{total}$ *[%]*
13.56	1630	*7.17*
13.74	1675	*6.80*
13.96	1645	*6.92*
14.19	1600	*7.45*
14.42	1644	*7.43*
14.61	1635	*6.76*
14.78	1728	*6.74*
Ref. CS is ^{93}Nb(n,2n)^{92m}Nb		

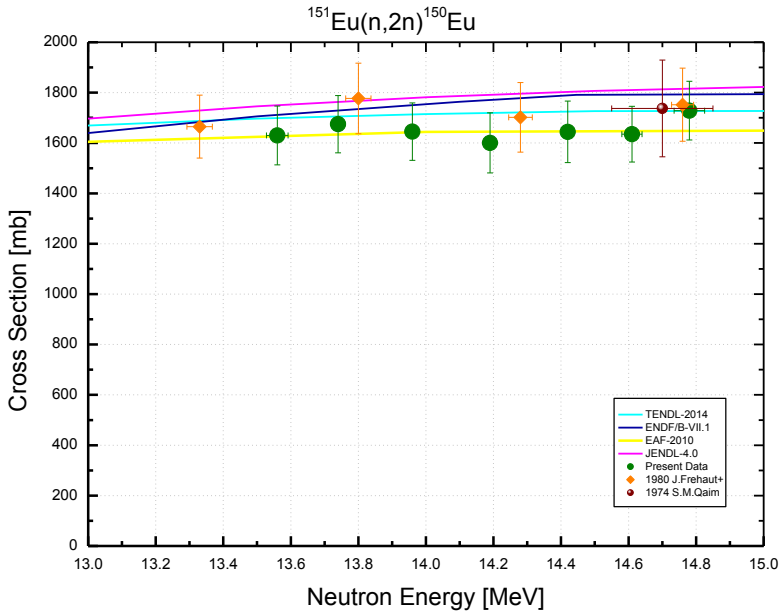

The ^{151}Eu(n, 2n)^{150}Eu cross-section was not measured in the experiment directly. This is the sum of the ^{151}Eu(n, 2n)^{150m}Eu and ^{151}Eu(n, 2n)^{150g}Eu cross-sections presented in the previous pages.

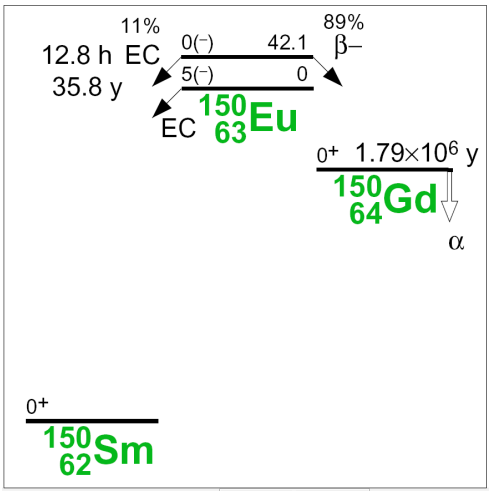

^{153}Eu(n, α)^{150}Pm

^{153}Eu(n, α)^{150}Pm			
E_n [MeV]	σ [mb]	$\pm\Delta\sigma_{total}$ [%]	$\pm\Delta\sigma_{ref}$ [%]
13.50	1.19	*18.5*	*6.82*
14.04	1.29	*10.1*	*6.81*
14.28	1.51	*10.5*	*6.81*
14.80	1.70	*8.19*	*6.82*
Ref. CS is ^{93}Nb(n,2n)^{92m}Nb;			α_d = *1.7*

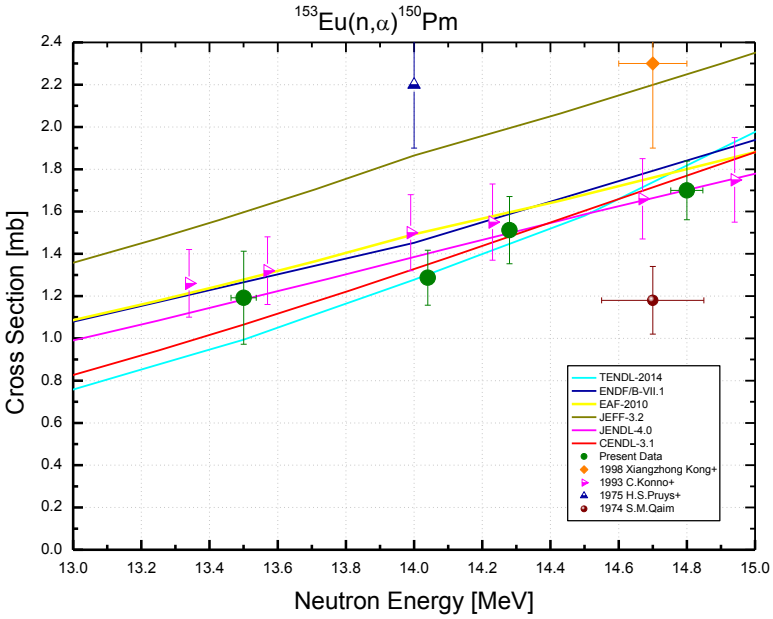

Three γ-lines given in the table at the page bottom were used for experiments with samples with separated isotopes of Europium. If samples of a natural abundance were irradiated then only the last γ-line 1324.5 keV was used for ^{153}Eu(n, α)^{150}Pm cross-section determination. This was done to avoid a possible interference of the ^{151}Eu(n, 2n)^{150m}Eu reaction where the first two γ-lines were also excited in a branch decay to ^{150}Sm.

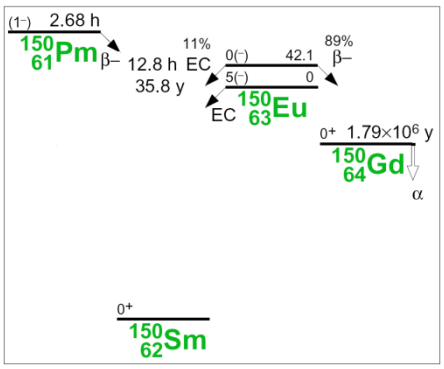

Decay data used for **^{153}Eu(n, α)^{150}Pm**.

Target nucleus	**Abundance [%]**	**Chemical form**	**Reaction product**	**$T_{1/2}$**	**E_γ [keV]**	**Y_γ [%]**
^{153}Eu	**52.19** *6*	Eu_2O_3	^{150}Pm	**2.698 h** *15*	831.9	11.9 *8*
	*99.20 *8*				1165.8	15.8 *11*
					1324.5	**17.5** *12*

*– refer to samples with separated isotopes of Europium

^{153}Eu(n, 2n)^{152m1}Eu

^{153}Eu(n, 2n)^{152m1}Eu			
E_n [MeV]	σ [mb]	$\pm\Delta\sigma_{total}$ [%]	$\pm\Delta\sigma_{ref}$ [%]
13.56	293	*14.3*	*11.3*
13.74	288	*13.6*	*11.3*
13.96	284	*13.8*	*11.3*
14.19	286	*14.0*	*11.3*
14.42	281	*13.8*	*11.3*
14.61	275	*14.5*	*11.3*
14.78	267	*14.6*	*11.3*
Ref. CS is ^{93}Nb(n,2n)^{92m}Nb;			α_d = *1.6*

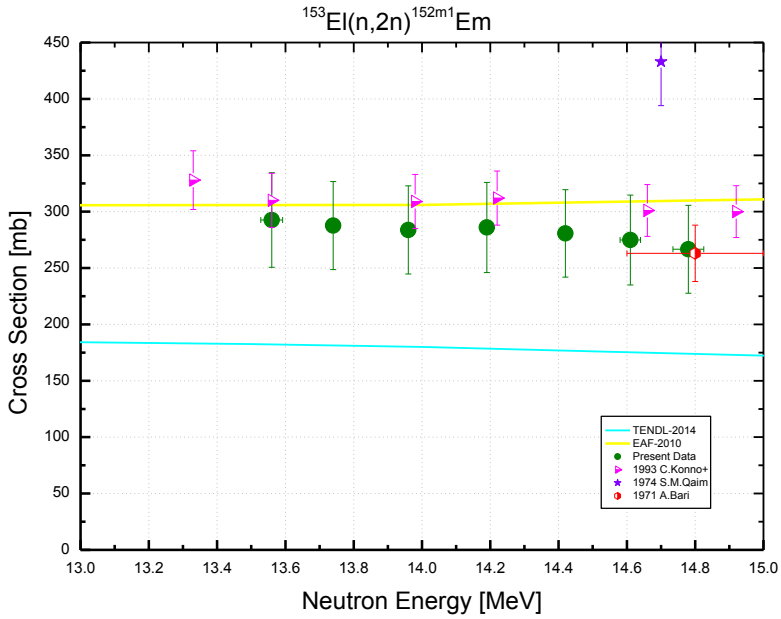

The metastable state ^{152m1}Eu (45.6 keV 0^-) is not populated from the higher lying metastable level ^{152m2}Eu (147.8 keV 8^-) which decays to the ^{152g}Eu ground state (0.0 keV 3^-). On the other hand, the ^{152m1}Eu does not populate the ^{152g}Eu in decay. Therefore, two independent experiments were carried out for measurement of cross-sections of ^{153}Eu(n, 2n)^{152m1}Eu (this page) and ^{153}Eu(n, 2n)$^{152m2+g}$Eu (next page).

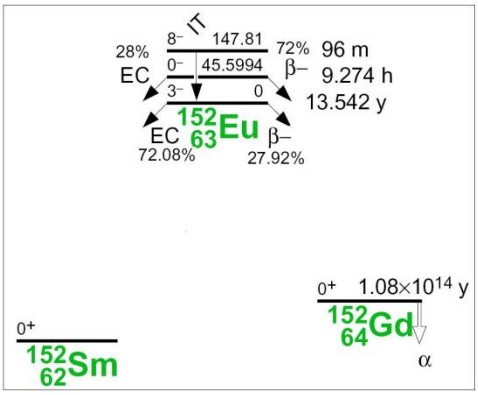

Decay data used for **^{153}Eu(n, 2n)^{152m1}Eu**.

Target nucleus	Abundance [%]	Chemical form	Reaction product	$T_{1/2}$	E_γ [keV]	Y_γ [%]
^{153}Eu	**52.19** *6*	Eu_2O_3	^{152m1}Eu	**9.3116 h** *13*	121.8	7.0 *8*
	*99.20 *8*				344.3	2.4 *4*
					841.6	**14.2** *16*
					963.4	11.6 *13*

* – refer to samples with separated isotopes of Europium

^{153}Eu(n, 2n)$^{152m2+g}$Eu

^{153}Eu(n, 2n)$^{150m2+g}$Eu			
E_n [MeV]	σ [mb]	$\pm\Delta\sigma_{total}$ [%]	$\pm\Delta\sigma_{ref}$ [%]
13.56	1467	*4.64*	*0.758*
13.74	1524	*4.74*	*0.735*
13.96	1526	*4.26*	*0.714*
14.19	1505	*4.92*	*0.706*
14.42	1443	*4.55*	*0.711*
14.61	1544	*3.89*	*0.723*
14.78	1464	*3.85*	*0.738*
Ref. CS is ^{93}Nb(n,2n)^{92m}Nb;			α_d = *1.05*

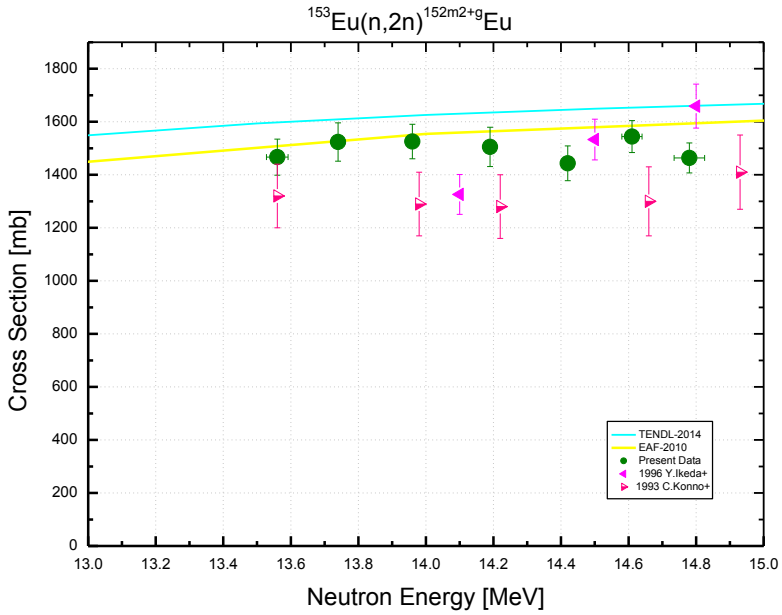

The main attention of the experiment was concentrated on the accurate measurement of cross-sections which lead to generating long-lived reaction products. The ^{152m2}Eu metastable level (147.8 keV 8$^-$) decays to the long-lived ^{152g}Eu with a 100% probability. The cross-section ^{153}Eu(n, 2n)$^{152m2+g}$Eu was determined in this work.

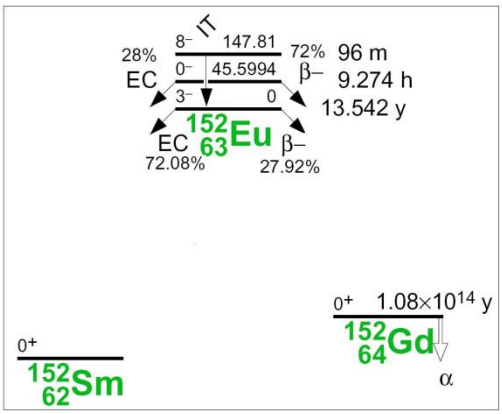

Decay data used for **^{153}Eu(n, 2n)$^{152m2+g}$Eu**.

Target nucleus	**Abundance [%]**	**Chemical form**	**Reaction product**	**$T_{1/2}$**	**E_γ [keV]**	**Y_γ [%]**
^{153}Eu	**52.19** *6* *99.20 *8*	Eu_2O_3	^{152g}Eu	**13.517 y** *9*	344.3	26.59 *20*
					778.9	12.93 *8*
					1112.1	13.67 *8*
					1408.0	**20.87** *9*

* – refer to samples with separated isotopes of Europium

^{153}Eu(n, 2n)^{152}Eu

^{153}Eu(n, 2n)^{152}Eu		
E_n [MeV]	σ [mb]	$\pm\Delta\sigma_{total}$ *[%]*
13.56	1759	*4.50*
13.74	1811	*4.49*
13.96	1809	*4.15*
14.19	1791	*4.66*
14.42	1724	*4.38*
14.61	1819	*3.92*
14.78	1730	*3.91*
Ref. CS is ^{93}Nb(n,2n)^{92m}Nb		

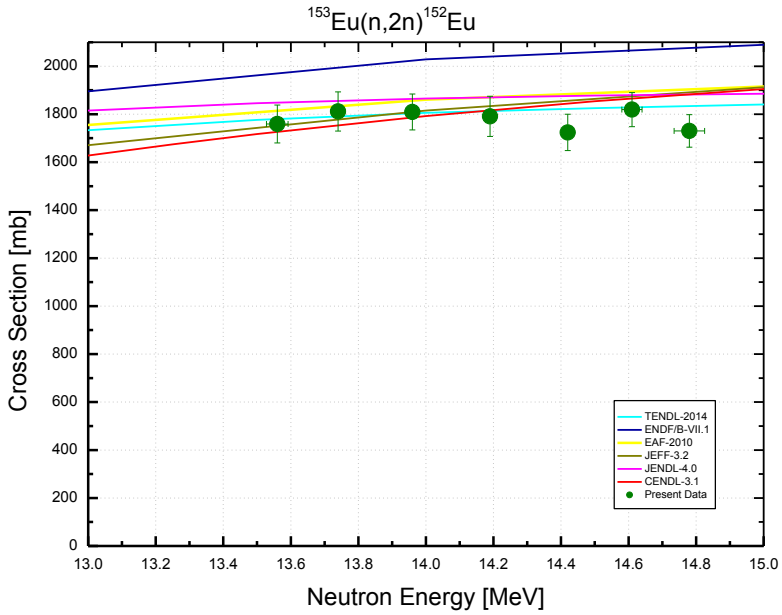

The ^{153}Eu(n, 2n)^{152}Eu cross-section was not measured in the experiment directly. This is the sum of the ^{153}Eu(n, 2n)^{152m1}Eu and ^{153}Eu(n, 2n)$^{152m2+g}$Eu cross-sections presented in the previous pages.

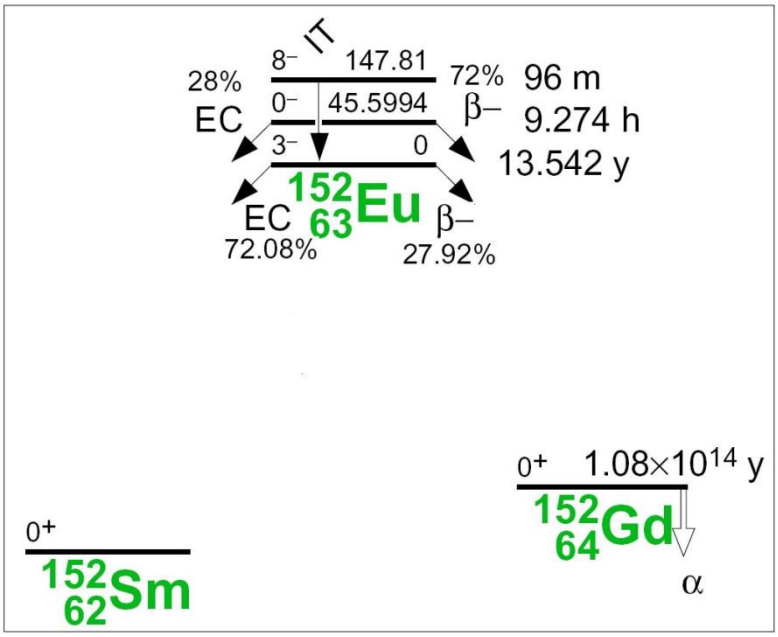

^{181}Ta(n, α)^{178m}Lu

^{181}Ta(n, α)^{178m}Lu			
E_n [MeV]	σ [mb]	$\pm\Delta\sigma_{total}$ [%]	$\pm\Delta\sigma_{ref}$ [%]
13.68	0.151	*9.23*	*2.94*
13.88	0.171	*8.78*	*2.93*
14.26	0.203	*7.29*	*2.92*
14.44	0.216	*6.91*	*2.91*
14.64	0.242	*12.5*	*2.92*
14.71	0.209	*9.56*	*2.92*
Ref. CS is ^{27}Al(n, α)^{24}Na;			$\alpha_d = 1.8$

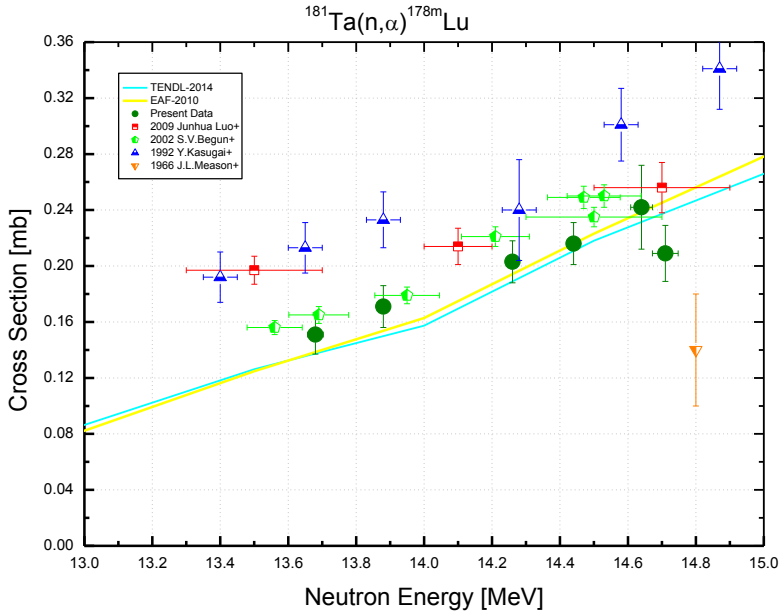

A separate determination of ^{181}Ta(n, α)^{178m}Lu and ^{181}Ta(n, α)^{178g}Lu cross-sections was based on the following circumstances.

There is no isomeric transition from the metastable state (9^-) to the ground state (1^+) of ^{178}Lu.

The remarkable spin difference cause also the different decay paths of the ^{178m}Lu and ^{178g}Lu inside the ^{178}Hf that are not crossed till the lowest states. The ^{178}Hf γ-transitions between the high spin states were chosen for characterization of the ^{178m}Lu decay, and those between the low spin states were used in processing the ^{178g}Lu data.

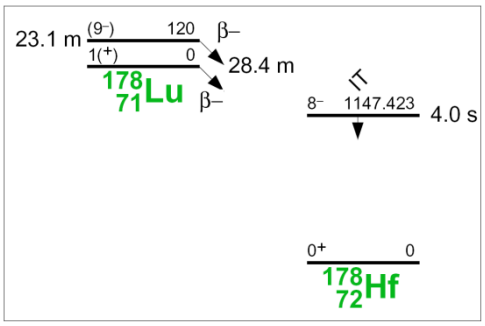

Decay data used **^{181}Ta(n, α)^{178m}Lu.**

Target nucleus	Abundance [%]	Chemical form	Reaction product	$T_{1/2}$	E_γ [keV]	Y_γ [%]
^{181}Ta	**99.988** *2*	Ta-metal	^{178m}Lu	**23.1 m** *3*	213.4	81.4 *15*
					325.6	**94.1** *16*
					426.4	97.0 *18*

^{181}Ta(n, α)^{178g}Lu

^{181}Ta(n, α)^{178g}Lu			
E_n [MeV]	σ [mb]	$\pm\Delta\sigma_{total}$ [%]	$\pm\Delta\sigma_{ref}$ [%]
13.68	0.303	55.1	*50.0*
13.88	0.403	55.9	*50.0*
14.26	0.422	50.9	*50.0*
14.44	0.423	52.7	*50.0*
14.71	0.524	52.9	*50.0*
Ref. CS is ^{27}Al(n, α)^{24}Na;			α_d = *1.7*

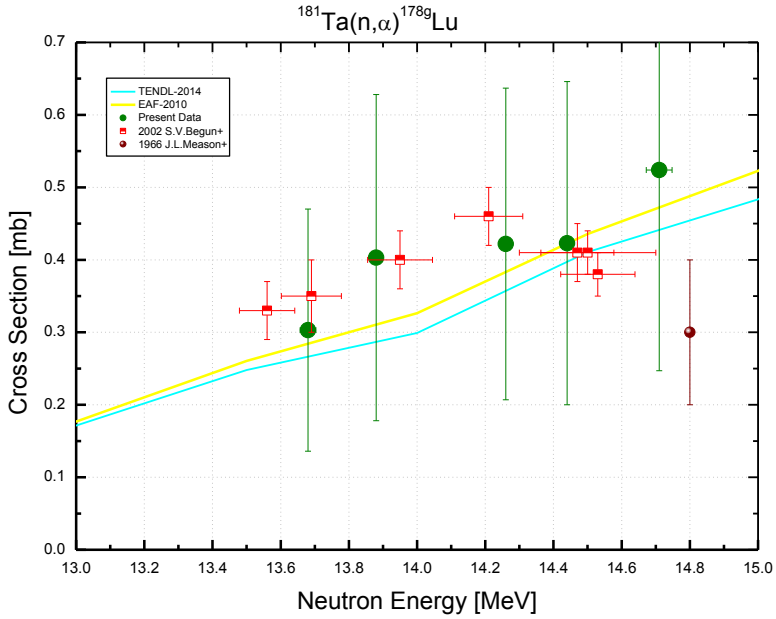

An essential difference between spins of ^{178m}Lu and ^{178g}Lu allows a separate determination of ^{181}Ta(n, α)^{178m}Lu and ^{181}Ta(n, α)^{178g}Lu cross-sections (see the previous page).

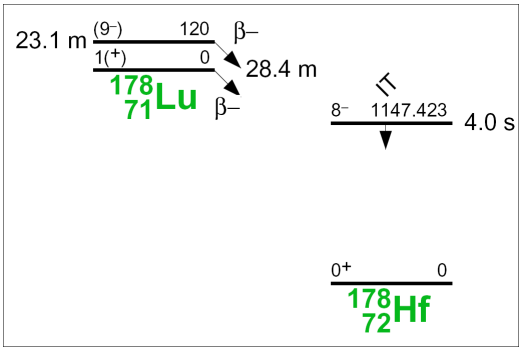

Decay data used for **^{181}Ta(n, α)^{178g}Lu**.

Target nucleus	Abundance [%]	Chemical form	Reaction product	$T_{1/2}$	E_γ [keV]	Y_γ [%]
^{181}Ta	**99.988** *2*	Ta-metal	^{178g}Lu	**28.4 m 2**	1309.5	1.1 *6*
					1340.8	**3.4** *17*

^{181}Ta(n, α)^{178}Lu

^{181}Ta(n, α)^{178}Lu		
E_n [MeV]	σ [mb]	$\pm\Delta\sigma_{total}$ *[%]*
13.68	0.454	*36.9*
13.88	0.575	*39.3*
14.26	0.625	*34.4*
14.44	0.638	*34.9*
14.71	0.733	*37.9*
Ref. CS is ^{27}Al(n, α)^{24}Na		

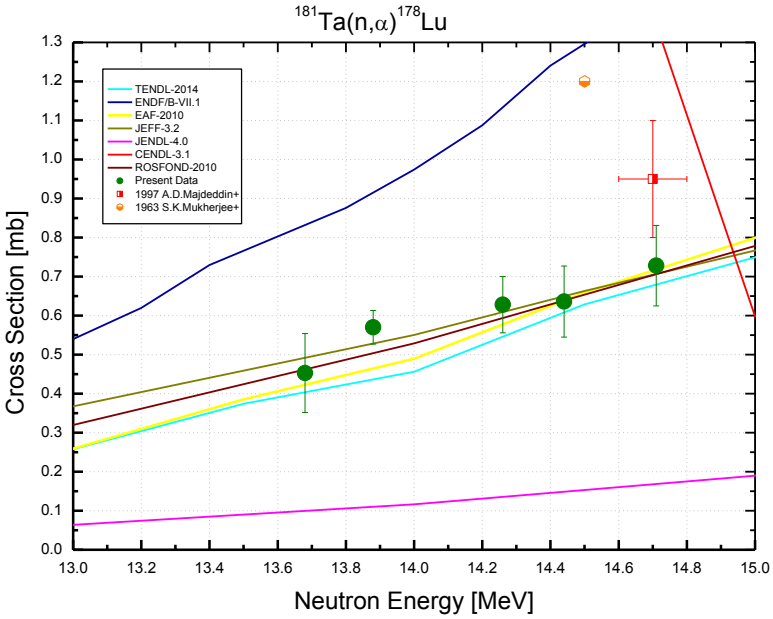

The ^{181}Ta(n, α)^{178}Lu cross-section was not measured in the experiment directly. This is the sum of cross sections ^{181}Ta(n, α)^{178m}Lu and ^{181}Ta(n, α)^{178g}Lu presented in the previous pages.

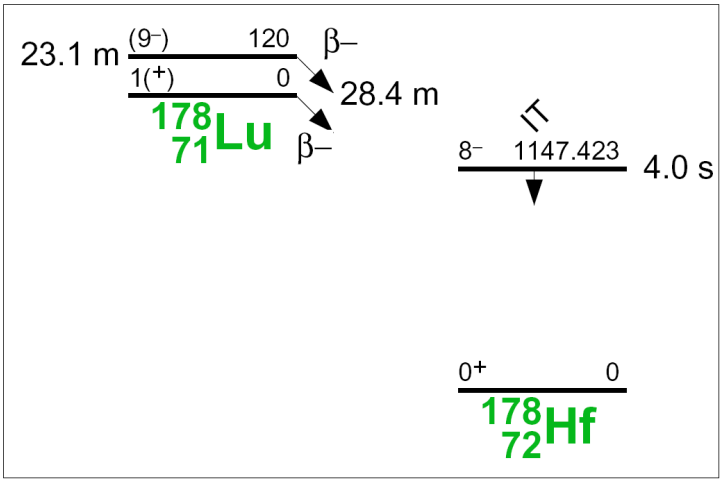

^{181}Ta[(n, np)+(n, d)]^{180m}Hf

^{181}Ta(n, x)^{180m}Hf			
E_n [MeV]	σ [mb]	$\pm\Delta\sigma_{total}$ [%]	$\pm\Delta\sigma_{ref}$ [%]
13.68	0.067	*14.9*	*14.6*
13.88	0.084	*11.9*	*11.5*
14.26	0.124	*8.06*	*7.49*
14.44	0.145	*20.7*	*20.5*
14.64	0.144	*10.4*	*10.0*
14.71	0.147	*13.6*	*13.3*
Ref. CS is ^{27}Al(n, α)^{24}Na;			$\alpha_d = 1.3$

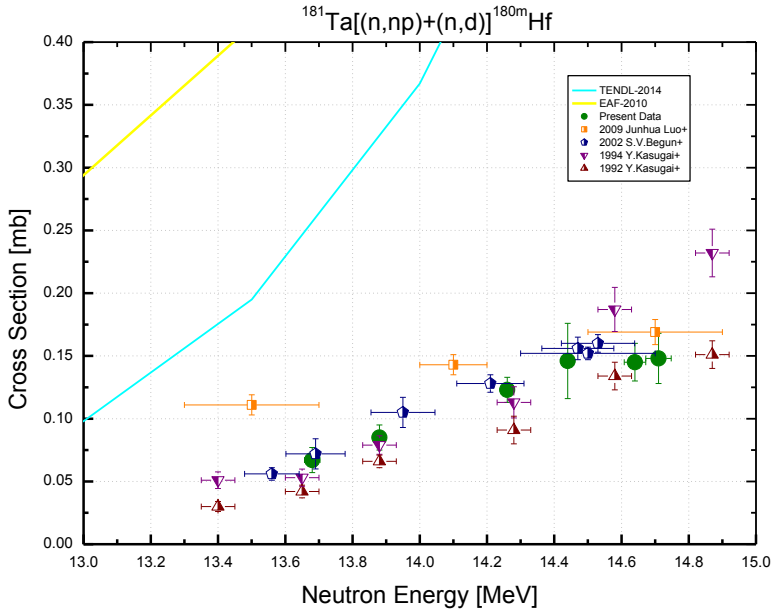

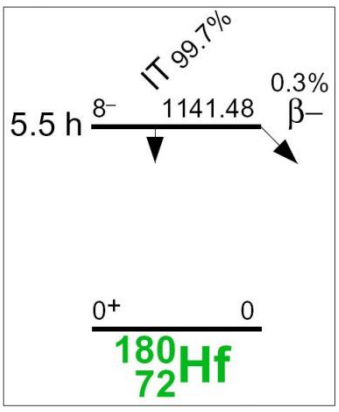

Decay data used for **^{181}Ta(n, x)^{180m}Hf**.

Target nucleus	Abundance [%]	Chemical form	Reaction product	$T_{1/2}$	E_γ [keV]	Y_γ [%]
^{181}Ta	**99.988** *2*	Ta-metal	^{180m}Hf	**5.53 h** *2*	**215.4**	**81.6** *20*
					332.3	94.0 *30*
					443.2	81.7 *25*

^{181}Ta(n, p)^{181}Hf

^{181}Ta(n, p)^{181}Hf			
E_n [MeV]	σ [mb]	$\pm\Delta\sigma_{total}$ [%]	$\pm\Delta\sigma_{ref}$ [%]
13.48	1.918	7.73	*0.82*
13.68	2.040	6.23	*0.79*
13.88	2.305	7.33	*0.77*
14.06	2.594	6.88	*0.76*
14.27	2.853	5.84	*0.76*
14.46	3.306	6.23	*0.76*
14.69	3.624	5.27	*0.77*
14.83	3.703	6.41	*0.79*
Ref. CS is ^{93}Nb(n,2n)^{92m}Nb;			α_d = *1.2*

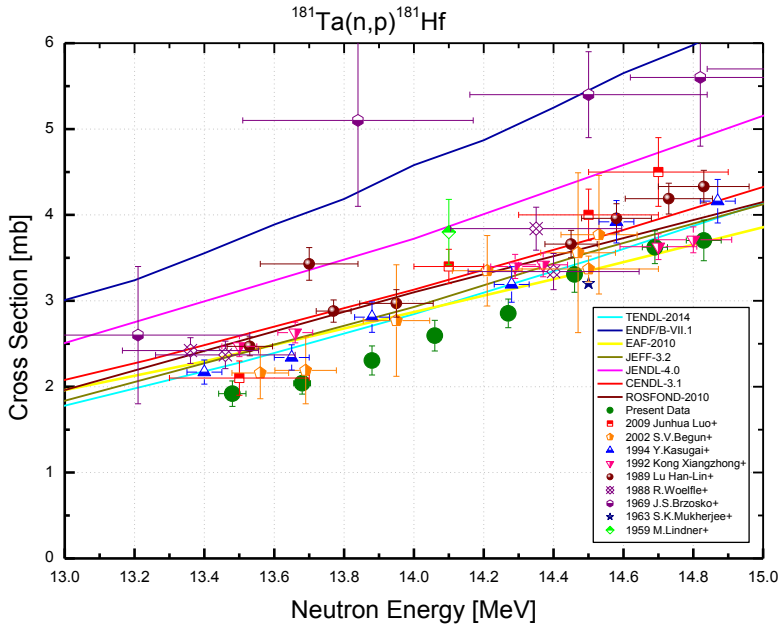

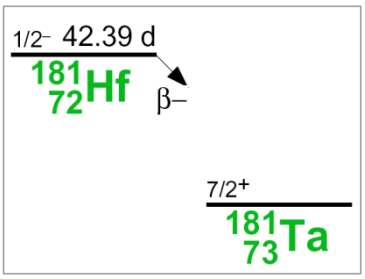

Decay data used for **^{181}Ta(n, p)^{181}Hf**.

Target nucleus	Abundance [%]	Chemical form	Reaction product	$T_{1/2}$	E_γ [keV]	Y_γ [%]
^{181}Ta	**99.988** *2*	Ta-metal	^{181}Hf	**42.39 d** *6*	345.9	15.12 *12*
					482.2	**80.5** *4*

^{181}Ta(n, 2n)^{180g}Ta

^{181}Ta(n, 2n)^{180g}Ta			
E_n [MeV]	σ [mb]	$\pm\Delta\sigma_{total}$ [%]	$\pm\Delta\sigma_{ref}$ [%]
13.47	1179	18.0	*3.60*
13.66	1238	12.0	*3.60*
13.88	1157	17.6	*3.59*
14.05	1190	17.4	*3.59*
14.27	1256	12.2	*3.59*
14.47	1224	17.3	*3.59*
14.69	1240	12.2	*3.59*
14.86	1190	17.6	*3.60*
Ref. CS is ^{93}Nb(n,2n)^{92m}Nb;			α_d = *1.4*

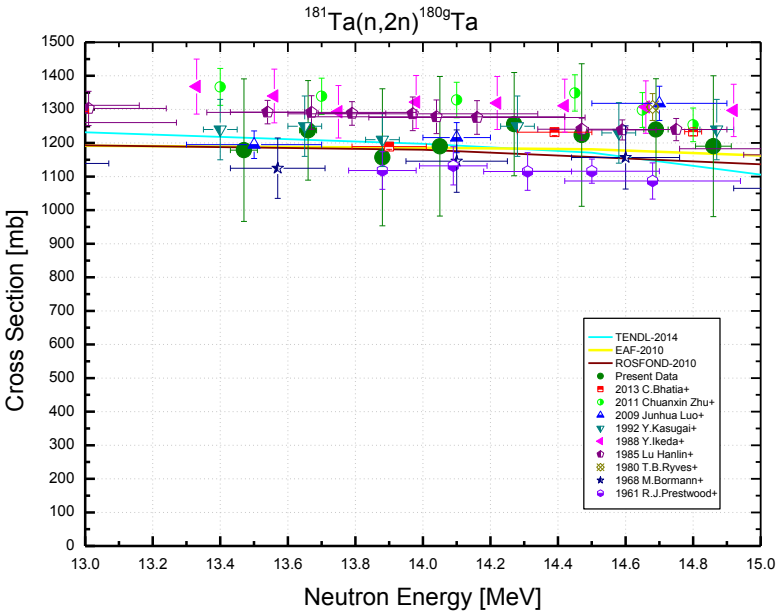

Decay data used for **^{181}Ta(n, 2n)^{180g}Ta**.

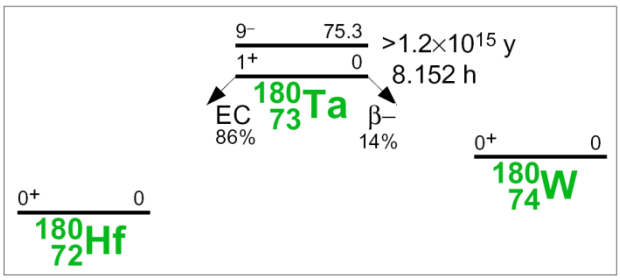

Target nucleus	Abundance [%]	Chemical form	Reaction product	$T_{1/2}$	E_γ [keV]	Y_γ [%]
^{181}Ta	**99.988** *2*	Ta-metal	^{180g}Ta	**8.154 h** *6*	**93.3**	**4.51** *16*
					103.6	0.87 *24*

^{180}W(n, 2n)^{179m}W

^{180}W(n, 2n)^{179m}W			
E_n [MeV]	σ [mb]	$\pm\Delta\sigma_{total}$ [%]	$\pm\Delta\sigma_{ref}$ [%]
13.48	540	*15.9*	*11.6*
13.64	573	*14.0*	*11.6*
13.88	490	*14.4*	*11.6*
14.28	498	*19.0*	*11.6*
14.47	501	*13.4*	*11.6*
14.68	459	*15.3*	*11.6*
14.82	476	*13.6*	*11.6*
Ref. CS is ^{27}Al(n, α)^{24}Na; $\alpha_d = 1.4$			

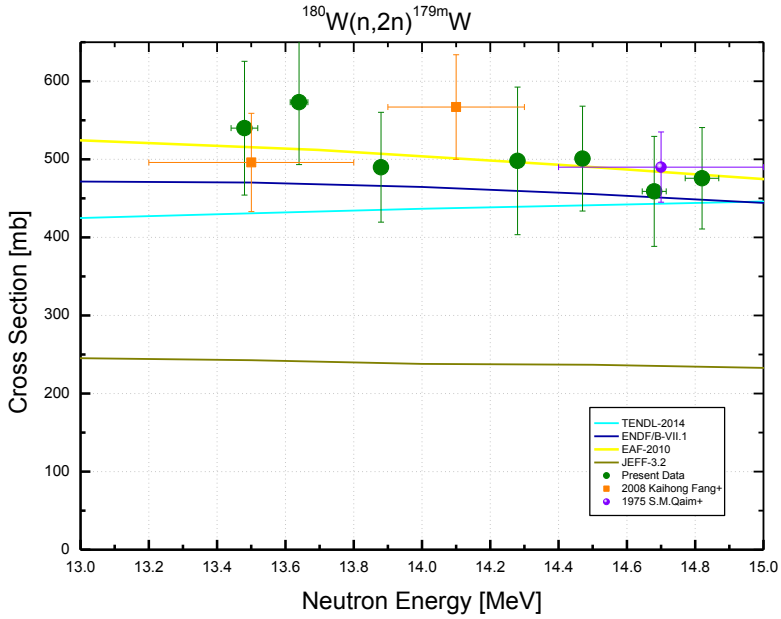

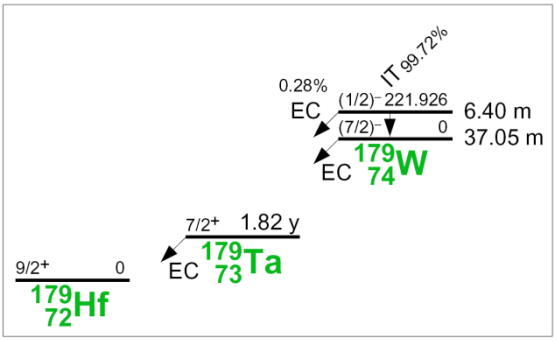

Decay data used for **^{180}W(n, 2n)^{179m}W.**

Target nucleus	**Abundance [%]**	**Chemical form**	**Reaction product**	$T_{1/2}$	**E_γ [keV]**	**Y_γ [%]**
^{180}W	**0.12** *1*	W-metal	^{179m}W	**6.40 m** *7*	**221.5**	**8.8** *7*

^{182}W(n, nα)^{178m2}Hf

^{182}W(n, nα)^{178m2}Hf			
E_n [MeV]	σ [mb]	$\pm\Delta\sigma_{total}$ [%]	$\pm\Delta\sigma_{ref}$ [%]
14.74	0.010	*60.0*	*3.77*
Ref. CS is ^{93}Nb(n,2n)^{92m}Nb; α_d = *1.01*			

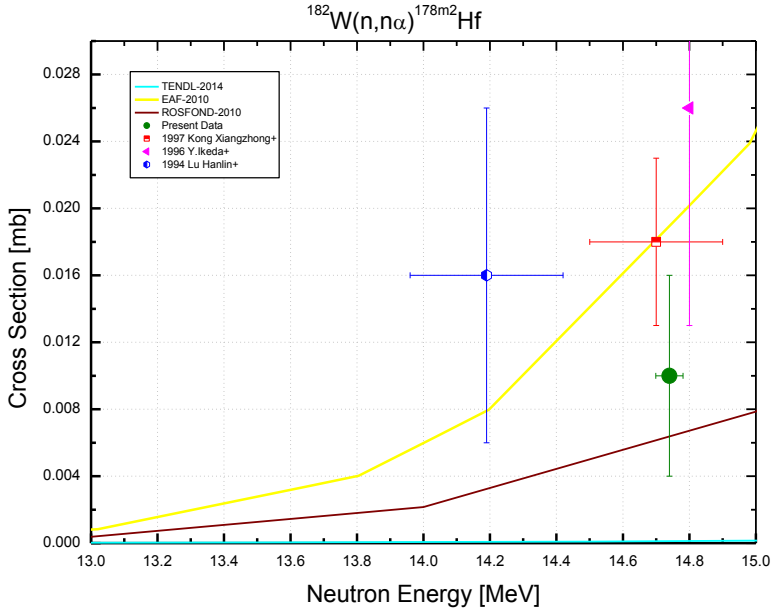

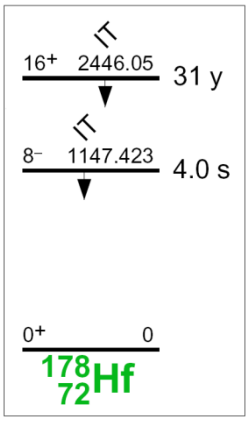

Decay data used for **^{182}W(n, nα)^{178m2}Hf**.

Target nucleus	Abundance [%]	Chemical form	Reaction product	$T_{1/2}$	E_γ [keV]	Y_γ [%]
^{182}W	**26.50** *16*	W-metal	^{178m2}Hf	**31 y 1**	**325.6**	**94.1** *16*
					426.4	96.5 *17*
					495.0	70.1 *16*
					574.2	88.6 *21*

^{182}W(n, α)^{179m2}Hf

^{182}W(n, α)^{179m2}Hf			
E_n [MeV]	σ [mb]	$\pm\Delta\sigma_{total}$ [%]	$\pm\Delta\sigma_{ref}$ [%]
14.28	0.0022	*59.1*	*3.71*
14.82	0.0080	*62.5*	*3.72*
Ref. CS is ^{93}Nb(n,2n)^{92m}Nb; α_d = *1.1*			

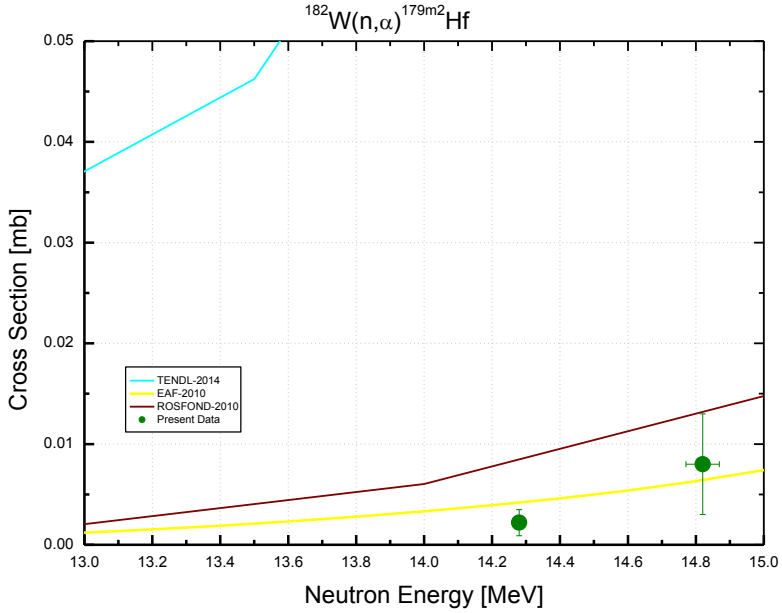

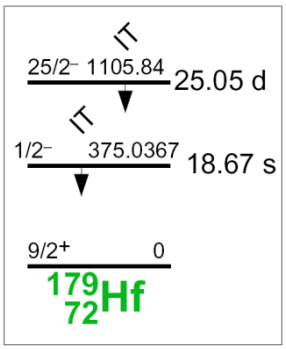

Decay data used for **^{182}W(n, α)^{179m2}Hf**.

Target nucleus	Abundance [%]	Chemical form	Reaction product	$T_{1/2}$	E_γ [keV]	Y_γ [%]
^{182}W	**26.50** *16*	W-metal	^{179m2}Hf	**25.05 d** *25*	**315.9**	**20.3** *7*
					362.6	39.6 *15*
					409.7	21.5 *8*
					453.6	68 *3*

^{182}W(n, p)^{182m2}Ta

^{182}W(n, p)^{182m2}Ta			
E_n [MeV]	σ [mb]	$\pm\Delta\sigma_{total}$ [%]	$\pm\Delta\sigma_{ref}$ [%]
13.48	0.040	*75.0*	*4.36*
13.64	0.052	*40.4*	*4.32*
13.88	0.079	*25.6*	*4.31*
14.28	0.115	*17.4*	*4.30*
14.47	0.115	*30.4*	*4.30*
14.68	0.126	*24.0*	*4.30*
14.82	0.150	*33.3*	*4.31*
Ref. CS is ^{27}Al(n, α)^{24}Na; $\alpha_d = 1.3$			

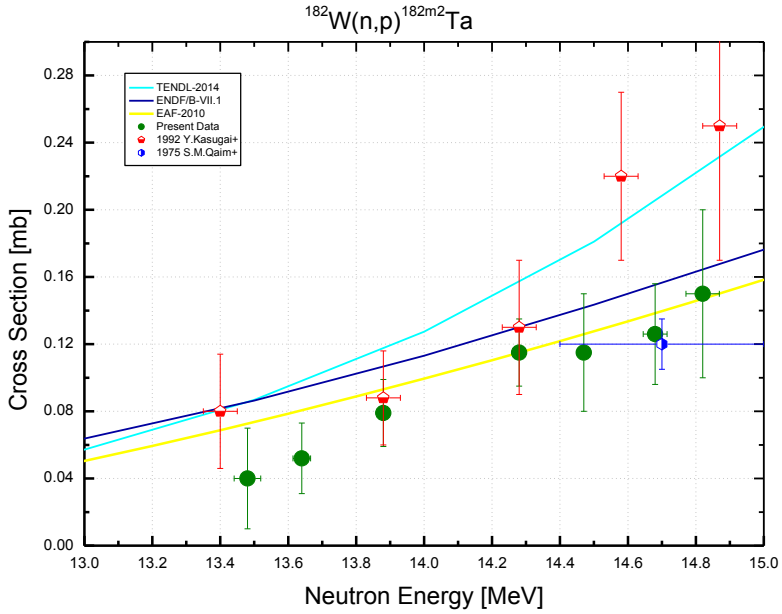

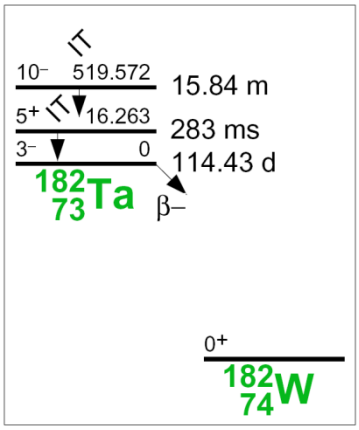

Decay data used for **^{182}W(n, p)^{182m2}Ta**.

Target nucleus	Abundance [%]	Chemical form	Reaction product	$T_{1/2}$	E_γ [keV]	Y_γ [%]
^{182}W	**26.50** ***16***	W-metal	^{182m2}Ta	**15.84 m** ***10***	146.8	36.5 *24*
					171.6	**48.0** ***20***

^{182}W(n, p)^{182}Ta

^{182}W(n, p)^{182}Ta			
E_n [MeV]	σ [mb]	$\pm\Delta\sigma_{total}$ [%]	$\pm\Delta\sigma_{ref}$ [%]
13.64	3.344	*8.93*	*3.55*
13.88	4.056	*17.3*	*3.55*
14.28	4.767	*5.33*	*3.54*
14.47	4.355	*20.6*	*3.55*
14.68	5.348	*9.27*	*3.55*
14.82	5.785	*5.79*	*3.55*
Ref. CS is ^{93}Nb(n,2n)^{92m}Nb; $\alpha_d = 1.1$			

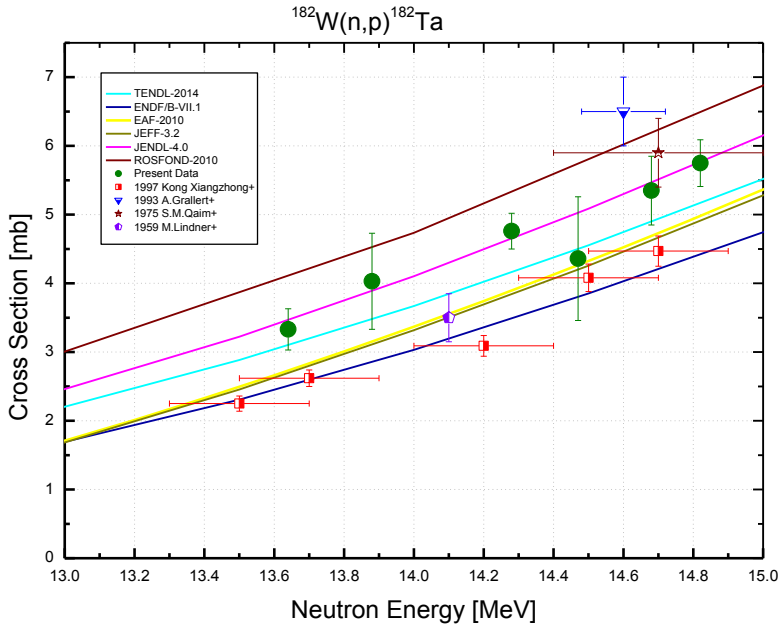

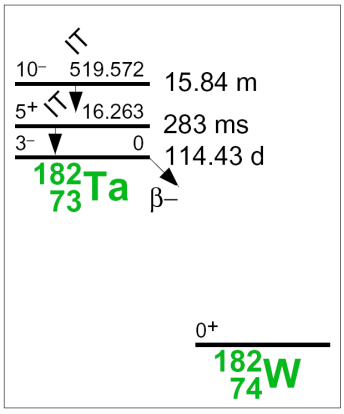

Decay data used for **^{182}W(n, p)^{182}Ta**.

Target nucleus	Abundance [%]	Chemical form	Reaction product	$T_{1/2}$	E_γ [keV]	Y_γ [%]
^{182}W	**26.50** *16*	W-metal	^{182}Ta	**114.74 d** *12*	**1121.3**	**35.24** *8*
					1221.4	27.23 *10*

^{183}W(n, α)^{180m}Hf

^{183}W(n, α)^{180m}Hf			
E_n [MeV]	σ [mb]	$\pm\Delta\sigma_{total}$ [%]	$\pm\Delta\sigma_{ref}$ [%]
13.64	0.025	*19.98*	*1.74*
13.88	0.033	*21.19*	*1.73*
14.28	0.039	*25.62*	*1.71*
14.47	0.060	*21.64*	*1.70*
14.68	0.047	*29.77*	*1.70*
14.82	0.071	*18.28*	*1.72*
Ref. CS is ^{27}Al(n, α)^{24}Na; $\alpha_d = 1.4$			

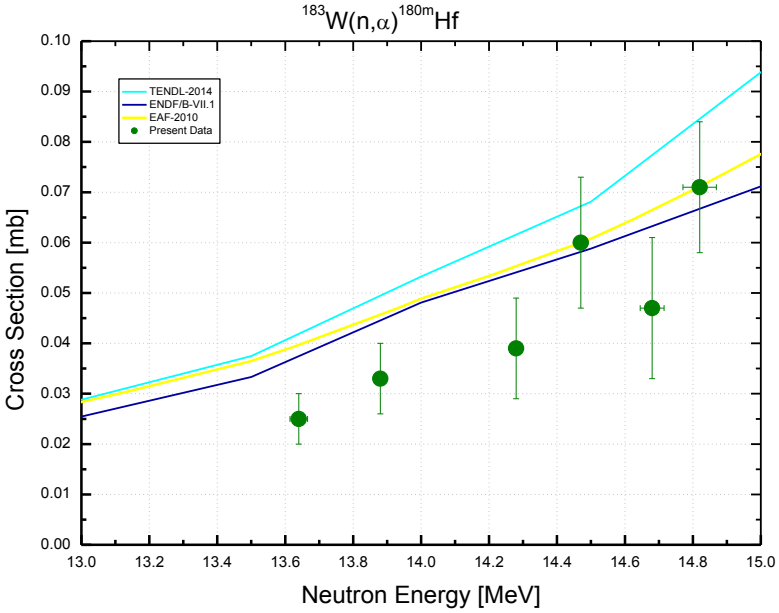

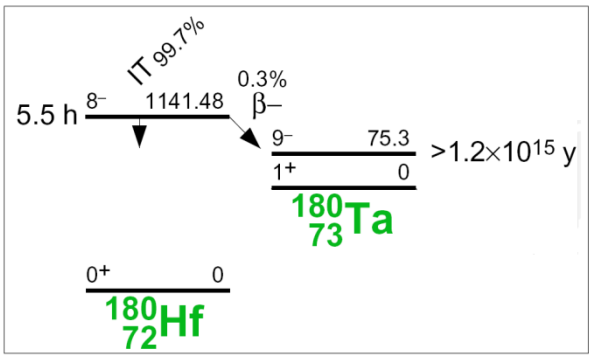

Decay data used for **^{183}W(n, α)^{180m}Hf.**

Target nucleus	Abundance [%]	Chemical form	Reaction product	$T_{1/2}$	E_γ [keV]	Y_γ [%]
^{183}W	**14.31** *4*	W-metal	^{180m}Hf	**5.53 h** *2*	**332.3**	**94.0** *30*
					443.2	81.7 *25*

^{183}W(n, p)^{183}Ta

^{183}W(n, p)^{183}Ta			
E_n [MeV]	σ [mb]	$\pm\Delta\sigma_{total}$ [%]	$\pm\Delta\sigma_{ref}$ [%]
13.64	3.77	*9.26*	*6.71*
13.88	4.49	*8.89*	*6.71*
14.28	5.71	*8.34*	*6.71*
14.47	5.43	*10.6*	*6.71*
14.68	6.86	*7.63*	*6.71*
14.82	7.19	*8.02*	*6.71*
Ref. CS is ^{93}Nb(n,2n)^{92m}Nb;			α_d = *1.2*

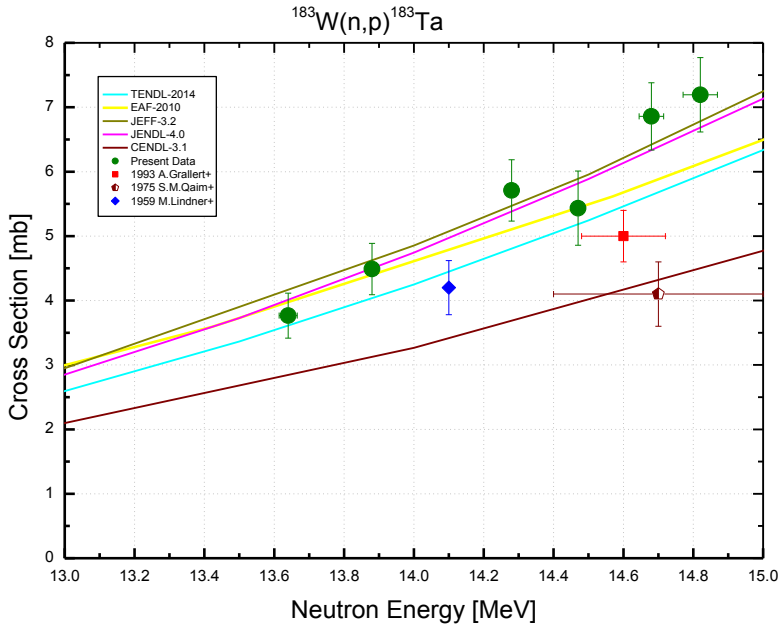

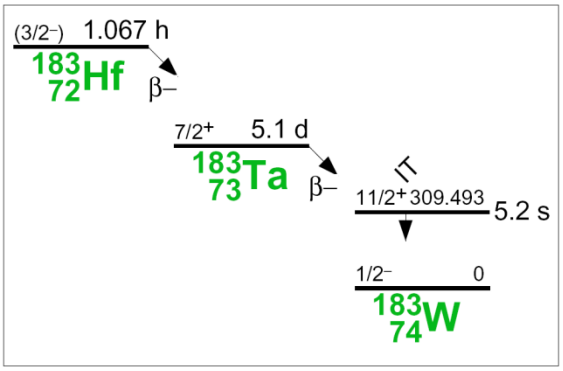

Decay data used for **^{183}W(n, p)^{183}Ta**.

Target nucleus	**Abundance [%]**	**Chemical form**	**Reaction product**	$T_{1/2}$	**E_γ [keV]**	**Y_γ [%]**
^{183}W	**14.31** *4*	W-metal	^{183}Ta	**5.1 d** *1*	**354.0**	**11.2** *7*

^{184}W(n, α)^{181}Hf

^{184}W(n, α)^{181}Hf			
E_n [MeV]	σ [mb]	$\pm\Delta\sigma_{total}$ [%]	$\pm\Delta\sigma_{ref}$ [%]
13.64	0.495	*8.64*	*0.79*
13.88	0.484	*8.65*	*0.77*
14.28	0.701	*4.56*	*0.75*
14.47	0.639	*15.6*	*0.76*
14.68	0.819	*5.48*	*0.77*
14.82	0.850	*5.18*	*0.79*
Ref. CS is ^{93}Nb(n,2n)^{92m}Nb; $\alpha_d = 1.1$			

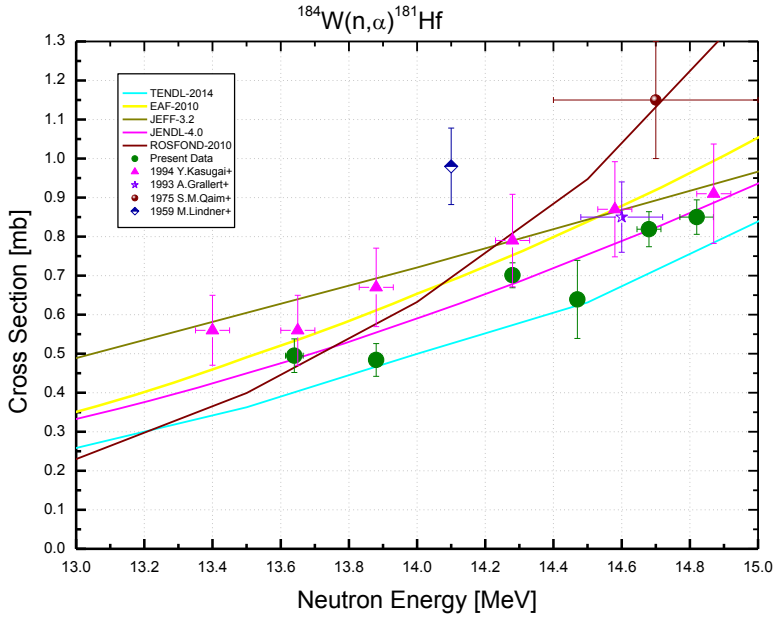

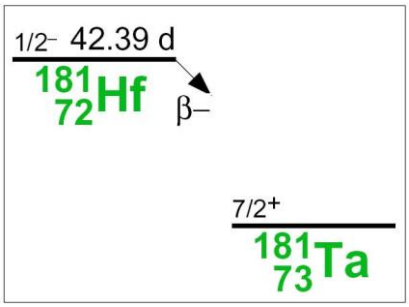

Decay data used for **^{184}W(n, α)^{181}Hf.**

Target nucleus	Abundance [%]	Chemical form	Reaction product	$T_{1/2}$	E_γ [keV]	Y_γ [%]
^{184}W	**30.64** *2*	W-metal	^{181}Hf	**42.39 d** *6*	133.0	43.3 *5*
					345.9	15.12 *12*
					482.2	**80.5** *4*

^{184}W(n, p)^{184}Ta

^{184}W(n, p)^{184}Ta			
E_n [MeV]	σ [mb]	$\pm\Delta\sigma_{total}$ [%]	$\pm\Delta\sigma_{ref}$ [%]
13.48	1.40	*6.71*	*4.50*
13.64	1.60	*6.00*	*4.46*
13.88	1.86	*6.19*	*4.45*
14.05	2.15	*7.39*	*4.45*
14.28	2.39	*5.71*	*4.45*
14.47	2.73	*5.03*	*4.44*
14.68	3.03	*5.05*	*4.44*
14.84	3.23	*4.97*	*4.45*
Ref. CS is ^{27}Al(n, α)^{24}Na; $\alpha_d = 1.4$			

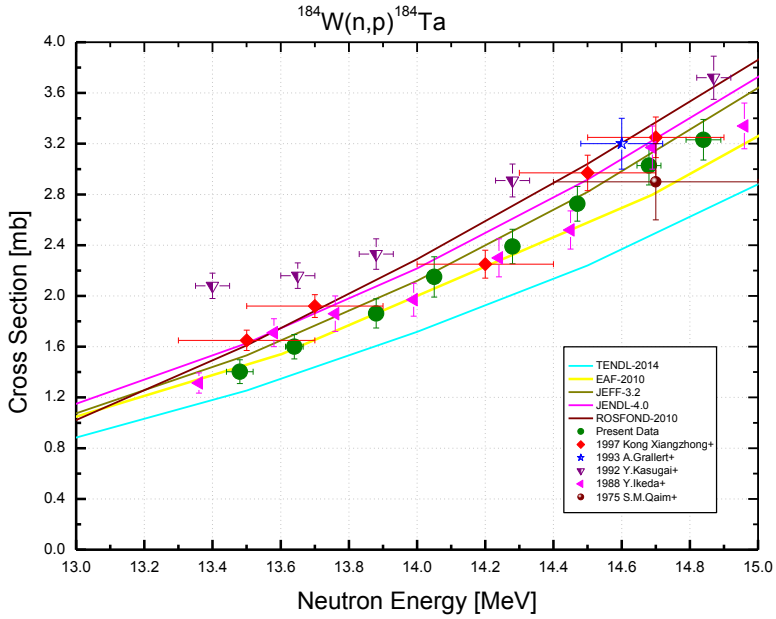

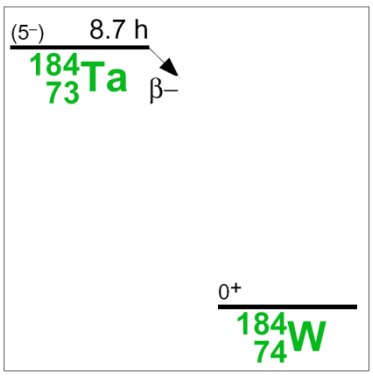

Decay data used for **^{184}W(n, p)^{184}Ta**.

Target nucleus	Abundance [%]	Chemical form	Reaction product	$T_{1/2}$	E_γ [keV]	Y_γ [%]
^{184}W	**30.64** *2*	W-metal	^{184}Ta	**8.7 h** *1*	252.9	44 *3*
					414.0	**72** *3*
					920.9	32.0 *15*

^{186}W(n, nα)^{182m}Hf

^{186}W(n, nα)^{182m}Hf			
E_n [MeV]	σ [mb]	$\pm\Delta\sigma_{total}$ [%]	$\pm\Delta\sigma_{ref}$ [%]
14.72	0.0063	*20.6*	*8.74*
14.81	0.0065	*23.1*	*8.74*
Ref. CS is ^{27}Al(n, α)^{24}Na; $\alpha_d = 1.5$			

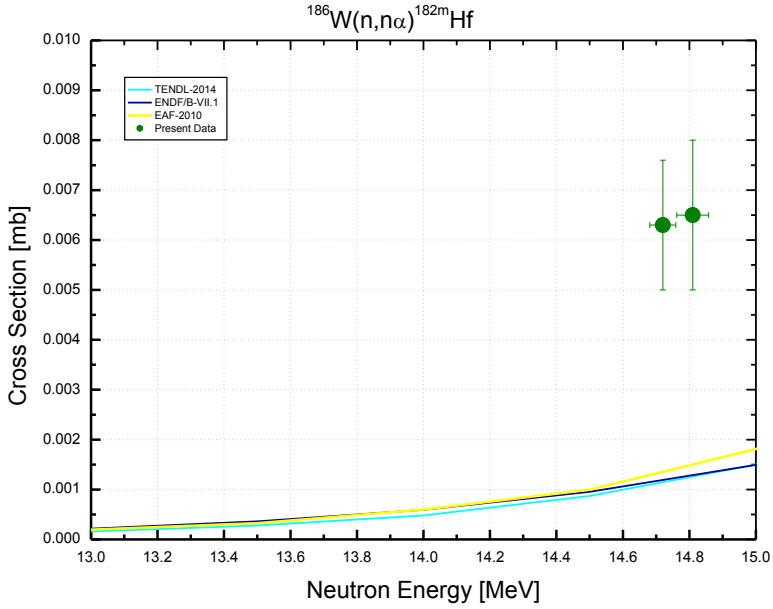

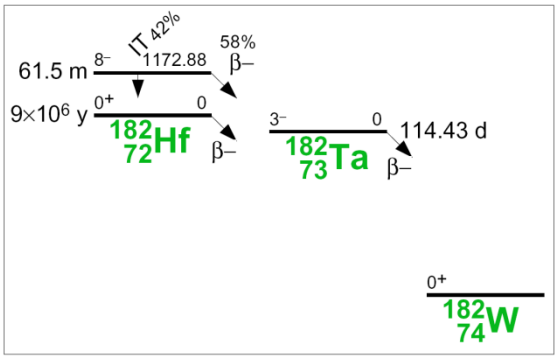

Decay data used for **^{186}W(n, nα)^{182m}Hf**.

Target nucleus	Abundance [%]	Chemical form	Reaction product	$T_{1/2}$	E_γ [keV]	Y_γ [%]
^{186}W	**28.43** *19*	W-metal	^{182m}Hf	**61.5 m** *15*	**224.4**	**38** *3*
					344.1	46 *6*
					455.8	20.0 *21*
					942.8	23 *3*

^{186}W(n, α)^{183}Hf

^{186}W(n, α)^{183}Hf			
E_n [MeV]	σ [mb]	$\pm\Delta\sigma_{total}$ [%]	$\pm\Delta\sigma_{ref}$ [%]
13.48	0.274	*22.9*	*13.9*
13.64	0.277	*18.5*	*13.9*
13.88	0.387	*15.6*	*13.9*
14.28	0.461	*17.3*	*13.9*
14.47	0.520	*14.4*	*13.9*
14.68	0.582	*19.0*	*13.9*
14.82	0.601	*14.1*	*13.9*
Ref. CS is ^{27}Al(n, α)^{24}Na; $\alpha_d = 1.5$			

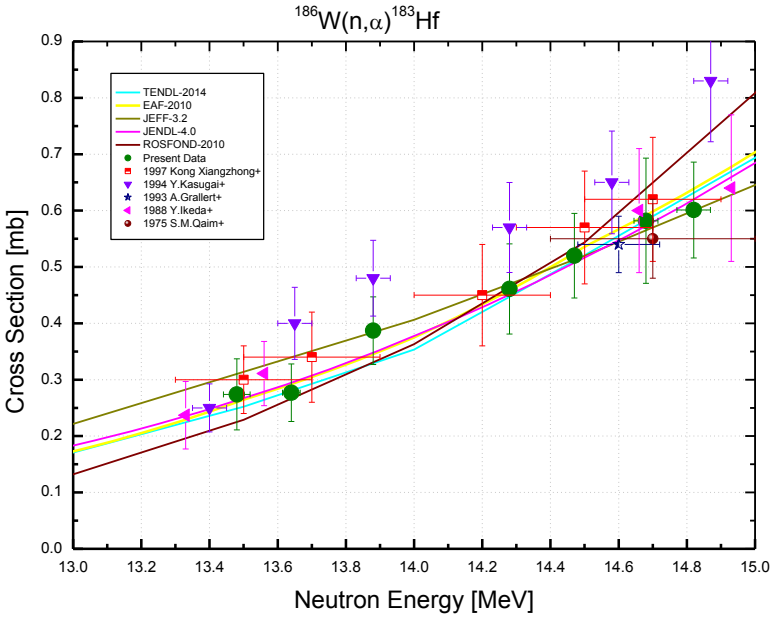

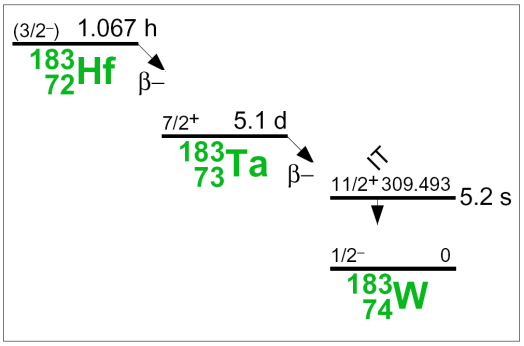

Decay data used for **^{186}W(n, α)^{183}Hf**.

Target nucleus	Abundance [%]	Chemical form	Reaction product	$T_{1/2}$	E_γ [keV]	Y_γ [%]
^{186}W	**28.43** *19*	W-metal	^{183}Hf	**1.067 h** *17*	459.1	27 *4*
					783.8	**66** *9*

^{186}W(n, p)^{186}Ta

^{186}W(n, p)^{186}Ta			
E_n [MeV]	σ [mb]	$\pm\Delta\sigma_{total}$ [%]	$\pm\Delta\sigma_{ref}$ [%]
13.48	0.80	*12.5*	*10.9*
13.65	0.93	*12.0*	*10.9*
13.88	1.02	*11.5*	*10.9*
14.04	1.25	*12.0*	*10.9*
14.27	1.55	*12.5*	*10.9*
14.46	1.59	*11.2*	*10.9*
14.67	1.83	*11.6*	*10.9*
14.82	1.97	*11.2*	*10.9*
Ref. CS is ^{27}Al(n, α)^{24}Na; $\alpha_d = 1.5$			

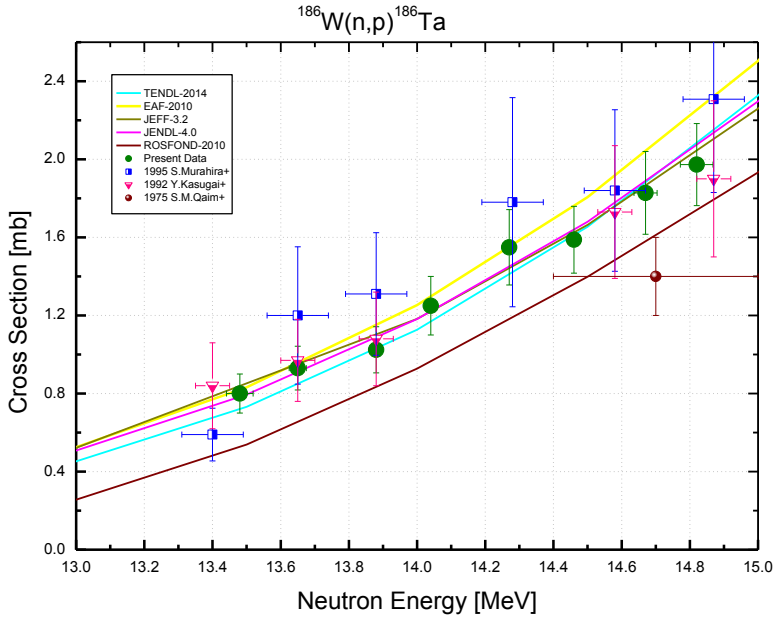

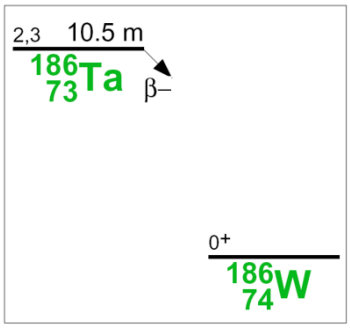

Decay data used for **^{186}W(n, p)^{186}Ta**.

Target nucleus	Abundance [%]	Chemical form	Reaction product	$T_{1/2}$	E_γ [keV]	Y_γ [%]
^{186}W	**28.43** *19*	W-metal	^{186}Ta	**10.5 m** *3*	**197.9**	**50** *5*
					615.3	28 *3*

^{186}W[(n, np)+(n,d)]^{185}Ta

^{186}W(n, x)^{185}Ta			
E_n [MeV]	σ [mb]	$\pm\Delta\sigma_{total}$ [%]	$\pm\Delta\sigma_{ref}$ [%]
14.72	0.155	*9.68*	*5.82*
14.81	0.250	*7.93*	*5.82*
14.88	0.270	*7.33*	*5.82*
Ref. CS is ^{27}Al(n, α)^{24}Na; α_d = *1.4*			

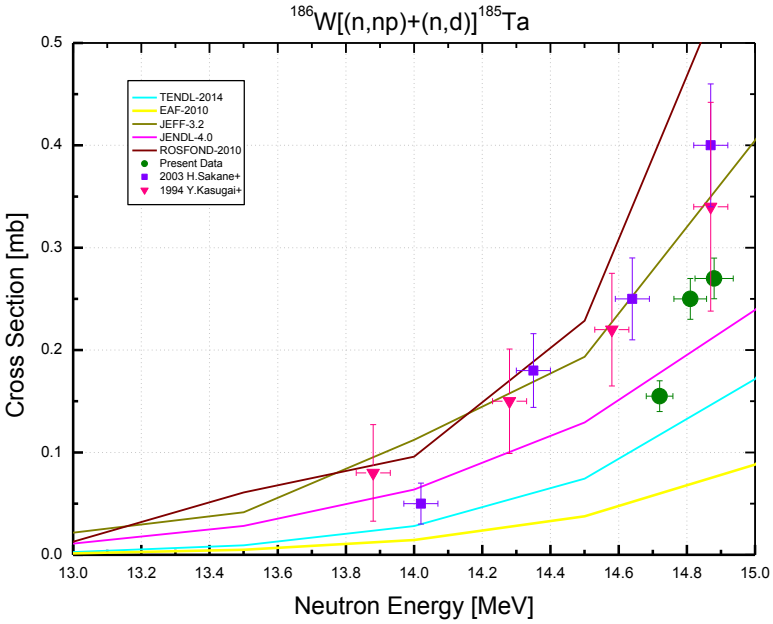

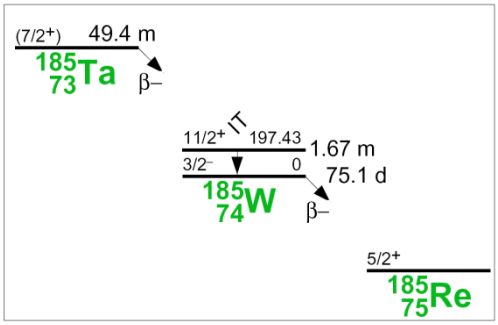

Decay data used for **^{186}W(n, x)^{185}Ta**.

Target nucleus	Abundance [%]	Chemical form	Reaction product	$T_{1/2}$	E_γ [keV]	Y_γ [%]
^{186}W	**28.43** ***19***	W-metal	^{185}Ta	**49.4 m** ***15***	173.9	22.6 *17*
					177.6	**25.7** ***10***

^{186}W(n, 2n)^{185m}W

^{186}W(n, 2n)^{185m}W			
E_n [MeV]	σ [mb]	$\pm\Delta\sigma_{total}$ [%]	$\pm\Delta\sigma_{ref}$ [%]
13.47	699	*8.53*	*5.72*
13.66	676	*8.86*	*5.69*
13.88	686	*8.77*	*5.68*
14.04	680	*8.78*	*5.68*
14.26	683	*8.69*	*5.68*
14.44	712	*9.26*	*5.68*
14.63	691	*8.70*	*5.68*
14.81	707	*7.72*	*5.68*
Ref. CS is ^{27}Al(n, α)^{24}Na; $\alpha_d = 1.8$			

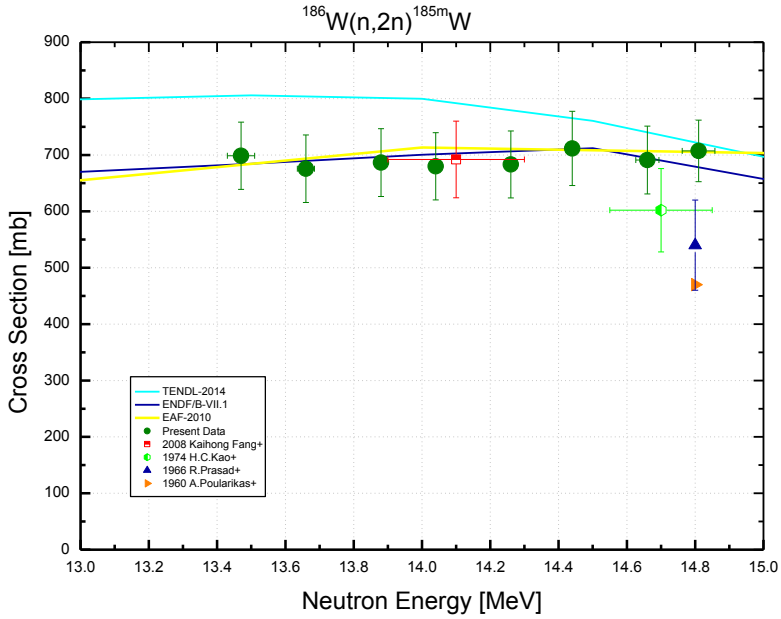

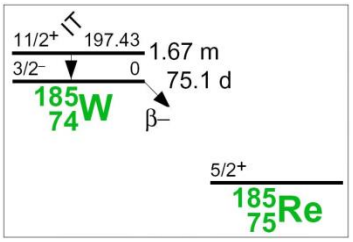

Decay data used for **^{186}W(n, 2n)^{185m}W**.

Target nucleus	Abundance [%]	Chemical form	Reaction product	$T_{1/2}$	E_γ [keV]	Y_γ [%]
^{186}W	**28.43** *19*	W-metal	^{185m}W	**1.67 m** *3*	131.6	4.33 *21*
					164.3	0.59 *3*
					173.7	**3.26** *15*
					187.9	0.81 *5*

^{186}W(n, 2n)^{185}W

^{186}W(n, 2n)^{185}W			
E_n [MeV]	σ [mb]	$\pm\Delta\sigma_{total}$ [%]	$\pm\Delta\sigma_{ref}$ [%]
13.64	1968	*17.8*	*3.76*
13.88	1892	*17.5*	*3.75*
14.28	1903	*12.0*	*3.75*
14.68	1969	*13.1*	*3.75*
14.82	2073	*11.6*	*3.76*
Ref. CS is ^{93}Nb(n,2n)^{92m}Nb;		α_d = *1.1*	

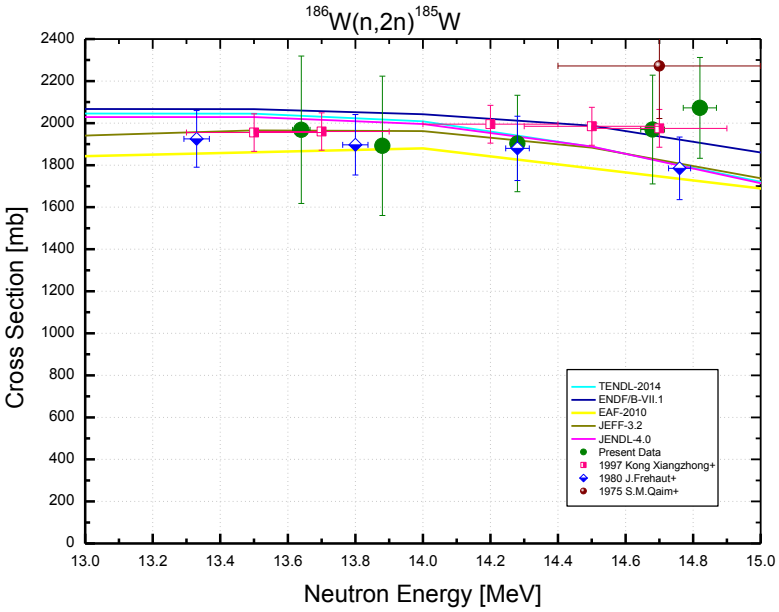

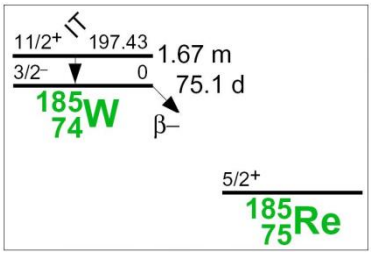

Decay data used for **^{186}W(n, 2n)^{185}W**.

Target nucleus	Abundance [%]	Chemical form	Reaction product	$T_{1/2}$	E_γ [keV]	Y_γ [%]
^{186}W	**28.43** *19*	W-metal	^{185}W	**75.1 d** *3*	**125.4**	**0.0192** *7*

^{185}Re(n, α)^{182}Ta

^{185}Re(n, α)^{182}Ta			
E_n [MeV]	σ [mb]	$\pm\Delta\sigma_{total}$ [%]	$\pm\Delta\sigma_{ref}$ [%]
14.48	1.40	*35.7*	*0.681*
Ref. CS is ^{93}Nb(n,2n)^{92m}Nb; α_d = *1.01*			

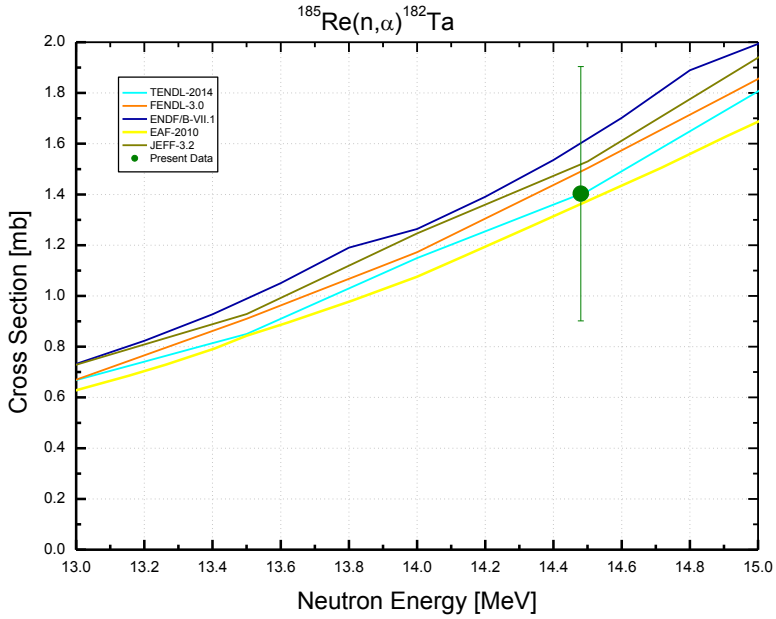

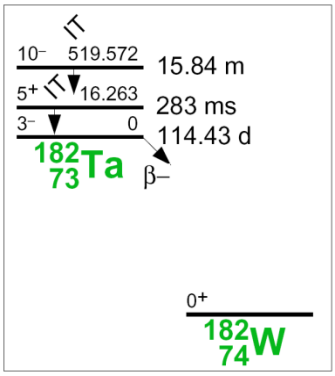

Decay data used for **^{185}Re(n, α)^{182}Ta**.

Target nucleus	Abundance [%]	Chemical form	Reaction product	$T_{1/2}$	E_γ [keV]	Y_γ [%]
^{185}Re	**37.40** *2*	K_2ReCl_6	^{182}Ta	**114.74 d** *12*	**1189.0**	**16.49** *5*
					1221.4	27.23 *10*

^{185}Re(n, 2n)^{184m}Re

^{185}Re(n, 2n)^{184m}Re			
E_n [MeV]	σ [mb]	$\pm\Delta\sigma_{total}$ [%]	$\pm\Delta\sigma_{ref}$ [%]
14.74	357	*9.19*	*6.01*
Ref. CS is ^{93}Nb(n,2n)^{92m}Nb; α_d = *1.1*			

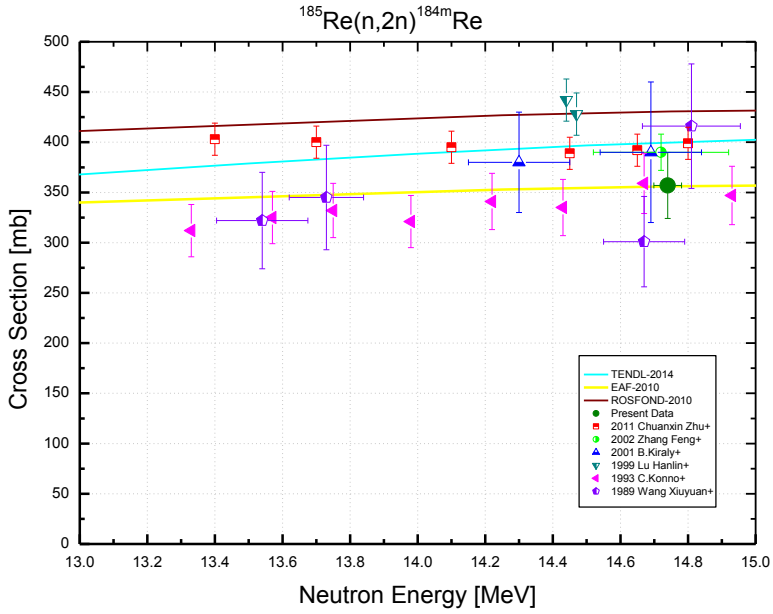

Most γ-rays used for ^{185}Re(n, 2n)^{184m}Re cross-section calculation belong to the ^{184}W. (An exception is a 104.7 keV γ-ray which belongs to the ^{184}Re). For γ-rays of the ^{184}W, a special care was taken to exclude γ-transitions which may accompany the ^{184}Re ground state decay.

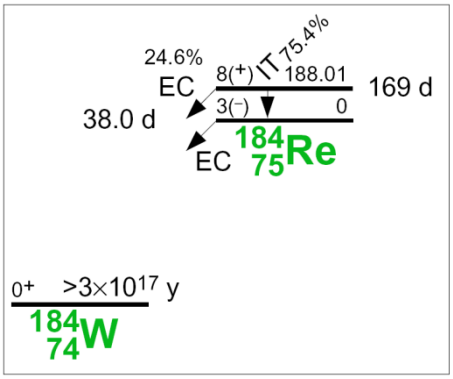

Decay data used for **^{185}Re(n, 2n)^{184m}Re**.

Target nucleus	Abundance [%]	Chemical form	Reaction product	$T_{1/2}$	E_γ [keV]	Y_γ [%]
^{185}Re	**37.40** *2*	K_2ReCl_6	^{184m}Re	**169 d** *8*	**104.7**	**13.6** *4*
					161.3	6.56 *23*
					536.7	3.33 *11*
					920.9	8.2 *3*

^{185}Re(n, 2n)^{184g}Re

^{185}Re(n, 2n)^{184g}Re			
E_n [MeV]	σ [mb]	$\pm\Delta\sigma_{total}$ [%]	$\pm\Delta\sigma_{ref}$ [%]
14.74	1488	*5.94*	*3.81*
Ref. CS is ^{93}Nb(n,2n)^{92m}Nb; α_d = *1.2*			

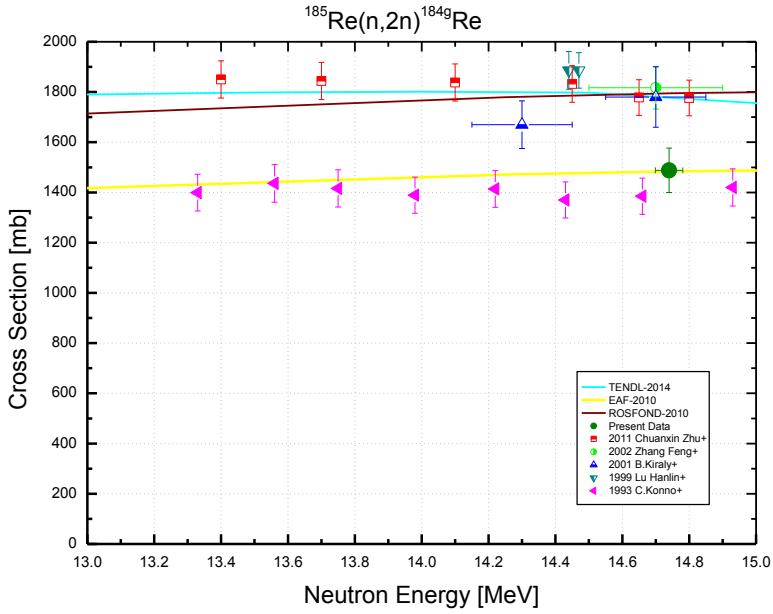

Gamma-rays used for ^{185}Re(n, 2n)^{184g}Re cross-section calculation are presented in the table at the page bottom. They all belong to the ^{184}W. In contrast to the case considered on the previous page, the γ-rays chosen to characterize the ^{185}Re(n, 2n)^{184g}Re reaction may accompany not only the decay of ^{184g}Re but also this of ^{184m}Re, with a far less intensity though.

The ^{185}Re(n, 2n)^{184g}Re cross-section data was corrected for a possible admixture of the ^{184m}Re decay.

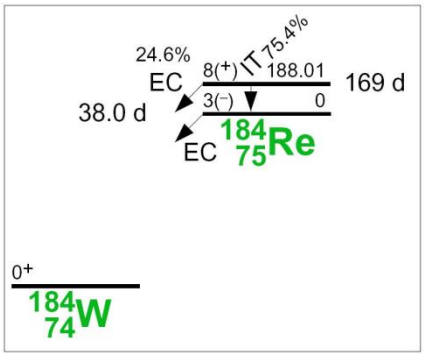

Decay data used for **^{185}Re(n, 2n)^{184g}Re**.

Target nucleus	Abundance [%]	Chemical form	Reaction product	$T_{1/2}$	E_γ [keV]	Y_γ [%]
^{185}Re	**37.40** *2*	K_2ReCl_6	^{184g}Re	**35.4 d** *7*	**792.1**	**37.7** *11*
					894.8	15.7 *5*
					903.3	38.1 *12*

^{185}Re(n, 2n)^{184}Re

^{185}Re(n, 2n)^{184}Re		
E_n [MeV]	σ [mb]	$\pm\Delta\sigma_{total}$ *[%]*
14.74	1845	*5.07*
Ref. CS is ^{93}Nb(n,2n)^{92m}Nb		

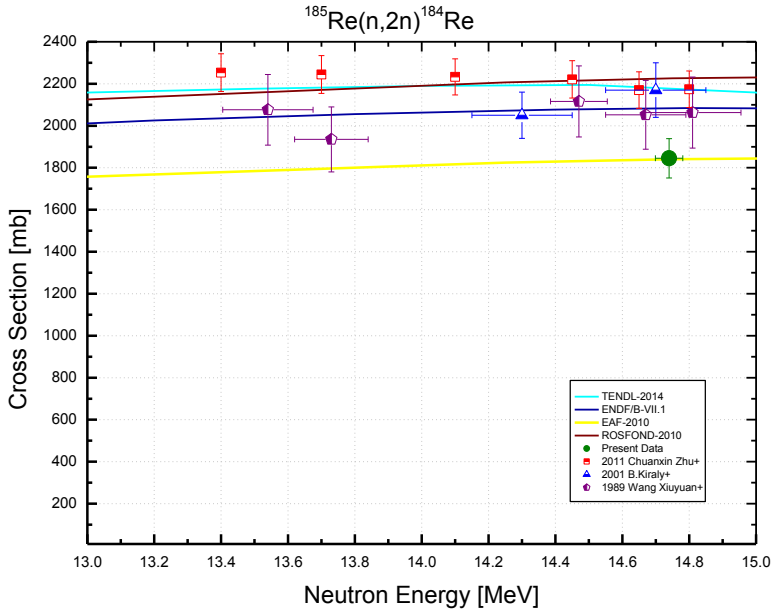

The ^{185}Re(n, 2n)^{184}Re cross-section was not measured in the experiment directly This is the sum of cross-sections ^{185}Re(n, 2n)^{184m}Re and ^{185}Re(n, 2n)^{184g}Re presented in the previous pages.

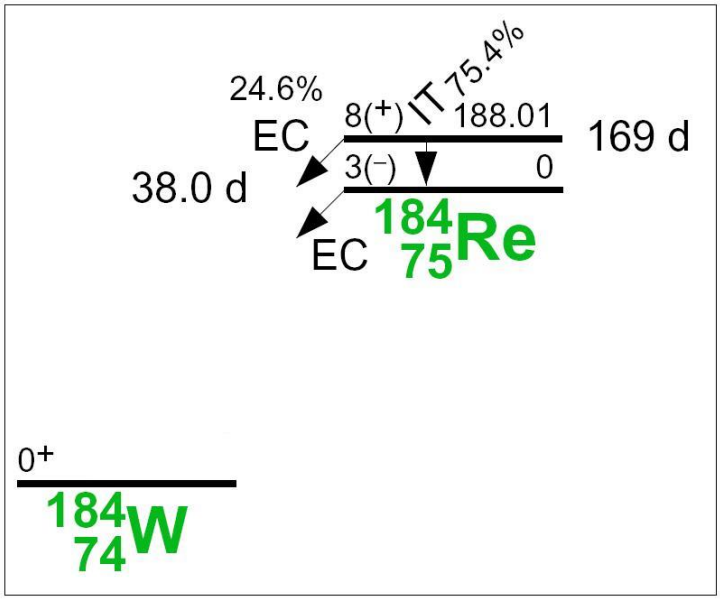

^{187}Re(n, α)^{184}Ta

^{187}Re(n, α)^{184}Ta			
E_n [MeV]	σ [mb]	$\pm\Delta\sigma_{total}$ [%]	$\pm\Delta\sigma_{ref}$ [%]
13.67	0.316	*15.2*	*4.80*
14.06	0.416	*10.6*	*4.79*
14.46	0.561	*7.74*	*4.79*
14.84	0.609	*7.97*	*4.80*
Ref. CS is ^{93}Nb(n,2n)^{92m}Nb;		α_d = *2.0*	

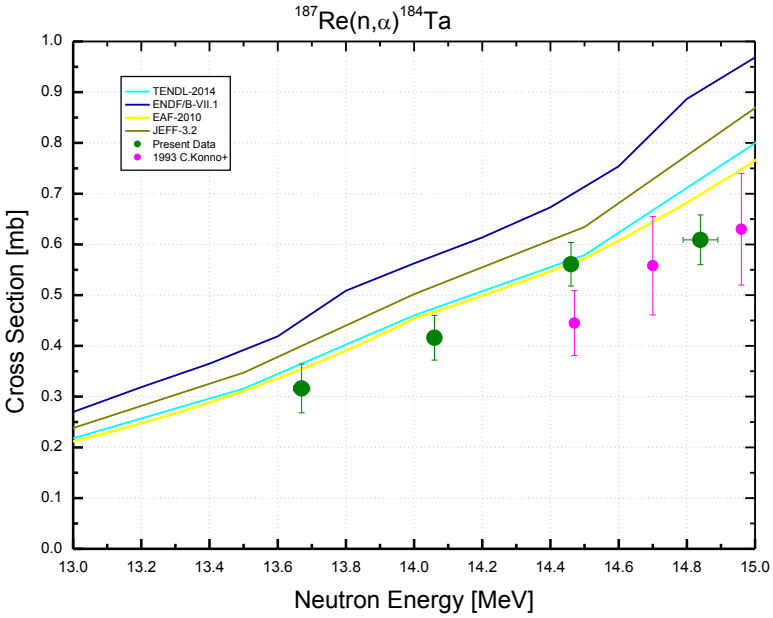

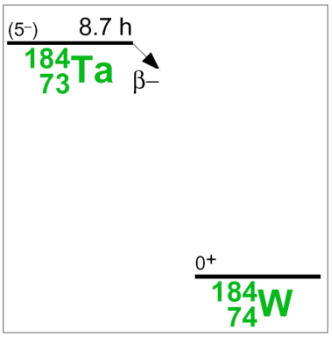

Decay data used for **^{187}Re(n, α)^{184}Ta**.

Target nucleus	**Abundance [%]**	**Chemical form**	**Reaction product**	$T_{1/2}$	**E_γ [keV]**	**Y_γ [%]**
^{187}Re	**62.60** *2*	K_2ReCl_6	^{184}Ta	**8.7 h** *1*	**414.0**	**72** *3*

^{187}Re(n, p)^{187}W

^{187}Re(n, p)^{187}W			
E_n [MeV]	σ [mb]	$\pm\Delta\sigma_{total}$ [%]	$\pm\Delta\sigma_{ref}$ [%]
13.67	2.75	*10.9*	*1.62*
14.06	3.18	*9.42*	*1.60*
14.46	3.45	*10.1*	*1.60*
14.84	3.94	*7.23*	*1.61*
Ref. CS is ^{93}Nb(n,2n)^{92m}Nb;		α_d = *1.5*	

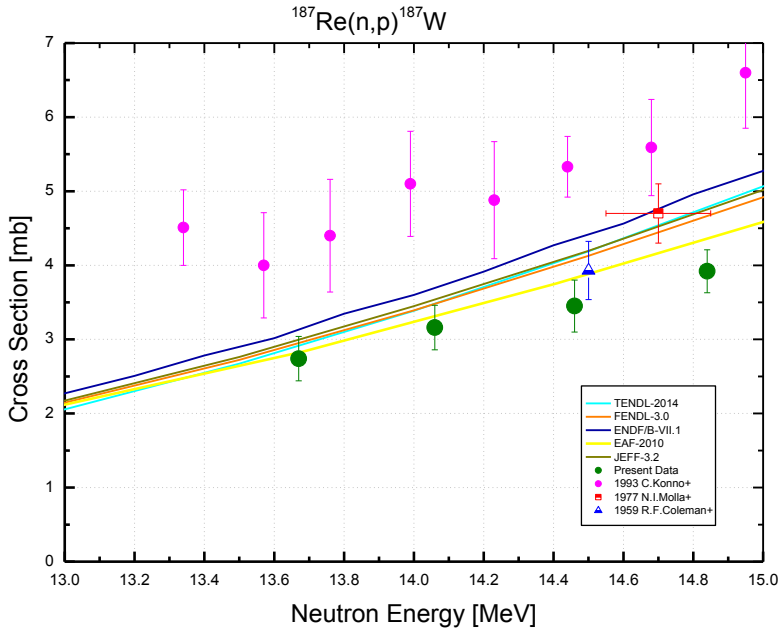

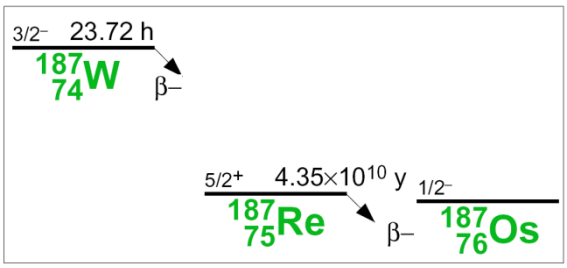

Decay data used for **^{187}Re(n, p)^{187}W**.

Target nucleus	Abundance [%]	Chemical form	Reaction product	$T_{1/2}$	E_γ [keV]	Y_γ [%]
^{187}Re	**62.60** *2*	K_2ReCl_6	^{187}W	**24.000 h** *4*	479.5	26.6 *4*
					685.8	**33.2** *5*

^{187}Re(n, 2n)^{186g}Re

^{187}Re(n, 2n)^{186g}Re			
E_n [MeV]	σ [mb]	$\pm\Delta\sigma_{total}$ [%]	$\pm\Delta\sigma_{ref}$ [%]
14.85	1680	*5.86*	*0.67*
Ref. CS is ^{93}Nb(n,2n)^{92m}Nb; $\alpha_d = 1.5$			

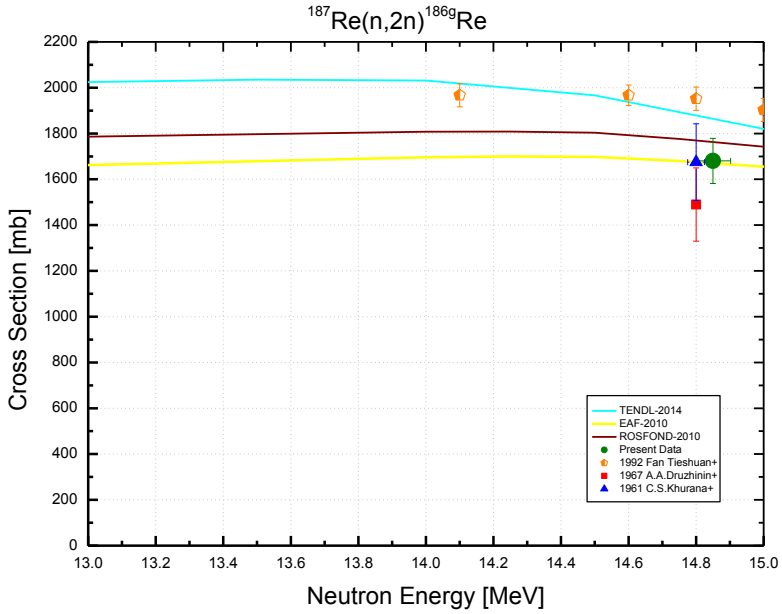

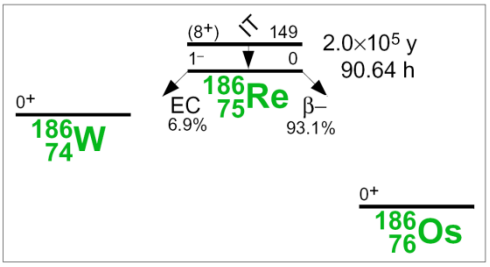

Decay data used for **^{187}Re(n, 2n)^{186g}Re**.

Target nucleus	Abundance [%]	Chemical form	Reaction product	$T_{1/2}$	E_γ [keV]	Y_γ [%]
^{187}Re	**62.60** *2*	K_2ReCl_6	^{186g}Re	**3.7183 d** *11*	**137.2**	**9.47** *3*

^{186}Os(n, p)^{186g}Re

^{186}Os(n, p)^{186g}Re			
E_n [MeV]	σ [mb]	$\pm\Delta\sigma_{total}$ [%]	$\pm\Delta\sigma_{ref}$ [%]
14.47	6.69	*22.4*	*1.99*
14.82	5.53	*27.2*	*2.00*
Ref. CS is ^{93}Nb(n,2n)^{92m}Nb;			α_d = *1.4*

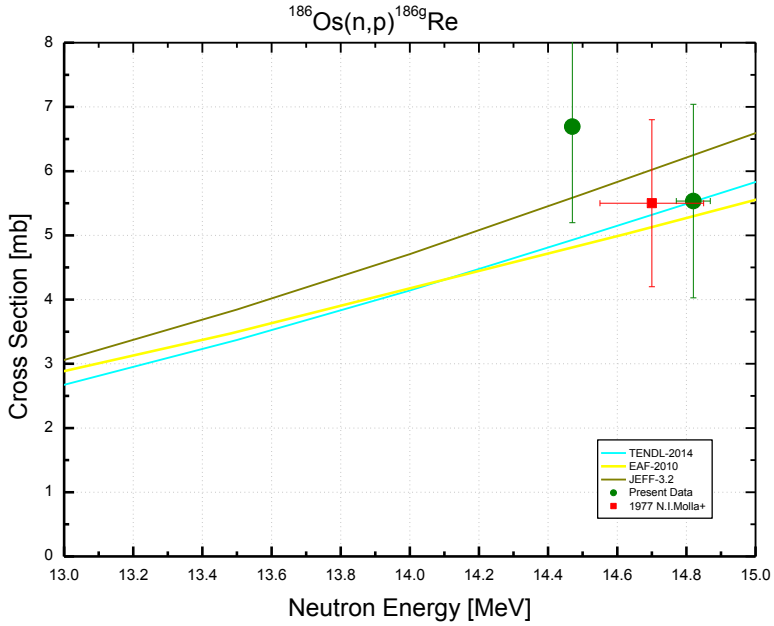

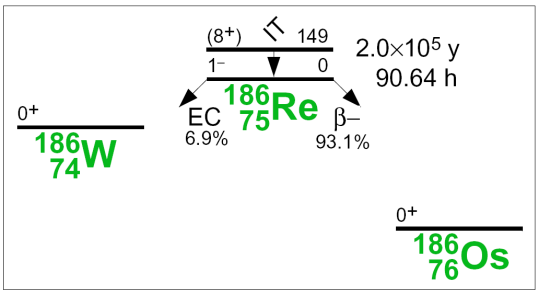

Decay data used for **^{186}Os(n, p)^{186g}Re**.

Target nucleus	Abundance [%]	Chemical form	Reaction product	$T_{1/2}$	E_γ [keV]	Y_γ [%]
^{186}Os	**1.59** *3*	Os-metal	^{186g}Re	**3.7183 d** *11*	**137.2**	**9.47** *3*

^{188}Os(n, p)^{188}Re

^{188}Os(n, p)^{188}Re			
E_n [MeV]	σ [mb]	$\pm\Delta\sigma_{total}$ [%]	$\pm\Delta\sigma_{ref}$ [%]
13.64	2.89	*11.4*	*1.43*
13.88	3.38	*11.2*	*1.42*
14.47	4.76	*11.3*	*1.41*
14.68	5.12	*11.1*	*1.42*
14.82	5.61	*10.7*	*1.43*
Ref. CS is ^{93}Nb(n,2n)^{92m}Nb; $\alpha_d = 1.6$			

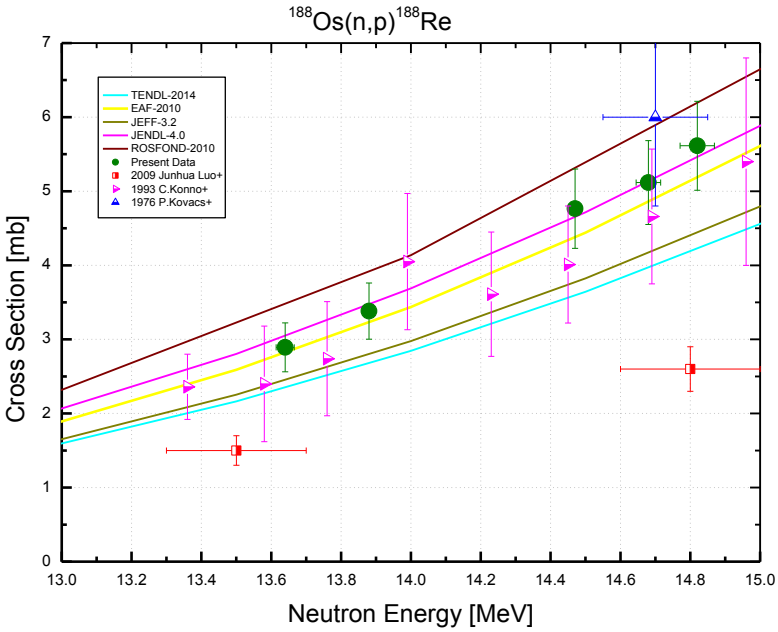

The possible contribution of ^{189}Os(n, np)^{188}Re + ^{189}Os(n, d)^{188}Re is expected to be as small as <1%.

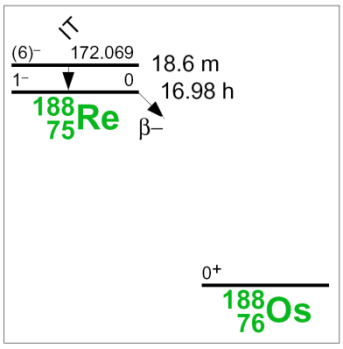

Decay data used for **^{188}Os(n, p)^{188}Re**.

Target nucleus	**Abundance [%]**	**Chemical form**	**Reaction product**	$T_{1/2}$	**E_γ [keV]**	**Y_γ [%]**
^{188}Os	**13.24** ***8***	Os-metal	^{188}Re	**17.0040 h** ***22***	**155.0**	**15.61** ***18***

^{189}Os(n, p)^{189}Re

^{189}Os(n, p)^{189}Re			
E_n [MeV]	σ [mb]	$\pm\Delta\sigma_{total}$ [%]	$\pm\Delta\sigma_{ref}$ [%]
13.64	5.62	*30.3*	*15.8*
13.88	6.74	*28.3*	*15.8*
14.47	9.29	*25.8*	*15.8*
14.68	10.1	*28.7*	*15.8*
14.82	11.4	*28.3*	*15.8*
Ref. CS is ^{93}Nb(n,2n)^{92m}Nb;		α_d = *1.6*	

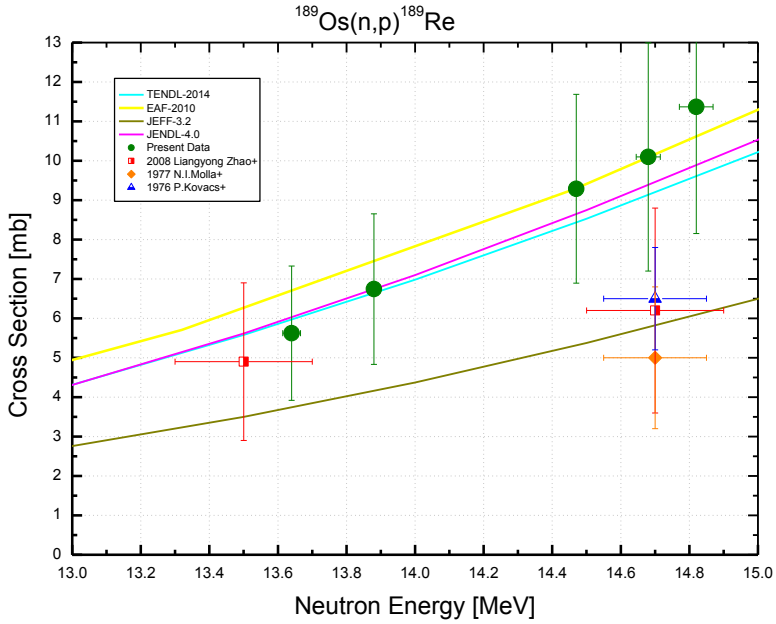

Possible contribution of ^{190}Os(n, np)^{189}Re + ^{190}Os(n, d)^{189}Re reactions is estimated as about 5% which is several times less than experimental uncertainties.

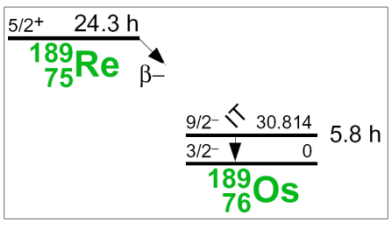

Decay data used for **^{189}Os(n, p)^{189}Re**.

Target nucleus	**Abundance [%]**	**Chemical form**	**Reaction product**	**$T_{1/2}$**	**E_γ [keV]**	**Y_γ [%]**
^{189}Os	**16.15** *5*	Os-metal	^{189}Re	**24.3 h** *4*	147.1	1.24 *21*
					216.7	5.5 *9*
					219.4	**4.5** *7*
					245.1	3.5 *7*

^{190}Os(n, α)^{187}W

^{190}Os(n, α)^{187}W			
E_n [MeV]	σ [mb]	$\pm\Delta\sigma_{total}$ [%]	$\pm\Delta\sigma_{ref}$ [%]
13.64	0.523	*7.98*	*1.62*
13.88	0.595	*8.38*	*1.61*
14.47	0.797	*6.15*	*1.60*
14.68	0.843	*6.05*	*1.61*
14.82	0.960	*6.38*	*1.62*
Ref. CS is ^{93}Nb(n,2n)^{92m}Nb;			α_d = *1.7*

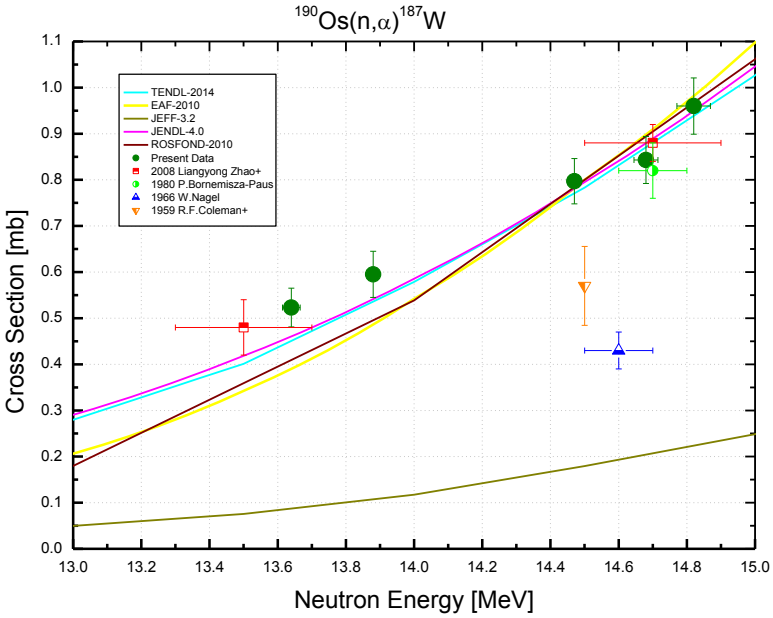

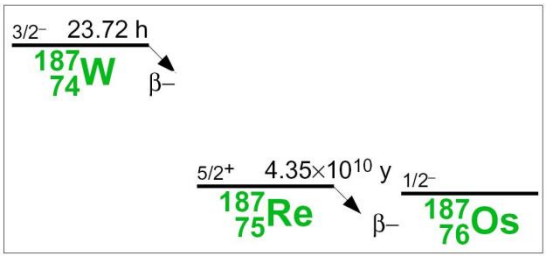

Decay data used for **^{190}Os(n, α)^{187}W.**

Target nucleus	Abundance [%]	Chemical form	Reaction product	$T_{1/2}$	E_γ [keV]	Y_γ [%]
^{190}Os	**26.26** *2*	Os-metal	^{187}W	**24.000 h** *4*	**479.5**	**26.6** *4*
					685.8	33.2 *5*

^{190}Os(n, p)^{190m}Re

^{190}Os(n, p)^{190m}Re			
E_n [MeV]	σ [mb]	$\pm\Delta\sigma_{total}$ [%]	$\pm\Delta\sigma_{ref}$ [%]
13.64	0.240	*28.8*	*12.4*
13.88	0.282	*15.3*	*12.4*
14.47	0.337	*13.3*	*12.4*
14.68	0.370	*21.6*	*12.4*
14.82	0.448	*16.4*	*12.4*
Ref. CS is ^{93}Nb(n,2n)^{92m}Nb;		α_d = *1.7*	

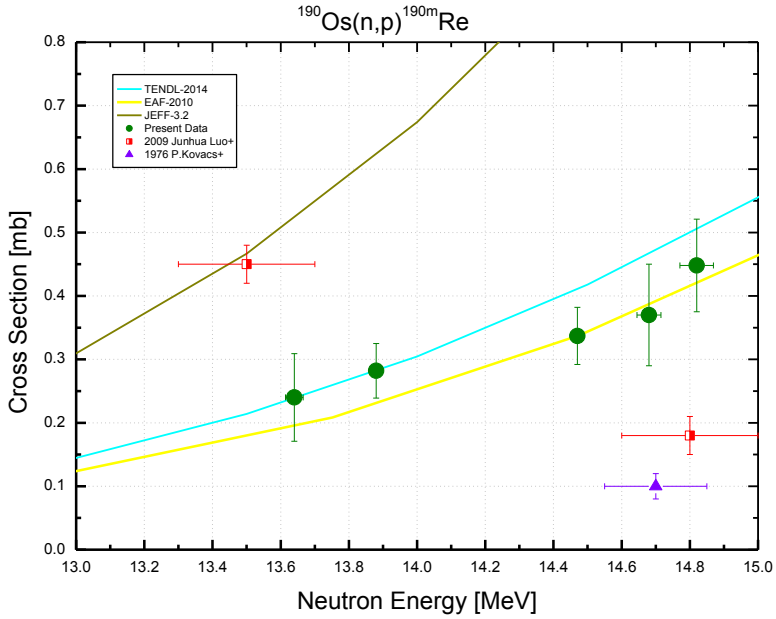

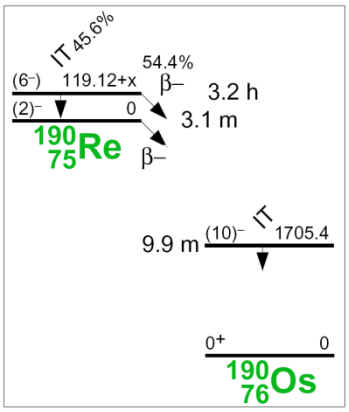

Decay data used for **^{190}Os(n, p)^{190m}Re**.

Target nucleus	Abundance [%]	Chemical form	Reaction product	$T_{1/2}$	E_γ [keV]	Y_γ [%]
^{190}Os	**26.26** *2*	Os-metal	^{190m}Re	**3.2 h** *2*	361.1	12.1 *11*
					569.3	13.7 *11*
					605.1	14.9 *11*
					673.1	**9.4** *6*

^{191}Ir(n, α)^{188}Re

^{191}Ir(n, α)^{188}Re			
E_n [MeV]	σ [mb]	$\pm\Delta\sigma_{total}$ [%]	$\pm\Delta\sigma_{ref}$ [%]
13.64	0.562	*26.8*	*1.40*
13.88	0.423	*16.6*	*1.39*
14.10	0.684	*20.6*	*1.38*
14.28	0.641	*15.6*	*1.38*
14.47	0.629	*31.7*	*1.39*
14.68	0.770	*15.5*	*1.39*
14.82	0.986	*22.4*	*1.40*
Ref. CS is ^{93}Nb(n,2n)^{92m}Nb;		α_d = *1.6*	

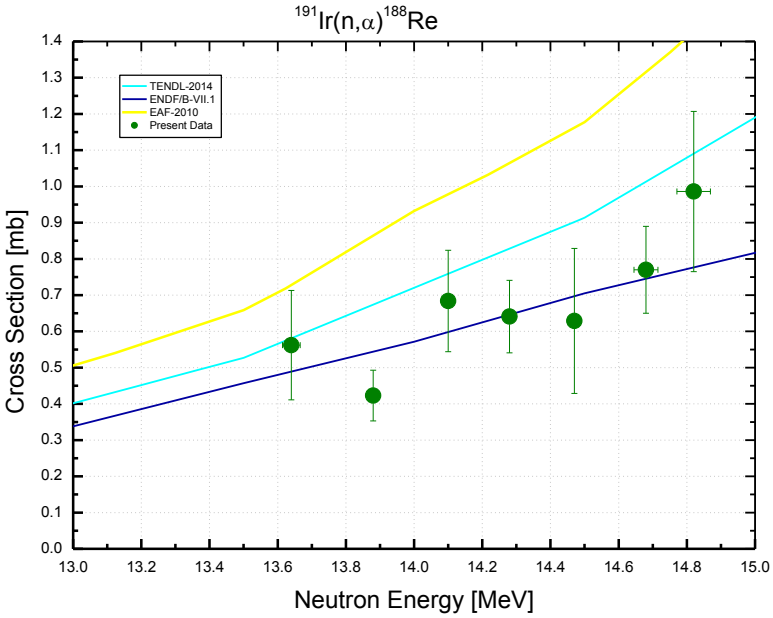

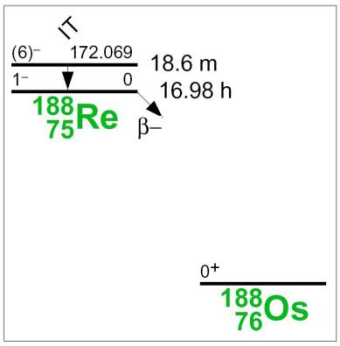

Decay data used for **^{191}Ir(n, α)^{188}Re**.

Target nucleus	Abundance [%]	Chemical form	Reaction product	$T_{1/2}$	E_γ [keV]	Y_γ [%]
^{191}Ir	**37.3** *2*	Ir-metal	^{188}Re	**17.0040 h** *22*	**155.0**	**15.61** *18*

^{191}Ir(n, p)^{191}Os

^{191}Ir(n, p)^{191}Os			
E_n [MeV]	σ [mb]	$\pm\Delta\sigma_{total}$ [%]	$\pm\Delta\sigma_{ref}$ [%]
13.64	3.56	*18.3*	*1.17*
13.88	3.62	*14.1*	*1.16*
14.10	3.72	*21.6*	*1.15*
14.28	4.37	*12.6*	*1.15*
14.47	4.38	*15.9*	*1.15*
14.68	4.13	*12.0*	*1.16*
14.82	5.31	*15.1*	*1.17*
Ref. CS is ^{93}Nb(n,2n)^{92m}Nb;		$\alpha_d = 1.3$	

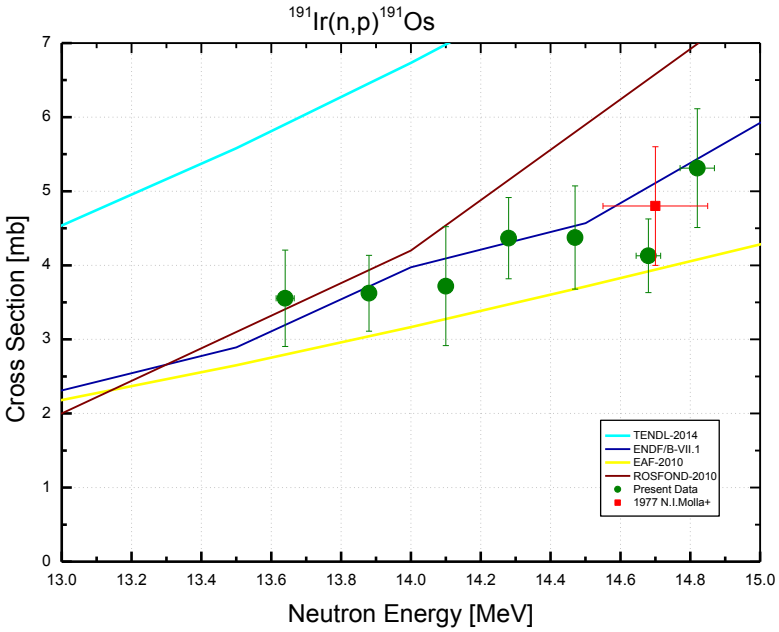

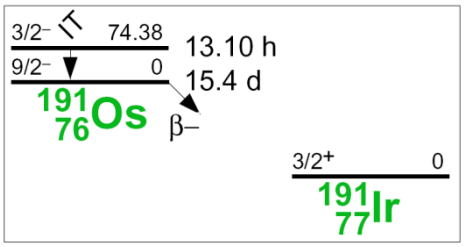

Decay data used for **^{191}Ir(n, p)^{191}Os**.

Target nucleus	**Abundance [%]**	**Chemical form**	**Reaction product**	$T_{1/2}$	**E_γ [keV]**	**Y_γ [%]**
^{191}Ir	**37.3** *2*	Ir-metal	^{191}Os	**15.4 d** *1*	**129.4**	**26.50** *4*

^{191}Ir(n, 2n)^{190m2}Ir

^{191}Ir(n, 2n)^{190m2}Ir			
E_n [MeV]	σ [mb]	$\pm\Delta\sigma_{total}$ [%]	$\pm\Delta\sigma_{ref}$ [%]
13.64	116	*6.80*	*1.11*
13.88	122	*6.51*	*1.09*
14.10	122	*6.45*	*1.09*
14.28	137	*6.46*	*1.09*
14.47	136	*6.51*	*1.09*
14.68	144	*6.13*	*1.10*
14.82	150	*6.60*	*1.11*
Ref. CS is ^{93}Nb(n,2n)^{92m}Nb;		α_d = *1.9*	

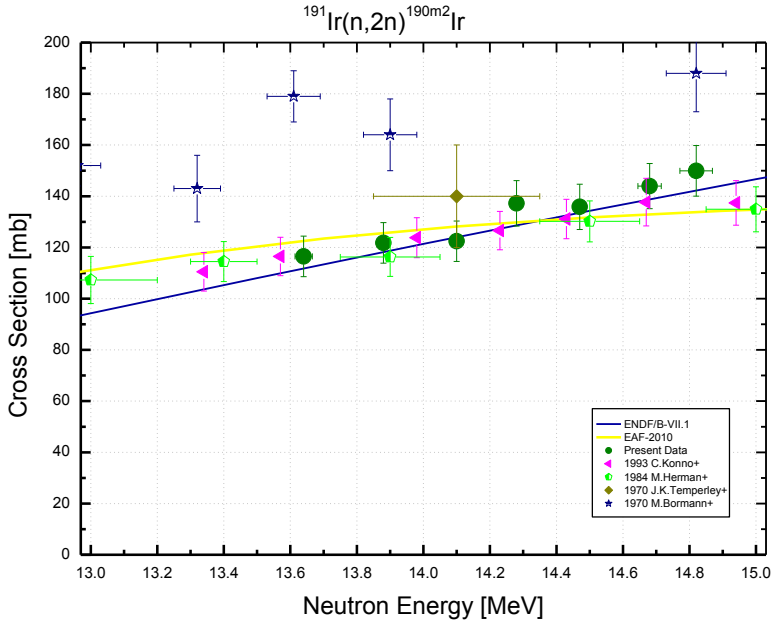

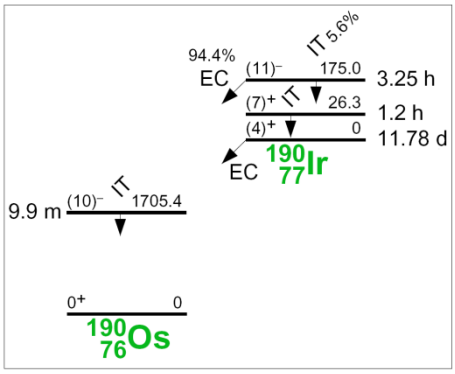

Decay data used for **^{191}Ir(n, 2n)^{190m2}Ir**.

Target nucleus	Abundance [%]	Chemical form	Reaction product	$T_{1/2}$	E_γ [keV]	Y_γ [%]
^{191}Ir	**37.3** *2*	Ir-metal	^{190m2}Ir	**3.087 h** *12*	361.2	86.72 *21*
					502.5	**89.35** *20*
					616.5	90.14 *22*

^{191}Ir(n, 2n)$^{190g+m1}$Ir

^{191}Ir(n, 2n)$^{190g+m1}$Ir			
E_n [MeV]	σ [mb]	$\pm\Delta\sigma_{total}$ [%]	$\pm\Delta\sigma_{ref}$ [%]
13.64	1726	*5.40*	*3.39*
13.88	1782	*5.52*	*3.38*
14.10	1736	*5.37*	*3.38*
14.28	1759	*5.57*	*3.38*
14.47	1764	*5.53*	*3.38*
14.68	1755	*5.56*	*3.38*
14.82	1738	*5.66*	*3.39*
Ref. CS is ^{93}Nb(n,2n)^{92m}Nb;		α_d = *1.4*	

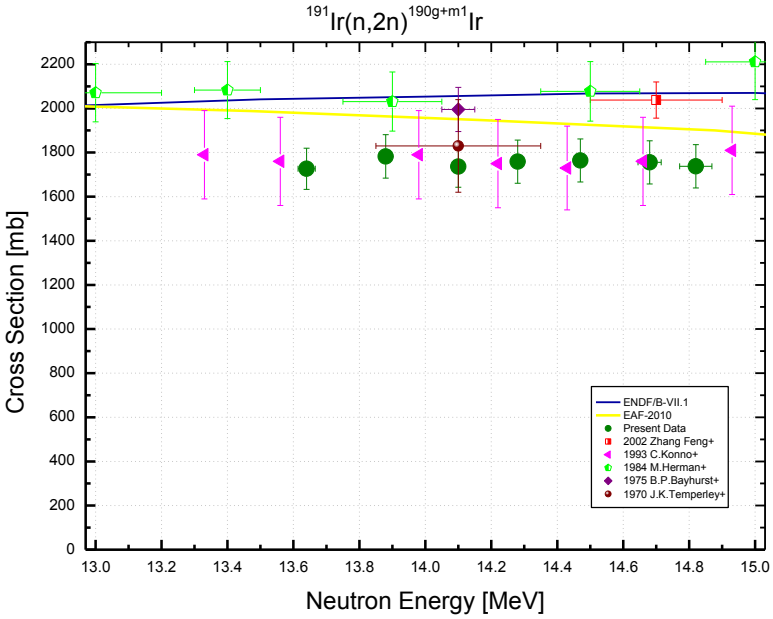

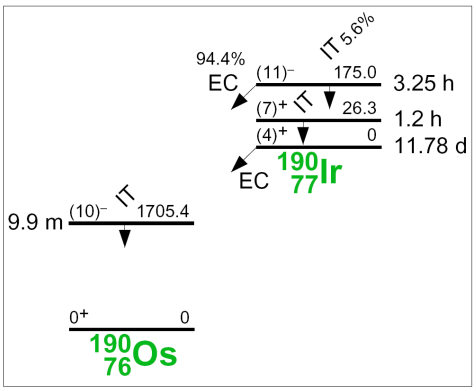

Decay data used for **^{191}Ir(n, 2n)$^{190g+m1}$Ir**.

Target nucleus	Abundance [%]	Chemical form	Reaction product	$T_{1/2}$	E_γ [keV]	Y_γ [%]
^{191}Ir	**37.3** *2*	Ir-metal	^{190g}Ir	**11.78 d** *10*	361.1	13.0 *6*
					371.2	**22.8** *7*
					518.6	34.0 *15*
					569.3	28.5 *13*

^{191}Ir(n, 2n)^{190}Ir

^{191}Ir(n, 2n)^{190}Ir		
E_n [MeV]	σ [mb]	$\pm\Delta\sigma_{total}$ *[%]*
13.64	1835	*5.06*
13.88	1892	*5.17*
14.10	1849	*5.02*
14.28	1893	*5.17*
14.47	1902	*5.14*
14.68	1900	*5.14*
14.82	1876	*5.22*
Ref. CS is ^{93}Nb(n,2n)^{92m}Nb		

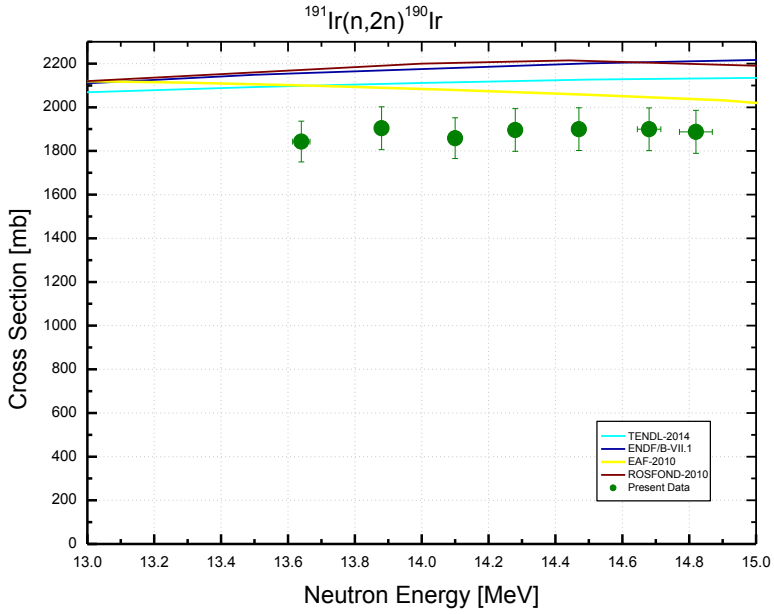

The ^{191}Ir(n, 2n)^{190}Ir cross-section was not measured in the experiment directly. This is the sum of cross sections ^{191}Ir(n, 2n)^{190m2}Ir and ^{191}Ir(n, 2n)$^{190m1+g}$Ir presented in the previous pages.

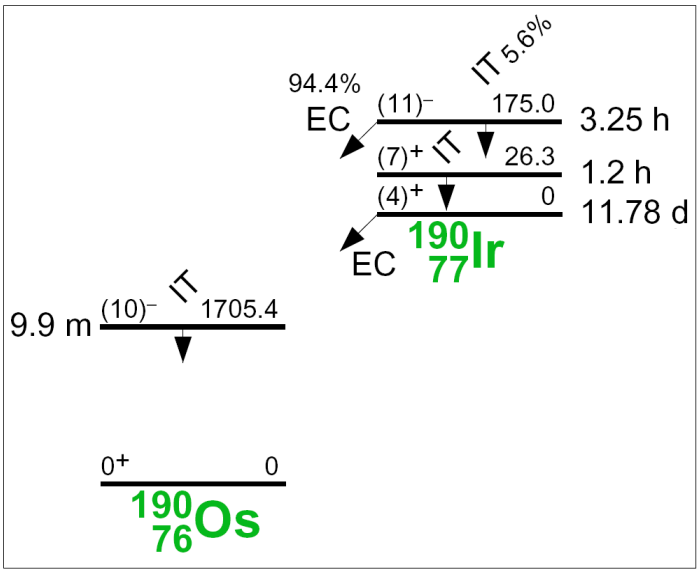

^{193}Ir(n, α)^{190m}Re

^{193}Ir(n, α)^{190m}Re			
E_n [MeV]	σ [mb]	$\pm\Delta\sigma_{total}$ [%]	$\pm\Delta\sigma_{ref}$ [%]
13.64	0.050	*60.0*	*13.0*
13.88	0.131	*46.1*	*13.0*
14.10	0.101	*50.0*	*13.0*
14.28	0.130	*38.4*	*12.9*
14.47	0.090	*55.5*	*13.0*
14.68	0.160	*37.5*	*13.0*
14.82	0.181	*33.3*	*13.0*
Ref. CS is ^{93}Nb(n,2n)^{92m}Nb;		α_d = *1.3*	

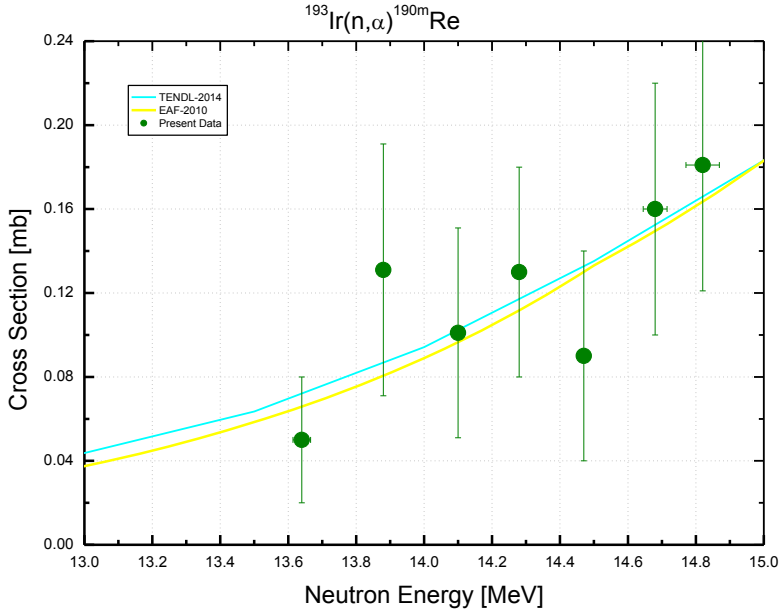

Gamma transitions with energies coinciding with those of the ^{191}Ir(n,2n)^{190m2}Ir reaction ($T_{1/2}$=3.087 h) were excluded.

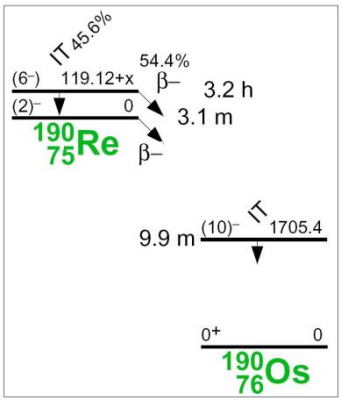

Decay data used for **^{193}Ir(n, α)^{190m}Re**.

Target nucleus	Abundance [%]	Chemical form	Reaction product	$T_{1/2}$	E_γ [keV]	Y_γ [%]
^{193}Ir	**62.7** *2*	Ir-metal	^{190m}Re	**3.2 h** *2*	119.1	11.1 *11*
					673.1	**9.4** *6*

^{193}Ir(n, p)^{193}Os

^{193}Ir(n, p)^{193}Os			
E_n [MeV]	σ [mb]	$\pm\Delta\sigma_{total}$ [%]	$\pm\Delta\sigma_{ref}$ [%]
13.88	1.43	*18.2*	*17.9*
14.28	2.10	*11.9*	*11.4*
14.47	2.44	*12.3*	*11.8*
14.68	2.90	*15.9*	*15.5*
14.82	3.54	*22.6*	*22.4*
Ref. CS is ^{93}Nb(n,2n)^{92m}Nb;		α_d = *1.3*	

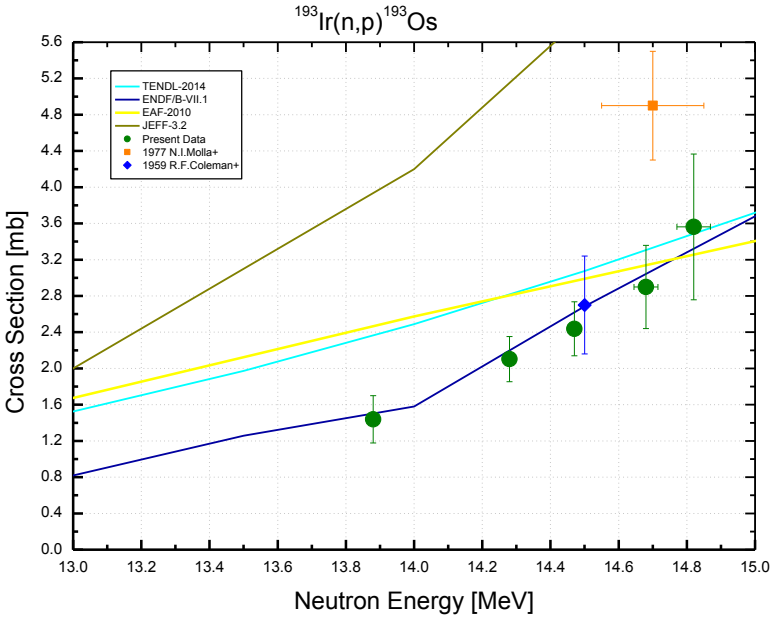

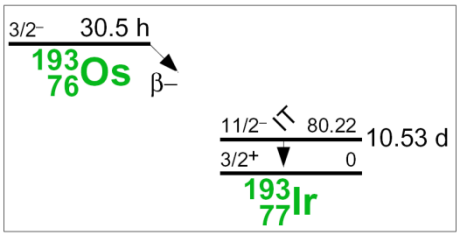

Decay data used for **^{193}Ir(n, p)^{193}Os**.

Target nucleus	**Abundance [%]**	**Chemical form**	**Reaction product**	**$T_{1/2}$**	**E_γ [keV]**	**Y_γ [%]**
^{193}Ir	**62.7** *2*	Ir-metal	^{193}Os	**30.11 h** *1*	321.6	1.251 *18*
					460.5	**3.88** *5*

^{193}Ir(n, 2n)$^{192g+m1}$Ir

^{193}Ir(n, 2n)$^{192g+m1}$Ir			
E_n [MeV]	σ [mb]	$\pm\Delta\sigma_{total}$ [%]	$\pm\Delta\sigma_{ref}$ [%]
13.64	2012	*4.85*	*0.674*
13.88	2075	*4.60*	*0.647*
14.10	1996	*4.63*	*0.634*
14.28	2040	*4.51*	*0.631*
14.47	2034	*4.56*	*0.636*
14.68	2032	*4.67*	*0.650*
14.82	2036	*4.53*	*0.670*
Ref. CS is ^{93}Nb(n,2n)^{92m}Nb; $\alpha_d = 1.2$			

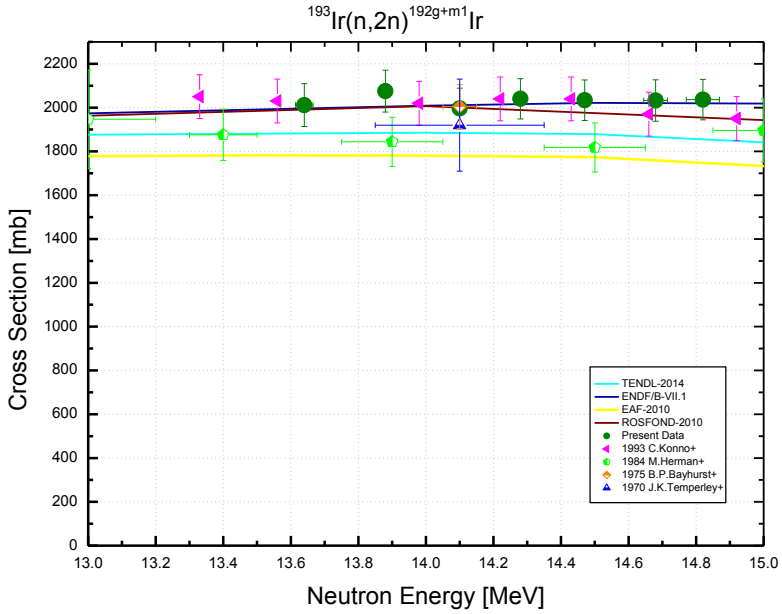

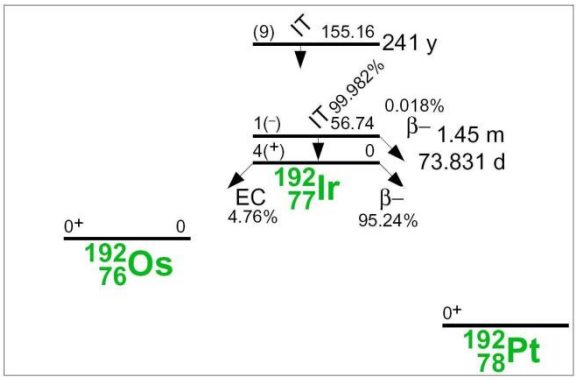

Decay data used for **^{193}Ir(n, 2n)$^{192g+m1}$Ir**.

Target nucleus	Abundance [%]	Chemical form	Reaction product	$T_{1/2}$	E_γ [keV]	Y_γ [%]
^{193}Ir	**62.7** *2*	Ir-metal	^{192g}Ir	**73.829 d** *11*	**316.5**	**82.86** *3*
					468.1	47.84 *3*

^{192}Pt(n, 2n)^{191}Pt

^{192}Pt(n, 2n)^{191}Pt			
E_n [MeV]	σ [mb]	$\pm\Delta\sigma_{total}$ [%]	$\pm\Delta\sigma_{ref}$ [%]
13.48	1919	*14.6*	*7.66*
13.64	1899	*13.8*	*7.66*
13.88	1909	*13.7*	*7.65*
14.10	1882	*13.9*	*7.65*
14.28	1897	*14.8*	*7.65*
14.47	1964	*13.2*	*7.65*
14.64	2005	*13.0*	*7.66*
14.82	2045	*14.3*	*7.66*
Ref. CS is ^{93}Nb(n,2n)^{92m}Nb;		α_d = *1.5*	

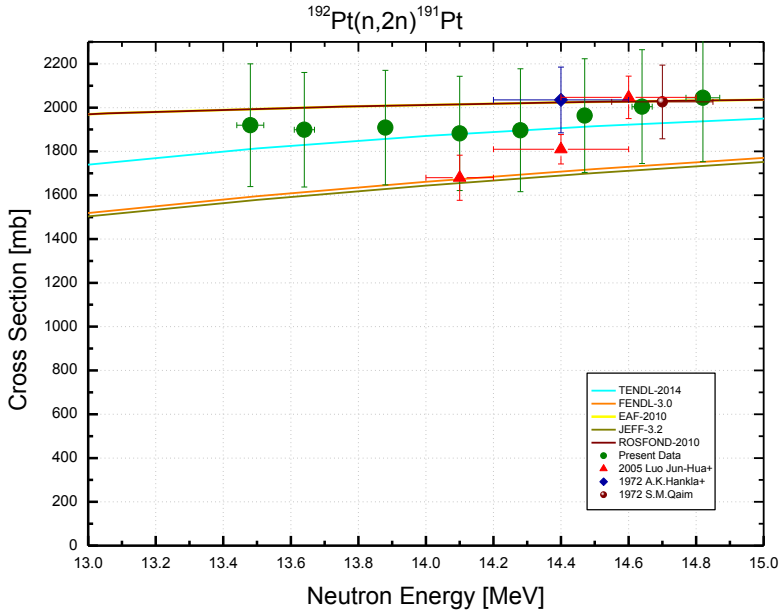

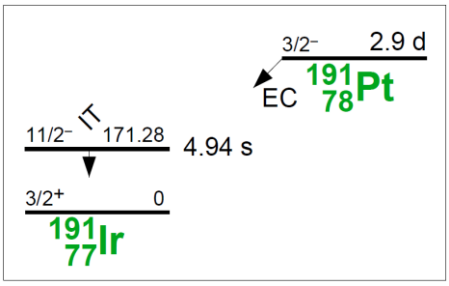

Decay data used for **^{192}Pt(n, 2n)^{191}Pt**.

Target nucleus	Abundance [%]	Chemical form	Reaction product	$T_{1/2}$	E_γ [keV]	Y_γ [%]
^{192}Pt	**0.782** *7*	Pt-metal	^{191}Pt	**2.83 d** *2*	129.4	3.3 *3*
					359.9	6.4 *5*
					409.4	8.8 *7*
					538.9	**15.9** *12*

^{194}Pt(n, α)^{191}Os

^{194}Pt(n, α)^{191}Os			
E_n [MeV]	σ [mb]	$\pm\Delta\sigma_{total}$ [%]	$\pm\Delta\sigma_{ref}$ [%]
14.68	1.15	*30.5*	*0.94*
Ref. CS is ^{93}Nb(n,2n)^{92m}Nb;		α_d = *1.1*	

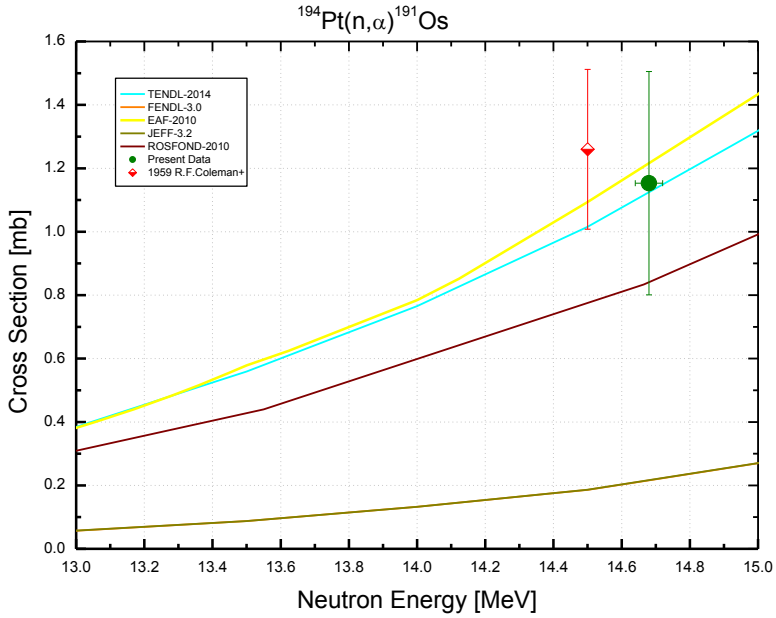

Poor statistics of the gamma peak located in the region of high background counts is the main reason for the large cross section uncertainty.

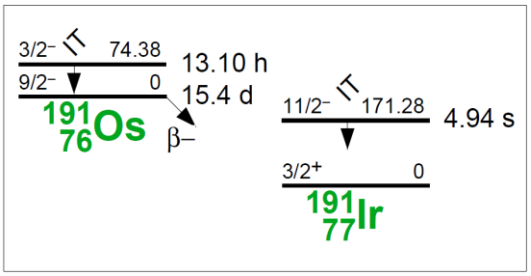

Decay data used for **^{194}Pt(n, α)^{191}Os**.

Target nucleus	**Abundance [%]**	**Chemical form**	**Reaction product**	$T_{1/2}$	**E_γ [keV]**	**Y_γ [%]**
^{194}Pt	**32.97** ***10***	Pt-metal	^{191}Os	**15.4 d** ***1***	**129.4**	**26.50** ***4***

^{194}Pt(n, p)^{194m2}Ir

^{194}Pt(n, p)^{194m2}Ir			
E_n [MeV]	σ [mb]	$\pm\Delta\sigma_{total}$ [%]	$\pm\Delta\sigma_{ref}$ [%]
13.88	0.059	*25.4*	*9.14*
14.05	0.046	*28.3*	*9.14*
14.82	0.104	*24.3*	*9.14*
Ref. CS is ^{93}Nb(n,2n)^{92m}Nb;		α_d = *1.01*	

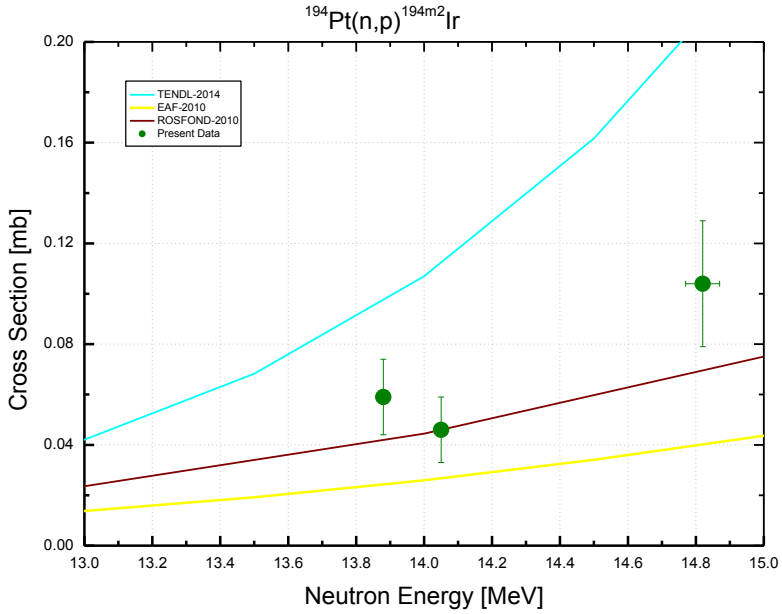

The reaction product is the nuclide of a high spin state (10^+). The main reason of the large uncertainty is the poor statistics of gamma peaks. The discharging gammas are in a cascade. Cross sections were corrected for gamma summing.

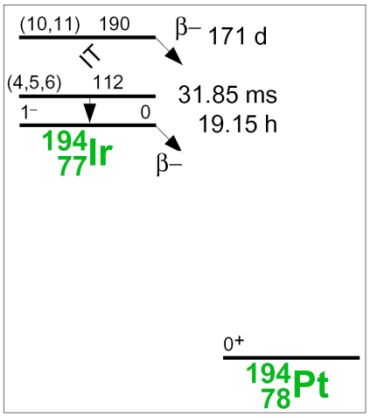

Decay data used for **^{194}Pt(n, p)^{194m2}Ir**.

Target nucleus	**Abundance [%]**	**Chemical form**	**Reaction product**	**$T_{1/2}$**	**E_γ [keV]**	**Y_γ [%]**
^{194}Pt	**32.97** ***10***	Pt-metal	^{194m2}Ir	**171 d** ***11***	328.5	93 *7*
					482.6	**97** ***7***
					600.5	62 *4*
					687.8	59 *4*

^{194}Pt(n, p)$^{194g+m1}$Ir

^{194}Pt(n, p)$^{194g+m1}$Ir			
E_n [MeV]	σ [mb]	$\pm\Delta\sigma_{total}$ [%]	$\pm\Delta\sigma_{ref}$ [%]
13.47	2.09	*21.0*	*12.0*
13.88	2.84	*15.9*	*12.0*
14.05	3.32	*15.1*	*12.0*
14.28	3.69	*16.3*	*12.0*
14.47	4.11	*14.1*	*12.0*
14.68	4.46	*13.5*	*12.0*
14.82	4.58	*15.4*	*12.0*
Ref. CS is ^{93}Nb(n,2n)^{92m}Nb;		α_d = *1.4*	

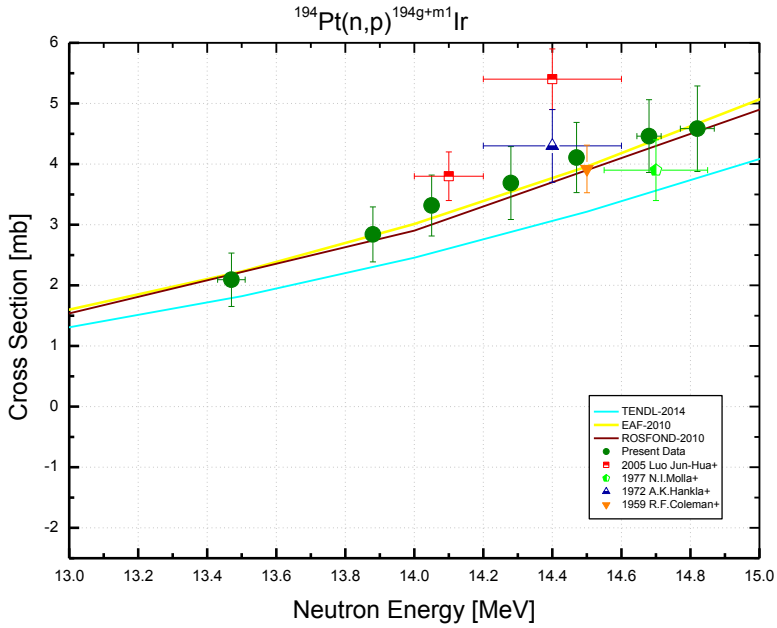

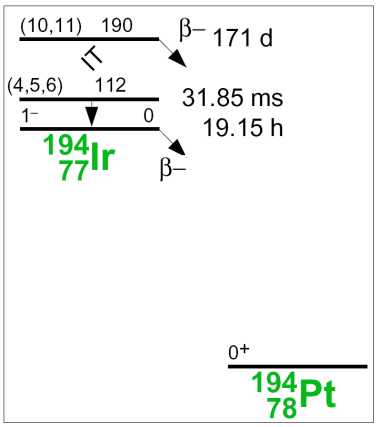

Decay data used for **^{194}Pt(n, p)$^{194g+m1}$Ir**.

Target nucleus	Abundance [%]	Chemical form	Reaction product	$T_{1/2}$	E_γ [keV]	Y_γ [%]
^{194}Pt	**32.97** *10*	Pt-metal	^{194g}Ir	**19.28 h** *13*	293.5	2.5 *3*
					328.4	**13.1** *17*
					645.1	1.18 *16*

^{194}Pt(n, p)^{194}Ir

^{194}Pt(n, p)^{194}Ir		
E_n [MeV]	σ [mb]	$\pm\Delta\sigma_{total}$ *[%]*
13.88	2.88	*15.2*
14.05	3.35	*13.4*
14.82	4.65	*12.8*
Ref. CS is ^{93}Nb(n,2n)^{92m}Nb		

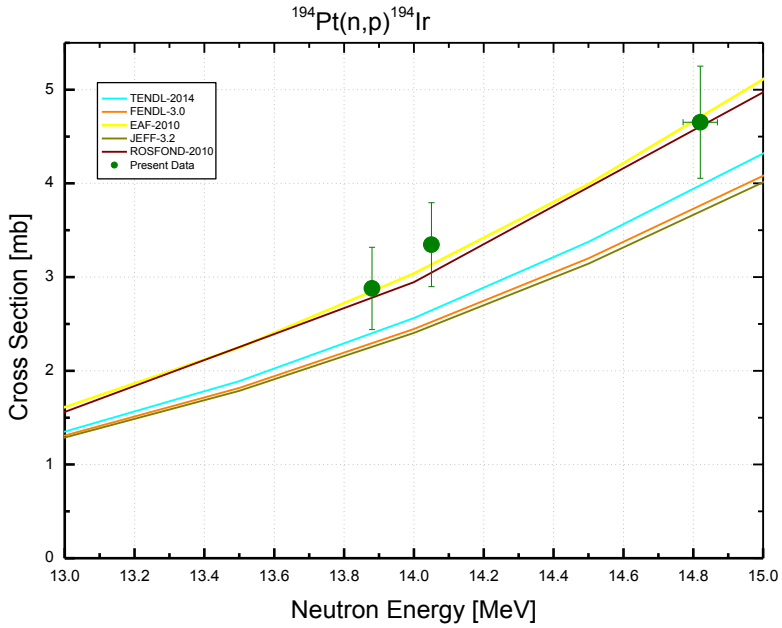

The present data for ^{194}Pt(n, p)^{194}Ir cross section were obtained by summing the experimental data measured separately for ^{194}Pt(n, p)$^{194g+m1}$Ir and ^{194}Pt(n, p)^{194m2}Ir. This was done for extending the comparative base because a limited number of evaluations exist in which the cross sections are split for ground and metastable states. Most evaluations contain the data for the total reaction cross-sections only.

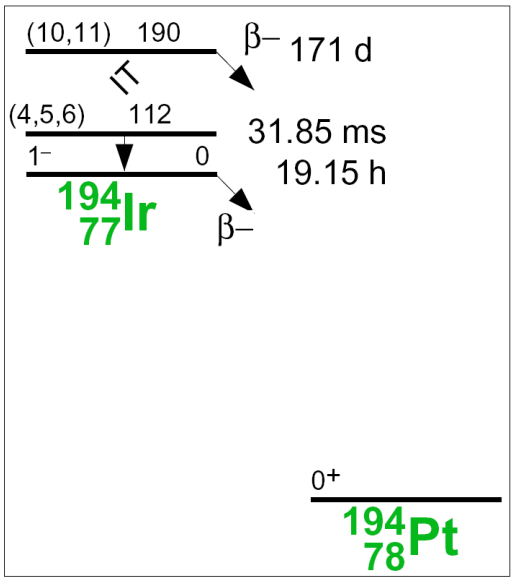

^{195}Pt(n, p)^{195m}Ir

^{195}Pt(n, p)^{195m}Ir			
E_n [MeV]	σ [mb]	$\pm\Delta\sigma_{total}$ [%]	$\pm\Delta\sigma_{ref}$ [%]
13.88	0.80	*16.2*	*15.5*
14.28	1.00	*23.0*	*15.5*
14.47	1.30	*17.7*	*15.5*
14.68	1.40	*24.3*	*15.5*
14.82	1.46	*15.7*	*15.5*
Ref. CS is ^{93}Nb(n,2n)^{92m}Nb;		$\alpha_d = 2.0$	

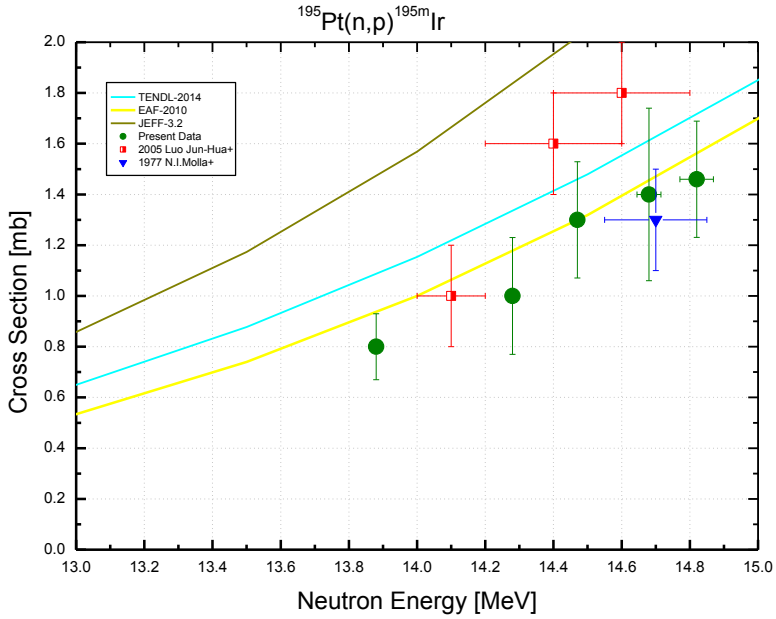

The data were not corrected for possible contribution of ^{196}Pt(n, np)^{195m}Ir + ^{196}Pt(n, d)^{195m}Ir. According to EAF-2010 evaluation, this contribution can be neglected.

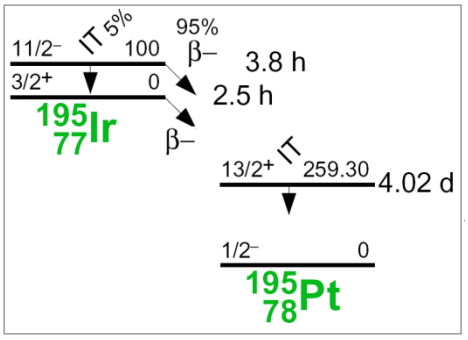

Decay data used for **^{195}Pt(n, p)^{195m}Ir**.

Target nucleus	Abundance [%]	Chemical form	Reaction product	$T_{1/2}$	E_γ [keV]	Y_γ [%]
^{195}Pt	**33.83** *1*	Pt-metal	^{195m}Ir	**3.67 h** *8*	319.9	9.8 *16*
					364.9	9.7 *15*
					432.9	**9.8** *15*
					684.9	9.8 *16*

^{196}Pt(n, α)^{193}Os

^{196}Pt(n, α)^{193}Os			
E_n [MeV]	σ [mb]	$\pm\Delta\sigma_{total}$ [%]	$\pm\Delta\sigma_{ref}$ [%]
13.88	0.43	*55.8*	*1.69*
14.05	0.44	*52.3*	*1.69*
14.28	0.62	*53.2*	*1.70*
14.47	0.53	*43.4*	*1.70*
14.68	0.80	*50.0*	*1.70*
14.82	0.82	*19.5*	*1.70*
Ref. CS is ^{93}Nb(n,2n)^{92m}Nb; $\alpha_d = 1.3$			

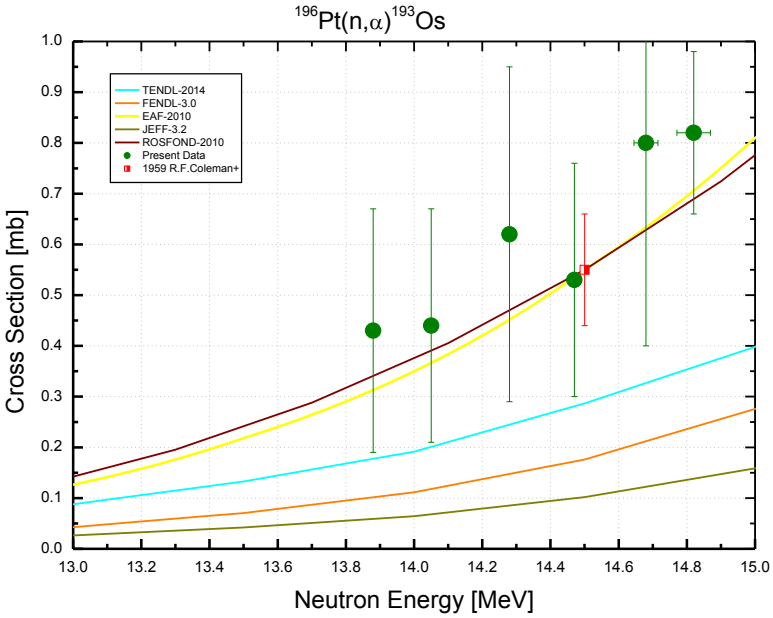

The large uncertainty of relevant gamma peak in the spectra propagates in the total cross section uncertainty.

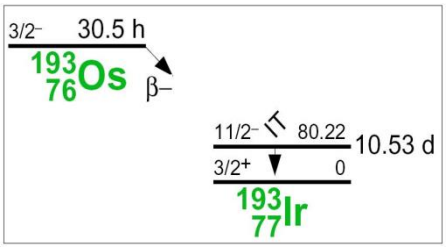

Decay data used for **^{196}Pt(n, α)^{193}Os**.

Target nucleus	**Abundance [%]**	**Chemical form**	**Reaction product**	$T_{1/2}$	**E_γ [keV]**	**Y_γ [%]**
^{196}Pt	**25.24** *4*	Pt-metal	^{193}Os	**30.11 h** *1*	**460.5**	**3.88** *5*

^{196}Pt(n, p)^{196m}Ir

^{196}Pt(n, p)^{196m}Ir			
E_n [MeV]	σ [mb]	$\pm\Delta\sigma_{total}$ [%]	$\pm\Delta\sigma_{ref}$ [%]
13.47	0.013	*26.5*	*3.57*
13.88	0.017	*22.5*	*3.57*
14.28	0.026	*29.8*	*3.58*
14.47	0.031	*15.4*	*3.58*
14.68	0.037	*10.7*	*3.58*
14.82	0.045	*10.7*	*3.58*
Ref. CS is ^{93}Nb(n,2n)^{92m}Nb;		$\alpha_d = 2.0$	

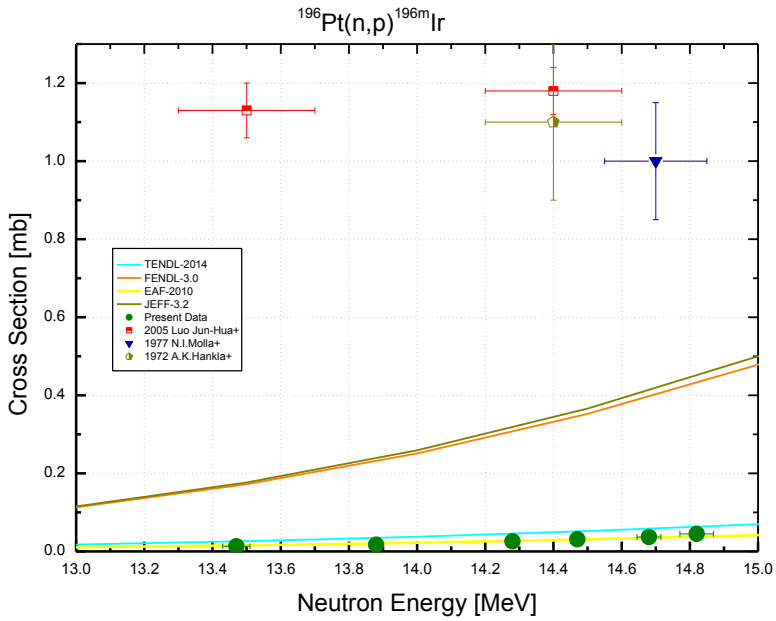

Two Figures are given to show the noticeable difference between our data and the data of three other experimental groups. The upper Figure presents all the data, the lower one gives the Figure fragment zoomed in.

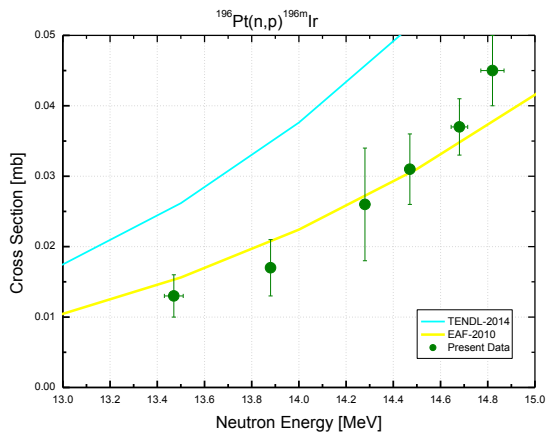

When analyzing possible reasons for the significant difference in the data, the following circumstances were revealed:

1. In other experiments, the γ-peak with energy 356 keV was used for cross section determination. Our γ-countings have indicated that this peak consists of three close γ-lines, two of which are not related to the reaction studied. In our work, γ-peak with energy 355.9 keV was not used for cross section determination

3. Four other γ-lines were used for cross section determination in our work (see Table below). Cross sections obtained for any of these four γ-lines agree within errors.

4. The recommended spin value of the metastable state ^{196m}Ir is high (10, 11$^-$). The isomeric ratio for the ^{196}Pt(n, p)^{196}Ir is expected to be low, about 0.01 [ref.24, p.23]. Our data agree well with the expected value.

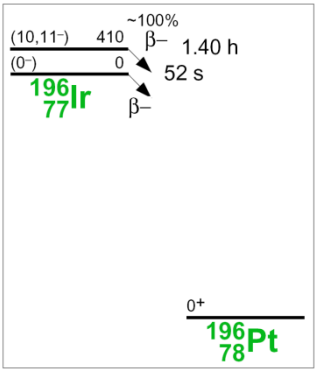

Decay data used for **^{196}Pt(n, p)^{196m}Ir**.

Target nucleus	Abundance [%]	Chemical form	Reaction product	$T_{1/2}$	E_γ [keV]	Y_γ [%]
^{196}Pt	**25.24** *4*	Pt-metal	^{196m}Ir	**1.40 h** *2*	393.5	97 *4*
					447.1	94 *4*
					521.4	**96** *3*
					647.3	91 *4*

^{196}Pt(n, p)^{196g}Ir

^{196}Pt(n, p)^{196g}Ir			
E_n [MeV]	σ [mb]	$\pm\Delta\sigma_{total}$ [%]	$\pm\Delta\sigma_{ref}$ [%]
14.77	1.40	*42.8*	*22.3*
Ref. CS is ^{27}Al(n, α)^{24}Na; $\alpha_d = 2.0$			

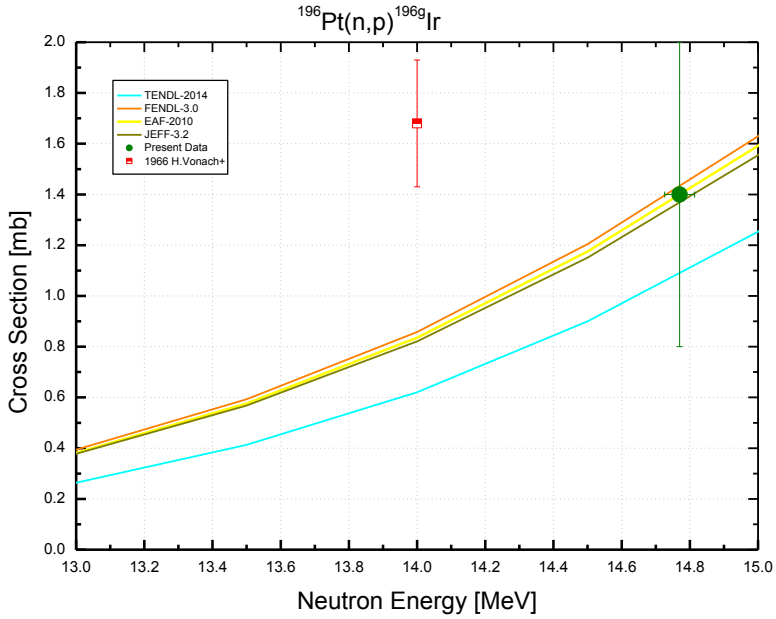

Only one experimental result obtained fifty years ago was presented in EXFOR-file for the ^{196}Pt(n, p)^{196g}Ir cross section. The aim of our experiment was to supplement the measurement results for the ^{196}Pt(n, p)^{196m}Ir reaction discussed above. The value agrees within errors with the EXFOR data and with the available evaluations. Also, the isomeric ratio determined in our measurements agrees with the branching ratio systematics [ref.24, p.23].

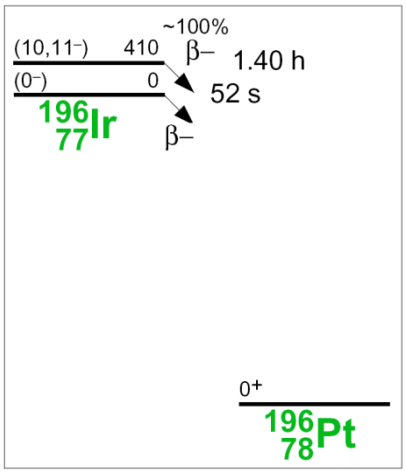

Decay data used for **^{196}Pt(n, p)^{196g}Ir**.

Target nucleus	Abundance [%]	Chemical form	Reaction product	$T_{1/2}$	E_γ [keV]	Y_γ [%]
^{196}Pt	**25.24** *4*	Pt-metal	^{196g}Ir	**52 s** *1*	332.9	3.9 *9*
					355.7	**18** *4*
					446.8	3.9 *9*
					779.6	10.9 *25*

^{196}Pt(n, p)^{196}Ir

^{196}Pt(n, p)^{196}Ir		
E_n [MeV]	σ [mb]	$\pm\Delta\sigma_{total}$ *[%]*
14.77	1.44	*41.6*
Ref. CS are ^{27}Al(n, α)^{24}Na and ^{93}Nb(n,2n)^{92m}Nb		

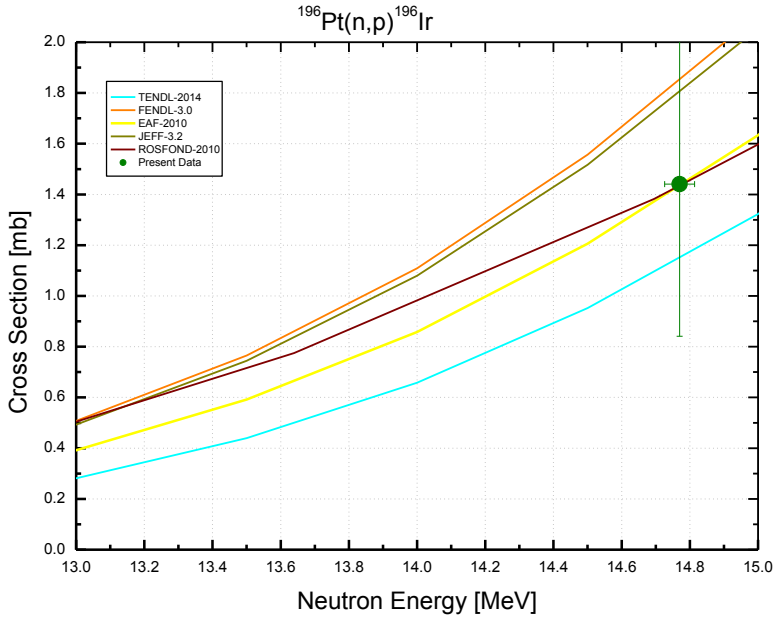

The present experimental data for ^{196}Pt(n, p)^{196}Ir cross section is the sum of ^{196}Pt(n, p)^{196m}Ir and ^{196}Pt(n, p)^{196m}Ir cross-sections measured separately.

The agreement of the sum experimental data with a more number of available evaluations can be considered as a strengthened evidence for the correctness of our results obtained for the ^{196}Pt(n, p)^{196m}Ir cross section where the prominent discrepancy with the results reported by other authors was revealed (see above).

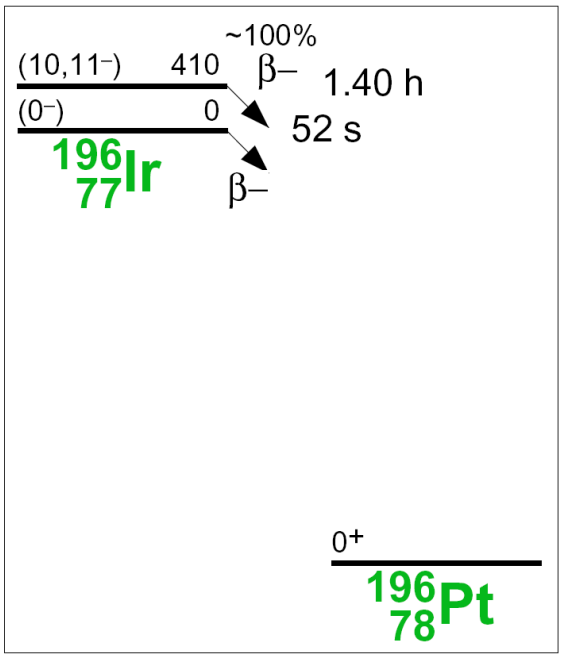

^{197}Au(n, α)^{194m2}Ir

^{197}Au(n, α)^{194m2}Ir			
E_n [MeV]	σ [mb]	$\pm\Delta\sigma_{total}$ [%]	$\pm\Delta\sigma_{ref}$ [%]
13.64	0.004	*50.0*	*9.17*
14.28	0.013	*23.0*	*9.18*
14.82	0.020	*35.0*	*9.18*
Ref. CS is ^{93}Nb(n,2n)^{92m}Nb;			α_d = *1.002*

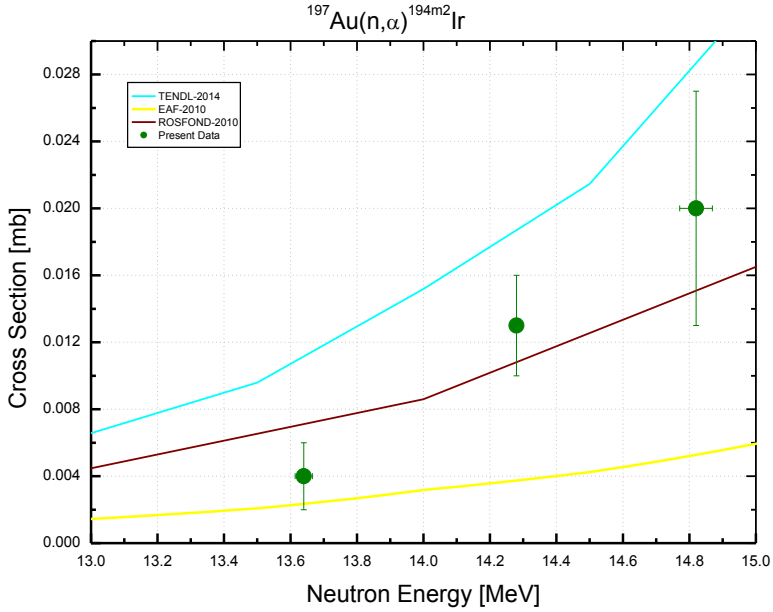

The studied reaction leads to population of a high spin state. The cross section is small and the main part of uncertainty is related to the poor peak statistics in the measured gamma spectra.

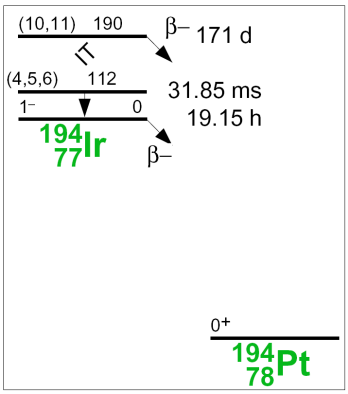

Decay data used for **^{197}Au(n, α)^{194m2}Ir**.

Target nucleus	Abundance [%]	Chemical form	Reaction product	$T_{1/2}$	E_γ [keV]	Y_γ [%]
^{197}Au	**100**	Au-metal	^{194m2}Ir	**171 d** *11*	328.5	93 *7*
					482.6	**97** *7*
					600.5	62 *4*
					687.8	59 *4*

^{197}Au(n, α)$^{194g+m1}$Ir

^{197}Au(n, α)$^{194g+m1}$Ir			
E_n [MeV]	σ [mb]	$\pm\Delta\sigma_{total}$ [%]	$\pm\Delta\sigma_{ref}$ [%]
13.64	0.22	*27.2*	*12.1*
13.88	0.28	*28.5*	*12.1*
14.28	0.36	*27.8*	*12.1*
14.47	0.65	*30.7*	*12.1*
14.68	0.38	*28.9*	*12.1*
14.82	0.54	*27.8*	*12.1*
Ref. CS is ^{93}Nb(n,2n)^{92m}Nb;		α_d = *1.4*	

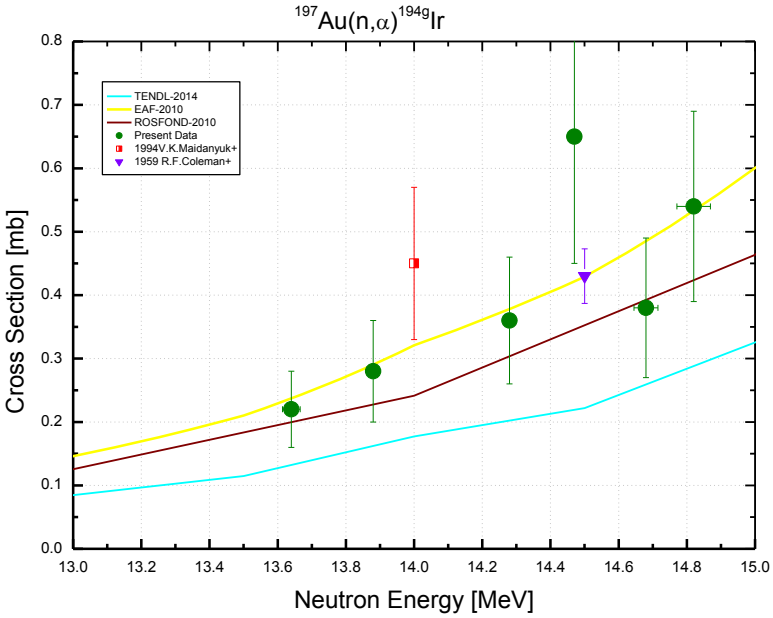

It should be noted that the first metastable state of ^{194}Ir with excitation energy 112 keV and half-life 31.85 ms was earlier omitted sometimes. This invoked the change of notation. So, the old ^{194m}Ir state can correspond to the present ^{194m2}Ir state and the ^{197}Au(n, α)^{194g}Ir cross-section in the old notation can be the ^{197}Au(n, α)$^{194g+m1}$Ir cross-section in the new notation. One must keep the attention to the possible variations of the used notations.

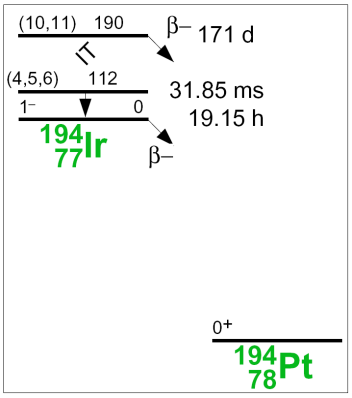

Decay data used for **^{197}Au(n, α)$^{194g+m1}$Ir**.

Target nucleus	Abundance [%]	Chemical form	Reaction product	$T_{1/2}$	E_γ [keV]	Y_γ [%]
^{197}Au	**100**	Au-metal	^{194g}Ir	**19.28 h** *13*	293.5	2.5 *3*
					328.4	**13.1** *17*
					645.1	1.18 *16*

^{197}Au(n, α)^{194}Ir

^{197}Au(n, α)^{194}Ir		
E_n [MeV]	σ [mb]	$\pm\Delta\sigma_{total}$ [%]
13.64	0.22	*26.8*
14.28	0.37	*26.8*
14.82	0.56	*26.8*
Ref. CS is ^{93}Nb(n,2n)^{92m}Nb		

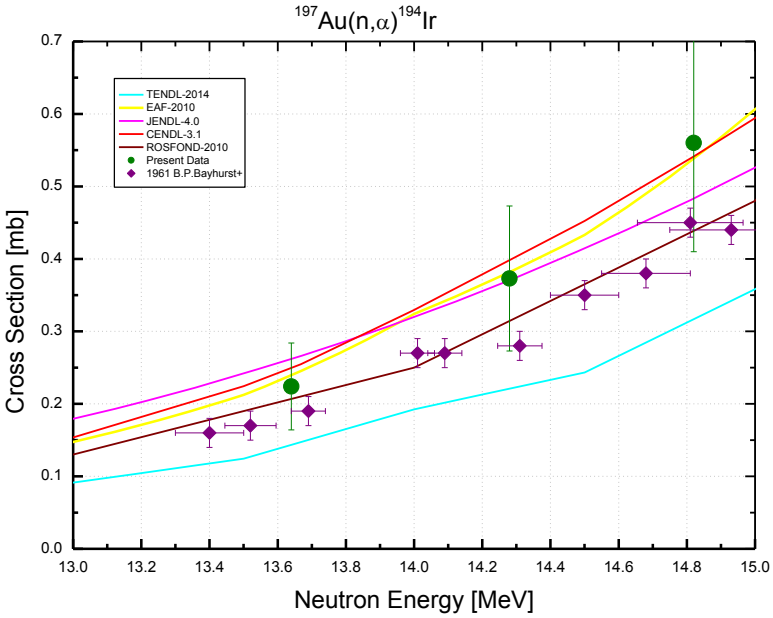

The ^{197}Au(n, α)^{194}Ir cross section presented on this page is the sum of the ^{197}Au(n, α)$^{194g+m1}$Ir and ^{197}Au(n, α)^{194m2}Ir cross sections measured separately (see above). This provides the comparison with a more number of evaluations. The present experimental data agree with most available evaluations within errors.

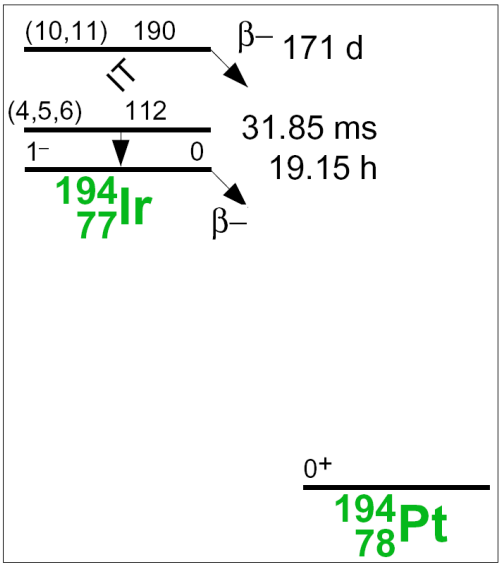

^{197}Au(n, p)^{197m}Pt

^{197}Au(n, p)^{197m}Pt			
E_n [MeV]	σ [mb]	$\pm\Delta\sigma_{total}$ [%]	$\pm\Delta\sigma_{ref}$ [%]
13.88	1.04	*6.63*	*2.92*
14.28	1.23	*7.22*	*2.92*
14.47	1.26	*6.23*	*2.92*
14.82	1.63	*6.01*	*2.93*
Ref. CS is ^{93}Nb(n,2n)^{92m}Nb;		$\alpha_d = 2.0$	

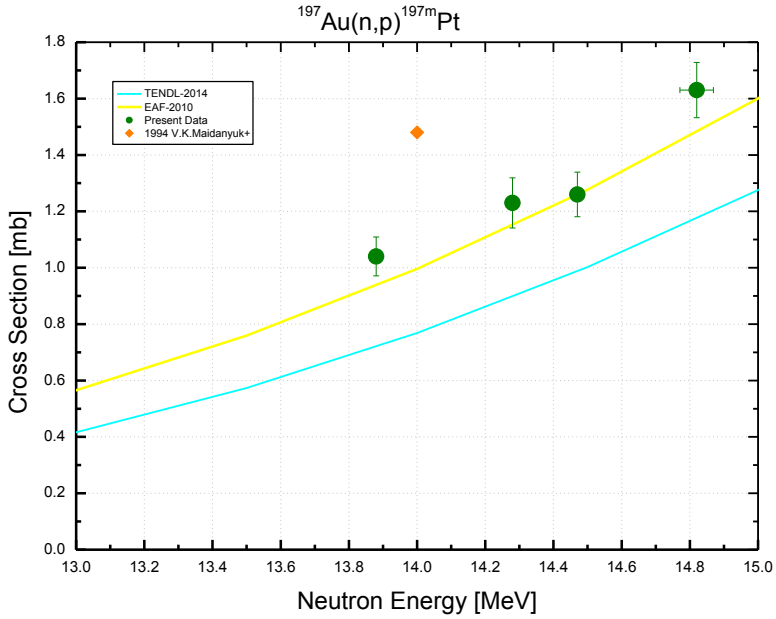

Two gamma lines are given in the Table of the decay data used. The first gamma line marked out by bold font had the determining influence on the total and reference uncertainty. The second one that has the energy 279 keV was used for increasing the result reliability.

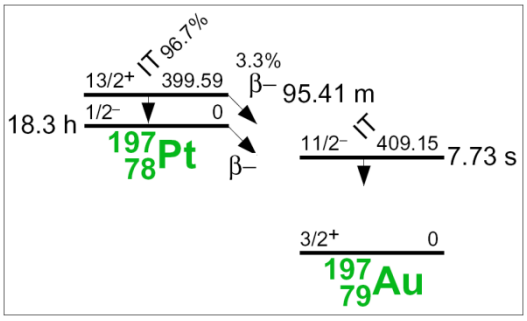

Decay data used for **^{197}Au(n, p)^{197m}Pt**.

Target nucleus	Abundance [%]	Chemical form	Reaction product	$T_{1/2}$	E_γ [keV]	Y_γ [%]
^{197}Au	**100**	Au-metal	^{197m}Pt	**95.41 m** *18*	**346.5**	**11.1** *3*
					279.0	2.4 *6*

^{197}Au(n, p)^{197}Pt

^{197}Au(n, p)^{197}Pt			
E_n [MeV]	σ [mb]	$\pm\Delta\sigma_{total}$ [%]	$\pm\Delta\sigma_{ref}$ [%]
13.64	2.54	*15.8*	*10.8*
13.88	2.95	*20.4*	*10.8*
14.28	3.45	*17.4*	*10.8*
14.47	3.94	*20.3*	*10.9*
14.68	3.85	*18.1*	*10.8*
14.82	4.28	*18.8*	*10.8*
Ref. CS is ^{93}Nb(n,2n)^{92m}Nb;		α_d = *1.4*	

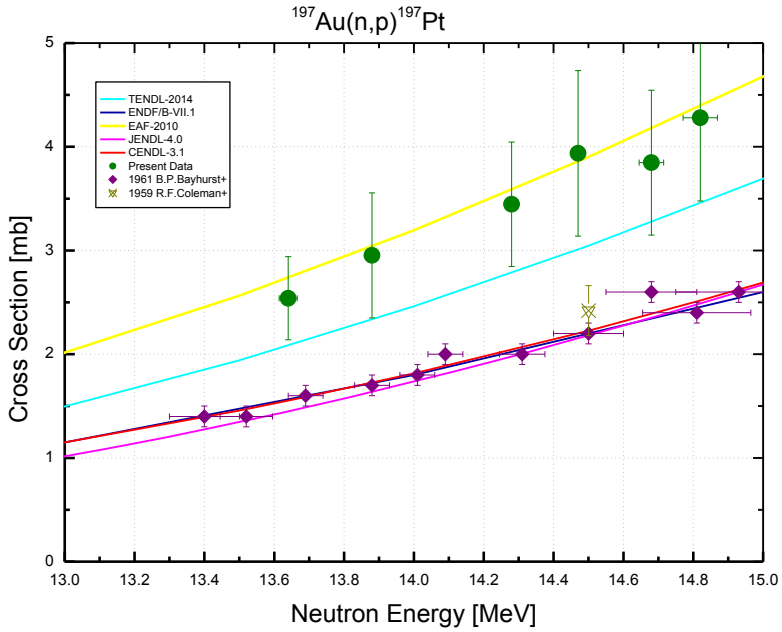

The ^{197}Au(n, p)^{197}Pt cross section was measured after the total discharge of the metastable excitation state ^{197m}Pt. In this process, 96.7% of the ^{197m}Pt have populated the ^{197}Pt ground state via isomeric transitions but other 3.3% of the ^{197m}Pt have decayed to the ^{197}Au levels directly. The gammas listed in the Table below correspond to decay of the ^{197}Pt ground state exclusively. When we used them, then the cross sections of [^{197}Au(n, p)^{197g}Pt + 0.967^{197}Au(n, p)^{197m}Pt] were determined. To obtain the ^{197}Au(n, p)^{197}Pt cross section, the data were added by the 0.033 ^{197}Au(n, p)^{197m}Pt cross section measured earlier (see the previous page).

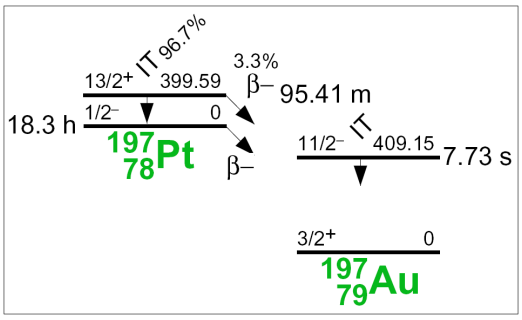

Decay data used for **^{197}Au(n, p)^{197}Pt**.

Target nucleus	Abundance [%]	Chemical form	Reaction product	$T_{1/2}$	E_γ [keV]	Y_γ [%]
^{197}Au	**100**	Au-metal	^{197g}Pt	**19.8915 h *19***	**191.4**	**3.7 *4***
					268.8	0.23 *3*

^{197}Au(n, 2n)^{196m2}Au

^{197}Au(n, 2n)^{196m2}Au			
E_n [MeV]	σ [mb]	$\pm\Delta\sigma_{total}$ [%]	$\pm\Delta\sigma_{ref}$ [%]
13.48	116	*5.05*	*3.44*
13.66	119	*4.82*	*3.44*
13.88	123	*4.85*	*3.43*
14.06	131	*4.70*	*3.43*
14.28	133	*4.60*	*3.43*
14.47	137	*4.47*	*3.43*
14.68	145	*4.62*	*3.43*
14.83	143	*4.59*	*3.43*
Ref. CS is ^{93}Nb(n,2n)^{92m}Nb;		α_d = *2.0*	

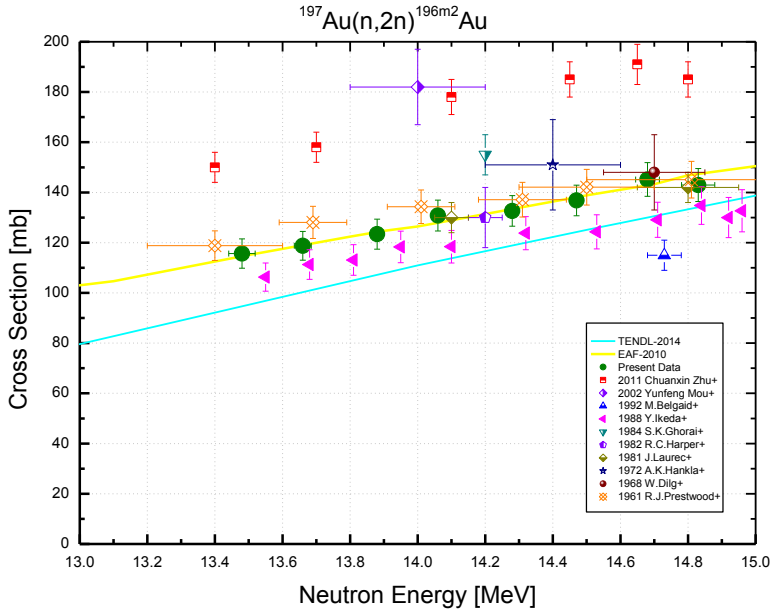

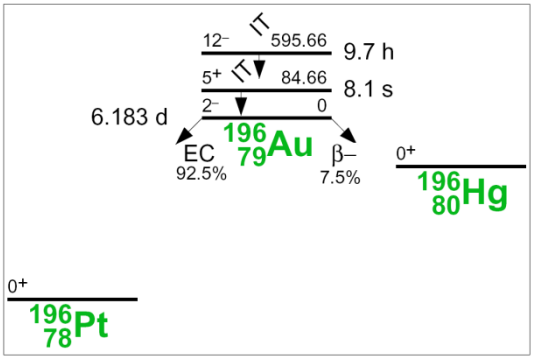

Decay data used for **^{197}Au(n, 2n)^{196m2}Au**.

Target nucleus	Abundance [%]	Chemical form	Reaction product	$T_{1/2}$	E_γ [keV]	Y_γ [%]
^{197}Au	**100**	Au-metal	^{196m2}Au	**9.6 h** *1*	**147.8**	**43.5** *15*
					188.3	30.0 *15*
					285.5	4.4 *5*
					316.2	3.0 *3*

^{197}Au(n, 2n)^{196}Au

^{197}Au(n, 2n)^{196}Au			
E_n [MeV]	σ [mb]	$\pm\Delta\sigma_{total}$ [%]	$\pm\Delta\sigma_{ref}$ [%]
13.48	2242	*4.30*	*3.28*
13.66	2184	*4.25*	*3.27*
13.88	2183	*4.30*	*3.27*
14.06	2252	*4.77*	*3.27*
14.28	2173	*4.08*	*3.27*
14.47	2213	*4.24*	*3.27*
14.68	2243	*4.16*	*3.27*
14.83	2220	*4.25*	*3.27*
Ref. CS is ^{93}Nb(n,2n)^{92m}Nb;		α_d = *1.05*	

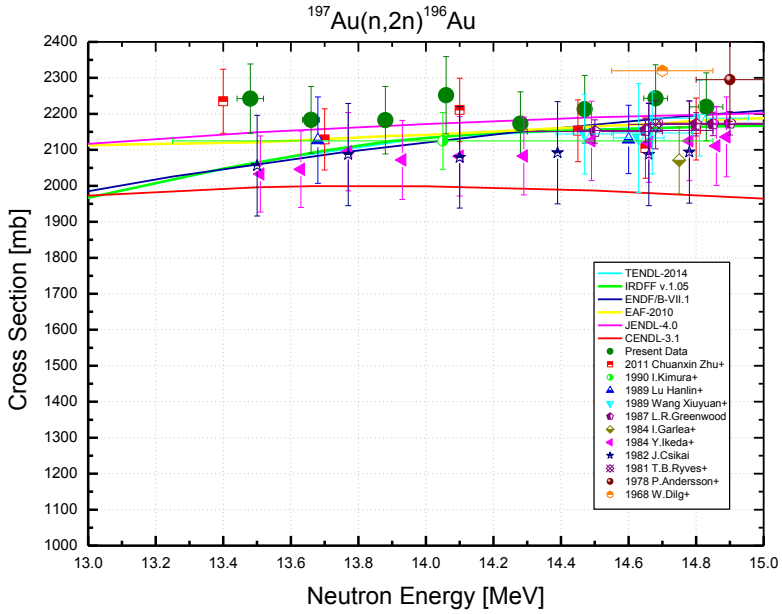

The cross-section data presented in the Table above are the weighted average of [1] and [3] corresponding data. The results were also corrected for the new reference data.

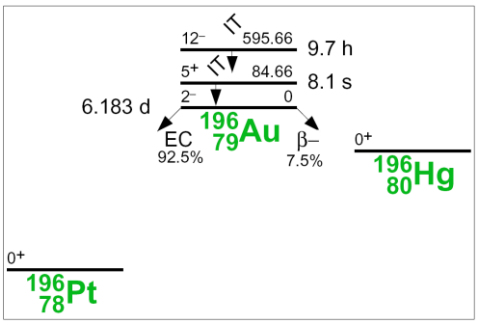

Decay data used for **^{197}Au(n, 2n)^{196}Au**.

Target nucleus	Abundance [%]	Chemical form	Reaction product	$T_{1/2}$	E_γ [keV]	Y_γ [%]
^{197}Au	**100**	Au-metal	^{196g}Au	**6.1669 d** *6*	333.0	22.9 *9*
					355.7	**87** *3*
					426.1	6.6 *3*

^{205}Tl(n, α)^{202}Au

^{205}Tl(n, α)^{202}Au			
E_n [MeV]	σ [mb]	$\pm\Delta\sigma_{total}$ [%]	$\pm\Delta\sigma_{ref}$ [%]
13.58	0.14	*64.3*	*5.16*
14.23	0.13	*69.2*	*5.15*
14.50	0.20	*75.0*	*5.16*
14.72	0.48	*64.6*	*5.16*
14.80	0.33	*24.2*	*5.16*
14.88	0.55	*92.6*	*5.16*
Ref. CS is ^{27}Al(n, α)^{24}Na; $\alpha_d = 1.5$			

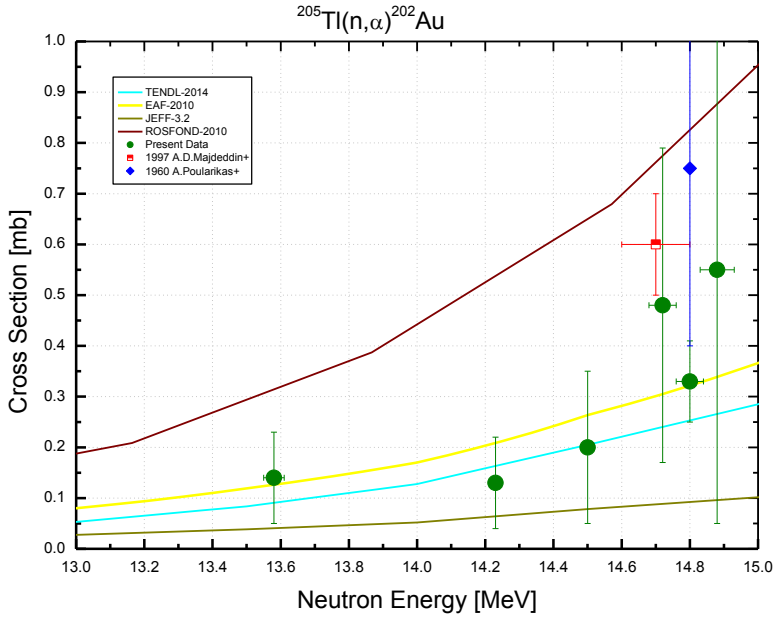

The data accuracy is limited by a very weak gamma peak statistics which is the result of the small cross section, the low gamma intensity and the short half-life. An additional problem was impossibility to use irradiated samples repeatedly because of high background of the competing reaction ^{203}Tl(n, 2n)^{202}Tl that produce gamma rays of the same energy. The half life of ^{202}Tl is 12.23 d.

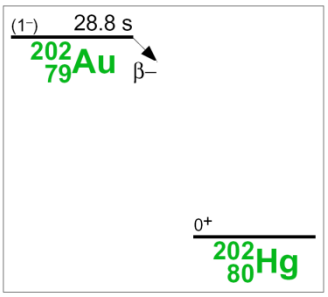

Decay data used for **^{205}Tl(n, α)^{202}Au**.

Target nucleus	Abundance [%]	Chemical form	Reaction product	$T_{1/2}$	E_γ [keV]	Y_γ [%]
^{205}Tl	**70.48** *1*	Tl-metal	^{202}Au	**28.4 s** *12*	439.5	9.2 *5*
					1125.3	2.12 *7*
					1306.4	**2.07** *6*

^{205}Tl(n, p)^{205}Hg

^{205}Tl(n, p)^{205}Hg			
E_n [MeV]	σ [mb]	$\pm\Delta\sigma_{total}$ [%]	$\pm\Delta\sigma_{ref}$ [%]
13.58	0.87	*91.9*	*45.5*
14.23	1.60	*81.2*	*45.5*
14.50	1.90	*89.5*	*45.5*
14.72	1.30	*61.5*	*45.5*
14.84	3.22	*56.2*	*45.5*
Ref. CS is ^{27}Al(n, α)^{24}Na; $\alpha_d = 1.3$			

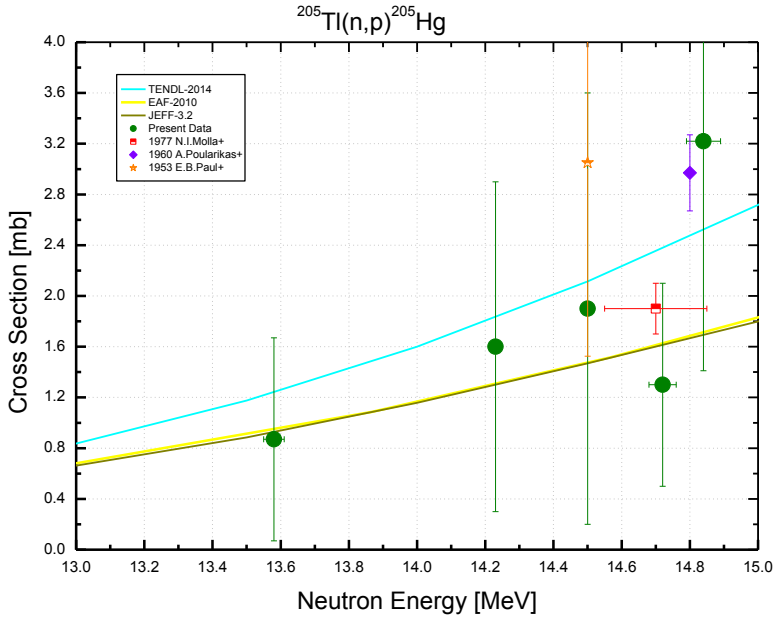

A large uncertainty in the reference γ-ray intensity and very weak peak statistics in the counted spectra are causes of high uncertainties in the measured cross section values.

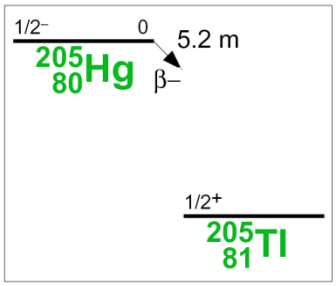

Decay data used for **^{205}Tl(n, p)^{205}Hg**.

Target nucleus	**Abundance [%]**	**Chemical form**	**Reaction product**	$T_{1/2}$	**E_γ [keV]**	**Y_γ [%]**
^{205}Tl	**70.48** *1*	Tl-metal	^{205}Hg	**5.14 m** *9*	**203.7**	**2.2** *10*

^{204}Pb(n, 2n)^{203}Pb

^{204}Pb(n, 2n)^{203}Pb			
E_n [MeV]	σ [mb]	$\pm\Delta\sigma_{total}$ [%]	$\pm\Delta\sigma_{ref}$ [%]
13.48	2045	*7.83*	*7.77*
13.67	2191	*7.98*	*7.76*
13.88	2172	*7.78*	*7.76*
14.06	2143	*8.43*	*7.76*
14.28	2205	*7.92*	*7.76*
14.50	2161	*7.98*	*7.76*
14.72	2220	*8.51*	*7.76*
14.88	2207	*8.29*	*7.77*
Ref. CS is ^{93}Nb(n,2n)^{92m}Nb;		α_d = *1.2*	

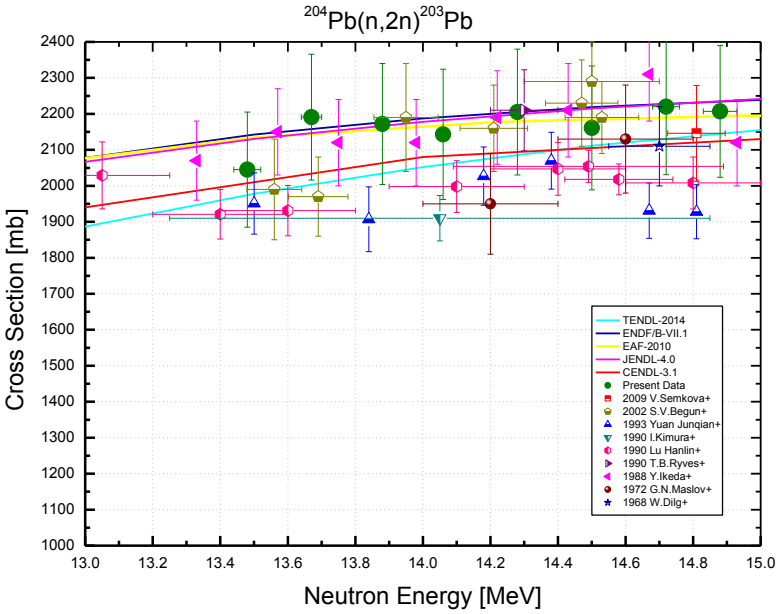

Although the cross-section is convenient for measurement, the experimental results are scattered significantly. Perhaps, this is caused by the remarkable uncertainty of ^{204}Pb abundance in the natural mixture. Anyway, the abundance uncertainty is a major contributor to the total uncertainty in our experiment.

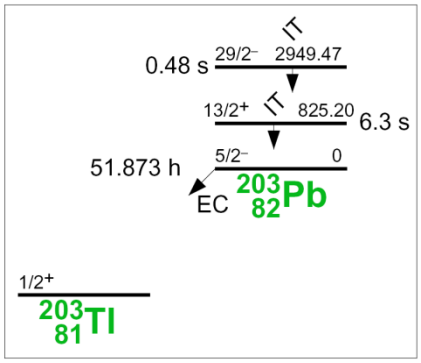

Decay data used for **^{204}Pb(n, 2n)^{203}Pb**.

Target nucleus	Abundance [%]	Chemical form	Reaction product	$T_{1/2}$	E_γ [keV]	Y_γ [%]
^{204}Pb	**1.4** *1*	Pb-metal	^{203}Pb	**51.92 h** *3*	**279.2**	**80.9** *19*
					401.3	3.35 *10*

^{206}Pb(n, α)^{203}Hg

^{206}Pb(n, α)^{203}Hg			
E_n [MeV]	σ [mb]	$\pm\Delta\sigma_{total}$ [%]	$\pm\Delta\sigma_{ref}$ [%]
13.48	0.283	*9.46*	*0.76*
13.67	0.348	*9.46*	*0.73*
13.88	0.403	*9.67*	*0.69*
14.06	0.408	*7.77*	*0.69*
14.28	0.523	*7.35*	*0.69*
14.50	0.615	*7.68*	*0.71*
14.72	0.653	*6.77*	*0.72*
14.88	0.739	*7.97*	*0.77*
Ref. CS is ^{93}Nb(n,2n)^{92m}Nb;		α_d = *1.04*	

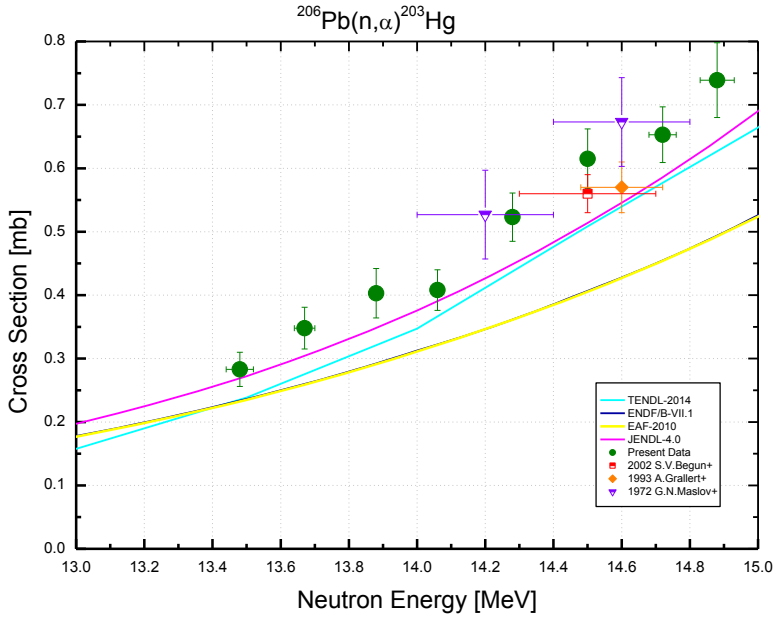

There are rather comfortable conditions for this cross-section measurement. The problem may arise from the intersection with the reaction ^{204}Pb(n, 2n)^{203}Pb which has a much higher cross-section, a coinciding gamma radiation but a shorter half-live. To provide the result reliability, the cooling time should be not less than 20 d. The main contribution to the data uncertainty is related to the weak gamma peak statistics.

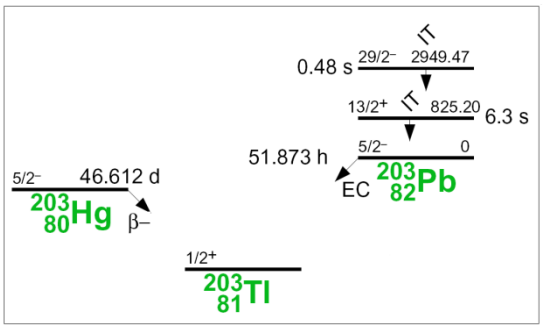

Decay data used for **^{206}Pb(n, α)^{203}Hg**.

Target nucleus	**Abundance [%]**	**Chemical form**	**Reaction product**	$T_{1/2}$	**E_γ [keV]**	**Y_γ [%]**
^{206}Pb	**24.1** *1*	Pb-metal	^{203}Hg	**46.594 d** *12*	**279.2**	**81.56** *5*

^{209}Bi(n, α)^{206m}Tl

^{209}Bi(n, α)^{206m}Tl			
E_n [MeV]	σ [mb]	$\pm\Delta\sigma_{total}$ [%]	$\pm\Delta\sigma_{ref}$ [%]
13.48	0.0076	*14.4*	*4.18*
13.95	0.0058	*22.4*	*4.17*
14.23	0.0117	*19.6*	*4.17*
14.71	0.0140	*17.1*	*4.17*
14.82	0.0170	*14.2*	*4.18*
14.88	0.0172	*23.5*	*4.18*
Ref. CS is ^{27}Al(n, α)^{24}Na; $\alpha_d = 1.3$			

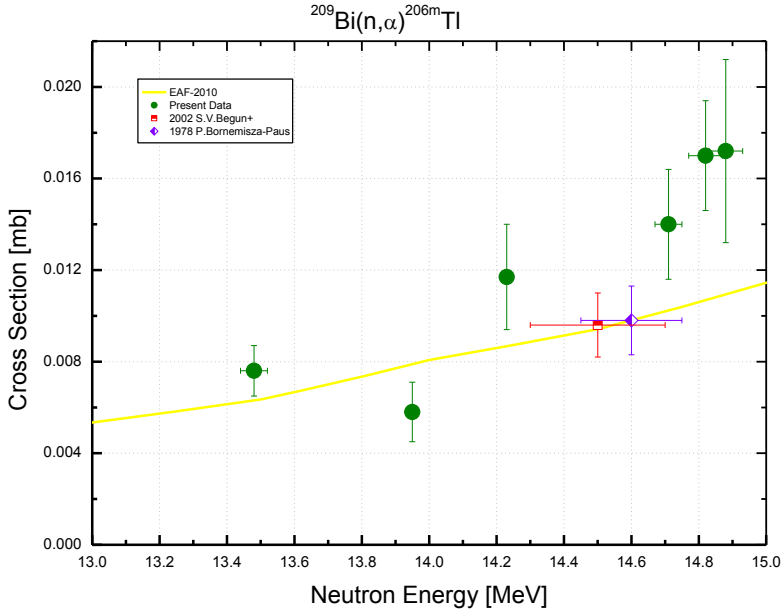

A very small cross section was measured. A possible contamination with ^{206}Pb that could generate a ^{206}Pb(n, p)^{206m}Tl reaction and disturb the data was found to be neglected for the bismuth sampes used. The weak gamma peak statistics is the main contributor to the experimental uncertainties. The gammas are cascading and corrections for gamma summing are necessary.

Only two evaluations were found for the ^{209}Bi(n, α)^{206m}Tl cross-section. EAF-2010 agrees satisfactory with the experimental data. TENDL-2014 evaluation is tens times higher (is not shown in the Figure). Note that the spin of the ^{206m}Tl is recommended as high as (12^-). If so then the isomeric ratio would be expected of order of 0.01. The corresponding value is approximately 0.012 in EAF-2010.

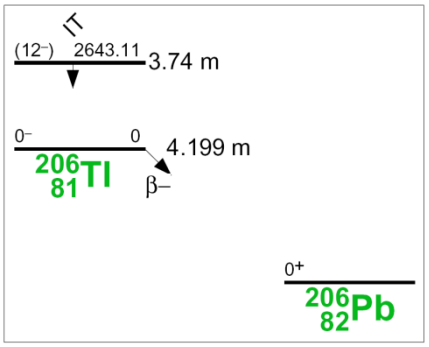

Decay data used for **^{209}Bi(n, α)^{206m}Tl**.

Target nucleus	Abundance [%]	Chemical form	Reaction product	$T_{1/2}$	E_γ [keV]	Y_γ [%]
^{209}Bi	**100**	Bi_2O_3	^{206m}Tl	**3.74 m** *3*	**216.4**	**74** *3*
					453.3	93 *5*
					457.2	22 *3*
					686.5	91 *5*

^{209}Bi(n, 2n)^{208}Bi

^{209}Bi(n, 2n)^{208}Bi			
E_n [MeV]	σ [mb]	$\pm\Delta\sigma_{total}$ [%]	$\pm\Delta\sigma_{ref}$ [%]
14.74	2293	*16.2*	*1.47*
Ref. CS is ^{93}Nb(n,2n)^{92m}Nb;		α_d = *1.001*	

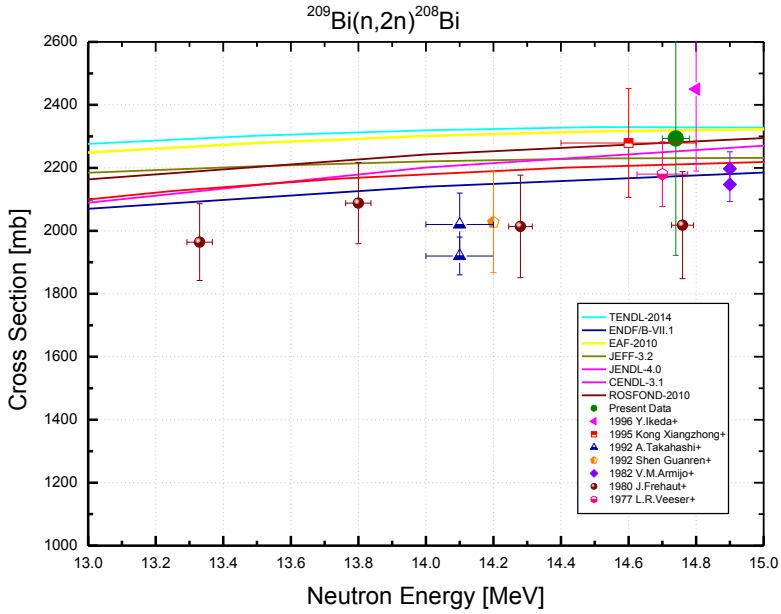

The main problems of the present measurement are the extremely long half-life of the ^{208}Bi and overlapping its radiation with the very power background γ-line 2614.5 keV.

The experimental result is inside the comparatively narrow band formed by many evaluations.

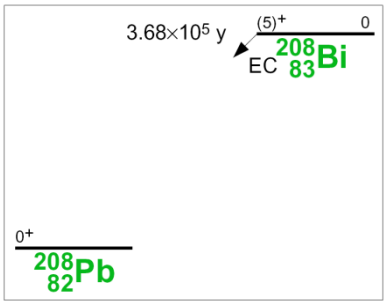

Decay data used for **^{209}Bi(n, 2n)^{208}Bi**.

Target nucleus	**Abundance [%]**	**Chemical form**	**Reaction product**	$T_{1/2}$	**E_γ [keV]**	**Y_γ [%]**
^{209}Bi	**100**	Bi_2O_3	^{208}Bi	**3.68•10^5 y** *4*	**2614.5**	**99.785** *2*

^{209}Bi(n, 3n)^{207}Bi

^{209}Bi(n, 3n)^{207}Bi			
E_n [MeV]	σ [mb]	$\pm\Delta\sigma_{total}$ [%]	$\pm\Delta\sigma_{ref}$ [%]
14.78	0.55	*9.01*	*0.77*
Ref. CS is ^{93}Nb(n,2n)^{92m}Nb;		α_d = *1.001*	

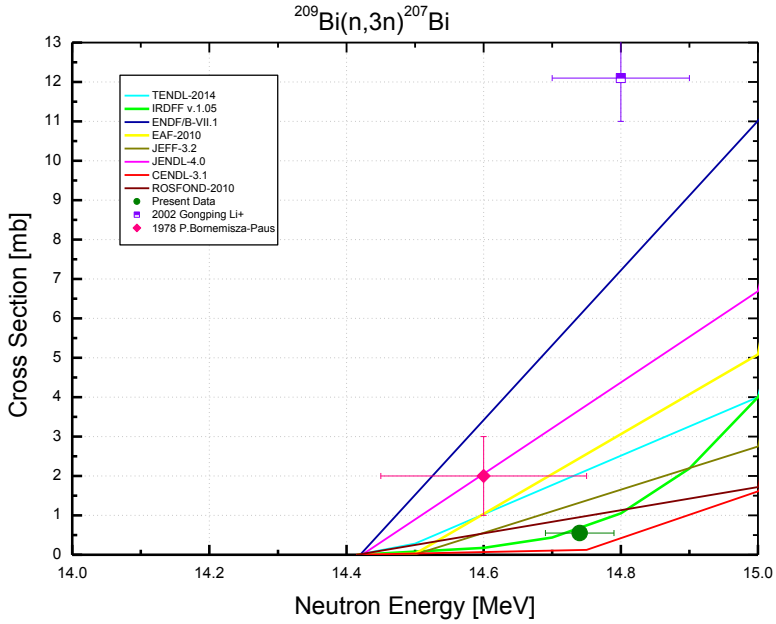

It is a rare situation for the neutron energy region covered in the present work when the (n, 3n) reaction can be excited.

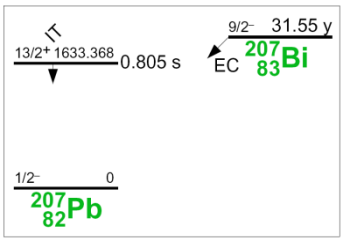

Decay data used for **^{209}Bi(n, 3n)^{207}Bi**.

Target nucleus	Abundance [%]	Chemical form	Reaction product	$T_{1/2}$	E_γ [keV]	Y_γ [%]
^{209}Bi	**100**	Bi_2O_3	^{207}Bi	**31.55 y** *4*	**569.7**	**97.75** *3*
					1063.7	74.5 *3*

^{232}Th(n, 2n)^{231}Th

^{232}Th(n, 2n)^{231}Th			
E_n [MeV]	σ [mb]	$\pm\Delta\sigma_{total}$ [%]	$\pm\Delta\sigma_{ref}$ [%]
13.48	1921	*7.22*	*5.54*
13.67	1799	*6.91*	*5.54*
13.88	1727	*7.52*	*5.53*
14.06	1521	*7.11*	*5.53*
14.28	1444	*6.90*	*5.53*
14.46	1308	*7.01*	*5.53*
14.67	1281	*6.83*	*5.54*
14.83	1150	*7.22*	*5.54*
Ref. CS is ^{93}Nb(n,2n)^{92m}Nb; $\alpha_d = 1.4$			

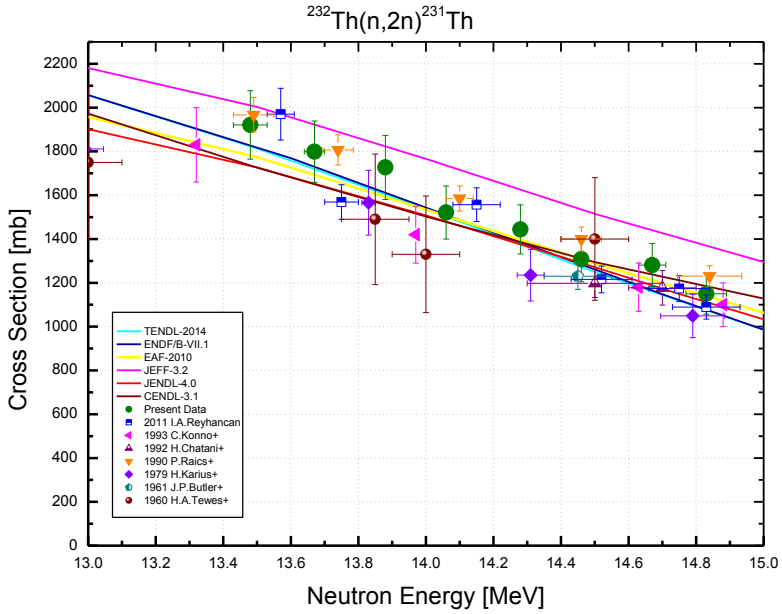

The main difficulty of the present experiment is high background and very high self absorption.

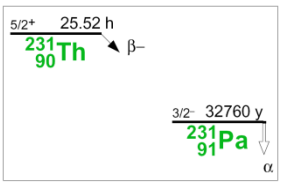

Decay data used for **^{232}Th(n, 2n)^{231}Th**.

Target nucleus	**Abundance [%]**	**Chemical form**	**Reaction product**	**$T_{1/2}$**	**E_γ [keV]**	**Y_γ [%]**
^{232}Th	**100**	Th-metal	^{231}Th	**25.52 h** *1*	**84.2**	**6.6** *4*
					102.3	0.436 *24*

^{238}U(n, 2n)^{237}U

^{238}U(n, 2n)^{237}U			
E_n [MeV]	σ [mb]	$\pm\Delta\sigma_{total}$ [%]	$\pm\Delta\sigma_{ref}$ [%]
13.47	1145	*8.30*	*1.55*
13.64	1056	*7.32*	*1.53*
13.88	1002	*7.34*	*1.52*
14.05	915	*7.82*	*1.52*
14.28	816	*7.22*	*1.52*
14.47	746	*7.39*	*1.52*
14.68	716	*8.41*	*1.53*
14.86	664	*7.42*	*1.55*
Ref. CS is ^{93}Nb(n,2n)^{92m}Nb; $\alpha_d = 1.1$			

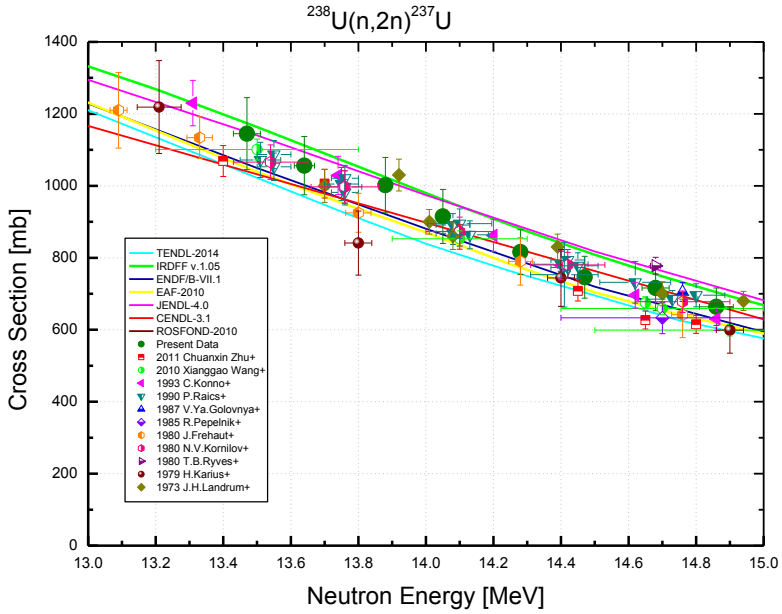

The reaction is studied rather well. The evaluations and experimental data are in a good accordance.

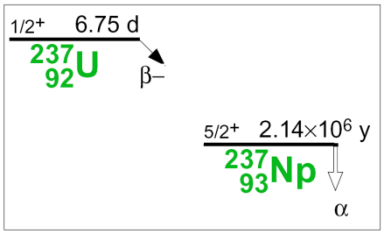

Decay data used for **^{238}U(n, 2n)^{237}U**.

Target nucleus	**Abundance [%]**	**Chemical form**	**Reaction product**	$T_{1/2}$	**E_γ [keV]**	**Y_γ [%]**
^{238}U	**99.2745** ***15***	U-metal	^{237}U	**6.752 d** ***2***	**208.0**	**21.2** ***3***

^{241}Am(n, α)^{238}Np

^{241}Am(n, α)^{238}Np		
E_n [MeV]	σ [mb]	$\Delta\sigma_{total}$ *[%]*
14.84	<1.5	*33.3*
Ref. CS is ^{93}Nb(n,2n)^{92m}Nb		

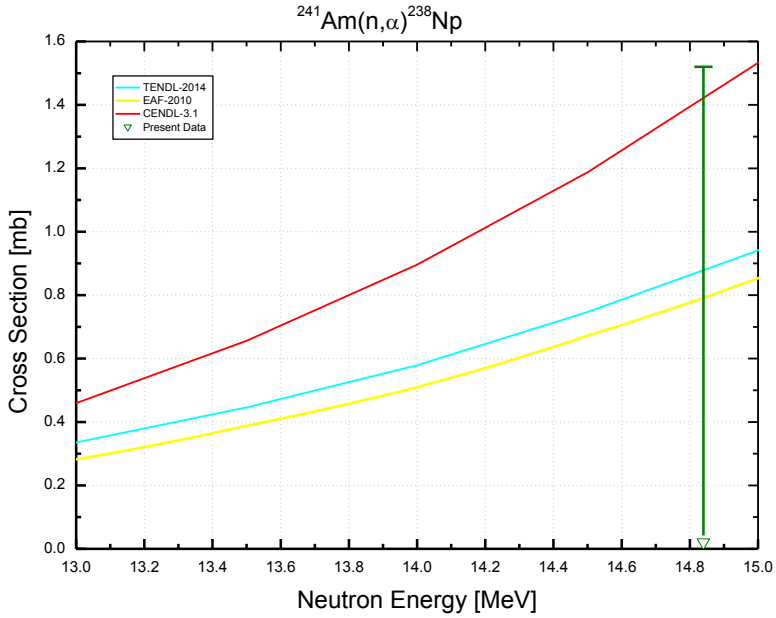

This is one of the results of the KRI pioneering cross section measurements with the ^{241}Am [4]. In more detail, the experiment of high complexity is described in pp.26-30 of this paper.

For the ^{241}Am(n, α)^{238}Np cross-section, we managed to determine only the upper limit. It is equal to 1.5 mb.

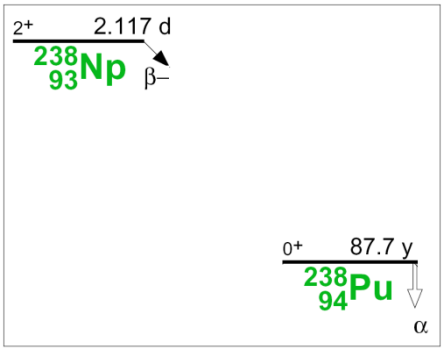

Decay data used for **^{241}Am(n, α)^{238}Np**.

Target nucleus	**Abundance [%]**	**Chemical form**	**Reaction product**	**$T_{1/2}$**	**E_γ [keV]**	**Y_γ [%]**
^{241}Am	**99.9** *1*	$Am(NO_3)_3$	^{238}Np	**2.099 d** *2*	984.5	25.2 *3*
					1025.9	8.75 *7*
					1028.5	**18.23** *12*

^{241}Am(n, 3n)^{239}Am

^{241}Am(n, 3n)^{239}Am			
E_n [MeV]	σ [mb]	$\pm\Delta\sigma_{total}$ [%]	$\pm\Delta\sigma_{ref}$ [%]
14.73	3	*66.7*	*11.8*
14.86	12	*25.0*	*11.8*
Ref. CS is ^{93}Nb(n,2n)^{92m}Nb;		$\alpha_d = 2.0$	

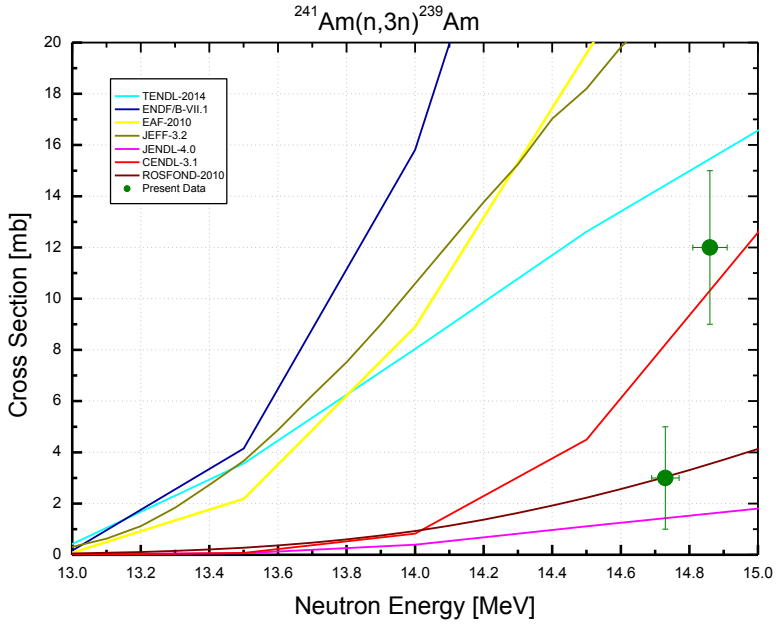

Experiment of high complexity is described in detail on pp.26-30 of this work.

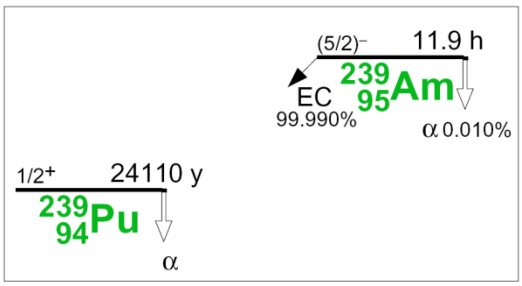

Decay data used for **^{241}Am(n, 3n)^{239}Am**.

Target nucleus	Abundance [%]	Chemical form	Reaction product	$T_{1/2}$	E_γ [keV]	Y_γ [%]
^{241}Am	**99.99**	$Am(NO_3)_3$	^{239}Am	**11.9 h** *1*	226.4	3.3 *4*
					228.2	11.3 *13*
					277.6	**15.0** *17*

^{241}Am(n, 2n)^{240}Am

^{241}Am(n, 2n)^{240}Am			
E_n [MeV]	σ [mb]	$\pm\Delta\sigma_{total}$ [%]	$\pm\Delta\sigma_{ref}$ [%]
13.48	247	*8.01*	*2.76*
13.56	240	*10.4*	*2.75*
14.09	208	*10.5*	*2.74*
14.21	229	*10.9*	*2.74*
14.69	199	*11.0*	*2.75*
14.84	194	*11.3*	*2.77*
14.86	217	*6.87*	*2.77*
Ref. CS is ^{93}Nb(n,2n)^{92m}Nb;		$\alpha_d = 1.2$	

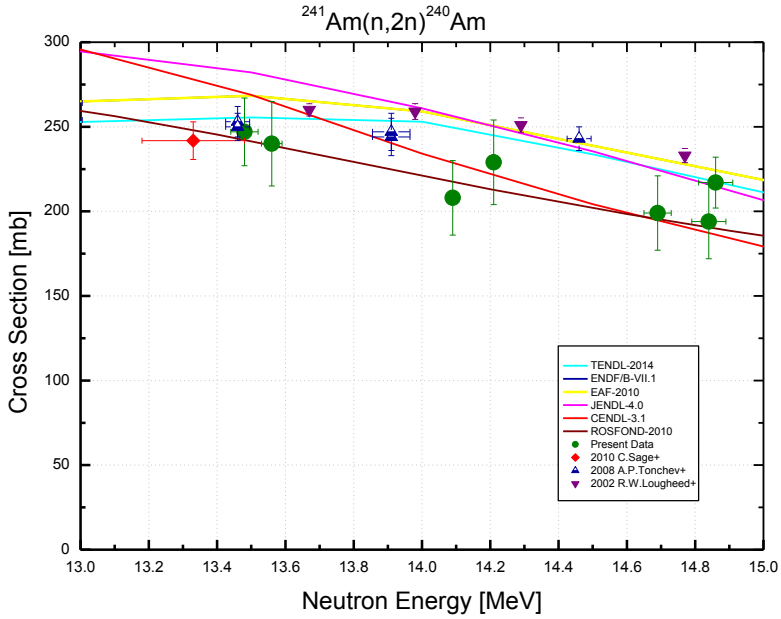

The pioneering neutron activation cross-section measurements with ^{241}Am [4] demonstrated the ability to obtain the cross section data for material of small mass ~3 mg but of very high own activity ~10^8 Bk. The experiment is described in detail in pp.26-30 of this paper.

Results of new experiments reported recently have generally confirmed the KRI data.

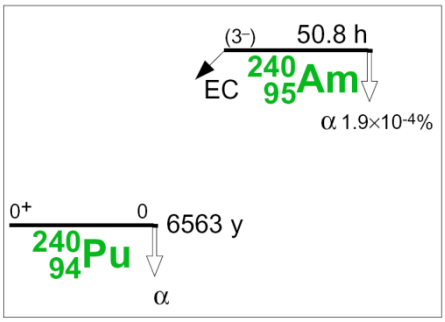

Decay data used for **^{241}Am(n, 2n)^{240}Am**.

Target nucleus	Abundance [%]	Chemical form	Reaction product	$T_{1/2}$	E_γ [keV]	Y_γ [%]
^{241}Am	**99.99**	$Am(NO_3)_3$	^{240}Am	**50.8 h** *3*	888.9	24.7 *5*
					987.8	**72.2** ***13***

ATTACHMENT. Reference cross sections

Table I. The $^{27}Al(n, \alpha)^{24}Na$ reference cross section

E_n [MeV]	**KRI** (old)		**IRDFF v1.05** (new)	
	CS [mb]	Relative Error [%]	CS [mb]	Relative Error [%]
13.45	125.8	1.13	125.46	0.795
13.46	125.8	1.12	125.46	0.795
13.47	125.7	1.11	125.46	0.795
13.48	125.7	1.11	125.46	0.795
13.49	125.6	1.10	125.46	0.795
13.50	125.5	1.09	125.46	0.795
13.56	125.2	1.04	125.33	0.525
13.58	125.0	1.04	125.29	0.525
13.64	124.6	1.04	125.07	0.525
13.65	124.5	1.04	125.03	0.525
13.66	124.4	1.05	124.98	0.525
13.67	124.3	1.05	124.94	0.525
13.68	124.2	1.05	124.89	0.525
13.70	124.0	1.05	124.80	0.525
13.72	123.8	1.05	124.67	0.525
13.73	123.7	1.05	124.60	0.525
13.74	123.6	1.05	124.53	0.525
13.75	123.5	1.05	124.47	0.525
13.87	122.7	0.98	123.51	0.491
13.88	122.6	0.98	123.43	0.491
13.89	122.6	0.98	123.34	0.491
13.95	122.3	0.98	122.72	0.491
13.96	122.3	0.98	122.62	0.491
14.04	121.9	0.98	121.71	0.462
14.05	121.9	0.98	121.59	0.462
14.06	121.8	0.99	121.47	0.462
14.07	121.7	0.99	121.35	0.462
14.09	121.4	0.99	121.12	0.462
14.10	121.3	0.99	121.00	0.462
14.19	120.3	1.00	119.83	0.462
14.21	119.9	1.00	119.56	0.410
14.23	119.6	1.00	119.29	0.410
14.25	119.2	1.01	119.02	0.410
14.26	119.1	1.01	118.88	0.410
14.27	118.9	1.01	118.74	0.410
14.28	118.7	1.01	118.61	0.410

E_n [MeV]	**KRI** (old)		**IRDFF v1.05** (new)	
	CS [mb]	Relative Error [%]	CS [mb]	Relative Error [%]
14.29	118.5	1.01	118.47	0.410
14.42	116.1	1.03	116.63	0.375
14.43	115.9	1.04	116.49	0.375
14.44	115.6	1.04	116.35	0.375
14.45	115.4	1.04	116.20	0.375
14.46	115.1	1.04	116.06	0.375
14.47	114.9	1.04	115.91	0.375
14.48	114.8	1.05	115.77	0.375
14.49	114.6	1.05	115.63	0.375
14.50	114.5	1.05	115.48	0.375
14.61	112.9	1.06	113.88	0.385
14.62	112.8	1.06	113.73	0.385
14.63	112.6	1.07	113.59	0.385
14.64	112.5	1.07	113.44	0.385
14.65	112.4	1.07	113.29	0.385
14.66	112.3	1.07	113.15	0.385
14.67	112.1	1.07	113.00	0.385
14.68	112.0	1.07	112.85	0.385
14.69	111.9	1.07	112.71	0.385
14.70	111.8	1.07	112.56	0.385
14.71	111.7	1.07	112.41	0.385
14.72	111.6	1.08	112.27	0.385
14.73	111.5	1.08	112.12	0.385
14.74	111.4	1.08	111.97	0.385
14.77	111.1	1.08	111.53	0.385
14.78	111.0	1.08	111.38	0.385
14.80	111.0	1.13	111.09	0.385
14.81	111.0	1.15	110.94	0.437
14.82	111.0	1.17	110.79	0.437
14.83	110.9	1.17	110.64	0.437
14.84	110.8	1.17	110.49	0.437
14.85	110.7	1.17	110.35	0.437
14.86	110.6	1.18	110.20	0.437
14.87	110.5	1.18	110.05	0.437
14.88	110.4	1.18	109.90	0.437

Table Ia. Decay data used at the $^{27}Al(n, \alpha)^{24}Na$ cross section determination.

Reaction product	**$T_{1/2}$**	**$E_{\square}$ [keV]**	**$Y_{\square}$ [%]**
^{24}Na	14.997 h *12*	1368.6	99.9936 *15*
		2754.0	99.855 *5*

Table II. The ^{93}Nb(n, 2n)^{92m}Nb reference cross section

E_n [MeV]	**KRI** (old)		**IRDFF v1.05** (new)	
	CS [mb]	Relative Error [%]	CS [mb]	Relative Error [%]
13.45	451.5	1.40	452.00	0.633
13.46	451.6	1.39	452.20	0.633
13.47	451.7	1.37	452.40	0.633
13.48	451.8	1.36	452.60	0.633
13.49	451.9	1.35	452.80	0.633
13.50	451.9	1.34	453.00	0.592
13.56	452.4	1.26	454.03	0.592
13.58	452.4	1.30	454.38	0.592
13.64	452.4	1.37	455.31	0.592
13.65	452.5	1.36	455.46	0.592
13.66	452.6	1.34	455.60	0.592
13.67	452.8	1.33	455.75	0.592
13.68	452.9	1.32	455.90	0.592
13.70	453.1	1.29	456.19	0.592
13.72	453.4	1.26	456.43	0.592
13.73	453.5	1.25	456.55	0.592
13.74	453.6	1.23	456.68	0.592
13.75	453.7	1.24	456.80	0.562
13.87	454.8	1.35	458.09	0.562
13.88	454.9	1.36	458.18	0.562
13.89	455.0	1.35	458.28	0.562
13.95	455.5	1.25	458.75	0.562
13.96	455.6	1.23	458.83	0.562
14.04	456.9	1.40	459.34	0.546
14.05	457.1	1.42	459.39	0.546
14.06	457.2	1.41	459.45	0.546
14.07	457.4	1.39	459.50	0.546
14.09	457.7	1.36	459.61	0.546
14.10	457.8	1.35	459.66	0.546
14.19	459.1	1.22	459.95	0.546
14.21	459.1	1.27	460.00	0.543
14.23	459.1	1.33	460.02	0.543
14.25	459.2	1.38	460.05	0.543
14.26	459.2	1.41	460.06	0.543
14.27	459.2	1.43	460.07	0.543
14.28	459.2	1.46	460.09	0.543

E_n [MeV]	**KRI** (old)		**IRDFF v1.05** (new)	
	CS [mb]	Relative Error [%]	CS [mb]	Relative Error [%]
14.29	459.3	1.44	460.10	0.543
14.42	460.2	1.22	460.12	0.549
14.43	460.2	1.26	460.12	0.549
14.44	460.3	1.30	460.12	0.549
14.45	460.3	1.35	460.13	0.549
14.46	460.4	1.39	460.13	0.549
14.47	460.4	1.43	460.13	0.549
14.48	460.4	1.42	460.13	0.549
14.49	460.3	1.40	460.13	0.549
14.50	460.3	1.39	460.13	0.549
14.61	459.9	1.22	460.15	0.565
14.62	459.8	1.25	460.15	0.565
14.63	459.6	1.29	460.16	0.565
14.64	459.5	1.32	460.16	0.565
14.65	459.3	1.36	460.16	0.565
14.66	459.2	1.39	460.16	0.565
14.67	459.0	1.43	460.16	0.565
14.68	458.9	1.46	460.17	0.565
14.69	458.7	1.43	460.17	0.565
14.70	458.6	1.41	460.17	0.565
14.71	458.4	1.38	460.17	0.565
14.72	458.3	1.36	460.18	0.565
14.73	458.1	1.33	460.18	0.565
14.74	457.9	1.31	460.18	0.565
14.77	457.5	1.23	460.19	0.565
14.78	457.3	1.20	460.19	0.565
14.80	457.1	1.28	460.20	0.565
14.81	456.9	1.32	460.21	0.588
14.82	456.8	1.36	460.21	0.588
14.83	456.4	1.36	460.22	0.588
14.84	456.1	1.36	460.23	0.588
14.85	455.7	1.36	460.24	0.588
14.86	455.3	1.36	460.24	0.588
14.87	454.9	1.36	460.25	0.588
14.88	454.6	1.36	460.26	0.588

Table IIa. Decay data used at the ^{93}Nb(n, 2n)^{92m}Nb cross section determination.

Reaction product	**$T_{1/2}$**	**$E_{\square}$ [keV]**	**$Y_{\square}$ [%]**
^{92m}Nb	10.15 d *2*	934.4	99.15 *4*

REFERENCES

1. A.A.Filatenkov, S.V.Chuvaev. Systematic Activation Cross-Section Measurements at Neutron Energies around 14 MeV. //Preprint RI-252, (1999) (in Russian).
2. A.A.Filatenkov, S.V.Chuvaev. Measurement of a Set of Insufficiently Known Neutron Induced Cross Sections. //Preprint KRI-258 (2001).
3. A.A.Filatenkov, S.V.Chuvaev. Experimental Determination of Cross Sections for Several Insufficiently Known Neutron Induced Reactions on Heavy Nuclei (Z = 74 – 79). //Preprint KRI-259 (2003).
4. A.A.Filatenkov, S.V.Chuvaev. Measurement of Cross Sections for the Reactions ^{241}Am(n, 2n) and ^{241}Am(n, 3n). //Physics of Atomic Nuclei, vol.63, No.9, pp.1504-1510 (2000).
5. A.Wallner, S.V.Chuvaev, A.A.Filatenkov, et. al. Precise measurement of the ^{27}Al(n, 2n)^{26g}Al excitation function near threshold and its relevance for fusion-plasma technology. //Eur. Phys. J. A 17, pp.285–296 (2003).
6. A.A.Filatenkov, S.V.Chuvaev, V.N.Aksenov, et. al. Systematic Measurement of Cross Sections at Neutron Energies from 13.4 to 14.9 MeV. //IAEA Report INDC(CCP)-402 (1997).
7. A.A.Filatenkov, S.V.Chuvaev, V.A.Jakovlev, V.P.Popik. Recent Nuclear Data Measurement at Khlopin Radium Institute. //Fusion Engineering and Design, vol.37, pp.151-158 (1997).
8. V.Avrigenau, S.Sudar, Cs.M.Buszko, et. al. Energy Dependence of the Isomeric Cross Section Ratio in the ^{58}Ni(n, p)^{58}Co^{m,g} Reaction. //Phys. Rev. C, vol. 60, pp.602-605 (1999).
9. P. Reimer, V. Avrigeanu, S.V. Chuvaev, A.A. Filatenkov, et. al. Reaction mechanisms of fast neutrons on stable Mo isotopes below 21 MeV. //Phys. Rev. C, vol.71, 044617, (2005).
10. V. Avrigeanu, S.V. Chuvaev, R. Eichin, A.A. Filatenkov, et. al Pre-equilibrium reactions on the stable tungsten isotopes at low energy. //Nucl. Phys. A765, pp.1-28 (2006).
11. M. Avrigeanu, S.V. Chuvaev, A.A. Filatenkov, et. al. Fast–neutron induced pre–equilibrium reactions on 55Mn and 63,65Cu at energies up to 40 MeV. //Nucl. Phys. A806, pp.17-39 (2008).
12. A.A.Filatenkov, S.V.Chuvaev, S.V.Jakovlev, et. al. Systematic Measurement of Cross Sections at Neutron Energies of 13.4-14.9 MeV. //In: Proc. of Int. Conf. on Nucl. Data for Science and Technology, 19-24 May 1997, Trieste, Italy. pp.598-602.
13. A.A.Filatenkov, S.V.Chuvaev, S.V.Jakovlev, et. al. Measurement and Analysis of the (n, p), (n, a), (n, 2n) and (n, np) Reaction Cross Sections of ^{59}Co and ^{58}Ni. //In: Proc. of Int. Conf. on Nucl. Data for Science and Technology, 19-24 May 1997, Trieste, Italy. pp.595-597.
14. A.Wallner, S.V.Chuvaev, A.A.Filatenkov, et. al. Study of the ^{27}Al(n, 2n)^{26}Al Reaction. //In: Proc. of Int. Conf. on Nucl. Data for Science and Technology, 19-24 May 1997, Trieste, Italy. pp.1248-1251.
15. A.A.Filatenkov, S.V.Chuvaev, D.L.Smith, et. al. Measurement of ^{241}Am Activation Cross Sections at Neutron Energies around 14 MeV. //In: Proc. of Int. Conf. on Nucl. Data for Science and Technology, 19-24 May 1997, Trieste, Italy. pp.1313-1316.
16. V.Avrigenau, S.Sudar, Cs.M.Buszko, et. al. Energy Dependence of the Isomeric Cross Section Ratio in the ^{58}Ni(n, p)^{58}Co^{m,g} Reactions. //In: Proc. of Int. Conf. on Nucl. Data for Science and Technology, 19-24 May 1997, Trieste, Italy. pp.1274-1276.

17. M.V.Blinov, A.A.Filatenkov, B.M.Shiryaev, S.V.Chuvaev. Measurements of Cross Sections of the ^{109}Ag(n,2n)^{108m}Ag, ^{151}Eu(n,2n)^{150m}Eu and ^{153Eu}(n,2n)^{152Eu} Reactions at Neutron Energy 14 MeV //IAEA Report INDC(NDS)-232L, p.87-94 (1990).

18. M.V.Blinov, A.A.Filatenkov, S.V.Chuvaev. Measurements of Activation Cross Sections for Some Long-lived Nuclides Important in Fusion Reactor Technology. // IAEA Report INDC(NDS)-263, p. 143-154. (1992).

19. M.V.Blinov, S.V.Chuvaev, A.A.Filatenkov, et al. Measurement of Cross Sections of Some Reactions of Importance in Fusion Reactor Technology. //IAEA Report INDC(NDS)-342, p. 53-64 (1996).

20. V.A.Jakovlev. Analytical expression for fast neutron spectra at finite experiment geometry. Preprint RI-211 (1988). (in Russian).

21. Yujiro Ikeda, Chikara Konno, Koji Oishi, et. al. Activation Cross Section Measurements for Fusion Reactor Structural Materials at Neutron Energy from 13.3 to 15.0 MeV Using FNS Facility. JAERI 1312 (1988).

22. Chikara Konno, Yujiro Ikeda, Koji Oishi, et. al. Activation Cross Section Measurements at Neutron Energy from 13.3 to 14.9 MeV Using the FNS Facility. JAERI 1329 (1993).

23. M.Wagner, H.Vonach, A.Pavlik et all. Evaluation of Cross Sections for 14 Important Neutron-Dosimetry Reactions. Physics Data, No. 13-5 (1990).

24. J.-Ch.Sublet, L.W.Packer, J.Kopecky, et al. The European Activation File: EAF-2010 neutron-induced cross section library. //CCFE-R (10) 05 (2010). available also on website: http://www.ccfe.ac.uk/tech_reports.aspx

25. Richard B. Firestone. Table of Isotopes, CD ROM Edition, version 1, March 1996.

26. Live Chart of Nuclides nuclear structure and decay data:
http://www-nds.ieae.org/relnsd/vcharthtml/VChartHTML.html or:
http://www.nndc.bnl.gov/nudat2/

27. Isotopic Compositions of the Elements:
https://www-nds.iaea.org/IRDFF/IRDFF-Abundancy-2012.pdf

28. Experimental Nuclear Reaction Data (EXFOR): http://www-nds.ieae.org/exfor/

29. Evaluated Nuclear Data File (ENDF): http://www-nds.iaea.org/endf/

Nuclear Data Section
International Atomic Energy Agency
Vienna International Centre, P.O. Box 100
A-1400 Vienna, Austria

E-mail: nds.contact-point@iaea.org
Fax: (43-1) 26007
Telephone: (43-1) 2600 21725
Web: http://www-nds.iaea.org